The Impact of Aging on Memory: a Behavioral Genetics Study

Inaugural-Dissertation

to obtain the academic degree

Doctor rerum naturalium (Dr. rer. nat.)

submitted to the Department of Biology, Chemistry, Pharmacy

of Freie Universität Berlin

by

Christine Brigitte Beuschel-Dang

2022

This thesis was accomplished from September 2013 to March 2022 under the supervision of Prof. Dr. Stephan J. Sigrist at the Institute of Biology/ Genetics of the Freie Universität Berlin and the CharitéCrossOver from the Charité Campus Mitte Berlin, Germany.

1st Reviewer: Prof. Dr. Stephan J. Sigrist

2nd Reviewer: Prof. Dr. Mathias F. Wernet

Date of Defense: 07.07.2022

State of Authorship

I hereby affirm that I wrote this thesis independently and without any inappropriate support. I performed all the experiments on my own. If there were sources from others, I referenced them as such. All used publications were declared.

Mehr Licht!

Johann Wolfgang von Goethe

The most exciting phrase to hear in science, the one that heralds new discoveries, is not 'Eureka!' but rather 'That's funny…'

Isaak Asimov

Table of contents

Summary

The question of how to decelerate aging will persist as long as humankind exists. Recently, healthy aging has come into focus. The mind should remain sharp in the same way as the body should stay agile. According to the World Health Organization, dementia will rise dramatically within the following decades, and the highest risk factor is aging. The problem is how to address this fundamental topic. Here, a tiny animal named *Drosophila melanogaster* is one solution. Due to its short lifespan, easy genetic access, and evolutionary conserved aging mechanisms between flies and humans, it serves as a suitable model organism.

In my studies, I used a classical pavlovian conditioning assay to draw connections between aging and cognitive decline. The flies were trained with an aversive olfactory approach. In the first part, I examined a potential anti-aging supplement, the natural-occurring flavonoid 4,4‘-Dimethoxychalcone. I found this substance prolonged the lifespan of treated animals and enhanced mobility yet did not improve memory performance. Spermidine, another anti-aging supplement, promotes longevity and also prevents age-induced memory decline. I discovered that a mild attenuation of the enzyme, which catalyzes the first step of the hypusination of the eukaryotic translation initiation factor 5A and needs Spermidine as a co-factor, already impaired the memory of young animals. Further, I examined some effects of autophagy. I could show that deficient macroautophagy, where an autophagosome engulfs cargo for degradation, provoked severe memory problems at a young age already, similar to aged animals. Analogously, an early memory decay occurred in animals lacking the neuropeptide sNPF (in mammals: NPY), which levels also decreased in macroautophagy-deficient animals or at advanced ages. However, further experiments demonstrated that a boost of either macroautophagy or sNPF could not protect from age-induced memory impairment. Other investigations revealed no memory benefit from a downregulated insulin-signaling pathway, which promotes longevity. Thus, a prolonged lifespan is not automatically accompanied by better cognitive abilities. Moreover, I investigated synaptic aspects of aging. The amount of scaffold proteins at the presynaptic active zone, where neurotransmitters are released, is enhanced in challenging situations like aging or sleep deprivation, seemingly leading to an operating peak of the system, followed by memory deficits. A moderate increase of one active zone component, the ELKS family member Bruchpilot, could prevent the memory issues of chronically sleep-deprived flies. Additionally, my examinations on another active zone protein, Unc13, the synaptic vesicle release factor, revealed its essential role in memory formation in the mushroom body, the learning center of the fly brain.

Taken together, my thesis sheds light on the mosaic of healthy aging, potentially supporting future preventive or therapeutic strategies for high-quality aging.

Zusammenfassung

Die Frage, wie das Leben verlängert werden kann, besteht seit Menschengedenken. Dabei rückt immer mehr ein gesundes Altern in den Fokus. Physische Fitness und kognitive Vitalität sind gefragt. Ein hohes Alter ist jedoch der größte Risikofaktor, um an Demenz zu erkranken. In meiner Doktorarbeit erforschte ich einige Zusammenhänge von Altern und Gedächtnisverlust. Hierbei diente *Drosophila melanogaster* als idealer Modellorganismus aufgrund seiner kurzen Lebenszeit, vieler Möglichkeiten der genetischen Modifikation und evolutionär hoch konservierter Alterungsmechanismen. Mit Hilfe der klassischen Konditionierung nach Pawlow überprüfte ich aversives olfaktorisches Lernverhalten. Zunächst entdeckte ich den positiven Einfluss des natürlich vorkommenden Flavonoids 4,4‘-Dimethoxychalcon auf Mobilität und Lebensspanne, was jedoch nicht mit einem verbesserten Gedächtnis im Alter einherging. Dagegen wirkt Spermidin, ein mit dem Alter abnehmendes endogenes Polyamin, als Nahrungsergänzungsmittel lebensverlängernd und gedächtniserhaltend. Ich konnte feststellen, dass eine milde Verringerung des Enzyms, das den ersten Schritt der Hypusinierung des eukaryotischen Translationsinitationsfaktors 5A katalysiert und Spermidin dafür als Co-Faktor benötigt, eine Gedächtnisbeeinträchtigung schon bei jungen Fliegen hervorrief. Die Untersuchung weiterer Alterungsprozesse zeigte vergleichbare Gedächtnisprobleme bei verminderter körpereigener Autophagozytose und erhöhtem Alter. In beiden Szenarien lag das Neuropeptid sNPF (bei Säugetieren: NPY) vermindert vor. Analog fand ich massive Erinnerungsschwierigkeiten in juvenilen, sNPF-defekten Fliegen. Jedoch konnten weder eine sNPF-Hochregulierung noch vermehrte Autophagie einen altersinduzierten Gedächtnisverlust verhindern. Zusätzliche Lernversuche mit Tieren, die durch Suppression insulin-ähnlicher Peptide langlebiger wurden, zeigten keinen bedingten Zusammenhang von Langlebigkeit und Gedächtniserhalt. Darüber hinaus untersuchte ich synaptische Aspekte des Alterns. Während der Kommunikation zwischen den Neuronen werden Neurotransmitter an der präsynaptischen aktiven Zone ausgeschüttet, wodurch an der Postsynapse das Signal weitergeleitet wird. Bestandteile dieser aktiven Zone sammeln sich in fordernden Situationen wie dem Altern oder Schlafentzug massiv an, sodass das System überladen wird und Prozesse wie das Lernen gestört werden. Jedoch konnte eine moderate Erhöhung der präsynaptischen Komponente Bruchpilot die Gedächtnisprobleme von chronisch schlaf-defizitären Tieren beheben. Lerntests mit einem weiteren präsynaptischen Protein, Unc13, einem Faktor für die Freisetzung synaptischer Vesikel, bestätigten dieses als essentiell im Mushroom Body, dem Lernzentrum bei Fliegen.
Meine Arbeit bringt einen konstruktiven Beitrag für die Altersforschung, um letztlich durch Prävention oder auch Therapien ein qualitativ hochwertiges Altern zu ermöglichen.

I. Introduction

1. Aging, a risk factor for physical and cognitive functions

Aging is a progressive process happening to all living beings. The time-dependent loss of physiological integrity and functionality causes reduced mobility, cognitive decline, and finally, the end of the individual's life (López-Otín et al., 2013; Mattson and Arumugam, 2018). However, human life expectancy increased enormously due to medical achievements in the last century. According to the World Health Organisation, the old-age dependency ratio (OADR), the percentage of persons older than 64 years in a population, will double in Europe within the next 30 years (United Nations Department of Economic and Social Affairs, Population Division, 2020). This entails several socio-economic challenges since becoming older is not automatically accompanied by staying healthy. Advancing age is the highest risk factor to suffer from several ailments, followed by a loss of self-determination and independence (Kulkarni et al., 2018). Thus, more than half of the age group beyond 65 is concerned about their cognitive fitness and life quality (Krivanek et al., 2021).

Aging itself starts in the organs and cells when the operating homeostasis, the equilibrium of synthesis and degradation, stumbles due to the accumulation of defective processes and damaged structures. The manifold hallmarks behind aging are highly conserved in the different species: Loss of proteostasis, cellular senescence, deregulated nutrient sensing, mitochondrial dysfunction, stem cell exhaustion, altered intercellular communication, genomic instability, and telomere attrition (Figure 1; López-Otín et al., 2013). All these senescence-promoting states are intertwined, making gerontology so complex.

Thus, protein homeostasis (proteostasis), a balanced proteome in a functioning and steady state, is a crucial player against aging (López-Otín et al., 2013). Its loss effects the accumulation of unfolded or misfolded proteins, and also cellular senescence (López-Otín et al., 2013). As housekeepers act the ubiquitin-proteasome and the autophagy-lysosome systems, which recycle faulty cellular components (more in detail in chapter I.3) (Liang and Sigrist, 2018; Loeffler, 2019). A balanced cleansing via autophagy supports neuronal maintenance and homeostasis (Liang and Sigrist, 2018). Additionally, autophagy facilitates mitochondrial homeostasis via the degradation of defective mitochondria (mitophagy), which are the energy factories within the cells (Liang and Sigrist, 2018). Their efficiency decreases with time, followed by enhanced electron leak and reduced ATP production (López-Otín et al., 2013). Regarding the coordination of autophagy, the insulin and insulin-like growth factor-1 (IGF-1) signaling (IIS) pathway interferes (more in detail in chapter I.2). The nutrient-sensing via the IIS coordinates the work of the transcription factor FOXO (forkhead box subgroup O) and its counterpart mTORC1 (mammalian target of rapamycin complex 1). Activation of FOXO, just like the inhibition of mTORC1, supports autophagy, metabolic control, and stress

resistance (Poloz and Stambolic, 2015; Kauwe et al., 2016). Several studies proved age-prolonging effects due to diminished IIS, FOXO polymorphism, or inhibition of mTORC1 via rapamycin administration in different species from *Drosophila* to mice and humans (Grönke et al., 2010; Cabo et al., 2014; Piper and Partridge, 2018).

Moreover, age-induced changes in intercellular communication disturb the balance of endocrine or neuroendocrine systems (López-Otín et al., 2013). For instance, the amount of

Figure 1: Hallmarks of aging.

Senescence is caused by several mechanisms, which are highly conserved in different species. They interact with each other and are mutually dependent: the loss of proteostasis, deregulated nutrient sensing, mitochondrial dysfunction, cellular senescence, stell cell exhaustion, altered intercellular communication, genomic instability, telomere attrition, and epigenetic alterations (López-Otín et al., 2013). Image taken from López-Otín et al., 2013.

the mammalian neuropeptide Y (NPY; in *Drosophila*: short neuropeptide F, sNPF), which mediates forage, growth, autophagy, and sleep, decreases with age (Lee et al., 2004; Chen et al., 2013; Aveleira et al., 2015b; Botelho and Cavadas, 2015). Further, an age-induced faulty sensitivity of the hormone insulin promotes insulin resistance of the cells, the first symptom of adult-onset diabetes (type-II diabetes; Silbernagl and Despopoulos, 1979). Such altered intercellular communications can impair the immunological response to pathogens and degenerated cells, and force the development of inflammation foci (López-Otín et al., 2013).
Directly concerning the DNA sequence, defects in the genomic stability, like replication errors, or the wear of telomeres, the repetitive nucleotide sequences at the end of the chromosomes, provoke an increase in genetic damage (López-Otín et al., 2013). These hazard signs also cause stem cell exhaustion, just like cellular senescence. Moreover, epigenetic alterations, such as histone modifications, DNA methylation, or chromatin remodeling, influence the DNA's readability (López-Otín et al., 2013). These are affected by life circumstances and environmental factors (Fraga et al., 2005). Concomitantly, all these elements of aging contribute to stem cell exhaustion, followed by the loss of tissues' regenerative abilities (López-Otín et al., 2013).

The question is how to address such a plethora of aging mechanisms. They raise not only with advancing age but also with an excessive lifestyle, smoking, continuing stress, inadequate sleep, or missing physical activity (Krivanek et al., 2021). Subsequently, several malady factors like metabolic syndrome, a cluster of obesity, insulin resistance, hypertension, and lipometabolic disorder, occur, followed by cardiovascular diseases, stroke, cancer, and early brain aging (Samson and Garber, 2014; Mattson and Arumugam, 2018). Additionally, neurodegenerative diseases such as Alzheimer's, Parkinson's, or Huntington's start with mild memory impairment and lead to severe physical and cognitive impairments with higher age (Mattson and Arumugam, 2018).

Already 1939, the first study about the favorable effects of caloric restriction, the reduction of caloric ingestion without malnutrition, on lifespan in mice and rats became published (McCay et al., 1939; Campisi et al., 2019; Madeo et al., 2019). Since then age research has discovered several underlying modes of action, highly conserved in different species and affecting hallmarks of aging like autophagy (López-Otín et al., 2013; Campisi et al., 2019). However, compliance with permanent or even intermittent fasting is relatively low.
Indeed, several substances were found to affect different or even some hallmarks of aging (Figure 2). For instance, Spermidine supports heart protection, neuroprotection, and memory and boosts the immune system and lifespan from invertebrates to mammals (Eisenberg et al., 2009; Gupta et al., 2013; Sigrist et al., 2014; Madeo et al., 2018). This endogenous substance

decreases with age, yet dietary supplementation can restore, for example, cognitive defects or lifespan (Gupta et al., 2013). Further naturally occurring compounds like flavonoids, secondary metabolites in plants, work anti-inflammatory, antioxidative, antibacterial, and antiviral (Kühnau, 1976; Rice-Evans and Miller, 1996; Badshah et al., 2021). Equally, old acquaintances in the human drug therapies such as the non-steroidal anti-inflammatory Aspirin (active ingredient: acetylsalicylic acid), the anti-diabetic Metformin, or the immunosuppressant medicament Rapamycin (also named Sirolimus), supports the body in various ways (Cabo et al., 2014; Campisi et al., 2019; Madeo et al., 2019).

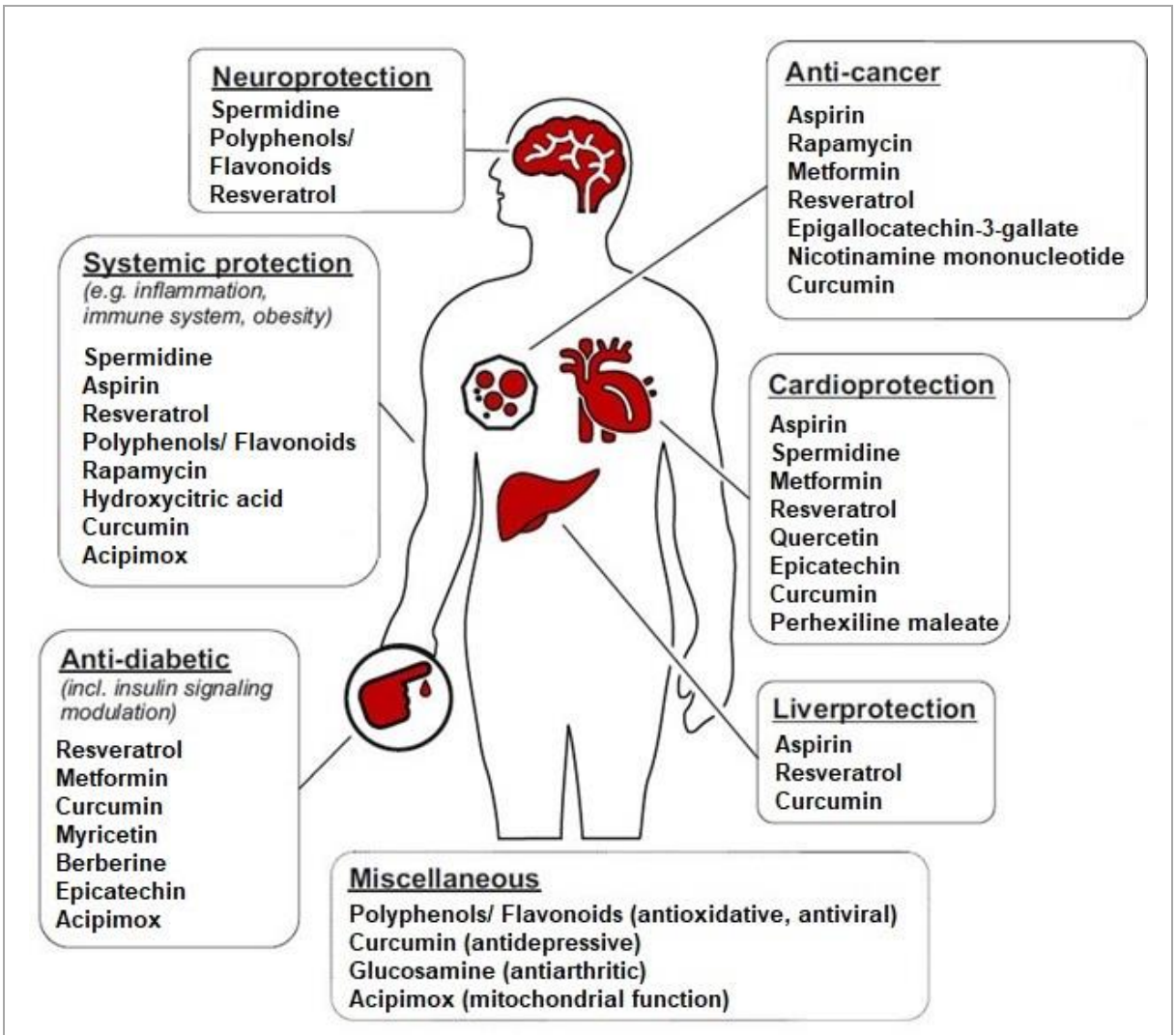

Figure 2: Substances interfering in aging pathways.

Several compounds are found to protect various tissues and combat age-associated diseases. They affect different or even some aging pathways. Thus, these substances can aid against inflammation, cancer, or misregulated insulin signaling and support the immune system or organs like neurons, the heart, or the liver. Image modified from Madeo et al., 2019

However, the search for compounds, targeting aging pathways and improving life expectancy, continues. In turn, such substances support not only human health but also shed light on the mosaic of healthy aging. Thus, more pathways and connections behind the beneficial effects become revealed.

2. The insulin signaling pathway

The impact of the insulin and insulin-like growth factor-1 (IGF-1) signaling (IIS) pathway on aging is proven in several studies and highly conserved in different species (López-Otín et al., 2013; Longo et al., 2015; Mattson et al., 2018). A downregulation of specific IIS components provides longevity in *C. elegans*, *Drosophila melanogaster*, mice, and humans (Piper and Partridge, 2018). This pathway regulates the nutritional circuit, especially glucose uptake into the cells, but is also involved in the development, reproduction, or stress response (Nässel et al., 2013).

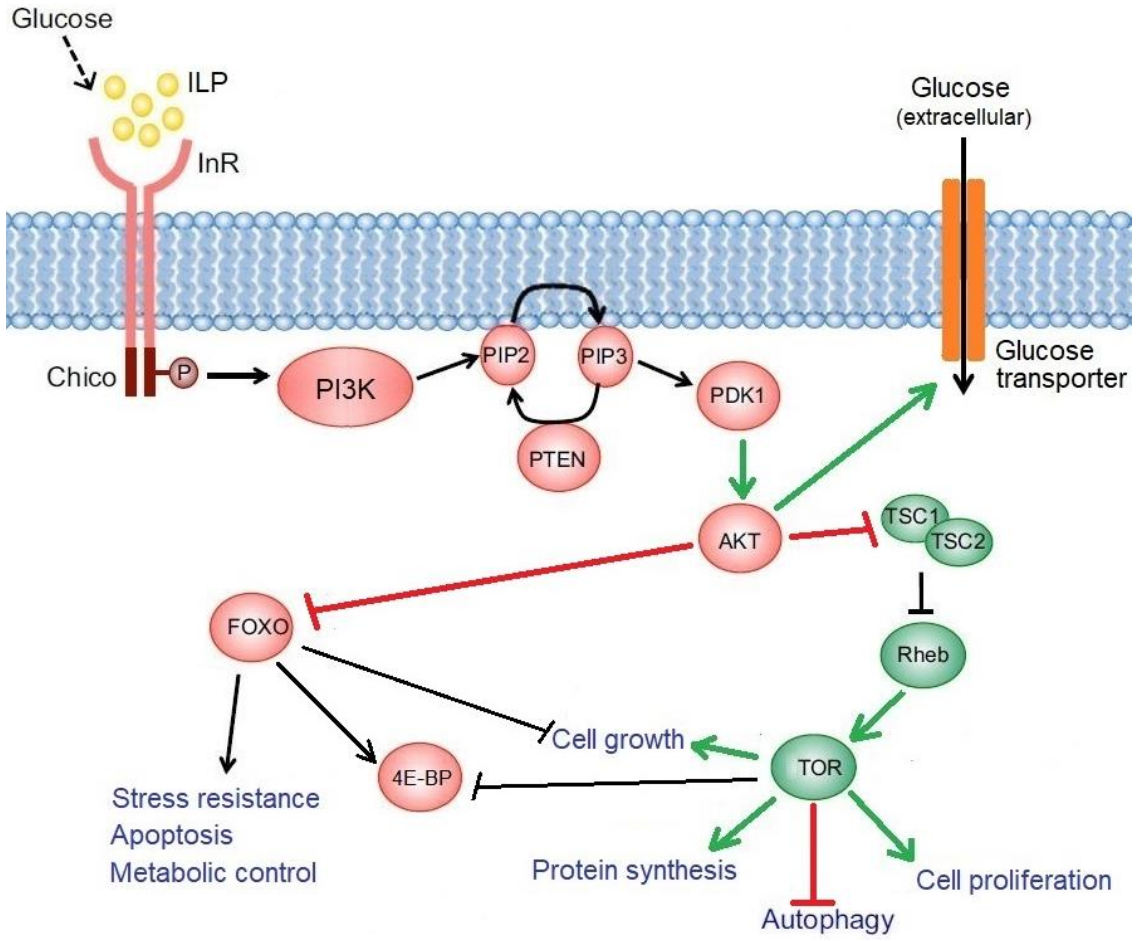

Figure 3: The insulin signaling pathway.

Free glucose in the hemolymph triggers the release of ILPs (insulin in mammals), which binds to the insulin receptor (InR). This, in turn, activates Chico (INSR in mammals), followed by a cascade of phosphorylations resulting in AKT activation. Additionally, this enables the glucose transporter to bring glucose into the cell. Further, AKT inhibits FOXO and activates TOR indirectly. Thus, insulin signaling triggers anabolic processes like cell growth, protein synthesis, and cell proliferation, plus it inhibits autophagy and stress resistance (Poloz and Stambolic, 2015; Kauwe et al., 2016; Pan and Finkel, 2017). Image modified from Shim et al., 2013.

The IIS pathway starts with the sensing of glucose, but also amino acids or fat in the hemolymph activate the release of insulin-like peptides (ILP, in *Drosophila*) (Figure 3; Shim et al., 2013). These bind to the insulin receptor (InR; INSR in mammals) on cells, which phosphorylates Chico (in mammals: insulin receptor substrate, IRS), followed by the activation of the phosphatidylinositol 3-kinase (PI3K) (Shim et al., 2013). This kinase catalyzes the phosphorylation of phosphatidylinositol-4,5-biphosphate (PIP2) to phosphatidylinositol-3,4,5-triphosphate (PIP3), in turn, to phosphorylate the 3-phosphoinositide-dependent protein kinase 1 (PDK1) and then AKT (a protein kinase B) (Poloz and Stambolic, 2015). Through AKT, the metabolic effects of the insulin pathway become generated (Poloz and Stambolic, 2015). Thus, the glucose transporter (GLUT in mammals) enables glucose intake into the cells. Additionally, AKT inhibits the transcription factor forkhead box subgroup O (FOXO), followed by decreased gluconeogenesis, reduced apoptosis, lower stress resistance, and less growth suppression (Shim et al., 2013). Additionally, FOXO activates the eukaryotic initiation factor 4E binding protein (4E-BP), which promotes inhibition of translational processes (Kauwe et al., 2016). Furthermore, AKT inhibits the tumor suppressor proteins TSC1 and TSC2 (tuberous sclerosis complex), which enables the activity of the GTPase Rheb (Ras homolog enriched in brain), followed by a stimulation of the kinase TOR (target of rapamycin; mTORC1 in mammals) (Poloz and Stambolic, 2015). TOR boosts transcription, protein synthesis, cell growth, and proliferation, but also inflammation, and it inhibits autophagy (Shim et al., 2013; Pan and Finkel, 2017). It operates as a counterpart to FOXO.
In this way, the IIS pathway lowers and buffers the blood glucose so that this is directly available for the highly glucose-dependent central nervous system, regardless of the food intake (Silbernagl and Despopoulos, 1979). Furthermore, IIS promotes anabolic processes like protein storage in muscle tissue and lipogenesis, the synthesis and storage of fatty acids in the form of triacylglycerides (TAG) (Silbernagl and Despopoulos, 1979). Additionally, IIS activates the distribution of potassium (K^+) by stimulating the Na^+-K^+-ATPase, a pump that transports K^+ into the cells and sodium (Na^+) out via the consumption of ATP, to maintain the resting potential of the cell membrane (Silbernagl and Despopoulos, 1979).

A lack of insulin (Diabetes mellitus type I) or a reduced insulin efficiency (Diabetes mellitus type II), mainly arising with senescence, results in an elevated blood sugar level, increased lipolysis, followed by the risk for a fatty liver (Silbernagl and Despopoulos, 1979). Long-term issues of diabetes are, *inter alia*, damage to the veins, the heart, and the nerves (Collaboration, 2010). Nowadays, connections between the IIS pathway with Alzheimer's, Parkinson's, or Huntington's disease are observed (Akhtar and Sah, 2020; Kellar and Craft, 2020).

3. Decreased autophagy, an essential parameter of aging

Autophagy comes from the Greek *autóphagos* and means ‘self-devouring’. In the context of aging, this essential cleaning system in eukaryotes seems to hold a key position (Rubinsztein et al., 2011; Liang and Sigrist, 2018). Indeed, it is highly conserved across different species (Bishop et al., 2010; Choi et al., 2013). Autophagy functions as the housekeeper of the cells and ensures the balance between synthesis and degradation to maintain cellular homeostasis (Levine and Kroemer, 2008; Yin et al., 2016). A malfunctioning of its adjusting nature can lead to inflammations, neurodegenerative diseases, and cancer (Yin et al., 2016). For instance, impaired autophagy is associated with the aggregation of malign proteins in mice, similar to accumulations in Alzheimer's or Huntington's disease (Hara et al., 2006; Liang and Sigrist, 2018). Furthermore, a downregulated expression of mitophagy genes (degradation of mitochondria via autophagy) can provoke inflammations (Okamoto, 2014).

Autophagy can be distinguished into three categories (Figure 4): chaperone-mediated autophagy (CMA), microautophagy, and macroautophagy. The CMA occurs in the cytosol, where the Hsc70 protein (heat shock cognate 70) recognizes proteins with the KFERQ motif and delivers them to the lysosome-associated membrane protein 2A (LAMP-2A), which binds the cargo. Subsequently, the supplied protein unfolds to cross the lysosomal membrane for its degradation (Singh and Cuervo, 2011). At microautophagy, a lysosome directly absorbs the substrates. The third and most complex type of autophagy is macroautophagy. In short, proteins and organelles, meant for degradation, are absorbed by multi-membrane vesicles, named autophagosomes, and transported to lysosomes for degradation (Bento et al., 2016; Bhukel and Beuschel et al., 2019). This process is regulated by autophagy-related proteins (Atg) (Menzies et al., 2017).

The machinery of macroautophagy starts with an initiation complex involving Atg1 (in mammals: Unc51-like kinase 1, Ulk1), which clusters and activates the subsequent complex of Atg6 (Beclin1 in mammals) and Vps34 (Figure 4). The latter works as a lipid kinase and builds the phagophore source via lipidation (Choi et al., 2013; Menzies et al., 2017). Additionally, this protein recruits complex factors from the conjugation cascades. Here, Atg5 conjugates with Atg12 and Atg16 to act within this formation as a ubiquitin-protein ligase-like (E3) complex, which facilitates the generation of activated, lipidated Atg8 (Atg8-II) (Hanada et al., 2007; Gelino and Hansen, 2012; Bento et al., 2016; Gui et al., 2019). In the second part of the conjugation cascade, Atg8 (in mammals LC3) is activated to its lipidated state Atg8-II, needed for elongation and ultimately for the phagophore's closure, forming an autophagosome with a double membrane. Here, the Atg5-Atg12-Atg16 complex supports Atg3 activity followed

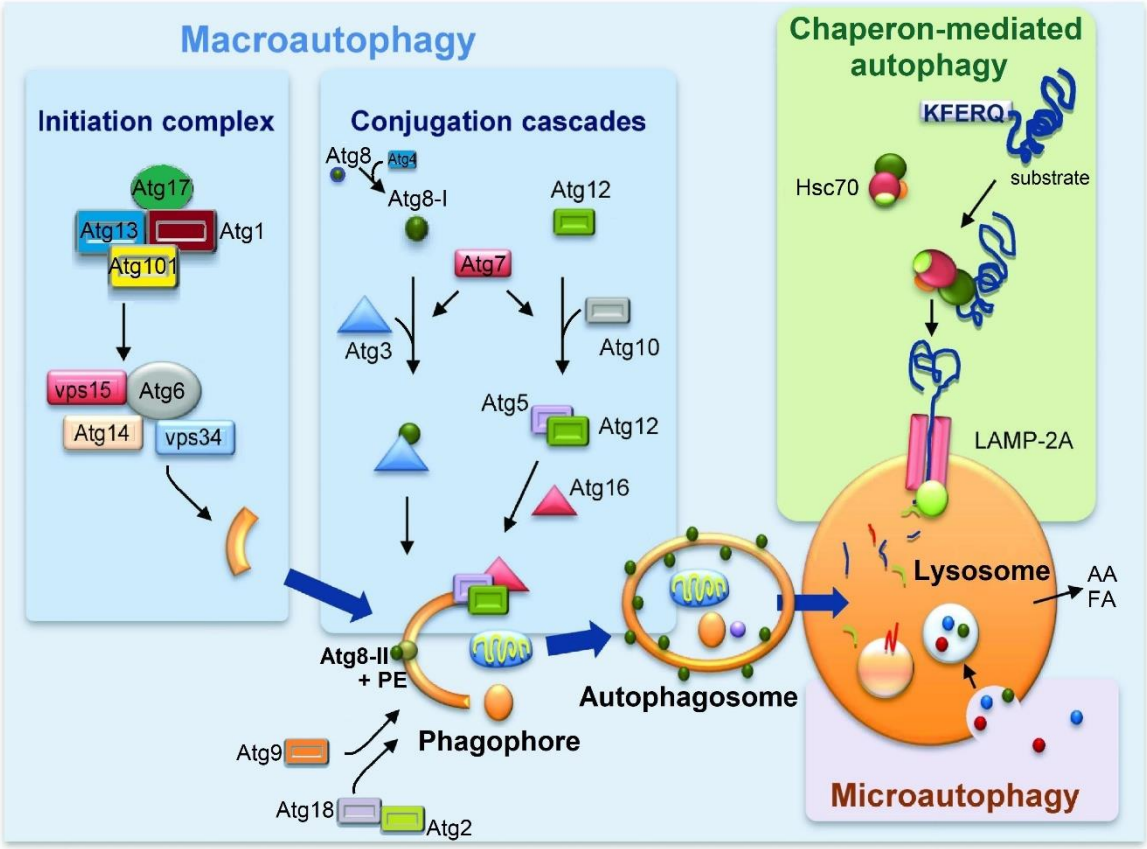

Figure 4: The three autophagy categories: macroautophagy, chaperon-mediated autophagy (CMA), and microautophagy.

Within macroautophagy, a phagophore (with a double-layered membrane) engulfs garbage, like damaged mitochondria or aggregated prone proteins, with the help of a cascade of autophagy-related proteins (Atg) and delivers its cargo as matured autophagosome to lysosomes for degradation. At chaperon-mediated autophagy (CMA), the cytosolic chaperon Hsc70 recognizes misfolded proteins with the KFERQ motif and provides them to the lysosome. At microautophagy, substrates are directly absorbed by lysosomes. AA: amino acids. FA: fatty acids. PE: phosphatidylethanolamine. Image modified from Singh and Cuervo, 2011.

by the conjugation of Atg8-II with phosphatidylethanolamine (PE) (Hanada et al., 2007). Another critical component, Atg9, serves as the transmembrane carrier for the required lipid bilayers (phosphatidylinositol 3-phosphate, PI3P) within the phagophore formation (Gelino and Hansen, 2012; Bento et al., 2016). The mature autophagosome engulfs cargo, marked for degradation with receptors like p62 (in *Drosophila*: Ref(2)p), binding ubiquitinated residues of proteins, and transports it to the lysosome. Via fusion with the lysosome, an autolysosome arises, where waste is digested (Bento et al., 2016).

Vice versa, p62/Ref(2)p, along with ubiquitinated proteins, serves as a marker for progressive autophagic damage and neuronal aging (Bartlett et al., 2011). Accumulations of these proteins are associated with several human diseases, which progress with age. Hence, pathological inclusions with these components can be found in tissues of patients with neurological ailments such as Alzheimer's disease (Bartlett et al., 2011). Of course, Alzheimer's is not the only neurodegenerative disease where autophagy is impaired. Misfolded protein aggregates due to reduced autophagy can also be detected for Parkinson's or Huntington's disease and amyotrophic lateral sclerosis (Frake et al., 2015; Menzies et al., 2017; Liang and Sigrist, 2018). Since these ailments show a link between impaired autophagy and aging, an operating cleaning system of the body seems to play a critical role in how we age.

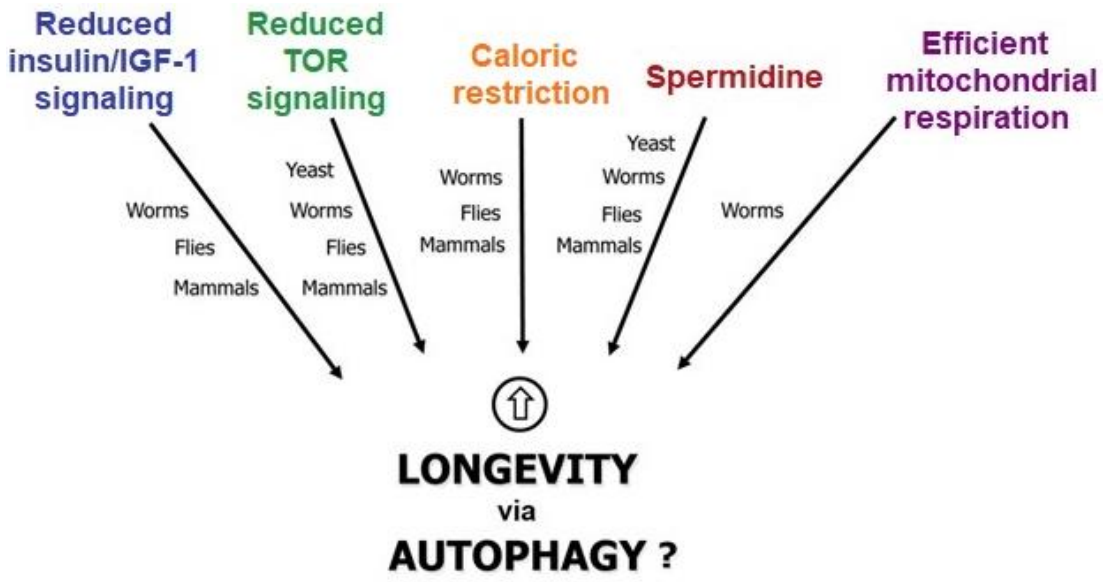

Figure 5: Conserved pathways, which induce longevity via autophagy.

Beneficial effects of increasing longevity are conserved over different species. Within them, autophagy plays a critical role. Thus, interventions like reducing insulin/ IGF-1 and TOR signaling, reducing ROS (reactive oxygen species) by more efficient mitochondrial respiration, caloric restriction, and supplementation of Spermidine show positive effects against aging (Gelino and Hansen, 2012). Image modified from Gelino and Hansen, 2012.

So far, we know several pathways to affect the longevity of organisms, presumably via autophagy (Figure 5; Simonsen et al., 2008; Gelino and Hansen, 2012; Leidal et al., 2018). Indeed, factors like caloric restriction, the reduced intake of nutrients with simultaneous prevention of malnutrition, or the supplementation of the polyamine Spermidine are protective against aging effects. Equally, suppression of insulin signaling or TOR (target of Rapamycin)

and a more efficient mitochondrial respiration are beneficial (Gelino and Hansen, 2012). In this study, some of these interventions were discussed.

4. The olfactory nervous system

Olfaction is evolutionary one of the oldest sensory systems. It allows to detect potentially dangerous situations like rotten food, noxious circumstances, or predators, but also supports foraging, mating behavior, or even provokes autobiographical memories (Chu and Downes, 2000; Asahina et al., 2008; Brattoli et al., 2011). Interestingly, a remarkable homology exists in the olfactory nervous system's fundamental anatomical organization and function between different species like invertebrates and mammals (Figure 6; Hildebrand and Shepherd, 1997; Matsunami and Amrein, 2003; Davis, 2004).

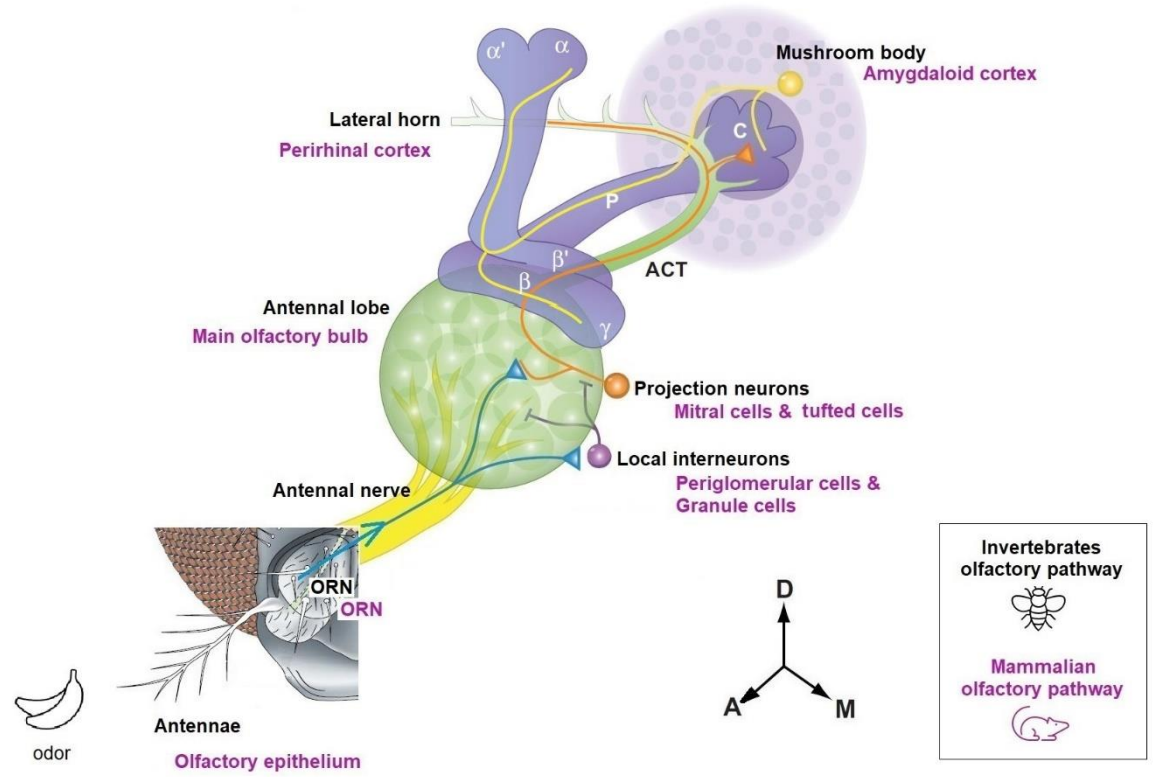

Figure 6: The olfactory pathway in *Drosophila melanogaster* and its mammalian equivalent. An odor signal becomes perceived by olfactory receptors in the antennae and the maxillary palps and is forwarded by olfactory receptor neurons (ORNs; blue line) via the antennal nerve to the antennal lobe (AL). The ORNs synapse with the projection neurons (PNs; orange line) or the local interneurons (LNs; purple line). The LNs, multiglomerular branched, transmit inhibiting signals within the AL. The PNs convey an excitatory signal via the antennal cerebral tract (ACT) to the mushroom body (MB) calyx (C), and the lateral horn. The MB compartments are the peduncle (P) and the different lobes, α/β, α'/β', and γ. Black: Invertebrates' olfactory pathway. Pink: Equivalents in the mammalian olfactory pathway. Axis directions: A = anterior, D = dorsal, M = medial. Image modified from Guven-Ozkan and Davis, 2014 and Heisenberg, 2003.

The olfactory pathway in adult *Drosophila melanogaster* starts with the percipience of an odor by olfactory receptors (OR; 62 types) and the universal olfactory co-receptor Or83b (Kaupp, 2010). These are localized on the dendrites of the olfactory receptor neurons (ORNs; ~ 1300 neurons; Figure 6, cyan track) in the antennae and maxillary palps (in mammals: olfactory epithelium) on each hemisphere of the fly head (Davis, 2005; Martin et al., 2013). The ORN axons forward the signal via the antennal nerve (AN) and form excitatory synapses with the projection neurons (PNs; Figure 6, orange track; in mammals: mitral and tufted cells) and the local interneurons (LNs; Figure 6, purple track; in mammals: periglomerular and granule cells) within the glomeruli (~ 50 in number), the synaptic areas of the antennal lobe (AL; mammalian main olfactory bulb) (Davis, 2005). Thereby, ORNs with one OR type convey to the same glomerulus in the AL, which forms a specific activation pattern of glomeruli per odor (Yu et al., 2004; Berry et al., 2008; Davis, 2011).

The axonless LNs are multiglomerular branched and provide via GABAergic inhibition an additional odor differentiation and intern control of the signal transmission (Davis, 2004; Olsen and Wilson, 2008; Amin and Lin, 2019). Analogously, this improved odor discrimination happens in the olfactory bulb in mice (Abraham et al., 2010).

The PNs (~ 180 neurons, cholinergic) convey the input via the antennal cerebral tract (ACT) to the mushroom body (MB; in mammals: amygdaloid cortex, sending signals to the dentate gyrus/ hippocampus) and the lateral horn (LH; in mammals: perirhinal cortex) (Davis, 2004; Berry et al., 2008; Amin and Lin, 2019). Additionally, reciprocal dendrodendritic connections between the LNs and the PNs, which are presynaptic and postsynaptic specializations on neurites and pervade the glomeruli, indicate a processing and computation location in the AL (Didier et al., 2001; Yu et al., 2004; Davis, 2011).

The MB (~ 2500 intrinsic neurons, also known as kenyon cells, KCs; Figure 6, yellow track) is the higher integration center for the generation and storage of memories in invertebrates (Heisenberg, 2003; McGuire et al., 2005; Aso et al., 2014; Wolff and Strausfeld, 2015). It is the functional homologous to the mammalian hippocampus (Wolff and Strausfeld, 2016). The PNs synapse with the KC dendrites in an area named calyx. From here, the KC axons, bundled in the peduncle, lead to the three classes of MB lobes, two branched as α'/β' and α/β, and one γ lobe (Crittenden et al., 1998; Berry et al., 2008).

In addition, several classes of extrinsic neurons are relevant to the MB (not indicated in Figure 6): the dorsal paired medial (DPM) neuron, the anterior paired lateral (APL) neuron, the dopaminergic neurons (DANs), and GABAergic neurons from the ellipsoid body (EB) (Berry et al., 2008; Liu and Davis, 2009; Mao and Davis, 2009; Davis, 2011; Zhang et al., 2013). Thereby, one DPM neuron per brain hemisphere, innervating the MB diffusely, signals mainly cholinergic to the MB but partly also GABAergic (sleep-promoting by then) (Yu et al., 2005; Haynes et al., 2015). The GABAergic APL neuron (one per hemisphere) provides an inhibitory

feedback loop to the MB activating the inhibitory $GABA_A$ receptor RDL (resistance to dieldrin) on the MB neurons (Liu et al., 2007; Liu and Davis, 2009; Davis, 2011). Further, three types of DAN clusters (PAM, PPL1, and PPL2ab) innervate the MB at various positions (Mao and Davis, 2009; Aso et al., 2012). They control the signal transmission from the KCs to the mushroom body output neurons (MBONs) dependent on the stimulus context (Cohn et al., 2015; Hige et al., 2015; Amin and Lin, 2019). Several studies found that a DAN inhibition blocks memory formation, while an artificial DAN activation together with pure odor stimulation triggers the development of memory (Claridge-Chang et al., 2009; Aso et al., 2010; Aso and Rubin, 2016; Amin and Lin, 2019). Additionally, DANs can overwrite obsolete memory information and regulate forgetting (Berry et al., 2012; Aso and Rubin, 2016; Berry et al., 2018; Aso and Rubin, 2020). In the MB, the KCs synapse with the MBON dendrites to forward the learned odor information and generate a behavioral reaction (Aso et al., 2014; Owald et al., 2015; Berry et al., 2018; Aso and Rubin, 2020).

Contradicting the traditional perception that the MB only coordinates the learning and memory, and the LH the innate behavior, newer findings reveal an MB intervention to the LH due to control conflict situations in foraging (Lewis et al., 2015; Tsao et al., 2018; Amin and Lin, 2019). Additionally, recent findings from Dolan et al., 2018, show a needed link from the MB to the LH for memory retrieval (Figure 7).

The LH is the principal processing center for responses to naïve odors, and controls the innate olfactory behavior (Belle and Heisenberg, 1994; Das Chakraborty and Sachse, 2021). Thereby, excitatory and inhibitory PNs send their axons to the LH, enabling further differentiation between naïve odors (Liang et al., 2013; Amin and Lin, 2019).

The olfactory nervous system in adult *Drosophila melanogaster* is less complex than the mammalian one yet holds remarkable homologies (Hildebrand and Shepherd, 1997; Davis, 2004; Haynes et al., 2015). A connectome of the olfactory learning circuit reveals widely ramified interactions (Figure 7; Amin and Lin, 2019; Li et al., 2020). These biological insights with the fruitfly as a suitable model organism can generate valuable points in investigating the neurobiology of learning and processes of memory acquisition, consolidation, and retrieval (Davis, 2005; van der Voet et al., 2014; Mariano et al., 2020). Several memory assays exist for flies, like visual or place memory, yet especially olfactory learning and memory is appealing due to its fundamental transferability to higher species (Davis, 2005; Kahsai and Zars, 2011; Liu et al., 2011). Additionally, experimental animals like flies or mice are guided through their environment, particularly by their olfaction and the resulting behavior (Davis, 2005).

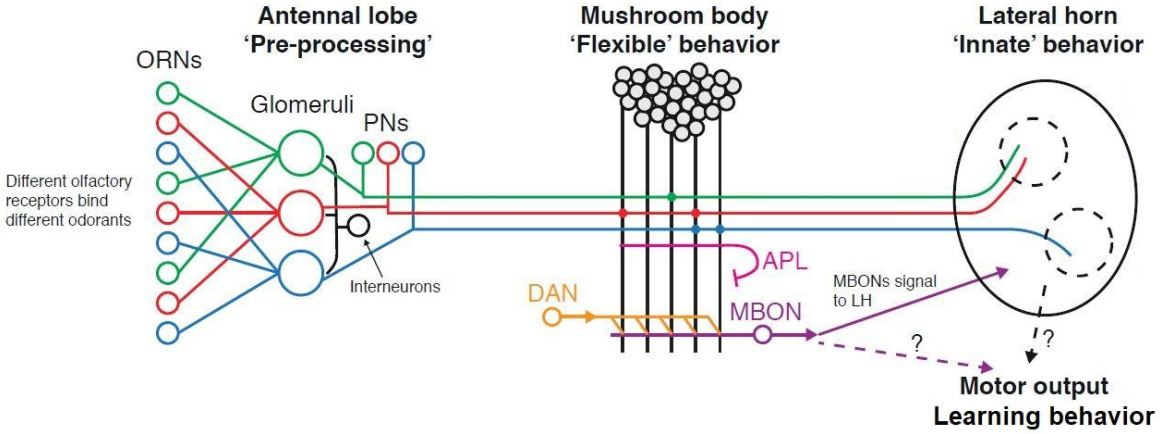

Figure 7: The connectome of the olfactory nervous system in *Drosophila melanogaster.*

During the coding of different odors, the olfactory receptor neurons (ORNs) with the same olfactory receptor (OR) gather the odor signal to one glomerulus, where they synapse to one projection neuron (PN) (the colors green, red and blue signify the different ORs) (Amin and Lin, 2019). Together with the local interneurons, pre-processing happens in the antennal lobe. The odor information becomes forwarded by the PNs to the mushroom body, where a flexible behavioral response together with a rewarded or punished trigger becomes coded, and the lateral horn (LH), the center for innate behavior. The dopaminergic neurons (DANs) and the inhibitory anterior paired lateral (APL) neuron adjust the odor code, which becomes forwarded by the mushroom body output neurons (MBONs). These mediate the response (learning, motor output) to the experienced trigger and partially modify innate behavior in the LH concerning conflict situations in foraging (Lewis et al., 2015). Image taken from Amin and Lin, 2019.

5. Learning and the generation of olfactory memory traces

Learning is the remaining behavioral change due to external circumstances (Kahsai and Zars, 2011). As a result, memory forms, the maintenance of the learned information over a longer period. These adaptations to the environment are essential and have to be adjustable (Kandel et al., 2014; Mattson and Arumugam, 2018). They are necessary for the animal's survival or even humans' daily routine. Typically, learning happens due to the connection of a stimulus with an experience. Of these associative learning, two types exist: operant and classical conditioning. In operant conditioning, the test subject chooses spontaneously between stimuli and learns due to the rewarded or punished experience (Skinner, 1950). Thus, learning through success via trial and error forms. In contrast, classical conditioning after Pavlov combines an unconditioned stimulus (US) with a neutral one, which becomes a conditioned stimulus (CS) thereupon (Pavlov, 1927). The US can be rewarding as an appetitive or punishing as an aversive assay. In this thesis, I focused on aversive classical conditioning.

On the molecular level, the coincidence of the US and the CS happens in the kenyon cells (KCs) of the mushroom body (MB) (Figure 8 for aversive olfactory memory formation) (Zars et al., 2000; Heisenberg, 2003; McGuire et al., 2003; Davis, 2005; Busto et al., 2010). Here, the projection neurons (PNs) transmit the CS (odor) via cholinergic synapses (neurotransmitter: acetylcholine, ACh), which opens voltage-gated calcium channels (VGCC) (Busto et al., 2010). The resulting intracellular calcium ion (Ca^{2+}) increase triggers the Ca^{2+} binding with the second messenger calmodulin (CaM), followed by activation of the adenylylcyclase (AC) and a cAMP increase. In parallel, the US information becomes transmitted via the dopaminergic neuron (DAN) clusters (PPL1 and PPL2ab) to the dopamine receptor (DAr) on the KCs, which is a G-protein coupled receptor. The following activation of the G-protein stimulates the AC, increasing cAMP production. Thus, AC, coded by *rutabaga*, serves as coincidence detector for US and CS (Tomchik and Davis, 2009; Gervasi et al., 2010; Christiansen et al., 2011). A cAMP increase activates the protein kinase A (PKA; coded by *DCO*), which phosphorylates transcription factors like the cAMP response element-binding (CREB) protein (important for long-term memories), target proteins (likewise for short-term memories), or ion channels (Davis, 2005; McGuire et al., 2005; Lee, 2015). Interestingly, the mechanism of cAMP signaling and the resulting regulation of synaptic plasticity are conserved in different species (Frey et al., 1993; Kandel, 2012; Lee, 2015).

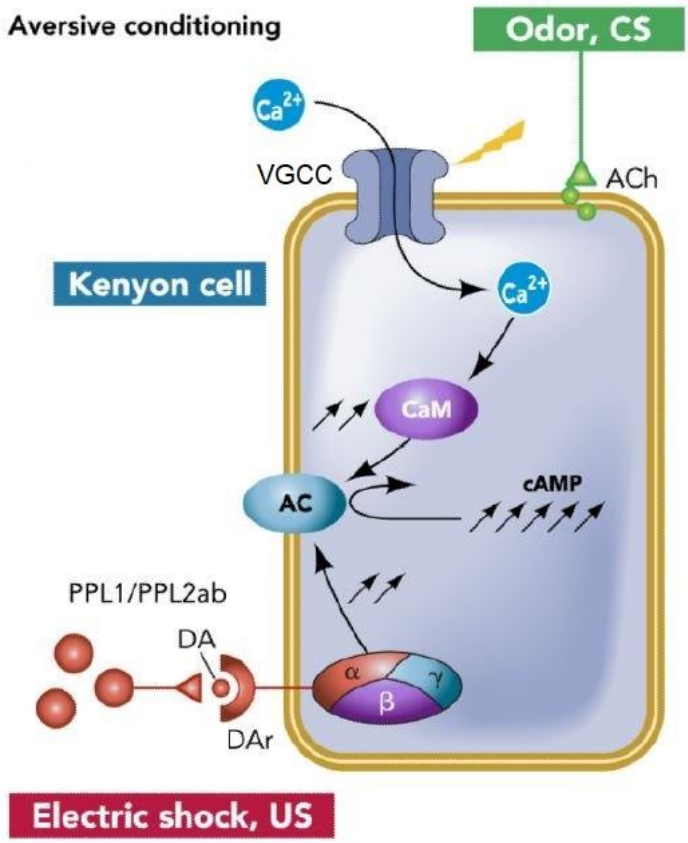

Figure 8: Molecular model for aversive olfactory conditioning in a kenyon cell of the mushroom body.

The coincidence of a former naive odor as conditioned stimulus (CS; green) and the electric shock as negative unconditioned stimulus (US; red) generates aversive olfactory conditioning and learned behavior. The cholinergic projection neurons (neurotransmitter: acetylcholine, ACh; green) transmit the CS to the kenyon cells (KCs) in the mushroom body. Accordingly, voltage-gated calcium channels (VGCCs) open, and the intracellular calcium ion (Ca^{2+}) concentration increases. The second messenger calmodulin (CaM) binds the Ca^{2+}, and this complex activates the adenylyl cyclase (AC; *rutabaga*-encoded), followed by an increased cAMP production (Davis, 2005). The US information becomes transmitted via the dopaminergic neuron (DAN) clusters (PPL1 and PPL2ab) to the dopamine receptor (DAr) on the KCs. This activates the heterotrimeric G-protein, which in turn stimulates the AC and generates more cAMP. This double AC induction due to the synergistic US and CS input leads to an increased protein kinase A (PKA) operation, which initiates downstream pathways to the different memory phases and behavior (Kandel, 2001; Heisenberg, 2003; Davis, 2005). Image taken from (Busto et al., 2010)

Memory traces are cellular and synaptic plasticity regarding changes in the neuronal network induced by learning (Christiansen et al., 2011; Davis, 2011). Thereby, a specific spatial code in the neurons of the olfactory *Drosophila* pathway causes different temporal memory phases, which are dynamic and can last from minutes to days (Figure 9).

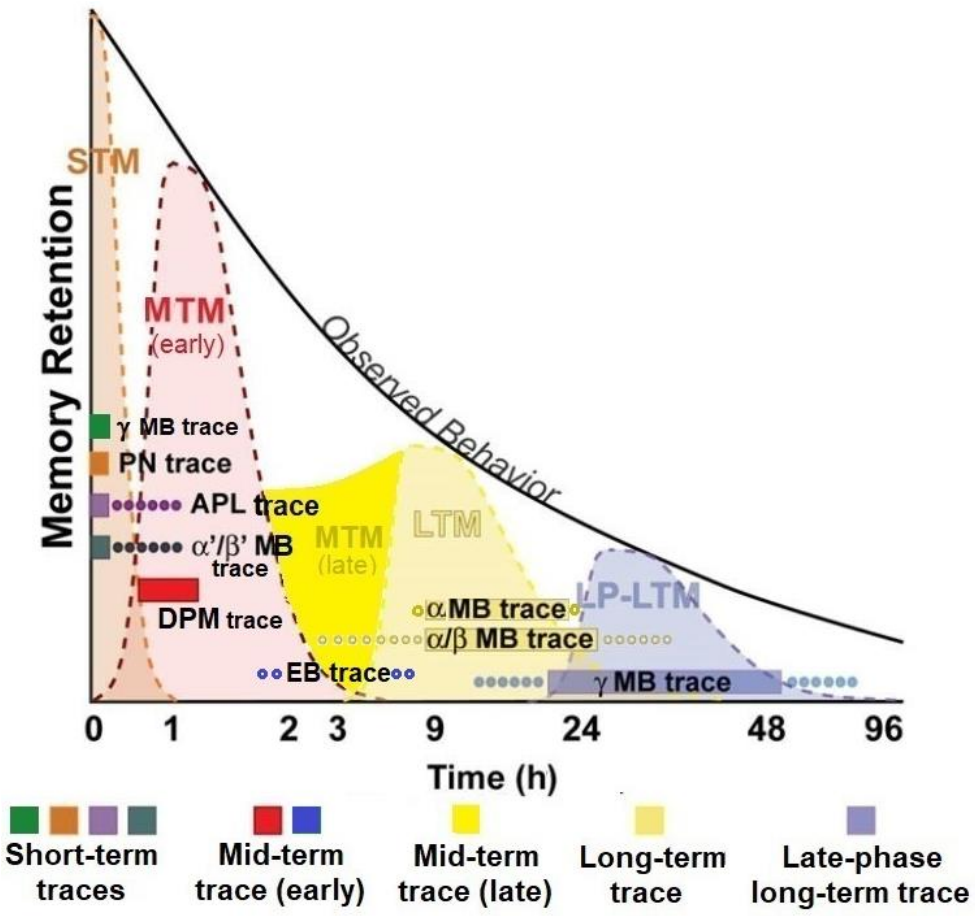

Figure 9: Memory traces in temporal memory phases.

The different aversive olfactory memory phases in *Drosophila melanogaster* occur temporally shifted from minutes to days. A spatial code in the neurons generates various memory traces, which partially coexist during the time. Short-term memory (STM; orange curve) develops in the projection neurons (PNs), the mushroom body (MB) a'/β' lobes, and γ lobe, and via a reduced activity of the anterior paired lateral (APL) neurons (Zars et al., 2000; Yu et al., 2004; Wang et al., 2008; Blum et al., 2009; Liu and Davis, 2009; Qin et al., 2012; Bouzaiane et al., 2015). Within the early phase of mid-term memory (MTM; red curve), a memory phase in the DPM neurons becomes active, lasting from 0.5 until 1.5 hours, and a trace in the ellipsoid body (EB) at around 3 hours (Keene et al., 2004; Zhang et al., 2013). The α/β MB trace generates late MTM and long-term memory (LTM), which overlap (yellow curve), while the α branch is the main area for LTM (McGuire et al., 2001; Yu et al., 2006; Blum et al., 2009). Finally, the late-phase of LTM (LP-LTM; blue curve) in the γ MB lasts from 18 hours until days (Akalal et al., 2010; Davis, 2011). Image modified from Davis, 2011.

Short-term memory (STM; also called initial learning) develops immediately and decreases within 30 minutes (Figure 9, orange curve). Its short traces are essential for memory acquisition. Yu et al., 2004, found that more glomeruli in the antennal lobes (ALs) were activated in response to an aversive conditioned odor compared to the naïve odor stimulus pattern. This trace in the PNs adds former inactive synapses and lasts 5 to 7 minutes (Yu et al., 2004). Additionally, Yu et al., 2004, detected the PNs as a recipient of electric shock as US. These discoveries imply the PNs as convergence areas for US and CS in STM (Davis, 2005; Berry et al., 2008). Further investigations from Wang et al., 2008, revealed a short-term trace in the α'/β' lobes of the MB, which lasts up to 1 hour, and depends on G-protein coupled receptors. Additionally, GABAergic APL neurons act as a suppressor of memory acquisition due to activating the inhibitory $GABA_A$ receptors RDL on the MB (Liu and Davis, 2009; Davis, 2011). Its GABA release decreases within the first 5 minutes after learning and enables memory formation (Liu et al., 2007; Liu and Davis, 2009; Davis, 2011). Concomitantly, the APLs are seen as a coincidence place for US and CS (Davis, 2011). Further, the γ lobe of the MB was also found to be essential for STM (Zars et al., 2000; Blum et al., 2009; Qin et al., 2012; Bouzaiane et al., 2015).

Memory can be dissected into two components: anesthesia-sensitive memory (ASM) decreases with retrograde anesthesia and is labile, while anesthesia-resistant memory (ARM) is consolidated and stays stable after anesthesia (Tamura et al., 2003; Scheunemann et al., 2012). Both are built after a single conditioning trial, yet ASM decreases with time, and ARM lasts several days (Heisenberg, 2003; Isabel et al., 2004). During STM retrieval, the early ASM, the major component at this timepoint, needs the γ lobe, while the early consolidated ARM trace recruits in the α/β lobes (Bouzaiane et al., 2015). Indeed, lesions in the human brain can extinguish not consolidated anesthesia-sensitive memory components like STMs, leading to retrograde amnesia (McGaugh, 2000).

Next, mid-term memory (MTM; also called intermediate-term memory) develops within 30 minutes and lasts for several hours (Figure 9, early and late MTM) (Davis, 2011). Additional to the acquisition and retrieval of memory, a phase of memory maintenance and further consolidation happens here (Tully and Quinn, 1985). One early MTM trace (red curve), lasting 0.5 to 1.5 hours, is generated in the DPM neurons, innervating the MB lobes. The DMPs are required in MTM consolidation via *amnesiac*, which is highly expressed here, and an *amnesiac* mutation in the DMP neurons was found to impair MTM (Quinn et al., 1979; Waddell et al., 2000; Keene et al., 2004). *amnesiac* codes the neuropeptide AMN, which stimulates cAMP production (Bhattacharya et al., 2004). Recent studies reveal *amnesiac* as important in the DPMs during development, and its protein AMN as necessary for MTM and long-term memory (LTM) in the MB α/β lobes (Turrel et al., 2018). The late MTM trace and the beginning LTM

start to overlap here (yellow curve). Memories become consolidated in the α/β lobes due to repeated activation in a loop between α'/β' lobes and the DMPs (Krashes et al., 2007). A disruption of the a/β MB trace impairs memory retrieval at 3 hours, while the acquisition and retention do not suffer (McGuire et al., 2001).
MTM consists of ASM and ARM in almost equal parts (Tamura et al., 2003; Scheunemann et al., 2012). While ARM is independent of protein synthesis, the ASM trace was found to be *rutabaga*-cAMP-PKA dependent in the MB KCs (Schwaerzel et al., 2007; Scheunemann et al., 2012). PKA even seems to suppress the building of ARM (Horiuchi et al., 2008). In contrast, ARM was found to develop via the signaling of *dunce* (coding the phosphodiesterase PDE4) between the local interneurons (LNs) of antennal lobes and the MB (Scheunemann et al., 2012). Thereby, PDE4 limits the cAMP signaling to specific areas (Houslay, 2010; Scheunemann et al., 2012). Several publications found traces, appearing time-dependent, to generate ARM and ASM separately. Thus at 2 hours, the retrieval of the labile ASM is built in the α/β lobes, while ARM consolidates in γ (Bouzaiane et al., 2015). Further, one ASM trace is created between the ellipsoid body (EB neurons) and the MB, where a release from the GABAergic EB block supports ASM formation (Zhang et al., 2013). Even in the synapses, a difference between ASM and ARM is visible. Two additional copies of the presynaptic active zone protein Bruchpilot diminish ASM, while a lack of Bruchpilot in the MB affects ARM (Knapek et al., 2011; Gupta et al., 2016). A convergence of ARM and ASM was found via the GTPase Rgk1, which stabilizes both MTM phases (Murakami et al., 2017).

Consolidated memory phases are longer-lasting. The late ARM develops with massed training cycles (no rest in between) but also a single training is sufficient (Heisenberg, 2003; Isabel et al., 2004). In contrast, LTM, the other consolidated long-lasting memory phase, requires at minimum three training sessions with timed intervals (spaced) and is formed via *de-novo* protein synthesis, typically with CREB (Tully et al., 1994; Heisenberg, 2003; Tully et al., 2003). The development of LTM is at the expense of ARM, yet both phases are present at 24 hours and later (Isabel et al., 2004). Investigations of Pascual and Préat, 2001, point towards a localization of the LTM trace in the vertical lobes α and α'. From these vertical lobes, especially the α trace (lasting 9 till 24 hours) was described as the main LTM retrieval area, while late ARM is located in the α/β lobes (Isabel et al., 2004; Yu et al., 2006; Blum et al., 2009). Further, the retrieval of ARM at 24 hours needs the α'/β' lobes (Bouzaiane et al., 2015).
At last, a late phase of LTM (LP-LT; blue curve) is formed in the γ lobe, lasting from 18 to days (Akalal et al., 2010; Bouzaiane et al., 2015).

A cognitive decline with advancing age is conserved in the different species (Saitoe et al., 2005; Burke and Barnes, 2010; Morrison and Baxter, 2012). The connectivity between the

DPM neurons and the MB α lobe declines with time, impeding the LTM trace in the α/β lobes (Tonoki and Davis, 2015). Additionally, aging erases the DMP memory trace, followed by a decrease in the ASM component (Tonoki and Davis, 2012). With age, the labile memory phases decrease, while the consolidated ones stay unaffected. Thus, the anesthesia-sensitive component in STM, MTM, and LTM is impaired, while ARM stays stable (Tamura et al., 2003; Mery, 2007; Tonoki and Davis, 2012; Gupta et al., 2013; Tonoki and Davis, 2015; Bhukel and Beuschel et al., 2019). New memories have to be consolidated, which needs neuronal and molecular operation (McGaugh, 2000). Advancing age impedes this memory consolidation step (Tonoki and Davis, 2015; Sander et al., 2021).

Since memory traces are built in neuronal tissues, they are dependent on modifications or reinforcement at the synapses. Cellular and plastic changes are necessary (Christiansen et al., 2011; Davis, 2011).

6. Neuronal information transfer via the synapse

The conditioned behavior of Pavlov's dog to bark when it heard a bell ringing was a marvelous learning process in the brain of this animal, which had its start in the nerves (Pavlov, 1927). A major part of learning happens through the transmission of impulses from neuron to neuron at their junction, the synapse. Synapse comes from the Greek *syn*, which means 'together', and *haptein*, translated 'clasp'. This junction between two nerves or a nerve and a muscle is a crucial part of the nervous system, and it is evolutionary conserved across species (Zhai and Bellen, 2004). The dendrites of a neuron capture stimuli, which are converted to electrical impulses due to the change of membrane properties (Figure 10). As soon as these signals sum over a threshold in the neuronal soma, an action potential is built at the axon hillock. This action potential is forwarded anterograde from the soma of the nerve via the axon to the synapse. Two types of synapses exist: The chemical synapse with the signal transfer via neurotransmitters, and the electrical synapse, which directly communicates by a current at gap junctions (Silbernagl and Despopoulos, 1979). In the following, I will focus on the chemical synapse.

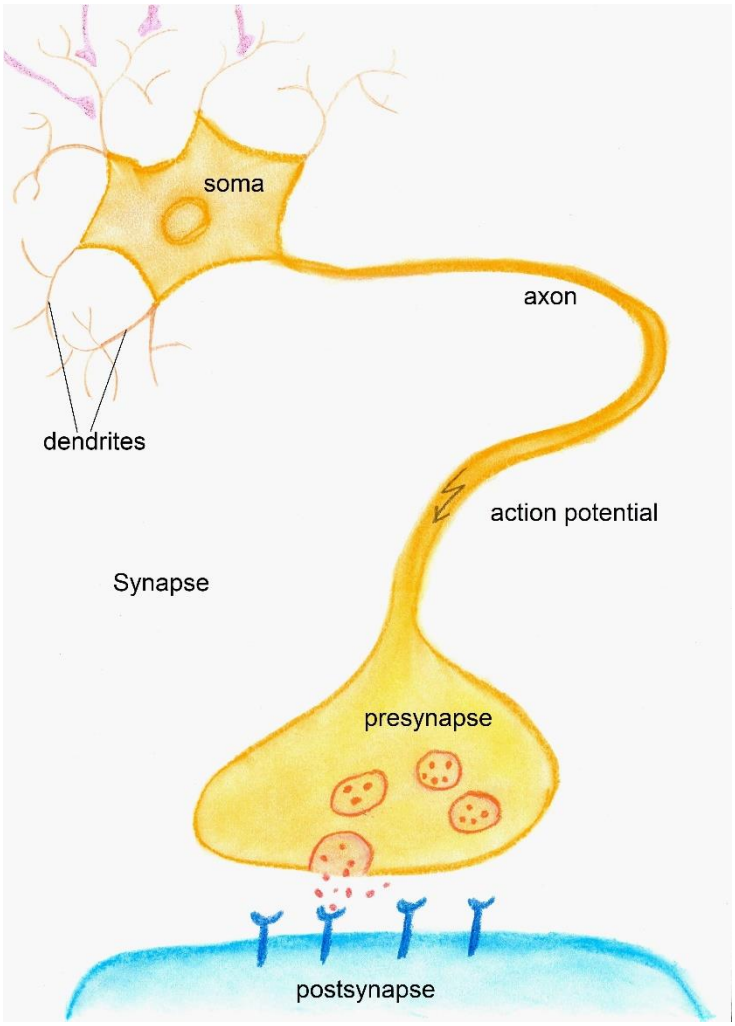

Figure 10: Scheme of a neuron.

The dendrites of a neuron receive input from the synapses of other neurons. When the sum of the signals comes over a threshold, an action potential is built at the axon hillock and sent along the axon to the synapse. Here, neurotransmitters (red dots) are set free through exocytosis from synaptic vesicles into the synaptic cleft and attach to receptors of the postsynapse.

When the action potential arrives at the synapse, presynaptic voltage-gated

calcium channels (VGCC) open for calcium (Ca^{2+}) influx from the synaptic cleft (Figure 11) (Südhof, 2012). This provokes the exocytosis of neurotransmitters, carried by synaptic vesicles (SVs), which is the essential process to convert an electrical signal (action potential) into a chemical signal (neurotransmitter) (Sigrist and Ohtsuka, 2018). The neurotransmitters diffuse into the synaptic cleft and bind to receptors in the membrane of the postsynapse, which transmits the signal further.

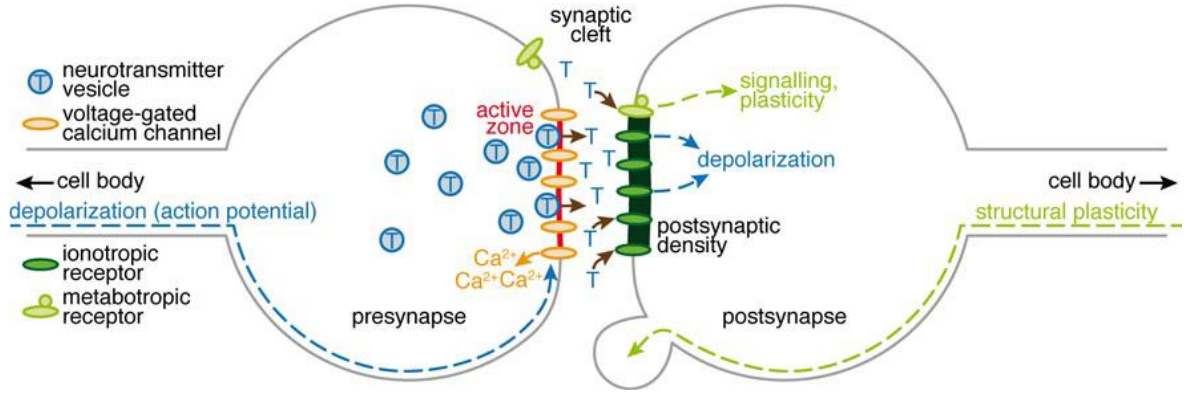

Figure 11: Scheme of a synapse (chemical), the synaptic cleft, and the postsynapse.

An action potential arrives at the synapse and triggers the opening of presynaptic voltage-gated Ca^{2+} channels, followed by Ca^{2+} influx. This causes the exocytosis of synaptic vesicles at the active zone, and thus neurotransmitters are released in the synaptic cleft. At the postsynapse, neurotransmitters activate receptors within the postsynaptic density, and the signal is forwarded. Image taken from Andlauer, 2013.

Three pools of SVs exist. The reserve pool with its biggest amount of SVs (around 80 – 90 %) maintains the stock of SVs, whereas the recycling pool (circa 10 – 15 %) conserves the SVs for release (Rizzoli and Betz, 2005). Finally, the readily releasable pool (RRP; around 1 %) supplies SVs, which are already docked near the release sites of the presynapse and primed in a mature condition, ready for exocytosis (Rizzoli and Betz, 2005; Reddy-Alla et al., 2017). The SV fusion with the presynaptic membrane happens in an electron-dense area, called the active zone (AZ) (Südhof, 2012). Here, a cluster of phylogenetically conserved proteins, the presynaptic cytomatrix at the AZ (CAZ; Figure 12), orchestrates the process of exocytosis. The core CAZ consists of the proteins Bruchpilot (BRP), Rab3-interaction molecules (RIM), RIM-binding protein (RIM-BP), Liprin-α, and Unc13 (Südhof, 2012). These proteins assemble and structure the AZ and coordinate the release of SVs as soon as an action potential arrives at the synapse. Thereby, BRP (mammalian homolog: CAST family (CAZ-associated structural protein), also ERC) builds the backbone of the CAZ, an electron-dense area with various shapes (plaques in *C. elegans*, T-bars in *Drosophila melanogaster*, ribbons in rats, pyramids

in humans; see Figure 15) (Wagh et al., 2006). This protein family is, together with RIM, responsible for an appropriate clustering of the Ca^{2+} channels within the AZ, the composition of the CAZ, and an operating SV release (Kittel et al., 2006b; Owald and Sigrist, 2009). Furthermore, BRP controls the size of the RRP of SVs (Matkovic et al., 2013). RIM proteins take part in the organization of the AZ and enable SV priming, thus, adjusting the RRP (Deng et al., 2011; Müller et al., 2012; Südhof, 2012). RIM-BP structures the AZ nanoarchitecture and anchors BRP within the AZ (Liu et al., 2011; Petzoldt et al., 2020). In addition, it binds Ca^{2+} channels to RIM and controls the SV refilling to release sites (Südhof, 2012; Petzoldt et al., 2020). Liprin-α assembles nascent AZs and helps to avert the random allocation of synaptic material in the axon (Fouquet et al., 2009; Owald et al., 2010; Li et al., 2014). The priming and release factor within the CAZ is Unc13 (in mouse Munc13; in humans UNC13) (Aravamudan

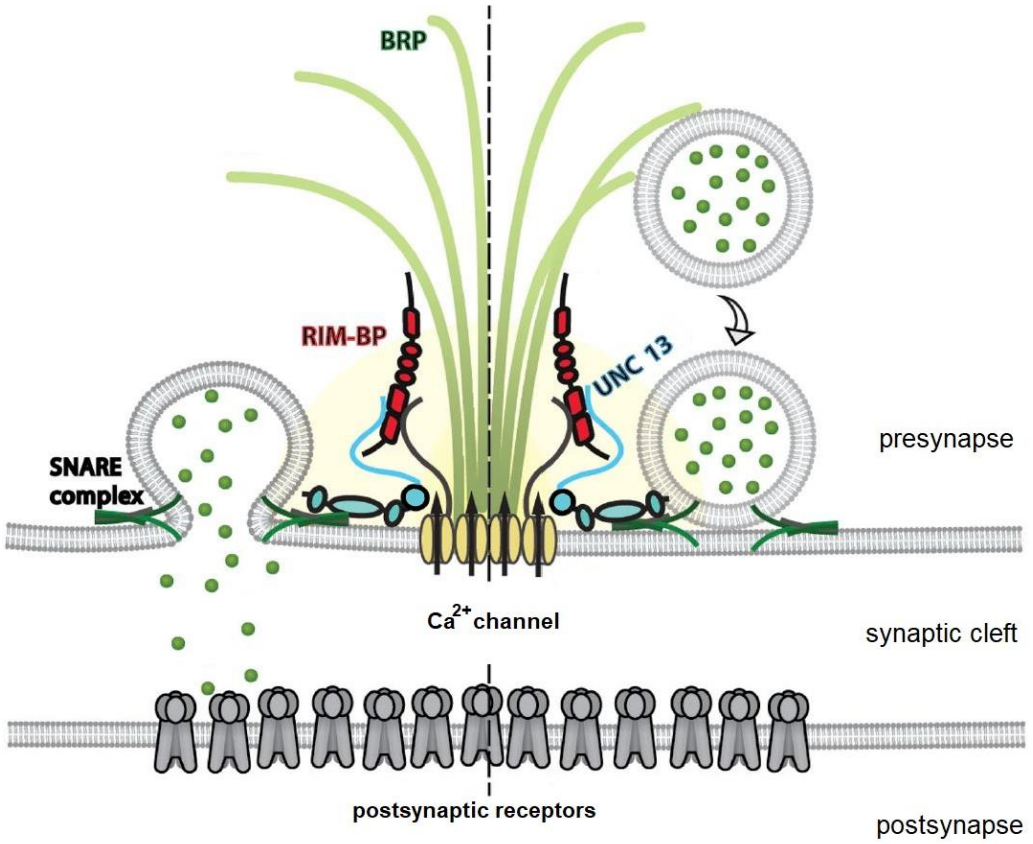

Figure 12: Synaptic vesicle release and the cytomatrix at the active zone.

After Ca^{2+} influx through Ca^{2+} channels within the active zone, synaptic vesicles of the readily releasable pool, primed by Unc13, are tethered by Bruchpilot (BRP). The SNARE complex links the synaptic vesicle to the presynaptic membrane. Thus, the membranes merge, and the neurotransmitters dispense into the synaptic cleft, where they activate receptors of the postsynapse (Südhof, 2012). Image modified from Petzoldt et al., 2020.

et al., 1999). It makes the SVs fusion-competent and controls short-term plasticity (Südhof, 2012). Furthermore, Unc13 promotes stability for the number and positions of SV release sites and an accurately timed neurotransmitter signaling (Reddy-Alla et al., 2017). Due to its two isoforms, Unc13 can cause different synaptic responses, which means a fast phasic answer or a slower tonic reply to a signal depending on a differential localization of its isoforms Unc13A or Unc13B (Fulterer et al., 2018; Böhme et al., 2019; Woitkuhn and Ender et al., 2020). Thus, under the control of the CAZ proteins, SVs of the RRP become activated for exocytosis by the Ca^{2+} sensor Synaptotagmin, located in their membrane, when an action potential triggers the Ca^{2+} influx (Haucke et al., 2011). The energy for the fusion of the vesicular membrane with the presynaptic membrane is provided by the SNARE complex (soluble NSF (N-ethylmaleimide-sensitive factor) attachment protein receptor) (Jahn and Fasshauer, 2012). This complex is built of one SV membrane protein, Synaptobrevin (in humans: VAMP (vesicle-associated membrane protein)), and two proteins in the presynaptic plasma membrane, Syntaxin-1 and SNAP-25 (synaptosomal-associated protein 25) (Haucke et al., 2011). After the SV membrane and the presynaptic membrane merge, neurotransmitters can dispense into the synaptic cleft and activate receptors at the postsynapse. Thus, the signal is passed on the postsynaptic cell. Via endocytosis, the SV membrane becomes recycled (Haucke et al., 2011).

In this way, information becomes transferred between the nervous network. However, learning stands for an adaptation to the environment and needs to be adjustable (Kandel et al., 2014). The system can react via synaptic plasticity, an experience-dependent modulation within the synapse (Ho et al., 2011; Takeuchi et al., 2014; Böhme et al., 2019). Thus, short-term plasticity operates within milliseconds to minutes, increases synaptic transmission, and is reversible (Alabi and Tsien, 2012; Jackman and Regehr, 2017). Here, an enhanced Ca^{2+} amount or sensitivity can increase exocytosis (Sigrist et al., 2003). Additionally, presynaptic homeostatic potentiation, a homeostatic regulation of neurotransmitter release, can adjust release sites (Böhme et al., 2019). In contrast, long-term potentiation lasts for hours and days and induces a persisting potentiation of synaptic strength (Nicoll and Roche, 2013; Jackman and Regehr, 2017). It can be adjusted via enrichment of postsynaptic areas, thus, incorporation of further postsynaptic receptors or a rise in the volume of dendritic spines (regions with postsynaptic density, located in the opposite of AZs) (Ho et al., 2011; Nicoll and Roche, 2013). Though, our recent study reveals that long-term potentiation also happens at the presynapse by a reconstruction of the AZ (Böhme et al., 2019). Here, more CAZ proteins become incorporated into the AZ step by step. Hence, chronic plasticity with augmented neurotransmitter release takes place (Böhme et al., 2019).

7. *Drosophila melanogaster* as an optimal model organism to investigate phylogenetically conserved aging pathways

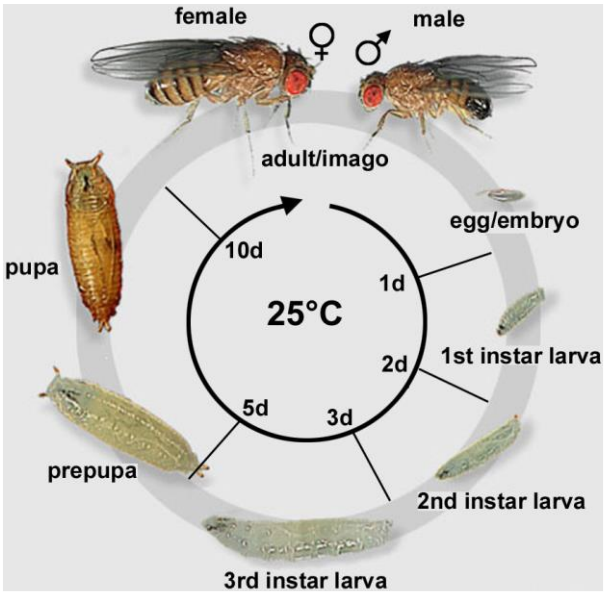

Figure 13: The life cycle of *Drosophila melanogaster* at 25 °C.

After the egg's eclosion, it takes five days from the larva to the pupa, where it goes through three instar stages. Finally, ten days after the oviposition, an adult fly encloses. Mated females lay around 100 eggs per day at 25 °C. Image taken from Roote and Prokop, 2013.

The fruit fly *Drosophila melanogaster* is a long-known genetic model. Since discovering the *white* gene through Thomas Hunt Morgan in 1910, this model system has helped to explore several research fields (Green, 2010). Due to straightforward genetics, flies are an effective system in the field of biology and medicine (Jennings, 2011). Thus, it was 1999 already possible to sequence the whole genome of *Drosophila melanogaster*, consisting of almost 13,600 genes on only four pairs of chromosomes (Adams et al., 2000). In addition, working with these animals holds benefits like the small amount of needed space, the large number of progeny, the short life cycle, and the brief lifetime (Figure 13).

As a genetic tool, the UAS-Gal4 system enables the expression of a single gene spatially and temporally. Discovered in yeast, this method uses the enhancer trap Gal4 to activate the expression of the gene of interest, targeted with UAS (Brand and Perrimon, 1993). As a technical improvement, Gal80 serves as a suppressor of Gal4 (Elliott and Brand, 2008; Roote and Prokop, 2013). Additionally, it is possible to gain the function of a gene through its targeted overexpression. Similarly, a reduction or even loss of the activation of a gene can be generated with the help of double-stranded RNA (RNA interference, RNAi). In this way, RNAi induces a specific posttranscriptional gene silencing (Hannon, 2002). Recently, a pioneering novel genetic tool, the enzyme mechanism CRISPR-Cas9 (clustered regularly interspaced palindromic repeats; CRISPR associated protein 9), was found with which it is possible to target any DNA sequence of interest (Doudna and Charpentier, 2014). This remarkable technique can efficiently redact Drosophila, providing many new possibilities (Gratz et al., 2015).

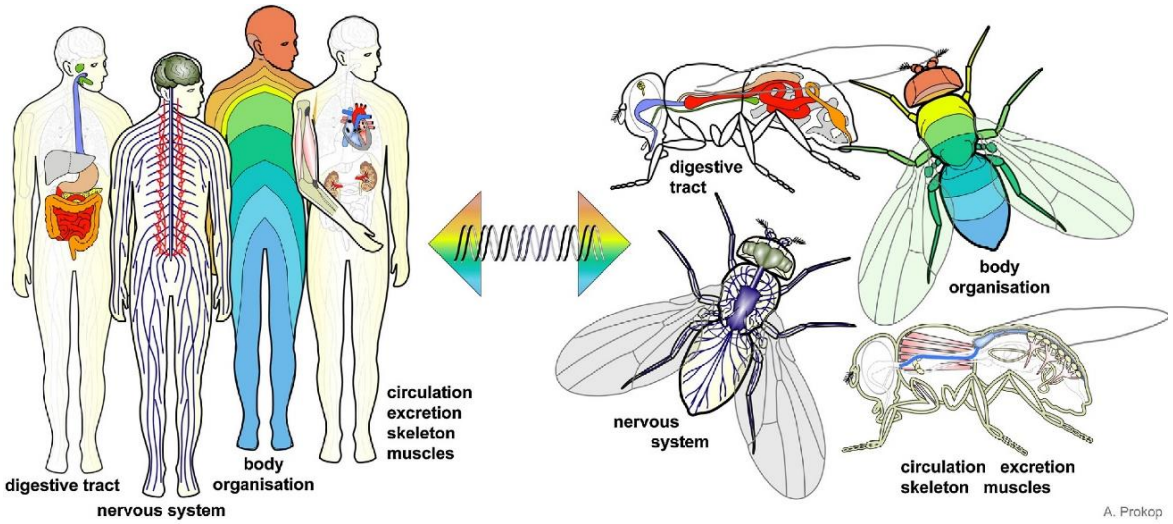

Figure 14: Conserved systems between humans and *Drosophila melanogaster*.

A similar assembly can be observed between humans and flies, starting with the whole body organization to the circulation, skeleton and muscles, digestive tract, and nervous system (Patel et al., 2017).

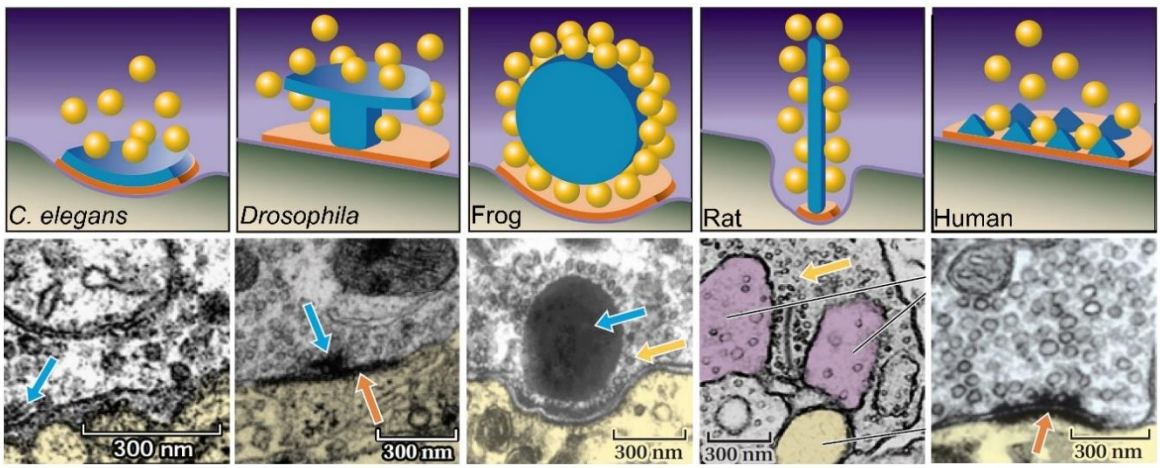

Figure 15: Active zones with their electron-dense structures in synapses of different species.

On the top: Schemata of the cytomatices at the active zones. At the bottom: Electron micrographs of the active zones of synapses. From left to right: *C.* elegans, *Drosophila* melanogaster, frog, rat human. Synaptic vesicles in yellow, electron-dense structures in blue, presynapses in orange, and postsynapses in green. Image modified from Zhai and Bellen, 2004.

In a large number, biological mechanisms and pathways are conserved across the different species (Jennings, 2011). Furthermore, when we compare humans and flies, a similar assembly can be found in the body organization, the digestive tract, the circulation, and the nervous system. Interestingly, even a look into the most minor parts of the nervous system, the synapses, reveal homologous structures across different species (Zhai and Bellen, 2004). Exemplarily, Figure 15 pictures the cytomatrices of synapse' active zones in *C. elegans*, *Drosophila melanogaster*, frogs, rats, and humans. Thus, even though the electron-dense structures in blue possess various shapes, the elemental composition of the active zones (AZs) show conserved presynapses across the species.

Around 75% of genes associated with human malady have orthologues in the flies' genome (Reiter et al., 2001). This state raises fascinating possibilities in researching diseases (van der Voet et al., 2014). With the fly, genes' role can be explored, also in the context of the parameter time. The origin of pathology *in vitro* and *in vivo*, a potential interaction partner or molecular pathways can be revealed (van der Voet et al., 2014). Even a screen for potential medicinal products is feasible (Cabo et al., 2014). Thus, the tiny fruit fly is a powerful tool to fight senescence-associated ailments.

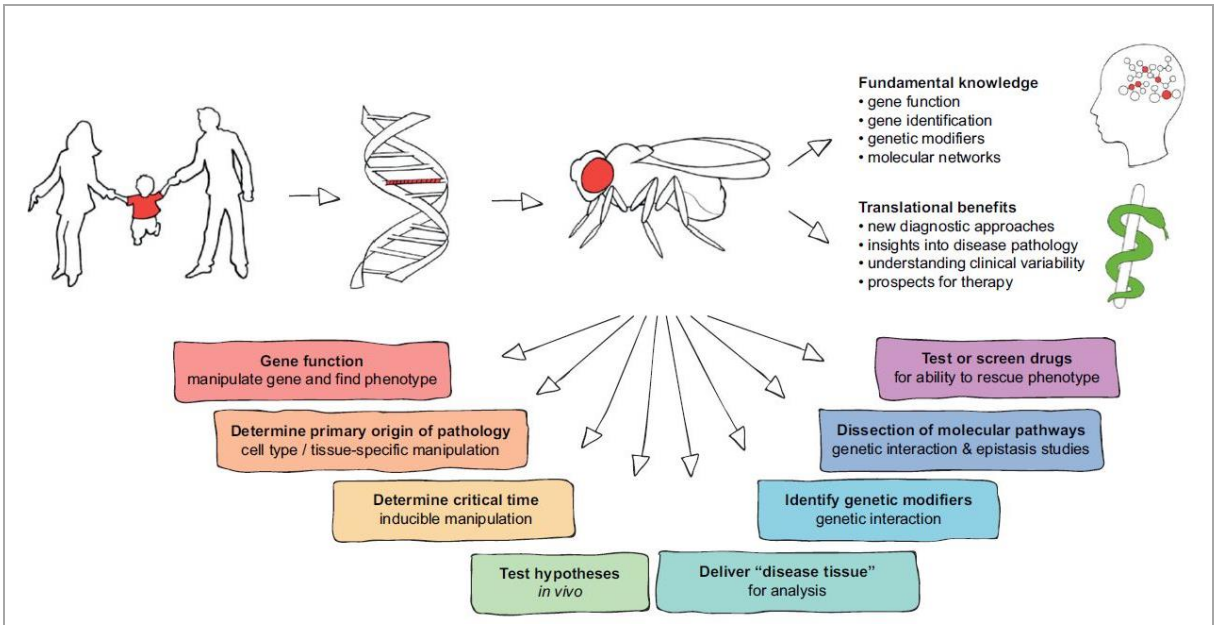

Figure 16: *Drosophila melanogaster* as model organism in the research of human diseases.

Since many genes associated with human ailments are conserved, the fruit fly serves as a powerful tool to explore the function of a gene *in vitro* and *in vivo,* just like a temporal context or potential interaction partner and molecular pathways. Additionally, it is possible to perform drug screens with these animals (van der Voet et al., 2014). This way, the immediate context becomes visible, which provides insights into the understanding of various maladies and a future remedy. Image taken from van der Voet et al., 2014.

II. Material and Methods

1. Fly stocks and their cultivation

Flies were reared under standard laboratory conditions of around 25 °C and 65 % humidity in a 12:12 hours light:dark cycle and kept on food after Bloomington recipe (https://bdsc.indiana.edu/information/recipes/bloomfood.html) with minor changes (in the following designated as normal food), if not declared otherwise (Sigrist et al., 2003).
In general, the parental generation was kept at 25 °C for egg deposition and placed on new food every second or third day to avoid larval overpopulation. Afterward, the progeny was stored until its emergence. Then, the adult flies were collected every other day in an appropriate population density. Until they reached their experimental age, the flies were placed on fresh food every second or third day. If not declared otherwise, all flies were raised under the same conditions. A short compilation of each genotype's method is added next to the results in the appendix.
In some trials, I combined the temperature-sensitive Gal-4 suppressor Gal80 ($Gal80^{ts}$; McGuire et al., 2003) with the Gal4-UAS-system to target the expression of RNA interference (RNAi) with UAS and exclude developmental effects due to genetic intervention (Brand and Perrimon, 1993). Here, the progeny was kept at 18 °C, where the $Gal80^{ts}$ operated until the flies' eclosion. Then, they were shifted to 29 °C so that the suppression of the enhancer trap Gal4 was terminated, and the gene of interest could be inhibited via RNAi (McGuire et al., 2003). Experimental animals treated under these conditions were designated in this study.

For Spermidine tests (Spd; source: Sigma-Aldrich [No. S4139]), a stock solution of 2 M in sterile distilled water was prepared and stored at - 20 °C. As soon as freshly prepared normal food cooled down to 40 °C, the Spd was added to the final concentration of 5 mM (designated as Spd food, + Spd). The flies were raised and developed on Spd food or the normal food as a control since egg deposition.

For tests with 4,4'-Dimethoxychalcone (DMC; source: ABCR [No. 179040], Extrasynthese [No. 1295]), DMC was freshly diluted in 0.1 % Dimethyl sulfoxide (DMSO; source: Sigma-Aldrich [No. 276855]). Afterward, this solution was added to freshly prepared normal food in different concentrations at a temperature of 55 °C. These were designated as 0.2 mM DMC (0.0537 µg/ml), 1.0 mM DMC (0.269 µg/ml), and 2.0 mM DMC (0.537 µg/ml). As control food served normal food containing the same concentration of DMSO as the DMC food without any DMC (designated as 0.1 % DMSO). The flies were raised and developed on normal food and were fed with the respective DMC concentrations or 0.1 % DMSO food after eclosion, if not declared otherwise. In an additional experiment to test a potential DMSO toxicity, the DMSO food concentrations 0.05 %, 0.1 %, and 0.5 % were used since egg deposition.

Table 1: Fly lines

fly stocks (source)	chromo-some	description / reference	previously described in
driver lines:			
appl-Gal4 (SL # 674)	X	pan-neuronal driver	Gupta et al., 2016
ilp2-Gal4 (SL # 5 / BL # 37516)	II	driver in the insulin producing cells in the brain	Bhukel and Beuschel et al., 2019
elaV(X)-Gal4 (SL # 10)	X	pan-neuronal driver (elaV-c155)	Lin and Goodman, 1994
gh146-Gal4 (SL # 1301 / BL # 30026)	II	projection neurons driver (excitatory projection neurons)	Stocker et al., 1997
gmr-Gal4 (SL # 504 / BL # 1104)	X	optic lobe driver	Hiesinger et al., 1999
mb247-Gal4 (SL # 2377)	III	mushroom body driver with α/β and γ lobes covered	Zars et al., 2000
mb247-Gal80 (SL # 1689 / BL # 64306)	II	Gal4-suppressor in the mushroom body lobes α/β and γ	Aso et al., 2014
mb247-Gal80;;*ok107*-Gal4	II ;; IV	diver profile of *ok107*-Gal4 minus the Gal80 suppression in the mushroom body lobes α/β and γ	kindly provided by Atefeh Pooryasin
ok107-Gal4 (SL # 2259 / BL # 854)	IV	mushroom body driver with all lobes covered (α/β, α'/β', γ) plus expression in pars intercerebralis, optic lobe, antennal lobe, and subesophageal ganglion	Connolly et al., 1996
or83b-Gal4 (SL # 1418)	III	expression in the odorant receptor co-receptors (Orco)	Fulterer et al., 2018

r13f02-Gal4 (BL # 48571)	III	mushroom body driver, all lobes	Bloomington Drosophila Stock Center
r58h05-Gal4 (BL # 39198)	III	expression in ellipsoid body ring 2 neurons (now renamed as R5 neurons)	Jenett et al., 2012
tub-Gal80^{ts} ;; *ok107*-Gal4	II ;; IV	diver profile of *ok107*-Gal4 minus temperature-sensitive Gal80 suppression	kindly provided by Atefeh Pooryasin
vt030559-Gal4 (VDRC # 206077)	III	mushroom body driver with α/β, α'/β' and γ lobes covered	Turrel et al., 2018
marker lines:			
UAS-EGFP (BL # 41556)	III	enhanced green fluorescent protein	Bloomington Drosophila Stock Center
mutants:			
aplip1^{ek4} , *Df(3L)BSC799* (SL # 2077+215 / BL # 24632)	III	App-like interacting protein 1, hypomorph (point mutation) in the background of Aplip1 deficiency (*Df(3L)BSC799*)	kindly provided by Mathias Böhme Horiuchi et al., 2005; Böhme et al., 2019
brp83	III	two endogenous plus two genomic *bruchpilo*t gene copies, coding four copies of Bruchpilot (4x BRP)	Gupta et al., 2016
brp83 , *r13f02*-Gal4	III	4x BRP combined with the mushroom body driver *r13f02*	kindly provided by Sheng Huang
brp^{c04298} (HMS #c04298)	II	null mutation of *bruchpilot*	Huang et al., 2020
CG8005^{DG05802}	III	deoxyhypusine synthase, necessary in the first step of hypusination	Liang et al., 2021

foxo^{EY11248} (BL # 20279)	III	P-element insertion of *foxo*, overexpression	Zhao et al., 2008
ilp2 (BL # 30881)	III	ends-out gene replacement of *ilp2* with w^+	Grönke et al., 2010
ilp2-3 (BL # 30888)	III	ends-out gene replacement of *ilp2* and *ilp 3* with w^+	Grönke et al., 2010
w^{Dah} ;; *ilp2-3,5* (SL # 23)	X ;; III	ends-out gene replacement of *ilp2, ilp3,* and *ilp5* with w^+, in the background of *white Dahomey*	kindly provided by Partridge lab Grönke et al., 2010
ilp3 (BL # 30882)	III	ends-out gene replacement of *ilp3* with w^+	Grönke et al., 2010
ilp5 (BL # 30884)	III	ends-out gene replacement of *ilp5* with w^+	Grönke et al., 2010
ilp7 (BL # 30887)	X	ends-out gene replacement of *ilp7* with w^+	Grönke et al., 2010
sNPF^{c00448} (SL # 2711 / BL # 85000)	II	short neuropeptide F (sNPF), hypomorph mutation	Hu et al., 2017
srpk79D^{VN} (SL # 1918)	III	serine-arginine protein kinase 79D (Srpk79D), null mutant	Nieratschker et al., 2009
sss (BL # 16588)	II	*sleepless*^{EY04063}, also named *sss*^{P1}; P-element insertion; *quiver* (*qvr*) is an allele of *sss*	Koh et al., 2008
sss ; 4x BRP	II ; III	*sleepless*^{EY04063} (also named *sss*^{P1}) combined with *brp83* (4x BRP)	kindly provided by Sheng Huang Huang et al., 2020

unc13B deletion *del100Bpacman*/+ ; *unc13*^{P84200} (SL # 784)	III ; IV	*unc13A* Pacman rescue (*del100Bpacman*) in the background of an *unc13* null allele (*unc13*^{P84200}, generated via EMS mutagenesis)	Böhme et al., 2016
unc13 rescue *unc13 pacman full*/+ ; *unc13*^{P84200}	III ; IV	*unc13* rescue with *unc13A* and *B* in the background of *unc13* null allele (*unc13*^{P84200})	Böhme et al., 2016
overexpression lines:			
UAS-*atg1*^{6B} OE (SL # 248 / BL # 51655)	III	overexpression of *autophagy-related 1*, core component of the Atg1 initiation complex within macroautophagy	Mohseni et al., 2009
UAS-*cellubrevin* OE	III	*cellubrevin* overexpression	Bhattacharya et al., 2002
UAS-*hdac6* OE		*histone deacetylase 6* overexpression	kindly provided by Patrik Verstreken
UAS-*hsc70-4*^{wt} OE (SL # 2682)	III	overexpression of the wild-type *heat shock protein cognate 4* (*hsc70-4*) with functional chaperone-mediated autophagy and endosomal microautophagy	Uytterhoeven et al., 2015
UAS-*hsc70-4*^{D10N} OE (SL # 2683)	III	*heat shock protein cognate 4* (*hsc70-4*) overexpression where the ATPase is not working, only the endosomal microautophagy is active	Uytterhoeven et al., 2015
UAS-*p62/Ref(2)p*-GFP OE (SL # 2667)	III	overexpression of mammalian *p62* protein receptor (*Ref(2)p* in *Drosophila*)	
UAS-*skywalker* OE (SL # 2642)	III	*skywalker*^{VKB3} overexpression	Uytterhoeven et al., 2011

UAS-*sNPF* OE		*short neuropeptide F* (*sNPF*) overexpression	kindly provided by Peter Soba
UAS-*sNPF* OE ; UAS-*sNPF* OE (SL # 2714)	II ; III	*short neuropeptide F* (*sNPF*) overexpression	kindly provided by Ilona Grunewald-Kadow
UAS-*sss* OE (BL # 30866)	III	overexpression of *sleepless*^{EY04063} (also named *sss*^{P1}); *quiver* (*qvr*) is an allele of *sss*	Bloomington Drosophila Stock Center
w ;; UAS-n-*synaptobrevin*-GFP OE (SL # 2649)	I ;; III	overexpression of neuronal *synaptobrevin* (with GFP tag)	Bhattacharya et al., 2002
UAS-*unc13A* C-term -GFP OE; *ok107*-Gal4 (SL # 599)	III ; IV	expressing Unc13A without the N-terminal end, driven by *ok107*-Gal4 in the mushroom body	kindly provided by Mathias Böhme Böhme et al., 2019
UAS-*unc13A* N-term^{DN} -GFP OE	III	dominant negative N-terminal end of Unc13A	Reddy-Alla et al., 2017
UAS-*unc-104* OE (BL # 24786)	X	*unc-104* overexpression	kindly provided by Tobias Rasse
RNAi lines:			
UAS-*aplip1* RNAi (SL # 2318 / VDRC # 50007)	III	App-like interacting protein (Aplip1), a scaffold protein with tasks in axonal transport	Böhme et al., 2019
UAS-*atg5* RNAi (BL # 34899)	III	*autophagy-related 5* (*atg5*); part of the Atg12 conjugation system within macroautophagy	Bhukel and Beuschel et al., 2019
UAS-*atg9* RNAi (BL # 34901)	III	*autophagy-related 9* (*atg9*); part of the PI3P binding complex within macroautophagy	Bhukel and Beuschel et al., 2019
UAS-*brp*^{B3} RNAi	III	Bruchpilot (BRP), a main scaffold protein of the presynaptic active zone	(Wagh et al., 2006)

UAS-*CG8005* RNAi (VDRC # 103593)	II	deoxyhypusine synthase, necessary in the first step of hypusination	Liang et al., 2021
UAS-*elp3* RNAi (BL # 35488)	III	elongator complex protein 3 (ELP3), a lysine acetyltransferase (KAT)	Bloomington Drosophila Stock Center
UAS-*elp3* RNAi (VDRC # 106128)	II	elongator complex protein 3 (ELP3), encodes a lysine acetyltransferase (KAT)	Vienna Drosophila Resource Center
UAS-*hdac6* RNAi (BL # 31053)	III	*histone deacetylase 6* (*hdac6*)	Gupta et al., 2016
UAS-*hdac6* RNAi (BL # 34702)	III	*histone deacetylase 6* (*hdac6*)	Bloomington Drosophila Stock Center
UAS-*p62/Ref(2)p* RNAi (BL # 33978)	III	mammalian p62 protein receptor (Ref(2)p in *Drosophila*)	Bloomington Drosophila Stock Center
UAS-*sss* RNAi (BL # 58061)	II	*sleepless*^{EY04063}, also named *sss*^{P1}; *quiver* (*qvr*) is an allele of *sss*	Bloomington Drosophila Stock Center
UAS-*sNPF* RNAi (SL # 2712)	X ; II	short neuropeptide F (sNPF)	Knapek et al., 2013
UAS-*sNPF R* RNAi (SL # 2717)	III	short neuropeptide F receptor	Knapek et al., 2013
UAS-*srpk79D* RNAi (VDRC # 47544)	III	serine-arginine protein kinase 79D (Srpk79D)	Nieratschker et al., 2009
UAS-*tomosyn* RNAi (SL # 2670 / VDRC # 43630)	II	RNAi for *tomosyn*	Chen et al., 2011

UAS-*unc13A* RNAi (SL # 1521)	III	RNAi for the isoform A of *unc13*	Fulterer et al., 2018
UAS-*unc13B* RNAi (SL # 1519)	III	RNAi for the isoform B of *unc13*	Fulterer et al., 2018
wild-type:			
Canton S (SL # 2136)		wild-type	Tully and Quinn, 1985
w^{Dah} (SL # 22)	X	*white Dahomey*, a natural host of the bacterium *Wolbachia pipientis*	kindly provided by Partridge lab (Grönke et al., 2010)
w^{1118}	X	with a *white* null allele	Hazelrigg et al., 1984; Diegelmann et al., 2006

2. Aversive olfactory assays

All aversive olfactory assays were performed at 25 ± 2 °C and relative humidity of 80 ± 5 % in dim red light. The experimental flies have been stored under these conditions for acclimation one hour before the tests. As olfactory cues, the odors 3-Octanol (OCT; source: Sigma-Aldrich [No. 218405]) and 4-Methylcyclohexanol (MCH; source: Sigma-Aldrich [No. 66360]) were used most frequently. The odors were applied in the concentration 1:100, diluted in Paraffin oil (source: Sigma-Aldrich [No. 18512]), and presented in 14 mm cups. In these concentrations, the odors are repulsive for the flies. In some experiments, different odor combinations were used in appropriate concentrations: 3-Octanol was combined with Ethylacetate (EA; source: Sigma-Aldrich [No. 270989]) and 4-Methylcyclohexanol with Benzaldehyde (BA; source: Sigma-Aldrich [No. 418099]). If necessary, the used concentrations were adapted using equal effectiveness between the odors. Each experimental setup and the according measured parameters are declared in the appendix, Table 25.

Following the Pavlovian principle from 1927, classical conditioning was performed to link a conditioned stimulus (CS) with punishment (e.g., electrical shock) as an unconditioned stimulus (US) (Kahsai and Zars, 2011). In this study, the electric shock as a negative reinforcer was used as an unconditioned stimulus with an alternating current of 120 volts (V) twelve times within one minute. Around 100 naïve flies were placed in the T-maze (one position; Figure 17) or a Tully Wheel (four positions, each with about 100 flies) (Tully and Quinn, 1985). The unconditioned stimulus was combined with one odor (A) as the conditioned stimulus (CS^+) in a single-cycle associative procedure (Figure 17). After one minute of rest, the other odor was presented to the flies as the non-shock associated odor (CS^-) for one minute. After this training session, the flies were either stored under experimental conditions separately to wait for the

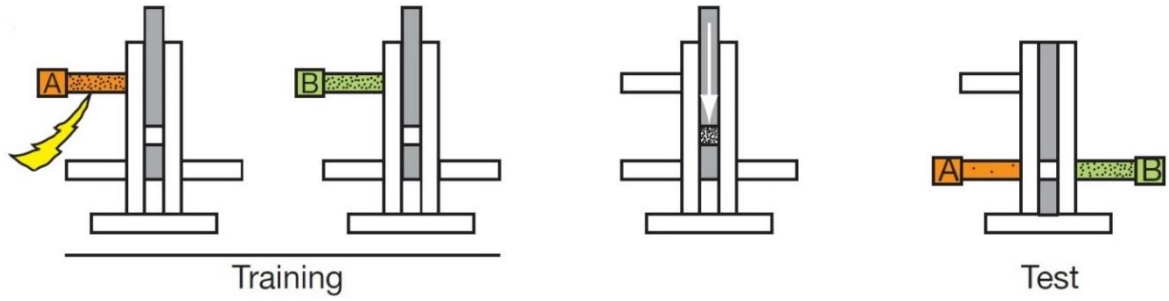

Figure 17: Aversive olfactory memory assay with a T-maze.

During the training session, one odor (A) is paired with an electric shock (unconditioned stimulus; US) to generate a conditioned stimulus (CS^+). Afterward, the second odor (B) is presented to the flies without reinforcement (CS^-). For the test situation, the flies were pushed into the choice position between the two odors (Tully and Quinn, 1985). Image taken from Vosshall, 2007.

test session or immediately lowered into the test position of the T-maze. In the test phase, the flies could choose between the two simultaneously presented odors for one minute (Figure 17). Afterward, the number of flies in the different tubes was counted, and the performance index (PI) was calculated as flies that avoided the shocked odor (CS^-) minus flies which choose the conditioned odor (CS^+), divided by the whole number of flies, and multiplied by 100 for the unit percentage. Hence, a distribution of 50:50 would give a PI of 0 %, meaning no learning, while a PI of 100 % would result in a distribution of 1:100 as total learning.

$$\mathrm{PI}_{\mathrm{A/B}}\,[\%] = \frac{\mathrm{CS}^- - \mathrm{CS}^+}{\mathrm{CS}^- + \mathrm{CS}^+} \cdot 100$$

To complete the trial, the second odor needs to be combined with the reinforcer within an additional reciprocal experiment with fresh flies. The resulting PI shows the learning with the second odor. The final performance index can be received via the means of both odors' PIs.

$$\mathrm{PI} = \frac{\mathrm{PI}_\mathrm{A} + \mathrm{PI}_\mathrm{B}}{2}$$

Different memory phases develop after the learning (Figure 18; Tully et al., 2003). At first, short-term memory (STM) emerges immediately after the training phase and lasts for minutes. Subsequently, mid-term memory (MTM) follows, which develops within minutes and lasts for hours. In this study, one and three hours MTM was performed. MTM can further be distinguished between anesthesia-resistant memory (ARM), which is the consolidated component of MTM, and its labile part, anesthesia-sensitive memory (ASM), which is sensitive to anesthesia (Tamura et al., 2003). To isolate these two phases, ARM was tested independently of MTM. Here, the training was run out regularly. 30 minutes before the testing, the experimental flies were kept in ice-cold water for 90 seconds. During this procedure, the labile ASM vanishes. Consequently, it is possible to calculate the value for ASM by subtracting the ARM value from the mid-term memory (median).

$$\mathrm{ASM} = \mathrm{MTM} - \mathrm{ARM}$$

Long-term memory (LTM) is tested 24 hours after training. It needs iterated, spaced training to develop after hours and persists for more than seven days (Tully et al., 2003). This test was not conducted in this thesis.

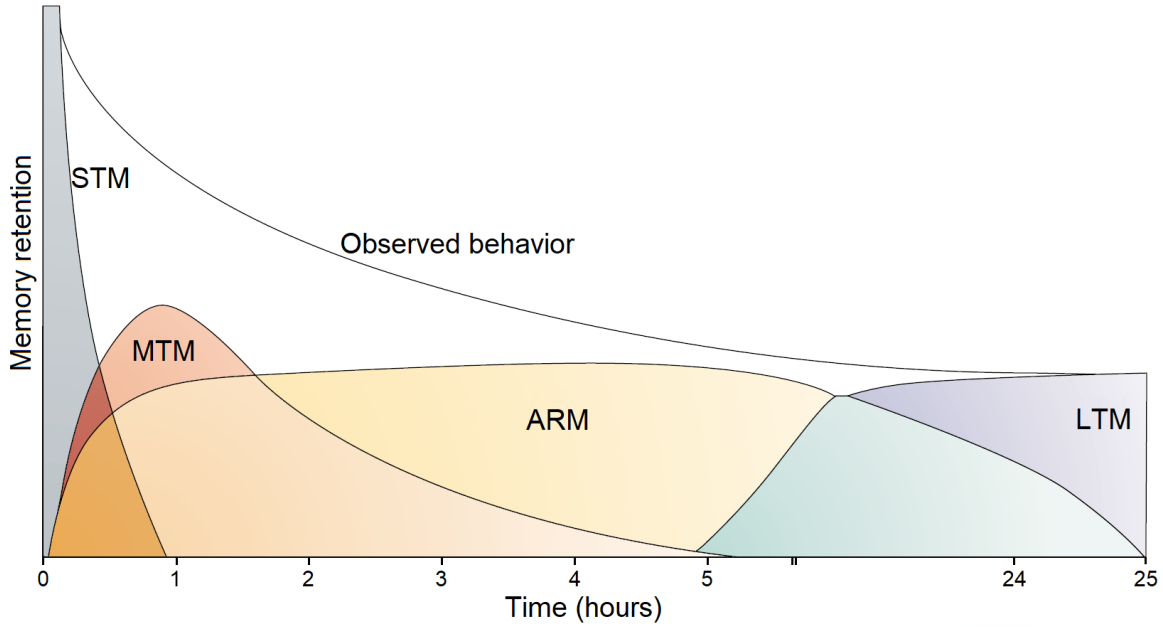

Figure 18: Memory phases

Aversive olfactory learning is assembled in different memory phases, which vary in function and genetics. Short-term memory (STM) develops immediately in the learning process but lasts only minutes. Mid-term memory (MTM) occurs within minutes and lasts for hours. MTM can be separated into anesthesia-resistant memory (ARM) as a more stable component of mid-term memory, which lasts for several days, and labile anesthesia-sensitive memory, decreasing with time. With iterated training, long-term memory (LTM) evolves after several hours and persists for more than a week. Image modified from Tully et al., 2003.

The following tests were conducted to check the experimental groups' innate behavior. First, the odor acuity to see the flies could sense the odors. For this, around 100 naïve flies were directly placed in the T-maze's choice position, where they could choose between one odor (A or B) and air for one minute. Since the odors were presented in aversive concentrations, flies should avoid these odors. The performance index for each odor acuity (PI_A / PI_B) was calculated as flies that choose the air (CS_{air}), minus flies from the odor side ($CS_{A\,/\,B}$), divided by the sum of the tested flies. The value was multiplied by 100 and stated in percentage.

$$\mathrm{PI_{A/B}\,[\%]} = \frac{\mathrm{CS_{air}} - \mathrm{CS_{A/B}}}{\mathrm{CS_{air}} + \mathrm{CS_{A/B}}} \cdot 100$$

For shock reactivity, around 100 naïve flies were put in the choice position between air and the running alternating current of 120 volts (V) for one minute. Afterward, the performance index (PI_{shock}) was calculated as the flies, which avoided the shock (CS_{air}), minus the shocked ones (CS_{shock}), divided by the whole number of tested flies. In the end, the result was multiplied by 100 and stated in percentage.

$$\mathrm{PI_{shock}}\,[\%] = \frac{\mathrm{CS_{air}} - \mathrm{CS_{shock}}}{\mathrm{CS_{air}} + \mathrm{CS_{shock}}} \cdot 100$$

In this study, if not dedicated otherwise, mid-term memory (1 and 3 hours) and anesthesia-resistant memory (1 and 3 hours) were performed with a T-maze, as well as odor acuity. In contrast, short-term memory and shock reactivity were mainly carried out with the Tully Wheel.

To test the experimental conditions, around 100 naïve wild-type flies were placed in the choice position, while one odor was presented on one side, the other one on the opposite. In a functional setup, equal distribution of around 50:50 for each odor was received (PI = 0). If necessary, the odor concentrations were adjusted depending on this direct comparison test in the T-maze or Tully Wheel. Usually, a concentration of 1:100 (diluted in paraffin oil) was used, if not declared otherwise (appendix, Table 25).
A short compilation of the methods (age, rearing temperature, apparatus, concentration) for each experiment is listed next to the measured parameter in the appendix.

3. Longevity assay

These trials were performed as a part of the research for 4,4'-Dimethoxychalcone (DMC). Here, wild-type *w*^{1118} flies were collected after their eclosion for three days. After one additional mating day, the flies were sorted, male and female separate, under CO_2 anesthesia, and portioned into 20 flies per vial for each cohort and concentration. Besides normal food and 0.1 % Dimethylsulfoxide (DMSO) food as controls, the following concentrations of DMC were used (each dissolved in 0.1 % DMSO): 0.2 mM (0.0537 µg/ml), 1.0 mM (0.269 µg/ml) and 2.0 mM (0.537 µg/ml). Subsequently, the flies were placed on fresh food of the appropriate DMC concentration every other day. Dead flies were noted and removed. Escaped flies were excluded. Additionally, test with different DMSO concentrations (0.05 %, 0.1 % and 0.5 % DMSO) were conducted.

4. Locomotor activity assay (negative geotaxis)

The locomotion capabilities of flies treated with 4,4'-Dimethoxychalcone (DMC) were tested with a locomotion activity assay (also called climbing assay; test for negative geotaxis) after Gupta et al., 2013: Wild-type *w*^{1118} flies were collected for one day, and sorted by sex under CO_2 anesthesia on the days 1, 8, 18, or 28. Groups of 15 flies were stored in separate vials with the different drug concentrations, split in sex and the different cohorts. After two days of recovery, the test animals were transferred into experimental vials, marked by a line at the height of seven centimeters from the bottom. Each trial was performed around the same time of the day, in natural light at room temperature (23 °C), and videotaped. One after the other, the respective flies with the age of 3, 10, 20, and 30 days were tapped down in the vial and allowed to climb for 5, 10, or 15 seconds. Thereby, each experimental group was tested only once.

The climbing success for each round was determined after 15 and 30 seconds. It was calculated as the whole number of flies plus the subtraction of the ones, which passed the seven centimeters (Ntop) within 15 or 30 seconds, substracted by the flies that failed the task (N_{bottom}). The result was divided by the number of flies (N_{total}), split in half, and multiplied by 100 for the unit percentage.

$$\text{Climbing Success } [\%] = \frac{N_{total} + (N_{top} - N_{bottom})}{N_{total}} \cdot \frac{1}{2} \cdot 100$$

In a second locomotion protocol following Inagaki et al., 2009, an apparatus as shown in Figure 19 was used to perform a negative geotaxis assay. This way, the gravity sensing of macroautophagy deficient flies was measured (see chapter III.2.4.1.b, Figure 47). In the trial, the flies migrated from the left position with test tube 1 to the right with test tube 6. A bad performance in locomotion would be visible with many animals in the left fraction and *vice versa*. In preparation for one test round, 20 female flies were collected and transferred to fresh food every second or third day until they reached their experimental age. The tests were performed at 25 ± 2 °C and relative humidity of 80 ± 5 % in dim red light. When the experimental flies were 10-day old, they were loaded in test tube 1 (step 1 in Figure 19) and fixed to the apparatus in its transfer state (slide right). After three minutes of resting time (to step 2), the device was strongly tapped down five times, and fast skidded to the testing state (slide left;

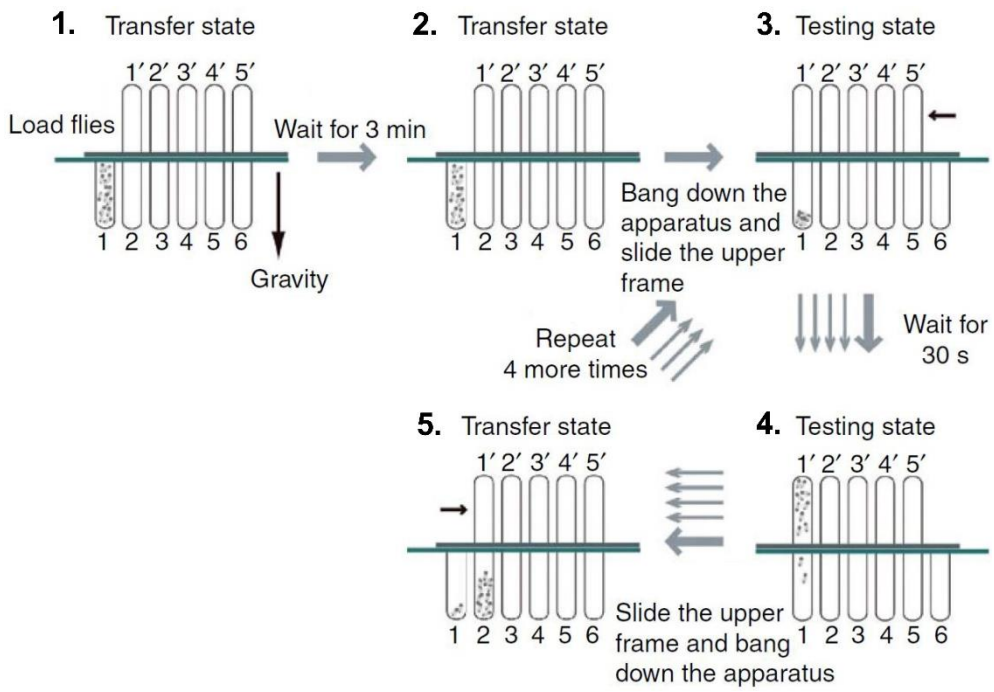

Figure 19: Apparatus and procedure for a negative geotaxis assay.

First (step 1), the flies were loaded in test tube 1 at the transfer state. After a break of 3 minutes (step 2), the whole device is tapped down five times, and the upper frame is fast slid to the testing state (test tubes 1 and 1' are in the opposite of each other; step 3). Now, the flies have 30 seconds to climb up into test tube 1' (step4). The climbing is stopped by sliding the upper frame back to the transfer state (step 5). Procedures 3 to 5 are repeated four more times. Image modified from Inagaki et al., 2009.

step 3). In this testing stage, the flies could climb from test tube 1 into 1' within 30 seconds (step 4). Next, the upper frame of the machine was set to the transfer state as at the beginning (slide right), and the apparatus was strongly tapped down five times. Most of the flies were in test tube number 2 by then (Figure 19). Once again, the apparatus is tapped down five times. Next, steps 3 to 5 were repeated four times until the flies could reach the last test tubes. The animals in the six test tubes of the lower row (1-6) were removed and counted. The coefficient Cf as the probability of the flies reaching successfully the last test tubes was calculated as below. Here, n was the number of the test tube.

$$Cf = \frac{n_2 + 2\,n_3 + 3\,n_4 + 4\,n_5 + 5\,n_6}{5\,(n_1 + n_2 + n_3 + n_4 + n_5 + n_6)}$$

5. Immunostainings and microscopy

The brains of female adults of the appropriate age were dissected in an ice-cold hemolymph-like solution (HL3) and immediately transferred for fixation to 4 % paraformaldehyde (4 % PFA in phosphate-buffered saline solution (PBS), pH = 7.4) on a shaker for one hour at room temperature. Afterward, the brains were washed in 0.6 % Triton X-100 in PBS solution (0.6 % PBT) on a shaker for 20 minutes at room temperature. Next, they were incubated in the blocking solution 10 % normal goat serum (NGS) in 0.6 % PBT on a shaker for two hours at room temperature. Finally, the primary antibodies were added in the needed concentrations to a solution of 0.6 % PBT containing 5 % NGS and 0.1 % sodium azide (NaN_3). In the darkness, the brains were incubated in this solution on a shaker at 4 °C for 48 hours. The used primary antibodies are listed in Table 2. After two days, the brains were washed six times in 0.6 % PBT at room temperature for 30 minutes. Next, the secondary antibodies were added in the necessary concentrations in a solution of 0.6 % PBT with 5 % NGS. The used secondary antibodies are listed in Table 2. In the darkness, the brains were incubated in that solution on a shaker at 4 °C for 24 hours. Afterward, the brains were washed six times in 0.6 % PBT at room temperature on a shaker for 30 minutes. After incubation in Vectashield® (Vector Laboratories) for 24 hours, they were mounted in Vectashield® and stored in darkness at 4 °C until the microscopy.

Images of the whole brain were acquired as described in Bhukel and Beuschel et al., 2019, with a 20 x 0.7 NA oil objective with a Leica TCS SP8 confocal microscope (Leica Microsystems). The images were acquired with an xy-resolution of 1024x1024, a z-resolution

of 0.3 µm, and a scan speed of 600 Hz using 4x line averaging. In this process, the software Leica LCS AF was used. Additional whole brain scans (chapter III.3.2.1, Figure 104) were performed with minor changes: z-resolution of 1.0 µm, scan speed 400 Hz. Furthermore, scans of the mushroom body were conducted with the following modifications (Böhme et al., 2019): 63 x 1.4 NA oil objective (immersion liquid type T), z-resolution of 0.8 µm, and a scan speed of 400 Hz using 2x line averaging.

For image acquisition, the software Fiji ImageJ 1.53c and Leica Application Suite X was used. Whole brain images were maximum projections, while the mushroom body pictures in Figure 101, chapter III.3.2.1, were single slide projections.

Table 2: Antibodies

antibody	Concentration	source	previously described in
primary antibodies:			
mouse anti-FasII^{1D4}	1:40	Developmental Studies Hybridoma Bank: AB_528235	Bhukel and Beuschel et al., 2019
mouse anti-BRP^{Nc82}	1:50	Developmental Studies Hybridoma Bank: AB_2314865	Bhukel and Beuschel et al., 2019
rabbit anti-p62/Ref(2)p	1:5000	Gabor Juhasz	Bhukel and Beuschel et al., 2019
rabbit anti-sNPF	1:2000	Jan Veenstra	Bhukel and Beuschel et al., 2019
chicken anti-GFP	1:2000 (Figure 101) 1:1500 (Figure 104)	Sigrist laboratory: # ab13970	Böhme et al., 2019
guineapig anti-unc13 A$^{N\text{-terminus}}$	1:500	Sigrist laboratory: # 14gp18	Böhme et al., 2019

secondary antibodies:			
goat anti-rabbit Alexa-488	1:500	Sigrist laboratory: # ab11008	Bhukel and Beuschel et al., 2019
goat anti-chicken Alexa-488	1:500	Sigrist laboratory	Huang et al., 2020
goat anti-guineapig Cy3	1:500	Sigrist laboratory	Böhme et al., 2019
goat anti-mouse Cy3	1:500	Sigrist laboratory: # ab97035	Bhukel and Beuschel et al., 2019
goat anti-mouse Alexa 633	1:500	Sigrist laboratory	Hussain et al., 2018

6. Statistics

To perform the statistic analysis and generate figures, GraphPad Prism 8.0.1 was used. Normal distribution was tested with the Shapiro-Wilk test, where all values are unique. Hence, if the results were parametric, an unpaired t-test was conducted for two groups to compare. For more than two groups, ordinary one-way ANOVA was conducted. As a multiple comparisons *post hoc* test, Sidak's analysis was performed for the belonging test groups, or Tukey's when comparing all experimental groups. In contrast, a Mann Whitney test was performed for two groups to compare, and a Kruskal-Wallis test with Dunn's multiple comparisons *post hoc* test for more than two groups if the values were distributed nonparametrically.

If more than one variable was included in a trial, the analysis was performed in a grouped table with two grouping variables, one parameter determined by rows and the other by columns. Then, the data was analyzed via two-way ANOVA and Sidak's multiple comparisons test.

Data sets were plotted as columns with the mean ± standard error of the mean (SEM) as the error bar and the individual values as points.

The survival curves were compared with a Log-rank (Mantel-Cox) test (conservative) for survival analyses.

Asterisks indicate statistical significance via *p*-values ($^{ns}p \geq 0.05$ $^{*}p < 0.05$; $^{**}p < 0.01$; $^{***}p < 0.001$; $^{****}p < 0.0001$). Each analysis with its used statistical tests and the results (mean ± SEM, median (n), p-value) were declared in the appendix.

III. Results

1. The quest for an anti-aging elixir and its advantages beyond

The search to combat aging and generate a long life with stable physical and mental health is as old as humankind. Nowadays, the mortality rate improved, but the increase in healthspan does not match the rising lifespan. Thus, the quest for an anti-aging elixir comes into focus.

1.1. Flavonoids as promising substances to prevent aging effects

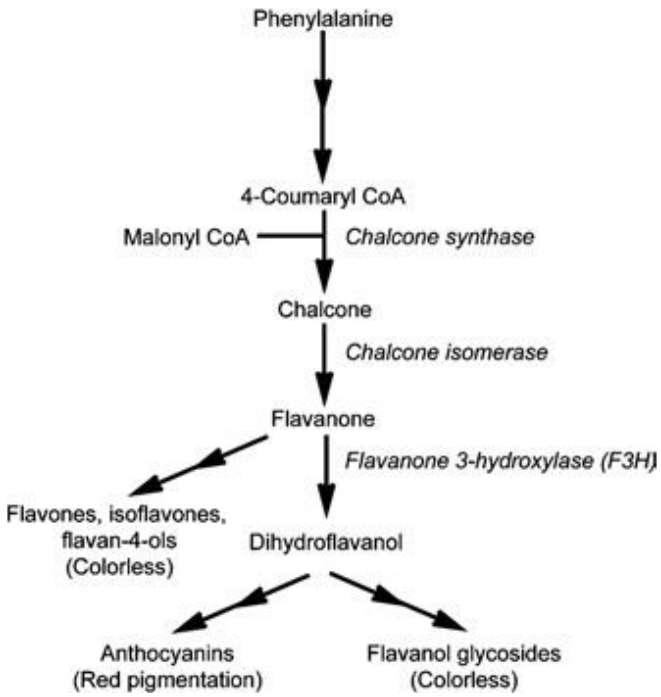

Figure 20: The biosynthesis of flavonoids.
From the basic module phenylalanine, further subgroups of the flavonoids are built. Among them are chalcones, flavanones, Isoflavones, and anthocyanins. Image taken from Rangarajan et al., 2004.

One substance group, which consistently comes to the fore, is flavonoids. They are the major subgroup of polyphenols (Carmona-Gutierrez et al., 2019), and many are ascribed as antioxidative, antibacterial and antiviral, anti-carcinogen, anti-inflammatory, and neuroprotective (Kühnau, 1976; Rice-Evans and Miller, 1996; Badshah et al., 2021).

Naturally occurring in plants as secondary metabolites, flavonoids are widespread compounds that trap free radicals. Due to two phenyl rings connected by a carbonyl structure, several free pairs of its electrons interact with reactive oxidative species (ROS). Thus, flavonoids are associated with various anti-aging and health-promoting effects, wherefore their beneficial value is used as a food supplement, in cosmetics, and even as medicine (Panche et al., 2016).

1.1.1. 4,4’-Dimethoxychalcone, a promising additive to delay aging

One promising flavonoid seemed to be 4,4’-Dimethodychalcone (DMC). Positive effects of this natural substance were found in a lifespan screen within various anti-aging flavonoid-subclasses via yeast in Professor Frank Madeo’s group (Carmona-Gutierrez et al., 2019). Here, DMC provided mitigated age-induced apoptosis and necrosis in cells plus a reduced impact of reactive oxygen species (ROS). This hints toward reproducible benefits in other species (Fontana et al., 2010). Additionally, DMC is a component in *Angelica keiskei koidzumi*, a well-known plant in Asian traditional medicine associated with health and longevity (Carmona-Gutierrez et al., 2019).

To verify these exciting findings, tests in higher organisms were mandatory. Accordingly, I used *Drosophila melanogaster* to perform a longevity assay with DMC. Indeed, I found a highly significant benefit for the DMC concentrations of 0.2 mM, 1.0 mM, and 2.0 mM (Figure 21). For female animals (Figure 21a), the median survival rose by 19 % from 52 days with the control food to 62 days for 0.2 mM DMC. Similarly, the health span improved by 11 % for 1.0 mM and 15 % for 2.0 mM DMC. The major increase in the maximal lifespan appeared for 0.2 mM DMC with 98 days compared to 87 days for the control food. Concomitantly, the male

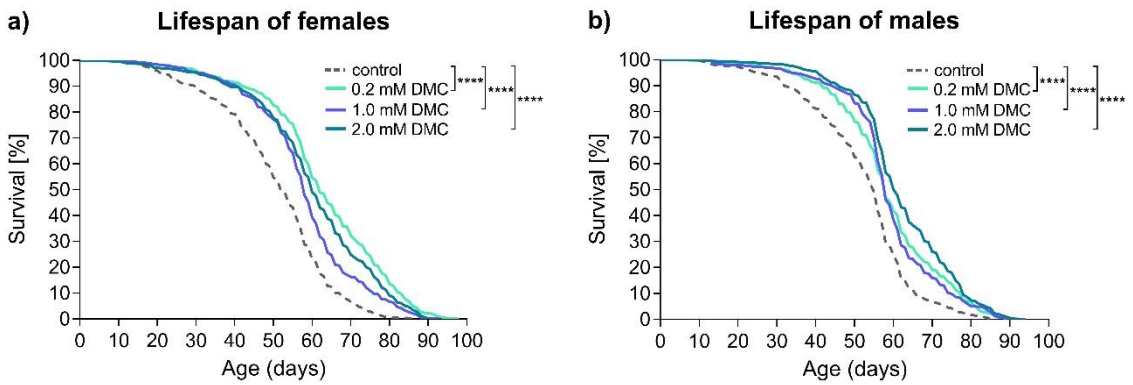

Figure 21: Lifespan for *Drosophila melanogaster* fed with different concentrations of 4,4’-Dimethoxychalcone.

a) Lifespan for w^{1118} females showed significant benefits for all DMC concentrations compared to the control food 0.1 % DMSO. Median survival: 52 days for control food (n = 581), 62 days for 0.2 mM DMC (n = 580), 58 days for 0.1 mM DMC (n = 584), 60 days for 2.0 mM (n = 590). Maximal lifespan: 87 days for control food, 98 days for 0.2 mM DMC, 93 days for 1.0 mM DMC, 91 days for 2.0 mM DMC. b) Lifespan for w^{1118} males showed a benefit for all DMC concentrations compared to the control food 0.1 % DMSO. Median survival: 55 days for control food (n = 581), 58 days for 0.2 mM DMC (n = 580), 58 days for 0.1 mM DMC (n = 584), 61 days for 2.0 mM DMC (n = 590). Maximal lifespan: 86 days for control food, 90 days for 0.2 mM DMC, 94 days for 1.0 mM DMC, 93 days for 2.0 mM DMC. Statistics: Log-rank (Mantel-Cox) test, ****$p < 0.0001$. Together with Sara Mertel.

performance was positive (Figure 21b), yet slightly weaker than the females. The maximal lifespan worked the best for 1.0 mM DMC with 91-day survival compared to 86 days for the control food.

The median survival for males appeared the best with 61 days for 2 mM DMC (11 %), followed by 5 % and 58 days for 0.2 and 1.0 mM DMC, compared to 55 days for control food. Possibly, the female flies showed a higher food intake due to augmented presence near the food for egg deposition. Differences in the DMC concentrations seemed to have less influence. Additional tests with a concentration of 1.0 mM DMC showed that even treatment from the earliest development, from the larval stage, was beneficial for female flies' health (Figure 22). In short, the median survival increased from 55 to 62 days (13 %), yet the maximal lifespan appeared similar with 83 (control food) to 85 days for 1.0 mM DMC. Thus, DMC possessed the ability to delay aging.

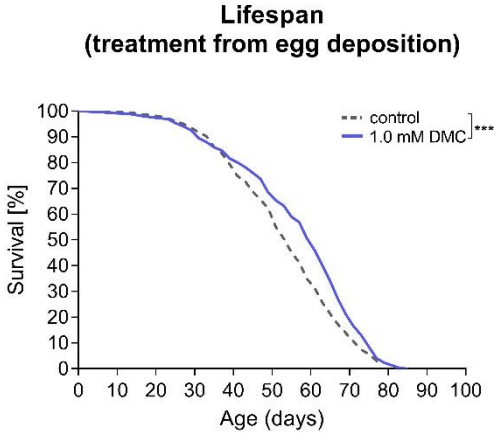

Figure 22: Lifespan for female flies treated with 0.1 mM DMC from the earliest development.

Significant beneficial effects for 0.1 mM DMC treatment since the larval state of w^{1118} females. Median survival: 55 days for control food (n = 390), 61 days for 1.0 mM DMC (n = 392). Maximal lifespan: 83 days for control food, 85 days for 1.0 mM DMC. Statistics: Log-rank (Mantel-Cox) test, ***$p < 0.001$.

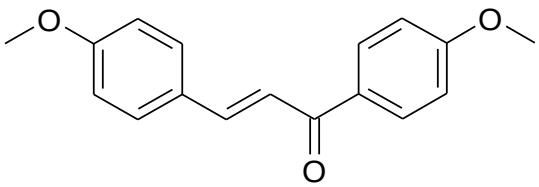

Figure 23: Structural formula of 4,4'-Dimethoxychalcone.

DMC is a highly lipophilic structure visible through the benzene rings and the three oxides (Figure 23). Thus, several free pairs of electrons are available, intercepting ROS and serving as antioxidants. DMC shows poor solubility in hydrophilic solvents due to its lipophilic characteristics. Accordingly, it appeared problematic to dissolve this substance in the water-based fly food. Thus, it was necessary to dispense DMC in 0.1 % Dimethylsulfoxide (DMSO), a dipolar dissolvent. This implied cytotoxic side effects and negative impacts on the reproductive and developmental properties of the experimental animals in the conducted longevity tests, since the critical concentration of DMSO seemed to be at 0.5 % (Nazir et al., 2003). Thus, the used concentration of 0.1 % DMSO could be non-

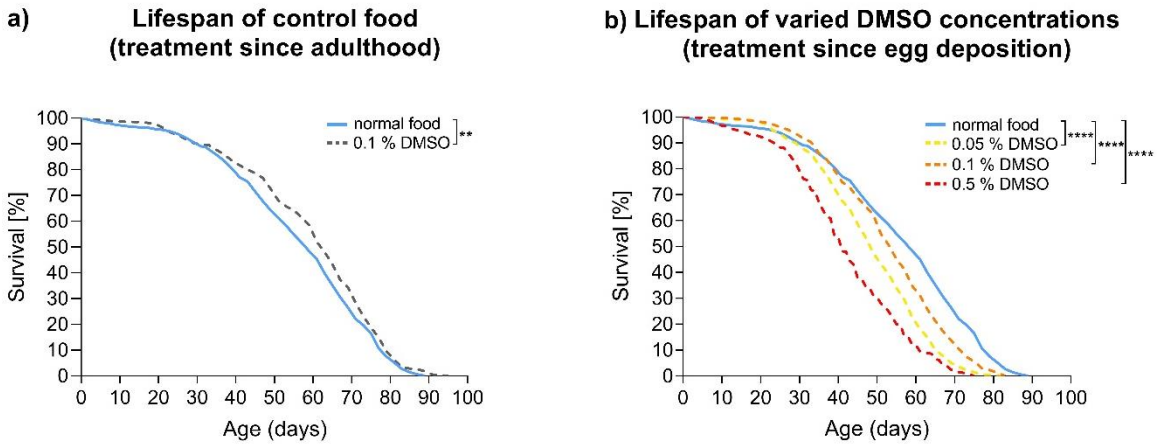

Figure 24: Exploration of a possible impact of Dimethylsulfoxide (DMSO), the solvent for DMC.

a) Lifespan for the experimental control food 0.1 % DMSO in comparison to normal food (treatment since eclosion of the w^{1118} female flies). Median survival: 59 days for normal food (n = 767), 63 days for 1.0 % DMSO (n = 383). Maximal lifespan: 85 days for normal food, 95 days for 1.0 % DMSO. b) Lifespan for different DMSO concentrations for w^{1118} female flies (treatment since the larval state). Median survival: 59 days for normal food (n = 767), 49 days for 0.05 % DMSO (n = 389), 55 days for 0.1 % DMSO (n = 390), 41 days for 0.5 % DMSO (n = 394). Maximal lifespan: 89 days for normal food, 95 days for 0.05 % DMSO, 83 days for 0.1 % DMSO, 83 days for 0.5 % DMSO. Statistics: Log-rank (Mantel-Cox) test, ****$p < 0.0001$, **$p < 0.01$.

toxic. For a toxicity check, I tested the effect of the concentration 0.1 % DMSO, which was the same concentration as for the DMC tests. In these longevity trials, I compared them to norma food

(Figure 24a). Flies were treated with 0.1 % DMSO from their eclosion so that the toxic effects had no bearing on the development (Figure 24a). Surprisingly, DMSO had a mild significant positive effect on the lifespan of females (median survival: 63 days; maximal lifespan: 95 days) compared to normal food (median survival: 59 days; maximal lifespan: 85 days). The median survival was 7 % better. In contrast, when I fed the experimental animals with different DMSO concentrations since their larval state (Figure 24b), the lifespan curves showed a more severe malign profile than the normal food (Figure 24b). Thus, the median survival dropped by 44 % for the critical concentration 0.5 % DMSO (median survival: 41 days; maximal lifespan: 83 days). The experimental DMSO concentration, 0.1 %, declined by 7 % (median survival: 55 days; maximal lifespan: 83 days). Oddly, the lifespan for the lowest concentration, 0.05 % DMSO, even falls by 20 % within its median lifespan (median survival: 55 days; maximal lifespan: 95 days). However, flies in these tests were already exposed to DMSO in their larval stage. The cytotoxic effects of DMSO tipped the scales. However, the adverse effects of DMSO

did not influence the longevity results obtained for DMC, fed since egg deposition. Even though DMSO is beneficial for survival, specifically at the adult stage (Figure 24a), the positive influence of the flavonoid had a much larger impact (Figure 21a). Furthermore, DMC possessed the potency to overcome DMSO's toxic effects on flies' development so that the median survival even increased by 13 % (Figure 22, Figure 24b).

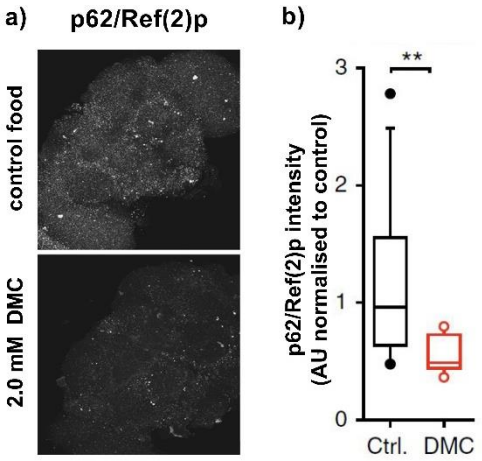

Figure 25: Immunostainings of fly brains, treated with 2.0 mM DMC, show a decreased amount of p62/Ref(2)p aggregates.

Immunostainings for p62/Ref(2)p (indicator for aging and deficient autophagy) showed reduced intensities with 4,4'-Dimethoxychalcone (DMC) treatment for 30-day old female w^{1118} flies. 0.1 % DMSO as control food, 2.0 mM DMC as treatment. a) Representative pictures, scale bar: 50 µm. b) Analysis of the brains as p62/Ref(2)p of control (n = 12) versus DMC therapy (n = 11) revealed a significant benefit. Statistics: unpaired t-test, $^{**}p = 0.0026$. Immunostainings and analysis by Sara Mertel from Carmona-Gutierrez et al., 2019.

Additionally, brain immunostainings of 30-day old flies showed reduced accumulations of p62/Ref(2) (p62 in mammals, Ref(2)p in *Drosophila*) when treated with 2.0 mM DMC (Figure 25). The autophagy receptor p627Ref(2)p was a marker for a functional autophagic system. It binds ubiquitinated proteins to label them for degradation (Bento et al., 2016). Notably, deficient autophagy due to advancing age is accompanied by an accumulation of p62 aggregates (Bartlett et al., 2011; Gupta et al., 2013; Mauvezin et al., 2014). Thus, DMC treatment prevented an age-induced accumulation of damaged proteins. Could DMC induce autophagy in aging animals? Tests in aging yeast showed that DMC could raise the autophagic flux (Carmona-Gutierrez et al., 2019). Furthermore, DMC supports autophagosome formation in *C. elegans* and conquers malign exposure of chloroquine on autophagosomal clearance in human cells (Carmona-Gutierrez et al., 2019).

To explore DMC's mechanism of action, macroautophagy deficient animals were tested. The autophagy-related gene *atg7* codes an E1 ubiquitin conjugase-like enzyme and activates Atg3 and Atg10 within the conjugation cascades, leading to autophagosome elongation (Figure 4; Singh and Cuervo, 2011; Choi et al., 2013). Thus, flies with missing *atg7* suffer from diminished macroautophagy. Interestingly, the beneficial longevity effects of DMC vanished within these animals (Figure 26). Here, the lifespan of female $atg7^{-/-}$ treated with various DMC concentrations stayed on the same level as the control food 0.1 % DMSO or was even slightly

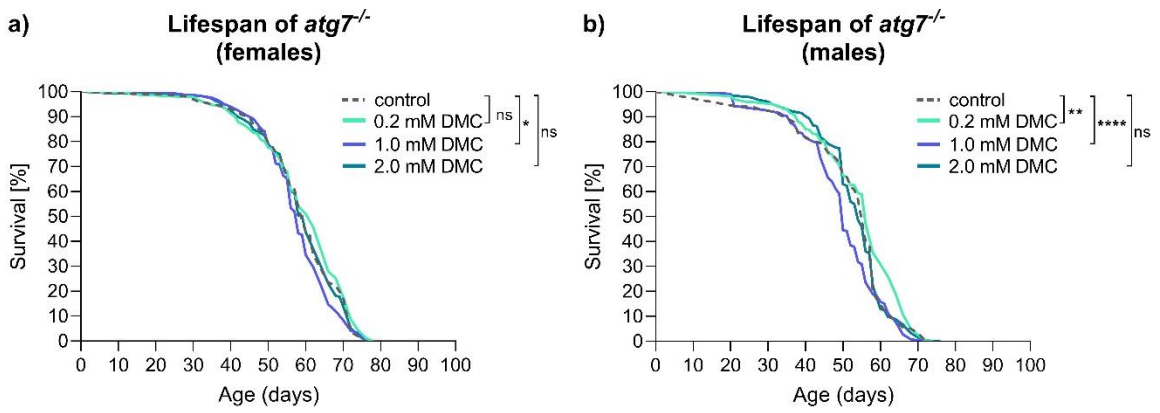

Figure 26: Flies with deficient macroautophagy demonstrate no improved longevity with 4,4'-Dimethoxychalcone.

Lifespan for *atg7*$^{-/-}$ deficient flies showed no significant benefits with DMC-treatment in comparison to 0.1 % DMSO as control food. a) Female median survival: 60 days for control food (n = 327), 62 days for 0.2 mM DMC (n = 329), 58 days for 0.1 mM DMC (n = 333), 60 days for 2.0 mM (n = 325). Female maximal lifespan: 76 days for control food, 78 days for 0.2 mM DMC, 78 days for 1.0 mM DMC, 76 days for 2.0 mM DMC. b) Male median survival: 56 days for control food (n = 331), 56 days for 0.2 mM DMC (n = 328), 50 days for 0.1 mM DMC (n = 330), 54 days for 2.0 mM DMC (n = 327). Male maximal lifespan: 72 days for control food, 74 days for 0.2 mM DMC, 72 days for 1.0 mM DMC, 76 days for 2.0 mM DMC. Statistics: Log-rank (Mantel-Cox) test, ****$p < 0.0001$, **$p < 0.01$, *$p < 0.5$, $^{ns}p > 0.05$. Together with Sara Mertel.

reduced for 0.1 mM DMC (median survival: 58 days; Figure 26a). The median survival for control food was 60 days, just like a treatment with 2.0 mM DMC. For all four different compositions, the maximal survival was from 76 until 78 days. Male *atg7*$^{-/-}$ flies lived shorter than the females but showed a similar picture with DMC (Figure 26b). Here, the lifespan was even significantly reduced for a DMC-administration of 0.2 mM (median survival: 56 days) and 1.0 mM (median survival: 50 days). Since no improvement upon DMC treatment could be observed in the absence of operating autophagy, DMC seems to operate via autophagic induction.

Notably, DMC showed not only in yeast and flies its potential to combat aging but also in other organisms. It decelerates aging in *C. elegans* and human cell cultures and prevents prolonged myocardial ischemia and ethanol-induced damage in mice (Carmona-Gutierrez et al., 2019). Interestingly, similar results as in macroautophagy-impaired *Drosophila melanogaster* appeared in macroautophagy reduced yeast and *C. elegans*, where the beneficial DMC impact on the lifespan was erased (Carmona-Gutierrez et al., 2019). Furthermore, a knockdown of autophagy in the heart of mice fails to prevent ischemia with DMC administration (Zimmermann

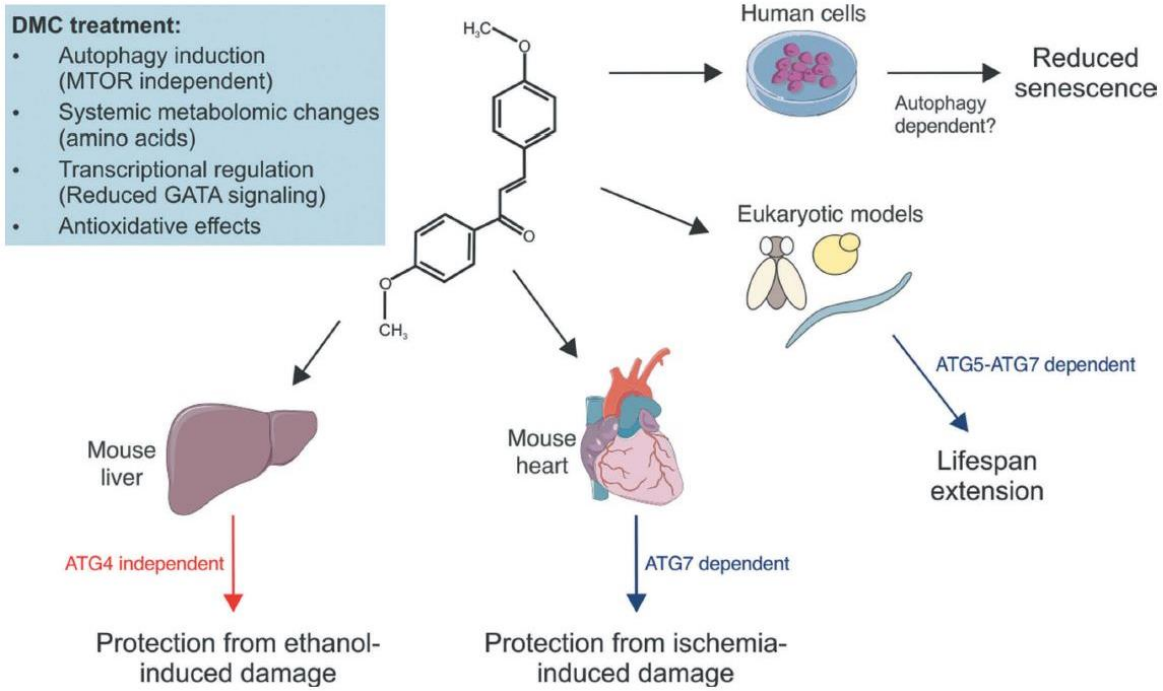

Figure 27: Salutary effects of 4,4'-Dimethoxychalcone in different organisms.

With the treatment of DMC, the longevity of yeast, *C. elegans*, and *Drosophila melanogaster* is extended. Equally, human cell culture survived longer. In mice, the flavonoid protected the heart from prolonged myocardial ischemia and the liver from ethanol-induced damage (Carmona-Gutierrez et al., 2019). DMC operates with versatile principles. Thus, it possesses antioxidative effects, induces autophagy and transcriptional regulation, and changes systemic metabolism (Zimmermann et al., 2019a). Image taken from Zimmermann et al., 2019a.

et al., 2019a). In short, DMC seemed to work via a phylogenetically conserved mechanism. But how does DMC steer macroautophagy? In our 2019 published paper, Carmona-Gutierrez et al. of the Madeo group found DMC operates by inhibiting the GATA transcription factor Gln3. This one is a transcriptional regulator within the nitrogen catabolite inhibition to intensify the biosynthesis of amino acids (Mitchell and Magasanik, 1984; Zimmermann et al., 2019b). In fact, deletion of *gln3* in yeast, *C. elegans* (homolog: *elt-1*), or humans (homolog: *gata2*) eliminated the beneficial effects of DMC (Carmona-Gutierrez et al., 2019). Thus, DMC manipulates autophagy via inhibition of Gln3, a phylogenetically conserved mechanism. Interestingly, this pathway reacts independently of TORC1 (target of rapamycin complex 1) since Rapamycin's autophagy-boosting and cytoprotective impact remained in Gln3 deficient yeast (Carmona-Gutierrez et al., 2019). Hence, the two substances DMC and Rapamycin can promote synergistic curative effects.

1.1.2. Behavioral assays reveal an ambivalent potential of 4,4'-Dimethoxychalcone to combat aging

A powerful drug for the control of aging should increase the lifetime and provide health during aging. Thus, features such as agility and performing memory are prerequisites of an anti-aging elixir. To test if 4,4'-Dimethoxychalcone (DMC) possessed such a supportive profile, I examined the negative geotaxis following the protocol in Gupta et al., 2013, for different DMC concentrations (0.2 mM, 1.0 mM, and 2.0 mM; 0.1 % DMSO as control). This food was used

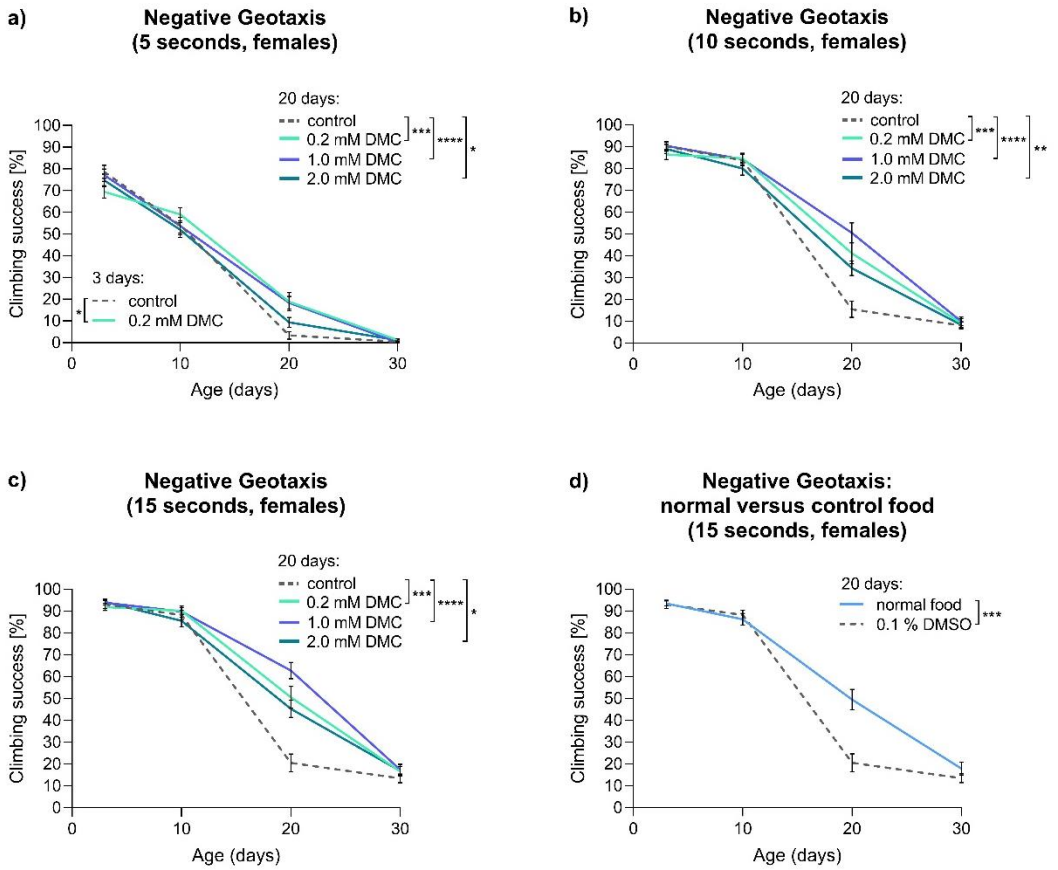

Figure 28: Negative geotaxis tests with female *w*^{1118} for different 4,4'-Dimethodychalcone concentrations.

a-c) Locomotion activity for female *w*^{1118} flies, fed with the DMC concentrations 0.2 mM, 1.0 mM, and 2.0 mM DMC compared to 0.1 % DMSO as control. Similar climbing success appeared for all tested compositions at 3, 10, and 30 days. A significant benefit compared to the control food appeared only at 20 days. a) 5 seconds climbing time. b) 10 seconds climbing time. c) 15 seconds climbing time. d) Comparison of the control food 0.1 % DMSO to normal food with female *w*^{1118} and15 seconds climbing time revealed a benefit for normal food at 20 days. Statistics: Mann-Whitney test, ****p < 0.0001, ***p < 0.001, **p < 0.01, *p < 0.05, $^{ns}p \geq 0.05$. Significant p-values indicated. Error bars: mean ± SEM. Together with Sara Mertel.

since the flies' adult stage. This assay gives a hint about the physical condition of the animals fed with varying food compositions.

Interestingly, DMC only appeared significantly beneficial for animals at 20 days. This was evident for all measured intervals in which the flies could succeed the climbing (5, 10, or 15 seconds). On the contrary, no significant benefit appeared for female *w*^{1118} flies with any DMC concentration at the age of 3, 10, and 30 days in comparison to control food 0.1 % Dimethyl sulfoxide (DMSO) (Figure 28a-c). Actually, 0.2 mM DMC was slightly worse than the control food for 5 seconds climbing with the age of three days (Figure 28a).

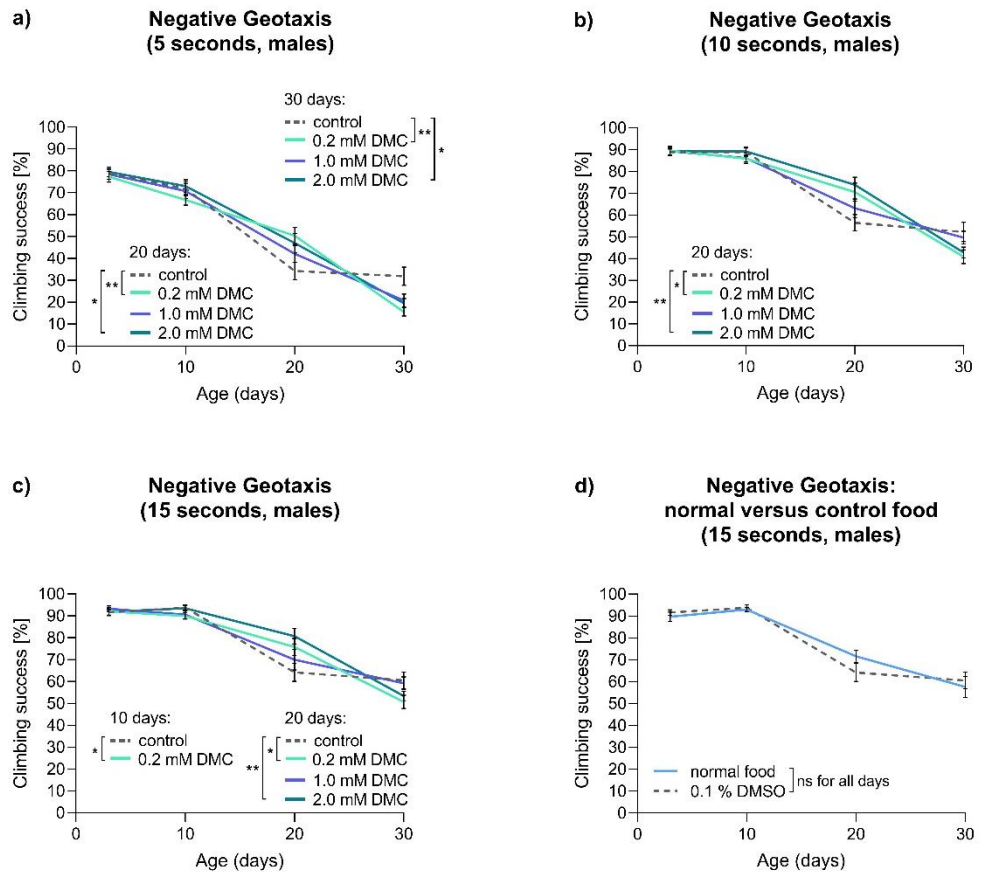

Figure 29: Negative geotaxis tests with male *w*^{1118} *for* different 4,4'-Dimethodychalcone concentrations.

a-c) Locomotion activity for male *w*^{1118} flies, fed with the DMC concentrations 0.2 mM, 1.0 mM, and 2.0 mM DMC compared to 0.1 % DMSO as control. Similar climbing success for all tested compositions at 3, 10, and 30 days, though with more discrepancies than female animals. A significant benefit compared to the control food appeared mostly at 20 days. a) 5 seconds climbing time. b) 10 seconds climbing time. c) 15 seconds climbing time. d) Comparison of the control food 0.1 % DMSO to normal food with male *w*^{1118} and15 seconds climbing time revealed no significant benefit at any age. Statistics: Mann-Whitney test, $^{**}p < 0.01$, $^{*}p < 0.05$, $^{ns}p \geq 0.05$. Significant p-values indicated. Error bars: mean ± SEM. Together with Sara Mertel.

It has to be noted that the control food 0.1% DMSO compared to normal food without any additive turned out to be highly harmful to the locomotion performance of flies (Figure 28d), although only at 20 days. Thus, DMSO seemed to have a detrimental impact on the agility of female flies. However, DMC did intercept this and even significantly surpassed the control values (Figure 28a-c).

I observed similar results for male w^{1118} animals, though these values were more ambiguous (Figure 29). Thus, the protective effect of DMC at 20 days was less pronounced for all tested climbing times (Figure 29a-c). Only 0.2 mM and 2.0 mM DMC gave a significantly better outcome. However, the locomotion performance for these concentrations dropped at 30 days for 5 seconds of climbing time. Additionally, a concentration of 0.2 mM DMC slightly worsened for 15 seconds climbing at ten days (Figure 29c). In contrast to the female performance, the male climbing success occurred at no time point significantly worse for the control food 0.1 % DMSO compared to normal food (Figure 29d). DMC probably affected female animals more stronger since females generally consume more food due to higher energy requirements in reproduction.

Since a performing memory is desirable with advancing age, I explored a possible supportive effect of 4,4'-Dimethoxychalcone on the ability to learn and form memories. The flies

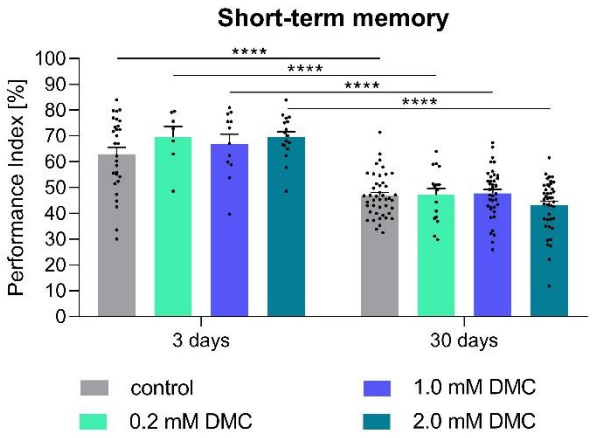

Figure 30: The short-term memory for 4,4'-Dimethoxychalcone fed animals decreases similarly to non-fed.

Aversive olfactory short-term memory (tested 3 min after training) for 3-day versus 30-day old w^{1118} flies fed with 0.2 mM, 1.0 mM, or 2.0 mM DMC in comparison to the control 0.1 % DMSO. 3 days: n = 29 for control, n = 7 for 0.2 mM DMC, n = 12 for 1.0 mM DMC, n = 17 for 2.0 mM DMC. 30 days: n = 44 for control, n = 16 for 0.2 mM DMC, n = 39 for 1.0 mM DMC, n = 42 for 2.0 mM DMC. Statistics: two-way ANOVA with Sidak's *post hoc* test, ****$p < 0.0001$, $^{ns}p \geq 0.05$. Error bars: mean ± SEM.

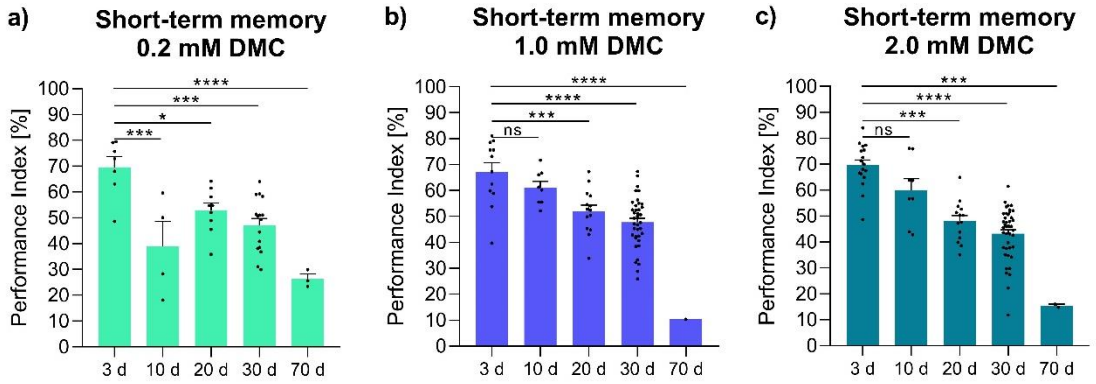

Figure 31: Gradual decrease of memory with advancing the age.

Aversive olfactory short-term memory of w^{1118} flies (tested 3 min after training) for different 4,4'-Dimethoxychalcone concentrations at 3, 10, 20, 30, and 70 days. 0.2 mM DMC: n = 7 for 3 d, n = 4 for 10 d, n = 9 for 20 d, n = 16 for 30 d, n = 3 for 70 d. 1.0 mM DMC: n = 12 for 3 d, n = 8 for 10 days, n = 14 for 20 d, n = 39 for 30 d, n = 1 for 70 d. 2 mM DMC: n = 17 for 3 d, n = 8 for 10 d, n = 14 for 20 d, n = 42 for 30 d, n = 2 for 70 d. Statistics: ordinary one-way ANOVA with Sidak's *post hoc* test for 0.2 mM and 1.0 mM DMC, Kruskal-Wallis with Dunn's *post hoc* test for 2.0 mM DMC, ****$p < 0.0001$, ***$p < 0.001$, *$p < 0.05$, $^{ns}p \geq 0.05$. Error bars: mean ± SEM.

developed on normal food and were fed with different DMC concentrations or 0.1% DMSO as control after eclosion.

Short-term memory of w^{1118} animals showed no beneficial impact in the concentrations of 0.2 mM, 1.0 mM, and 2.0 mM DMC compared to the control 0.1 % DMSO, neither for three days nor 30 days (Figure 30). A highly significant decrease in memory performance was visible for all food compositions with age. For each DMC concentration, the memory performance dropped with advancing age (Figure 31). The retention gradually decreased from three days over ten and 20 days to 30. With 70 days, the memory performance was at circa 10 %. Only for 0.2 mM, a drop occurred within ten days, which would intercept with more values (Figure 31a). At 20 days, the results stabilize at a higher level. On the contrary, no significant decrease appeared between three and ten days for 1.0 and 2.0 mM DMC. The memory performance falls from age 20 days significantly for all three concentrations (Figure 31).

Additionally, I examined the short-term memory of the control food in the DMC tests, 0.1 % DMSO, compared to normal food without any additives (Figure 32). The used control food performed similarly to normal food. Thus, 0.1 % DMSO had no additional influence on memory.

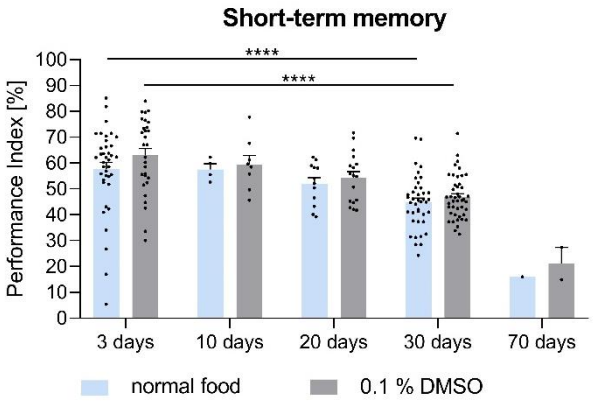

Figure 32: No short-term memory difference of the control food to normal food.

Aversive olfactory short-term memory of w^{1118} flies (tested 3 min after training) for the control food 0.1 % Dimethyl sulfoxide (DMSO) compared to normal food without any additive at 3, 10, 20, 30, and 70 days. Normal food: n = 38 for 3 d, n = 4 for 10 d, n = 12 for 20 d, n = 40 for 30 d, n = 1 for 70 d. 0.1 % DMSO: n = 29 for 3 d, n = 8 for 10 days, n = 17 for 20 d, n = 44 for 30 d, n = 2 for 70 d. Statistics: two-way ANOVA with Sidak's *post hoc* test, ****$p < 0.0001$, **$p < 0.01$, $^{ns}p \geq 0.05$. Error bars: mean ± SEM.

Even though DMC had significant benefits in extending lifespan, there was no protective effect on physical or mental health. An impact on agility was only transient at the age of 20 days (Figure 28, Figure 29). Furthermore, exploring DMC-treated flies' cognitive conditions revealed no protection from age-induced memory impairment (Figure 30). Additionally, memory tests for mid-term or long-term memory could be conducted. However, DMC possibly can not pass the blood-brain barrier due to its structure (Figure 23). Despite its lipophilic character, DMC did not seem to affect the central nervous system, hence no memory benefit. Its size or active efflux transport could be the reason (Begley, 2004). Maybe the link to a vehicle, which reaches the brain, could solve that problem. Thus, further investigations of this scenario would reveal if DMC is a promising substance only to enhance lifespan or if mobility and memory performance benefits as well.

1.2. The remedy Spermidine is a powerful tool to explore potential candidates for anti-aging pathways

One potent substance, of which anti-aging effects were already proven in a growing body of publications, is Spermidine (Spd). This natural polyamine appears endogenous in various species like humans, mice, and *Drosophila* and decreases with age (Pucciarelli et al., 2012; Gupta et al., 2013). Dietary sources are, for example, wheat germs, aged cheese, mushrooms, or the Japanese nattō (Madeo et al., 2018). Spd could be shown to prolong lifespan in invertebrates and mammals (Eisenberg et al., 2009) and protect from age-induced memory impairment in fruit flies, mice, and humans (Gupta et al., 2013; Schroeder et al., 2021).
Thus, Spd can be used as a tool to detect unknown proteins and pathways against aging. Combined with a SILAC label (Stable Isotope Labelling of Amino Acids in Cell culture), several promising candidates were identified in a screen, which compared the protein turnover rate of untreated and Spd-fed flies (Bhukel, 2018). Hence, a higher turnover rate upon Spd treatment indicated increased degradation and synthesis of a number of proteins. Among these, I tested the memory of some identified candidates' overexpression (OE).

The presynaptic protein Synaptobrevin is a member of the SNARE (soluble N-ethylmaleimide-sensitive-factor attachment protein (SNAP) receptor) complex, which is involved in the fusion of synaptic vesicles with the presynaptic membrane (Bhattacharya et al., 2002; Böhme et al., 2021). Thus, it is taking part in the release of neurotransmitters. Synaptobrevin's mammalian orthologue is the vesicle-associated membrane protein (VAMP) (Böhme et al., 2021). This family of proteins is associated with neurological disorders, and a lack of these can cause diseases like spastic ataxia or congenital myasthenic syndrome (Nystuen et al., 2007; Salpietro et al., 2017).
Since Synaptobrevin showed an increased turnover upon Spd-treatment (Bhukel, 2018), I tested the short-term memory of a pan-neuronal overexpression of this protein (Figure 33). Interestingly, the neuronal Synaptobrevin demonstrated significantly better memory performance than its control at 20 days (Figure 33a). However, a drop with age was still visible (5 versus 20 days). The homolog of Synaptobrevin, Cellubrevin, is present in all cells and responsible for membrane trafficking (McMahon et al., 1993). In contrast to Synaptobrevin, a pan-neuronal overexpression of Cellubrevin could not rescue memory from age-induced memory impairment (Figure 33b). Thus, Synaptobrevin seems to affect mental aging in neuronal tissue. Newest findings even show that glial Synaptobrevin is involved in the myelination of neurons in the peripheral nervous system (Böhme et al., 2021).

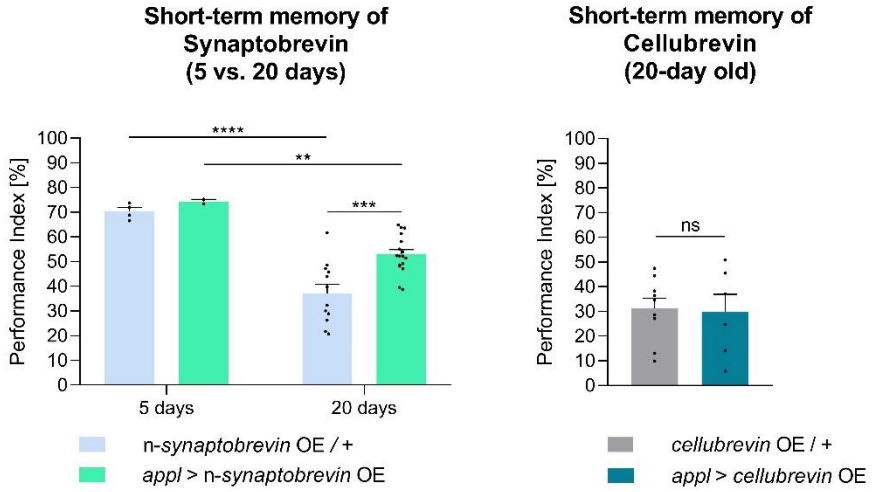

Figure 33: Aversive olfactory memory of the pan-neuronal lack of the SNARE protein Synaptobrevin.

Short-term memory (test 3 min after training) for the pan-neuronal overexpression (OE) of the presynaptic protein a) Synaptobrevin (neuronal; n-*syb*), and it's equivalent in all cells b) Cellubrevin. a) n = 4 for 5-day old and n = 12 for 20-day old n-*syb* OE / +, n = 2 for 5-day old and n = 17 for 20-day old *appl* > n-*syb* OE. b) n = 9 for 20-day old *cellubrevin* OE / +, n = 6 for 20-day old *appl* > *cellubrevin* OE. Statistics: unpaired t-test for 2 genotypes to analyze, for 2 groups two-way ANOVA with Sidak's *post hoc* test, ****$p < 0.0001$, ***$p < 0.001$, **$p < 0.01$, $^{ns}p \geq 0.05$. Error bars: mean ± SEM.

Another hit in the SILAC screen with an accelerated turnover rate was Unc-104 (in humans: KIF1A) (Bhukel, 2018). This protein is a member of the kinesin superfamily (KIFs), essential for intracellular transport (Miki et al., 2005). Unc-104 itself is involved in the axonal

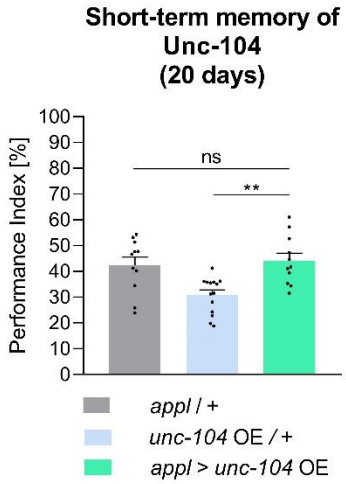

Figure 34: Aversive olfactory memory of the pan-neuronal lack of the anterograde transport protein Unc-104.

Short-term memory (test 3 min after training) for the pan-neuronal overexpression (OE) of Unc-104: n = 11 for *appl* / +, n = 14 for *unc-104* OE / +, n = 11 for *appl* > *unc-104* OE. Statistics: ordinary one-way ANOVA with Sidak's *post hoc* test, **$p < 0.01$, $^{ns}p \geq 0.05$. Error bars: mean ± SEM.

anterograde transport, which brings cargo like neurotransmitters or, for example, the autophagy protein Atg9 from the cell body to the synapse (Stavoe et al., 2016; Lim et al., 2017). Additionally, this motor protein is necessary for presynaptic maturation (Zhang et al., 2016). Short-term memory tests with a pan-neuronal overexpression of *unc-104* in 20-day old animals revealed no rescue from age-induced memory impairment (Figure 34). Even though the memory was significantly increased compared to the control *unc-104* OE / +, the driver control *appl* / + showed a similar performance index level as *appl* > *unc-104* OE. Thus, Unc-104 failed to be protective against age-induced memory impairment.

The mammalian autophagy receptor p62 (in *Drosophila*: Ref(2)p) binds ubiquitinated residues of proteins to label them for autophagosomal degradation (Bento et al., 2016). Indeed, the short-term memory performance of the pan-neuronal overexpression of p62/Ref(2)p was slightly better than control animals at 20 days, though with no statistical significance (Figure 35a). The decay with age was still visible with a probability value of $p = 0.0690$, yet insignificant. Oddly, the control *p62/Ref(2)p* OE / + showed no drop with age. The memory of 5-day old flies was probably already too low so a further decrease did not appear with age.

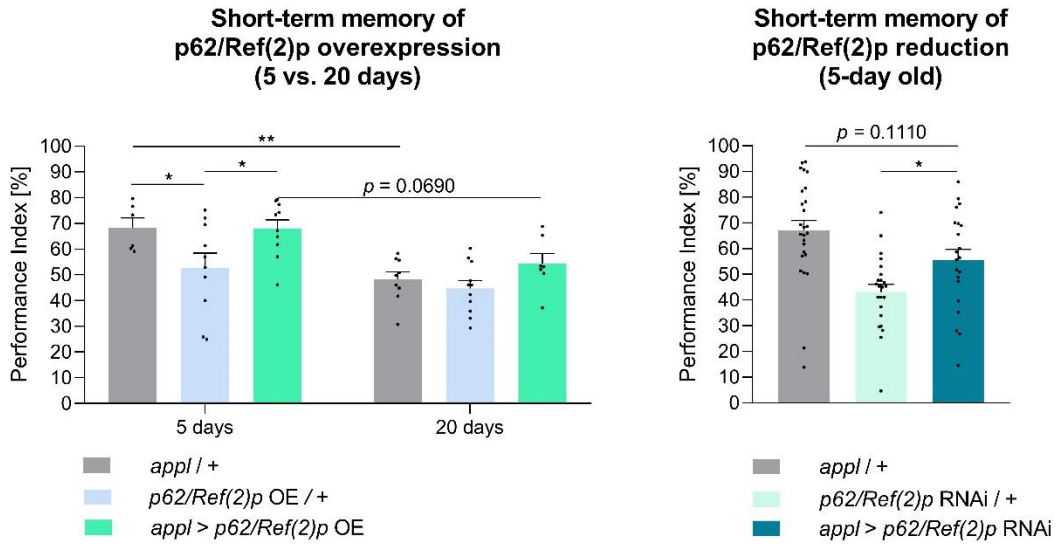

Figure 35: Aversive olfactory memory of the pan-neuronal lack of the autophagy receptor p62/Ref(2)p.

Short-term memory (test 3 min after training) for pan-neuronal p62/Ref(2)p. a) *p62/Ref(2)p* overexpression (OE) for 5- and 20-day old animals: n = 6 for 5-day old and n = 9 for 20-day old *appl* / +, n = 10 for 5-day old and n = 11 for 20-day old *p62/Ref(2)*p OE / +, n = 10 for 5-day old and n = 7 for 20-day old *appl* > *p62/Ref(2)p* OE. b) Reduced *p62/Ref(2)p* in 5-day old animals: n = 26 for *appl* / +, n = 23 for *p62/Ref(2)p* RNAi / +, n = 21 for *appl* > *p62/Ref(2)p* RNAi. Statistics: Kruskal-Wallis with Dunn's *post* hoc test for the 3 genotypes to analyze, for 2 ages of 3 genotypes two-way ANOVA with Sidak's *post hoc* test, $^{**}p < 0.01$, $^{*}p < 0.05$, $^{ns}p \geq 0.05$. Error bars: mean ± SEM.

The protein turnover rate of p62 increased in Spd-fed flies (Bhukel, 2018). In contrast, accumulations of p62 aggregates were connected to deficient autophagy and neuronal aging in several publications (Bartlett et al., 2011; Bhukel and Beuschel et al., 2019). Additionally, they are associated with human diseases such as Alzheimer's, Parkinson's, or amyotrophic lateral sclerosis (Bartlett et al., 2011; Menzies et al., 2017; Liang and Sigrist, 2018). Thus, I tested a pan-neuronal reduction of p62/Ref(2)p via RNAi (Figure 35b). The short-term memory of 5-day old appl > p62/Ref(2)p RNAi learned significantly better than its RNAi control. In contrast, they showed a slightly reduced performance than its driver control, yet not substantially. Obviously, less p2/Ref(2)p also did not tip the scales.

However, proteins with a significantly decreased metabolic turnover rate upon Spd treatment indicated a reduced degradation and a slowed synthesis. Here, I tested the pan-neuronal reduction of the candidate Tomosyn via RNAi (Bhukel, 2018). This protein (in humans: syntaxin binding protein 5, STXBP5) is a negative regulator of the SNARE complex, which Synaptobrevin, Syntaxin, and SNAP-25 are part of (Li et al., 2018). Within the exocytosis, Tomosyn is capturing Syntaxin-1, followed by a block of vesicle priming, thus the synaptic transmission (Ashery et al., 2009). Consequently, less amount of this protein could support synaptic plasticity. Indeed, a pan-neuronal reduction revealed a significant benefit compared to the RNAi control and a trend towards better performance than the driver control in 20-day old animals. Interestingly, Chen et al. published in 2011 that the short-term memory of pan-neuronal reduction in Tomosyn was equal to its controls in young flies. They observed a 50 % drop in the late memory (3 hours mid-term memory), more precisely, in the anesthesia-sensitive memory. This component of longer-lasting retention is labile with age (Tamura et al., 2003). Since I observed potential protection of age-induced memory decline in 20-day old pan-neuronal Tomosyn deficient animals, further investigation of aging animals in late memory could be interesting.

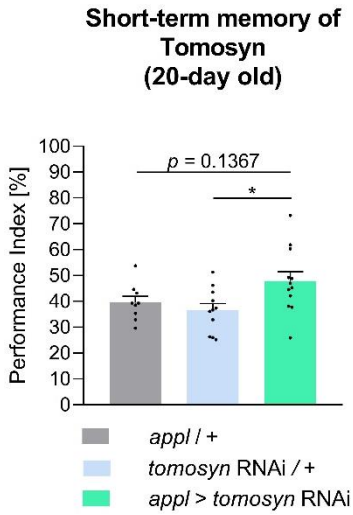

Figure 36: Aversive olfactory memory of the pan-neuronal lack of Tomosyn.

Short-term memory (test 3 min after training) for the pan-neuronal reduced Tomosyn in 20-day old flies: n = 9 for *appl* / +, n = for *tomosyn* RNAi / +, n = 12 for *appl* > *tomosyn* RNAi. Statistics: ordinary one-way ANOVA with Sidak's *post hoc* test, $*p < 0.05$, $^{ns}p \geq 0.05$. Error bars: mean ± SEM.

2. Approaches to combat aging - Mediation of effects

To discover further potent therapeutics, basic research is irreplaceable. Several hallmarks of aging have been revealed (see chapter I.1, Figure 1; López-Otín et al., 2013), yet the impact of these pathways and involved proteins on cognitive decline often remains in the dark. Operating neuronal maintenance and homeostasis promote flexible learning and memory as an adaptation to the environment (Kandel et al., 2014; Liang and Sigrist, 2018). Here, the cleaning systems of the body work as the housekeeper of the cells (Levine and Kroemer, 2008). Thus, recycling at the synapses, microautophagy, chaperone-mediated autophagy, or macroautophagy ensures the balance between synthesis and degradation to maintain cellular homeostasis (Yin et al., 2016). The following chapters shall enlighten some junctions in the context of age-induced memory impairment.

2.1. Spermidine protects from age-induced memory impairment via hypusination

One powerful remedy in the fight against aging is Spermidine (Spd). I worked on this naturally occurring substance already on a screen to reveal further unknown proteins and pathways involved in the aging memory process (see chapter III.1.2).

Spd is an endogenous polyamine in flies, mice, and humans, and its levels in the body decrease with age (Pucciarelli et al., 2012; Gupta et al., 2013). Relatively high Spd amounts in food can be found in wheat germs or the Japanese nattō (Madeo et al., 2018). Spd supplementation itself can counteract age-induced memory impairment and physical degeneration due to aging in flies, mice, and humans (see Figure 37; Gupta et al., 2013; Madeo et al., 2018; Schroeder et al., 2021). Additionally, it possesses pleiotropic effects: antioxidant and anti-inflammatory skills, protecting mitochondrial functionality, proteostasis, homeostasis, and promoting autophagic clearance (Liang and Sigrist, 2018; Madeo et al., 2018).

During aging, nerves lose their flexible neuroplasticity, neuronal homeostasis, and operating network activity (Liang and Sigrist, 2018; Mattson and Arumugam, 2018). This starts already in the connections of the nerves, the synapses. Gupta et al. found in 2016 that Spd protects from an age-induced severe increase of main components of the presynaptic active zone, such as Bruchpilot, followed by relief from an overloading system towards a functional state. Thus, the generation of memories recovered (Gupta et al., 2016).

However, several operating principles of the polyamine Spd can be announced, yet not all aspects can be explained.

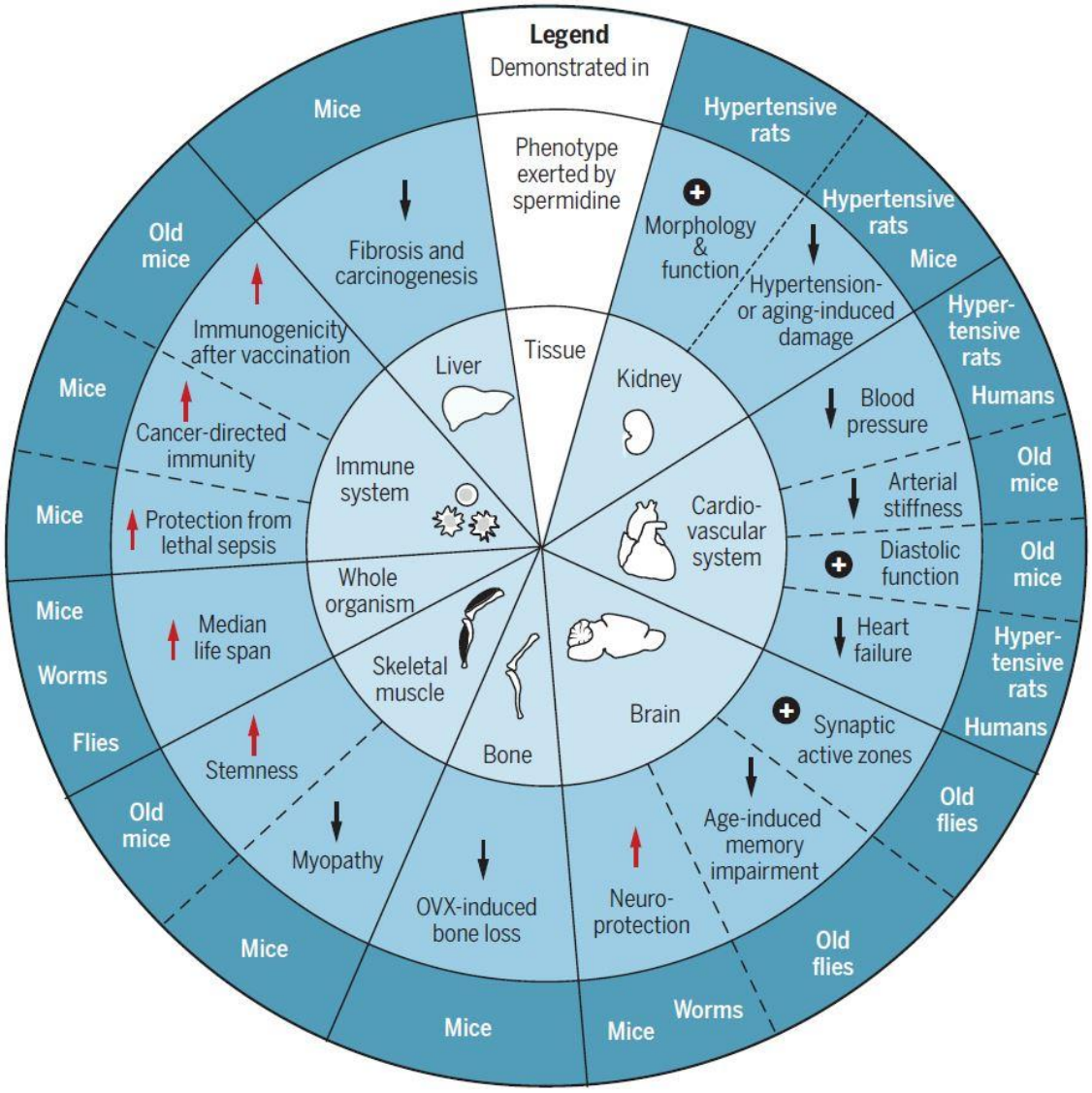

Figure 37: Beneficial effects of Spermidine on different tissues.

Spermidine supplementation reveals several positive processes on tissues, which suffer from aging, like the brain, the cardiovascular system, or the immune system. These protective effects of Spermidine seem to be conserved over various species. Image taken from Madeo et al., 2018.

In this chapter, I focused on the mechanism of hypusination and its importance in age-induced memory impairment. Spermidine gives its amino-butyl residue as a co-factor for this unique pathway, conserved over different species (Hofer et al., 2021; Schroeder et al., 2021). Here, the eukaryotic translation initiation factor 5A (eIF5A) becomes reversibly deoxyhypusinated via the deoxyhypusine synthase (DHS in mammals; CG8005 in *Drosophila*) at its lysine chain (see Figure 38; Liang et al., 2021). In the second step of the hypusination, the deoxyhypusine hydroxylase (DHHO in mammals; nero in *Drosophila*) hydroxylases eIF5A to its activated form

with a hypusine chain. Subsequently, the hypusinated eIF5A boosts autophagy and mitochondrial function (Hofer et al., 2021). Besides others, these lose their competence with age (Liang and Sigrist, 2018). Interestingly, the amount of Sperminide also decreases with time, and the same happens to the hypusination mechanism (Gupta et al., 2013; Liang et al., 2021).

I attenuated the rate-limiting first hypusination step with a loss-of-function allele of *CG8005* in

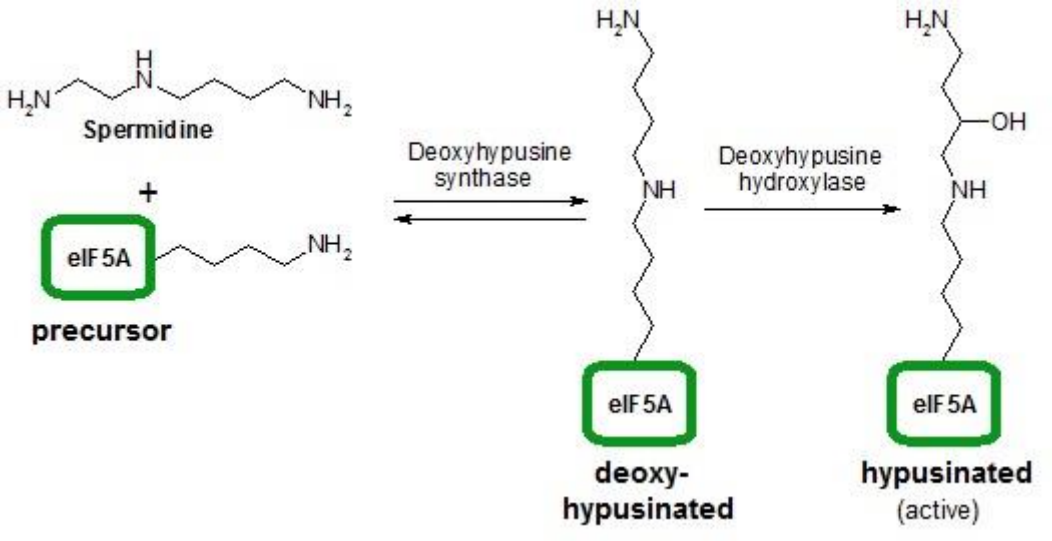

Figure 38: Spermidine gives as the co-factor for the hypusination of the translation initiation factor eIF5A.

Spermidine spends its amino-butyl residue to the lysine chain of eIF5A. Here, the deoxyhypusine synthase (DHS in mammals; CG8005 in Drosophila) catalyzes the build of deoxyhypusinated eIF5A in a reversible way in the first step of hypusination. With the second unreversible step, eIF5a becomes its hypusinated active form via the deoxyhypusine hydroxylase (DHHO in mammals; nero in Drosophila) (Liang et al., 2021).

Drosophila (Templin et al., 2011; Liang et al., 2021). A homozygous lack of this highly conserved enzyme led to lethality in the larval state (Liang et al., 2021). In contrast, the heterozygous animals *CG8005* / + reached adulthood yet showed a reduced amount of hypusine in the brain at 5 days already. Aversive olfactory memory tests revealed a significantly impaired memory performance for short-term memory (Figure 39a) and decreased learning for 3 hours mid-term memory (Figure 39c). An Spd supplementation had no effect in 5-day old flies. Intriguingly, 30-day old *CG8005* / + animals still showed a worse short-term memory than the wild-type w^{1118}, and contrary to controls, a supplementation of Spd could not improve the performance (Figure 39b). Similarly, dietary Spd had beneficial effects

on 30-day old w^{1118} flies in 3 hours mid-term memory, while the hypusination impaired animals experienced no protection (Figure 39d). Other positive Spd effects on age, like an increased hypusination level, enhanced locomotion, or an improved lifespan, also failed to appear in these animals (Liang et al., 2021).

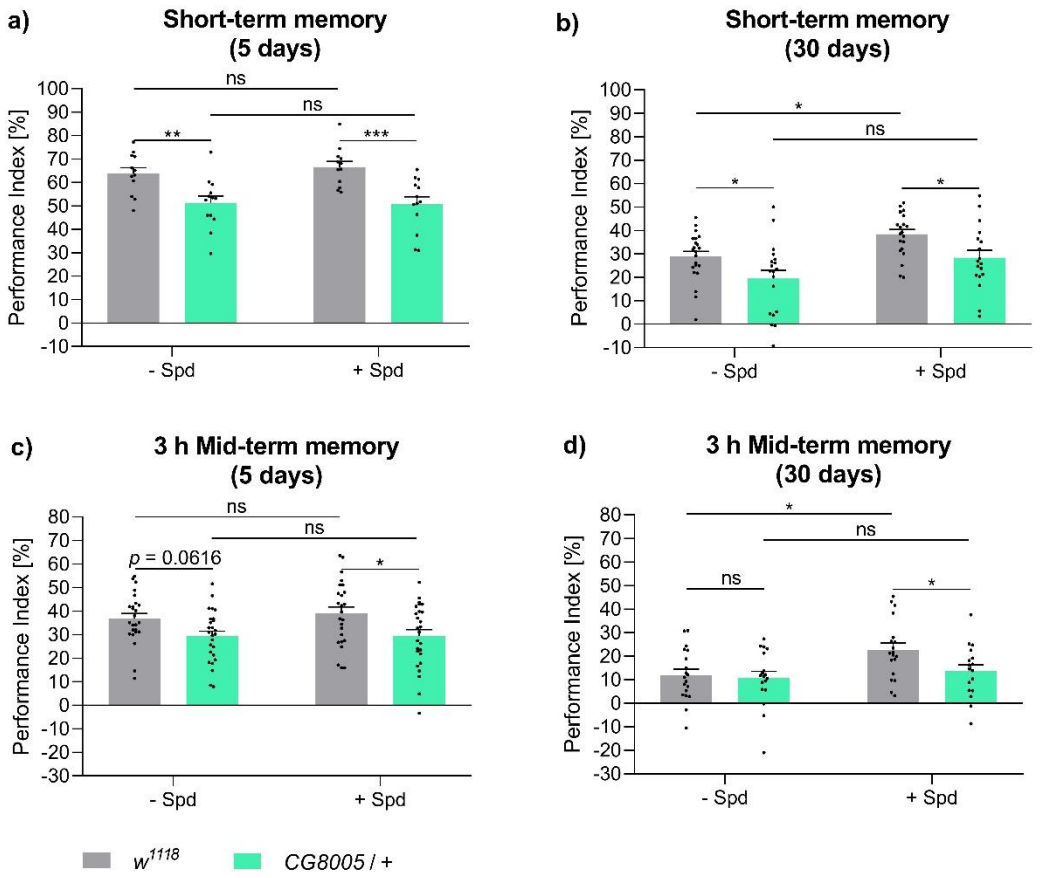

Figure 39: Heterozygous loss-of-function in the first and rate-limiting hypusination step impairs the memory performance of young flies and inhibits a beneficial effect of Spermidine at a higher age.

Aversive olfactory memory of *CG8005* / + compared to w^{1118} as control. a) Short-term memory (test 3 min after training) for 5-day old flies: n = 12 for w^{1118} and n = 13 for *CG8005* / + without Spd supplementation, n = 12 for w^{1118} and n = 13 for *CG8005* / + with Spd supplementation. b) Short-term memory (test 3 min after training) for 30-day old flies: n = 22 for w^{1118} and n = 19 for *CG8005* / + without Spd supplementation, n = 21 for w^{1118} and n = 18 for *CG8005* / + with Spd supplementation. c) 3 hours mid-term memory (test 3 hours after training) for 5-day old flies: n = 25 for w^{1118} and n = 26 for *CG8005* / + without Spd supplementation, n = 25 for w^{1118} and n = 26 for *CG8005* / + with Spd supplementation. d) 3 hours mid-term memory (test 3 hours after training) for 30-day old flies: n = 19 for w^{1118} and n = 18 for *CG8005* / + without Spd supplementation, n = 19 for w^{1118} and n = 17 for *CG8005* / + with Spd supplementation. Statistics: two-way ANOVA with Sidak's *post hoc* test, ***p < 0.001, **p < 0.01, *p < 0.05, $^{ns}p \geq 0.05$. Error bars: mean ± SEM.

Additionally, I tested the effects of pan-neuronally diminished activity of the deoxyhypusine synthase (*elaV(X)* > *CG8005* RNAi; Liang et al., 2021). These animals showed a significant decrease in short-term memory compared to both controls (Figure 40a). Immunostainings of brains revealed a reduced hypusine level (Figure 40b, Liang et al., 2021). However, the mushroom body, the higher integration center for learning in the *Drosophila* brain, where learning and memory storage happens (Aso et al., 2014), showed developmental malformations in these flies (Liang, 2019). Thus, a functional hypusination in the neurons seems to be irreplaceable.

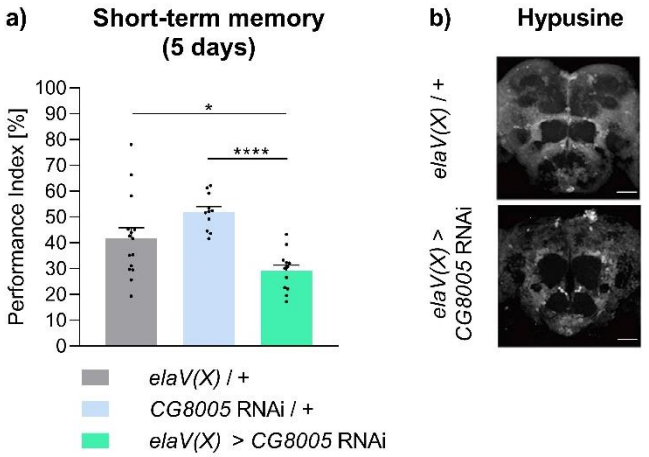

Figure 40: Pan-neuronal diminished CG8005 entails a reduced memory plus a lower hypusine level in the brain.

a) Short-term memory (test 3 min after training) for 5-day old pan-neuronal reduced CG8005 and its controls: n = 15 for *elaV(X)* / +, n = 11 for *CG8005* RNAi / +, n = 12 for *elaV(X)* > *CG8005* RNAi. Statistics: ordinary one-way ANOVA with Sidak's *post hoc* test, ****p < 0.0001, *p < 0.05. Error bars: mean ± SEM. b) Immunostainings for hypusine showed a reduced intensity in brains of 5-day old *elaV(X)* > *CG8005* RNAi animals compared to the control *elaV(X)* / +, scale bar: 50 µm. Immunostainings by Chengji Piao from Liang et al., 2021.

In summary, Spd proved to be a limiting factor in hypusination, which is important for memory formation and the effects of Spd on older animals. Thus, Spd supplementation shows protective effects against aging, partially based on increased hypusination levels.

The innate smell scores for *CG8005* deficiencies showed comparable performance indices to their controls (Table 3). Both odor acuities for 3-Octanol and 4-Methylcyclohexanol were insignificant. Thus, the preconditions for generating memory are present.

	Olfactory acuity	
Genotype	3-Octanol (n)	4-Methylcyclohexanol (n)
w^{1118}, - Spd, 5 days	28.89 ± 4.754 (11)	41.46 ± 5.885 (14)
CG8005 / +, - Spd, 5 days	18.70 ± 4.751 (11)	49.73 ± 7.955 (12)
w^{1118}, + Spd, 5 days	26.44 ± 5.417 (11)	53.05 ± 5.793 (13)
CG8005 / +, + Spd, 5 days	31.28 ± 4.123 (11)	48.67 ± 5.068 (16)
w^{1118}, - Spd, 30 days	41.44 ± 4.111 (14)	59.36 ± 5.680 (22)
CG8005 / +, - Spd, 30 days	34.59 ± 3.465 (14)	66.10 ± 4.586 (23)
w^{1118}, + Spd, 30 days	32.81 ± 3.621 (14)	55.00 ± 5.229 (22)
CG8005 / +, + Spd, 30 days	33.67 ± 2.623 (12)	57.28 ± 4.449 (22)

Table 3: Innate behavior of *CG8005* / +.

As tests for innate behavior, olfactory acuity gave no significant difference for the experimental groups. Statistics: two-way ANOVA with Sidak's *post hoc* test, $^{ns}p \geq 0.05$. Mean ± SEM.

2.2. Recycling at the synapse

Synapses are important institutions in the neuronal network since, based on their dynamics, the neurons can convey information through the whole body and the brain (Liang and Sigrist, 2018). Such a structure needs an operating cleaning system.

The GTPase activating protein (GAP) Skywalker supports the transport of synaptic vesicles to the endosome (Uytterhoeven et al., 2011). It regulates the GTPase activity of Rab35, which in turn controls the synaptic versicle cycling (Fernandes et al., 2014). Skywalker mutation leads to an uncontrolled movement of the synaptic vesicles to the endosomes, which induces disturbed protein turnover and enhanced neurotransmitter release (Uytterhoeven et al., 2011; Fischer et al., 2016). In humans, the ortholog to Skywalker is TBC1D24, which mutation is associated with epilepsy and the DOORS syndrome (deafness, onychodystrophy, osteodystrophy, mental retardation, seizures; Fischer et al., 2016).

The pan-neuronal overexpression (OE) of Skywalker already performed significantly better than its control at 5 days (Figure 41a). This increase persisted with even a higher difference at 20 days. Curiously, neither the control nor the pan-neuronal *skywalker* overexpression showed decay in memory. Though, the performance of the control was already low, with 53 % for 5-day short-term memory. Hence, more Skywalker in the neurons could protect from age-

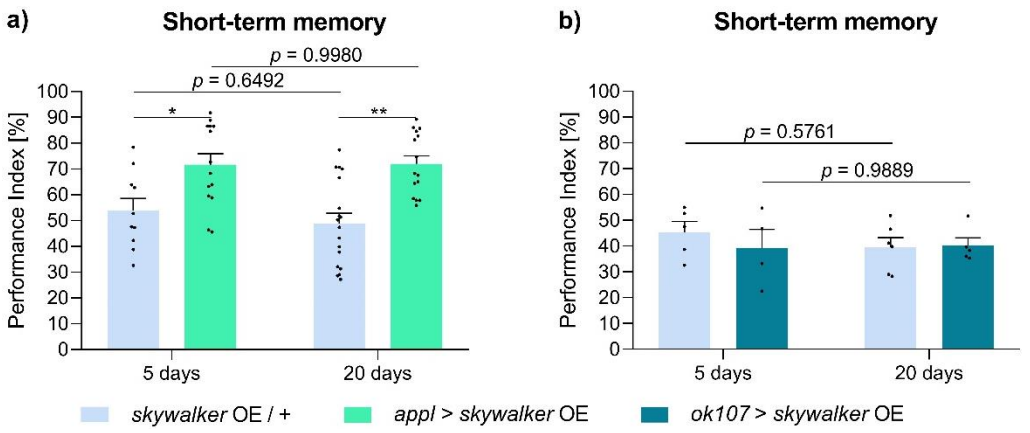

Figure 41: A pan-neuronal *skywalker* overexpression boosts aversive olfactory memory.

Short-term memory (test 3 min after training) of *skywalker* overexpression (OE) at 5 and 20 days. a) Pan-neuronal overexpression shows increased memory: n = 10 for 5-day old and n = 18 for 20-day old *skywalker* OE / +, n = 14 for 5-day old and n = 15 for 20-day old *appl* > *skywalker* OE. b) Overexpression in the mushroom body gives no memory benefit: n = 5 for 5-day old and n = 6 for 20-day old *skywalker* OE / +, n = 4 for 5-day old and n = 5 for 20-day old *ok107* > *skywalker* OE. Statistics: two-way ANOVA with Sidak's *post hoc* test, *p < 0.05, ^{ns}p ≥ 0.05. Error bars: mean ± SEM.

induced memory impairment. Next, I tested the effect on the mushroom body, the principal center of learning in the fly brain. In contrast to the pan-neuronal expression, no benefit appeared compared to the control, neither at 5 nor 20 days (Figure 41b).

In the end, the Skywalker recycling system at the synapses seems to be a promising mechanism of action for further investigations, since its pan-neuronal overexpression provided a boost in short-term memory.

2.3. Chaperone-mediated autophagy and endosomal microautophagy

The central recycling system in the body is autophagy, which is essential for neuronal homeostasis and retention (Liang and Sigrist, 2018). Additionally, it is a key regulator to combat aging. In this chapter, I focused on chaperon-mediated autophagy, which occurs in the cytosol. Here, the heat shock protein family A member 8 (Hspa8, in mammals) recognizes individual proteins with the KFERQ motif and delivers them to the lysosome-associated membrane protein 2A (LAMP-2A), which binds the cargo (Mukherjee et al., 2016). Subsequently, the substrate unfolds to cross the lysosomal membrane for its degradation (Singh and Cuervo, 2011).
In *Drosophila*, six orthologs of the mammalian Hspa8, the heat shock cognate 70 (Hsc70) protein family, exist, whereby Hsc70-4 owns the highest similarity to the human Hspa8 (Mukherjee et al., 2016). Additionally to the activity in chaperon-mediated autophagy, Hsc70-4 facilitates endosomal microautophagy, where the KFERQ motif also serves as a marker for protein embedding within endosomal membrane (Uytterhoeven et al., 2015). This endosomal microautophagy via Hsc70-4 supports protein turnover, for example, at the synapse (Uytterhoeven et al., 2015).

First, I tested the effects of a pan-neuronal overexpressed chaperone-mediated autophagy with the wild-type Hsc70-4 (*appl > hsc70-4^{wt}* OE) on age-induced memory impairment (Figure 42a). Here, endosomal microautophagy became also enhanced. This neuronal boost could not prevent a memory decline with age, similar to the tested controls. In contrast, an increase of HSC70-4^{wt} in the mushroom body, the center of learning and memory storage, showed slightly reduced memory in young flies (5 days) and a milder memory drop with age than in the control (Figure 42b). Though, this benefit of *ok107 > hsc704^{wt}* OE could be illusive since these flies already suffered in their memory performance at 5 days, and a driver control is missing here.
Additionally, I tested a pan-neuronal overexpression (OE) of a *hsc70-4* mutant, which only promoted endosomal microautophagy (Figure 43). The short-term memory of *appl > hsc70-4^{D10N}* OE presented a reduced memory decay compared to its controls. Thus, a slight benefit with age could be possible, yet the driver control *appl* / + was on the same performance level. Taken together, neither augmented chaperone-mediated autophagy nor increased endosomal microautophagy could protect from age-induced memory impairment. Certainly, Hsc70-4 promotes protein turnover and regulates quality control at the synapses, yet this boost seemed not enough to counteract a cognitive decline with age (Uytterhoeven et al., 2015; Liang and Sigrist, 2018).

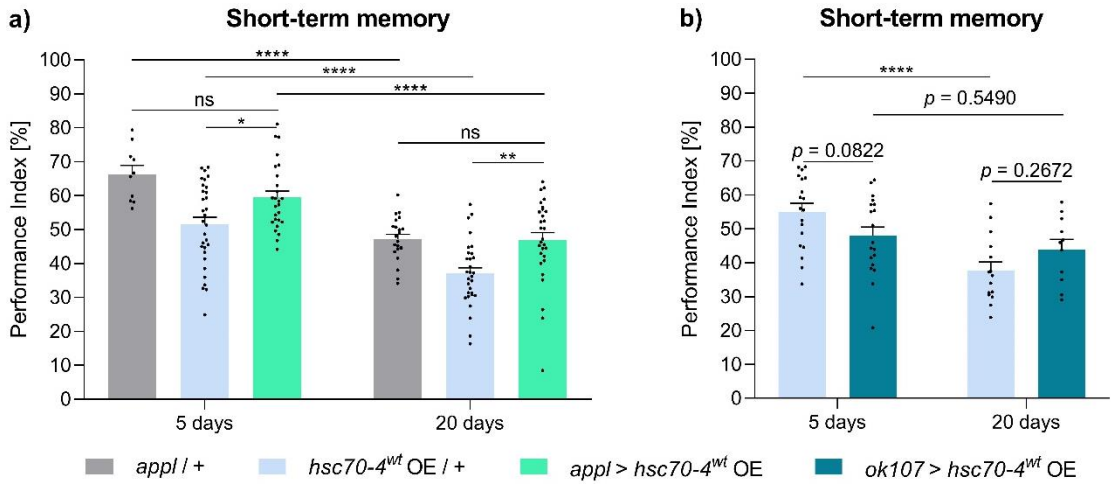

Figure 42: Memory of boosted chaperone-mediated autophagy and endosomal microautophagy via hsc70-4.

Short-term memory (test 3 min after training) for wild-type Hsc70-4 at 5 and 20 days. a) Pan-neuronal overexpression (OE) promotes no memory benefits: n = 10 for 5-day and n = 22 for 20-day old appl / +, n = 31 for 5-day and n = 30 for 20-day old hsc70-4wt OE / +, n = 26 for 5-day and n = 29 for 20-day old appl > hsc70-4wt OE. b) Overexpression in the mushroom body: n = 19 for 5-day and n = 15 for 20-day old hsc70-4wt OE / +, n = 19 for 5-day and n = 11 for 20-day old ok107 > hsc70-4wt OE. Statistics: two-way ANOVA with Sidak's post hoc test, ****p < 0.0001, ***p < 0.001, **p < 0.01, *p < 0.05, nsp ≥ 0.05. Error bars: mean ± SEM.

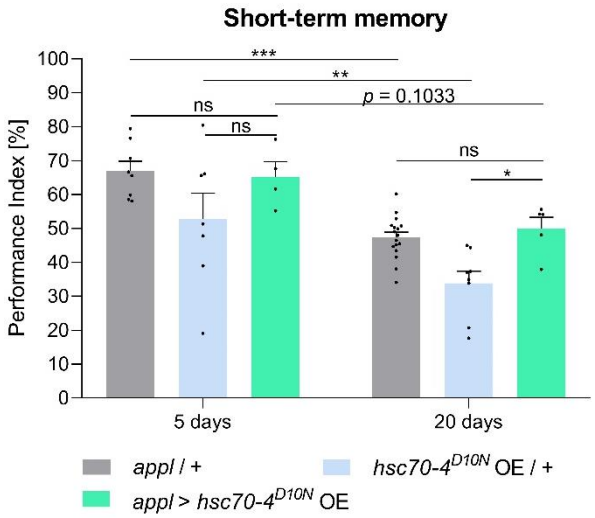

Figure 43: Memory of pan-neuronal overexpressed endosomal microautophagy.

Short-term memory for the pan-neuronal overexpression (OE) of Hsc70-4^{D10N}: n = 8 for 5-day and n = 17 for 20-day old *appl* / +, n = 7 for 5-day and n = 8 for 20-day old *hsc70-4^{D10N}* OE / +, n = 4 for 5-day and n = 5 for 20-day old *appl* > *hsc70-4^{D10N}* OE. Statistics: two-way ANOVA with Sidak's *post hoc*, ***p < 0.001,**p < 0.01, *p < 0.05, ^{ns}p ≥ 0.05. Error bars: mean ± SEM.

2.4. Macroautophagy influences the ability to learn and form memories

With the Hsc70-4 overexpression, we already had an impression of chaperone-mediated autophagy and endosomal microautophagy on learning and memory. In the following part, I will concentrate on another type of autophagy, the macroautophagy. Here, proteins and organelles, meant for degradation, are absorbed by multi-membrane vesicles, named autophagosomes, and transported to lysosomes for digestion (Bento et al., 2016; Bhukel and Beuschel et al., 2019). This process is regulated by a cascade of autophagy-related (Atg) proteins (Menzies et al., 2017). In this chapter, I will show the effects on memory of genetically compromised macroautophagy in the nervous system of *Drosophila melanogaster*. I used RNA interference (RNAi) to downregulate two independent core components in this degradation machinery, *atg5* and *atg9*, to provoke a state of senescence at young age (Bhukel and Beuschel et al., 2019).

2.4.1. Modification at the level of autophagosome elongation within macroautophagy

The assembling and elongation of an autophagosome is an essential step in the macroautophagy machinery (Bento et al., 2016). Thus, Atg8 lipidation via the ubiquitin-protein ligase (E3) like complex, built of Atg5 together with Atg12 and Atg16, is essential during autophagosome formation (Hanada et al., 2007; Gelino and Hansen, 2012; Bento et al., 2016; Gui et al., 2019). In the following chapter, I show, focusing on aversive olfactory memory, the consequences of an early impairment in the macroautophagy pathway by an *atg5* knockdown in diverse neuronal tissues.

2.4.1.a Pan-neuronal *atg5* knockdown affects the ability to form memory at young age already

In the paper Bhukel and Beuschel et al., 2019, we used immunolabelling of the autophagy receptor p62 (also named sequestome 1; *Drosophila*'s homolog: Ref(2)p) as a read-out for autophagic inefficiency. p62 binds ubiquitinated residues of proteins to label them for degradation (Bento et al., 2016). The lipidated, activated Atg8 binds p62/Ref(2)p to encourage the engulfment by the autophagosome (Pankiv et al., 2007; Gelino and Hansen, 2012). Hence,

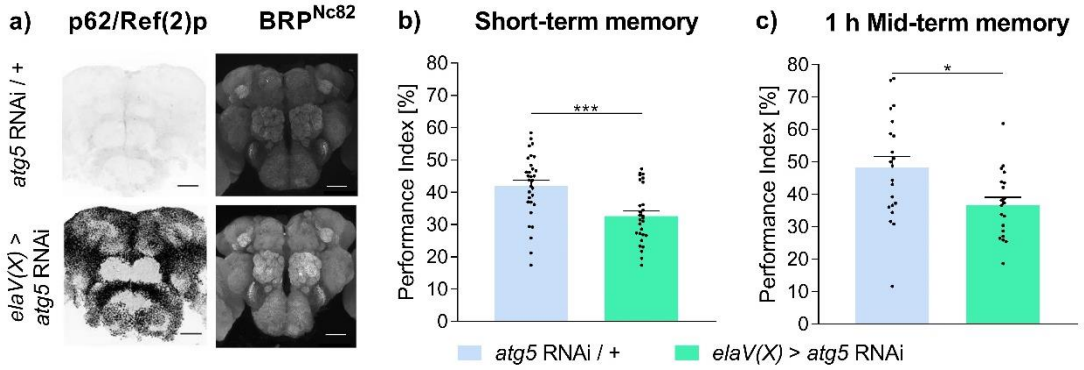

Figure 44: Pan-neuronal knockdown of *atg5* reduces short-term and mid-term memory at young age already.

a) Immunostainings for p62/Ref(2)p (indicator for deficient macroautophagy) and Bruchpilot (BRP^{Nc82}; marker for synaptic plasticity) showed increased intensities in brains of 10-day old *elaV(X)* > *atg5* RNAi animals compared to the control *atg5* RNAi / +, scale bar: 50 µm. b-c) Aversive olfactory memory declined for 10-day old flies of *elaV(X)* > *atg5* RNAi compared to the control *atg5* RNAi / +. b) Performance Index for short-term memory (test 3 min after training): n = 31 for *atg5* RNAi / +, n = 28 for *elaV(X)* > *atg5* RNAi. c) Performance Index for 1 hour mid-term memory (test 1 hour after training): n = 21 for *atg5* RNAi / +, n = 20 for *elaV(X)* > *atg5* RNAi. Statistics: unpaired t-test, ****p* < 0.001, **p* < 0.05. Error bars: mean ± SEM. Immunostainings by Anuradha Bhukel from Bhukel and Beuschel et al., 2019.

deficient macroautophagy is accompanied by an accumulation of p62 aggregates (Bjørkøy et al., 2009; Bartlett et al., 2011; Mauvezin et al., 2014). Accordingly, when we knocked down *atg5* pan-neuronal (*elaV(X)*-Gal4) via RNAi, we could observe a dramatic increase of p62/Ref(2) in the brain of 10-day old flies (Figure 44a; Bhukel and Beuschel et al., 2019). Interestingly, this accumulation of p62/Ref(2)p as a sign of lacking macroautophagy is usually associated with the age of 30 days (Gupta et al., 2013). Additionally, a brain-wide increase of the presynaptic active zone (AZ) occurs with rising age measurable via immunolabelling of the AZ scaffold protein Bruchpilot (Gupta et al., 2016). Intriguingly, a pan-neuronal *atg5* knockdown triggered presynaptic plasticity brain-wide in already 10-day old animals (Figure 44a; Bhukel and Beuschel et al., 2019). When I tested these flies for their aversive olfactory memory performance, I could measure severe deficits (Figure 44b-c). With the loss of Atg5 in the nerves, a severe reduction in short-term memory, tested immediately after the memory training, was visible (Figure 44b). Furthermore, I found a decline in the longer-lasting 1 hour mid-term memory, where the test is conducted 1 hour after the drill (Figure 44c).

Next, I wanted to compare deficient macroautophagy directly to senescence. With increasing age, bodily functions gradually decrease, and the ability to form memories is no exception

(Tamura et al., 2003; Gupta et al., 2013). Indeed, the macroautophagy system also becomes less functional with time (Gupta et al., 2013; Stavoe et al., 2019). Thus, a comparison of wild-type like *atg5* RNAi / + flies at ten days versus 30 days revealed severe accumulations of p62/Ref(2)p aggregates in immunostainings of old brains (Figure 45a.). Additionally, presynaptic plasticity, visible as increasing intensity of Bruchpilot (BRP^{Nc82}), could be observed

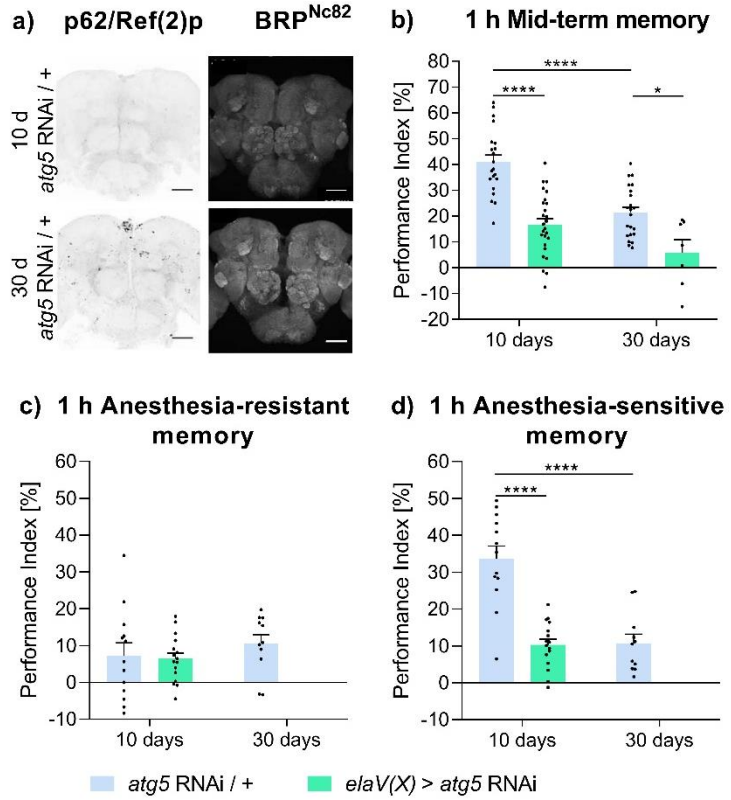

Figure 45: Anesthesia-sensitive memory of young pan-neuronal *atg5* knockdown animals drops to a similar low level as aged control flies.

a) Immunostainings for p62/Ref(2)p (indicator for deficient macroautophagy) and Bruchpilot (BRP^{Nc82}; marker for synaptic plasticity) showed increased intensities in brains of 30-day old wild-typic *atg5* RNAi / + compared to 10-day young flies, scale bar: 50 µm. b-d) Aversive olfactory memory for 10- and 30-day old flies of *atg5* RNAi / + and *elaV(X)* > *atg5* RNAi. b) Performance Index for 1 hour mid-term memory (test 1 hour after training): n = 21 for 10-day old and n = 22 for 30-day old *atg5* RNAi / +, n = 26 for 10-day old and n = 7 for 30-day old *elaV(X)* > *atg5* RNAi. c) Performance Index for 1-hour anesthesia-resistant memory (ice-bad 30 min and test 1 hour after training): n = 13 for 10-day old and n = 16 for 30-day old *atg5* RNAi / +. n = 11 for 10-day old *elaV(X)* > *atg5* RNAi. d) Performance Index for 1 hour anesthesia-sensitive memory: Results received via calculation of the median of 1 hour mid-term memory minus the individual performance indices of 1 hour anesthesia-resistant memory. Statistics: two-way ANOVA with Sidak's *post hoc* test to compare two groups and ordinary one-way ANOVA with Tukey's *post hoc* test, ****$p < 0.0001$, *$p < 0.05$, $^{ns}p \geq 0.05$. Error bars: mean ± SEM. Immunostainings by Anuradha Bhukel from Bhukel and Beuschel et al., 2019.

in 30-day old fly brains (Figure 45a). When I had a look at the aversive olfactory memory of young versus 30-day old wild-type like flies (*atg5* RNAi / +), I could observe a decline in memory with age. Furthermore, the performance of 10-day old pan-neuronal *atg5* deficient flies was comparable to the senescent ones (see Figure 45b-d). While the control *atg5* RNAi / + showed a performance index of circa 40 % at the juvenile age of 10-day in 1 hour mid-term memory (Figure 45b), this decreased by 50 % for 30-day old flies. In contrast, the pan-neuronal *atg5* knockdown demonstrated at already the age of ten days a performance index of only around 16 %, and at 30 days even less with 6 % (Figure 45b). It was also interesting to see that the pan-neuronal knockdown's survival was dramatically reduced at 30 days. Based on this, and since the performance index for 1 hour mid-term memory was already near zero, I had to abandon further experiments on aging macroautophagy deficient flies. Hence, I had a closer look at the aging wild-type like control *atg5* RNAi / +. 1 hour mid-term memory can be separated into two components. One is the consolidated component, anesthesia-resistant memory (ARM), and the other is anesthesia-sensitive memory (ASM), with its more labile nature (DeZazzo and Tully, 1995; Isabel et al., 2004). ASM can be calculated by deducting the anesthesia-resistant memory value from the median mid-term memory. Interestingly, these two phases can be differentiated by the impact of age. While ARM stays the same with age, ASM appears vulnerable to it (Tamura et al., 2003; Gupta et al., 2013). The same I observed for *atg5* RNAi / + flies. The typically stable 1 hour ARM memory was nearly the same for the 30-day old wild-typic flies as for the young ones. Interestingly, the pan-neuronal *atg5* knockdown also showed no decrease in the consolidated memory (Figure 45c). In contrast, 1 hour ASM was impaired with age and lacking macroautophagy (Figure 45d). Here, the memory dramatically drops from a value around 35 % for 10-day old *atg5* RNAi / + to a performance index of 10 % for 30-day old flies. Intriguingly, flies with erased macroautophagy already had the same reduced memory level at young age as 30-day old control flies. In short, a lack of macroautophagy mimicked the memory of aged flies in juvenile animals already. Even when I tested the *elaV(X)* > *atg5* RNAi flies at the younger age of 5 days, I still could observe a severe impairment of short-term memory (Figure 46). Accordingly, a

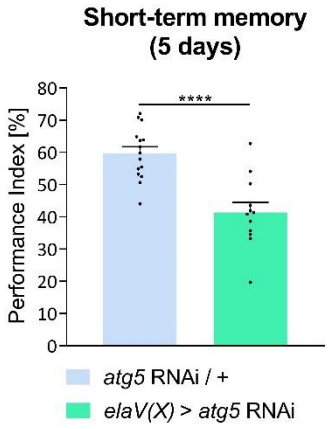

Figure 46: Short-term memory for younger Atg5 deficient flies.

Aversive olfactory memory for 5-day old flies, measured directly after training: n = 15 for *atg5* RNAi / +, n = 12 for *elaV(X)* > *atg5* RNAi. Statistics: unpaired t-test, ****$p < 0.0001$. Error bars: mean ± SEM.

macroautophagy deficit shows similar changes in p62/Ref(2p) accumulation, presynaptic plasticity, and memory performance as aged animals.

Additionally, I performed a negative geotaxis assay according to Inagaki et al., 2009 to test the climbing/ locomotor ability of macroautophagy deficient animals (Figure 47). The final distribution of the pan-neuronal *atg5* knockdown in the different fractions showed no obvious distinction to the control *atg5* RNAi / +. The flies showed adequate mobility for the conducted memory tests.

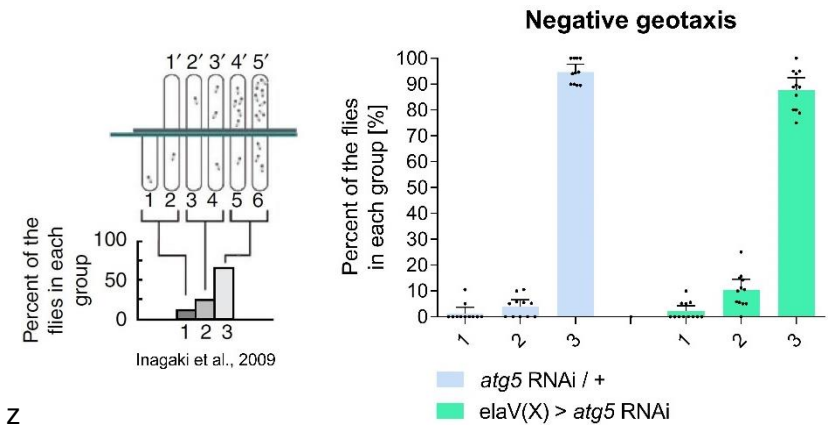

Figure 47: Negative geotaxis performance for pan-neuronal macroautophagic deficiency.

Negative geotaxis after Inagaki et al., 2009, for female 10-day old *elaV(X)* > *atg5* RNAi flies plus the control *atg5* RNAi / +, final distribution of the flies in the different tubes as bar graph: n = 12 for *atg5* RNAi / +, n = 12 for *elaV(X)* > *atg5* RNAi. Cf (partition coefficient for final distribution): Cf_{mean} = 0.9577 ± 0.01282 for *atg5* RNAi / +, Cf_{mean} = 0.9042 ± 0.01467 for *elaV(X)* > *atg5* RNAi.

The innate behavior scores for the pan-neuronal *atg5* knockdown showed comparable performance indices to their controls (Table 4). Both odor acuities for 3-Octanol and 4-Methylcyclohexanol were insignificant, as well as shock reactivity.

		Olfactory acuity	
Genotype	Shock reactivity (n)	3-Octanol (n)	4-Methylcyclohexanol (n)
atg5 RNAi / +	77.68 ± 4.012 (9)	22.63 ± 4.085 (9)	24.59 ± 6.726 (13)
elaV(X) > *atg5* RNAi	77.31 ± 2.626 (12)	21.22 ± 5.824 (6)	19.55 ± 6.205 (11)

Table 4: Innate behavior of pan-neuronal *atg5* knockdown.

Shock reactivity and olfactory acuity showed no significant difference in the pan-neuronal knockdown of *atg5*, *elaV(X)* > *atg5* RNAi, compared to its control *atg5* RNAi / +. Statistics: unpaired t-test, $^{ns}p \geq 0.05$. Mean ± SEM.

2.4.1.b Restriction of Atg5 deficiency to specific neuronal areas

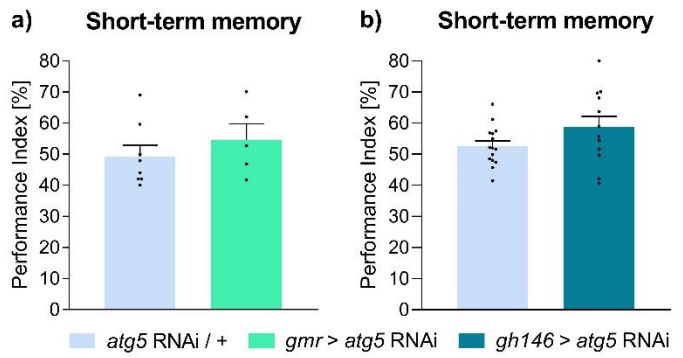

Figure 48: Decreased macroautophagy does not affect short-term memory when restricted to the optic lobes or the olfactory projection neurons.

Aversive olfactory short-term memory (tested 3 min after training) for 10-day old flies of *gmr* > *atg5* RNAi and *gh146* > *atg5* RNAi and their control *atg5* RNAi / +. a) Performance Index for *atg5* knockdown in the optic lobes: n = 8 for *atg5* RNAi / +, n = 5 for *gmr* > *atg5* RNAi. b) Performance Index for *atg5* knockdown in the projection neurons: n = 15 for *atg5* RNAi / +, n = 12 for *gh146* > *atg5* RNAi. Statistics: unpaired t-test, $^{ns}p \geq 0.05$. Error bars: mean ± SEM.

Next, I asked where the protective effects of macroautophagy are localized in the brain of *Drosophila melanogaster*. For this, I knocked down *atg5* with different enhancer trap lines. A notable short-term memory defect was not visible with *gmr*-Gal4 (Figure 48a) which addresses the optic lobes as visual centers, filling almost the half brain of *Drosophila* (Hiesinger et al., 1999). Similarly, I observed no memory decay for the *atg5* knockdown with *gh146*-Gal4 (Figure 48b), which covers the olfactory projection neurons, the conveyor of the olfactory cue to the higher brain centers (Stocker et al., 1997).

In contrast, an intervention of missing macroautophagy at the level of autophagosome elongation in the mushroom body seemed to have a massive impact on the ability to form memories. The mushroom body is a higher integration center in the *Drosophila* brain, where the generation of learning and memory storage happens (Aso et al., 2014; Bhukel and Beuschel et al., 2019). Accordingly, as soon as a functioning mushroom body is not available anymore, for example, via chemical ablation, associative conditioned odor learning vanishes (Belle and Heisenberg, 1994). Here, a restriction of missing macroautophagy to the mushroom body with the Gal4 driver *vt030559* impacted memory. With a reduction of *atg5* in the mushroom body, short-term memory dropped dramatically by 20 % (Figure 49b). Similar results could be observed for 1 hour mid-term memory (Figure 49c). Additionally, a severe buildup of p62/Ref(2)p aggregates in the mushroom body's cell bodies occurred in these flies (Figure 49a; Bhukel and Beuschel et al., 2019). Surprisingly, the Bruchpilot intensity level (BRP^{Nc82}) in the brain's immunostainings was not only increased in the expression domain of *vt030559*, the mushroom body, but also over the whole brain in a non-cell autonomous manner (Figure 49a; Bhukel and Beuschel et al., 2019). A similar brain-wide increase of Bruchpilot

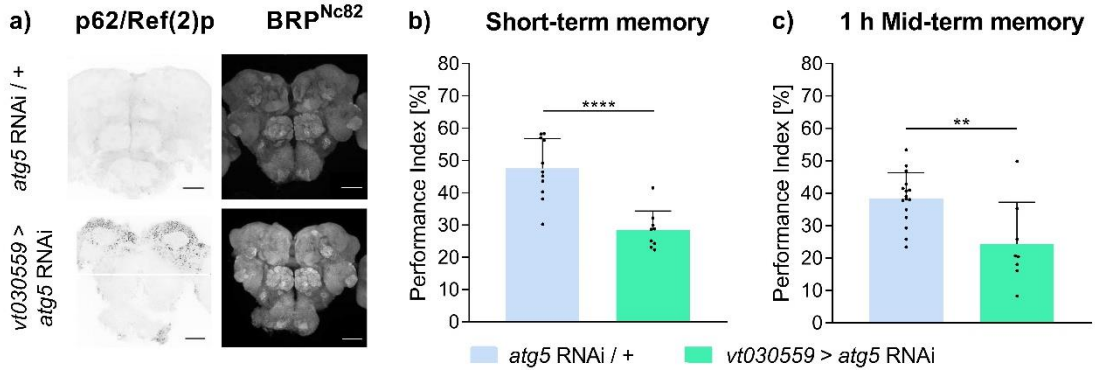

Figure 49: Deficient macroautophagy in the mushroom body impairs memory formation.

a) Immunostainings for p62/Ref(2)p (indicator for deficient macroautophagy) and Bruchpilot (BRP^{Nc82}; marker for synaptic plasticity) showed increased intensities in brains of 10-day old *vt030559* > *atg5* RNAi animals compared to the control *atg5* RNAi / +, scale bar: 50 µm. b-c) Aversive olfactory memory declined for 10-day old flies of *vt030559* > *atg5* RNAi compared to the control *atg5* RNAi / +. b) Performance Index for short-term memory (test 3 min after training): n = 11 for *atg5* RNAi / +, n = 9 for *vt030559* > *atg5* RNAi. c) Performance Index for 1 hour mid-term memory (test 1 hour after training): n = 16 for *atg5* RNAi / +, n = 8 for *vt030559* > *atg5* RNAi. Statistics: unpaired t-test, ****p < 0.0001, **p < 0.01. Error bars: mean ± SEM. Immunostainings by Anuradha Bhukel from Bhukel and Beuschel et al., 2019.

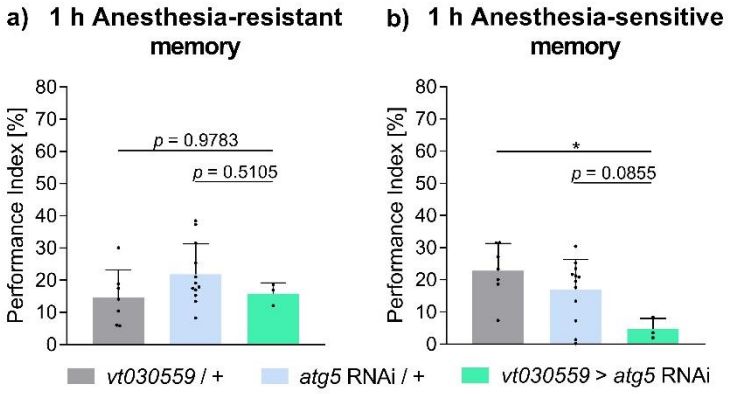

Figure 50: Macroautophagy restricted to the mushroom body results in reduced 1 hour anesthesia-sensitive memory.

Aversive olfactory memory for 10-day old flies of *vt030559* > *atg5* RNAi and the controls *vt030559* / + and *atg5* RNAi / +. a) Performance Index for 1 hour anesthesia-resistant memory (ice-bad 30 min and test 1 hour after training): n = 7 for *vt030559* / +, n = 12 for *atg5* RNAi / +, n = 3 for *vt030559* > *atg5* RNAi. b) Performance Index for 1 hour anesthesia-sensitive memory: Results received via calculation of the median of 1 hour mid-term memory minus the individual performance indices of 1 hour anesthesia-resistant memory. Statistics: ordinary one-way ANOVA with Sidak's *post hoc* test, *p < 0.05, ^{ns}p ≥ 0.05. Error bars: mean ± SEM.

occurred in pan-neuronal diminished macroautophagy (Figure 44a) and aged animals (Figure 45a). I was curious about which 1 hour memory phase would be impaired, so I explored 1 hour anesthesia-resistant memory (ARM) and 1 hour anesthesia-sensitive memory (ASM). As expected, reduced macroautophagy in the mushroom body revealed no significant memory deficit for the typically robust ARM (Figure 50a). However, a significant reduction was visible when I compared this knockdown's ASM to its driver control vt030559 / +. Similarly, the memory of this cross was reduced compared to its RNAi control *atg5* / +, though with a tendency of $p = 0.0855$ (Figure 50b). Here, a larger number of *vt030559* > *atg5* RNAi tests would probably result in a significant outcome.

Indeed, a repetition of associative olfactory memory tests using another mushroom body specific driver line, *ok107*-Gal4, gave similar results for short-term memory, although in a minor significance (Figure 51b). Comparable to *vt030559*, an accumulation of p62/Ref(2)p was visible in the area of the mushroom body (Bhukel and Beuschel et al., 2019), as well as a brain-wide increase in the intensity of Bruchpilot (Figure 51a; Bhukel and Beuschel et al., 2019). When I performed short-term memory with 5-day old flies of this genotype, they also showed a memory deficit, even at a younger age (Figure 51c). Consequently, autophagy seems crucial for associative olfactory memory performance when expressed only in the mushroom body.

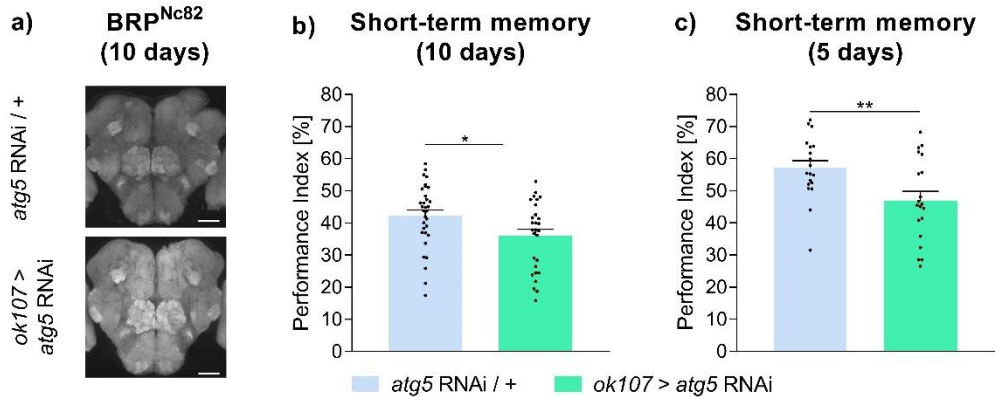

Figure 51: Deficient macroautophagy with a further mushroom body specific driver shows reduced short-term memory, even at a very young age.

a) Immunostainings for Bruchpilot (BRP^{Nc82}; marker for synaptic plasticity) showed an increased intensity in brains of 10-day old *ok107* > *atg5* RNAi animals compared to the control *atg5* RNAi / +, scale bar: 50 µm. a-b) Short-term memory (tested 3 min after training). a) 10-day old flies: n = 32 for *atg5* RNAi / +, n = 29 for *ok107* > *atg5* RNAi. b) 5-day old flies: n = 19 for *atg5* RNAi / +, n = 20 for *ok107* > *atg5* RNAi. Statistics: unpaired t-test, $^{**}p < 0.01$, $^{*}p < 0.05$. Error bars: mean ± SEM. Immunostainings by Anuradha Bhukel from Bhukel and Beuschel et al., 2019.

In addition, this mushroom body-specific driver also showed a brain-wide non-cell autonomous increase of the Bruchpilot intensity (Bhukel and Beuschel et al., 2019). With the driver vt030559 and ok107, the whole mushroom body is aimed (Aso et al., 2009; Plaçais et al., 2017). How would an attenuation of macroautophagy in a subset of the mushroom body operate? It consists of diverse regions, assigned with partly differential functions in the memory process (Krashes et al., 2007).

First, I aimed only a subset of the mushroom body, the α'/β' lobes, via expression with *ok107*-Gal4 plus its partly suppression with *mb247*-Gal80 (Figure 52). These lobes are especially required for memory acquisition, which lasts up to 1 hour (Wang et al., 2008). In contrast to our previous results about the mushroom body, no increase in synaptic plasticity via Bruchpilot could be observed (Figure 52a; Bhukel and Beuschel et al., 2019). The short-term memory of *mb247*-Gal80 ;; *ok107* > *atg5* RNAi only dropped to the driver control *mb247*-Gal80 / + ;; *ok107*-Gal4 / +, yet a namely difference to the RNAi control *atg5* RNAi / + was not apparent (Figure 52b). Additionally, the performance for 1 hour mid-term memory showed similar results for all tested genotypes, around 50 % (Figure 52c). Thus, is a macroautophagy deficit not

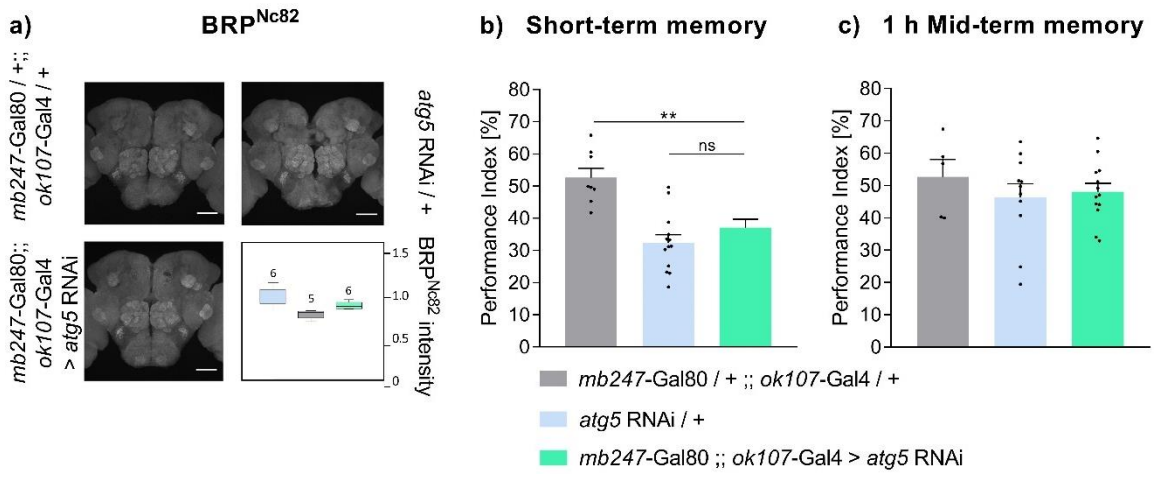

Figure 52: Sole expression of deficient macroautophagy via *atg5* RNAi in the α'/β' lobes of the mushroom body gives no memory decay.

a) Brain immunostainings showed similar Bruchpilot intensities (BRP^{Nc82}; a marker for synaptic plasticity) at 10-day flies with *atg5* RNAi expressed in the mushroom body via *ok107*-Gal4 and simultaneous suppression in the α/β and γ lobes (*mb247*-Gal80), controls: *mb247*-Gal80 / + ;; *ok107*-Gal4 / +, *atg5* RNAi / +. Scale bar: 50 µm. b) Short-term memory (test 3 min after training): n = 8 for *mb247*-Gal80 / + ;; *ok107*-Gal4 / +, n = 13 for *atg5* RNAi / +, n = 12 for *mb247*-Gal80 ;; *ok107*-Gal4 > *atg5* RNAi. c) 1 hour mid-term memory (test 1 hour after training): n = 5 for *mb247*-Gal80 / +;; *ok107*-Gal4 / +, n = 11 for *atg5* RNAi / +, n = 13 for *mb247*-Gal80 ;; *ok107*-Gal4 > *atg5* RNAi. Statistics: ordinary one-way ANOVA with Sidak's *post hoc* test, $^{**}p < 0.01$, $^{ns}p \geq 0.05$. Error bars: mean ± SEM. Immunostainings by Anuradha Bhukel from Bhukel and Beuschel et al., 2019.

crucial for functional memory acquisition in the prime lobes? Or was the Gal4 suppression via Gal80 inefficient? p62/Ref(2)p immunostainings showed an operating *mb247*-Gal80 with suppression in the α/β, and γ lobes, while a strong p62/Ref(2)p aggregation was visible in other regions like the *pars intercerebralis*, which *ok107*-Gal4 covers (Bhukel, 2018). Consequently, suppressing the *atg5* deficit in the α/β and γ lobes seemed to be functional and strong enough to prevent a non-cell autonomous increase of presynaptic plasticity via Bruchpilot over the whole brain and a memory decay (Figure 52; Bhukel and Beuschel et al., 2019). Only a macroautophagy lack in the prime lobes did not show early aging-like effects.

Could it be that active macroautophagy, particularly in the α/β and γ lobes, is essential for working memory performance? Hence, I tested attenuated macroautophagy driven by *mb247*-Gal4 as a mushroom body driver with expression only in the α/β and γ lobes (Aso et al., 2009). Curiously, I could not observe any memory deficit in short-term memory and 1 hour mid-term memory (Figure 53). p62/Ref(2)p immunostainings of *mb247* > *atg5* RNAi showed aggregates in the α/β and γ lobes, though with a weaker expression than *ok107*-Gal4 (Bhukel, 2018). Aso et al., 2009, also described *mb247*-Gal4 as a relative weak driver. Thus, only an intense inhibition of macroautophagy in the α/b and γ lobes seemed to result in the observed memory drop as seen with *vt030559*-Gal4 and *ok107*-Gal4 (Figure 49, Figure 51). A weaker expression with the diver *mb247*-Gal4 could be insufficient (Figure 53). Though, maybe an expression of missing macroautophagy in all the mushroom body lobes is necessary.

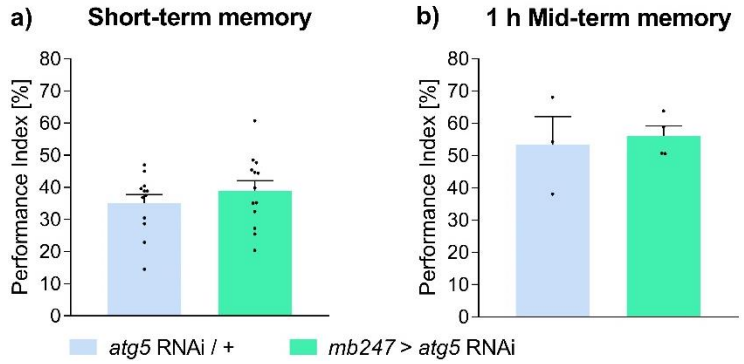

Figure 53: Missing macroautophagy in the α/β and γ lobes of the mushroom body shows no memory deficit.

Aversive olfactory memory for 10-day old flies with deficient macroautophagy expression only in the α/β and γ lobes. a) Performance index for short-term memory (measured directly after training): n = 12 for *atg5* RNAi / +, n = 13 for *mb247* > *atg5* RNAi. b) Performance Index for 1 hour mid-term memory (test 1 hour after training): n = 3 for *atg5* RNAi / +, n = 4 for *mb247* > *atg5* RNAi. Statistics: unpaired t-test, $^{ns}p \geq 0.05$. Error bars: mean ± SEM.

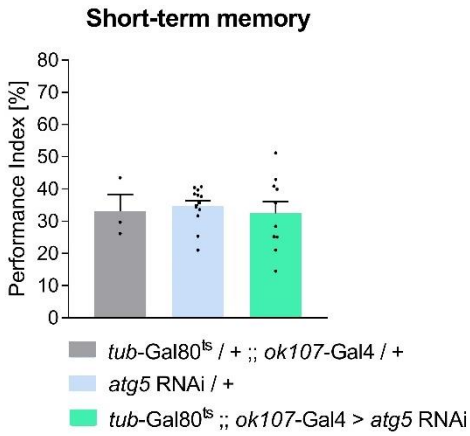

Figure 54: No memory impairment when deficient macroautophagy was only expressed in adulthood.

Short-term memory for 10-day old flies with the deficient macroautophagy in the mushroom body expressed from adulthood (measured directly after training): n = 3 for *tub*-Gal80^{ts} / + ;; *ok107*-Gal4 / +, n = 13 for *atg5* RNAi / +, n = 10 for *tub*-Gal80^{ts} ;; *ok107*-Gal4 > *atg5* RNAi. Statistics: Kruskal-Wallis with Dunn's *post hoc* test, $^{ns}p \geq 0.05$. Error bars: mean ± SEM.

To prevent developmental effects, I performed temperature-sensitive Gal80 experiments, where the macroautophagy deficit in the mushroom body (via *ok107*-Gal4) was suppressed at 18 °C until the adulthood of the flies. By shifting them to 29 °C after the eclosion, the Gal4 suppressor Gal80^{ts} was not active anymore (McGuire et al., 2003). Curiously, this procedure demonstrated no detectable accumulation of p62/Ref(2)p (Bhukel and Beuschel et al., 2019), and, concomitantly, no short-term memory deficit could be observed (Figure 54). Likely, the knockdown of *atg5* could not be sufficiently achieved when restricting the RNA interference only to the post-eclosion adult stages, and a remaining turnover of developmentally expressed Atg5 occurred (Bhukel and Beuschel et al., 2019).

The innate smell scores for the *atg5* knockdown in the relevant areas showed comparable performance indices to their controls (Table 5). Only for the 3-Octanol acuity of the *atg5* knockdown in the projection neurons (*gh146* > *atg5* RNAi), a slight significance ($^{*}p = 0.0303$) could be observed compared to its control. Since this cross's memory performance showed no memory deficit, this observation did not affect the memory results.

	Olfactory acuity	
Genotype	3-Octanol (n)	4-Methylcyclohexanol (n)
atg5 RNAi / +	52.14 ± 5.870 (12)	38.07 ± 5.315 (15)
gh146 > *atg5* RNAi	36.70 ± 3.845 (16)	29.16 ± 5.910 (14)
atg5 RNAi / +	34.56 ± 10.220 (8)	61.54 ± 6.915 (8)
vt030559 > *atg5* RNAi	39.15 ± 13.200 (6)	54.88 ± 5.965 (4)
atg5 RNAi / +	22.63 ± 4.085 (9)	24.59 ± 6.726 (13)
ok107 > *atg5* RNAi	20.32 ± 5.798 (5)	18.97 ± 5.136 (11)
mb247-Gal80 / + ;; *ok107*-Gal4 / +	52.77 ± 4.117 (7)	57.93 ± 3.425 (8)
atg5 RNAi / +	44.03 ± 9.636 (6)	58.00 ± 8.286 (8)
mb247-Gal80 ;; *ok107*-Gal4 > *atg5* RNAi	56.24 ± 5.648 (10)	42.31 ± 5.420 (9)
tub-Gal80^{ts} / + ;; *ok107*-Gal4 / +	63.74 ± 10.86 (5)	71.80 ± 9.503 (3)
atg5 RNAi / +	49.46 ± 9.698 (8)	33.43 ± 5.040 (9)
tub-Gal80^{ts} ;; *ok107*-Gal4 > *atg5* RNAi	42.23 ± 12.33 (6)	46.20 ± 6.229 (7)

Table 5: Innate behavior of *atg5* knockdown for the experimental groups.

As tests for innate behavior, olfactory acuity gave no significant difference for the experimental groups but *gh146* > *atg5* RNAi. A significant decay for the 3-Octanol could be observed here. However, since an *atg5* knockdown in the projection neurons gave no learning deficit, this was inconsequential for the memory. Statistics: unpaired t-test for two genotypes and one-way ANOVA with Sidak's multiple comparisons *post hoc* test for three genotypes, $*p < 0.05$, $^{ns}p \geq 0.05$. Mean ± SEM.

2.4.2. Intervening at the phase of phagophore assembly

To compare two independent steps of macroautophagy, I went on with Atg9, a transmembrane protein that assists by transporting lipid bilayers to the emerging phagophore (Gelino and Hansen, 2012; Bhukel and Beuschel et al., 2019). In contrast to the earlier discussed Atg5, this protein is marginal for the lipidation of Atg8, which is conducted by the E3 ligase-like complex, built of Atg5 together with Atg12 and Atg16 (Hanada et al., 2007; Gelino and Hansen, 2012; Bento et al., 2016; Gui et al., 2019). The lipidated, activated Atg8-II binds p62/Ref(2)p, a receptor marking cargo for degradation, to encourage the engulfment by the autophagosome (Pankiv et al., 2007; Gelino and Hansen, 2012). However, Atg9 serves as the carrier for the required membrane in the process of phagophore elongation (Gelino and Hansen, 2012; Bento et al., 2016).

In the paper Bhukel and Beuschel et al., 2019, we showed that Atg8 had two bands in brain Western blots of a pan-neuronal *atg9* knockdown, similar to all its controls. In contrast, the *atg5* deficient brains did not hold the second band of Atg8, its lipidated modification. Thus, the effects of an *atg9* knockdown suited perfectly as a second strategy to examine the consequences of macroautophagy in different neuronal tissues, focusing on aversive olfactory memory.

2.4.2.a Pan-neuronal *atg9* knockdown affects the ability to form memory at young age already

As described before, the autophagy receptor p62/Ref(2)p is usable as a marker for macroautophagic inefficiency, in this chapter caused by a pan-neuronal knockdown of *atg9* (Bhukel and Beuschel et al., 2019). Missing macroautophagy is associated with an aggregation of p62/Ref(2)p since a cluster of this receptor reveals malfunctioning autophagic systems (Bjørkøy et al., 2009; Bartlett et al., 2011; Mauvezin et al., 2014). Hence, a severe increase of p62/Ref(2)p occurred in the brains of 10-day old *elav(X) > atg9* RNAi animals (Figure 55a). An accumulation of p62/Ref(2)p aggregates like this were already visible in the pan-neuronal knockdown of *atg5* (Figure 44) as well as in aging animals (Gupta et al., 2013). Moreover, increased intensity of Bruchpilot (BRP^{Nc82}), a presynaptic active zone scaffold protein, could be detected in the brains of these young animals, comparable to aged 30-day old ones (Figure 55a; Gupta et al., 2016). Again, this was similar in *atg5* deficient 10-day old flies (Figure 44). Accordingly, these *atg9* deficient flies performed poorly in aversive olfactory memory. At the young age of 10 days, they already displayed a memory performance like old animals in short-term memory (Figure 55c; Figure 48c) and 1 hour mid-term memory (Figure 55d; Figure 45).

Moreover, even younger flies like 5-day old ones could not prevent this memory impairment (Figure 55b).

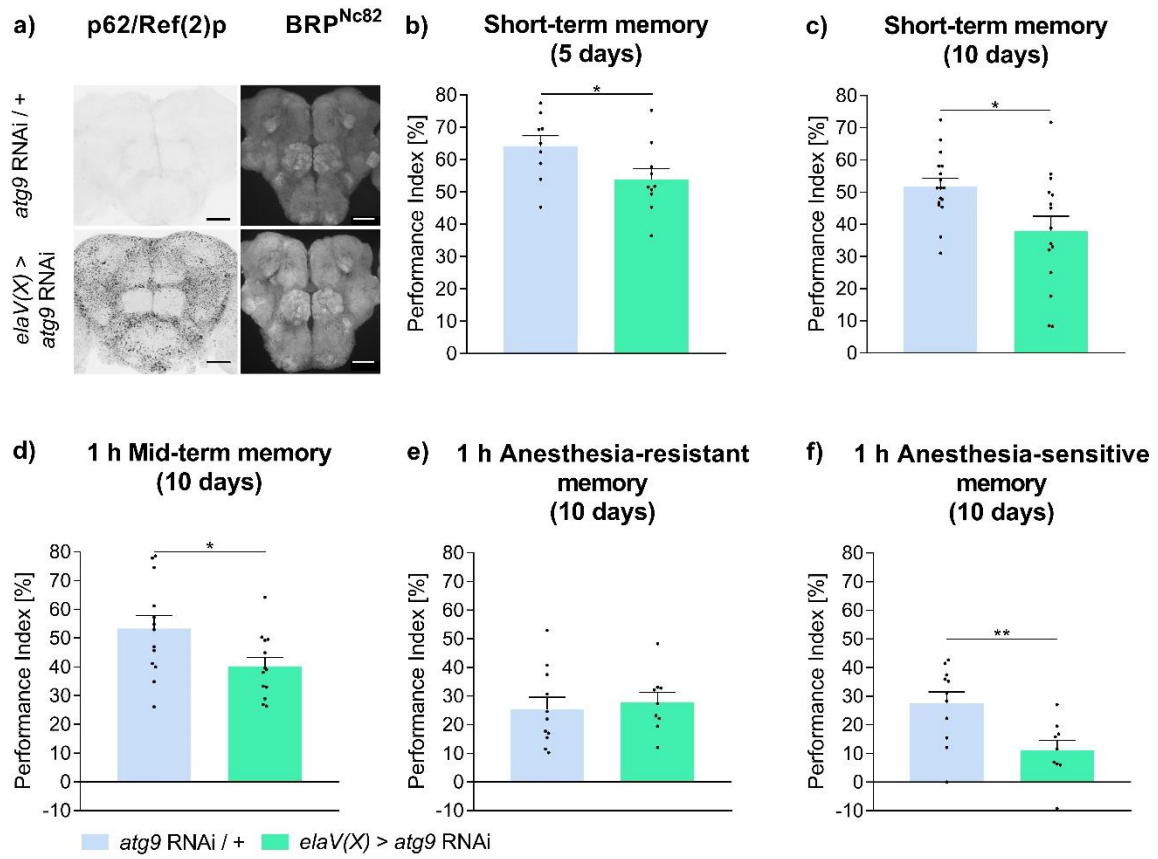

Figure 55: Pan-neuronal knockdown of *atg9* reduces aversive olfactory memory.

a) Immunostainings for p62/Ref(2)p (indicator for deficient macroautophagy) and Bruchpilot (BRP^{Nc82}; marker for synaptic plasticity) showed increased intensities for brains of 10-day old *elaV(X)* > *atg9* RNAi animals compared to the control *atg9* RNAi / +, scale bar: 50 µm. b) Aversive olfactory memory (short-term memory, measured directly after training) for 5-day old *elaV(X)* > *atg9* RNAi flies plus its control: n = 9 for *atg9* RNAi / +, n = 10 for *elaV(X)* > *atg9* RNAi. c-f) Aversive olfactory memory declined for 10-day old flies of *elaV(X)* > *atg9* RNAi compared to its control *atg9* RNAi / +. c) Performance Index for short-term memory: n = 17 for *atg9* RNAi / +, n = 15 for *elaV(X)* > *atg9* RNAi. d) Performance Index for 1 hour mid-term memory (test 1 hour after training): n = 13 for *atg9* RNAi / +, n = 13 for *elaV(X)* > *atg9* RNAi. e) Performance Index for 1 hour anesthesia-resistant memory (ice-bad 30 min and test 1 hour after training): n = 11 for *atg9* RNAi / +, n = 9 for *elaV(X)* > *atg9* RNAi. f) Performance Index for 1 hour anesthesia-sensitive memory: Results received via calculation of the median of 1 hour mid-term memory minus the individual performance indices of 1 hour anesthesia-resistant memory. Statistics: unpaired t-test, $^{**}p < 0.01$, $^{*}p < 0.05$, $^{ns}p \geq 0.05$. Error bars: mean ± SEM. Immunostainings by Anuradha Bhukel from Bhukel and Beuschel et al., 2019.

To see if the age-sensitive 1 hour memory component, anesthesia-sensitive memory (ASM), was comparable to pan-neuronal *atg9* deficient animals, I performed 1 hour anesthesia-resistant memory (ARM). This way, the ASM values could be calculated according to the median of 1 hour mid-term memory of this genotype. Similar to the behavior tests for aged animals (Figure 45), these flies revealed no behavioral differences for the ARM (Figure 55e), which is stable with age (Figure 45c, Gupta et al., 2013). Consequently, the labile memory phase ASM showed a massive memory decrease (Figure 55f), again similar to the behavior of aging flies and pan-neuronal *atg5* deficient animals (Figure 45Figure 45d; Tamura et al., 2003).

Innate behavior was normal for *elaV(X)* > *atg9* RNAi flies when compared to their controls (Table 6). Both odor acuities with 3-Octanol and 4-Methylcyclohexanol were insignificant, as well as the shock reactivity.

		Olfactory acuity	
Genotype	Shock reactivity (n)	3-Octanol (n)	4-Methylcyclohexanol (n)
atg9 RNAi / +	88.62 ± 2.648 (6)	27.26 ± 3.823 (14)	50.28 ± 8.450 (10)
elaV(X) > *atg9* RNAi	85.14 ± 2.302 (8)	23.34 ± 3.853 (17)	49.11 ± 7.583 (13)

Table 6: Innate behavior of pan-neuronal *atg9* knockdown.

Shock reactivity and olfactory acuity showed no significant difference in the pan-neuronal *atg9* knockdown *elaV(X)* > *atg9* RNAi compared to its control *atg9* RNAi / +. Statistics: unpaired t-test, $^{ns}p \geq 0.05$. Mean ± SEM.

2.4.2.b Restriction of Atg9 deficiency to specific neuronal areas

To locate the protective effects of macroautophagy in specific neuronal populations, I investigated deficient macroautophagy in different fly brain divisions (Bhukel and Beuschel et al., 2019). Considering the olfactory pathway, an odor's cue is sent via the projection neurons to the higher processing centers, the mushroom body and the lateral horn (Stocker et al., 1997). Moreover, one short-term trace goes through the projection neurons and generates short-term memory (Yu et al., 2004). Though, neither an increase of Bruchpilot (BRP^{Nc82}, Figure 56a) nor any short-term memory deficit could be found in *gh146* > *atg9* RNAi flies (Figure 56b). However, accumulated p62/Ref(2) was visible in these neurons when *atg9* was downregulated there (Figure 56a). Hence, functional RNAi expression was present in the projection neurons. These results were similar to the Atg5 deficiency in the projection neurons (Figure 48). The Bruchpilot increase in the brain or the missing memory acquisition due to inoperative macroautophagy seemed not to be mediated by these neurons.

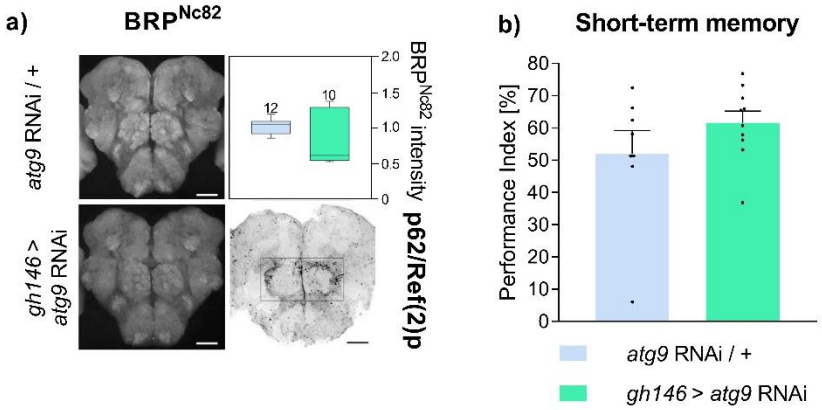

Figure 56: An *atg9* knockdown in the projection neurons reveals no change in presynaptic plasticity or short-term memory.

a) Immunostainings for Bruchpilot (BRP^{Nc82}; a marker for synaptic plasticity) showed no increased intensity for brains of 10-day old *gh146* > *atg9* RNAi animals compared to the control *atg9* RNAi / +. Quantification of BRP^{Nc82} intensity for the brain normalized to the control (Mann Whitney test). Immunostaining for p62/Ref(2)p (indicator for deficient macroautophagy) for 10-day old *gh146* > *atg9* RNAi flies, scale bar: 50 µm. b) Short-term memory for 10-day old flies of *gh146* > *atg9* RNAi compared to the control *atg9* RNAi / + (test 3 min after training): n = 8 for *atg9* RNAi / +, n = 10 for *gh146* > *atg9* RNAi. Statistics: unpaired t-test, $^{ns}p \geq 0.05$. Error bars: mean ± SEM. Immunostainings and their quantification by Anuradha Bhukel from Bhukel and Beuschel et al., 2019.

Focusing on the brain's olfactory learning center, I performed short-term memory for *vt030559* > *atg9* RNAi flies. This restriction of deficient macroautophagy to the mushroom body revealed a significant memory impairment compared to the driver control vt030559 / + and the RNAi control *atg9* RNAi / + for 10-day old flies (Figure 57b). Similarly, younger animals aged 5 days showed a significant malfunctioning short-term memory, in contrast to their RNAi control *atg9* RNAi / + and their driver control *vt030559* / + (Figure 57a).

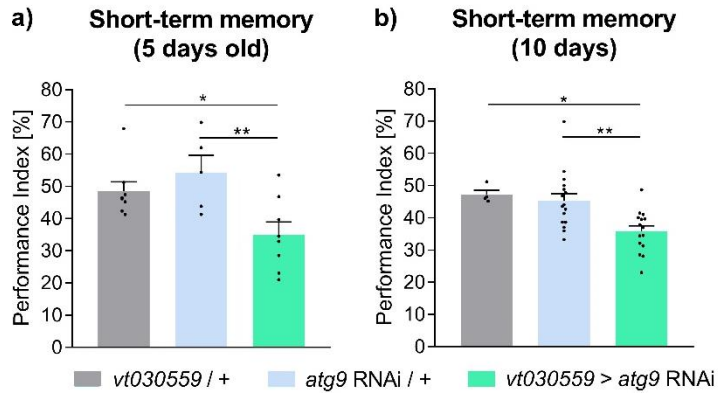

Figure 57: Deficient macroautophagy via *atg9* RNAi, expressed in the mushroom body, impairs memory formation.

Aversive olfactory short-term memory (test 3 min after training) for *vt030559* > *atg9* RNAi and its controls *vt030559* / + and *atg9* RNAi / +. a) Performance Index for 5-day old flies: n = 8 for *vt030559* / +, n = 5 for *atg9* RNAi / +, n = 8 for *vt030559* > *atg9* RNAi. b) Performance Index for 10-day old flies: n = 4 for *vt030559* / +, n = 16 for *atg9* RNAi / +, n = 15 for *vt030559* > *atg9* RNAi. Statistics: ordinary one-way ANOVA with Sidak's *post hoc* test, $^{**}p < 0.01$, $^{*}p < 0.05$, $^{ns}p \geq 0.05$. Error bars: mean ± SEM.

Further tests on missing Atg9 with an additional mushroom body driver, *ok107*-Gal4, confirmed the importance of an operating macroautophagic system in these neurons to prevent aging's malignant effects. Immunostainings for *ok107* > *atg9* RNAi showed a severe buildup of p62/Ref(2)p aggregates in the cell bodies of the mushroom body, a sign of impaired macroautophagy (Figure 58a; Mauvezin et al., 2014; Bhukel and Beuschel et al., 2019). Interestingly, immunostainings of Bruchpilot (BRP), a core component of the presynaptic active zone, showed a massive brain-wide increase of the BRP^{Nc82} intensity in the brains of 10-day old flies, beyond the area of the mushroom body brain-wide (Figure 58a). Additionally, investigations of this area with transmission emission electron microscopy (EM) and super-resolution light microscopy (STED) revealed the presynaptic status of the active zones in the mushroom body (Bhukel and Beuschel et al., 2019). The active zone's architecture contains an electron-dense structure, visible with EM, which appears for *Drosophila melanogaster* as a T-shaped structure, called T-bar (Figure 15; Zhai and Bellen, 2004; Bhukel and Beuschel et al., 2019). This T-bar increases massively with age, just like *ok107* > *atg9* RNAi flies (Figure 58b; (Gupta et al., 2016)). In Atg9 deficient mushroom body neurons, the T-bar shaped wide

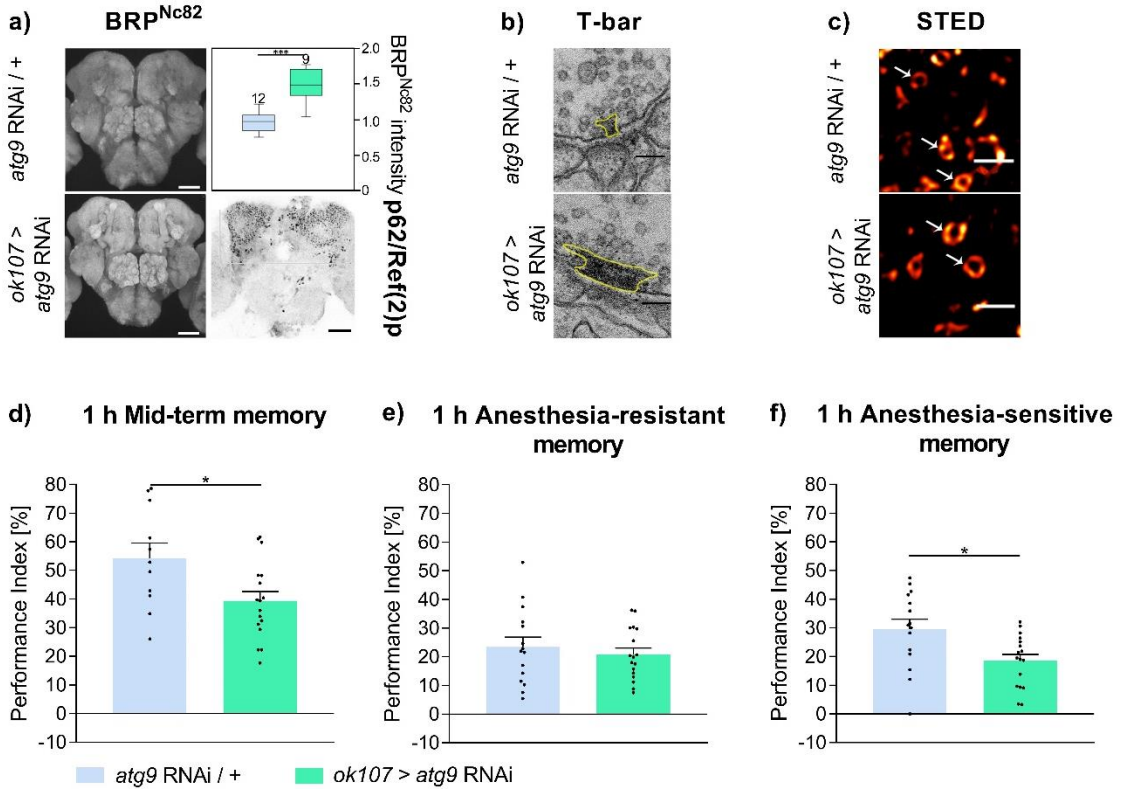

Figure 58: Deficient macroautophagy via *atg9* knockdown enlarges presynaptic plasticity and decreases the age-sensitive memory component.

a) Immunostainings for Bruchpilot (BRP^{Nc82}; marker for synaptic plasticity) showed increased intensity for brains of 10-day old *ok107* > *atg9* RNAi animals compared to the control *atg9* RNAi / +. Quantification of BRP^{Nc82} intensity for the brain, normalized to the control (Mann Whitney test, ***$p < 0.001$). Immunostaining for p62/Ref(2)p (indicator for deficient macroautophagy) for 10-day old *ok107* > *atg9* RNAi flies, scale bar: 50 µm. b) Electron micrographs showing the T-bar of the mushroom body's calyx for 10-day old *ok107* > *atg9* RNAi and *atg9* RNAi / + flies, scale bar: 100 nm. c) STED images of BRP uncover ring-shaped structures (arrows) within the calyx of the mushroom body for 10-day old *ok107* > *atg9* RNAi and *atg9* RNAi / + flies, scale bar: 500 nm. d-f) Aversive olfactory memory for 10-day old *ok107* > *atg9* RNAi flies plus their control *atg9* / +. d) Performance Index for 1 hour mid-term memory (test 1 hour after training): n = 11 for *atg9* RNAi / +, n = 17 for *ok107* > *atg9* RNAi. e) Performance Index for 1 hour anesthesia-resistant memory (ice-bad 30 min and test 1 hour after training): n = 15 for *atg9* RNAi / +, n = 17 for *ok107* > *atg9* RNAi. f) Performance Index for 1 hour anesthesia-sensitive memory: Results received via calculation of the median of 1 hour mid-term memory minus the individual performance indices of 1 hour anesthesia-resistant memory. Statistics: unpaired t-test, *$p < 0.05$, $^{ns}p \geq 0.05$. Error bars: mean ± SEM. Immunostainings plus their quantification, electron micrographs, and STED images by Anuradha Bhukel from Bhukel and Beuschel et al., 2019.

and loose at the young age of ten days already, in contrast to the compact and small shape of the control *ok107* / +. With STED, it is possible to display the nano-architecture of planar-oriented active zones as a ring-shaped BRP structure, increasing their diameter with age (Gupta et al., 2016). However, these BRP rings occurred similarly with a broader ring diameter in macroautophagy deficient neurons (arrows in Figure 58c; Bhukel and Beuschel et al., 2019). The diameter of BRP rings seemed to correlate with the physical size of the T-bars in the corresponding animals as well as the BRP intensity (Figure 58a-c; Gupta et al., 2016). Thus, the mushroom body's macroautophagic status appeared to affect ultrastructural conditions, the functional state of the active zone, and the olfactory system (Bhukel and Beuschel et al., 2019). Consequently, I could observe an impairment in 1 hour mid-term memory for *ok107* > *atg9* RNAi flies (Figure 58d). To determine the involved 1 hour memory phase, I performed 1 hour anesthesia-resistant memory (ARM) and anesthesia-sensitive memory (ASM). Like Atg5 deficient and aging flies, the *atg9* knockdown animals had a stable memory performance for ARM (Figure 58e) though a memory impairment with ASM (Figure 58f).

Though, the enhancer trap like *ok107*-Gal4 drives not only in the mushroom body but also in other neuronal tissues like the median neurosecretory cells (mNSCs), also known as insulin-producing cells (IPCs) (Aso et al., 2009; Nässel et al., 2013; Bhukel and Beuschel et al., 2019).

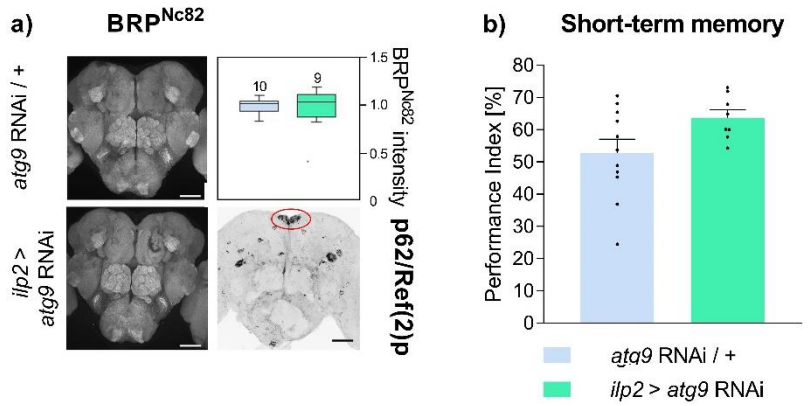

Figure 59: Expression of deficit macroautophagy in *pars intercerebralis* reveals no change in presynaptic plasticity nor short-term memory.

a) Immunostainings for Bruchpilot (BRP^{Nc82}; marker for synaptic plasticity) showed increased intensity for brains of 10-day old *ilp2* > *atg9* RNAi animals compared to the control *atg9* RNAi / +. Quantification of BRP^{Nc82} intensity for the brain normalized to the control (Mann Whitney test). Immunostaining for p62/Ref(2)p (indicator for deficient macroautophagy) for 10-day old *ilp2* > *atg9* RNAi flies, scale bar: 50 µm. b) Short-term memory for 10-day old flies of *ilp2* > *atg9* RNAi compared to the control *atg9* RNAi / + (test 3 min after training): n = 11 for *atg9* RNAi / +, n = 8 for *ilp2* > *atg9* RNAi. Statistics: unpaired t-test, $^{ns}p \geq 0.05$. Error bars: mean ± SEM. Immunostainings and their quantification by Anuradha Bhukel from Bhukel and Beuschel et al., 2019.

Since the signaling of *Drosophila* insulin-like peptide (Ilp) could be the reason for the non-cell autonomous effects of macroautophagy, additional tests were conducted with *ilp2*-Gal4, expressed in the IPCs (Ulgherait et al., 2014; Minnerly et al., 2017; Bhukel and Beuschel et al., 2019). Expression of deficient macroautophagy in the *pars intercerebralis* via *ilp2*-Gal4 revealed no change in the presynaptic plasticity (BRP^{Nc82} in Figure 59a), although a strong buildup of p62/Ref(2)p could be observed in the IPCs (Figure 59a; Bhukel and Beuschel et al., 2019). When these flies were examined with short-term memory, no memory decay could be seen. They even performed slightly better with a tendency of $p = 0.0597$ compared to their control (Figure 59b).

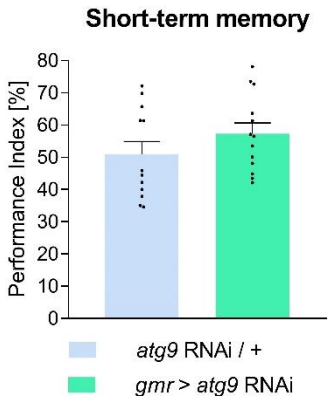

Figure 60: Downregulation of *atg9* in the optic lobes shows no memory deficit.

Short-term memory for 10-day old flies of *gmr* > *atg9* RNAi compared to the control *atg9* RNAi / + (test 3 min after training): n = 12 for *atg9* RNAi / +, n = 13 for *gmr* > *atg9* RNAi. Statistics: unpaired t-test, $^{ns}p \geq 0.05$. Error bars: mean ± SEM.

Further aversive olfactory memory tests addressed the optic lobes. These neurons hold almost half of *Drosophila's* brain, though there was no memory decay for short-term memory visible as well (Figure 60; Hiesinger et al., 1999). *gmr* > *atg9* RNAi even performed slightly better than its control.

Similar to the Atg5 deficiency tests, I aimed only a subset of the mushroom body, the α'/β' lobes, via expression of *ok107*-Gal4 plus partly its suppression with *mb247*-Gal80 (Figure 61). These prime lobes are required for memory acquisition, which lasts up to 1 hour (Wang et al., 2008). Even though I could observe a significant memory drop of *mb247*-Gal80 ;; *ok107*-Gal4 > *atg9* RNAi compared to its driver control (*mb247*-Gal80 / + ;; *ok107*-Gal4 / +), this was not the case for the second control *atg9* RNAi /+. Short-term memory (Figure 61a) and 1 hour mid-term memory (Figure 61b) of deficient macroautophagy in the α'/β' lobes were non significantly different from both controls. p62/Ref(2)p immunostainings showed an operating *mb247*-Gal80 with suppression in the α/β, and γ lobes, while a strong p62/Ref(2)p aggregation was visible in the *pars intercerebralis*, which *ok107*-Gal4 covers (Bhukel, 2018). Consequently, suppressing the *atg9* deficit in the α/β and γ lobes seemed to be functional. When I tested the opposite situation by attenuating only the α/β and γ lobes via *mb247*-Gal4, no memory decay appeared for 10- and 5-day old flies (Figure 62). I could observe similar results for *atg5* RNAi

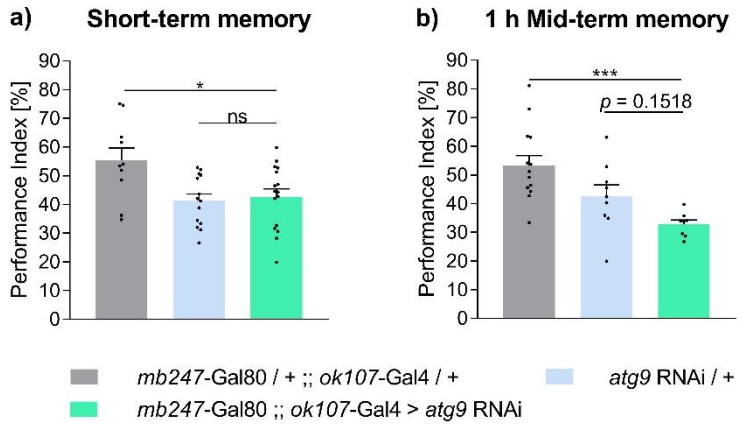

Figure 61: Sole expression of deficient macroautophagy via *atg9* RNAi in the α'/β' lobes of the mushroom body shows no significant memory decay.

a-b) Aversive olfactory memory for *atg9* RNAi, expressed in the mushroom body via *ok107*-Gal4 with simultaneous suppression in the α/β and γ lobes (*mb247*-Gal80), 10-day old, *mb247*-Gal80 / + ;; *ok107*-Gal4 / + as driver control, *atg9* RNAi / + as RNAi control. a) Performance Index for short-term memory (test 3 min after training): n = 10 for *mb247*-Gal80 / + ;; *ok107*-Gal4 / +, n = 14 for *atg9* RNAi / +, n = 16 for *mb247*-Gal80 ;; *ok107*-Gal4 > *atg9* RNAi. b) Performance Index for 1 hour mid-term memory (test 1 hour after training): n = 14 for *mb247*-Gal80 / + ;; *ok107*-Gal4 / +, n = 9 for *atg9* RNAi / +, n = 8 for *mb247*-Gal80 ;; *ok107*-Gal4 > *atg9* RNAi. Statistics: ordinary one-way ANOVA with Sidak's *post hoc* test, ***p < 0.001, *p < 0.05, ^{ns}p ≥ 0.05. Error bars: mean ± SEM.

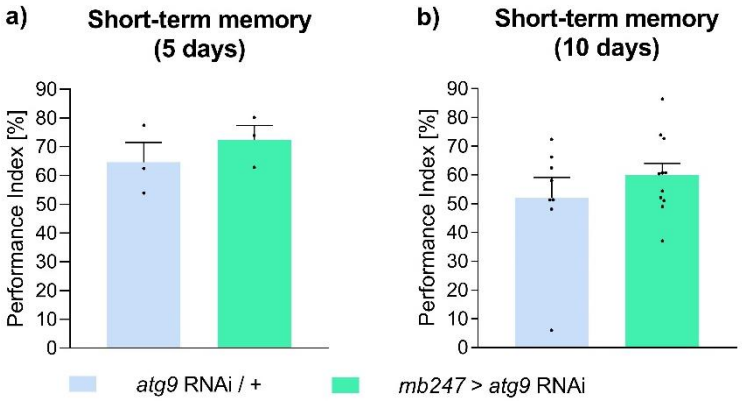

Figure 62: Missing macroautophagy in the α/β and γ lobes of the mushroom shows no memory deficit.

Short-term memory (test 3 min after training) for *atg9* RNAi expressed in α/β and γ lobes of the mushroom body via *mb247*-Gal4. a) Performance Index for 5-day old flies: n = 3 for *mb247* / +, n = 3 for *mb247* > *atg9* RNAi. b) Performance Index for 10-day old flies: n = 8 for *mb247* / +, n = 11 for *mb247* > *atg9* RNAi. Statistics: unpaired t-test, ^{ns}p ≥ 0.05. Error bars: mean ± SEM.

in this scenario (Figure 52, Figure 53). Indeed, *mb247*-Gal4 is a mushroom body driver with a relatively weak expression (Aso et al., 2009). p62/Ref(2)p immunostainings of *mb247* > *atg9* RNAi showed very weak aggregates in the α/β and γ lobes (Bhukel, 2018). Thus, this driver's expression in Figure 62 could be inadequate for successful macroautophagy inhibition in the mushroom body. Curiously, BRP^{Nc82} immunostainings with *mb247* > *atg9* even showed a decreased intensity for Bruchpilot (Bhukel, 2018).

Argumentum e contrario, the α/β and γ lobes seemed hold the key role in the effect of early memory impairment due to deficient macroautophagy, since no memory loss occurred with suppression of *atg9* RNAi expression in these lobes (Figure 61).

To avert developmental effects, I performed temperature-sensitive Gal80 experiments. Here, the *atg9* RNAi expression was suppressed until the flies' adulthood by shifting them to a higher temperature after the eclosion. This way, the Gal4 activity was restricted to these flies' maturity (McGuire et al., 2003). Curiously, these flies showed neither a detectable accumulation of p62/Ref(2)p (Bhukel and Beuschel et al., 2019) nor any memory defect in their performance (Figure 63). The short-term memory (Figure 63a) and 1 hour mid-term memory (Figure 56b) for *atg9* knockdown flies exhibited no memory decay compared to their controls. Similar was already visible in Atg5 deficient flies (Figure 54). Probably, the degradation of developmentally built Atg9 proteins was not completed until the memory testing days (10 days after eclosion). The RNAi could only inhibit the *atg9* transcription in the post-eclosion adult

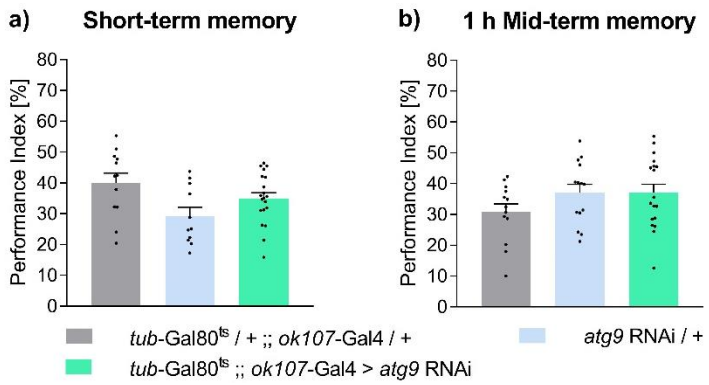

Figure 63: No memory impairment, when *atg9* RNAi is only expressed in the adulthood.

Aversive olfactory memory for 10-day old flies of *atg9* RNAi expressed in the mushroom body only from adulthood on. a) Performance Index for short-term memory (test 3 min after training): n = 12 for *tub*-$Gal80^{ts}$ / + ;; *ok107*-Gal4 / +, n = 11 for *atg9* RNAi / +, n = 20 for *tub*-$Gal80^{ts}$;; *ok107*-Gal4 > *atg9* RNAi. b) Performance Index for 1 hour mid-term memory (test 1 hour after training): n = 13 for for *tub*-$Gal80^{ts}$ / + ;; *ok107*-Gal4 / +, n = 14 for *atg9* RNAi / +, n = 18 for *tub*-$Gal80^{ts}$;; *ok107*-Gal4 > *atg9* RNAi. Statistics: ordinary one-way ANOVA with Sidak's *post hoc* test, $^{ns}p \geq 0.05$. Error bars: mean ± SEM.

stages. In this way, a remaining Atg9, expressed during development, was maybe enough to fulfill its macroautophagic tasks (Bhukel and Beuschel et al., 2019).

The innate smell scores for Atg9 deficiencies in the relevant areas showed comparable performance indices to their controls (Table 7). Both odor acuities for 3-Octanol and 4-Methylcyclohexanol were insignificant. Only the 3-Octanol and 4-Methylcyclohexanol acuity of the *atg9* knockdown in the α'/β' lobes of the mushroom body displayed significance (3-Octanol: $^{*}p = 0.0103$; MCH: $*p = 0.0418$) when compared to its control. Since this cross's memory performance showed no memory deficits, this observation did not affect the memory results.

	Olfactory acuity	
Genotype	3-Octanol (n)	4-Methylcyclohexanol (n)
atg9 RNAi / +	22.74 ± 5.672 (17)	36.55 ± 5.867 (22)
gh146 > *atg9* RNAi	23.84 ± 5.540 (16)	33.17 ± 4.863 (19)
atg9 RNAi / +	27.26 ± 3.823 (14)	50.28 ± 8.450 (10)
ok107 > *atg9* RNAi	23.34 ± 3.853 (17)	49.11 ± 7.583 (13)
atg9 RNAi / +	31.64 ± 7.345 (14)	27.25 ± 7.087 (14)
ilp2 > *atg9* RNAi	37.08 ± 5.098 (13)	33.94 ± 6.010 (11)
mb247-Gal80 / + ;; *ok107*-Gal4 / +	63.03 ± 3.664 (8)	80.33 ± 5.647 (8)
atg9 RNAi / +	55.01 ± 4.433 (9)	73.10 ± 5.499 (9)
mb247-Gal80 ;; *ok107*-Gal4 > *atg9* RNAi	41.14 ± 4.401 (5)	54.74 ± 8.696 (5)
tub-Gal80^{ts} /+ ;; *ok107*-Gal4 / +	74.78 ± 10.05 (5)	78.16 ± 6.858 (7)
atg9 RNAi / +	61.97 ± 3.831 (9)	57.13 ± 9.724 (9)
tub-Gal80^{ts} ;; *ok107*-Gal4 > *atg9* RNAi	68.51 ± 1.808 (10)	66.50 ± 6.313 (8)

Table 7: Innate behavior of *atg9* knockdown for the experimental groups.

As tests for innate behavior, olfactory acuity gave no significant difference for the experimental groups, but for *mb247*-Gal80 ;; *ok107*-Gal4 > *atg9* RNAi compared to the control *mb247*-Gal80 / + ;; *ok107*-Gal4 / +. Here, a significant decay for the 3-Octanol and 4-Methylcyclohexanol could be observed. However, since an *atg9* knockdown in the α'/β' lobes of the mushroom body gave no learning deficit, this is inconsequential for the memory. Statistics: unpaired t-test for two genotypes to analyze, for three genotypes one-way ANOVA with Sidak's multiple comparisons *post hoc* test (parametric) or Kruskal-Wallis with Dunn's *post hoc* test (nonparametric), $*p < 0.05$, $^{ns}p \geq 0.05$. Mean ± SEM.

2.4.3. Increased macroautophagy at the level of phagophore initiation does not benefit aversive olfactory memory

In the last chapters, I outlined the effects of deficient macroautophagy on two independent steps of its machinery. Knockdowns of macroautophagic core components, especially in the mushroom body, mimicked age-typical manifestations like p62/Ref(2)p aggregates, increased synaptic plasticity, and memory deficits in young animals already (Bhukel and Beuschel et al., 2019). Hence, would a boost of the cleaning system in the fly brain's learning center protect them from age-induced memory impairment? An interesting target seemed to be Atg1 (homolog in mammals: Ulk1), which belongs to the initiation complex of macroautophagy (Gelino and Hansen, 2012). Atg1 clusters and activates the subsequent complex around Atg6 (homolog in mammals: Beclin 1), followed by the buildup of the phagophore's source via lipidation (Choi et al., 2013; Menzies et al., 2017). With its link to mTOR, Atg1 works as a transcriptional regulator of macroautophagy (Menzies et al., 2017). An increase of nutrients or growth factors activates mTOR, which subsequently inhibits Atg1, thus macroautophagy (Chang and Neufeld, 2009). Additionally, Atg1 affects starvation-induced macroautophagy, and the cycling of mammalian Atg9 (Young et al., 2006; Lamb et al., 2013). Furthermore, Ulgherait et al., 2014, showed an increased lifespan with a pan-neuronal *atg1* overexpression. Hence, Atg1 appeared a suitable candidate to protect from age-induced memory impairment via overexpressed macroautophagy.

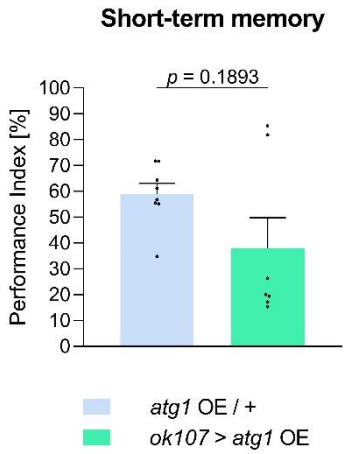

Figure 64: a*tg1* overexpression in the mushroom body impairs memory performance at an already young age.

Short-term memory for 5-day old flies with overexpression (OE) of macroautophagy in the mushroom body (measured directly after training): n = 8 for *atg1* OE / +, n = 7 for *ok107* > *atg1* OE. Statistics: Mann-Whitney test, $^{ns}p \geq 0.05$. Error bars: mean ± SEM.

When I performed short-term memory for the *atg1* overexpression (OE) in the mushroom body (*ok107*-Gal4), I could observe no benefit in these flies' memory performance at 5 days already (Figure 64). Even though one trial showed an increased memory with a performance index of 80 % compared to the control with around 55 %, further tests could not confirm these results. In total, the short-term memory appeared with a lower memory tendency for *ok107* > *atg1* OE.

At least via *atg1*, an up-regulation of macroautophagy resulted in no protective effect for memory. Possibly, the intervention at the initial phase of macroautophagy with Atg1 as its central figure interfered far too much in the system's machinery, followed by no memory gains. Indeed, an *atg1* overexpression could improve lifespan, yet processes to generate memories are costly. Strategic considerations about the energy-intensive cognitive abilities and a longer life could have interfered here.

2.5. The impact of short Neuropeptide F on age-induced memory impairment

2.5.1. Reduced short neuropeptide F in aging animals

In the last chapters, aging's effects were mimicked via deficient macroautophagy in the mushroom body in young flies (Bhukel and Beuschel et al., 2019). Thus, these animals owned overloaded presynaptic plasticity and failed to develop for their age typical aversive olfactory memory. To ascertain a putative mechanism underlying the crucial role of operating macroautophagy in the mushroom body, I searched for a promising candidate, linking autophagy with the emerging effects.

The neuropeptide Y (NPY) occurs in a large amount in the central nervous system of mammals (Botelho and Cavadas, 2015) and plays a role in the learning and memory process (Beck and Pourié, 2013). Interestingly, NPY also has a massive influence on autophagy. For instance, Aveleira et al. have shown in their 2015 paper that NPY acts as an inducer for hypothalamic autophagy. They blocked NPY receptors via the antagonist chloroquine with the consequence of an accumulation of LC3B-II (in *Drosophila*: Atg8-II) and SQSTM1 (idem p62; in *Drosophila*: Ref(2)p), both indicators for deficient macroautophagy. Furthermore, they could show stimulation of autophagy via elevated NPY-levels in mice. The hypothalami of these animals hold increased levels of LC3B-I and a reduced amount of SQSTM1, pointing towards operating autophagic flux (Aveleira et al., 2015b).
The orthologue of NPY in *Drosophila* is short neuropeptide F (sNPF). In this animal model, the gene *sNPF* expresses the ancestor of the four types of sNPF peptides, which all bind one G-protein coupled sNPF-specific receptor (Nässel et al., 2008). This causes a cascade of reactions affecting odor-driven feeding behavior (Lee et al., 2004; Root et al., 2011), growth (Lee et al., 2008), and sleep (Chen et al., 2013). Interestingly, sNPF is generated by manifold neurons in the central nervous system of flies, among them the mushroom body (Johard et al., 2008; Nässel et al., 2008).

As shown before, presynaptic plasticity, denoted via the main scaffold protein Bruchpilot (BRP), increases with age in a brain-wide fashion (Figure 45a, Figure 65a, Gupta et al., 2016; Bhukel and Beuschel et al., 2019). Contrarily, the amount of sNPF decreases dramatically in the mushroom body of 30-day old flies (Figure 65a). Even more intriguingly, 10-day old flies with deficient macroautophagy in the mushroom body (*vt030550* > *atg5* RNAi) also exhibited a reduced sNPF intensity in the target area (Figure 65b). This was an intriguing connection

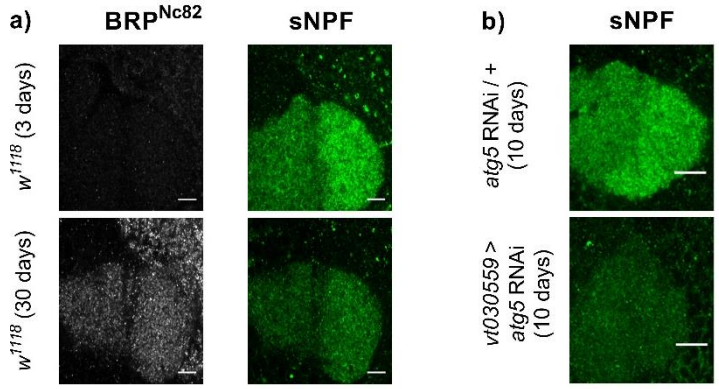

Figure 65: The neuropeptide sNPF decreases with age and deficient macroautophagy.

a) Immunostaingings for Bruchpilot (BRP^{Nc82}; marker for presynaptic plasticity) showed increased intensities for brains of 30-day compared to 3-day old w^{1118} flies. In contrast, short neuropeptide F (sNPF) displayed decreased intensities in the mushroom body, scale bar: 10 µm. b) Immunostainings for sNPF showed decreased intensities in the mushroom body for brains of 10-day old macroautophagy deficient flies (*vt030559* > *atg5* RNAi) compared to the control *atg5* RNAi / +, scale bar: 10 µm. Immunostainings by Anuradha Bhukel from Bhukel and Beuschel et al., 2019.

between sNPF and macroautophagy (Bhukel and Beuschel et al., 2019). Therefore, sNPF was a promising candidate for autocrine signaling in the mushroom body and could help steer presynaptic plasticity to a state of operating memory function (Bhukel and Beuschel et al., 2019).

First, I examined the sNPF-hypomorph $sNPF^{c00448}$. This mutant possessed a similar reduced intensity of sNPF as aging flies plus an increased amount of BRP in the fly brain of 5-day old animals (Figure 66a-b; Bhukel and Beuschel et al., 2019). Comparable to a deficit in macroautophagy, I could observe a decay in the aversive olfactory memory. Thus, short-term memory, tested directly after the training, decreased significantly compared to the wild-type control w^{1118} (Figure 66c). Addressing longer-lasting memory, 1 hour mid-term memory performed similarly (Figure 66d). This memory decay had its origin in the reduced 1 hour anesthesia-sensitive memory (ASM; Figure 66f) since mid-term memory is the sum of two components, the ASM and the anesthesia-resistant memory (ARM). $sNPF^{c00448}$ flies showed no decrease in 1 hour ARM (Figure 66e).

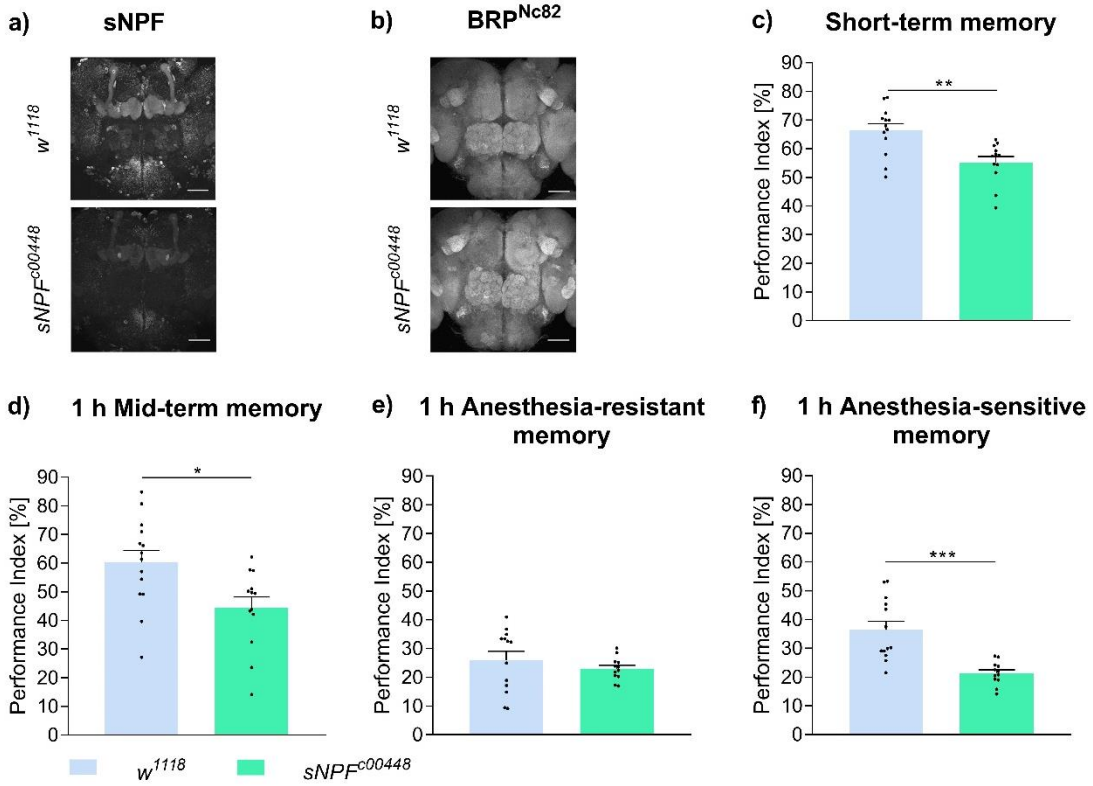

Figure 66: The hypomorph *sNPF^{c00448}* mutant influences presynaptic plasticity and memory formation.

a-b) Immunostaings for 5-day old hypomorph short neuropeptide F flies (*sNPF^{c00448}*), *w^{1118}* as control: a) sNPF intensity decreased in *sNPF^{c00448}*, scale bar: 50 µm. b) Bruchpilot (BRP^{Nc82}; marker for presynaptic plasticity) increased in *sNPF^{c00448}*, scale bar: 50 µm. c-f) Aversive olfactory memory for 5-day old hypomorph short neuropeptide F flies (*sNPF^{c00448}*), *w^{1118}* as control: c) Performance Index for short-term memory (test 3 min after training): n = 13 for *w^{1118}*, n = 12 for *sNPF^{c00448}*. d) Performance Index for 1 hour mid-term memory (test 1 hour after training): n = 14 for *w^{1118}*, n = 13 for *sNPF^{c00448}*. e) Performance Index for 1 hour anesthesia-resistant memory (ice-bad 30 min and test 1 hour after training): n = 13 for *w^{1118}*, n = 12 for *sNPF^{c00448}*. f) Performance Index for 1 hour anesthesia-sensitive memory: Results received via calculation of the median of 1 hour mid-term memory minus the performance indices of 1 hour anesthesia-resistant memory. Statistics: unpaired t-test, $^{**}p < 0.01$, $^{ns}p \geq 0.05$. Error bars: mean ± SEM. Immunostaining by Anuradha Bhukel from Bhukel and Beuschel et al., 2019.

Oddly, the innate behavior of the sNPF-hypomorph *sNPF*^{c00448} mutants showed severe defects (Table 8). Accordingly, the odor acuity was significantly reduced for 4-Methylcyclohexanol (**p = 0.0014) and even more dramatically for 3-Octanol (****p < 0.0001) compared to wild-type *w*^{1118} animals. These results impede the evaluation of the aversive olfactory memory. The appearing deficits in STM, 1 hour MTM and 1 hour ASM could originate in these flies' lack of genuine smell ability. Though, 1 hour ARM was unaffected (Figure 66e). Consequently, all memory results can be taken as true since this memory phase was not affected by the reduced odor acuity. Memory formation seemed to be possible.

	Olfactory acuity	
Genotype	3-Octanol (n)	4-Methylcyclohexanol (n)
w^{1118}	33.21 ± 6.258 (17)	48.33 ± 3.852 (12)
sNPF^{c00448}	- 4.118 ± 4.783 (17)	27.83 ± 4.110 (11)

Table 8: Innate behavior of *sNPF*^{c00448}.

Olfactory acuity of 5-day old sNPF-hypomorph *sNPF*^{c00448} animals was significantly reduced for 3-Octanol and 4-Methylcyclohexanol compared to wild-type *w*^{1118} flies. These results impeded the analysis of the memory phases. Statistics: unpaired t-test, ****p < 0.0001, **p < 0.01. Mean ± SEM.

To address the learning center in the fly brain, I attenuated sNPF in the mushroom body via the driver *ok107*-Gal4. Curiously, these flies showed no reduced deficit in short-term memory or 1 hour mid-term memory (data in Appendix). Immunostainings revealed a missing reduction of the sNPF with this RNAi line (Bhukel, 2018).

To verify our previous results with *sNPF*^{c00448} via a different approach, I investigated the sNPF receptor (sNPF R) and generated a reduction of this in the mushroom body (Figure 67; Bhukel and Beuschel et al., 2019). Similar to deficient macroautophagy in this region and the hypomorph sNPF mutant flies, a decimation of the sNPF receptor lead to a dramatically increased presynaptic plasticity, visible by an increased Bruchpilot (BRP^{Nc82}) intensity in 10-day young flies (Figure 58a, Figure 66b, Figure 67a). As a further look into the presynaptic state of the active zone, I inspected the T-bars in the mushroom body. These electron-dense structures, visible via transmission emission electron microscopy (EM), enlarged with age (Gupta et al., 2016) and defective macroautophagy (Figure 58b). Just the same, I saw in 10-day old animals with a reduced sNPF receptor in the mushroom body (Figure 67b; Bhukel and Beuschel et al., 2019). The T-bar shapes were wide and loose compared to the compact and

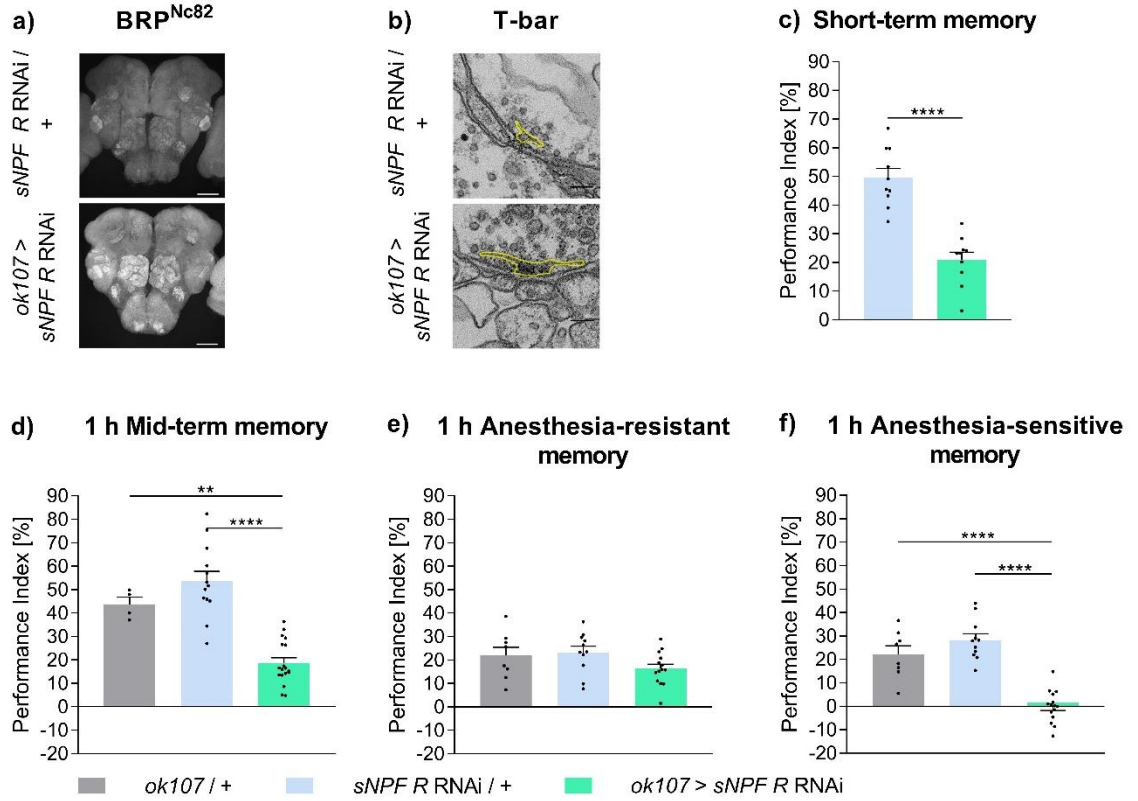

Figure 67: Reduced sNPF receptor in the mushroom body increases presynaptic plasticity and impairs memory formation.

a) Immunostaings for Bruchpilot (BRP^{Nc82}; marker for presynaptic plasticity) showed an increased intensity for brains of 10-day old *ok107 > sNPF R* RNAi animals compared to the control *sNPF R* RNAi / +, scale bar: 50 µm. b) Electron micrographs showing the T-bar of the mushroom body's calyx for 10-day old *ok107 > sNPF R* RNAi and *sNPF R* RNAi / + flies, scale bar: 100 nm. c-f) Aversive olfactory memory for 10-day old *ok107 > sNPF R* RNAi animals plus their controls *ok107* / + and *sNPF R* RNAi / +. c) Performance Index for short-term memory (test directly after the training): n = 10 for *sNPF R* RNAi / +, n = 10 for *ok107 > sNPF R* RNAi. d) Performance Index for 1 hour mid-term memory (test 1 hour after training): n = 4 for *ok107* / +, n = 13 for *sNPF R* RNAi / +, n = 18 for *ok107 > sNPF R* RNAi. e) Performance Index for 1 hour anesthesia-resistant memory (ice-bad 30 min and test 1 hour after training): n = 8 for *ok107* / +, n = 11 for *sNPF R* RNAi / +, n = 14 for *ok107 > sNPF R* RNAi. f) Performance Index for 1 hour anesthesia-sensitive memory: Results received via calculation of the median of 1 hour mid-term memory minus the individual performance indices of 1 hour anesthesia-resistant memory. Statistics: unpaired t-test for 2 genotypes to analyze, for 3 genotypes one-way ANOVA with Sidak's multiple comparisons *post hoc* test, ****$p < 0.0001$, **$p < 0.01$, $^{ns}p \geq 0.05$. Error bars: mean ± SEM. Immunostainings and electron micrographs by Anuradha Bhukel from Bhukel and Beuschel et al., 2019.

sharp contours in the controls. Next, I tested aversive olfactory memory for these flies. They performed poorly at the young age of ten days already. Short-term memory showed a 30 % lower performance index than its control. Similarly, 1 hour mid-term memory (MTM) and its labile component 1 hour anesthesia-sensitive memory (ASM) hold severe defects, for ASM even around zero (Figure 67d, f). In contrast, these animals possessed stable 1 hour anesthesia-resistant memory (ARM) (Figure 67e). Thereupon, I reproduced these memory results with another mushroom body-specific diver, *vt030559*-Gal4. Short-term memory decreased grossly by 20 % and 1 hour mid-term memory by 12 % performance index (Figure 68a-b). Contrarily, sNPF receptor loss in the mushroom body revealed no significant memory deficit in the ARM, the more robust component with age (Figure 68c). Again, 1 hour ASM

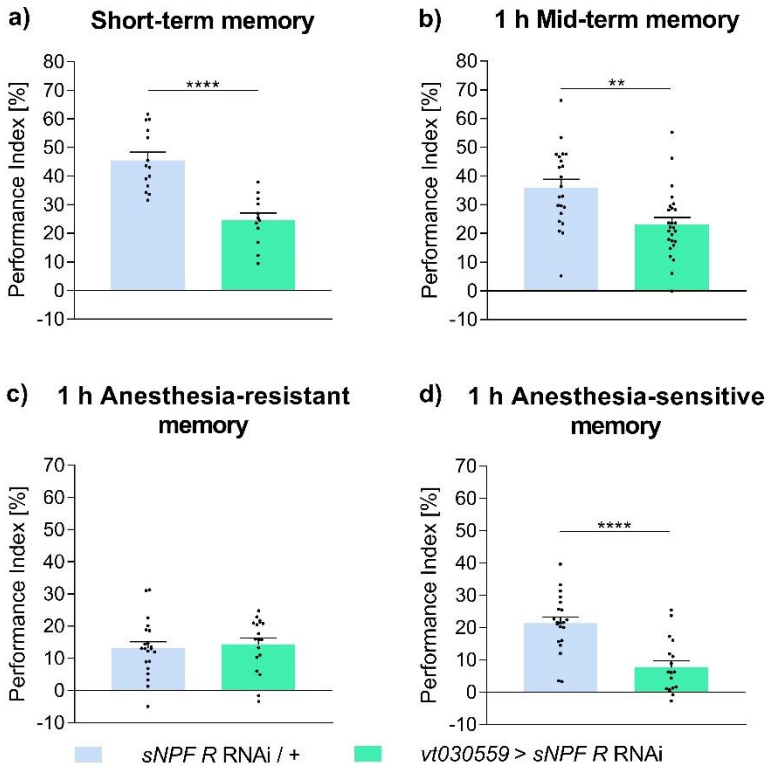

Figure 68: Memory of deficient sNPF receptor with another mushroom body Gal4 driver.

Aversive olfactory memory for 10-day old *vt030559 > sNPF R* RNAi animals plus their control *sNPF R* RNAi / +. a) Performance Index for short-term memory (test directly after the training): n = 14 for *sNPF R* RNAi / +, n = 12 for *vt030559 > sNPF R* RNAi. b) Performance Index for 1 hour mid-term memory (test 1 hour after training): n = 22 for *sNPF R* RNAi / +, n = 26 for *vt030559 > sNPF R* RNAi. c) Performance Index for 1 hour anesthesia-resistant memory (ice-bad 30 min and test 1 hour after training): n = 21 for *sNPF R* RNAi / +, n = 18 for *vt030559 > sNPF R* RNAi. d) Performance Index for 1 hour anesthesia-sensitive memory: Results received via calculation of the median of 1 hour mid-term memory minus the individual performance indices of 1 hour anesthesia-resistant memory. Statistics: unpaired t-test, ****$p < 0.0001$, **$p < 0.01$, $^{ns}p \geq 0.05$. Error bars: mean ± SEM.

dropped, comparable to the labile memory of 30-day old flies and macroautophagy-missing 10-day old flies (Figure 68d, Figure 45d, Figure 50b).

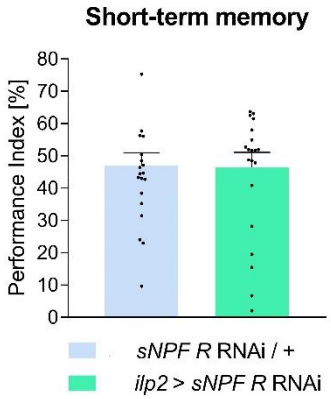

Figure 69: Reduced sNPF receptor in *pars intercerebralis* shows no memory decay.

Short-term memory for 10-day old flies of *ilp2* > *sNPF R* RNAi compared to the control *sNPF R* RNAi / + (test 3 min after training): n = 21 for *sNPF R* RNAi / +, n = 21 for *ilp2* > *sNPF R* RNAi. Statistics: Mann-Whitney test, $^{ns}p \geq 0.05$. Error bars: mean ± SEM.

To nail down these effects of attenuated memory as a consequence of missing sNPF signaling in the mushroom body, I examined other sNPF receptor expressing tissues like the *pars intercerebralis*. This region in the central nervous system of adult *Drosophila* possesses sNPF receptors, comparable to the mushroom body (Nässel et al., 2008; Nässel et al., 2013). When I attenuated the sNPF receptor in the *pars intercerebralis* via *ilp2*-Gal4, no deficit in short-term memory could be observed (Figure 69). Additionally, these flies showed even a significantly reduced presynaptic plasticity, visible via a decreased intensity of Bruchpilot in immunostainings (Bhukel, 2018). Thus, the effects of lowered sNPF signaling seemed to originate in the mushroom body.

Within a further dissection of the mushroom body, I suppressed the lobes α, β, and γ with *mb247*-Gal80 so that the focus was set on the prime lobes α' and β'. In contrast to my previous results about the mushroom body signaling, I could find no decrease in the memory performance. Even though the short-term memory was significantly reduced compared to the driver control *mb247*-Gal80 ;; *ok107*-Gal4, a namely difference to the RNAi control *sNPF R* RNAi / + was missing (Figure 70a). Furthermore, 1 hour mid-term memory and 1 hour anesthesia-resistant memory showed no salience (Figure 70b-c). For 1 hour anesthesia-sensitive memory, a significant rise could be observed compared to the driver control. However, the RNAi control appeared with a similar performance index as the sNPF receptor reduction in the a' and β' lobes (Figure 70d). Thus, the prime lobes seemed to be no key area for sNPF signaling, although these parts of the mushroom body are required to obtain and maintain aversive olfactory memory (Krashes et al., 2007).

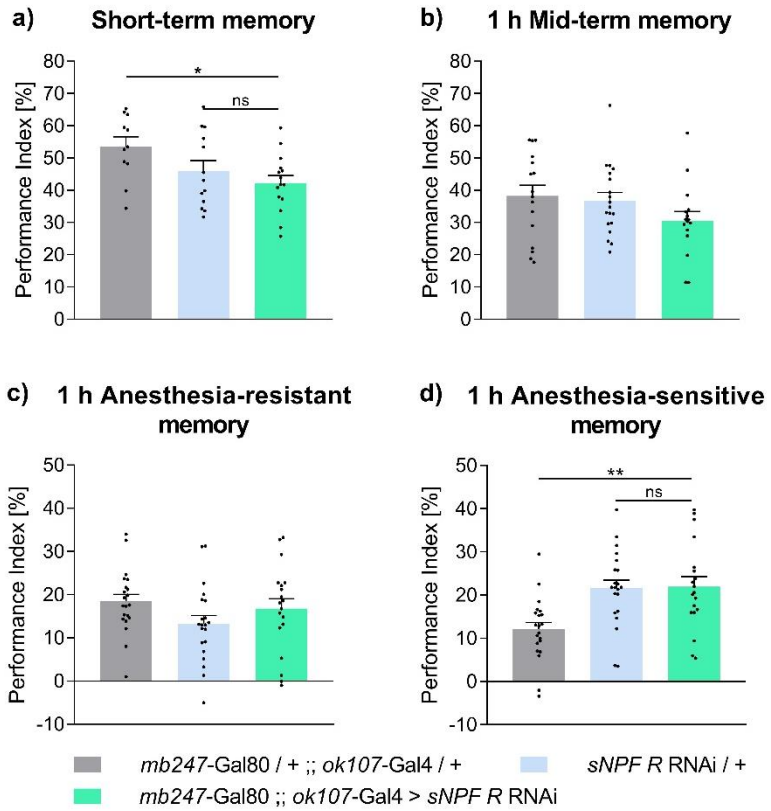

Figure 70: Deficient sNPF signaling, only diminished in the α'/β' lobes of the mushroom body, shows no memory decay.

Aversive olfactory memory for *sNPF R* RNAi expressed in the mushroom body via *ok107*-Gal4 with simultaneous suppression in the α/β and γ lobes (*mb247*-Gal80), 10-day old, *mb247*-Gal80 / + ;; *ok107*-Gal4 / + as driver control, *sNPF R* RNAi / + as RNAi control. a) Performance Index for short-term memory (test 3 min after training): n = 11 for *mb247*-Gal80 / + ;; *ok107*-Gal4 / +, n = 13 for *sNPF R* RNAi / +, n = 15 for *mb247*-Gal80 ;; *ok107*-Gal4 > *sNPF R* RNAi. b) Performance Index for 1 hour mid-term memory (test 1 hour after training): n = 16 for *mb247*-Gal80 / + ;; *ok107*-Gal4 / +, n = 19 for *sNPF R* RNAi / +, n = 16 for *mb247*-Gal80 ;; *ok107*-Gal4 > *sNPF R* RNAi. c) Performance Index for 1 hour anesthesia-resistant memory (ice-bad 30 min and test 1 hour after training): n = 21 for *mb247*-Gal80 / + ;; *ok107*-Gal4 / +, n = 21 for *sNPF R* RNAi / +, n = 19 for *mb247*-Gal80 ;; *ok107*-Gal4 > *sNPF R* RNAi . b) Performance Index for 1 hour anesthesia-sensitive memory: Results received via calculation of the median of 1 hour mid-term memory minus the individual performance indices of 1 hour anesthesia-resistant memory.Statistics: ordinary one-way ANOVA with Sidak's *post hoc* test, $^{**}p < 0.01$, $^{*}p > 0.05$, $^{ns}p \geq 0.05$. Error bars: mean ± SEM.

To avert developmental effects, I performed temperature-sensitive Gal80 memory experiments. Here, the sNPF receptor RNAi was suppressed until the flies' adulthood by shifting them to a higher temperature after the eclosion. This way, the Gal4 suppression was restricted to these flies' maturity (McGuire et al., 2003). Oddly, these flies showed no detectable defect in their short-term memory performance (Figure 71). Thus, the depletion of downregulation of the sNPF receptor could probably not be sufficiently achieved when restricting the RNA interference to only the post-eclosion adult stages. In this way, a remaining turnover of developmentally expressed sNPF receptors could remain, and interfere with the results.

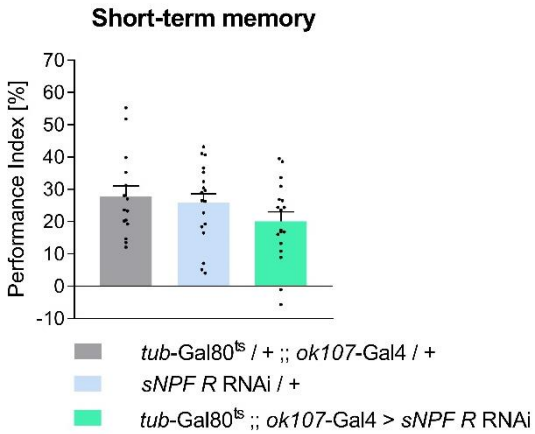

Figure 71: No memory impairment when deficient sNPF signaling was only expressed to adulthood.

Short-term memory for 10-day old flies with the deficient sNPF receptor in the mushroom body expressed from adulthood on (measured directly after training): n = 15 for *tub*-Gal80^{ts} / + ;; *ok107*-Gal4 / +, n = 18 for *sNPF R* RNAi / +, n = 18 for *tub*-Gal80^{ts} ;; *ok107*-Gal4 > *sNPF R* RNAi. Statistics: ordinary one-way ANOVA with Sidak's *post hoc* test, $^{ns}p \geq 0.05$. Error bars: mean ± SEM.

Oddly, the innate smell behavior with both odors showed severe defects for the mushroom body-specific *sNPF R* attenuation, and slightly with 4-Methylcyclohexanol for the downregulation in the *pars intercerebralis*. I already saw similar results with sNPF-hypomorph *sNPF*^{c00448} flies (Table 9). This made the interpretation of the memory findings complicated since the measured defects could be reasoned by the missing genuine smell ability. However, the 1 hour ARM was unaffected for sNPF receptor reduced flies, comparable to *sNPF*^{c00448}, indicating general learning and memory formation was possible (Figure 67e, Figure 68c; Figure 66e).

Genotype	Olfactory acuity	
	3-Octanol (n)	4-Methylcyclohexanol (n)
sNPF R RNAi / + (2 replicates)	70.44 ± 3.513 (17)	87.04 ± 2.267 (12)
	72.00 ± 8.729 (8)	88.22 ± 1.790 (9)
ok107 > *sNPF R* RNAi (2 replicates)	37.40 ± 3.636 (22)	59.03 ± 4.683 (28)
	24.71 ± 7.449 (9)	40.14 ± 4.157 (9)
sNPF R RNAi / +	70.33 ± 5.857 (12)	76.08 ± 4.885 (14)
vt030559 > *sNPF R* RNAi	36.94 ± 6.466 (12)	53.26 ± 8.863 (12)
sNPF R RNAi / +	60.39 ± 5.068 (9)	93.88 ± 1.076 (8)
ilp2 > *sNPF R* RNAi	49.50 ± 6.892 (12)	86.66 ± 2.830 (8)
mb247-Gal80 / + ;; *ok107*-Gal4 / +	54.87 ± 7.412 (10)	63.94 ± 7.238 (10)
sNPF R RNAi / +	57.13 ± 5.541 (7)	65.40 ± 6.073 (8)
mb247-Gal80 ;; *ok107*-Gal4 > *sNPF R* RNAi	39.01 ± 10.41 (12)	33.02 ± 13.41 (12)
tub-Gal80^{ts} / + ;; *ok107*-Gal4 / +	79.16 ± 4.305 (14)	70.43 ± 7.699 (16)
sNPF R RNAi / +	67.02 ± 5.510 (16)	69.30 ± 6.143 (16)
tub-Gal80^{ts} ;; *ok107*-Gal4 > *sNPF R* RNAi	73.55 ± 5.054 (13)	82.03 ± 4.681 (13)

Table 9: Innate behavior of the attenuated sNPF receptor in different tissues.

Olfactory acuities for 3-Octanol (OCT) and 4-Methylcyclohexanol (MCH) for a deficient sNPF receptor in different tissues in 10 day-old flies. Both odor acuities were significantly impaired with a downregulation in the mushroom body, and additionally MCH in the *pars intercerebralis* (*ilp2*-Gal4) (see Table 25). Relevant *p*-values compared to the controls: *ok107* > *sNPF R* RNAi: replicate 1: OCT ****$p < 0.0001$, MCH ***$p = 0.0005$; replicate 2: OCT ***$p = 0.0009$, MCH ****$p < 0.0001$. *vt030559* > *sNPF R* RNAi: OCT ***$p = 0.0009$, MCH *$p = 0.0277$. *ilp2* > *sNPF R* RNAi: MCH *$p = 0.0319$.

Statistics: unpaired t-test for 2 genotypes to analyze, for 3 genotypes one-way ANOVA with Sidak's multiple comparisons *post hoc* test (parametric) or Kruskal-Wallis with Dunn's *post hoc* test (nonparametric), ****$p < 0.0001$, ***$p < 0.001$ *$p < 0.05$, $^{ns}p \geq 0.05$. Mean ± SEM.

2.5.2. An overexpression of short neuropeptide F fails to protect from age-induced memory impairment

When sNPF decreases with age and an early memory impairment occurs in sNPF-deficient flies (Figure 65, Figure 66), could a genetic increase of this protein protect from age-induced

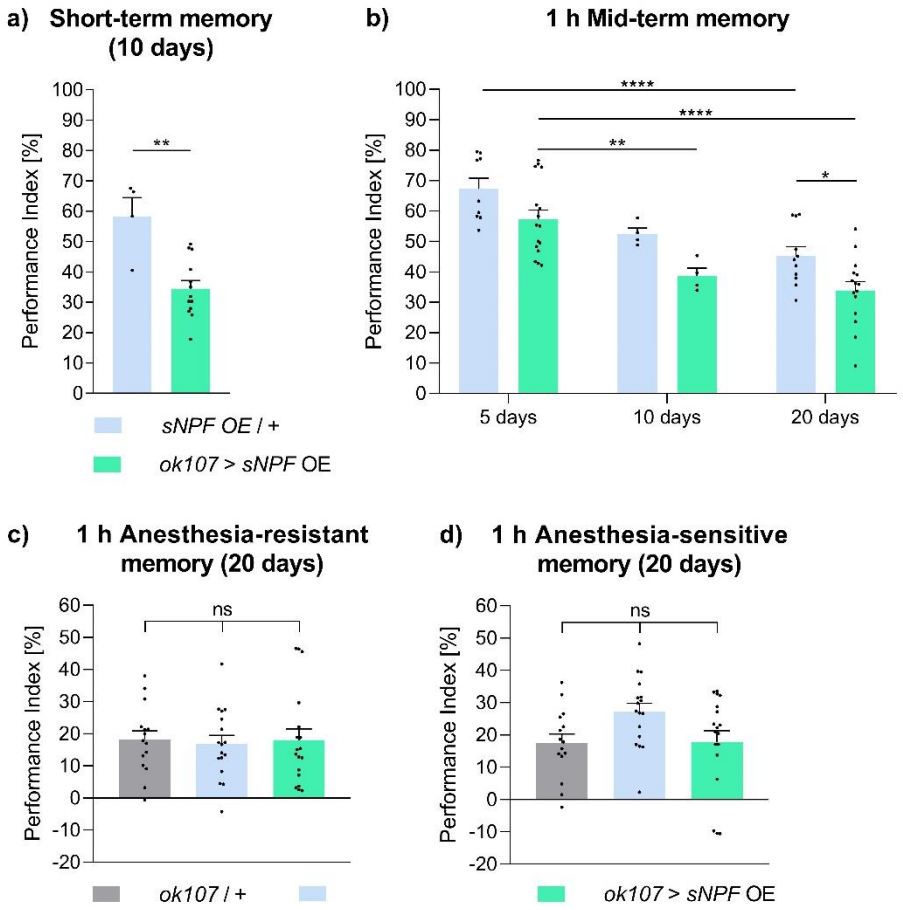

Figure 72: An overexpression of *sNPF* does not prevent age-induced memory impairment.

Aversive olfactory memory for an overexpression (OE) of sNPF in the mushroom body. a) Short-term memory (test directly after training) for 10-day old flies: n = 4 *sNPF* OE / +, n = 13 for old *ok107 > sNPF* OE. b) Performance Index for 1 hour mid-term memory (test 1 hour after training): n = 9 for 5-day old, n = 4 for 10-day and n = 11 for 20-day old *sNPF* OE / +, n = 16 for 5-day old, n = 4 for 10-day old and n = 15 for 20-day old *ok107 > sNPF* OE. c) Performance Index for 1-hour anesthesia-resistant memory (ice-bad 30 min and test 1 hour after training) of 20-day old flies: n = 15 for *ok107* / +, n = 17 for *sNPF* OE / +, n = 18 for *ok107 > sNPF* OE. d) Performance Index for 1 hour anesthesia-sensitive memory: Results received via calculation of the median of 1 hour mid-term memory minus the individual performance indices of 1 hour anesthesia-resistant memory. Statistics: unpaired t-test for a, two-way ANOVA with Sidak's post hoc test for b, ordinary one-way ANOVA with Sidak's post hoc test for c and d, ****$p < 0.0001$, **$p < 0.01$, *$p < 0.05$, $^{ns}p \geq 0.05$. Error bars: mean ± SEM.

memory decay? For this reason, we examined an overexpression (OE) of short neuropeptide F (sNPF) in the mushroom body, which is the center of generating learning and memory storage. Interestingly, brain immunostainings of 5- versus 20-day old *ok107* > sNPF OE flies showed a similar intensity for Bruchpilot, which serves as a marker for age-induced increased synaptic plasticity (Gupta et al., 2016; Bhukel, 2018). In contrast, the control *sNPF* OE / + had more Bruchpilot in 20-day than in 5-day old animals (Bhukel, 2018). Thus, protection could be possible. When I examined the short-term memory, flies with an sNPF overexpression in the mushroom body already performed worse than their control at 10 days (Figure 72a).
Additionally, these animals showed slightly decreased 1 hour mid-term memory at 5 days, which drops significantly further at 10 days and stays lower than the control at 20 days (Figure 72b). At 20 days, the performance of the tested groups could not be distinguished for 1 hour anesthesia-resistant and anesthesia-sensitive memory (Figure 72c-d). Hence, an *sNPF* overexpression seems valid to block the age-induced Bruchpilot increase, yet not enough to protect the memory from aging effects.

Thus, I tested the flies' memory with two copies *sNPF* overexpression in the mushroom body (Figure 73). Again, the memory could not be protected. It already dropped significantly for 1 hour mid-term memory at 5 days and was still reduced with more age (Figure 73a). Curiously, neither the control *sNPF* OE/+;*sNPF* OE/+ nor *ok107* > *sNPF* OE;*sNPF* OE showed a decay with age. Though, the performance of the control was already low with 46 % for 5-day 1 hour memory. Furthermore, no difference to the control appeared in 1 hour anesthesia-resistant memory (Figure 73b), and only a drop could be observed for 5-day old animals, yet not at 20 days (Figure 73c). Oddly, 1 hour anesthesia-resistant memory decreases for both groups with age, plus the anesthesia-sensitive component stays the same for the control and even increases for the *sNPF* overexpression.
Taken together, overexpression of *sNPF* in the mushroom body could not prevent age-induced memory impairment, neither with one nor with two overexpression constructs.

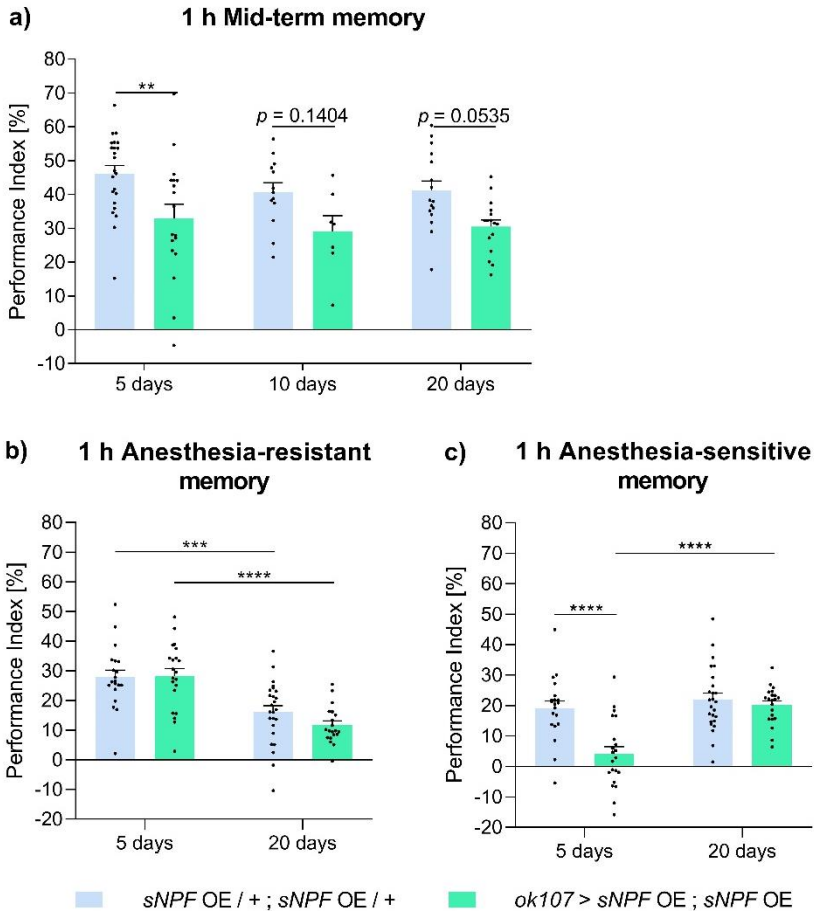

Figure 73: No memory benefit with two copies of *sNPF* overexpression.

Aversive olfactory memory for a two copies overexpression (OE) of sNPF in the mushroom body. a) Performance Index for 1 hour mid-term memory (test 1 hour after training): n = 23 for 5-day old, n = 13 for 10-day and n = 16 for 20-day old *sNPF* OE/+;*sNPF* OE/+, n = 18 for 5-day old, n = 7 for 10-day old and n = 16 for 20-day old *ok107* > *sNPF* OE;*sNPF* OE. c) Performance Index for 1-hour anesthesia-resistant memory (ice-bad 30 min and test 1 hour after training): n = 20 for 5-day old and n = 25 for 20-day old *sNPF* OE/+;*sNPF* OE/+, n = 21 for 5-day old and n = 21 for 20-day old *ok107* > *sNPF* OE;*sNPF* OE. d) Performance Index for 1 hour anesthesia-sensitive memory: Results received via calculation of the median of 1 hour mid-term memory minus the individual performance indices of 1 hour anesthesia-resistant memory. Statistics: two-way ANOVA with Sidak's *post hoc* test, ****p < 0.0001, ***p < 0.001, **p < 0.01, ^{ns}p ≥ 0.05. Error bars: mean ± SEM.

2.6. A reduced insulin signaling pathway protects from aging yet does not have any benefit on memory

Several laboratories have proven that reducing the insulin signaling pathway can extend lifetime. Thus, the lifespan can be increased due to a mutation in the insulin receptor or its substrate Chico (Clancy et al., 2001; Tatar et al., 2001). Furthermore, the ablation of the median neurosecretory cells (MNC) in the *pars intercerebralis*, which harbor the insulin-producing cells (IPC), shows similar results (Figure 74; Broughton et al., 2005). The IPCs are homolog to the pancreatic beta cells in mammals, and the *Drosophila* insulin-like peptides (ILP) of the brain, 2, 3, and 5, become produced here (Nässel et al., 2013). In flies, one insulin receptor (InR) exists while eight ILPs are active in flies (Nässel et al., 2013). Thereby, each

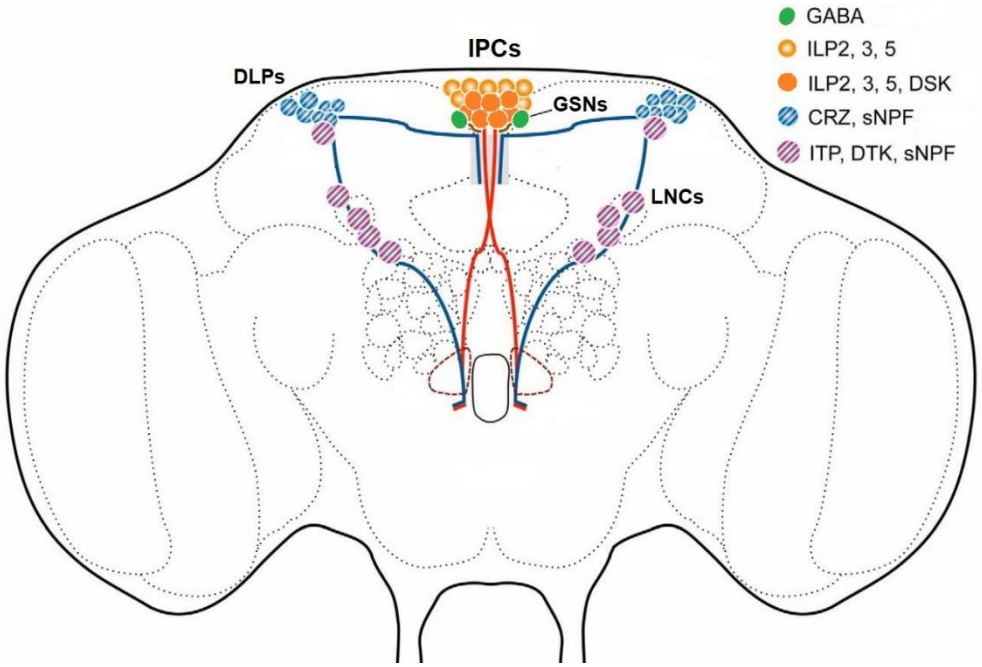

Figure 74: Insulin-producing cells (IPC) in the fly brain, a homolog to the pancreatic beta cells in mammals.

Embedded in the *pars* intercerebralis, the IPCs (orange) produce the brain insulin-like peptides (ILP 2, 3, and 5) and some the saturation hormone drosulfakinin (DSK) (Söderberg et al., 2012). The IPCs are controlled by the dorsal lateral peptidergic neurons (DLP, blue), expressing short neuropeptide F (sNPF) and corazonin (CRZ), and the lateral neurosecretory cells (LNC, purple), which release the ion transport peptide (ITP), *Drosophila* tachykinin (DTK), and also sNPF (Kahsai et al., 2010; Kapan et al., 2012; Gáliková et al., 2018). Additionally, GABAergic neurons (GSN, green) inhibit the IPCs, which, in turn, are suppressed by the postprandial from the fat body released Upd2 (Enell et al., 2010). Image modified from Nässel et al., 2013.

ILP has its individual spatio-temporal expression in the tissues and different answers to nutritional stimulation (Grönke et al., 2010; Piper and Partridge, 2018).

Interestingly, within longevity experiments of lacking ILPs, solely a mutation in ILP2, plus its combination with an ILP3 mutation, could delay aging (Grönke et al., 2010). Thus, only some ILPs seem to be involved in aging processes. Do they also possess different memory patterns? Could lifespan protection be accompanied by a robust memory performance at an older age? Instead, short-term memory (STM) tests revealed a severe memory decrease for *ilp2* and *ilp2-3* at the young age of 5 days already (Figure 75a, b). The sole *ilp3* mutation showed a similar severe memory drop as *ilp2* (Figure 75c). Interestingly, the combined *ilp2-3* demonstrated no

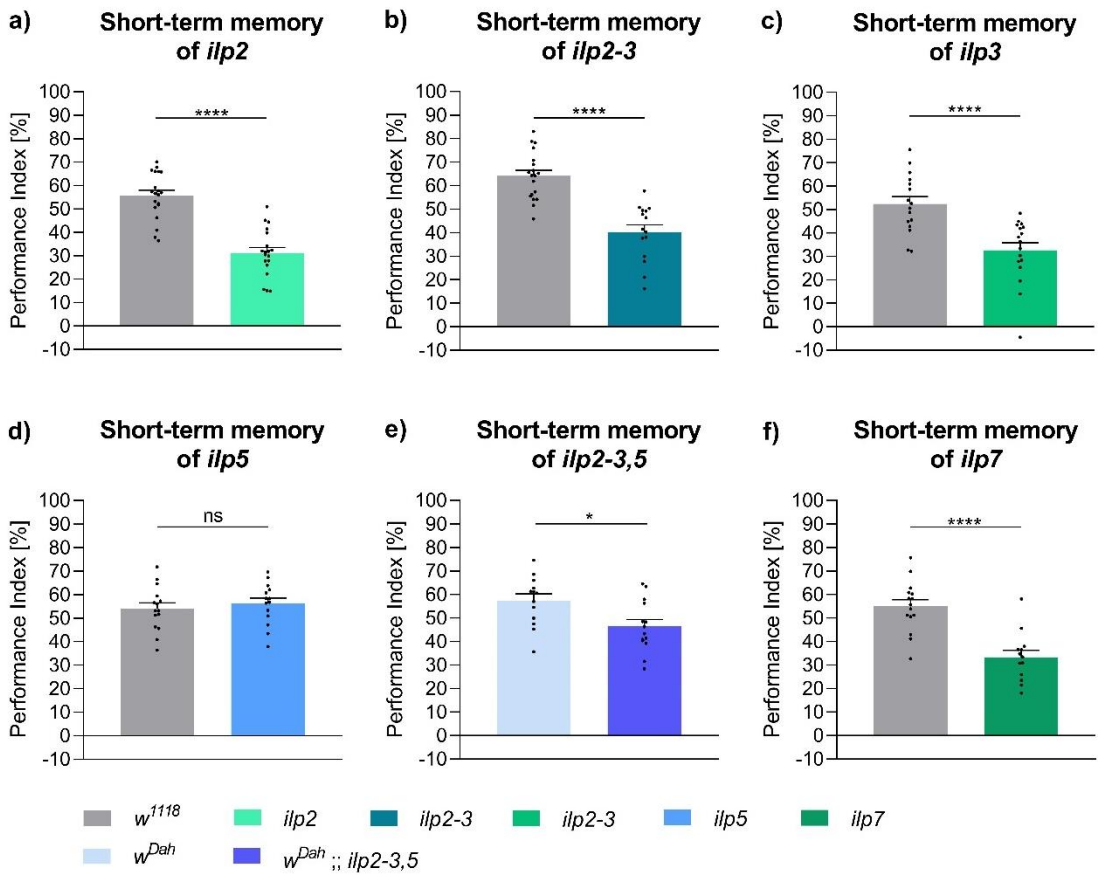

Figure 75: Various short-term memory profiles of the different *ilp* mutants.

Aversive olfactory short-term memory (test directly after training) of different ILP deficient mutants with their isogenetic background as control, 5-day old: a) n = 20 for w^{1118}, n = 19 for *ilp2*. b) n = 19 for w^{1118}, n = 15 for *ilp2-3*. c) n = 16 for w^{1118}, n = 17 for *ilp3*. d) n = 15 for w^{1118}, n = 14 for *ilp5*. e) n = 13 for w^{Dah}, n = 14 for w^{Dah} ;; *ilp2-3,5*. f) n = 15 for w^{1118}, n = 13 for *ilp7*. Statistics: unpaired t-test (parametric) or Mann-Whitney test (nonparametric), ****$p < 0.0001$, *$p < 0.05$, $^{ns}p \geq 0.05$. Error bars: mean ± SEM.

additive memory decay of its two missing components (see Table 10). Among the brain ILPs, only the STM for *ilp5* stayed on the same level as its wild-type control w^{1118} (Figure 75d, Table 10). It seems like a lack of ILP5 could be compensated by the other two brain ILPs. Grönke et al., 2010, saw a raised expression level of ILP3 in *ilp5*, yet ILP2 stayed the same (Table 10). Was ILP3 the driving force for a wild-type memory performance? In *ilp2*, the mutant with the enhanced lifespan, ILP3 and 5 are dramatically increased, though more ILP3 could not compensate the memory issues of *ilp2 (*Figure 75a, Table 10; Grönke et al., 2010). In contrast, an *ilp3* knockout entails a decreased expression of ILP2 and 5 (Table 10; Grönke et al., 2010). Accordingly, ILP2 is automatically down here. In conclusion, ILP2 could be the critical player for memory, and maybe a standard ILP2 amount in *ilp5* is adequate to reach a wild-type memory level. Likewise, ILP5 is perhaps not needed for memory acquisition.

Grönke et al., 2010, also observed an immensely increased longevity through the downregulation of all brain ILPs, *ilp2-3,5*, combined with a *Wolbachia*-infection, whereas uninfected *ilp2-3,5* mutants did not hold this effect. Here, the used wild-type strain *white Dahomey* (w^{Dah}) served as a natural host of the endosymbiotic bacterium *Wolbachia pipientis* (Grönke et al., 2010). However, STM tests of *ilp2-3,5* in w^{Dah} background revealed worse memory than w^{Dah} alone (Figure 75e), though this memory drop turned out to be lower than for

knockout mutants	*ilp2*	*ilp2-3*	*ilp3*	*ilp5*	w^{Dah} ; *ilp2-3,5*	*ilp7*
Short-term memory	↓	↓	↓	=	↓	↓
Relative STM change	- 45 %	- 37 %	- 37 %	+ 4 %	- 19 %	- 40 %
Relative expression level of the brain ILPs (Grönke et al., 2010)	3 ↑, 5 ↑	5 ↑	2 ↓, 5 ↓	2 =, 3 ↑	-	(2 ↓), 3 ↓
Lifespan (Grönke et al., 2010)	↑	↑	=	=	↑	=
localization (Nässel et al., 2013)	brain	brain	brain	brain, renal tubules	brain	ventral nerve cord

Table 10: Overview of the tested ilp knockouts.

Short-term memory (STM) trend and its relative change (each STM mean normalized to the respective control mean performance index (see Table 25)), plus some parameters from the literature. ‘ = ’ means no change, ‘ ( ) ‘ means change but not significant.

ilp2 or *ilp2-3* mutants (Table 10). Could the better STM, compared to *ilp2* or *ilp3* mutations, result from the additional downregulation of *ilp5* or the *Wolbachia* infection? The *Wolbachia*-positive control w^{Dah} and the uninfected w^{1118} performed similarly. Thus, a reduction of ILP5 could support memory acquisition, as we saw for the *ilp5* knockout (Figure 75d). Interestingly, a lack of ILP7, expressed outside of the brain by IPCs in the abdominal ventral nerve cord, showed severe STM deficits as well (Figure 75f, Table 10; Nässel et al., 2013).

A look into 1 hour mid-term memory (MTM) revealed a similar performance as in STM. The 1 hour MTM decayed dramatically by 30 % performance index (PI) for *ilp2* mutants (Figure 76a) and by 22 % PI for *ilp2-3* mutants (Figure 76b). Contrarily, the *ilp5* mutation again owned the same memory level as w^{1118} (Figure 76c). The differentiation of 1 hour MTM in its components, anesthesia-resistant (ARM) and anesthesia-sensitive memory (ASM), exhibited a massive ARM drop for *ilp2-3* (17 % PI, Figure 76e) and a moderate one for *ilp2* (9 % PI, Figure 76d). Consequently, 1 hour ASM was severely reduced for *ilp2* (17 % PI, Figure 76f), and no deficit could be observed for *ilp2-3* (Figure 76g). Thus, a lack of ILP2 could namely prolong life (Grönke et al., 2010), yet memory acquisition and maintenance were dramatically reduced in all memory phases at a young age already. ARM and especially ASM decreased significantly. On the contrary, the combined mutation of *ilp2-3* suffered only in STM and the normally consolidated ARM, yet not in the labile ASM component. Possibly, a lack of ILP3 stabilizes ASM, and ILP3 is especially needed for ARM. This was also seen in flies with downregulated ILP3 in the IPCs (Tanabe et al., 2017), where a significant decrease occurred in repetitive massed training ARM after 24 hours.

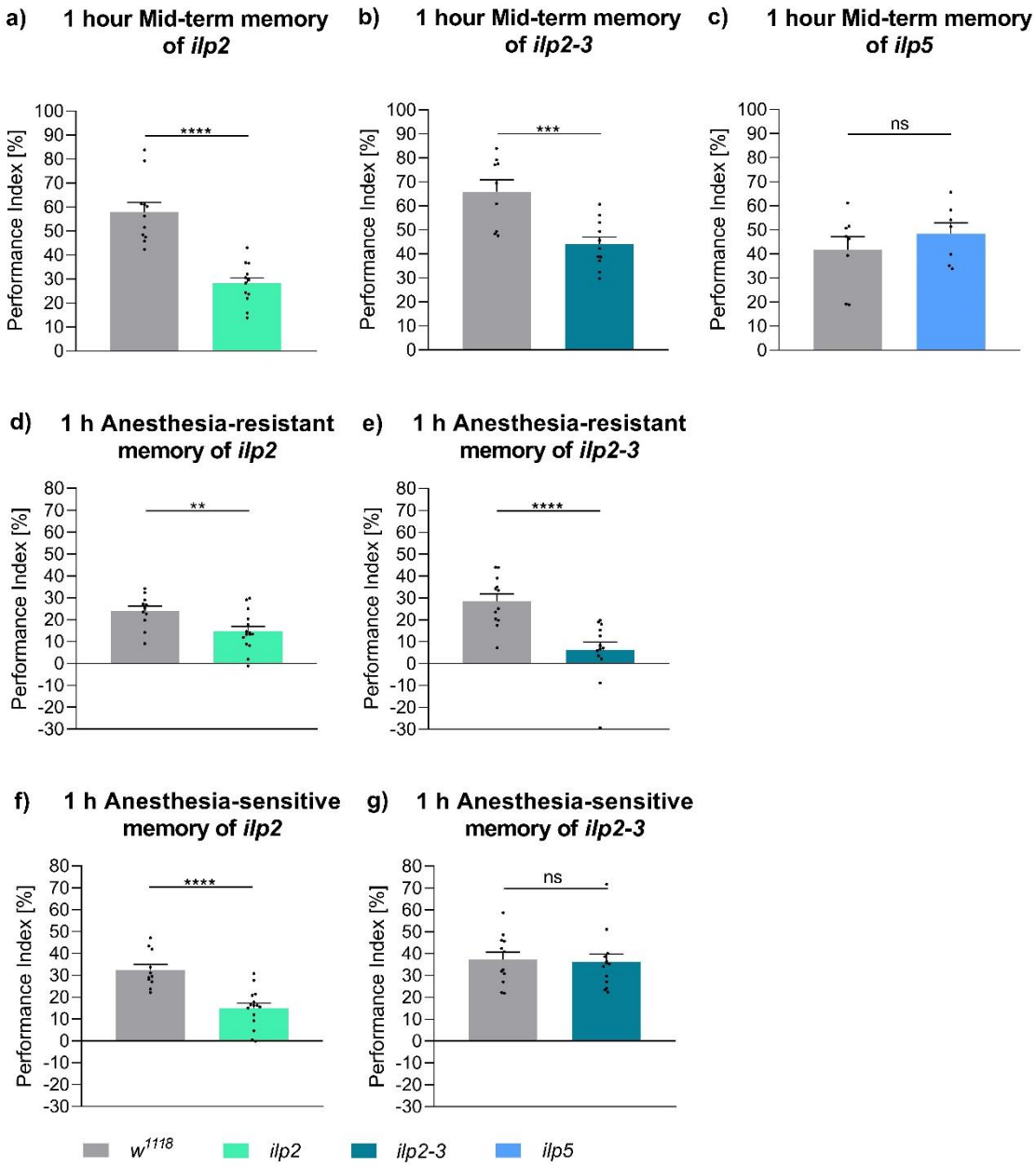

Figure 76: *ilp* mutants exhibit similar long-lasting memory as their short-term pattern.

a-c) 1 hour Mid-term memory (test 1 hour after training) for 5 -day old ILP mutants with their isogenic background as control. a) n = 11 for w^{1118}, n = 13 for *ilp2*. b) n = 9 for w^{1118}, n = 11 for *ilp2-3*. c) n = 8 for w^{1118}, n = 7 for *ilp5*. d-e) 1 hour anesthesia-resistant memory (ice-bad 30 min and test 1 hour after training) for 5-day old *ilp2* and *ilp2-3* mutants: d) n = 11 for w^{1118}, n = 15 for *ilp2*. e) n = 12 for w^{1118}, n = 13 for *ilp2-3*. f-g) 1 hour anesthesia-sensitive memory for 5-day old *ilp2* and *ilp2-3* mutants.: Results were received via calculation of the median of 1 hour mid-term memory minus the individual performance indices of 1 hour anesthesia-resistant memory. Statistics: unpaired t-test (parametric) or Mann-Whitney test (nonparametric), ****p < 0.0001, ***p < 0.001, **p < 0.01 $^{ns}p \geq 0.05$. Error bars: mean ± SEM.

Next, I explored the memory of aged animals. Only a lack of ILP5 demonstrated no memory decay (Figure 75d, Figure 76c). Though, this mutant could not profit from an improved longevity effect (Grönke et al., 2010). Investigations of 30-day old *ilp5* mutants revealed neither increased nor decreased STM and 1 hour MTM compared to aged w^{1118} (Figure 77, c).

To test if an enhanced life expectancy could protect memory at a higher age, I tried the *Wolbachia*-positive *ilp2-3,5* animals. Their STM appeared less severe dropped than *ilp2* or *ilp2-3* mutants in young animals (Figure 75; Table 10). However, tests with 30-day old flies showed no benefit as well. Similar to young animals (Figure 75e), older *Wolbachia*-positive *ilp2-3,5* had decreased STM (Figure 77b), and 1 hour MTM dropped as well (Figure 77d). Like for an *ilp2* mutation, a connection between increased longevity and better memory at higher

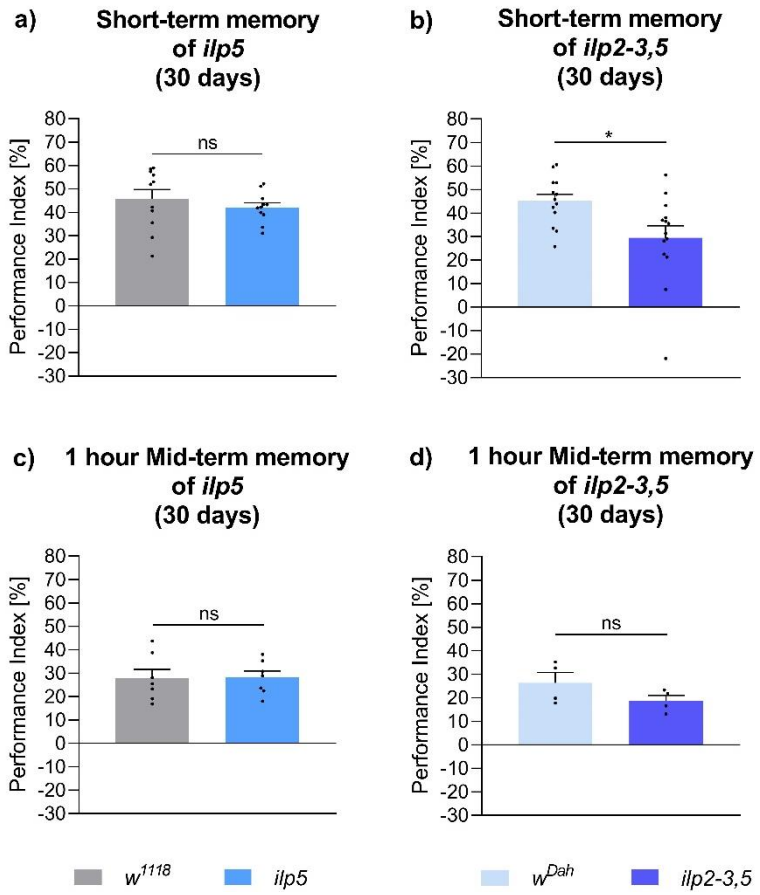

Figure 77: *ilp* mutations can not protect from age-induced memory impairment.

The aversive olfactory memory of *ilp5* or *ilp2-3,5* show similar reduced memory at 30 days as their isogenic background control. a-b) Short-term memory (test directly after training): a) n = 11 for w^{1118}, n = 11 for *ilp5*. b) n = 13 for w^{Dah}, n = 14 for *ilp2-3,5*. c-d) 1 hour mid-term memory (test 1 hour after training): c) n = 7 for w^{1118}, n = 7 for *ilp5*. d) n = 4 for w^{Dah}, n = 4 for *ilp2-3,5*. Statistics: unpaired t-test, *$p < 0.05$, $^{ns}p \geq 0.05$. Error bars: mean ± SEM.

age via a restriction of the brain ILPs could not be confirmed. Additionally, the investigated ILP mutations could not prevent age-induced memory impairment.

Of course, the tested mutants missed the respective ILPs during the developmental stages, and the insulin and insulin-like growth factor-1 (IGF-1) signaling pathway is essential during larval growth (Kannan and Fridell, 2013). Even if the other ILPs could compensate for the missing ones, some functions seem to be connected to single ILPs (Broughton et al., 2008; Grönke et al., 2010). However, the innate behavior showed comparable performance indices to the controls (Table 11). Both odor acuities for 3-Octanol and 4-Methylcyclohexanol were insignificant, just like the shock reactivities. The *ilp5* mutants revealed a reduced MCH olfactory acuity, yet this was not significant. Additionally, a lack of ILP5 showed no memory decay (Figure 75e, Figure 76c), thus the slightly decreased odor perception was not relevant.

		Olfactory acuity	
Genotype	Shock reactivity (n)	3-Octanol (n)	4-Methylcyclohexanol (n)
w^{1118}	91.02 ± 1.666 (9)	61.74 ± 6.908 (10)	70.10 ± 4.717 (13)
ilp2	91.00 ± 1.946 (10)	57.78 ± 7.608 (10)	80.13 ± 4.757 (10)
w^{1118}	83.40 ± 3.929 (12)	46.74 ± 3.025 (14)	60.41 ± 6.641 (15)
ilp3	86.80 ± 3.857 (10)	39.92 ± 2.709 (13)	56.37 ± 4.231 (15)
w^{1118}	78.30 ± 1.713 (21)	78.38 ± 3.615 (10)	81.51 ± 3.140 (10)
ilp2-3	70.05 ± 2.173 (24)	75.65 ± 4.301 (10)	87.35 ± 1.703 (10)
w^{1118}	71.85 ± 3.686 (10)	43.78 ± 3.843 (14)	60.58 ± 5.883 (17)
ilp5	80.01 ± 3.309 (10)	51.90 ± 5.535 (12)	46.13 ± 7.443 (18)
w^{Dah}	89.16 ± 2.562 (10)	39.36 ± 8.668 (8)	69.28 ± 7.964 (10)
ilp2-3,5	92.44 ± 1.145 (9)	40.61 ±7.387 (10)	73.98 ± 3.572 (9)

Table 11: Innate behavior of ILP mutations.

Shock reactivity and olfactory acuities showed no significant differences in their controls. Statistics: unpaired t-test (parametric) or Mann-Whitney test (nonparametric), $^{ns}p \geq 0.05$. Error bars: mean ± SEM.

3. Presynaptic aspects of age protection strategies

Aging is not only accompanied by decreased autophagy (Bishop et al., 2010; Bhukel and Beuschel et al., 2019) or changes in insulin sensitivity (Frazier et al., 2019) but also by changes in the synapses of neurons. Here, the transmission of signals becomes impaired due to inoperable presynaptic plasticity (Gupta et al., 2016) or a reduced postsynaptic density (Burke and Barnes, 2010). For instance, T-bars, electron-dense structures of the presynaptic active zone in *Drosophila melanogaster*, enlarge dramatically with age to a broad and loose shape (Gupta et al., 2016). They are composed of Bruchpilot, a key player within the presynaptic scaffold, and this protein increases with age drastically over the whole fly brain, accompanied by severe memory deficits (Gupta et al., 2016; Bhukel and Beuschel et al., 2019). Concomitantly, the connection to BRP stabilizes Unc13A, priming and release factor for synaptic vesicles, and the amount of Unc13A in the brain increases with age as well (Aravamudan et al., 1999; Fulterer et al., 2018; Huang et al., 2020). In the following, I will focus on the presynaptic scaffold and how changes in its structure can affect age-induced effects like memory decay.

3.1. Bruchpilot as potential modulator of aging conditions

The protein Bruchpilot (BRP) is a central component of the presynaptic active zone (AZ) in *Drosophila melanogaster*. As a member of the CAST family (cytomatrix at the AZ associated structural proteins), it is highly conserved in different species and possesses homologies to the mammalian ERC (ELKS/ RAB6-interacting/ CAST family) and ELKS in *C. elegans* (Wagh et al., 2006). A null mutation of BRP results in a lack of T-bars and lethality at the larval stage (Kittel et al., 2006b; Fouquet et al., 2009). Additionally, the BRP null mutant possesses a reduced density of Ca^{2+} channels and a larger distance of them to the synaptic vesicles (SVs) due to the inhibited Ca^{2+} channel clustering in the presynaptic membrane, regularly mediated through BRP (Kittel et al., 2006a; Kittel et al., 2006b). Accordingly, it shows an impaired SV release probability, hence changes in the short-term plasticity (Kittel et al., 2006b). Concerning the composition of a T-bar, the two isoforms, BRP-190 and BRP-170, are equally distributed in an alternating array, both needed to form an AZ scaffold (Figure 78; Matkovic et al., 2013). Their N-termini, responsible for an ordinary, complete T-bar, are oriented to the Ca^{2+} channels within the presynaptic membrane (Fouquet et al., 2009). In contrast, the C-terminus, common in both isoforms and the location of the antibody BRP^{Nc82} epitope, reaches towards the interior of the presynapse (Fouquet et al., 2009). This end is necessary for the T-bar assembly, and it tethers SVs to the presynaptic membrane (Fouquet et al., 2009; Hallermann et al., 2010). Additionally, BRP controls the SV's readily releasable pool size and is responsible for accessible release slots (Matkovic et al., 2013).

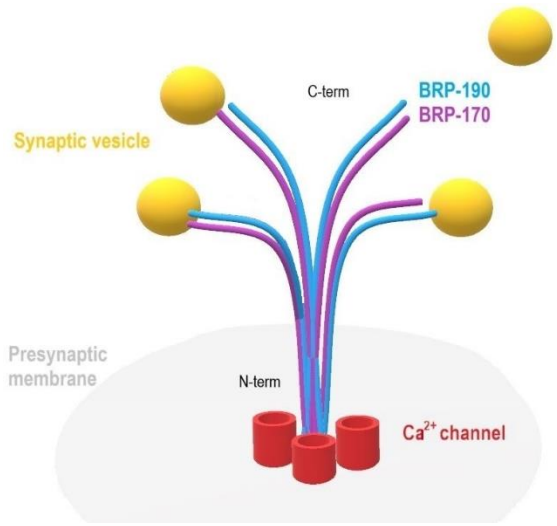

Figure 78: Model of Bruchpilot at the presynapse.
Bruchpilot (BRP) organizes the active zone scaffold and builds the T-bar structure, with the N-terminus near the Ca^{2+} channels (red) and the C-terminus towards the inner cell. Its two isoforms, BRP-170 (purple) and BRP-190 (blue), are equally distributed in an alternating array and tether synaptic vesicles (yellow) to the presynaptic membrane (grey) (Hallermann et al., 2010; Matkovic et al., 2013).

With age, the T-bar becomes more broad and loose, and BRP increases (Figure 79; Gupta et al., 2016; Bhukel and Beuschel et al., 2019). In parallel, different phases of memory decrease

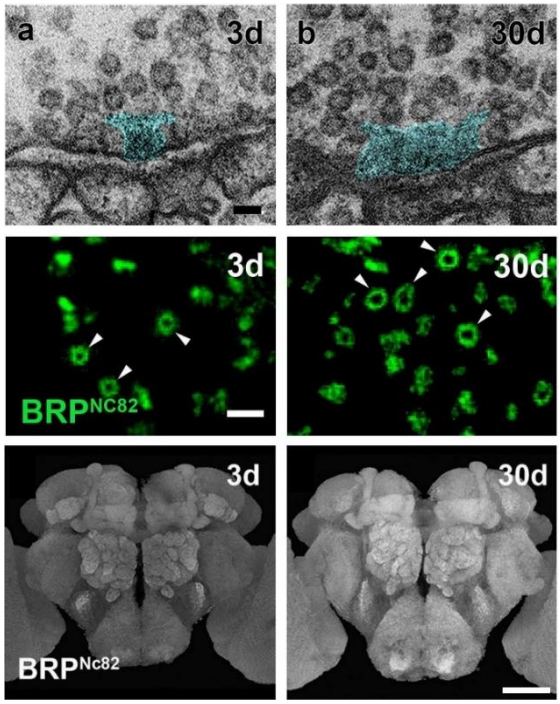

Figure 79: BRP increases with age.

Columns: a) 3-day old flies. b) 30-day old flies. First row: The T-bar becomes more broad and loose with age; electron micrographs of the calyx region, scale bar: 50 nm. Second row: BRP ring diameter increase with age; STED images with BRP^{Nc82} antibody in the calyx, scale bar: 500 nm. Third row: The BRP intensity raises with age; whole-brain confocal immunostainings with BRP^{Nc82}, scale bar: 50 µm. All images taken from Gupta et al., 2016.

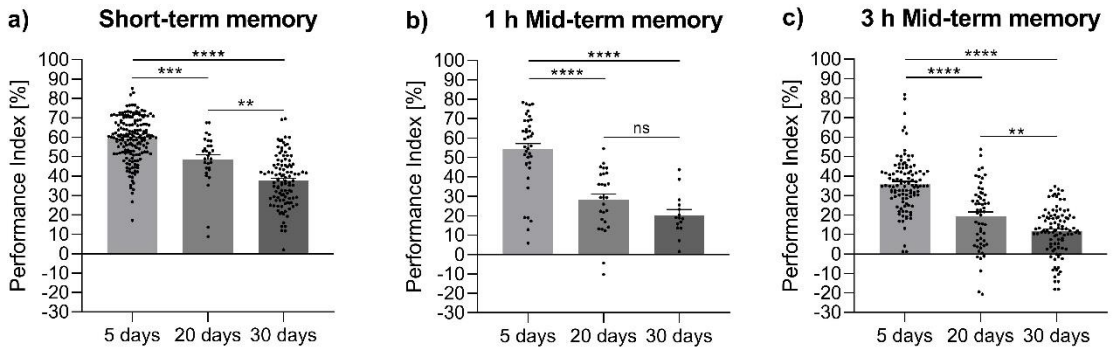

Figure 80: Memory decreases with age.

Aversive olfactory memory of *w*^{1118} for 5, 20, and 30 days. a) Short-term memory (test directly after training): n = 176 for 5-day, n = 29 for 20-day, n = 107 for 30-day old animals. b) 1 hour Mid-term memory (test 1 hour after training): n = 38 for 5-day, n = 27 for 20-day, n = 15 for 30-day old animals. c) 3 hours id-term memory (test 3 hours after training): n = 107 for 5-day, n = 56 for 20-day, n = 97 for 30-day old animals. Statistics: one-way ANOVA with Tukey's multiple comparisons *post hoc* test (parametric) or Kruskal-Wallis with Dunn's *post hoc* test (nonparametric), ****$p < 0.0001$, ***$p < 0.001$, **$p < 0.01$, $^{ns}p \geq 0.05$. Error bars: mean ± SEM.

(Tamura et al., 2003; Gupta et al., 2013). The memory formation of 20- and 30-day old animals dropped dramatically in short-term memory (STM), 1 and 3 hours mid-term memory (MTM), compared to 5-day old flies (Figure 80). Furthermore, all tested memory phases also decreased between 20 and 30 days, yet not significantly for 1 hour mid-term memory.

Thus, could a higher amount of BRP be associated with aging? Could a reduced amount of it prevent aging-accompanied conditions? To test this, I conducted short-term memory for animals with only one BRP copy (1x BRP) and found these flies' memory was not protected from age-induced memory impairment (Figure 81). The memory decrease appeared comparable to 2x BRP (two endogenous copies in wild-type) at 20 days. However, the BRP intensity in 1x BRP stayed similarly low for 3- and 30-days old flies (Gupta et al., 2016). Therefore, a reduced amount of BRP seemed not to compensate the adverse effects of aging.

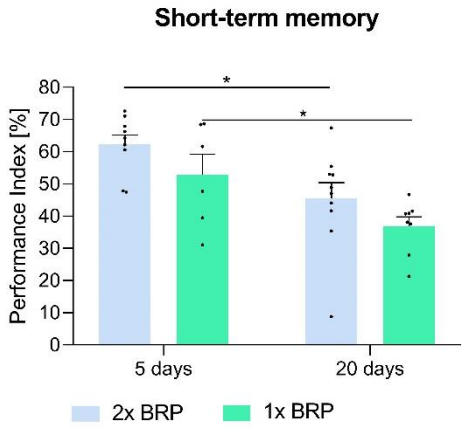

Figure 81: One copy of BRP does not prevent age-induced memory impairment.

Aversive olfactory short-term memory of 1x BRP and as the control w^{1118} (2x BRP) for the age 5 and 20 days (test directly after training): n = 9 for 5-day and n = 10 for 20-day old 2x BRP, n = 6 for 5-day old and n = 8 for 20-day old 1x BRP. Statistics: two-way ANOVA with Sidak's *post hoc* test, *p < 0.05, $^{ns}p \geq 0.05$. Error bars: mean ± SEM.

Worthy of note, premature aging can be induced by adding two additional gene copies of BRP to the two endogenous copies (Gupta et al., 2016). This 4x BRP mutant mimics aged flies in several aspects: an increase of BRP in the whole brain, a bigger BRP ring diameter, and reduced memory (Gupta et al., 2016). Here, STM and 3 hours MTM drop at a young age and stay low for 30 days (Gupta et al., 2016). This can be traced to the labile anesthesia-sensitive memory (ASM) component of 3 hours MTM, which decreases for 4x BRP, similar to ASM's decrease with age (Tamura et al., 2003; Gupta et al., 2016).

Could a BRP elimination in the higher integration center for generation and storage of memory, the mushroom body (MB) (Aso et al., 2014), rescue a memory deterioration? Knapek et al., 2011, attenuated *brp* in the mushroom body and found reduced STM, 3 hours MTM, and anesthesia-resistant memory (ARM), the consolidated component of MTM, while the ASM component stayed unaffected. This is intriguing since the two components of MTM seem to be

dosage-dependent on BRP. ASM vanished with a high BRP amount (4x BRP animals), generating early aging-like memory impairment, while a lack of BRP in the learning center diminished ARM (Knapek et al., 2011; Gupta et al., 2016).

Interestingly, a state of sleep deprivation causes dramatically increased BRP levels, plus sleep-deprived flies as well as 4x BRP show an extreme sleep drive (Gilestro et al., 2009; Huang et al., 2020). The 'synaptic homeostasis hypothesis' says that sleep is needed to reinforce what has been learned and sleeping allows to form new memories via changes in brain plasticity (Tononi and Cirelli, 2016). Thus, like 4x BRP mutants, sleep-deprived flies seem to bring the synapses to an operating peak and overload the system (Gilestro et al., 2009; Gupta et al., 2016; Huang et al., 2020). In this state, memory generation seems inoperable.
Notably, the BRP amount in sleep-deprived flies raises dramatically in the R2 neurons (now renamed as R5 neurons; aimed with the driver *r58h05*-Gal4), a subset of the fly brain's ellipsoid body (Liu et al., 2016). These neurons are responsible for homeostatic sleep drive after sleep depression (Liu et al., 2016). What effect on 4x BRP flies would a lack of BRP in these neurons reveal? Our recent study shows that the sleep phenotype of 4x BRP was partially rescued when *brp* was knocked down in the R2 neurons (Huang et al., 2020). 4x BRP, *r58h05* > brp^{B3} RNAi could partly rebuild the sleep pattern of 4x BRP to a normal level (Huang et al., 2020). 4x BRP animals show an extreme sleep drive, comparable to the sleep rebound of sleep-deprived flies, and have extra sleep, especially during the daytime (Huang et al., 2020). Thus, a homeostatic sleep drive, seeming to be continuously present in 4x BRP, could be regulated down due to absent presynaptic plasticity by BRP in the R2 neurons (Liu et al., 2016; Huang et al., 2020). Thus, I tested the aversive olfactory memory of 4x BRP, *r58h05* > brp^{B3} RNAi (Figure 82). Indeed, no BRP in the R2 neurons could negate the severe STM deficits of 4x BRP, restored to the wild-type level of w^{1118} (2x BRP) (Figure 82a). Equally, 1 hour MTM could be rescued, yet not to the same level as the wild-type 2x BRP (Figure 82b). Even if deficient BRP in R2 neurons in a 2x BRP background could not reach the wild-typic memory, it performed similarly to its genetic controls (Figure 82c-d). Indeed, this scenario did rescue the memory of 4x BRP (Figure 82).

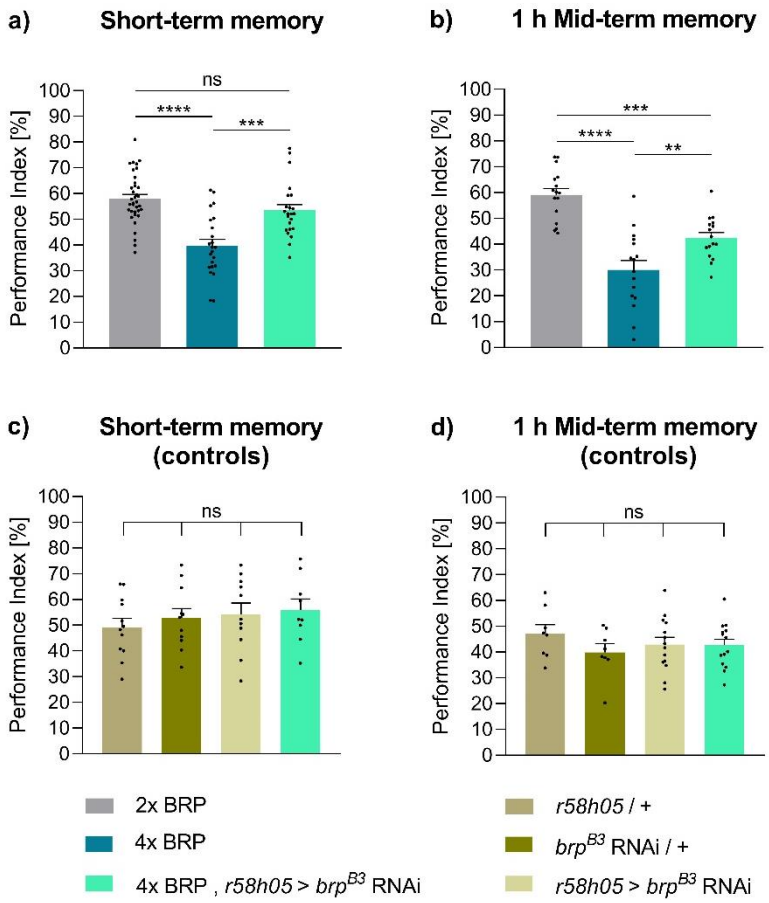

Figure 82: A lack of BRP in the R2 neurons improves the memory of 4x BRP.

Aversive olfactory memory tests for 5-day old animals with no BRP in the R2 neurons in a 4x BRP background. a) Short-term memory (test directly after training): n = 36 for 2x BRP, n = 23 for 4x BRP, n = 23 for 4x BRP , *r58h05* > *brp*^{B3} RNAi. b) Performance Index for 1 hour mid-term memory (test 1 hour after training): n = 16 for 2x BRP, n = 16 for 4x BRP, n = 16 for 4x BRP , *r58h05* > *brp*^{B3} RNAi. c-d) 4x BRP , *r58h05* > *brp*^{B3} RNAi compared to its genetic controls: c) Short-term memory: n = 12 for *r58h05* / +, n = 11 for *brp*^{B3} RNAi / +, n = 11 for *r58h05* > *brp*^{B3} RNAi, n = 9 for 4x BRP , *r58h05* > *brp*^{B3} RNAi. d) 1 hour mid-term memory: n = 8 for *r58h05* / +, n = 8 for *brp*^{B3} RNAi / +, n = 14 for *r58h05* > *brp*^{B3} RNAi, n = 14 for 4x BRP , *r58h05* > *brp*^{B3} RNAi. Statistics: one-way ANOVA with Sidak's multiple comparisons *post hoc* test, ****$p < 0.0001$, ***$p < 0.001$, **$p < 0.01$, $^{ns}p \geq 0.05$. Error bars: mean ± SEM.

Intriguingly, via genetics chronically sleep-deprived flies show a drastic BRP increase in themselves (Huang et al., 2020). Chronic sleep loss is particularly predominant in the gene mutation *sleepless* (*sss*), which causes a severe reduction in sleep (more than 80 %) (Koh et al., 2008). The protein SSS is a glycosylphosphatidylinositol-anchored membrane protein, enriched in *Drosophila melanogaster*'s brain, promoting sleep and rebound sleep after sleep deprivation (Koh et al., 2008). SSS facilitates sleep by regulating the level and function of the voltage-gated potassium (K^+) channel Shaker, followed by an attenuation of neuronal excitability (Koh et al., 2008).

Examining the chronically sleep-deprived *sss* mutant for their memory performance (Figure 83, left column), I found the STM normal but dramatically reduced 3 hours MTM (Figure 83a, d). The decreased longer-lasting memory resulted from an extreme lack of 3 hours anesthesia-sensitive memory (ASM), which even became appetitive towards the shocked odor (Figure 83j). The 3 hours anesthesia- resistant memory (ARM) stayed unchanged (Figure 83g). As the only one of the tested short sleep mutants in Huang et al., 2020, this one lost its intrinsic ability to undergo presynaptic scaling via BRP.

Huang et al., 2020, found that the combination of *sss* with 4 x BRP could compensate the extreme contrary sleep patterns of these two genotypes. Thus, especially daytime sleep was normalized to the level of 2x BRP (wild-type) in *sss* ; 4x BRP (Huang et al., 2020). Could a restoration with 4x BRP help *sss* to balance its intrinsic plasticity with missing presynaptic plasticity? Could the memory deficit in 3 hours ASM be rebuilt in these animals? Conversely, the STM of *sss* ; 4x BRP dropped dramatically by 20 % (Figure 83b). Thus, the upper level of homeostatic plasticity via 4x BRP negated the regular STM performance of *sss* (Figure 83a). Next, I tested longer-lasting memory. Similar to *sss*, its combination with 4x BRP could not bring the 3 hours MTM back (Figure 83e). The performance indices of 4x BRP, *sss*, and *sss* ; 4x BRP ranged all low around 19 %, whereas the wild-type 2x BRP reacted 9 % higher at 28 %. Here, 4x BRP was lower than 2x BRP, yet not significantly. However, a significant decrease was evident in the direct comparison via unpaired t-test (*p = 0.0331). In Figure 83e, *sss*'s 3 MTM occurred better than in Figure 83d, which could stem from slight variations in behavioral performances during the different seasons since the tests were conducted at different times of the year (Dubruille and Emery, 2008; Ferguson and Maier, 2013; Gleason et al., 2019). The 3 hours ARM was for all tested genotypes similar, *sss* ; 4x BRP only slightly reduced but insignificantly (Figure 83h). Consequently, the combination of *sss* with 4x BRP performed marginally better than 2x BRP in 3 hours ASM due to the calculative property of ASM (Figure 83k).

Taken together, the combination of *sss* with 4x BRP impaired the STM and could not improve longer-lasting memory. Possibly, 4x BRP reaches the ceiling of the operational range and

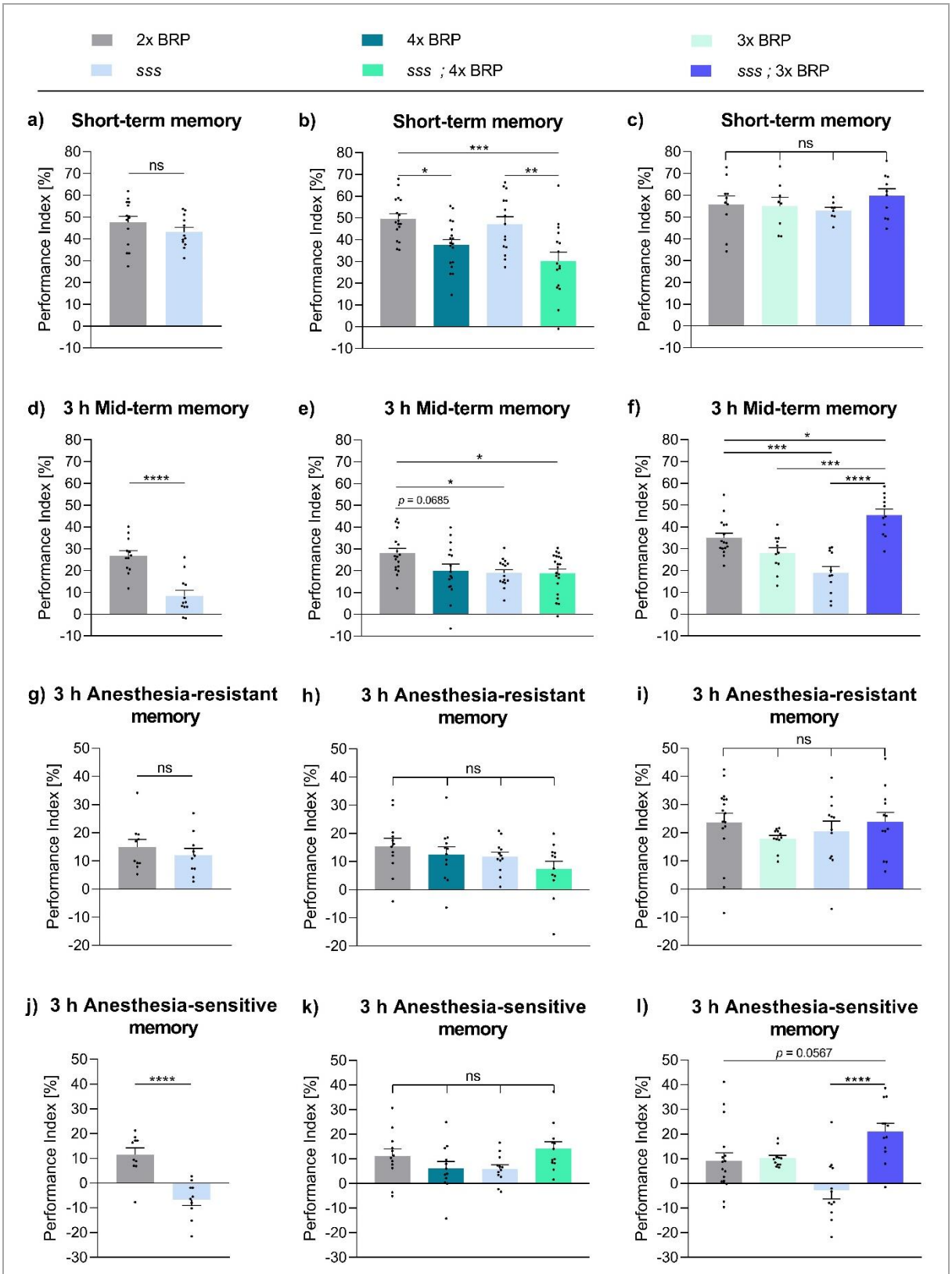

Figure 83: One additional BRP copy restores the memory deficits in the sleep-deprived mutant *sleepless.*

Aversive olfactory memory tests for the chronically sleep-deprived *sss* mutants and its combinations with 4x BRP or 3x BRP for 5-day old flies. a-c) Short-term memory (test directly after training): a) n

= 14 for 2x BRP, n = 12 for *sss*. b) n = 17 for 2x BRP, n = 18 for 4x BRP, n = 15 for *sss*, n = 16 for *sss* ; 4x BRP. c) n = 10 for 2x BRP, n = 8 for 3x BRP, n = 8 for *sss*, n = 10 for *sss* ; 3x BRP. d-f) Performance Index for mid-term memory (test 3 hours after training): d) n = 12 for 2x BRP, n = 12 for *sss*. e) n = 18 for 2x BRP, n = 16 for 4x BRP, n = 15 for *sss*, n = 21 for *sss* ; 4x BRP. f) n = 16 for 2x BRP, n = 11 for 3x BRP, n = 11 for *sss*, n = 11 for *sss* ; 3x BRP. g-i) Performance Index for anesthesia-resistant memory (ice-bad 2.5 hours and test 3 hours after training): g) n = 10 for 2x BRP, n = 10 for *sss*. h) n = 12 for 2x BRP, n = 12 for 4x BRP, n = 12 for *sss*, n = 12 for *sss* ; 4x BRP. i) n = 17 for 2x BRP, n = 11 for 3x BRP, n = 12 for *sss*, n = 12 for *sss* ; 3x BRP. j-l) Performance Index for anesthesia-sensitive memory: Results received via calculation of the median of 3 hours mid-term memory minus the individual performance indices of 3 hours anesthesia-resistant memory. Statistics: unpaired t-test for two genotypes, one-way ANOVA with Sidak's multiple comparisons *post hoc* test (parametric) or Kruskal-Wallis with Dunn's *post hoc* test (nonparametric) for four genotypes, ****$p < 0.0001$, ***$p < 0.001$, **$p < 0.01$, *$p < 0.05$, $^{ns}p \geq 0.05$. Error bars: mean ± SEM.

results in an overload of the system, which could be incompatible with memory generation (Gupta et al., 2016; Huang et al., 2020).

Thus, I examined 3x BRP in combination with *sss* (Figure 83, right column). The STM of *sss* ; 3x BRP, as well as the pure 3x BRP, appeared with a similar performance index as 2x BRP or *sss* (Figure 83c). Astonishingly, *sss* ; 3x BRP's 3 hours MTM increased dramatically with a highly significant improvement to *sss* and 3x BRP and even a better performance than the wild-type 2x BRP (Figure 83f). This effect came from the massive gain in 3 hours ASM, while 3x BRP stayed similar to 2x BRP (Figure 83l). 3 hour ARM was equal for all tested genotypes (Figure 83i). Accordingly, one additional BRP copy to the two endogenous ones (3x BRP) seemed to increase the synaptic plasticity of *sss* to an operational level, which supported the ability to form memories.

The next question was if this improvement was still present with higher age. STM appeared at the same level for 30-days old 2x BRP and *sss* ; 3x BRP and was significantly higher for these two genotypes than 3x BRP (Figure 84a). Longer-lasting memory phases were similar between all tested groups (Figure 84b-d). 3x BRP seemed to perform slightly better in 3 hours ASM (around 6 %), yet this could be due to the calculative property of ASM (Figure 84d). Therefore, neither 3x BRP nor the combination of *sss* and 3x BRP could prevent age-induced memory impairment.

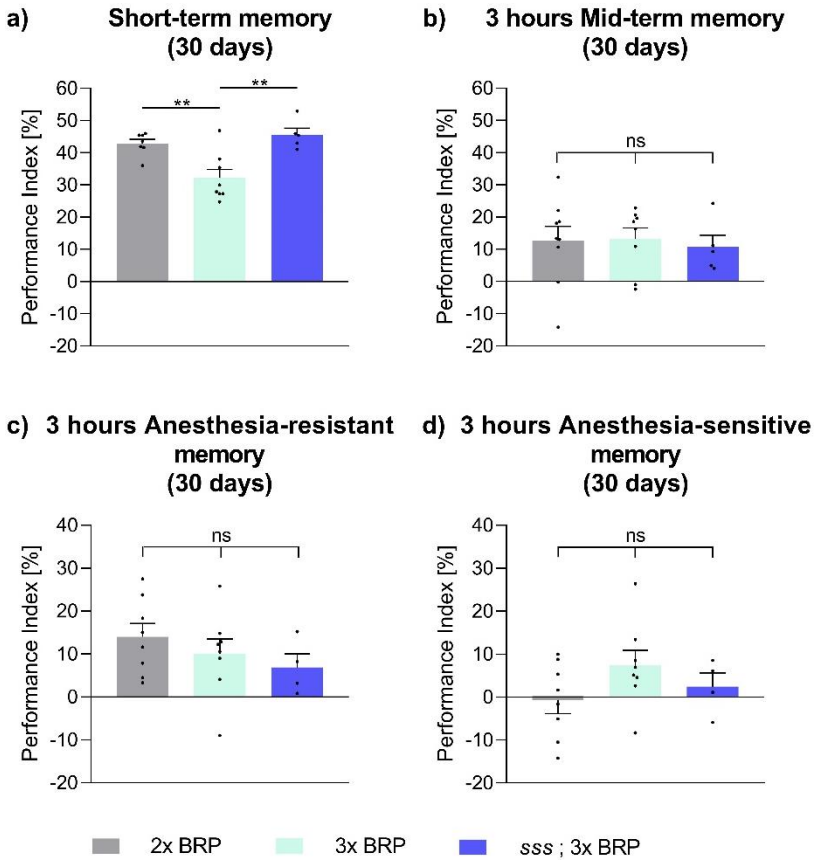

Figure 84: 3x BRP can not protect from age-induced memory impairment.

Aversive olfactory memory tests for *sss* ; 3x BRP and its controls for 30-day old flies. a) Short-term memory (test directly after training): n = 7 for 2x BRP, n = 8 for 3x BRP, n = 5 for *sss* ; 3x BRP. b) Performance Index for mid-term memory (test 3 hours after training): n = 9 for 2x BRP, n = 8 for 3x BRP, n = 5 for *sss* ; 3x BRP.c) Performance Index for anesthesia-resistant memory (ice-bad 2.5 hours and test 3 hours after training): n = 8 for 2x BRP, n = 8 for 3x BRP, n = 4 for *sss* ; 3x BRP. d) Performance Index for anesthesia-sensitive memory: Results received via calculation of the median of 3 hours mid-term memory minus the individual performance indices of 3 hours anesthesia-resistant memory. Statistics: one-way ANOVA with Tukey's multiple comparisons *post hoc* test, $^{**}p < 0.01$, $^{ns}p \geq 0.05$. Error bars: mean ± SEM.

Could 3x BRP combined with reduced SSS in the mushroom body, the higher integration center for learning and memory, mimic the results of *sss* ; 3x BRP? As expected STM of this combination revealed a similar performance compared to the wild-type 2x BRP or the driver control 3xBRP <, *r13f02* / + (Figure 85a). Only the RNAi control *sss* RNAi / + ; 3x BRP performed significantly lower than *r13f02* > *sss* RNAi ; 3x BRP. Interesting was if 3 hours MTM would go down as for the *sss* mutant or if a memory boost would appear like for *sss* ; 3x BRP. However, all tested genotypes performed at the same level in 3 hours MTM (Figure 85b). The overshooting beneficial memory effect via slightly increased plasticity with 3x BRP was not present when *sss* RNAi was only expressed in the mushroom body, but also not the memory defects of *sss*. Interesting would be if the memory deficits of missing SSS are located in the mushroom body (via *r13f02* > *sss* RNAi). That would reveal if the *sss* knockdown in the mushroom body did profit from higher presynaptic plasticity via 3x BRP, at least to the level of the controls. Or came the *sss* mutant's 3 hours MTM deficits due to missing SSS in another region than the mushroom body? Further investigations would be interesting.

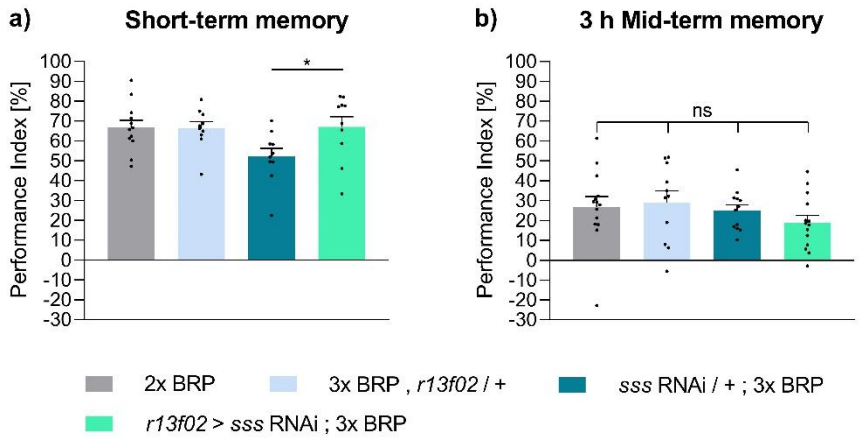

Figure 85: The deficiency of SSS only in the mushroom body with 3x BRP background can not mimic *sss* ; 3x BRP.

Aversive olfactory memory tests for deficient *sss* only in the mushroom body with 3x BRP background and its controls for 5-day old flies. a) Short-term memory (test directly after training): n = 12 for 2x BRP, n = 10 for 3x BRP , *r13f02* / +, n = 10 for *sss* RNAi / +; 3x BRP, n = 10 for *r13f02* > *sss* RNAi ; 3x BRP. b) Performance Index for mid-term memory (test 3 hours after training): n = 14 for 2x BRP, n = 11 for 3x BRP , *r13f02* / +, n = 12 for *sss* RNAi / +; 3x BRP, n = 14 for *r13f02* > *sss* RNAi ; 3x BRP. Statistics: one-way ANOVA with Sidak's multiple comparisons *post hoc* test, $^{ns}p \geq 0.05$. Error bars: mean ± SEM.

Surprisingly, an overexpression (OE) of *sss* only in the mushroom body with *sss* ; 3x BRP background possessed impaired STM compared to the controls (Figure 86a). The sole expression of the SSS protein, especially in the mushroom body as the learning center, maybe attenuated neuronal excitability due to a higher K^+ channel activity in this neuropile via SSS's control, (Zars et al., 2000; Koh et al., 2008; Blum et al., 2009).

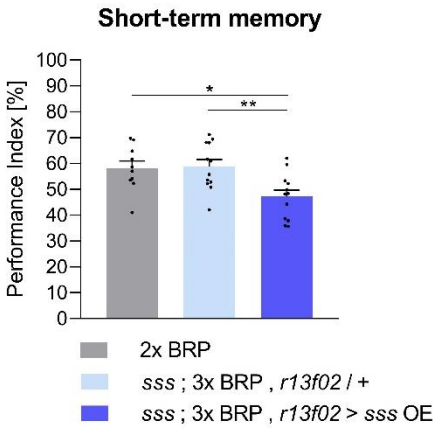

Figure 86: *sss* overexpression restricted to the mushroom body in an *sss* ; 3xBRP background shows decreased short-term memory.

Short-term memory (test directly after training) for the overexpression (OE) of *sss* in the mushroom body with *sss* ; 3x BRP background and its controls for 5-day old flies: n = 10 for 2x BRP, n = 12 for sss ; 3x BRP , *r13f02* / +, n = 12 for *sss* ; 3x BRP , *r13f02* > *sss* OE. Statistics: one-way ANOVA with Tukey's multiple comparisons *post hoc* test, $**p < 0.01$, $*p < 0.05$. Error bars: mean ± SEM.

The innate behavior for this chapter is listed in Table 12 and in more detail in the appendix, Table 25. All genotypes of interest showed comparable or even higher performance indices to at least one of their controls in both odor acuities (3-Octanol, OCT, and 4-Methylcyclohexanol, MCH) and the shock reactivity. Only the chronically sleep-deprived mutant *sss* possessed severe avoidance problems with MCH. However, *sss*' ability to learn and form memories is available since its performance in STM appeared at the same height as the wild-type 2x BRP (Figure 83a). Notably, 4x BRP and its combination with *sss* obtained a 20 % higher OCT odor acuity than 2x BRP and pure *sss*. This increase vanished for 3x BRP and *sss* ; 3x BRP. The highest range of BRP (4x BRP) maybe supports the detection of the odor OCT. Gupta et al., 2016, showed a higher odor-evoked synaptic vesicle release in 30-day old animals, which possess a similarly high level of BRP as 4x BRP. Though, this was visible for OCT and MCH (Gupta et al., 2016).

Genotype	Shock reactivity (n)	Olfactory acuity	
		3-Octanol (n)	4-Methyl-cyclohexanol (n)
2x BRP (*w*^{1118})	-	38.37 ± 4.341 (23)	65.09 ± 5.586 (15)
4x BRP	-	40.29 ± 5.220 (13)	64.20 ± 5.220 (13)
4x BRP , r58h05 > *brp*^{B3} RNAi	-	44.44 ± 5.013 (14)	76.25 ± 5.356 (14)
r58h05 / +	-	35.50 ± 3.838 (12)	70.43 ± 3.206 (11)
brp^{B3} RNAi / +	-	46.17 ± 6.096 (13)	63.90 ± 7.265 (12)
r58h05 > *brp*^{B3} RNAi	-	35.20 ± 5.837 (13)	73.07 ± 2.873 (11)
4x BRP , *r58h05* > *brp*^{B3} RNAi	-	38.26 ± 5.476 (8)	73.07 ± 9.182 (3)
2x BRP (*w*^{1118})	-	36.98 ± 2.556 (32)	38.17 ± 3.411 (41)
sss	-	31.36 ± 4.062 (30)	27.20 ± 3.907 (31)
2x BRP (*w*^{1118})	79.76 ± 2.863 (14)	17.39 ± 4.873 (16)	71.31 ± 5.086 (14)
4x BRP	81.61 ± 3.886 (10)	41.12 ± 5.237 (13)	51.24 ± 7.933 (12)
sss	73.80 ± 1.296 (12)	16.66 ± 3.862 (9)	38.46 ± 7.043 (12)
sss ; 4x BRP	76.80 ± 4.467 (10)	43.52 ± 4.635 (12)	62.75 ± 7.376 (12)
2x BRP (*w*^{1118})	78.48 ± 3.831 (10)	18.66 ± 4.771 (16)	50.55 ± 7.643 (14)
3x BRP	82.79 ± 2.698 (8)	24.82 ± 6.386 (12)	44.31 ± 8.520 (13)
sss	74.58 ± 2.216 (8)	13.00 ± 6.447 (9)	5.250 ± 7.603 (10)
sss ; 3x BRP	81.82 ± 3.154 (10)	22.22 ± 6.054 (11)	51.63 ± 9.293 (12)
2x BRP (*w*^{1118})	50.01 ± 4.289 (10)	27.61 ± 6.400 (10)	48.38 ± 11.91 (12)
3x BRP , *r13f02* / +	57.69 ± 4.474 (10)	34.50 ± 4.813 (12)	48.63 ± 8.200 (12)
sss RNAi / + ; 3x BRP	60.01 ± 3.439 (10)	47.05 ± 4.399 (10)	44.59 ± 9.340 (14)
r13f02 > *sss* RNAi ; 3x BRP	67.33 ± 3.095 (10)	27.59 ± 4.975 (10)	48.98 ± 10.07 (12)
2x BRP (*w*^{1118})	74.89 ± 4.109 (7)	18.21 ± 7.434 (14)	64.45 ± 4.255 (8)
sss ; 3x BRP , *r13f02* / +	71.68 ± 3.523 (8)	24.71 ± 4.958 (14)	80.01 ± 4.504 (10)
sss ; 3x BRP , *r13f02* > *sss* OE	70.25 ± 3.465 (8)	17.48 ± 4.578 (14)	71.47 ± 7.796 (10)

Table 12: Innate behavior for the examined memory tests regarding BRP.

Shock reactivity and olfactory acuity of the genotypes of interest showed no significant differences than at least one of their control. Only the mutant *sss* performed significantly worse in the MCH odor acuity. Since *sss*'s STM stayed similar high as the wild-type 2x BRP, the flies seemed able to learn (Figure 83a). Statistics: one-way ANOVA with Sidak's/ Tukey's multiple comparisons *post hoc* test (parametric) or Kruskal-Wallis with Dunn's *post hoc* test (nonparametric), $^{**}p < 0.01$ $^{*}p < 0.05$, $^{ns}p \geq 0.05$. Mean ± SEM.

3.1.1. Deacetylation of the T-bar induces an aging-like configuration

With age, the T-bar, located at the presynaptic active zone and composed of Bruchpilot (BRP), enlarges dramatically to a broad and loose shape (Gupta et al., 2016). This age-induced increase is accompanied by severe memory deficits (Gupta et al., 2016; Bhukel and Beuschel et al., 2019). The elongator protein 3 (ELP3) is a lysine acetyltransferase (KAT), which acetylates lysine sites of the BRP C-terminus, leading to a bundled and compact shape of the T-bar and a reduced synaptic vesicle (SV) release, similar to young flies (Figure 87; Miśkiewicz et al., 2011; Gupta et al., 2016). A lack of ELP3 results in a T-bar phenotype like old animals or 4x BRP (see Figure 87) and is associated with amyotrophic lateral sclerosis (ALS) (Simpson et al., 2009; Miśkiewicz et al., 2011; Gupta et al., 2016). Its counterpart, the histone deacetylase 6 (HDAC6), increases the deacetylation of BRP, followed by a broader and looser shape of the T-bar with more SV tethering and release (Figure 87; Miskiewicz et al., 2014). This was also seen in old flies and 4x BRP animals (Gupta et al., 2016). Notably, HDAC6 inhibitors act neuroprotective and improve memory in rodents (Toonen and Verhage, 2011).

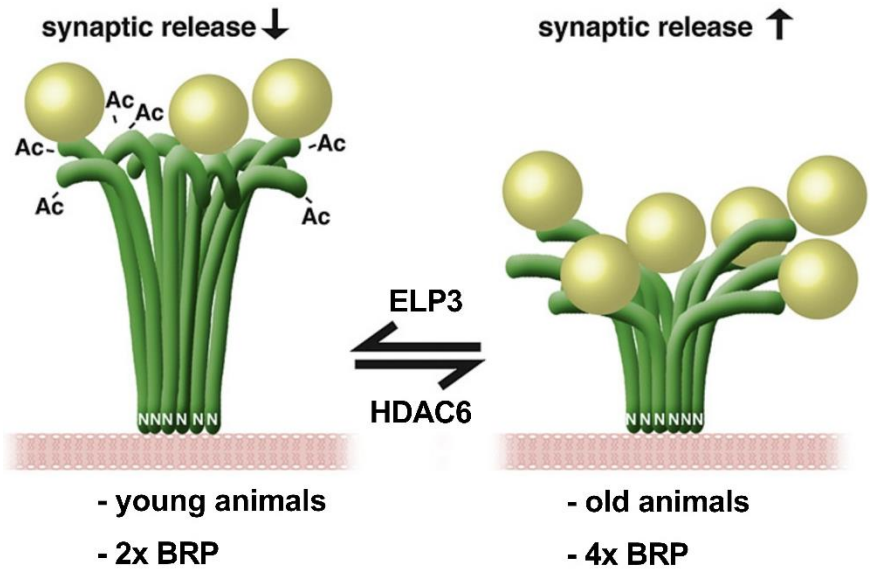

Figure 87: Deacetylation of the T-bar causes a broad and loose shape comparable to old animals

In young animals, the C-termini of Bruchpilot (BRP) are acetylated by ELP3, followed by a sharp and condensed structure at the presynaptic active zone (Gupta et al., 2016). In contrast, aged animals possess a wide and loose T-bar, accompanied by increased synaptic vesicle release. HDAC6 mediates this deacetylation. Similar to young versus old flies are wildtype and 4x BRP with a rampant T-bar for 4x BRP. Image modified from Toonen and Verhage, 2011.

Like HDAC inhibitors, a pan-neuronal reduction of HDAC6 did improve memory at 5 and 30 days significantly, yet the age-induced memory impairment was still apparent, here from a higher memory level (Figure 88). The short-term memory (STM) performance was 15 % higher for *appl* > *hdac6* RNAi in young and old flies (Figure 88a). This positive effect did not appear when the diminished HDAC6 was restricted to the mushroom body (Figure 88b). A second tested *hdac6* RNAi line could not enhance the memory, neither pan-neuronal nor in the mushroom body (Figure 88c-d). The innate shock reactivity was significantly decreased for all

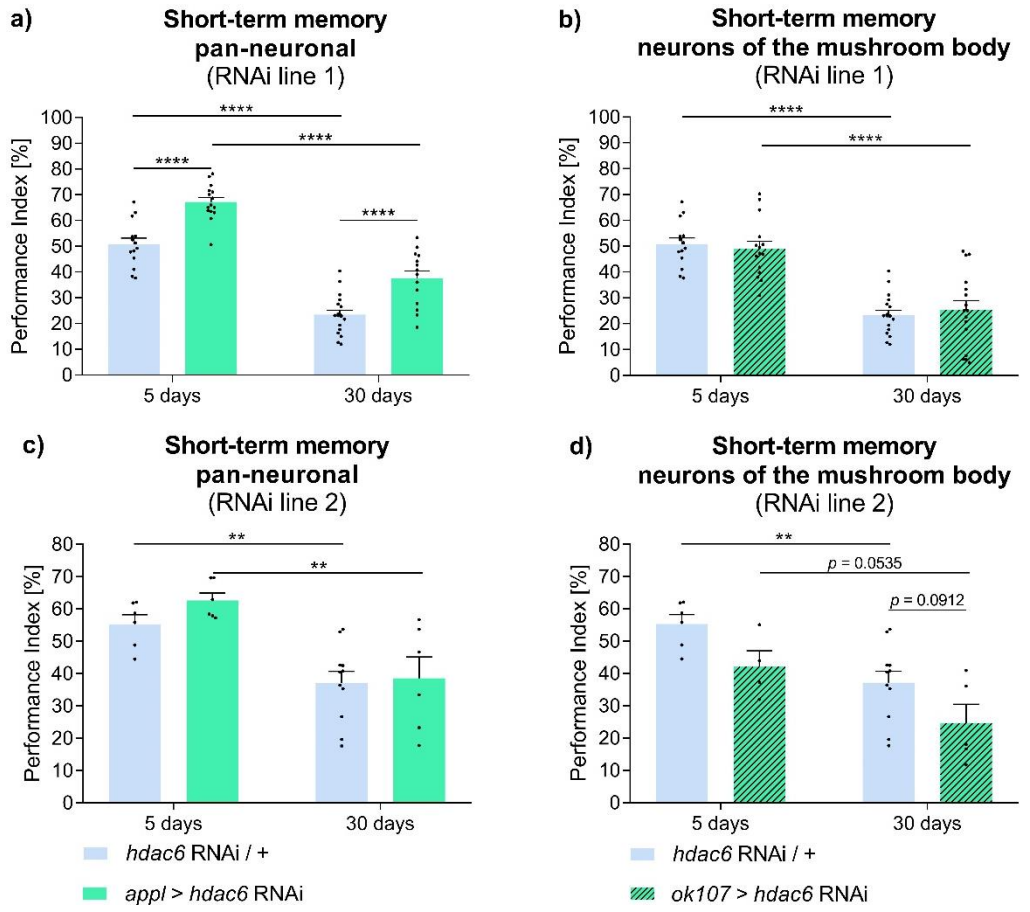

Figure 88: A pan-neuronal lack of HDAC6 improves memory in young and old flies.

Short-term memory (test directly after training) for deficient HDAC6 (two different RNAi lines), 5- and 30-days old flies. a-b) RNAi line 1 (BL # 31503): a) pan-neuronal: n = 14 for 5-day and n = 18 for 30-day old *hdac6* RNAi / +, n = 15 for 5-day and n = 14 for 30-day old *appl* > *hdac6* RNAi. b) mushroom body: n = 14 for 5-day and n = 18 for 30-day old *hdac6* RNAi / +, n = 15 for 5-day and n = 16 for 30-day old *ok107* > *hdac6* RNAi. c-d) RNAi line 2 (BL # 34702): c) pan-neuronal: n = 6 for 5-day and n = 11 for 30-day old *hdac6* RNAi / +, n = 6 for 5-day and n = 6 for 30-day old *appl* > *hdac6* RNAi. d) mushroom body: n = 6 for 5-day and n = 11 for 30-day old *hdac6* RNAi / +, n = 4 for 5-day and n = 5 for 30-day old *ok107* > *hdac6* RNAi. Statistics: two-way ANOVA with Sidak's multiple comparisons post hoc test, ****p < 0.0001, **p < 0.01, nsp ≥ 0.05. Error bars: mean ± SEM.

aged flies compared to the young ones in these tests (Table 13; Appendix, Table 25). Thus, the aged flies seemed less sensitive to electrical punishment. It could be possible that the aged flies could perform even better without that detriment. Further, a drop with age appeared in the 4-Methylcyclohexanol (MCH) innate acuity tests for mushroom body driven *hdac6* RNAi flies (*ok107*-Gal4). It could be that the nonexistent memory protection in these flies came from their decreased smell ability. Though this can be excluded since both parts of the memory tests, the results of the memory performances for 3-Octanol (OCT) and MCH were equally high. Thus, the flies learned with shocked MCH just like with OCT. Taken together, pan-neuronal diminished *hdac6* could boost memory but not protect from an age-induced decline. *hdac6* RNAi driven in den mushroom body could not improve memory.

Would an increase of HDAC6, thus enhanced deacetylation of the T-bar, negatively influence the memory performance? STM tests with a pan-neuronal overexpression (OE) revealed no detrimental effects (Figure 89). Neither *hdac6* OE driven with *appl*-Gal4 nor with *elaV(X)*-Gal4 showed any benefit compared to their controls.

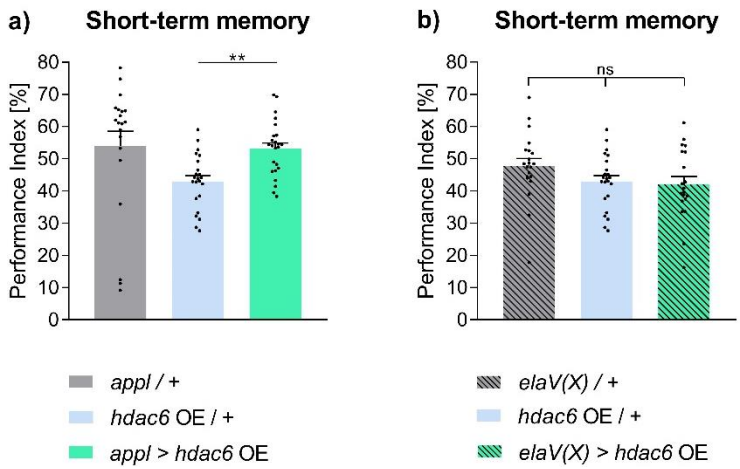

Figure 89: More deacetylation via overexpressed *hdac6* does not affect memory.

Short-term memory (test directly after training) for the pan-neuronal overexpression (OE) *hdac6* for 5-days old flies. a) n = 20 for *appl* / +, n = 23 for *hdac6* OE / +, n = 24 for *appl* > *hdac6* OE. b) n = 21 for *elaV(X)* / +, n = 23 for *hdac6* OE / +, n = 20 for *elaV(X)* > *hdac6* OE. Statistics: one-way ANOVA with Sidak's multiple comparisons *post hoc* test (parametric) or Kruskal-Wallis with Dunn's *post hoc* test (nonparametric), **p < 0.01, nsp ≥ 0.05. Error bars: mean ± SEM.

Taken together, the pan-neuronal *hdac6* attenuation positively affected aversive olfactory memory at all ages (Figure 88a). An overloaded T-bar, occurring with aging, seemed to burden the operational state of the presynapse. Thus, its relief due to reduced HDAC6 activity in all neurons brought boosted the memory acquisition phase, interestingly also in young flies. A pan-neuronal elevation via *hdac6* OE gave no changes in memory.

Surprisingly, reducing ELP3, which acetylates the T-bar to its more compact configuration, thus it is the antagonistically operating enzyme of HDAC6, showed no memory defects. 5-day old flies of one tested pan-neuronally expressed *elp3* RNAi line performed even better in STM than their controls, while 3 hours mid-term memory (MTM) showed no improvement (Figure 90a). In contrast, the second *elp3* RNAi line showed no memory improvement in STM, neither

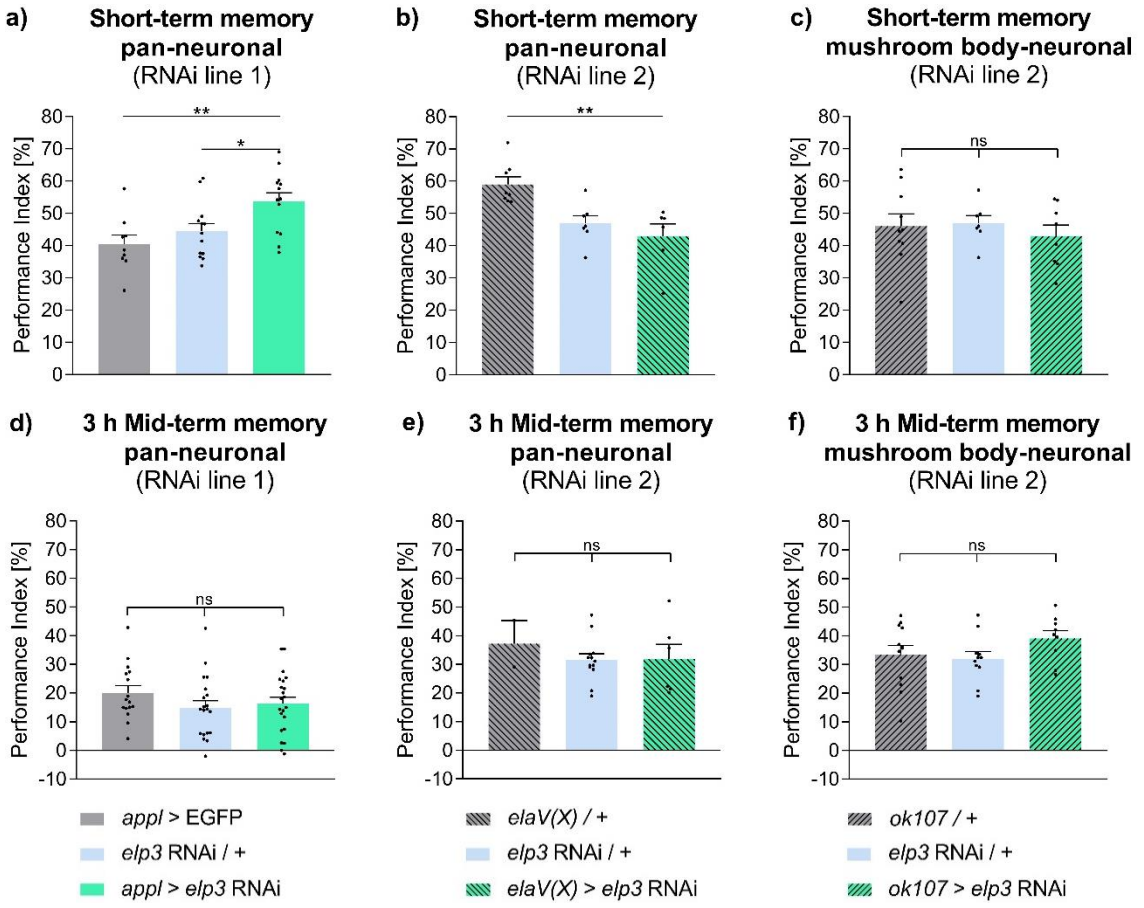

Figure 90: Memory for pan-neuronal and in the mushroom body attenuated *elp3*.

Aversive olfactory memory tests of diminished ELP3 (two different RNAi lines, 1: BL # 35488, 2: VDRC # 106128), pan-neuronal and in the mushroom body, for 5-day old flies. a-c) Short-term memory (test directly after training): a) RNAi line 1, pan-neuronal: n = 9 for *appl* > EGFP, n = 13 for *elp3* RNAi / +, n = 13 for *appl* > *elp3* RNAi. b) RNAi line 2, pan-neuronal: n = 8 for *elaV(X)* / +, n = 7 for *elp3* RNAi / +, n = 6 for *elaV(X)* > *elp3* RNAi. c) RNAi line 2, in the mushroom-body: n = 10 for *ok107* / +, n = 7 for *elp3* RNAi / +, n = 8 for *ok107* > *elp3* RNAi. d-f) 3 hours mid-term memory (test 3 hours after training): d) RNAi line 1, pan-neuronal: n = 16 for *appl* > EGFP, n = 20 for *elp3* RNAi / +, n = 22 for *appl* > *elp3* RNAi. e) RNAi line 2, pan-neuronal: n = 2 for *elaV(X)* / +, n = 13 for *elp3* RNAi / +, n = 6 for *elaV(X)* > *elp3* RNAi. f) RNAi line 2, in the mushroom-body: n = 12 for *ok107* / +, n = 11 for *elp3* RNAi / +, n = 9 for *ok107* > *elp3* RNAi. Statistics: one-way ANOVA with Sidak's multiple comparisons *post hoc* test, $^{**}p < 0.01$, $^{*}p < 0.05$, $^{ns}p \geq 0.05$. Error bars: mean ± SEM.

pan-neuronal (Figure 90b) nor in the mushroom body (Figure 90c). Further examinations with longer-lasting 3 hours MTM revealed no defect or improvement for *elp3* RNAi line 2, pan-neuronal or in the mushroom body driven, similar to line 1 (Figure 90d-f).
The STM benefit in 5 day old *appl* > *elp3* RNAi flies was surprising, since the T-bar would be less acetylated here. Maybe in particular the repulsion of the BRP C-termini in their deacetylated state gave more space for synaptic vesicle tethering. With age (similar T-bar confirmation), a higher synaptic vesicle release could be seen (Gupta et al., 2016). Possibly, especially memory acquisition with STM was boosted this way, while these flies were enabled to react otherwise normally in the remaining system due to their young age and no further detrimental scenarios. Further examinations, like tests of longer-lasting memory, would be interesting.

The shock reactivity and MCH acuity decreased for 5- compared to 30-day old *hdac6* RNAi animals (Table 13). These results were discussed in specific above. In short, age-induced memory impairment appeared severely. Thus, the minor innate behavior deficits did not affect the memory results. *elp3* RNAi's innate behavior occurred unobtrusively (Table 13).

		Olfactory acuity	
Genotype	Shock reactivity (n)	3-Octanol (n)	4-Methylcyclohexanol (n)
hdac6 RNAi line 1:			
hdac6 RNAi / + (5 days)	85.97 ± 2.050 (10)	25.30 ± 6.071 (6)	53.15 ± 5.467 (6)
appl > *hdac6* RNAi (5 days)	94.86 ± 1.020 (9)	29.67 ± 8.024 (6)	40.92 ± 4.859 (6)
hdac6 RNAi / + (30 days)	65.10 ± 5.303 (9)	20.98 ± 6.292 (6)	21.28 ± 5.857 (6)
appl > *hdac6* RNAi (30 days)	82.88 ± 4.993 (8)	25.10 ± 5.526 (6)	23.02 ± 6.656 (6)
hdac6 RNAi line 1:			
hdac6 RNAi / + (5 days)	85.97 ± 2.050 (10)	25.30 ± 6.071 (6)	53.15 ± 5.467 (6)
ok107 > *hdac6* RNAi (5 days)	94.86 ± 1.020 (9)	10.73 ± 6.931 (6)	36.04 ± 9.411 (5)
hdac6 RNAi / + (30 days)	65.10 ± 5.303 (9)	20.98 ± 6.292 (6)	21.28 ± 5.857 (6)
ok107 > *hdac6* RNAi (30 days)	82.88 ± 4.993 (8)	16.10 ± 2.722 (7)	6.586 ± 6.971 (7)

elp3 RNAi line 1:			
appl > EGFP	-	28.23 ± 4.983 (4)	22.85 ± 5.818 (4)
elp3 RNAi / +	-	24.88 ± 8.481 (4)	43.05 ± 10.22 (4)
appl > *elp3* RNAi	-	26.40 ± 7.938 (8)	31.29 ± 8.162 (8)

Table 13: Innate behavior to the conducted HDAC6 and ELP3 crosses.

Shock reactivity and olfactory acuity of the genotypes of interest showed no significant difference from at least one of their control or were performed even better. Only the *hdac6* RNAi animals showed decreased shock reactivity with age (discussed in the text). *hdac6* RNAi driven in the mushroom body showed reduced MCH acuity at all ages compared to the controls (discussed in the text). Statistics: two-way (genotypes and ages to compare) or one-way ANOVA (genotypes to compare) with Sidak's multiple comparisons *post hoc* test, ***$p < 0.001$, **$p < 0.01$, *$p < 0.05$, nsp ≥ 0.05. Mean ± SEM.

3.1.2. Anterograde transport of presynaptic scaffold proteins

Functional synaptic plasticity is dependent on the transport of the scaffold compounds from the soma over the axon to the presynaptic active zone. The co-transport of Bruchpilot (BRP), RIM-binding protein (RIM-BP), and Unc13 along the axon is coordinated by transport proteins, thus a lack of proteins like Aplip1 or SRPK79D lead to a block of rapid presynaptic homeostatic potentiation (PHP) (Siebert et al., 2015; Böhme et al., 2019; Driller et al., 2019). This mechanism is necessary for an immediate adjustment of the neurotransmitter release, the presynaptic plasticity, and a fast answer to changes in the environment (Ortega et al., 2018).

The APP (β-amyloid precursor protein) -like protein interacting protein 1 (Aplip1) is involved in the fast axonal transport (Taru et al., 2002; Böhme et al., 2019). Its mammalian homolog, JNK (c-jun NH_2 terminal kinase) interacting protein 1 (JIP1), is taking part in the modulation of APP phosphorylation, thus associated with Alzheimer's disease and diabetes (Taru et al., 2002; Beeler et al., 2009). Additionally, it links the cargo to the kinesin family motor protein (here: Unc104) for anterograde transport along the axon (Siebert et al., 2015; Driller et al., 2019). Within the co-transport of BRP-Unc13-RIM-BP, Aplip1 serves as an adapter to RIM-BP for complex' transportation, yet the BRP delivery is not inhibited in the absence of RIM-BP (Siebert et al., 2015; Driller et al., 2019). However, since mutant *aplip1*^{ek4} possesses severe problems in rapid presynaptic homeostatic potentiation, I tested its aversive olfactory short-term memory.

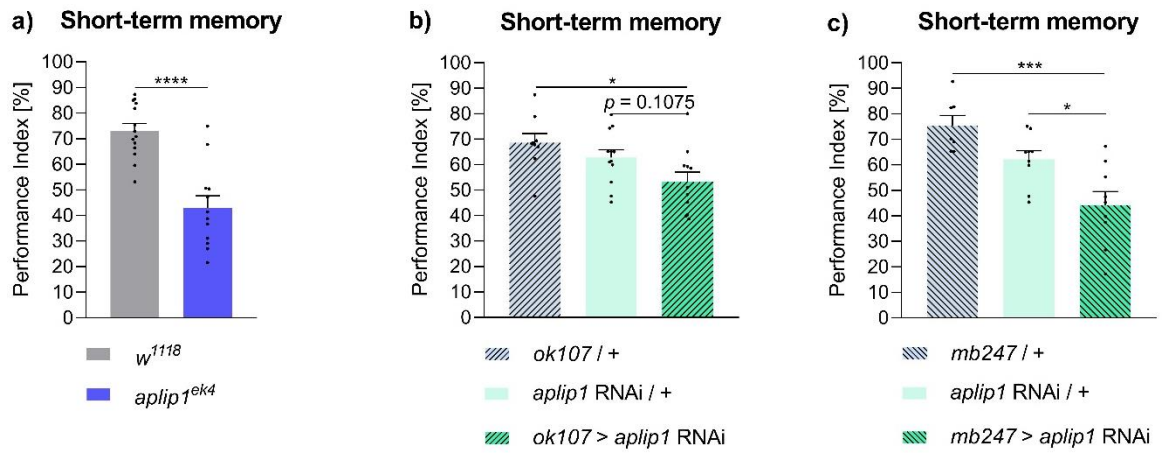

Figure 91: The short-term memory is reduced with a lack of Aplip1.

Short-term memory (test directly after training) of deficient Aplip1 for 5-days old flies. a) point mutation: n = 14 for w^{1118}, n = 12 for *aplip*^{ek4}. b-c) *aplip1* RNAi in the mushroom body: b) n = 9 for *ok107* / +, n = 12 for *aplip1* / +, n = 11 for *ok107* > *aplip1* RNAi. c) n = 7 for *mb247* / +, n = 9 for *aplip1* / +, n = 9 for *mb247* > *aplip1* RNAi. Statistics: unpaired t-test for two, and one-way ANOVA with Sidak's multiple comparisons *post hoc* test for three genotypes, ****$p < 0.0001$, ***$p < 0.001$, $^{ns}p \geq 0.05$. Error bars: mean ± SEM.

Indeed, the memory was dramatically reduced, while the innate smell behavior appeared unremarkable (Figure 91a, Table 14). Next, I examined the effect of deficient *aplip1* in the mushroom body, the learning center of the fly brain, with two driver lines (Figure 91b-c; Aso et al., 2014). *ok107*-Gal4 covers all lobes, while *mb247*-Gal4 drives in the α/ β and γ lobes (Connolly et al., 1996; Zars et al., 2000). Both knockdowns of *aplip1* learned significantly poorer than their controls, yet *ok107* > *aplip1* RNAi was only slightly reduced than its RNAi control. Thus, a fast cognitive reaction was dependent on the mushroom body functional transport adapter protein Aplip1. Though, further experiments to exclude developmental defects would be interesting.

The innate smell scores with diminished *aplip1* showed comparable performance indices to at least one of their controls (Table 14Table 16). Both odor acuities for 3-Octanol and 4-Methylcyclohexanol were insignificant. Only *mb247* > *aplip1* RNAi was slightly reduced, yet not significantly.

	Olfactory acuity	
Genotype	3-Octanol (n)	4-Methylcyclohexanol (n)
w^{1118}	40.78 ± 5.316 (17)	86.90 ± 1.418 (9)
aplip1^{ek4} *, Df(3L)BSC799*	47.31 ± 6.886 (11)	88.20 ± 2.660 (9)
ok107 / +	24.60 ± 3.504 (37)	76.28 ± 3.656 (9)
aplip1 RNAi / +	37.87 ± 3.493 (57)	71.21 ± 76.70 (15)
ok107 > *aplip1* RNAi	23.91 ± 3.254 (54)	72.90 ± 3.360 (14)
mb247 / +	16.26 ± 4.200 (32)	70.02 ± 6.238 (9)
aplip1 RNAi / +	37.87 ± 3.493 (57)	71.21 ± 76.70 (15)
mb247 > *aplip1* RNAi	29.45 ± 3.947 (36)	57.40 ± 7.355 (9)

Table 14: Innate behavior to the conducted Aplip1 tests.

The olfactory acuities for diminished *aplip1* showed no significant differences than at least one of its controls. Statistics: one-way ANOVA with Sidak's multiple comparisons *post hoc* test (parametric) or Kruskal-Wallis with Dunn's *post hoc* test (nonparametric), $^{**}p < 0.01$ $^{*}p < 0.05$, $^{ns}p \geq 0.05$. Mean ± SEM.

Another protein involved in the axonal transport of presynaptic scaffold proteins is the serine-arginine protein kinase 79D (SRPK79D) (Siebert et al., 2015). Its null mutation *srpk79D*^{VN} evokes aggregates of BRP-RIM-BP-Unc13 accompanied by a reduced life span and an impaired flight ability, whereas the synaptic transmission seems normal (Nieratschker et al., 2009; Driller et al., 2019). Driller et al., 2019, found that SRPK79D phosphorylates the N-terminus of the isoform BRP-190, which is evolutionary conserved in mammals and *C. elegans*. This post-translational adjustment enables an ensured transport to the presynaptic active zone along the axon (Driller et al., 2019). Interestingly, a complete lack of SRPK showed severe memory problems (Figure 92). In aversive olfactory memory tests, the short-term memory

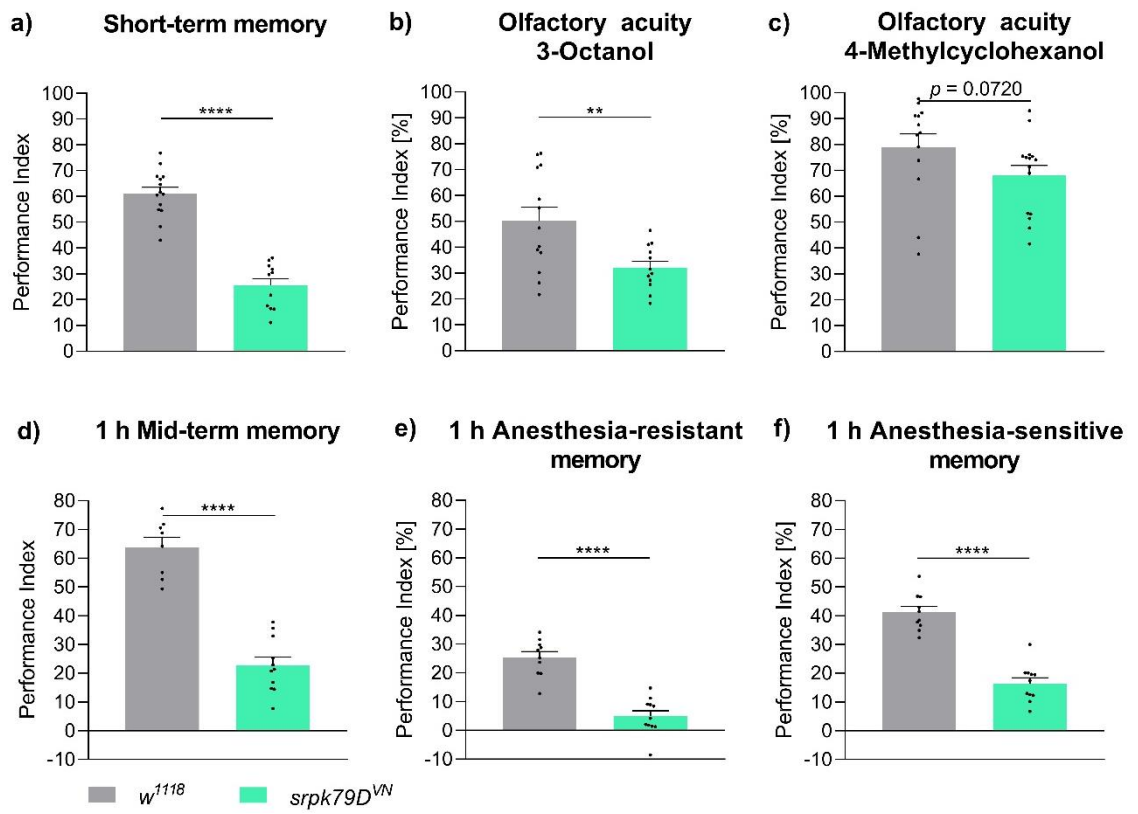

Figure 92: A null mutation of *srpk79D* possesses severe memory deficits.

Aversive olfactory memory tests for 5-day old *srpk79D*^{VN}. a) Short-term memory (test directly after training): n = 14 for *w*^{1118}, n = 11 for *sprk79D*^{VK}. b-c) Odor acuity. b) 3-Octanol: n = 13 for *w*^{1118}, n = 12 for *sprk79D*^{VK}. c) 4-Methylcyclohexanol: n = 13 for *w*^{1118}, n = 15 for *sprk79D*^{VK}. d-f) 1 hour memory. d) Mid-term memory (test 1 hour after training): n = 8 for *w*^{1118}, n = 11 for *sprk79D*^{VK} . e) Anesthesia-resistant memory (ice-bad 30 min and test 1 hour after training): n = 10 for *w*^{1118}, n = 11 for *sprk79D*^{VK}. f) Anesthesia-sensitive memory: Results received via calculation of the median of 1 hour mid-term memory minus the individual performance indices of 1 hour anesthesia-resistant memory. Statistics: unpaired t-test (parametric) or Mann-Whitney test (nonparametric), , ****p < 0.0001, **p < 0.01, ^{ns}p ≥ 0.05. Error bars: mean ± SEM.

(STM) of the *srpk79D*^{VN} null mutation was severely impaired by 36 % compared to the wild-type control (Figure 92a). Similarly, the 1 hour mid-term memory dropped by 41 %, whereby its component anesthesia-sensitive memory dropped by 25 %, and anesthesia-resistant memory appeared near zero (Figure 92d-f). Of course, these memory defects could be caused by a reduced odor acuity (Figure 92b-c). The innate smell behavior declined significantly for 3-Octanol, yet this drop occurred less grave than the memory deficits (Figure 92b). Additionally, the performance index against 4-Methylcyclohexanol (MCH) was slightly decreased, nevertheless insignificant (Figure 92c). Notably, Nieratschker et al., 2009, saw no issues for olfactory conditioning with larvae, though a walking deficit in adult *srpk79D*^{VN} animals. However, the flies seemed mobile enough for the behavior tests with the T-maze since the MCH avoidance occurred insignificantly. Overall, the memory decay was so dramatic a memory deficit can be taken for sure.

Further tests with diminished *srpk79D* restricted to the mushroom body demonstrated no short-term memory defects (Figure 93a-b) or any innate smell deficits (Table 15). Thus, the memory defects were only apparent in the *srpk79D* mutant (Figure 92).

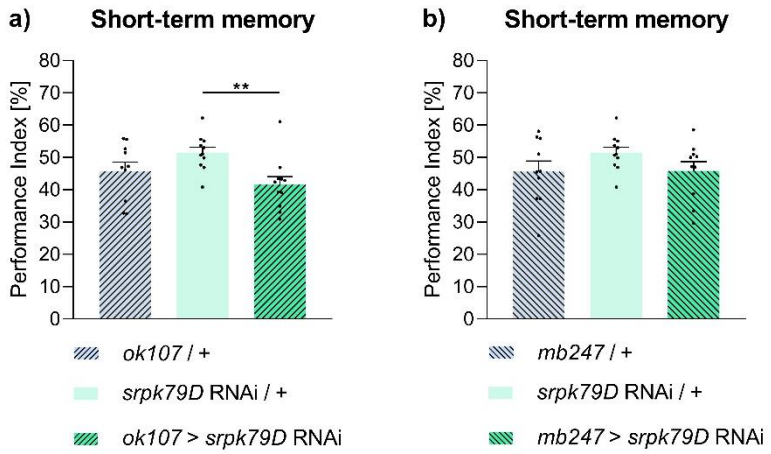

Figure 93: A restriction of attenuated *srpk79D* to the mushroom body shows no memory deficits.

Short-term memory (test directly after training) of deficient Aplip1 in the mushroom body for 5-days old flies. a) n = 10 *ok107* / +, n = 11 for *srpk79D* RNAi / +, n = 11 for *ok107* > *srpk79D* RNAi. b) n = 10 *mb247* / +, n = 11 for *srpk79D* RNAi / +, n = 10 for *mb247* > *srpk79D* RNAi. Statistics: one-way ANOVA with Sidak's multiple comparisons *post hoc* test, $^{**}p < 0.01$, $^{ns}p \geq 0.05$. Error bars: mean ± SEM.

Obviously, SRPK79D missing only in the mushroom body was not sufficient to reach the memory deficits of the null mutant. It could be that SRPK79D was necessary in other neurons. Developmental deficits must be considered since SRPK79D was lacking in the null mutant. Further tests with a restricted reduction in different tissues or Gal80^{ts}, forcing the srpk79D knockdown to adulthood, would be interesting. Longer-lasting memory phases could be examined as well.

	Olfactory acuity	
Genotype	3-Octanol (n)	4-Methylcyclohexanol (n)
ok107 / +	28.73 ± 7.479 (7)	53.71 ± 8.064 (8)
srpk79D RNAi / +	33.84 ± 8.324 (8)	78.73 ± 7.558 (7)
ok107 > *sprk79D* RNAi	61.82 ± 6.944 (6)	82.86 ± 4.263 (7)
mb247 / +	28.73 ± 10.18 (8)	50.40 ± 7.226 (8)
srpk79D RNAi / +	33.84 ± 8.324 (8)	78.73 ± 7.558 (7)
mb247 > *srpk79D* RNAi	44.53 ± 4.616 (7)	73.89 ± 6.490 (7)

Table 15: Innate behavior of diminished *srpk79D* in the mushroom body.

The olfactory acuities for diminished *srpk79D* in the mushroom body revealed no smell deficit compared to the controls. *ok107* > *srpk79D* RNAi performed significantly better against 3-Octanol than controls. Statistics: one-way ANOVA with Sidak's multiple comparisons *post hoc* test (parametric) or Kruskal-Wallis with Dunn's *post hoc* test (nonparametric), *$p < 0.05$, ns$p \geq 0.05$. Mean ± SEM.

3.2. Unc13, a regulating factor for the synaptic vesicle release at the presynapse

The gene *unc13* was first identified as 'uncoordinated mutant number 13' with an EMS-induced (Ethyl methanesulphonate) mutant screen in *C. elegans* in 1974 (Brenner, 1974). Unc13 was found to be highly conserved across different species, explicitly expressed in the nervous system, and as a critical synaptic vesicle (SV) release factor at the presynaptic active zone (AZ) (Aravamudan et al., 1999; Südhof, 2012). Unc13 makes SVs fusion-competent (priming) and defines the number and positions of SV release sites for an accurately timed neurotransmitter release (Reddy-Alla et al., 2017). Mutations in its mammalian ortholog (MUnc13) are associated with alcohol abuse and a higher risk for amyotrophic lateral sclerosis (Xu et al., 2018; Yang et al., 2019).

The ortholog in *Drosophila melanogaster*, DUnc13 (here referred to as Unc13), holds one lipid-binding C1 domain (reducing the energy-need for SV fusion), two calcium-binding C2 motifs (C2B binding Ca^{2+}, C2C bridging SVs to the plasma membrane), and one MUN domain,

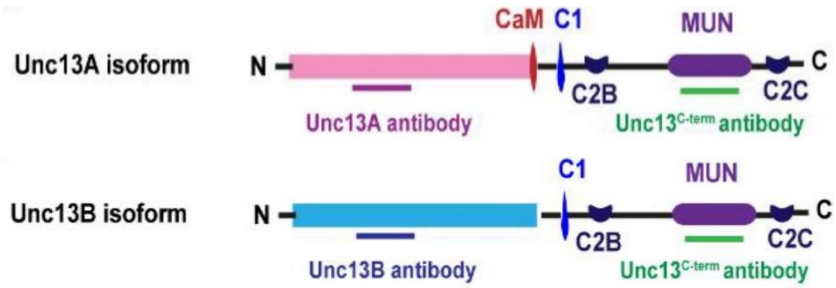

Figure 94: The two dominant isoforms of Unc13.

The C-termini of Unc13 A and Unc13B are equal with one C1 domain plus the two C2 motifs and the MUN domain. In contrast, the N-termini differ, and Unc13A possesses an additional calmodulin (CaM) motif in it (Aravamudan et al., 1999; Stevens et al., 2005). Epitopes for antibodies of Unc13A, Unc13B, or the Unc13 C-terminus are indicated. Schemes taken from Pooryasin et al., 2021.

responsible for SV priming (Figure 94; Aravamudan et al., 1999; Stevens et al., 2005; Basu et al., 2007; Quade et al., 2019; Piao and Sigrist, 2021). Two dominant isoforms of Unc13 exist, Unc13A and B, which differ at their N-termini. During the genesis of an AZ, BRP clusters Unc13A, while Syd-1 gathers Unc13B (Fulterer et al., 2018). In contrast to Unc13B, Unc13A possesses a calmodulin-binding site (CaM) which controls the SV refilling from the readily releasable pool (RRP) and thus short-term plasticity (STP) (Lipstein et al., 2013). This process is a fast adaptation within the synapse to alterations in action potential transmissions due to learning, and adjustment to the environment (Kandel et al., 2014; Böhme et al., 2019).

Additionally, Unc13A localizes at around 70 nm from the AZ center (marked by calcium channels). Unc13B clusters further away from the center at a distance of about 120 nm (Böhme et al., 2016; Fulterer et al., 2018). Taken together, Unc13A supports a fast, phasic probability of release to individual action potentials, whereas Unc13B promotes a slower, tonic release (Böhme et al., 2016; Fulterer et al., 2018; Woitkuhn and Ender et al., 2020). My question was how reducing such a crucial component of the presynaptic AZ interfered with learning and memory.

A null mutant of *unc13* does not survive beyond the embryonal stage (Aravamudan et al., 1999). Its synaptic transmission vanishes, accompanied by SV clusters near the AZ (Aravamudan et al., 1999; Böhme et al., 2016). Equally, *unc13A* null mutants show an impaired SV release with a decreased Bruchpilot amount (Böhme et al., 2016). The larvae can barely move but sometimes develop into a few weak adults (Böhme et al., 2016). In contrast, *unc13B* deletions survive easily until adulthood and possess only a slightly reduced evoked excitatory current (Böhme et al., 2016). An *unc13* Pacman rescue in the background of the *unc13* null allele, reexpressing both isoforms, was vital and developed until the adult phase. Equally, only the reexpression of *unc13A* (from now on named *unc13B* deletion) was vital. Thus, it was possible to conduct behavioral experiments with the *unc13B* deletion and the *unc13* rescue (A and B) (Figure 95; Böhme et al., 2016).

First, tests of innate behavior revealed a 3-Octanol odor acuity deficit for the Unc13 rescue, though recovery of only Unc13A (*unc13B* deletion) did not show this problem (Figure 95a). Similar with 4-Methylcyclohexanol, a significant failure in the smell ability of the Unc13 rescue occurred, yet no deficit could be observed between the wild-type w^{1118} and the *unc13B* deletion (Figure 95b). Results from Pooryasin et al., 2021, revealed Unc13A as necessary for appetitive and aversive innate smell behavior, while Unc13B was only essential for aversive smell abilities. Thus, the odor avoidances in Figure 95 appeared odd. Notably, the Pacman constructs brought only one unc13A and unc13B copy in the *unc13* rescue and one copy of *unc13A* in the *unc13B* deletion (Böhme et al., 2016). The wild-type typical two copies were not inserted.

Additionally, I tested short-term memory (STM) of these animals (Figure 95c). Here, the *unc13* rescue did not perform as well as the wild-type. Possibly, this was the impact of the missing gene copies, or the reason was the defect innate behavior so that these flies could not distinguish between the odors as well as w^{1118}. Interestingly, the bare *unc13A* component (*unc13B* deletion) performed even worse and showed a significant memory decrease compared to the rescue with both isoforms. Since this construct had no problems with its smell abilities, the memory decay to the full rescue (*unc13A* and *B*) was evident. Thus, mainly

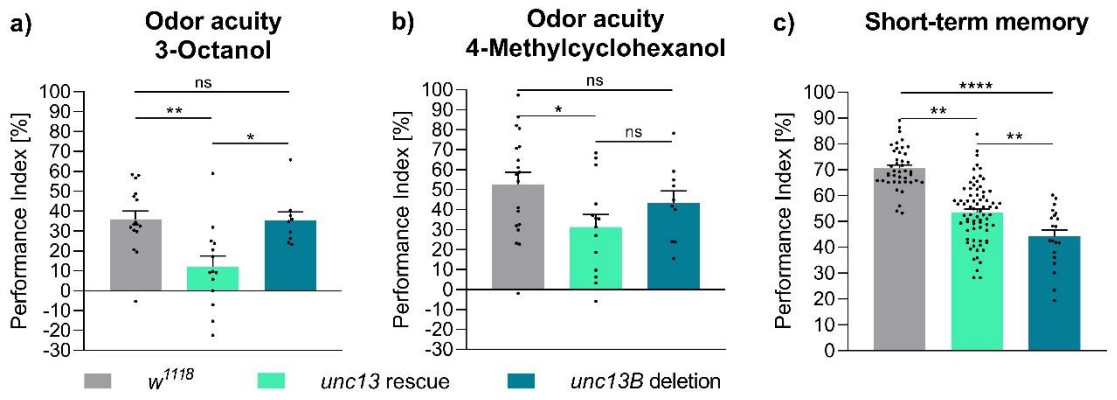

Figure 95: Behavior tests for *unc13* rescues in an *unc13* null mutation background.

Behavioral tests for rescues of *unc13* (with each one copy A and B) and its isoform *unc13A* (*unc13B* deletion) in the background of *unc13* null mutation. a-b) odor acuity tests. a) against 3-Octanol: n = 16 for w^{1118}, n = 14 for *unc13* rescue, n = 9 for *unc13B* deletion. b) against 4-Methylcyclohexanol: n = 19 for w^{1118}, n = 14 for *unc13* rescue, n = 10 for *unc13B* deletion. c) Short-term memory (test directly after training): n = 42 for w^{1118}, n = 74 for *unc13* rescue, n = 20 for *unc13B* deletion. Statistics: one-way ANOVA with Sidak's multiple comparisons *post hoc* test (parametric) or Kruskal-Wallis with Dunn's *post hoc* test (nonparametric), ****$p < 0.0001$, **$p < 0.01$, *$p < 0.05$, $^{ns}p \geq 0.05$. Error bars: mean ± SEM.

Unc13A influenced the memory formation in STM, yet both isoforms seemed essential to reach the memory of the full rescue.

Next, I separately attenuated *unc13A* or *unc13B* expression with RNAi, specifically in different regions involved in the olfactory memory system. First, I tested the STM of these animals (Figure 96). To target the first step of the odor recognition pathway, I drove *unc13A* RNAi and *unc13B* RNAi with *or83b*-Gal4. This olfactory co-receptor generates an olfactory signal with the olfactory receptors due to an odor (Fulterer et al., 2018). Neither attenuated *unc13A* (Figure 96a) nor *unc13B* (Figure 96d) showed a different memory performance than the control. The innate smell was slightly reduced for both deficient isoforms, yet not significantly (Table 16). Next, I targeted excitatory projection neurons, which forward the olfactory signal to the higher integration center for learning (Pooryasin et al., 2021). Interestingly, the reduced *unc13A* expression showed a significant loss of STM (Figure 96b). On the contrary, *gh146* > *unc13B* RNAi demonstrated no significant reduction in memory performance compared to the driver control (*gh146* / +) (Figure 96e). Thus, only Unc13A seemed to affect the memory formation in the projection neurons.

Furthermore, I examined the effect of missing Unc13A (Figure 96c) or B (Figure 96f) in the mushroom body, the memory formation region. Interestingly, both isoforms were essential for

the STM, which is the critical phase for memory acquisition. *ok107* > *unc13A* RNAi dropped by half, and *ok107* > *unc13B* RNAi by one-third.

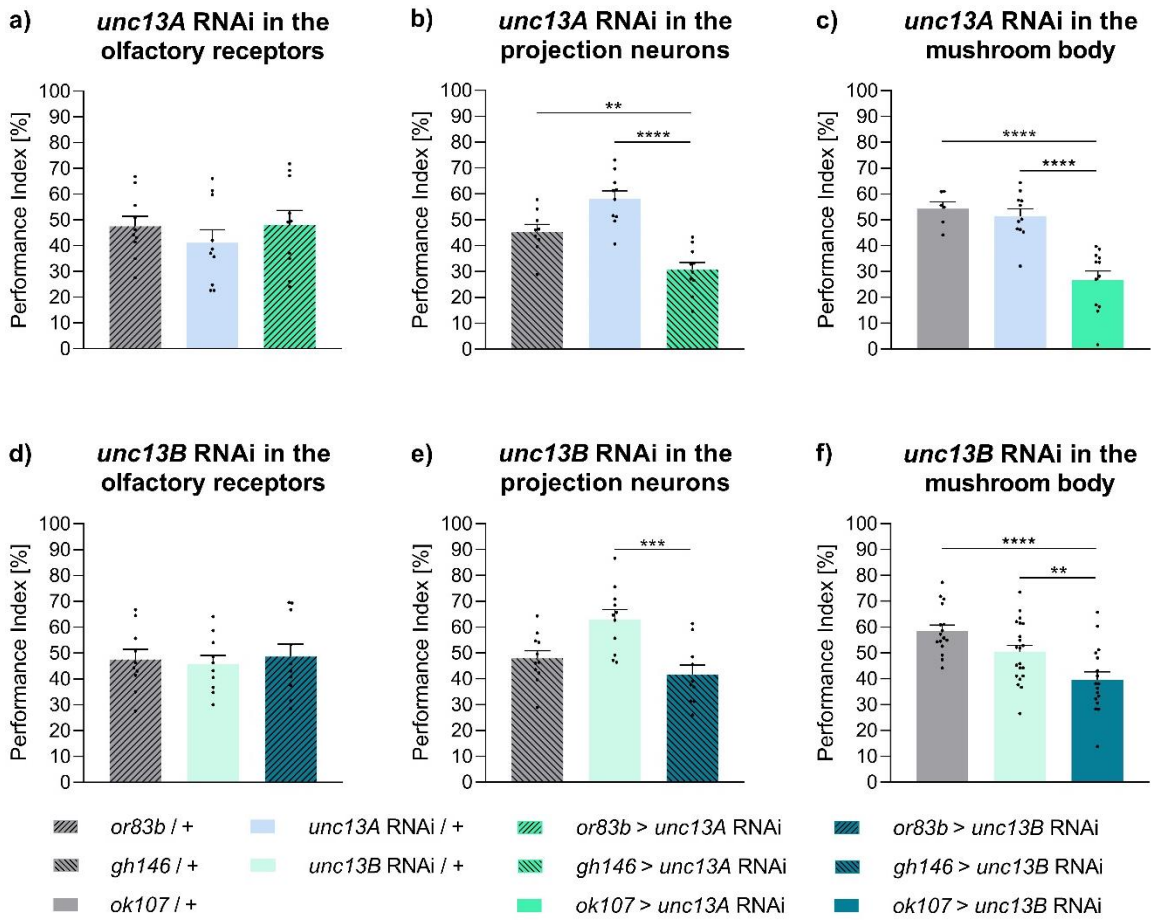

Figure 96: Short-term memory of unc13A or B RNAi in different regions of the olfactory learning pathway.

Aversive olfactory short-term memory (test directly after training) of 5- to 7-day old animals with reduced Unc13 A or B. a-c) *unc13A* RNAi with its controls. a) in the olfactory co-receptors: n = 10 for *or83b* / +, n = 10 for *unc13A* RNAi / +, n = 10 for *or83b* > *unc13A* RNAi. b) in the projection neurons: n = 9 for *gh146* / +, n = 10 for *unc13A* RNAi / +, n = 10 for *gh146* > *unc13A* RNAi. c) in the mushroom body: n = 6 for *ok107* / +, n = 11 for *unc13A* RNAi / +, n = 12 for *ok107* > *unc13A* RNAi. d-f) *unc13B* RNAi with its controls. d) in the olfactory co-receptors: n = 10 for *or83b* / +, n = 10 for *unc13B* RNAi / +, n = 10 for *or83b* > *unc13B* RNAi. e) in the projection neurons: n = 11 for *gh146* / +, n = 11 for *unc13B* RNAi / +, n = 10 for *gh146* > *unc13B* RNAi. f) in the mushroom body: n = 17 for *ok107* / +, n = 21 for *unc13B* RNAi / +, n = 17 for *ok107* > *unc13B* RNAi. Statistics: ordinary one-way ANOVA with Sidak's *post hoc* test, ****$p < 0.0001$, ***$p < 0.001$, **$p < 0.01$, $^{ns}p \geq 0.05$. Error bars: mean ± SEM.

Since attenuated *unc13A* in the projection neurons decreased memory performance, I examined longer-lasting memory in these flies. Indeed, significantly worse 3 hours mid-term memory (MTM) could be observed compared to the RNAi control (*unc13A* RNAi / +), yet there was no difference to the driver control (*gh146* / +) (Figure 97a). Neither 3 hours anesthesia-

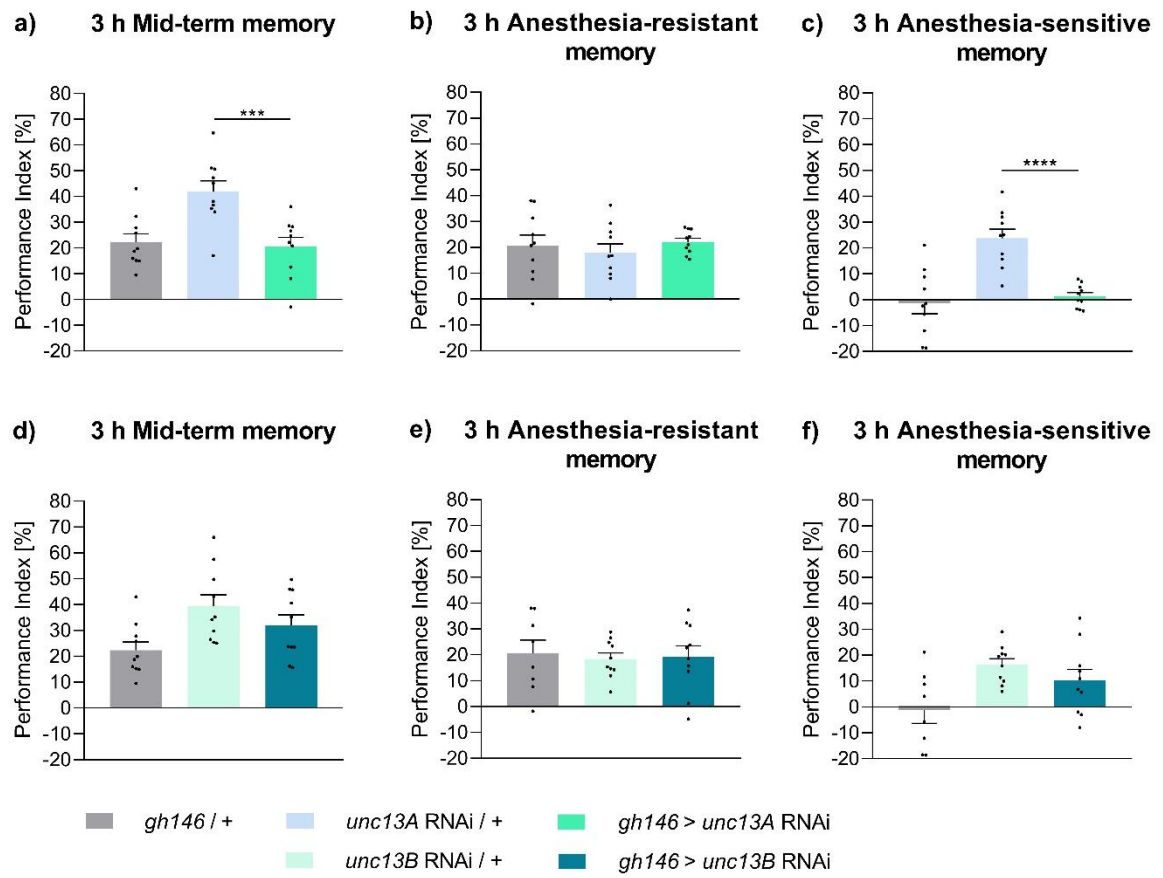

Figure 97: Longer-lasting memory shows no deficit for attenuated *unc13* isoforms in the projection neurons.

Aversive olfactory memory for 7-day old animals with reduced Unc13 A or B in the projection neurons. a-c) *unc13A* RNAi in the projection neurons. a) 3 hours mid-term memory (MTM; test 3 hours after training): n = 10 for *gh146* / +, n = 10 for *unc13A* RNAi / +, n = 10 for *gh146* > *unc13A* RNAi. b) 3 hours anesthesia-resistant memory (ARM; ice-bad 2.5 and test 3 hours after training): n = 10 for *gh146* / +, n = 10 for *unc13A* RNAi / +, n = 10 for *gh146* > *unc13A* RNAi. c) 3 hours anesthesia-sensitive memory (ASM): Results received via calculation of the median of 3 hours MTM minus the individual performance indices of 3 hours ARM. d-f) *unc13B* RNAi in the projection neurons. d) 3 hours MTM: n = 10 for *gh146* / +, n = 10 for *unc13B* RNAi / +, n = 10 for *gh146* > *unc13B* RNAi. e) 3 hours ARM: n = 8 for *gh146* / +, n = 10 for *unc13B* RNAi / +, n = 10 for *gh146* > *unc13B* RNAi. f) 3 hours ASM of *gh146* > *unc13B* RNAi and its controls. Statistics: one-way ANOVA with Sidak's multiple comparisons *post hoc* test, ****$p < 0.0001$, ***$p < 0.001$, $^{ns}p \geq 0.05$. Error bars: mean ± SEM.

resistant memory (ARM) nor 3 hours anesthesia-sensitive memory (ASM) showed a significantly diverging performance from both controls (Figure 97b-c). Additionally, I tested the 3 hours MTM, ARM, and ASM for *unc13B* RNAi in the projection neurons (Figure 97d-f). The longer-lasting memories did not differ from the controls. Thus, Unc13A seemed to be essential for the STM in the projection neurons (Figure 96b), while long-time memory phases were not affected (Figure 97a-c). Additionally, a reduction of Unc13's isoform B possessed no influence on any memory phase when expressed in the projection neurons (Figure 96e, Figure 97d-f).

Next, I focused on the mushroom body, the higher integration center for the generation and storage of memory in the brain of *Drosophila melanogaster* (Aso et al., 2014). Here, the mean performance index (PI) of 3 hours MTM was under zero (– 3.7 %) for *ok107* > *unc13A* RNAi (Figure 98a). This dramatic decrease resulted from severe memory impairment in 3 hours ASM (Figure 98c) and a lower performance in 3 hours ARM (Figure 98b). Despite using electric shock as a negative reinforcer, the 3 hours ASM even turned from aversive into appetitive behavior (mean PI – 7.8 %). According to Quinn et al., 1974, this behavior is called masochism. Interestingly, reduced Unc13 B showed a different memory profile. Even though its 3 hours MTM was significantly lower than the controls by 50 %, *ok107* > *unc13B* RNAi flies still avoided the negative connotated odor (Figure 98d). Additionally, neither the 3 hours ARM nor the 3 hours ASM showed any significant memory impairment compared to the controls (Figure 98e-f).

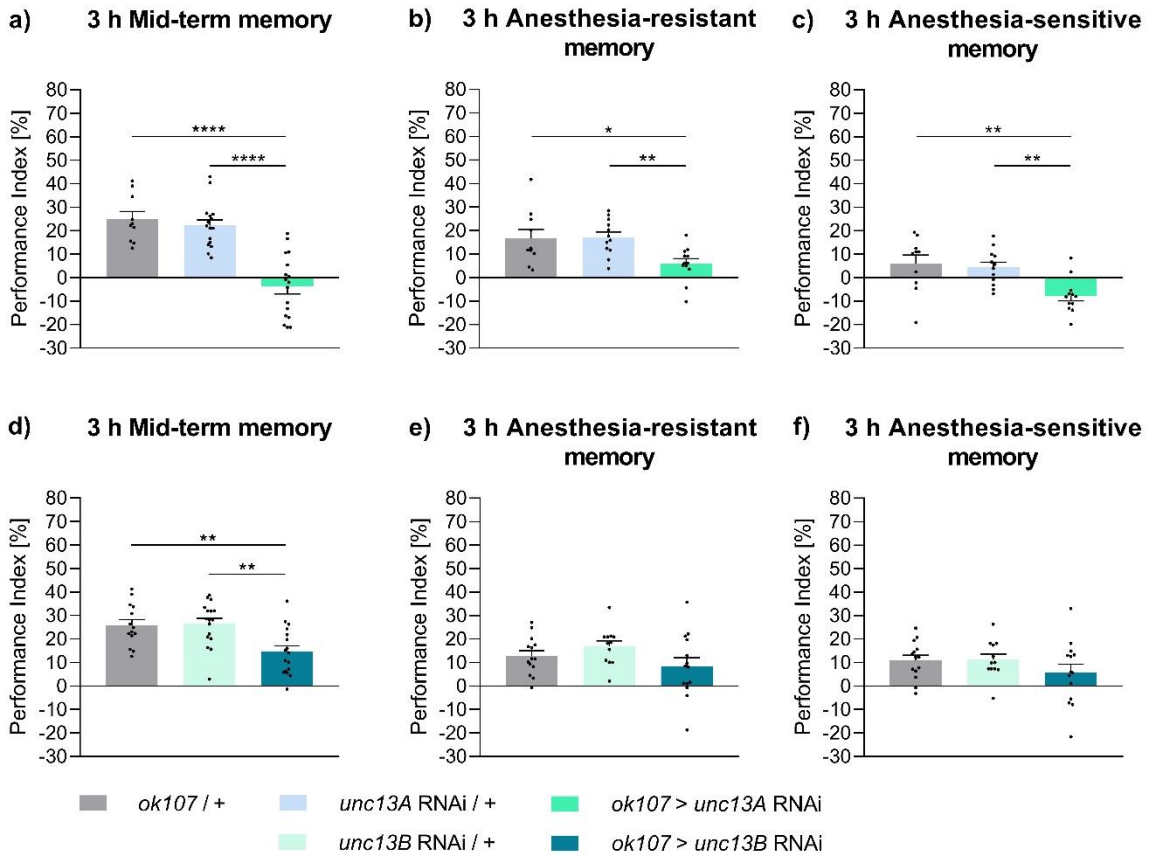

Figure 98: A deficit of Unc13 A in the learning center of the fly brain results in severe loss of 3 hours mid-term memory, while reduced Unc13 B shows milder defects.

Aversive olfactory memory for 6-day old animals with reduced Unc13 A or B in the mushroom body. a-c) *unc13A* RNAi in the mushroom body. a) 3 hours mid-term memory (MTM; test 3 hours after training): n = 10 for *ok107* / +, n = 16 for *unc13A* RNAi / +, n = 17 for *ok107* > *unc13A* RNAi. b) 3 hours anesthesia-resistant memory (ARM; ice-bad 2.5 hours and test 3 hours after training): n = 10 for *ok107* / +, n = 12 for *unc13A* RNAi / +, n = 12 for *ok107* > *unc13A* RNAi. c) 3 hours anesthesia-sensitive memory (ASM): Results received via calculation of the median of 3 hours MTM minus the individual performance indices of 3 hours ARM. d-f) *unc13B* RNAi in the mushroom body. d) 3 hours MTM: n = 14 for *ok107* / +, n = 17 for *unc13B* RNAi / +, n = 17 for *ok107* > *unc13B* RNAi. e) 3 hours ARM: n = 14 for *ok107* / +, n = 12 for *unc13B* RNAi / +, n = 14 for *ok107* > *unc13B* RNAi. f) 3 hours ASM for *ok107* > *unc13B* RNAi and its controls. Statistics: one-way ANOVA with Sidak's multiple comparisons *post hoc* test, ****$p < 0.0001$, **$p < 0.01$, *$p < 0.05$, $^{ns}p \geq 0.05$. Error bars: mean ± SEM.

In addition, I examined 1 hour MTM for each Unc13 isoform's RNAi expressed in the mushroom body. *ok107* > *unc13A* RNAi had severe memory problems, yet still above zero (Figure 99a). Similarly, animals with reduced *unc13B* in the mushroom body showed a significantly lower 1 h MTM than the controls (Figure 99d), though a milder drop than *unc13A* RNAi. Overall, even though the memory values were higher, the memory profile was similar to the 3 hours memory tests. Thus, 1 hour ARM and 1 hour ASM were both significantly lower after diminished *unc13A* knockdown in the mushroom body (Figure 99b-c). In contrast, *ok107* > *unc13B* RNAi appeared comparable to its controls in 1 hour ARM and 1 hour ASM (Figure 99e-f). Notably, 1 hour ARM was in both attenuated isoforms near zero, but only for *ok107* > *unc13A* RNAi significantly (Figure 99b, e). Interestingly, 1 hour ASM behavior showed a much clearer aversive memory performance than the 3 hours ASM values, especially visible in 3 hours ASM of *ok107* > *unc13A* RNAi appeared appetitive towards the negatively conditioned odor (Figure 98c). Though, memory performances also decreased for the controls from 1 to 3-hours tests.

The shock reactivities for *unc13A* RNAi and *unc13B* RNAi in the mushroom body appeared insignificant compared to the controls (Table 16). Additionally, the innate smell scores for Unc13A and Unc13B deficiencies in the relevant areas showed comparable performance indices to at least one of their controls for the used learning concentrations (Table 16). All odor acuities appeared insignificant.

Notably, Pooryasin et al., 2021, examined *unc13A* RNAi and *unc13B* RNAi in the projection neurons and found significantly decreased odor acuities to 4-Methylcyclohexanol and Benzaldehyde for both downregulations Though, they also demonstrated that enhanced odor concentrations could improve the smell acuity. The odor concentrations used for the memory tests were higher and saturated. The here conducted odor acuity tests (Table 16) were performed with these higher concentrations and appeared insignificant to at least one control.

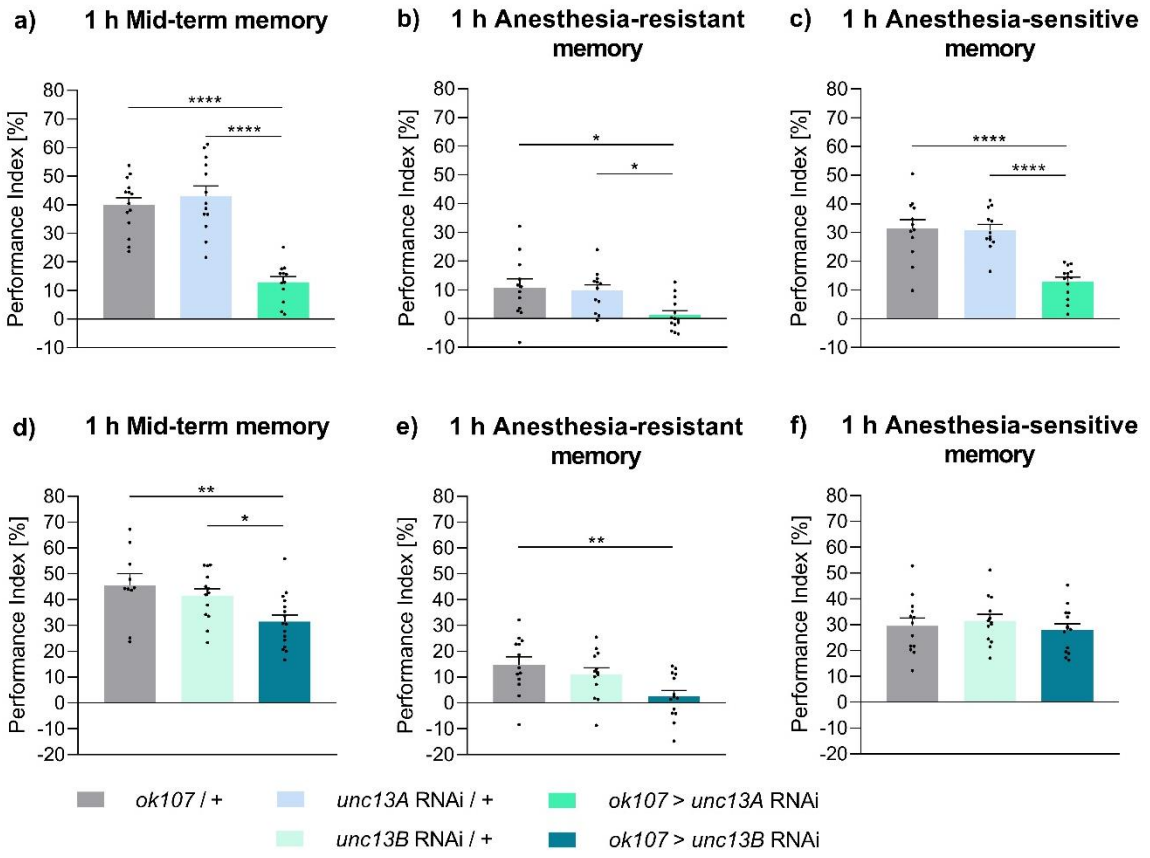

Figure 99: Decreased Unc13 isoforms in the mushroom body show a similar memory profile for 1 hour and 3 hours mid-term memory.

Aversive olfactory memory for 6-day old animals with reduced Unc13 A or B in the mushroom body. a-c) *unc13A* RNAi in the mushroom body. a) Performance Index for 1 hour mid-term memory (test 1 hour after training): n = 14 for *ok107* / +, n = 13 for *unc13A* RNAi / +, n = 12 for *ok107* > *unc13A* RNAi. b) Performance Index for 1 hour anesthesia-resistant memory (ice-bad 30 min and test 1 hour after training): n = 12 for *ok107* / +, n = 12 for *unc13A* RNAi / +, n = 14 for *ok107* > *unc13A* RNAi. c) Performance Index for 1 hour anesthesia-sensitive memory: Results received via calculation of the median of 1 hour mid-term memory minus the individual performance indices of 1 hour anesthesia-resistant memory. d-f)) *unc13B* RNAi in the mushroom body. d) Performance Index for 1 hour mid-term memory (test 1 hour after training): n = 10 for *ok107* / +, n = 13 for *unc13B* RNAi / +, n = 16 for *ok107* > *unc13B* RNAi. e) Performance Index for 1 hours anesthesia-resistant memory (ice-bad 30 min and test 1 hour after training): n = 13 for *ok107* / +, n = 13 for *unc13B* RNAi / +, n = 14 for *ok107* > *unc13B* RNAi. f) Performance Index for 1 hour anesthesia-sensitive memory: Results received via calculation of the median of 1 hour mid-term memory minus the individual performance indices of 1 hour anesthesia-resistant memory. Statistics: one-way ANOVA with Sidak's multiple comparisons *post hoc* test, ****$p < 0.0001$, **$p < 0.01$, *$p < 0.05$, $^{ns}p \geq 0.05$. Error bars: mean ± SEM.

		Olfactory acuity	
Genotype	Shock reactivity (n)	Benzaldehyde (n)	4-Methylcyclohexanol (n)
or83b / +	-	45.53 ± 8.583 (6)	49.60 ± 9.651 (4)
unc13A RNAi / +	-	42.82 ± 5.614 (6)	41.50 ± 12.63 (4)
or83b > *unc13A* RNAi	-	34.20 ± 7.071 (6)	27.88 ± 12.38 (4)
or83b / +	-	45.53 ± 8.583 (6)	49.60 ± 9.651 (4)
unc13B RNAi / +	-	36.58 ± 7.290 (6)	41.15 ± 7.609 (6)
or83b > *unc13B* RNAi	-	31.87 ± 8.460 (6)	36.77 ± 9.811 (6)
gh146 / +	-	42.00 ± 7.004 (19)	43.86 ± 5.224 (24)
unc13A RNAi / +	-	65.33 ± 5.361 (18)	66.03 ± 5.432 (22)
gh146 > *unc13A* RNAi	-	44.88 ± 5.857 (18)	42.46 ± 6.325 (22)
gh146 / +	-	42.00 ± 7.004 (19)	43.86 ± 5.224 (24)
unc13B RNAi / +	-	65.33 ± 5.361 (18)	66.03 ± 5.432 (22)
gh146 > *unc13B* RNAi	-	44.88 ± 5.857 (18)	42.46 ± 6.325 (22)
Genotype	Shock reactivity (n)	3-Octanol (n)	4-Methylcyclohexanol (n)
ok107 / +	90.95 ± 2.387 (12)	45.52 ± 5.280 (10)	71.71 ± 4.584 (16)
unc13A RNAi / +	87.07 ± 2.445 (13)	44.90 ± 4.163 (10)	64.60 ± 5.519 (21)
ok107 > *unc13A* RNAi	89.42 ± 2.045 (13)	49.83 ± 3.048 (10)	71.40 ± 4.197 (19)
ok107 / +	90.95 ± 2.387 (12)	45.40 ± 3.920 (14)	71.71 ± 4.584 (16)
unc13B RNAi / +	91.46 ± 1.530 (13)	37.24 ± 3.330 (14)	67.12 ± 4.763 (18)
ok107 > *unc13B* RNAi	95.05 ± 1.188 (13)	38.54 ± 5.680 (14)	71.16 ± 4.233 (16)

Table 16: Innate behavior of *unc13A* and *B* RNAi in different areas of the olfactory memory system.

Shock reactivity and olfactory acuities for attenuated *unc13A* or *unc13B* showed no significant differences than at least one of their controls when expressed in the specific regions involved in olfactory memory (olfactory co-receptor with *or83b*-Gal4, projection neurons with *gh146*-Gal4, mushroom body with *ok107*-Gal4). Statistics: one-way ANOVA with Sidak's multiple comparisons *post hoc* test (parametric) or Kruskal-Wallis with Dunn's *post hoc* test (nonparametric), ***$p < 0.001$, **$p < 0.01$ *$p < 0.05$, $^{ns}p \geq 0.05$. Mean ± SEM.

3.2.1. The isoform Unc13A in focus

Since Unc13A was the more crucial isoform to build memories in all tested categories of aversive olfactory memory, I conducted further experiments with constructs missing either the N- or C-terminal region of the protein. The Unc13A C-terminus construct possesses the lipid-binding C1 domain, two calcium-binding C2 motifs, and one MUN domain, responsible for the priming of synaptic vesicles (SVs) and the generation of SV release sites (Figure 100; Aravamudan et al., 1999; Stevens et al., 2005; Reddy-Alla et al., 2017). The N-terminus construct holds the calmodulin site (CaM) of Unc13A, which controls the SV refilling of the readily releasable pool (Lipstein et al., 2013). Additionally, the N-terminus anchors Unc13A to the active zone (Reddy-Alla et al., 2017). Both constructs were tagged with a GFP tag.

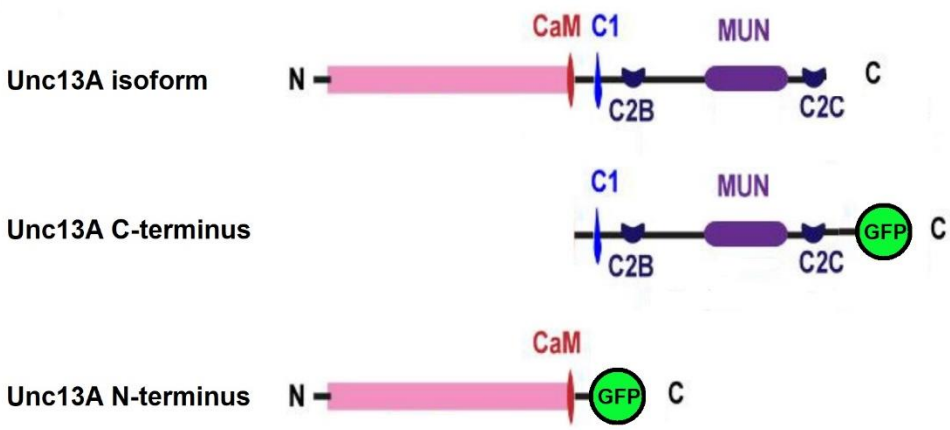

Figure 100: Schemes of Unc13A and its constructs from the C- and N-termini.

The C-terminus of Unc13A possesses one lipid-binding C1 motif, two calcium-binding C2 domains, and the MUN domain, responsible for the synaptic vesicle priming activity and the generation of release sites (Aravamudan et al., 1999; Stevens et al., 2005). In contrast, Unc13A's N-terminus holds a calmodulin site (CaM), which controls the synaptic vesicle refilling of the readily releasable pool (Lipstein et al., 2013). Additionally, it anchors Unc13A to the active zone (Reddy-Alla et al., 2017). Schemes taken from Pooryasin et al., 2021.

First, I examined a rescue with the Unc13A C-terminus in the background of *unc13A* RNAi in the mushroom body. This area is a higher integration center, where learning and memory storage happens (Aso et al., 2014). Immunostainings demonstrated a typical shaped mushroom body for all tested groups and validated the presence of the respective compositions in the experimental flies (Figure 101). Here, Bruchpilot's (BRP) C-terminus, labeled with the antibody Nc82, served as the marker for the mushroom body structure (Figure 101, first column, cyan). The second column (Figure 101, magenta) indicated the GFP-tag,

thus the presence of the C-terminus. The third column (Figure 101, yellow) with immunostainings against the N-terminus of Unc13A demonstrated the existence of endogenous Unc13A (no GFP-tag). Curiously, the overexpression of the C-terminus in the mushroom body seemed to hold no endogenous Unc13A (last row, third column). Only the heel of the mushroom body was visible in the lower left, but vaguely. Likely, the genetically overexpressed C-terminus overlayed the endogenous Unc13A and disturbed the labeling of its N-terminus. The last column was a merge of the other three.

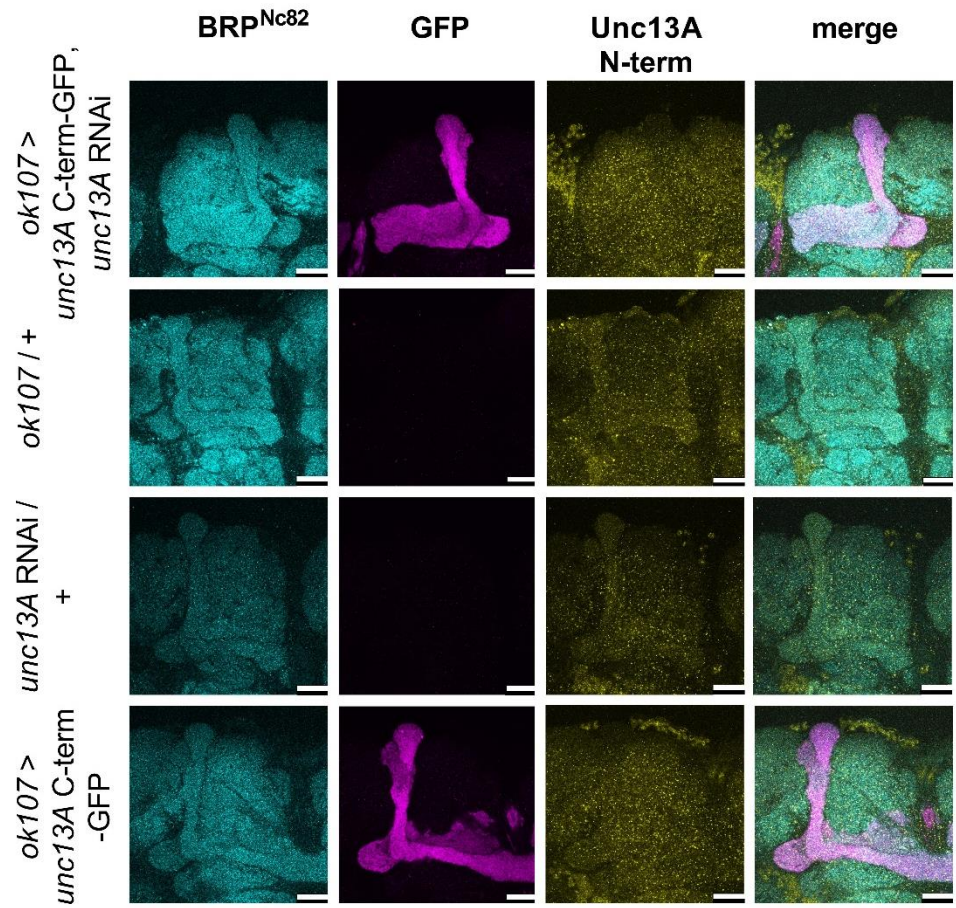

Figure 101: Immunostainings of the mushroom body, indicating the different experimental situations.

Immunostainings of the Unc13A C-terminus rescue in the mushroom body, with *unc13A* RNAi as background. Rows show the genotypes (from top to bottom): *ok107* > *unc13A* C-term-GFP,*unc13A* RNAi (only Unc13A C-terminus driven in the mushroom body, endogenous *unc13A* downregulated), *ok107* / + (endogenous Unc13A present), *unc13A* RNAi / + (endogenous Unc13A present), *ok107* > *unc13A* C-term-GFP (overexpression of Unc13A C-terminus, endogenous Unc13A present). Columns show the used antibodies (from left to right): Bruchpilot (BRP^{Nc82}; marker for the mushroom body), GFP, Unc13A N-terminus (marker for the endogenous Unc13A), and merge of the three antibodies. Images: single slide. Scale bar: 20 µm.

I already showed that a deficit of Unc13A in the mushroom body could reduce all tested memory components (Figure 96c, Figure 98, Figure 99). Next, I wanted to know if the reexpression of the Unc13A C-terminus could rescue this memory impairment. The pur C-terminus in the mushroom body (*ok107* > *unc13A* C-term-GFP,*unc13A* RNAi) could not bring the short-term memory (STM) back. The driver control (*ok107* / +), the RNAi control (*unc13A* RNAi / +), and the Unc13A C- terminus overexpression in the mushroom body (*ok107* > *unc13A* C-term-GFP) performed comparable around 50 % (Figure 102a). A similar profile was visible for longer-lasting memory. 1 and 3 hours mid-term memory (MTM) was significantly reduced for the C-terminus rescue in the *unc13A* RNAi background. The other tested flies possessed normal memory (Figure 102d, g). These findings were consistent with the memory for *unc13A* knockdown in the mushroom body (Figure 96c, Figure 98a, Figure 99a). Just like the full *unc13A* knockdown, the consolidated 1 hour anesthesia-resistant memory (ARM) and the labile 1 hour anesthesia-sensitive memory (ASM) went down (Figure 102e-f, Figure 99b-c). Thus, the C-terminus in the mushroom body alone could not rescue the earlier memory impairment. In contrast, 3 hours ARM and ASM were severely reduced, yet there was no significant drop to one control in each case (Figure 102h-i, Figure 98b-c). Maybe the memory phases after 3 hours become less affected. Interestingly, the genetically expressed C-terminus on the top of the endogenous Unc13A increased 1 hour ARM massively but impaired 1 hour ASM to the same height as the C-terminus alone (Figure 102e-f). Likewise, 3 hours ARM was raised due to the C-terminus overexpression, again increased significantly to its control (Figure 102h). Concomitantly, 3 hours ASM was low, yet the control *unc13A* RNAi / + as well (Figure 102i). According to Reddy-Alla et al., 2017, an expression of only the C-terminus fragment increases the release sites dramatically but shows a low release probability and inefficient transmission at the synapses. Possibly, the additional C-terminus construct, with endogenous Unc13A in its background, facilitated further SV release sites, here improving the signal transfer, which affected the ARM component positively yet not the ASM. Notably, the innate smell behavior was comparable among all tested groups (Figure 102b-c).

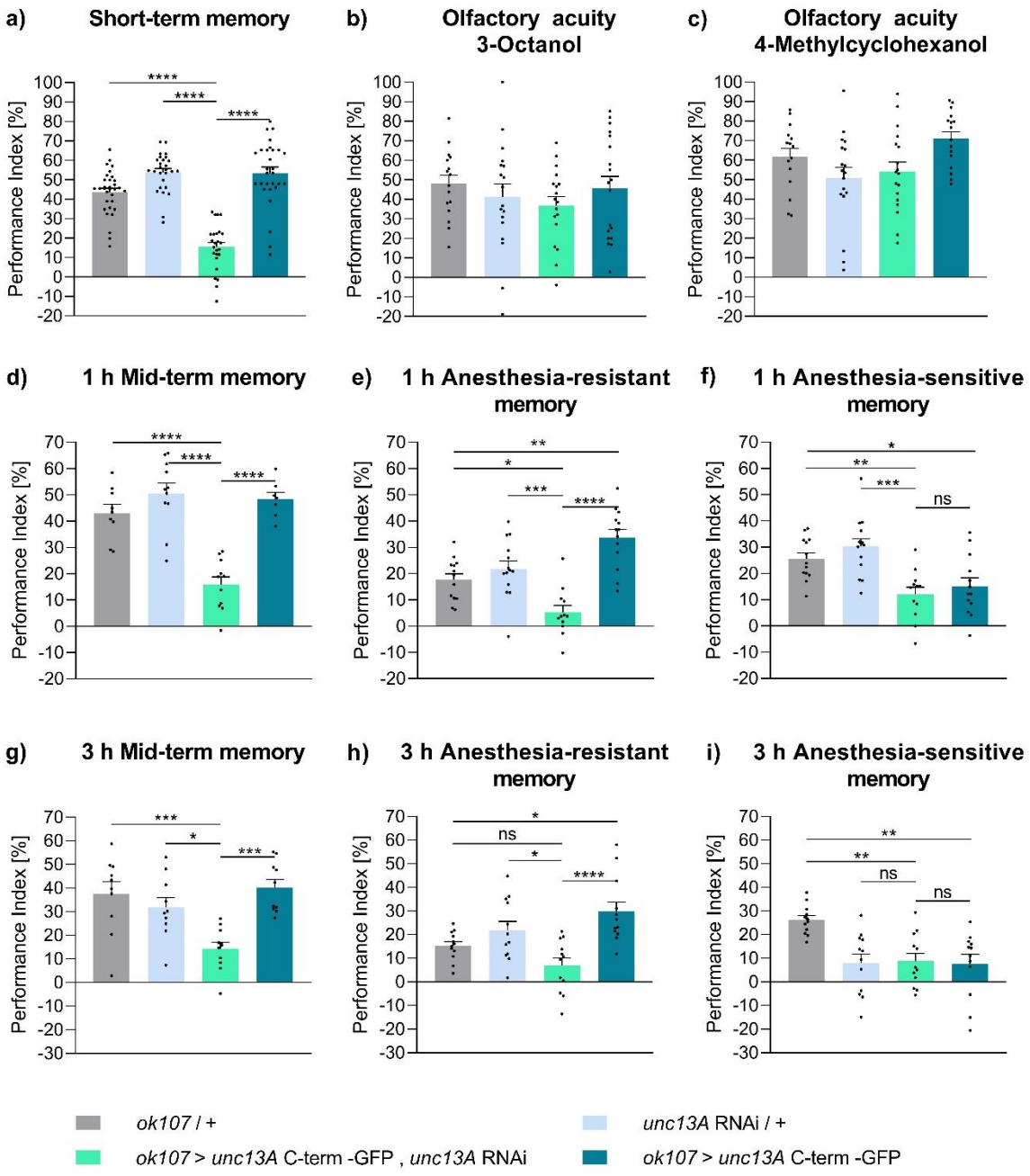

Figure 102: Memory phases and innate behavior of the Unc13A C-terminus rescue.

Aversive olfactory memory tests for 6-day old animals with Unc13A C-terminus in the mushroom body. a) Short-term memory (test directly after training): n = 32 for *ok107* / +, n = 27 for *unc13A* RNAi / +, n = 25 for *ok107* > *unc13A* C-term-GFP , *unc13A* RNAi, n = 29 for *ok107* > *unc13A* C-term-GFP. b-c) Odor acuity. b) 3-Octanol: n = 16 for *ok107* / +, n = 18 for *unc13A* RNAi / +, n = 18 for *ok107* > *unc13A* C-term-GFP , *unc13A* RNAi, n = 19 for *ok107* > *unc13A* C-term-GFP. c) 4-Methylcyclohexanol: n = 15 for *ok107* / +, n = 18 for *unc13A* RNAi / +, n = 18 for *ok107* > *unc13A* C-term-GFP , *unc13A* RNAi, n = 16 for *ok107* > *unc13A* C-term-GFP. d-f) 1 hour memory: d) Mid-term memory (MTM; test 1 hour after training): n = 9 for *ok107* / +, n = 11 for *unc13A* RNAi / +, n = 11 for *ok107* > *unc13A* C-term-GFP , *unc13A* RNAi, n = 7 for *ok107* > *unc13A* C-term-GFP. e)

Anesthesia-resistant memory (ARM; ice-bad 30 min and test 1 hour after training): n = 13 for *ok107* / +, n = 14 for *unc13A* RNAi / +, n = 12 for *ok107* > *unc13A* C-term-GFP , *unc13A* RNAi, n = 13 for *ok107* > *unc13A* C-term-GFP. f) Anesthesia-sensitive memory (ASM): Results received via calculation of the median of 1 hour MTM minus the individual performance indices of 1 hour ARM. g-i) 3 hours memory: g) MTM (test 3 hours after training): n = 10 for *ok107* / +, n = 10 for *unc13A* RNAi / +, n = 11 for *ok107* > *unc13A* C-term-GFP , *unc13A* RNAi, n = 10 for *ok107* > *unc13A* C-term-GFP. h) ARM (ice-bad 2.5 hours and test 3 hours after training): n = 12 for *ok107* / +, n = 12 for *unc13A* RNAi / +, n = 12 for *ok107* > *unc13A* C-term-GFP , *unc13A* RNAi, n = 12 for *ok107* > *unc13A* C-term-GFP. i) ASM: Results received via calculation of the median of 3 hours MTM minus the individual performance indices of 3 hours ARM. Statistics: one-way ANOVA with Sidak's multiple comparisons *post hoc* test (parametric) or Kruskal-Wallis with Dunn's *post hoc* test (nonparametric), ****$p < 0.0001$, ***$p < 0.001$, **$p < 0.01$, *$p < 0.05$, $^{ns}p \geq 0.05$. Error bars: mean ± SEM.

Next, I focused on the N-terminus of Unc13A. The N-terminal Unc13A construct displaces the endogenous Unc13A due to competition within the AZ (Reddy-Alla et al., 2017). Thus, the endogenous Unc13A does not function normally, and the Unc13A N-terminus operates dominant negatively. I expressed this construct in the mushroom body. These flies performed dramatically worse in short-term memory than the controls (Figure 103a). Though, a severe impairment appeared also in the innate smell behavior (Figure 103b-c). The olfactory acuity of 3-Octanol dropped significantly compared to both controls and was decreased for 4-Methylcyclohexanol as well, although not significantly. Accordingly, the results for the short-term memory could be due to defective odor acuity. Additionally, immunostainings of these flies revealed a misshaped mushroom body (Huang, 2019).

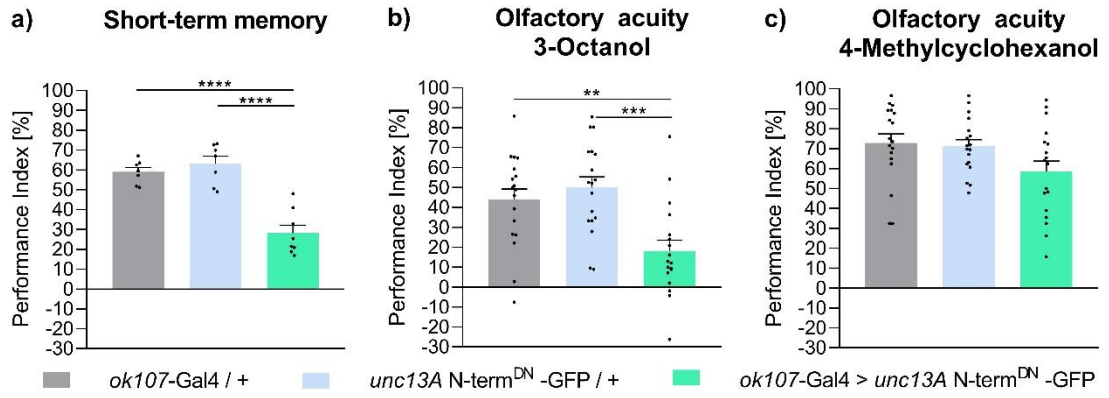

Figure 103: Only Unc13A N-terminus in the mushroom body shows odor acuity and memory deficits.

Aversive olfactory memory tests for 6-day old animals with only the N-terminus of Unc13A active in the mushroom body. a) Short-term memory (test directly after training): n = 7 for *ok107* / +, n = 7 for *unc13A* N-term^{DN} -GFP / +, n = 8 for *ok107* > *unc13A* N-term^{DN} -GFP. b) 3-Octanol odor acuity: n = 18 for *ok107* / +, n = 18 for *unc13A* N-term^{DN} -GFP / +, n = 18 for *ok107* > *unc13A* N-term^{DN} -GFP. c) 4-Methylcyclohexanol odor acuity: n = 18 for *ok107* / +, n = 18 for *unc13A* N-term^{DN} -GFP / +, n = 18 for *ok107* > *unc13A* N-term^{DN} -GFP. Statistics: one-way ANOVA with Sidak's multiple comparisons *post hoc* test (parametric) or Kruskal-Wallis with Dunn's *post hoc* test (nonparametric), ****$p < 0.0001$, ***$p < 0.001$, **$p < 0.01$, $^{ns}p \geq 0.05$. Error bars: mean ± SEM.

In contrast, the odor acuity was not diminished when I expressed Unc13A N-terminus solely during the flies' adulthood via temperature-sensitive inhibition of the expression during development (*tub*-Gal80^{ts}) (Table 17). Immunostainings of the fly brains with FasII as mushroom body marker revealed a typically shaped mushroom body in confocal images (Figure 104a). The expression of the Unc13A N-terminus was indicated through its GFP tag. Interestingly, short-term memory was no longer significantly reduced in these flies. Thus, the former memory deficit for *ok107* > *unc13A* N-term^{DN}-GFP resulted from the deformed mushroom body or the diminished odor acuity (Figure 103). However, *tub*-Gal80^{ts} ;; *ok107*-Gal4 > *unc13A* N-term^{DN}-GFP performed significantly lower than the driver control in the 1 hour mid-term memory and slightly lower than *unc13A* N-term^{DN}-GFP/+ (Figure 104c). 1 hour ARM appeared comparable to the controls (Figure 104d). Intriguingly, these animals possessed clearly reduced 1 hour ASM with a lower memory than both controls (Figure 104e). Reddy-Alla et al., 2017, showed the presence of the pure N-terminus of Unc13A inhibits functional SV release sites and has adverse effects on synaptic transmission. Thus, the impeded labile memory, 1 h ASM, could come from a decreased availability of SV release sites. Taken together, the sole Unc13A N-terminus in the mushroom body, restricted to adulthood, impaired only 1 h ASM.

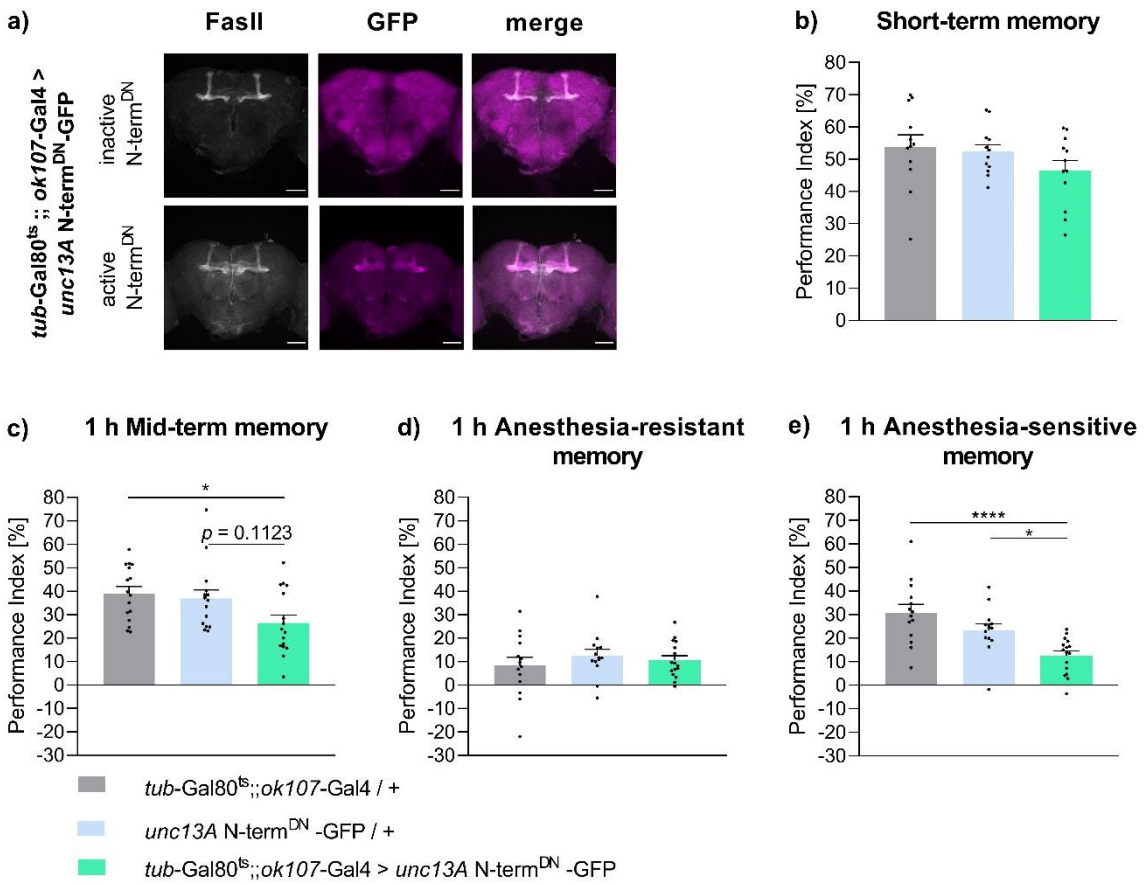

Figure 104: Restricted to adulthood, only the Unc13A N-terminus active in the mushroom shows a drop in anesthesia-sensitive memory.

Immunostainings and aversive olfactory memory tests, restricted to adulthood, only the Unc13A N-terminus active in the mushroom body, 6-day old. a) Immunostainings: First row with the inactive *unc13A* N-term^{DN}-GFP as control. Second row with the active *unc13A* N-term^{DN}-GFP expressed in the mushroom body. Columns present with FasII (a marker for the mushroom body) and GFP (showing the Unc13A N-terminus), plus their merge. Scale bar: 50 µm. b) Short-term memory (test directly after training): n = 12 for *tub*-Gal80^{ts} / + ;; *ok107* / +, n = 12 for *unc13A* N-term^{DN}-GFP / +, n = 12 for *tub*-Gal80^{ts} ;; *ok107* > *unc13A* N-term^{DN}-GFP. c) 1 hour mid-term memory (test 1 hour after training): n = 16 for *tub*-Gal80^{ts} / + ;; *ok107* / +, n = 15 for *unc13A* N-term^{DN}-GFP / +, n = 16 for *tub*-Gal80^{ts} ;; *ok107* > *unc13A* N-term^{DN}-GFP. d) 1 hour anesthesia-resistant memory (ice-bad 30 min and test 1 hour after training): n = 14 for *tub*-Gal80^{ts} / + ;; *ok107* / +, n = 14 for *unc13A* N-term^{DN}-GFP / +, n = 16 for *tub*-Gal80^{ts} ;; *ok107* > *unc13A* N-term^{DN}-GFP. e) 1 hour anesthesia-sensitive memory: Results received via calculation of the median of 1 hour mid-term memory minus the individual performance indices of 1 hour anesthesia-resistant memory. Statistics: one-way ANOVA with Sidak's multiple comparisons *post hoc* test (parametric) or Kruskal-Wallis with Dunn's *post hoc* test (nonparametric), , ****$p < 0.0001$, *$p < 0.05$, $^{ns}p \geq 0.05$. Error bars: mean ± SEM. Immunostainings by Sheng Huang.

Since diminished Unc13A in the mushroom body possessed drastically reduced 1 hour memory for all components (Figure 99a-c), both termini of Unc13A could have an additive effect. The N-terminus affected only the labile memory (Figure 104e), while the C-terminus impacted all memory phases (Figure 102) to a lesser degree than the *unc13A* knockdown in the mushroom body. However, the C-terminus' expression was not restricted to the adulthood of the flies as the N-terminus in Figure 104, and the defective memory could have its origin in developmental stages (Figure 102). In contrast to a life-long expression of the N-terminus in the mushroom body (Figure 103, Huang, 2019), the life-long C-terminus expression did not evoke a misshaped mushroom body nor any deficits in innate smell behavior (Figure 101, Figure 102b-c). Thus, the preconditions for functional learning and memory acquisition existed. Additionally, it would be interesting to reexpress both constructs, the Unc13A C- and N-terminus, in the background of *ok107* > *unc13A* RNAi to see if they could fulfill all functions of full-length Unc13A.

All residual innate behavior showed comparable performances to at least one of their controls for the used learning concentrations (Table 17). Both odor acuities for 3-Octanol and 4-Methylcyclohexanol were insignificant, except for the former mentioned chronically expressed Unc13A N-terminus in the mushroom body (*ok107* > *unc13A* N-term^{DN} -GFP; Figure 103b-c). Additionally, the shock reactivities appeared normal compared to at least one control (Table 17).

Genotype	Shock reactivity (n)	Olfactory acuity	
		3-Octanol (n)	4-Methylcyclohexanol (n)
1) *ok107* / +	85.49 ± 1.639 (12)	48.03 ± 4.372 (16)	61.65 ± 4.438 (15)
2) *unc13A* RNAi / +	73.70 ± 2.689 (12)	41.32 ± 6.658 (18)	50.72 ± 5.599 (18)
3) *ok107* > *unc13A* C-term-GFP, *unc13A* RNAi	79.52 ± 2.734 (12)	36.84 ± 4.578 (18)	54.14 ± 4.945 (18)
4) *ok107* > *unc13A* C-term -GFP	79.48 ± 3.372 (12)	45.76 ± 6.002 (19)	71.03 ± 3.557 (16)
1) *ok107* / +	91.42 ± 2.136 (6)	43.80 ± 5.499 (18)	72.81 ± 4.607 (18)
2) *unc13A* N-term^{DN} -GFP / +	81.85 ± 3.155 (6)	49.91 ± 5.386 (18)	71.22 ± 3.272 (18)
3) *ok107* > *unc13A* N-term^{DN} -GFP	88.91 ± 1.691 (10)	18.08 ± 5.476 (18)	58.41 ± 5.403 (18)
1) *tub*-Gal80^{ts} / + ;;	95.08 ± 1.045 (10)	44.03 ± 9.953 (12)	43.23 ± 5.946 (12)
ok107 / +	85.13 ± 1.794 (10)	38.93 ± 8.790 (12)	42.79 ± 3.546 (12)
2) *unc13A* N-term^{DN}-GFP / +	93.32 ± 1.068 (10)	26.60 ± 10.15 (12)	44.72 ± 5.438 (12)
3) *tub*-Gal80^{ts} ;; ok107 > *unc13A* N-term^{DN} -GFP			

Table 17: Innate behavior of the conducted C- or N-terminus of Unc13A, expressed in the mushroom body.

The shock reactivities were not significantly different from at least one of the belonging controls. The olfactory acuities appeared insignificant, but ok107 > unc13A N-termDN-GFP appeared significantly lower for 3-Octanol. Statistics: one-way ANOVA with Sidak's multiple comparisons *post hoc* test (parametric) or Kruskal-Wallis with Dunn's *post hoc* test (nonparametric), ***p < 0.001, **p < 0.01 *p < 0.05, nsp ≥ 0.05. Mean ± SEM.

IV. Discussion

1. Learning and memory formation in the context of aging

Learning is a fundamental ability to deal with the environment and external circumstances to survive. Depending on the importance and repetition, this learned information becomes consolidated and lasts longer, or fades with time. Though, the older we get, the harder it becomes to form new memories. The problem is how to address age-induced memory impairment in research. One solution is using a relatively simpler animal model like *Drosophila melanogaster* due to its short lifespan, easy genetic access, and evolutionary conserved aging mechanisms between flies and humans (Tamura et al., 2003; Davis, 2005; Mery, 2007; Bishop et al., 2010). With aversive olfactory conditioning, I investigated the impact of several aging mechanisms on memory formation. The olfactory system in adult *Drosophila melanogaster* is less complex than the mammalian one yet holds remarkable homologies in the fundamental anatomical organization and function (Hildebrand and Shepherd, 1997; Davis, 2004).

Memories themselves can be seen as traces in the neuronal tissues, cellular and synaptic plasticity regarding changes in the neuronal network induced by experiences (Christiansen et al., 2011; Davis, 2011). Thereby, presynaptic plasticity is the flexibility of the synaptic organization to adjust itself for the needed transmission strength. Though with aging, the presynaptic plasticity changes with dramatic increases of active zone components like Unc13A, Bruchpilot (BRP), and RIM-binding protein (RIM-BP) (Gupta et al., 2016; Huang et al., 2020). Thus, the transmission of signals becomes impaired, and the generation of memories is hindered (Gupta et al., 2016; Huang et al., 2020).

2. The nano-architecture in the presynapse

The probability of releasing synaptic vesicles (SVs), thus transmitting signals can vary extremely between different neuronal tissues, even though the elementary composition of the presynaptic active zones (AZs) stays the same (Akbergenova et al., 2018; Piao and Sigrist, 2021). Unc13 is the SV priming and release factor within the presynaptic AZ and generates SV release sites (Reddy-Alla et al., 2017). Several studies revealed a nanoscopic stable distribution of Unc13's two dominant isoforms, Unc13A and B, to the presynaptic AZ center: Unc13A clusters closer to the Ca^{2+} channels while Unc13B localizes at a larger distance (Böhme et al., 2016; Fulterer et al., 2018; Woitkuhn and Ender et al., 2020; Pooryasin et al., 2021). Interestingly, this goes along with Unc13A, supporting a high phasic release probability to individual action potentials, and Unc13B, promoting a lower tonic release (Fulterer et al., 2018; Woitkuhn and Ender et al., 2020). A varying ratio of Unc13A and B in the different tissues promotes an adjustable system with different functions in release probability and short-term plasticity (Fulterer et al., 2018; Woitkuhn and Ender et al., 2020). Since Unc13A was found to increase with age, what principle role play the Unc13 isoforms for memory formation?

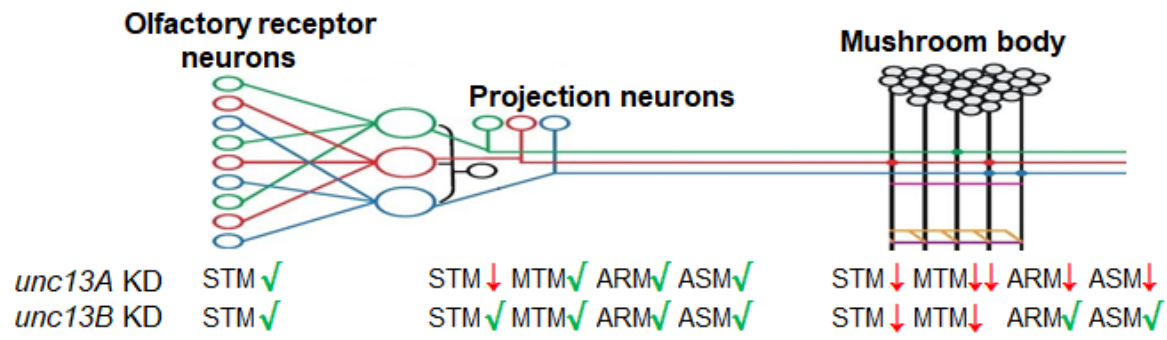

Figure 105: The memory impact of Unc13's isoforms along the olfactory nervous system.

An odor cue is sensed by the olfactory receptor neurons (ORNs), which synapse the projection neurons (PNs) in the antennal lobe. The PNs forward the signal to higher integration centers like the mushroom body (MB) or the lateral horn (not included in the image).

Knockdowns (KD) of *unc13 A* or *B* in the different tissues revealed various behaviors for aversive olfactory conditioning. The ORNs' short-term memory (STM) was not inhibited, while the *unc13A* KD in the PNs decreased STM. Severe deficits in all measured memory phases showed *unc13A* KD in the MB. Here, STM, mid-term memory (MTM; 1 and 3 hours), and its components, labile anesthesia-resistant memory (ASM; 1 and 3 hours) and anesthesia-resistant memory (ARM; 1 and 3 hours) dropped dramatically. *unc13B* KD in the MB also performed with reduced STM and MTM (1 and 3 hours), though the deficits were milder. ASM and ARM were not affected.

I investigated the relevance of Unc13's isoforms in different neuronal tissues involved in the olfactory pathway to gather aversive conditioned memories (Figure 105). In a first step, the olfactory receptors perceive an odor cue at the olfactory receptor neurons (ORNs). Here, neither a knockdown of *unc13A* nor *unc13B* generated a short-term memory (STM) deficit. Additionally, the scores for innate smell behavior were slightly reduced in these flies, yet did not differ from their controls significantly. The ORNs synapse in the antennal lobe (AL) with the projection neurons (PNs). These strengthen weak ORN signals while attenuating an overshooting firing, and convey the received signal less roaring, to avoid sensory noise and support odor differentiation (Bhandawat et al., 2007; Amin and Lin, 2019). Possibly, one isoform was enough to transmit the signal when knocking down *unc13A* or *B* in the ORNs, and the PNs processed this weaker information like a faint odor, still recognizable to generate memories.

From the AL, the odor cue is forwarded via the PNs, which convey their signal to higher integration centers like the mushroom body (MB). Interestingly, Unc13A seemed necessary in the PNs during STM formation. Generally, due to the stimulus of an aversive conditioned odor, a spatial code of activated glomeruli in the ALs creates a short-term trace in the PNs, involving former inactive synapses (Yu et al., 2004). Likely, since Unc13A promotes a high phasic release probability, facilitating short-term plasticity, the knockdown of *unc13A* in the PNs inhibited STM (Lipstein et al., 2013; Jackman and Regehr, 2017; Woitkuhn and Ender et al., 2020). On the contrary, longer-lasting memory phases did not suffer (Figure 105). Unc13B, supporting a lower SV release probability, showed no memory decay when it was reduced in the PNs. Notably, the belonging innate smell behavior tests revealed no deficits for these animals in the used odor concentrations. Pooryasin et al., 2021 showed a significant odor acuity decrease for the same genotypes, though with lower concentrations. Further, they demonstrated a normalized smell acuity with higher concentrations. The used odor concentrations in my conducted innate behavior and memory tests were relatively high and saturated, thus they had normal smell abilities. Such odor intensities provide the greatest chance to receive optimal memory performances (Yarali et al., 2009).

In my Unc13 memory tests, I found the strongest effects with the Unc13A deficiency in the MB, the principle integration center for generating and storing memories (Heisenberg, 2003; McGuire et al., 2005; Aso et al., 2014). Here, Unc13A seemed to play a fundamental role in memory formation since all measured memory phases decreased dramatically for *ok107* > *unc13A* RNAi. STM, MTM (1 and 3 hours), plus its components, the labile anesthesia-sensitive memory (ASM), and even the typically stable anesthesia-resistant memory (ARM) declined. Partially, this correlated with the Unc13A expression pattern in the MB lobes, enriched in the α'/β' and γ lobes (Woitkuhn and Ender et al., 2020). The initial learning phase, where the

memory is acquired, needs the γ lobe immediately, but also a memory trace in the α'/β' lobes is built, which lasts up to 1 hour (Wang et al., 2008; Bouzaiane et al., 2015). Accordingly, I found STM and 1 hour MTM severely reduced. However, the most severe memory lack occurred for 3 hours MTM and ASM, where the flies even showed a so-called masochistic behavior (Quinn et al., 1974), preferring the shocked odor. Of course, the ASM values were calculated by the subtraction of the ARM values from the median MTM, thus the flies did not perform the received masochistic behavior actively. Still, the performance indices were so low for MTM and ARM that the ASM component was erased.
In contrast, Unc13B seemed to have a less fundamental role in memory formation. The *unc13B* knockdown in the MB possessed milder memory deficits for STM and MTM (1 and 3 hours) than the *unc13A* knockdown. ASM and ARM (1 and 3 hours) were not affected.

Further dismantling the Unc13A's influence on memory, I found that its C-terminus alone in the MB could not restore STM or 1 hour MTM, nor its components ASM and ASM were also reduced. This was surprising since the *unc13A* C-terminus reexpression could largely restore the dramatic decrease of evoked exocytosis with the *unc13A* null mutant at the NMJ (Böhme et al., 2016; Böhme et al., 2019). Indeed, the 3 hours MTM decline seemed milder than for the complete *unc13A* knockdown, and 3 hours ASM and ARM showed no significant differences from the controls. Reddy-Alla et al., 2017, revealed that a pure C-terminus expression increases the release sites dramatically, but they were allocated in the presynapse, often further away from the AZ's center. Thus, the SV release probability was low, the release time changed massively, and an imprecise, inefficient transmission happened due to this uncoordinated release site positioning (Reddy-Alla et al., 2017; Pooryasin et al., 2021). In the sole C-terminus neurons, rapid presynaptic homeostatic potentiation was hindered, which impeded the immediate plastic increase of SV release (Böhme et al., 2019).
Interestingly, the C-terminus construct on the top of the endogenous Unc13A (thus a C-terminus overexpression) increased 1 hour ARM massively but impaired 1 hour ASM to the same lowness as the C-terminus alone in the MB. This boost of ARM was also visible at 3 hours. Possibly, the C-terminus overexpression primed additional SVs and facilitated further SV release site expressions, which improved the signal transfer and affected the ARM positively, yet inhibited the ASM component. Could this increased ARM intensity be at the expense of ASM? Pooryasin et al., 2021, saw that the C-terminus overexpression in the PNs possessed no smell response anymore, neither aversive nor appetitive, thus they performed even more worse than the pure C-terminus in the PNs. Seemingly, the proper localization of Unc13A at the AZ, defined by its N-terminus, is crucial for sensory information processing, and excessive release sites generated by an overshooting Unc13A C-terminus block the sensory

coding for innate smell behavior. The sensible ASM component maybe suffered from this Unc13A C-terminus proliferation as well.

Furthermore, my analyses of only the Unc13A N-terminus active in the MB revealed problems with innate behavior and a misshaped MB. Thus, I restricted this scenario to the flies' adulthood. Interestingly, only 1 hour ASM declined, while STM, 1 hour MTM and ARM were not significantly different from their controls. The N-terminus anchors Unc13A to the AZ, thus a precise, synchronise signal transmission is possible (Reddy-Alla et al., 2017). The used Unc13A N-terminus construct blocks the accessibility of SV release sites due to its competition with the endogenous Unc13A binding slots, which reduces the SV release probability in NMJs (Reddy-Alla et al., 2017; Pooryasin et al., 2021). Thus, the impeded labile 1 h ASM could result from a decreased availability of functional SV release sites. Does the ASM formation need a robust signal transmission? Knapek et al., 2010, saw for a mutant of *synapsin*, a phosphoprotein involved in the SV release under high-frequency nerve stimulation, in particular, the ASM component decreased. However, the number of active release slots seemed enough to rescue STM and ARM.

Taken together, a lack of the full-length Unc13A in the mushroom body showed severe deficits for all memory components, which a sole expression of the C-terminus seemed to copy. The MB's intrinsic neurons, the kenyon cells, filter the broader input from the PNs due to a sparse coding, where only a few KCs become activated (Honegger et al., 2011; Amin and Lin, 2019). A precise, synchronized SV release seemed required to forward a proper memory signal to the MB output neurons. N-terminus tests supported this since STM, ARM, and partially MTM were restored. Only the labile memory phase at 1 hour, ASM, decreased. An appropriate amount of functional release sites is possibly needed for this memory component, though the C-terminus overexpression showed ASM deficits as well. Overshooting SV release site expressions seemed to facilitate and strengthen the consolidated memory component ARM, maybe at the expense of ASM. The wild-typic combination of both parts seems indispensable to restore ASM, which appears to need a strong and precise release. It would be interesting to reexpress both constructs in one fly to see if each part could rescue the memory totally to mimic this additive effect. Notably, the *unc13A* knockdown and C-terminus manipulations were chronic. Developmental deficits could interfere with the observed results. Further tests would be interesting, restricting the treatment to the flies' adulthood.

My findings indicate Unc13A as a general switch for memory formation in the mushroom body. Interestingly, this seems to be the case in the sensory information processing. Pooryasin et al., 2021, found the fundamental odor detection decreased, with missing sensory coding for aversive and appetitive scents, upon an *unc13A* knockdown in the PNs (Pooryasin et al.,

2021). By contrast, PN deficient Unc13B caused only a lacking avoidance to aversive odors, indicating Unc13B is implementing “go-away” information (Pooryasin et al., 2021).

Even though the basic memory formation is dependent on Unc13A, the B isoform modified the memory behavior in the mushroom body in a milder form as well. The presynaptic nano-architecture, causing different competencies to conduct short-term plasticity, generated a diverse memory pattern with the fast, phasic release component as the main actor in memory formation. Further investigation on long-term memory could be promising to see a possible role for the slower, tonic release factor Unc13B.

3. Learning is dependent on plastic adjustments at the synapses

With advancing age, the ability to form new memories decreases dramatically, which is conserved in the different species (Mery, 2007; Tonoki and Davis, 2012; Konar et al., 2016). Short-term memory (STM), mid-term memory (MTM), and in particular anesthesia-sensitive memory (ASM) decrease, while the consolidated anesthesia-resistant memory (ARM) stays the same (Tamura et al., 2003; Gupta et al., 2013; Bhukel and Beuschel et al., 2019).
Notably, memory formation but also the inability to get new ones is highly dependent on the condition of the synapses. Gupta et al., 2016, found a massive upregulation of the presynaptic active zone (AZ) scaffold upon aging. This presynaptic upscaling is visible in dramatically increased intensities for AZ proteins like Bruchpilot (BRP), Unc13A, or RIM-binding protein (RIM-BP) in aged brains (Gupta et al., 2016). Aging neurons show enlarged BRP rings in the nano-architecture of planar-oriented AZs (STED), and broad and loose T-bars, the electron-dense structures at the AZ, composed of BRP (electron microscopy) (Zhai and Bellen, 2004; Wagh et al., 2006; Gupta et al., 2016). *Argumentum e contrario*, these findings revealed aging-typical conditions, which can serve as a suitable marker for aging and help to define aging pathways and connections on cellular levels (Figure 106). Equally, accumulations of p62/Ref(2)p, an autophagy receptor marking cargo for degradation, occur with advancing age, thus they can be exploited as a perfect aging indicator (more on page 186; Bartlett et al., 2011; Gupta et al., 2013; Mauvezin et al., 2014).
Astonishingly, Gupta et al., 2016, mimicked some of these aging-typical effects by adding two additional gene copies of BRP to the two endogenous copies in young animals already. Thus, they could link presynaptic increase with memory impairment in young animals. The 4x BRP mutant possesses a premature aging state with symptoms like BRP increase in the whole brain, an aging-typical T-bar shape, and severely reduced memory in STM, MTM, and ASM (Gupta et al., 2016). In these mutants, the presynaptic plasticity seems to become non-malleable, followed by impaired signal transmission and hindered memory generation.

One question appeared upon these findings, which is fundamental in age research: How can we differentiate between age-induced defects and the compensation by the system to counteract aging? What is beneficial, what is detrimental?

I investigated different scenarios. First, I examined the acetylation status of the T-bars since the more they become deacetylated with advancing age, the broader and looser their structure is (Figure 106; Miskiewicz et al., 2014). I found that a pan-neuronal knockdown of the BRP deacetylase *hdac6* boosted the STM in young and old flies immensely. Notably, HDAC6 inhibitors act neuroprotective, support the genesis of dendrites and synapses, and improve

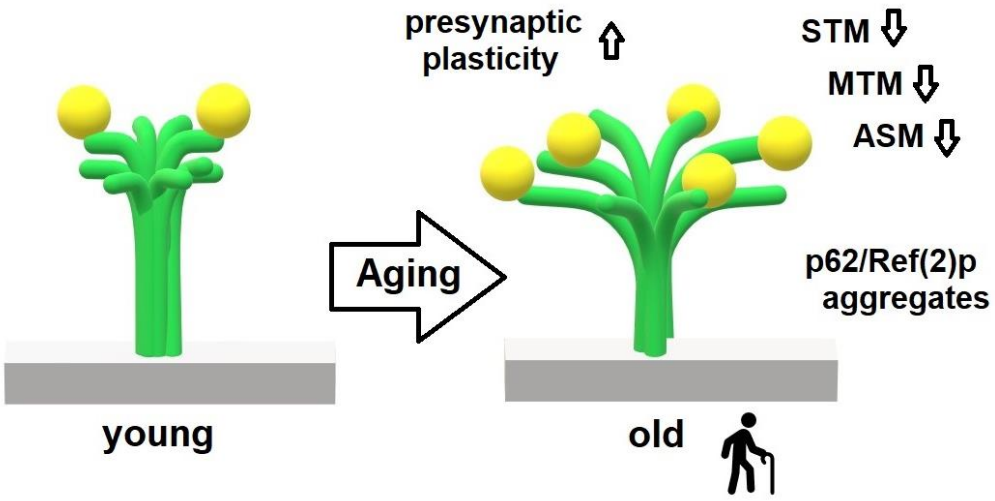

Figure 106: Indicators for aging.

How to define aging? In Drosophila melanogaster, age-typical changes in the brain like a broad and loose T-bar, increased presynaptic plasticity (more Bruchpilot, Unc13A, and RIM-BP), and multiplied p62/Ref(2)p aggregates are accompanied by reduced short-term memory (STM), mid-term memory (MTM), and its component anesthesia-sensitive memory (ASM) (Tamura et al., 2003; Gupta et al., 2013; Gupta et al., 2016; Bhukel and Beuschel et al., 2019).

memory in rodents (Fischer et al., 2007; Toonen and Verhage, 2011; Krukowski et al., 2017). They are promising substances against neurodegenerative diseases like Alzheimer's or Parkinson's (Li et al., 2021; Onishi et al., 2021). Even though I observed age-induced memory impairment in HDAC6 diminished flies, the substantial protective effect on memory was equally present in young and old animals.

Further, assuming that the current state of presynaptic plasticity for 4x BRP or aging was harmful, I wanted to see if a reduced BRP expression could prevent age-induced memory impairment. Thus, I examined STM for young and old 1x BRP animals. Surprisingly, they tended towards lower memory values than the wild-type 2x BRP at the young state already, which decreased further with higher age. A reason could the reduced sleep level of 1x BRP be (Huang et al., 2020). Our recent study detected a gradual increase in the sleep quantity according to a dosage-dependent enhancement of presynaptic plasticity via BRP (Huang et al., 2020): 1x BRP showed less sleep than the wild-type 2x BRP, followed by more with 3x BRP and an extreme sleep drive for 4x BRP. The harmful effects of sleep withdrawal on cognitive performances are familiar (Goel et al., 2009; Diekelmann and Born, 2010; Dissel et al., 2015; Donlea, 2019). Thus, was there a connection between the lower sleep in 1x BRP

animals and the tendency to lower memory? Reversely, sleep deprivation causes dramatically increased BRP levels, and sleep-deprived flies show an extreme sleep drive, comparable to 4x BRP (Gilestro et al., 2009; Huang et al., 2020). The 'synaptic homeostasis hypothesis' says that sleep is needed to reinforce what has been learned, and sleeping allows to form new memories via changes in brain plasticity (Tononi and Cirelli, 2016). Could the massive amount of BRP, like in 4x BRP mutants or sleep-deprived flies, hold the synapse at an operating peak and overload the system (Gilestro et al., 2009; Gupta et al., 2016; Huang et al., 2020)? And the high sleep drive is the try of the system to reset? Was the maximum of BPR maybe not the detrimental aspect but an adaptation of the synapse to a challenging scenario? With age, a higher SV release could be observed (Foster et al., 1991; Rosenzweig and Barnes, 2003; Gupta et al., 2016). Thus, an age-induced high tuning of the presynaptic AZ facilitates synaptic vesicle release, likely keeping it in an operating state and providing synaptic plasticity (Peled and Isacoff, 2011; Gupta et al., 2016). Typically, a system reacts with this experience-dependent modulation within the synapse as an adaptation to the environment, which needs to stay adjustable (Ho et al., 2011; Kandel et al., 2014; Takeuchi et al., 2014; Böhme et al., 2019). Though, when the compensatory upregulation reaches the upper limit of a functional system, it becomes overloaded and seems to block neuronal flexibility (Gilestro et al., 2009; Gupta et al., 2016; Huang et al., 2020). In this state of presynaptic metaplasticity, memory formation becomes inoperable.

Thus, I tested the memory for animals, where the presynaptic plasticity was seemingly not at the operational limit. In sleep examinations, 3x BRP shows slightly increased sleep per day, yet the sleep performance resembled more the wild-type 2x BRP than the extreme sleep quantity of 4x BRP (Huang et al., 2020). Additionally, 3x BRP boosts the life expectancy over the level of 2x BRP in male and female flies (Huang et al., in submission). Though, my memory tests revealed no benefit with 3x BRP animals compared to the wild-type 2x BRP.

Intriguingly, I found a link between a beneficial impact of presynaptic plasticity and memory in another context. Typically, chronic sleep-deprived flies show a presynaptic upscaling innately (Huang et al., 2020). However, Huang et al., 2020, found the sleep-deprived mutant *sleepless* as unable to undergo such a presynaptic scaling. Notably, this mutant possesses, in particular, a severe sleep reduction of more than 80 %, and I found dramatic memory deficits in MTM and ASM (Koh et al., 2008). Indeed, the combination of *sleepless* with 4x BRP compensates the extreme converse sleep characteristics of these two genotypes. Thus, especially daytime sleep was normalized to the level of 2x BRP (wild-type) (Huang et al., 2020). However, their memory performance was low to the level of sole 4x BRP.

Astonishingly, a moderate upscaling of the presynaptic plasticity improved 3 hours MTM and even boosted the ASM component. One additional BRP copy to the two endogenous ones (3x

BRP) seemed to restore the missing presynaptic plasticity of *sleepless* and balance its intrinsic plasticity to a functional level, which facilitated memory formation.

Interestingly, the loss of the overshooting presynaptic plasticity in neurons responsible for homeostatic sleep drive can create a remedy scenario. Thus, the sleep phenotype of 4x BRP is partially rescued when *brp* is knocked down in the R5 neurons (Huang et al., 2020). Notably, the BRP amount in sleep-deprived flies raises dramatically in this subset of the ellipsoid body, which is, in particular, responsible for homeostatic sleep drive after sleep depression (Liu et al., 2016). Thus, the continuous sleep drive in 4x BRP was regulated down due to absent presynaptic plasticity by BRP in the R5 neurons (Liu et al., 2016; Huang et al., 2020). How would these flies behave in memory tests? Indeed, this scenario rescued the severe memory defects of 4x BRP. STM and 1 hour MTM improved to the levels of their controls.

Taken together, presynaptic upregulation seems to be a try of the system to confront challenging circumstances like sleep loss or aging. Such plastic processes are crucial for adaptations to the environment and animals need to stay adjustable to generate new memories (Kandel et al., 2014). However, sleep resets presynaptic plasticity to an operational level (Spano et al., 2019; Vivo et al., 2019; Huang and Sigrist, 2021).

4. Missing autophagy provokes early cognitive decline in an age-typical manner

The autophagic pathway is one of the most important targets to prevent aging effects (Rubinsztein et al., 2011; Liang and Sigrist, 2018). Autophagic clearance, which is highly conserved in the different species, functions as the cellular housekeeper and ensures the balance between synthesis and degradation to maintain cellular homeostasis (Levine and Kroemer, 2008; Bishop et al., 2010; Yin et al., 2016). Though, autophagic efficiency declines with higher age, increasing the risk for accumulations of misfolded proteins like the aggregates in Alzheimer's (amyloid-beta plaques and tau neurofibrillary tangles) or Parkinson's (Lewy bodies) disease (Gupta et al., 2013; Yang et al., 2014; Yu et al., 2017; Liang and Sigrist, 2018; Mattson and Arumugam, 2018; Bhukel and Beuschel et al., 2019).
One type of autophagy, macroautophagy, is essential for the degradation of proteins and organelles. Here, the receptor p62 (also named sequestome 1; *Drosophila*'s homolog: Ref(2)p) binds ubiquitinated residues of these proteins, which marks them to become absorbed by multi-membrane vesicles, named autophagosomes. Afterward, the autophagosomes fuse with lysosomes for their cargo's digestion (Bento et al., 2016; Bhukel and Beuschel et al., 2019). This macroautophagic machinery is regulated by a cascade of autophagy-related (Atg) proteins (Menzies et al., 2017).

In my thesis, I used two strategies, Atg5 and Atg9, to investigate the influence of deficient macroautophagy on memory. These two proteins interfere in independent phases of macroautophagy: Atg5 is involved in the autophagosome assembly and elongation (Gelino and Hansen, 2012; Gui et al., 2019). In contrast, Atg9 serves as the carrier for the required lipid bilayers to the autophagosome construction site (Singh and Cuervo, 2011; Gelino and Hansen, 2012; Bento et al., 2016). Brain Western blots detecting Atg8 showed two bands for the pan-neuronal *atg9* knockdown (just like the controls), while pan-neuronal *atg5* deficient brains did not possess the second band of the lipidated Atg8 modification (Bhukel and Beuschel et al., 2019). Thus, the effects of the *atg5* and *atg9* knockdowns targeted different autophagic steps to examine the consequences of attenuated macroautophagy in neuronal tissues, focusing on aversive olfactory memory.
Concomitantly, a sufficient downregulation of the macroautophagy machinery in the respective areas was monitored via immunolabelling with p62/Ref(2)p. Deficient macroautophagy is accompanied by accumulations of p62/Ref(2)p, and such aggregates also occur with advancing age (Bjørkøy et al., 2009; Bartlett et al., 2011; Gupta et al., 2013; Mauvezin et al., 2014). As further readout served the immunolabelling of Bruchpilot. Gupta et al., 2016, found

a dramatic increase of the Bruchpilot (BRP^{Nc82}) intensity in fly brains with higher age. Thus, p62/Ref(2)p and BRP^{Nc82} labeling served as markers for age-like changes in the fly brain.

My results revealed that reduced macroautophagy was accompanied by early memory impairment. Deficits occurred in short-term memory (STM), essential for the acquisition of memory, and 1 hour mid-term memory (MTM), where memory maintenance and consolidation happen (Tully and Quinn, 1985). Intriguingly, even though I downregulated macroautophagy in two different ways, the observed memory decline was similar. These cognitive defects appeared in pan-neuronal downregulations of *atg5* and *atg9*, accompanied by p62/Ref(2)p accumulations in the whole brain and an increased BRP^{Nc82} intensity brain-wide.
Interestingly, functional macroautophagy in the mushroom body seemed to be crucial for memory formation. The memory performance dropped with the expression of *atg5* or *atg9* RNAi using the mushroom body drivers *ok107*-Gal4 or *vt030559*-Gal4. Both STM and MTM were affected. More precisely, MTM's anesthesia-sensitive, labile component (ASM) vanished, while the stable, consolidated anesthesia-resistant memory (ARM) remained. Thus, deficient macroautophagy in the mushroom body mimicked the memory performance of aged animals (Tamura et al., 2003; Scheunemann et al., 2012; Bhukel and Beuschel et al., 2019). Cellular observations with p62/Ref(2)p immunostainings revealed massive aggregates in the area of the mushroom body (Bartlett et al., 2011; Bhukel and Beuschel et al., 2019). Astonishingly, the presynaptic plasticity indicated by BRP levels increased not only in the mushroom body region but brain-wide. This non-cell autonomous upregulation of BRP seemed dependent on the mushroom body's autophagic status (Bhukel and Beuschel et al., 2019).

Could a subset of the mushroom body be necessary for these effects in particular? The different memory phases are generated due to the co-activation of memory traces, cellular and plasticity changes in the neurons induced by learning (Christiansen et al., 2011; Davis, 2011). Here, the three classes of mushroom body lobes, α'/β', α/β, and γ, entail various traces and memory processes (Krashes et al., 2007; Davis, 2011). An attenuation of macroautophagy only in the prime lobes, especially required for memory acquisition and maintenance until 1 hour (Wang et al., 2008), caused no memory deficits or presynaptic increases. The readout with p62/Ref(2)p demonstrated accumulations in other brain regions like *pars intercerebralis*, where *ok107*-Gal4 also expresses. Though the α/β and γ lobes seemed free from p62/Ref(2)p aggregates, likely due to functional macroautophagy (Bhukel, 2018). Thus, these lobes appeared to hold a key position for functional macroautophagy to prevent a brain-wide non-cell autonomous BRP increase and memory decay.
The opposing experiment with deficient Atg5 or Atg9 in the α/β and γ lobes also showed no memory impairment. Here, p62/Ref(2)p immunostainings with *mb247*-Gal4 showed

aggregates in the α/β and γ lobes, though with a weaker expression than *ok107*-Gal4 (Bhukel, 2018). Indeed, Aso et al., 2009, also described *mb247*-Gal4 as a relative weak driver. Thus, only an intense inhibition of macroautophagy in the α/b and γ lobes seemed to result in the effects of early memory impairment due to deficient macroautophagy.

To exclude developmental defects due to chronic downregulation of *atg5* or *atg9*, I restricted macroautophagic attenuation to the adulthood of the flies via Gal80^{ts}. In this test situation, I could not observe a memory decrease in STM or 1 hour MTM. Though, immunostainings with p62/Ref(2)p revealed an insufficient suppression of macroautophagic processes since no p62/Ref(2)p aggregates were visible in the kenyon cells of the mushroom body (Bhukel and Beuschel et al., 2019). Deficient macroautophagy would be accompanied by accumulations of p62/Ref(2)p, which were massively present in the pan-neuronal and mushroom-body specific downregulations of macroautophagy. Likely, the turnover of the proteins Atg5 or Atg9 was not sufficiently achieved when restricting missing macroautophagy via RNAi to only the post-enclosing adult stages. The stability period of these two proteins could be longer lasting than the 10 days when the flies were tested, and developmentally expressed remainings of Atg5 and Atg9 could generate a functional macroautophagic machinery. Kinetic analysis of the protein stability could reveal a suitable moment to test memory in these animals, yet the age-induced decrease of memory starts around day 15 in *Drosophila melanogaster* and would interfere with the results at this age (Gupta et al., 2013; Liang et al., 2021). Similarly, missing macroautophagy could be no longer important for memory formation in the mushroom body at the timepoint of the adult stages. Thus, limiting deficient macroautophagy only to the adult stage did not answer the question of developmental deficits. Indeed, these findings could also support that an intense inhibition of macroautophagy is needed to entail early memory impairment.

In conclusion, inoperative macroautophagy provoked severe conditions at a young age already. The synapse suffered from premature aging, triggering presynaptic metaplasticity, followed by early memory impairment. Thereby, the current macroautophagic status in the mushroom body seemed to affect the ultrastructural situation of the presynaptic active zone brain-wide (Bhukel and Beuschel et al., 2019).

5. Mediation of early memory impairment by reduced short neuropeptide F signaling?

How could a mediation from a small neuropile region to the whole brain work? Intercellular communication happens via messenger molecules like hormones or neuropeptides (Silbernagl and Despopoulos, 1979). The mammalian neuropeptide Y (NPY; in *Drosophila*: short neuropeptide F, sNPF) was a promising candidate since it expresses broadly in the central nervous system, mediating foraging, inducing autophagy, and decreasing with age (Lee et al., 2004; Aveleira et al., 2015a; Botelho and Cavadas, 2015). Additionally, the hypothalamus in mammals, or rather the mushroom body (MB) in *Drosophila melanogaster* was shown as NPY/ sNPF secreting tissues (Hahn et al., 1998; Johard et al., 2008; Nässel et al., 2008).

My results revealed that early memory impairment seems to be caused by a mechanism of deficient macroautophagy in the MB, which depressed sNPF signaling to an aging-typical state. Young flies, missing Atg5 in the MB, showed dramatically reduced amounts of sNPF. Moreover, reduced sNPF via a hypomorph mutant (*sNPF*^{c00448}) possessed a dramatic brain-wide increase of presynaptic plasticity and decreased short- (STM), mid-term (MTM), and anesthesia-sensitive memory (ASM), all aging-typical indicators (Figure 106). This mutant mimicked the missing macroautophagy phenotype and aging. Though the animals showed severe problems with innate smell behavior, thus I looked for another option to decrease sNPF signaling. However, the anesthesia-resistant memory (ARM) appeared similar to the wild-type, indicating general learning and memory formation was possible.
Nailing the effect on the MB, I downregulated the *sNPF receptor* with RNAi in this neuropile. This receptor is, *inter alia*, expressed on the MB, generating autocrine signaling to this tissue (Nässel et al., 2008; Bhukel and Beuschel et al., 2019). Intriguingly, the investigations with MB-specific lines copied the results of diminished macroautophagy in the MB: the missing sNPF receptor in this neuropile increased the presynaptic plasticity and the T-bar size dramatically, accompanied by a massive drop of STM, MTM, and ASM (near zero %). Notably, this memory decrease was even more massive than the memory phenotype of the decreased macroautophagy MB-specific examinations. Again, innate smell behavior also occurred critically here. However, general memory formation seemed possible since ARM was functional.
Indeed, a reduced smell ability in the hypomorph *sNPF* mutant was not surprising since sNPF signaling mediates foraging (Lee et al., 2004). A low level of insulin signaling, like during starvation or caloric restriction, mediates the expression of sNPF receptors in the olfactory receptor neurons (ORNs) to induce the food search (Root et al., 2011). Thus, odor perception is boosted via sNPF signaling's increase of presynaptic transmission from the ORNs to the

projection neurons. The intrinsic sNPF signaling mediates the innate smell behavior, and the *sNPF*^{c00448} mutants seemed unable to go through this upregulation in the ORNs. However, why could the flies also not smell properly when the *sNPF* receptor knockdown was restricted to the MB? Newer findings reveal an influence of the MB in the lateral horn, the principle processing center for naïve odor perception, to control the food-search and conflict situations in foraging (Lewis et al., 2015; Tsao et al., 2018; Amin and Lin, 2019; Das Chakraborty and Sachse, 2021).

Notably, reducing the *sNPF receptor* expression in other brain regions like the *pars intercerebralis* showed no memory decay. Indeed, Bruchpilot intensity in immunostainings was even significantly reduced (Bhukel, 2018). Investigations on rodents reveal that NPY's effects on memory can be highly divergent, depending on the region where NPY was increased (Beck and Pourié, 2013). In aged animals, the hippocampal areas dentate gyrus and CA1-CA3 lose their NPY amount (Hattiangady et al., 2005). Furthermore, NPY injection in the rostral (mouth direction) or the causal (tail direction) region of the hippocampus improved or impaired memory (Flood et al., 1989). My examinations of *sNPF* overexpression in the MB revealed no benefits for memory, neither with one nor with two additional *sNPF* transgenic copies. The STM and MTM tests showed instead declined performance values. Even though sNPF decreases with age in the mushroom body, boosted sNPF in this neuropile was detrimental to memory formation. Possibly, other regions along the olfactory memory pathway would be interesting, like the projection neurons, where an STM trace is built, or earlier, in the ORNs, thus they could boost the signal transmission to the PNs (Yu et al., 2004; Root et al., 2011). Of course, the missing beneficial effect could also be the sole boost of sNPF, which may not obstruct the age-induced autophagy reduction. p62/Ref(2)p immunostainings would be interesting to see the flies' autophagic status. However, the presynaptic plasticity in *sNPF* overexpressions was at a young level, showing at least a partial benefit (Bhukel 2018). Could these flies possess higher life expectancy? Michalkiewicz et al., 2003, saw a boosted lifespan in rats overexpressing NPY. Actually, caloric restriction (CR) increases the levels of NPY, and the favorable effects seem to be mediated through the NPY stimulation on autophagy (Aveleira et al., 2015b; Botelho and Cavadas, 2015; Ferreira-Marques et al., 2016). Chiba et al., 2014, could not find a CR-mediated lifespan extension in NPY deficient flies. Additionally, NPY/ sNPF signaling interacts with the insulin-signaling pathway, and higher levels of sNPF decrease the expression of insulin-like peptides and *vice versa* (Lee et al., 2008; Root et al., 2011).

Possibly, the MB controls the costly ability of memory formation depending on the energy level in the body via crosstalk of sNPF signaling and the autophagic status in the MB (Plaçais et al., 2017; Bhukel and Beuschel et al., 2019). With age, autophagy decreases, also in the MB, which reduces the sNPF signaling and brings the whole brain to the state of the presynaptic

plasticity increase in a non-cell autonomous manner, which impairs memory formation (Gupta et al., 2013; Liang and Sigrist, 2018; Bhukel and Beuschel et al., 2019).

Another aspect is that sNPF signaling is a negative regulator of sleep (Chen et al., 2013; Shang et al., 2013). The hypomorph mutant *sNPF*^{c00448} and *sNPF receptor* knockdowns in the mushroom body rest more, while a gain of function in the mushroom body via two *sNPF* copies decreased the total sleep amount (Chen et al., 2013). Though, another paper shows sNPF expressing neurons as sleep-promoting (Shang et al., 2013). However, in sleep-deprived flies, sNPF transcription levels increased (Chen et al., 2013). sNPF signaling raises cAMP, possibly driving sleep via the cAMP-PKA-CREB pathway (Chen et al., 2013). It could be that the sleep in the sNPF diminished flies is the try of the system to reset. Sleep-deprived flies show overshooting presynaptic plasticity, scaling during the waking state (Gilestro et al., 2009; Bushey et al., 2011; Vivo et al., 2017; Huang et al., 2020). Maybe, the boosted cAMP-PKA-CREB pathway due to increased sNPF signaling enables the improvement of longer-lasting memory since long-term memories (LTM) are dependent on CREB activation (Tully et al., 1994; Heisenberg, 2003; Tully et al., 2003). Further trials investigating sNPF overexpression in different tissues with LTM could be promising.

6. Longevity at the expense of memory formation?

During my investigations about aging and memory, I examined several mechanisms involved in aging processes. Surprisingly, counteracting these aging hallmarks, which were shown to prolong the lifespan, could often not improve memory performances.
Thus, a moderate increase of presynaptic plasticity, 3x BRP, boosts lifespan (Huang et al., in submission), yet could not prevent a cognitive decline with age. The STM of 30 days old 3x BRP animals was significantly reduced compared to the same-aged wild-type 2x BRP. Seemingly, their presynapses could not achieve the needed short-term plasticity to generate memories anymore.
Equally, missing macroautophagy induced premature aging like early memory impairment. *Vice versa*, Shen and Ganetzky, 2009, found an intense synaptic development upon boosted Atg1, and Ulgherait et al., 2014, could improve lifespan via *atg1* overexpression. Atg1 (in mammals: Ulk1) is a critical player in the macroautophagic initiation complex (Gelino and Hansen, 2012). Though, short-term memory (STM) of *atg1*'s overexpression in the mushroom body had lower values than its control in young animals already. The flies did not benefit from additional autophagy in this neuropile. Possibly, the intervention at this initial phase of macroautophagy, with Atg1 as its central figure, interfered too much in the system's machinery, followed by no memory gains. However, enhancing other types of autophagy, like chaperone-mediated autophagy via Hsc70-4, could also not prevent age-induced memory impairment.

Indeed, several studies proved the beneficial effects on life expectancy by downregulating the insulin signaling pathway (Clancy et al., 2001; Tatar et al., 2001; Broughton et al., 2005; Grönke et al., 2010; Piper and Partridge, 2018; Fabian et al., 2021). However, the memory did not profit from the reduction of any insulin-like peptide (ILP). Almost all *ilp* mutants suffered from early memory impairment (Figure 75), and *ilp5* mutants finally experienced an age-induced cognitive decline as well. Actually, several neurological ailments like stroke, Alzheimer's, or Parkinson's disease are linked to insulin resistance and type-II diabetes (Frazier et al., 2019; Akhtar and Sah, 2020). Insulin resistance causes inflammation, oxidative stress, and neurodegeneration, whereas intranasal insulin administration supports neurogenesis, synaptic density, and transmission (Ott et al., 2012; Verdile et al., 2015; Akhtar and Sah, 2020). However, hyperinsulinemia also causes an increase in misfolded proteins (Qiu and Folstein, 2006). A balanced household of insulin signaling seems to be important.
Moreover, the flavonoid 4,4'-Dimethoxychalcone improves the lifespan in *C. elegans*, *Drosophila melanogaster*, and human cell cultures and shows protective effects in mice against myocardial ischemia and ethanol-induced damage (Carmona-Gutierrez et al., 2019). However, a benefit against the aging effect did not appear for STM nor locomotion at 30 days.

Even though DMC had significant advantages in extending lifespan and is cardioprotective and cytoprotective, there was no protective effect on physical or mental health (Carmona-Gutierrez et al., 2019).

In summary, beneficial effects on longevity are not automatically accompanied by memory improvement. The processes to form memories need energy and are costly. Indeed, Plaçais et al., 2017, showed the need for a high energy level in the brain to obtain long-term memory. Indeed, under starvation, the system prefers survival at the expense of the energy-intensive formation of long-term memories, and Ca^{2+} oscillations from two specific dopamine neurons on the mushroom body vanish in this scenario (Pierre-Yves Plaçais et al., 2012; Plaçais and Preat, 2013). Strategic considerations about the “expensive” cognitive abilities or a more extended life seem to interfere. Indeed, Burger et al., 2008, found in fly populations with improved learning abilities a 15 % shorter lifespan in females and 10 % in male flies, while another long-lived population showed a 15 % lower memory performance index. What is the consequence of these results? Could there be a timeframe when the question, what to favor, cognitive flexibility or survival, is still open? However, a strategy, which boosts both the energy level and the life-supporting aspects, could allow for healthy aging with a conserved ability to form memories.

One promising allrounder in healthy aging seems to be the endogenous polyamine Spermidine (Spd). It decreases with age, but dietary Spd supplementation was shown to boost autophagy, improve mitochondrial respiration, and lower insulin signaling (Gupta et al., 2013; Tain et al., 2020; Liang et al., 2021). Aiming at these aging hallmarks, it boosts life expectancy, and it is cardioprotective and neuroprotective from invertebrates to mammals (Eisenberg et al., 2009; Gupta et al., 2013; Sigrist et al., 2014; Madeo et al., 2018; Wirth et al., 2018; Maglione et al., 2019; Hofer et al., 2021; Schroeder et al., 2021). Additionally, dietary Spd also prevents age-induced memory impairment (Gupta et al., 2013; Sigrist et al., 2014; Wirth et al., 2018; Wirth et al., 2019; Hofer et al., 2021; Schroeder et al., 2021).
I investigated the underlying mechanism of the beneficial Spermidine effects. Spd serves as a co-factor in the hypusination of the eukaryotic translation initiation factor 5A (eIF5A), which is a unique pathway conserved in the different species (Hofer et al., 2021; Liang et al., 2021; Schroeder et al., 2021). Hypusinated eIF5A boosts autophagy and mitochondrial function (Hofer et al., 2021). In this mechanism, I attenuated the rate-limiting first step with Spd as co-factor, where the deoxyhypusine synthase (DHS; in *Drosophila*: CG8005) catalyzes the built of deoxyhypusinated eIF5A. Already with a mild reduction of this mechanism via the heterozygous *CG8005* mutants, STM and MTM decreased at a young age, and Spd treatment could not bring the memory back. In contrast, dietary Spd improved STM and MTM of old wild-

type flies in the same trials. Thus, this first step of hypusination, where Spd is a rate-limiting donor, seems to be the crucial mechanism for memory formation in this scenario. The Spd supplementation prolongs lifespan and seems to promote a healthy high energy level via boosted mitochondrial respiration and autophagy, enabling the ability to form memories (Liang et al., 2021). Notably, the hypusination activity decreases with age, just like endogenous Spd levels do. Both, the availability of the enzymatic function and Spd as a co-factor, were important to protect from age-induced memory impairment.

However, the exact pathway, how the hypusinated eIF5A improves mitochondrial and autophagic functions still needs to be explored. Further analysis will help to understand the whole picture and support potential preventive or therapeutic strategies for healthy aging.

References

Abraham, N.M., Egger, V., Shimshek, D.R., Renden, R., Fukunaga, I., Sprengel, R., Seeburg, P.H., Klugmann, M., Margrie, T.W., and Schaefer, A.T., et al. (2010). Synaptic inhibition in the olfactory bulb accelerates odor discrimination in mice. Neuron *65*, 399-411. https://doi.org/10.1016/j.neuron.2010.01.009.

Adams, M.D., Celniker, S.E., Holt, R.A., Evans, C.A., Gocayne, J.D., Amanatides, P.G., Scherer, S.E., Li, P.W., Hoskins, R.A., and Galle, R.F., et al. (2000). The genome sequence of Drosophila melanogaster. Science (New York, N.Y.) *287*, 2185-2195. https://doi.org/10.1126/science.287.5461.2185.

Akalal, D.-B.G., Yu, D., and Davis, R.L. (2010). A late-phase, long-term memory trace forms in the γ neurons of Drosophila mushroom bodies after olfactory classical conditioning. J. Neurosci. *30*, 16699-16708. https://doi.org/10.1523/JNEUROSCI.1882-10.2010.

Akbergenova, Y., Cunningham, K.L., Zhang, Y.V., Weiss, S., and Littleton, J.T. (2018). Characterization of developmental and molecular factors underlying release heterogeneity at Drosophila synapses. eLife *7*. https://doi.org/10.7554/eLife.38268.

Akhtar, A., and Sah, S.P. (2020). Insulin signaling pathway and related molecules: Role in neurodegeneration and Alzheimer's disease. Neurochemistry international *135*, 104707. https://doi.org/10.1016/j.neuint.2020.104707.

Alabi, A.A., and Tsien, R.W. (2012). Synaptic vesicle pools and dynamics. Cold Spring Harbor perspectives in biology *4*, a013680. https://doi.org/10.1101/cshperspect.a013680.

Amin, H., and Lin, A.C. (2019). Neuronal mechanisms underlying innate and learned olfactory processing in Drosophila. Current opinion in insect science *36*, 9-17. https://doi.org/10.1016/j.cois.2019.06.003.

Andlauer, T. (2013). Structural and Functional Diversity of Synapses in the Drosophila CNS. PhD Thesis *2013*.

Aravamudan, B., Fergestad, T., Davis, W.S., Rodesch, C.K., and Broadie, K. (1999). Drosophila UNC-13 is essential for synaptic transmission. Nature neuroscience *2*, 965-971. https://doi.org/10.1038/14764.

Asahina, K., Pavlenkovich, V., and Vosshall, L.B. (2008). The survival advantage of olfaction in a competitive environment. Current Biology *18*, 1153-1155. https://doi.org/10.1016/j.cub.2008.06.075.

Ashery, U., Bielopolski, N., Barak, B., and Yizhar, O. (2009). Friends and foes in synaptic transmission: the role of tomosyn in vesicle priming. Trends in neurosciences *32*, 275-282. https://doi.org/10.1016/j.tins.2009.01.004.

Aso, Y., Grübel, K., Busch, S., Friedrich, A.B., Siwanowicz, I., and Tanimoto, H. (2009). The mushroom body of adult Drosophila characterized by GAL4 drivers. Journal of neurogenetics *23*, 156-172. https://doi.org/10.1080/01677060802471718.

Aso, Y., Hattori, D., Yu, Y., Johnston, R.M., Iyer, N.A., Ngo, T.-T.B., Dionne, H., Abbott, L.F., Axel, R., and Tanimoto, H., et al. (2014). The neuronal architecture of the mushroom body provides a logic for associative learning. eLife *3*, e04577. https://doi.org/10.7554/eLife.04577.

Aso, Y., Herb, A., Ogueta, M., Siwanowicz, I., Templier, T., Friedrich, A.B., Ito, K., Scholz, H., and Tanimoto, H. (2012). Three dopamine pathways induce aversive odor memories with different stability. PLoS genetics *8*, e1002768. https://doi.org/10.1371/journal.pgen.1002768.

Aso, Y., and Rubin, G.M. (2016). Dopaminergic neurons write and update memories with cell-type-specific rules. eLife *5*. https://doi.org/10.7554/eLife.16135.

Aso, Y., and Rubin, G.M. (2020). Toward nanoscale localization of memory engrams in Drosophila. Journal of neurogenetics *34*, 151-155. https://doi.org/10.1080/01677063.2020.1715973.

Aso, Y., Siwanowicz, I., Bräcker, L., Ito, K., Kitamoto, T., and Tanimoto, H. (2010). Specific dopaminergic neurons for the formation of labile aversive memory. Current biology : CB *20*, 1445-1451. https://doi.org/10.1016/j.cub.2010.06.048.

Aveleira, C.A., Botelho, M., Carmo-Silva, S., Pascoal, J.F., Ferreira-Marques, M., Nóbrega, C., Cortes, L., Valero, J., Sousa-Ferreira, L., and Álvaro, A.R., et al. (2015a). Neuropeptide Y stimulates autophagy in hypothalamic neurons. Proceedings of the National Academy of Sciences of the United States of America *112*, E1642-51. https://doi.org/10.1073/pnas.1416609112.

Aveleira, C.A., Botelho, M., and Cavadas, C. (2015b). NPY/neuropeptide Y enhances autophagy in the hypothalamus: a mechanism to delay aging? Autophagy *11*, 1431-1433. https://doi.org/10.1080/15548627.2015.1062202.

Badshah, S.L., Faisal, S., Muhammad, A., Poulson, B.G., Emwas, A.H., and Jaremko, M. (2021). Antiviral activities of flavonoids. Biomedicine & pharmacotherapy = Biomedecine & pharmacotherapie *140*, 111596. https://doi.org/10.1016/j.biopha.2021.111596.

Bartlett, B.J., Isakson, P., Lewerenz, J., Sanchez, H., Kotzebue, R.W., Cumming, R.C., Harris, G.L., Nezis, I.P., Schubert, D.R., and Simonsen, A., et al. (2011). p62, Ref(2)P and ubiquitinated proteins are conserved markers of neuronal aging, aggregate formation and

progressive autophagic defects. Autophagy *7*, 572-583. https://doi.org/10.4161/auto.7.6.14943.

Basu, J., Betz, A., Brose, N., and Rosenmund, C. (2007). Munc13-1 C1 domain activation lowers the energy barrier for synaptic vesicle fusion. J. Neurosci. *27*, 1200-1210. https://doi.org/10.1523/JNEUROSCI.4908-06.2007.

Beck, B., and Pourié, G. (2013). Ghrelin, neuropeptide Y, and other feeding-regulatory peptides active in the hippocampus: role in learning and memory. Nutr Rev *71*, 541-561. https://doi.org/10.1111/nure.12045.

Beeler, N., Riederer, B.M., Waeber, G., and Abderrahmani, A. (2009). Role of the JNK-interacting protein 1/islet brain 1 in cell degeneration in Alzheimer disease and diabetes. Brain research bulletin *80*, 274-281. https://doi.org/10.1016/j.brainresbull.2009.07.006.

Begley, D.J. (2004). ABC transporters and the blood-brain barrier. Current pharmaceutical design *10*, 1295-1312. https://doi.org/10.2174/1381612043384844.

Belle, J.S. de, and Heisenberg, M. (1994). Associative odor learning in Drosophila abolished by chemical ablation of mushroom bodies. Science (New York, N.Y.) *263*, 692-695. https://doi.org/10.1126/science.8303280.

Bento, C.F., Renna, M., Ghislat, G., Puri, C., Ashkenazi, A., Vicinanza, M., Menzies, F.M., and Rubinsztein, D.C. (2016). Mammalian Autophagy: How Does It Work? Annual review of biochemistry *85*, 685-713. https://doi.org/10.1146/annurev-biochem-060815-014556.

Berry, J., Krause, W.C., and Davis, R.L. (2008). Chapter 18 Olfactory memory traces in Drosophila. In Essence of Memory (Elsevier), pp. 293–304.

Berry, J.A., Cervantes-Sandoval, I., Nicholas, E.P., and Davis, R.L. (2012). Dopamine is required for learning and forgetting in Drosophila. Neuron *74*, 530-542. https://doi.org/10.1016/j.neuron.2012.04.007.

Berry, J.A., Phan, A., and Davis, R.L. (2018). Dopamine Neurons Mediate Learning and Forgetting through Bidirectional Modulation of a Memory Trace. Cell reports *25*, 651-662.e5. https://doi.org/10.1016/j.celrep.2018.09.051.

Bhandawat, V., Olsen, S.R., Gouwens, N.W., Schlief, M.L., and Wilson, R.I. (2007). Sensory processing in the Drosophila antennal lobe increases reliability and separability of ensemble odor representations. Nature neuroscience *10*, 1474-1482. https://doi.org/10.1038/nn1976.

Bhattacharya, A., Lakhman, S.S., and Singh, S. (2004). Modulation of L-type calcium channels in Drosophila via a pituitary adenylyl cyclase-activating polypeptide (PACAP)-

mediated pathway. The Journal of biological chemistry *279*, 37291-37297. https://doi.org/10.1074/jbc.M403819200.

Bhattacharya, S., Stewart, B.A., Niemeyer, B.A., Burgess, R.W., McCabe, B.D., Lin, P., Boulianne, G., O'Kane, C.J., and Schwarz, T.L. (2002). Members of the synaptobrevin/vesicle-associated membrane protein (VAMP) family in Drosophila are functionally interchangeable in vivo for neurotransmitter release and cell viability. Proceedings of the National Academy of Sciences *99*, 13867-13872. https://doi.org/10.1073/pnas.202335999.

Bhukel, A. (2018). Autophagy protects memory formation by tuning presynaptic metaplasticy through NPY signaling.

Bhukel, A., and Beuschel, C.B., Maglione, M., Lehmann, M., Juhász, G., Madeo, F., and Sigrist, S.J. (2019). Autophagy within the mushroom body protects from synapse aging in a non-cell autonomous manner. Nature communications *10*, 1318. https://doi.org/10.1038/s41467-019-09262-2.

Bishop, N.A., Lu, T., and Yankner, B.A. (2010). Neural mechanisms of ageing and cognitive decline. Nature *464*, 529-535. https://doi.org/10.1038/nature08983.

Bjørkøy, G., Lamark, T., Pankiv, S., Øvervatn, A., Brech, A., and Johansen, T. (2009). Monitoring Autophagic Degradation of p62/SQSTM1 *2009*, 181-197. https://doi.org/10.1016/S0076-6879(08)03612-4.

Blum, A.L., Li, W., Cressy, M., and Dubnau, J. (2009). Short- and long-term memory in Drosophila require cAMP signaling in distinct neuron types. Current biology : CB *19*, 1341-1350. https://doi.org/10.1016/j.cub.2009.07.016.

Böhme, M.A., Beis, C., Reddy-Alla, S., Reynolds, E., Mampell, M.M., Grasskamp, A.T., Lützkendorf, J., Bergeron, D.D., Driller, J.H., and Babikir, H., et al. (2016). Active zone scaffolds differentially accumulate Unc13 isoforms to tune Ca(2+) channel-vesicle coupling. Nature neuroscience *19*, 1311-1320. https://doi.org/10.1038/nn.4364.

Böhme, M.A., McCarthy, A.W., Blaum, N., Berezeckaja, M., Ponimaskine, K., Schwefel, D., and Walter, A.M. (2021). Glial Synaptobrevin mediates peripheral nerve insulation, neural metabolic supply, and is required for motor function. Glia *69*, 1897-1915. https://doi.org/10.1002/glia.24000.

Böhme, M.A., McCarthy, A.W., Grasskamp, A.T., Beuschel, C.B., Goel, P., Jusyte, M., Laber, D., Huang, S., Rey, U., and Petzoldt, A.G., et al. (2019). Rapid active zone remodeling consolidates presynaptic potentiation. Nature communications *10*, 1085. https://doi.org/10.1038/s41467-019-08977-6.

Botelho, M., and Cavadas, C. (2015). Neuropeptide Y: An Anti-Aging Player? Trends in neurosciences *38*, 701-711. https://doi.org/10.1016/j.tins.2015.08.012.

Bouzaiane, E., Trannoy, S., Scheunemann, L., Plaçais, P.-Y., and Preat, T. (2015). Two independent mushroom body output circuits retrieve the six discrete components of Drosophila aversive memory. Cell reports *11*, 1280-1292. https://doi.org/10.1016/j.celrep.2015.04.044.

Brand, A.H., and Perrimon, N. (1993). Targeted gene expression as a means of altering cell fates and generating dominant phenotypes. Development (Cambridge, England) *118*, 401-415.

Brattoli, M., Gennaro, G. de, Pinto, V. de, Loiotile, A.D., Lovascio, S., and Penza, M. (2011). Odour detection methods: olfactometry and chemical sensors. Sensors (Basel, Switzerland) *11*, 5290-5322. https://doi.org/10.3390/s110505290.

Brenner, S. (1974). The genetics of Caenorhabditis elegans. Genetics *77*, 71-94. https://doi.org/10.1093/genetics/77.1.71.

Broughton, S.J., Piper, M.D.W., Ikeya, T., Bass, T.M., Jacobson, J., Driege, Y., Martinez, P., Hafen, E., Withers, D.J., and Leevers, S.J., et al. (2005). Longer lifespan, altered metabolism, and stress resistance in Drosophila from ablation of cells making insulin-like ligands. Proceedings of the National Academy of Sciences *102*, 3105-3110. https://doi.org/10.1073/pnas.0405775102.

Burger, J.M.S., Kolss, M., Pont, J., and Kawecki, T.J. (2008). Learning ability and longevity: a symmetrical evolutionary trade-off in Drosophila. Evolution; international journal of organic evolution *62*, 1294-1304. https://doi.org/10.1111/j.1558-5646.2008.00376.x.

Burke, S.N., and Barnes, C.A. (2010). Senescent synapses and hippocampal circuit dynamics. Trends in neurosciences *33*, 153-161. https://doi.org/10.1016/j.tins.2009.12.003.

Bushey, D., Tononi, G., and Cirelli, C. (2011). Sleep and synaptic homeostasis: structural evidence in Drosophila. Science *332*, 1576-1581. https://doi.org/10.1126/science.1202839.

Busto, G.U., Cervantes-Sandoval, I., and Davis, R.L. (2010). Olfactory learning in Drosophila. Physiology (Bethesda, Md.) *25*, 338-346. https://doi.org/10.1152/physiol.00026.2010.

Cabo, R. de, Carmona-Gutierrez, D., Bernier, M., Hall, M.N., and Madeo, F. (2014). The search for antiaging interventions: from elixirs to fasting regimens. Cell *157*, 1515-1526. https://doi.org/10.1016/j.cell.2014.05.031.

Campisi, J., Kapahi, P., Lithgow, G.J., Melov, S., Newman, J.C., and Verdin, E. (2019). From discoveries in ageing research to therapeutics for healthy ageing. Nature *571*, 183-192. https://doi.org/10.1038/s41586-019-1365-2.

Carmona-Gutierrez, D., Zimmermann, A., Kainz, K., Pietrocola, F., Chen, G., Maglioni, S., Schiavi, A., Nah, J., Mertel, S., and Beuschel, C.B., et al. (2019). The flavonoid 4,4'-dimethoxychalcone promotes autophagy-dependent longevity across species. Nature communications *10*, 651. https://doi.org/10.1038/s41467-019-08555-w.

Chang, Y.-Y., and Neufeld, T.P. (2009). An Atg1/Atg13 complex with multiple roles in TOR-mediated autophagy regulation. Molecular biology of the cell *20*, 2004-2014. https://doi.org/10.1091/mbc.e08-12-1250.

Chen, K., Richlitzki, A., Featherstone, D.E., Schwärzel, M., and Richmond, J.E. (2011). Tomosyn-dependent regulation of synaptic transmission is required for a late phase of associative odor memory. Proceedings of the National Academy of Sciences *108*, 18482-18487. https://doi.org/10.1073/pnas.1110184108.

Chen, W., Shi, W., Li, L., Zheng, Z., Li, T., Bai, W., and Zhao, Z. (2013). Regulation of sleep by the short neuropeptide F (sNPF) in Drosophila melanogaster. Insect biochemistry and molecular biology *43*, 809-819. https://doi.org/10.1016/j.ibmb.2013.06.003.

Chiba, T., Tamashiro, Y., Park, D., Kusudo, T., Fujie, R., Komatsu, T., Kim, S.E., Park, S., Hayashi, H., and Mori, R., et al. (2014). A key role for neuropeptide Y in lifespan extension and cancer suppression via dietary restriction. Scientific reports *4*, 4517. https://doi.org/10.1038/srep04517.

am Choi, Ryter, S.W., and Levine, B. (2013). Autophagy in Human Health and Disease. N Engl J Med *368*, 1845-1846. https://doi.org/10.1056/NEJMc1303158.

Christiansen, F., Zube, C., Andlauer, T.F.M., Wichmann, C., Fouquet, W., Owald, D., Mertel, S., Leiss, F., Tavosanis, G., and Luna, A.J.F., et al. (2011). Presynapses in Kenyon cell dendrites in the mushroom body calyx of Drosophila. J. Neurosci. *31*, 9696-9707. https://doi.org/10.1523/JNEUROSCI.6542-10.2011.

Chu, S., and Downes, J.J. (2000). Odour-evoked autobiographical memories: psychological investigations of proustian phenomena. Chemical senses *25*, 111-116. https://doi.org/10.1093/chemse/25.1.111.

Clancy, D.J., Gems, D., Harshman, L.G., Oldham, S., Stocker, H., Hafen, E., Leevers, S.J., and Partridge, L. (2001). Extension of life-span by loss of CHICO, a Drosophila insulin receptor substrate protein. Science *292*, 104-106. https://doi.org/10.1126/science.1057991.

Claridge-Chang, A., Roorda, R.D., Vrontou, E., Sjulson, L., Li, H., Hirsh, J., and Miesenböck, G. (2009). Writing memories with light-addressable reinforcement circuitry. Cell *139*, 405-415. https://doi.org/10.1016/j.cell.2009.08.034.

Cohn, R., Morantte, I., and Ruta, V. (2015). Coordinated and Compartmentalized Neuromodulation Shapes Sensory Processing in Drosophila. Cell *163*, 1742-1755. https://doi.org/10.1016/j.cell.2015.11.019.

Collaboration, T.E.R.F. (2010). Diabetes mellitus, fasting blood glucose concentration, and risk of vascular disease: a collaborative meta-analysis of 102 prospective studies. The Lancet *375*, 2215-2222. https://doi.org/10.1016/S0140-6736(10)60484-9.

Connolly, J.B., Roberts, I.J., Armstrong, J.D., Kaiser, K., Forte, M., Tully, T., and O'Kane, C.J. (1996). Associative learning disrupted by impaired Gs signaling in Drosophila mushroom bodies. Science (New York, N.Y.) *274*, 2104-2107. https://doi.org/10.1126/science.274.5295.2104.

Crittenden, J.R., Skoulakis, E.M., Han, K.A., Kalderon, D., and Davis, R.L. (1998). Tripartite mushroom body architecture revealed by antigenic markers. Learning & Memory *5*, 38-51.

Das Chakraborty, S., and Sachse, S. (2021). Olfactory processing in the lateral horn of Drosophila. Cell and tissue research *383*, 113-123. https://doi.org/10.1007/s00441-020-03392-6.

Davis, R.L. (2004). Olfactory learning. Neuron *44*, 31-48. https://doi.org/10.1016/j.neuron.2004.09.008.

Davis, R.L. (2005). Olfactory memory formation in Drosophila: From molecular to systems neuroscience *2005*.

Davis, R.L. (2011). Traces of Drosophila memory. Neuron *70*, 8-19. https://doi.org/10.1016/j.neuron.2011.03.012.

Deng, L., Kaeser, P.S., Xu, W., and Südhof, T.C. (2011). RIM proteins activate vesicle priming by reversing autoinhibitory homodimerization of Munc13. Neuron *69*, 317-331. https://doi.org/10.1016/j.neuron.2011.01.005.

DeZazzo, J., and Tully, T. (1995). Dissection of memory formation: from behavioral pharmacology to molecular genetics. Trends in neurosciences *18*, 212-218. https://doi.org/10.1016/0166-2236(95)93905-d.

Didier, A., Carleton, A., Bjaalie, J.G., Vincent, J.D., Ottersen, O.P., Storm-Mathisen, J., and Lledo, P.M. (2001). A dendrodendritic reciprocal synapse provides a recurrent excitatory

connection in the olfactory bulb. Proceedings of the National Academy of Sciences *98*, 6441-6446. https://doi.org/10.1073/pnas.101126398.

Diegelmann, S., Zars, M., and Zars, T. (2006). Genetic dissociation of acquisition and memory strength in the heat-box spatial learning paradigm in Drosophila. Learning & memory (Cold Spring Harbor, N.Y.) *13*, 72-83. https://doi.org/10.1101/lm.45506.

Diekelmann, S., and Born, J. (2010). The memory function of sleep. Nature reviews. Neuroscience *11*, 114-126. https://doi.org/10.1038/nrn2762.

Dissel, S., Melnattur, K., and Shaw, P.J. (2015). Sleep, Performance, and Memory in Flies. Current sleep medicine reports *1*, 47-54. https://doi.org/10.1007/s40675-014-0006-4.

Dolan, M.-J., Belliart-Guérin, G., Bates, A.S., Frechter, S., Lampin-Saint-Amaux, A., Aso, Y., Roberts, R.J.V., Schlegel, P., Wong, A., and Hammad, A., et al. (2018). Communication from Learned to Innate Olfactory Processing Centers Is Required for Memory Retrieval in Drosophila. Neuron *100*, 651-668.e8. https://doi.org/10.1016/j.neuron.2018.08.037.

Donlea, J.M. (2019). Roles for sleep in memory: insights from the fly. Current opinion in neurobiology *54*, 120-126. https://doi.org/10.1016/j.conb.2018.10.006.

Doudna, J.A., and Charpentier, E. (2014). Genome editing. The new frontier of genome engineering with CRISPR-Cas9. Science (New York, N.Y.) *346*, 1258096. https://doi.org/10.1126/science.1258096.

Driller, J.H., Lützkendorf, J., Depner, H., Siebert, M., Kuropka, B., Weise, C., Piao, C., Petzoldt, A.G., Lehmann, M., and Stelzl, U., et al. (2019). Phosphorylation of the Bruchpilot N-terminus in Drosophila unlocks axonal transport of active zone building blocks. Journal of cell science *132*. https://doi.org/10.1242/jcs.225151.

Dubruille, R., and Emery, P. (2008). A plastic clock: how circadian rhythms respond to environmental cues in Drosophila. Molecular neurobiology *38*, 129-145. https://doi.org/10.1007/s12035-008-8035-y.

Eisenberg, T., Knauer, H., Schauer, A., Büttner, S., Ruckenstuhl, C., Carmona-Gutierrez, D., Ring, J., Schroeder, S., Magnes, C., and Antonacci, L., et al. (2009). Induction of autophagy by spermidine promotes longevity. Nature cell biology *11*, 1305-1314. https://doi.org/10.1038/ncb1975.

Elliott, D.A., and Brand, A.H. (2008). The GAL4 system : a versatile system for the expression of genes. Methods in molecular biology (Clifton, N.J.) *420*, 79-95. https://doi.org/10.1007/978-1-59745-583-1_5.

Enell, L.E., Kapan, N., Söderberg, J.A.E., Kahsai, L., and Nässel, D.R. (2010). Insulin signaling, lifespan and stress resistance are modulated by metabotropic GABA receptors on insulin producing cells in the brain of Drosophila. PloS one *5*, e15780. https://doi.org/10.1371/journal.pone.0015780.

Fabian, D.K., Fuentealba, M., Dönertaş, H.M., Partridge, L., and Thornton, J.M. (2021). Functional conservation in genes and pathways linking ageing and immunity. Immunity & ageing : I & A *18*, 23. https://doi.org/10.1186/s12979-021-00232-1.

Ferguson, S.A., and Maier, K.L. (2013). A review of seasonal/circannual effects of laboratory rodent behavior. Physiology & behavior *119*, 130-136. https://doi.org/10.1016/j.physbeh.2013.06.007.

Fernandes, A.C., Uytterhoeven, V., Kuenen, S., Wang, Y.-C., Slabbaert, J.R., Swerts, J., Kasprowicz, J., Aerts, S., and Verstreken, P. (2014). Reduced synaptic vesicle protein degradation at lysosomes curbs TBC1D24/sky-induced neurodegeneration. The Journal of cell biology *207*, 453-462. https://doi.org/10.1083/jcb.201406026.

Ferreira-Marques, M., Aveleira, C.A., Carmo-Silva, S., Botelho, M., Pereira de Almeida, L., and Cavadas, C. (2016). Caloric restriction stimulates autophagy in rat cortical neurons through neuropeptide Y and ghrelin receptors activation. Aging *8*, 1470-1484. https://doi.org/10.18632/aging.100996.

Fischer, A., Sananbenesi, F., Wang, X., Dobbin, M., and Tsai, L.-H. (2007). Recovery of learning and memory is associated with chromatin remodelling. Nature *447*, 178-182. https://doi.org/10.1038/nature05772.

Fischer, B., Lüthy, K., Paesmans, J., Koninck, C. de, Maes, I., Swerts, J., Kuenen, S., Uytterhoeven, V., Verstreken, P., and Versées, W. (2016). Skywalker-TBC1D24 has a lipid-binding pocket mutated in epilepsy and required for synaptic function. Nat Struct Mol Biol *23*, 965-973. https://doi.org/10.1038/nsmb.3297.

Flood, J.F., Baker, M.L., Hernandez, E.N., and Morley, J.E. (1989). Modulation of memory processing by neuropeptide Y varies with brain injection site. Brain research *503*, 73-82. https://doi.org/10.1016/0006-8993(89)91706-x.

Fontana, L., Partridge, L., and Longo, V.D. (2010). Extending healthy life span--from yeast to humans. Science (New York, N.Y.) *328*, 321-326. https://doi.org/10.1126/science.1172539.

Foster, T.C., Barnes, C.A., Rao, G., and McNaughton, B.L. (1991). Increase in perforant path quantal size in aged F-344 rats. Neurobiology of aging *12*, 441-448. https://doi.org/10.1016/0197-4580(91)90071-Q.

Fouquet, W., Owald, D., Wichmann, C., Mertel, S., Depner, H., Dyba, M., Hallermann, S., Kittel, R.J., Eimer, S., and Sigrist, S.J. (2009). Maturation of active zone assembly by Drosophila Bruchpilot. Journal of Cell Biology *186*, 129-145. https://doi.org/10.1083/jcb.200812150.

Fraga, M.F., Ballestar, E., Paz, M.F., Ropero, S., Setien, F., Ballestar, M.L., Heine-Suñer, D., Cigudosa, J.C., Urioste, M., and Benitez, J., et al. (2005). Epigenetic differences arise during the lifetime of monozygotic twins. Proceedings of the National Academy of Sciences *102*, 10604-10609. https://doi.org/10.1073/pnas.0500398102.

Frake, R.A., Ricketts, T., Menzies, F.M., and Rubinsztein, D.C. (2015). Autophagy and neurodegeneration. The Journal of clinical investigation *125*, 65-74. https://doi.org/10.1172/JCI73944.

Frazier, H.N., Ghoweri, A.O., Anderson, K.L., Lin, R.-L., Porter, N.M., and Thibault, O. (2019). Broadening the definition of brain insulin resistance in aging and Alzheimer's disease. Experimental neurology *313*, 79-87. https://doi.org/10.1016/j.expneurol.2018.12.007.

Frey, U., Huang, Y.Y., and Kandel, E.R. (1993). Effects of cAMP simulate a late stage of LTP in hippocampal CA1 neurons. Science *260*, 1661-1664. https://doi.org/10.1126/science.8389057.

Fulterer, A., Andlauer, T.F.M., Ender, A., Maglione, M., Eyring, K., Woitkuhn, J., Lehmann, M., Matkovic-Rachid, T., Geiger, J.R.P., and Walter, A.M., et al. (2018). Active Zone Scaffold Protein Ratios Tune Functional Diversity across Brain Synapses. Cell reports *23*, 1259-1274. https://doi.org/10.1016/j.celrep.2018.03.126.

Gáliková, M., Dircksen, H., and Nässel, D.R. (2018). The thirsty fly: Ion transport peptide (ITP) is a novel endocrine regulator of water homeostasis in Drosophila. PLoS genetics *14*, e1007618. https://doi.org/10.1371/journal.pgen.1007618.

Gelino, S., and Hansen, M. (2012). Autophagy - An Emerging Anti-Aging Mechanism. Journal of clinical & experimental pathology *Suppl 4*. https://doi.org/10.4172/2161-0681.s4-006.

Gervasi, N., Tchénio, P., and Preat, T. (2010). PKA dynamics in a Drosophila learning center: coincidence detection by rutabaga adenylyl cyclase and spatial regulation by dunce phosphodiesterase. Neuron *65*, 516-529. https://doi.org/10.1016/j.neuron.2010.01.014.

Gilestro, G.F., Tononi, G., and Cirelli, C. (2009). Widespread changes in synaptic markers as a function of sleep and wakefulness in Drosophila. Science (New York, N.Y.) *324*, 109-112. https://doi.org/10.1126/science.1166673.

Gleason, J.M., Roy, P.R., Everman, E.R., Gleason, T.C., and Morgan, T.J. (2019). Phenology of Drosophila species across a temperate growing season and implications for behavior. PloS one *14*, e0216601. https://doi.org/10.1371/journal.pone.0216601.

Goel, N., Rao, H., Durmer, J.S., and Dinges, D.F. (2009). Neurocognitive consequences of sleep deprivation. Seminars in neurology *29*, 320-339. https://doi.org/10.1055/s-0029-1237117.

Gratz, S.J., Rubinstein, C.D., Harrison, M.M., Wildonger, J., and O'Connor-Giles, K.M. (2015). CRISPR-Cas9 Genome Editing in Drosophila. Current protocols in molecular biology / edited by Frederick M. Ausubel … [et al.] *111*, 31.2.1-31.2.20. https://doi.org/10.1002/0471142727.mb3102s111.

Green, M.M. (2010). 2010: A century of Drosophila genetics through the prism of the white gene. Genetics *184*, 3-7. https://doi.org/10.1534/genetics.109.110015.

Grönke, S., Clarke, D.-F., Broughton, S., Andrews, T.D., and Partridge, L. (2010). Molecular evolution and functional characterization of Drosophila insulin-like peptides. PLoS genetics *6*, e1000857. https://doi.org/10.1371/journal.pgen.1000857.

Gui, X., Yang, H., Li, T., Tan, X., Shi, P., Li, M., Du, F., and Chen, Z.J. (2019). Autophagy induction via STING trafficking is a primordial function of the cGAS pathway. Nature *567*, 262-266. https://doi.org/10.1038/s41586-019-1006-9.

Gupta, V.K., Pech, U., Bhukel, A., Fulterer, A., Ender, A., Mauermann, S.F., Andlauer, T.F.M., Antwi-Adjei, E., Beuschel, C., and Thriene, K., et al. (2016). Spermidine Suppresses Age-Associated Memory Impairment by Preventing Adverse Increase of Presynaptic Active Zone Size and Release. PLoS biology *14*, e1002563. https://doi.org/10.1371/journal.pbio.1002563.

Gupta, V.K., Scheunemann, L., Eisenberg, T., Mertel, S., Bhukel, A., Koemans, T.S., Kramer, J.M., Liu, K.S.Y., Schroeder, S., and Stunnenberg, H.G., et al. (2013). Restoring polyamines protects from age-induced memory impairment in an autophagy-dependent manner. Nature neuroscience *16*, 1453-1460. https://doi.org/10.1038/nn.3512.

Guven-Ozkan, T., and Davis, R.L. (2014). Functional neuroanatomy of Drosophila olfactory memory formation. Learning & memory (Cold Spring Harbor, N.Y.) *21*, 519-526. https://doi.org/10.1101/lm.034363.114.

Hahn, T.M., Breininger, J.F., Baskin, D.G., and Schwartz, M.W. (1998). Coexpression of Agrp and NPY in fasting-activated hypothalamic neurons. Nature neuroscience *1*, 271-272. https://doi.org/10.1038/1082.

Hallermann, S., Kittel, R.J., Wichmann, C., Weyhersmüller, A., Fouquet, W., Mertel, S., Owald, D., Eimer, S., Depner, H., and Schwärzel, M., et al. (2010). Naked dense bodies provoke depression. The Journal of neuroscience : the official journal of the Society for Neuroscience *30*, 14340-14345. https://doi.org/10.1523/JNEUROSCI.2495-10.2010.

Hanada, T., Noda, N.N., Satomi, Y., Ichimura, Y., Fujioka, Y., Takao, T., Inagaki, F., and Ohsumi, Y. (2007). The Atg12-Atg5 conjugate has a novel E3-like activity for protein lipidation in autophagy. The Journal of biological chemistry *282*, 37298-37302. https://doi.org/10.1074/jbc.C700195200.

Hannon, G.J. (2002). RNA interference. Nature *418*, 244-251. https://doi.org/10.1038/418244a.

Hara, T., Nakamura, K., Matsui, M., Yamamoto, A., Nakahara, Y., Suzuki-Migishima, R., Yokoyama, M., Mishima, K., Saito, I., and Okano, H., et al. (2006). Suppression of basal autophagy in neural cells causes neurodegenerative disease in mice. Nature *441*, 885-889. https://doi.org/10.1038/nature04724.

Hattiangady, B., Rao, M.S., Shetty, G.A., and Shetty, A.K. (2005). Brain-derived neurotrophic factor, phosphorylated cyclic AMP response element binding protein and neuropeptide Y decline as early as middle age in the dentate gyrus and CA1 and CA3 subfields of the hippocampus. Experimental neurology *195*, 353-371. https://doi.org/10.1016/j.expneurol.2005.05.014.

Haucke, V., Neher, E., and Sigrist, S.J. (2011). Protein scaffolds in the coupling of synaptic exocytosis and endocytosis. Nature reviews. Neuroscience *12*, 127-138. https://doi.org/10.1038/nrn2948.

Haynes, P.R., Christmann, B.L., and Griffith, L.C. (2015). A single pair of neurons links sleep to memory consolidation in Drosophila melanogaster. eLife *4*. https://doi.org/10.7554/eLife.03868.

Hazelrigg, T., Levis, R., and Rubin, G.M. (1984). Transformation of white locus DNA in Drosophila: Dosage compensation, zeste interaction, and position effects. Cell *36*, 469-481. https://doi.org/10.1016/0092-8674(84)90240-X.

Heisenberg, M. (2003). Mushroom body memoir: from maps to models. Nature reviews. Neuroscience *4*, 266-275. https://doi.org/10.1038/nrn1074.

Hiesinger, P.R., Reiter, C., Schau, H., and Fischbach, K.-F. (1999). Neuropil Pattern Formation and Regulation of Cell Adhesion Molecules in Drosophila Optic Lobe Development Depend on Synaptobrevin. J. Neurosci. *19*, 7548-7556. https://doi.org/10.1523/JNEUROSCI.19-17-07548.1999.

Hige, T., Aso, Y., Modi, M.N., Rubin, G.M., and Turner, G.C. (2015). Heterosynaptic Plasticity Underlies Aversive Olfactory Learning in Drosophila. Neuron *88*, 985-998. https://doi.org/10.1016/j.neuron.2015.11.003.

Hildebrand, J.G., and Shepherd, G.M. (1997). Mechanisms of olfactory discrimination: converging evidence for common principles across phyla. Annual review of neuroscience *20*, 595-631. https://doi.org/10.1146/annurev.neuro.20.1.595.

Ho, V.M., Lee, J.-A., and Martin, K.C. (2011). The cell biology of synaptic plasticity. Science *334*, 623-628. https://doi.org/10.1126/science.1209236.

Hofer, S.J., Liang, Y., Zimmermann, A., Schroeder, S., Dengjel, J., Kroemer, G., Eisenberg, T., Sigrist, S.J., and Madeo, F. (2021). Spermidine-induced hypusination preserves mitochondrial and cognitive function during aging. Autophagy, 1-3. https://doi.org/10.1080/15548627.2021.1933299.

Honegger, K.S., Campbell, R.A.A., and Turner, G.C. (2011). Cellular-resolution population imaging reveals robust sparse coding in the Drosophila mushroom body. J. Neurosci. *31*, 11772-11785. https://doi.org/10.1523/JNEUROSCI.1099-11.2011.

Horiuchi, D., Barkus, R.V., Pilling, A.D., Gassman, A., and Saxton, W.M. (2005). APLIP1, a kinesin binding JIP-1/JNK scaffold protein, influences the axonal transport of both vesicles and mitochondria in Drosophila. Current biology : CB *15*, 2137-2141. https://doi.org/10.1016/j.cub.2005.10.047.

Horiuchi, J., Yamazaki, D., Naganos, S., Aigaki, T., and Saitoe, M. (2008). Protein kinase A inhibits a consolidated form of memory in Drosophila. Proceedings of the National Academy of Sciences *105*, 20976-20981. https://doi.org/10.1073/pnas.0810119105.

Houslay, M.D. (2010). Underpinning compartmentalised cAMP signalling through targeted cAMP breakdown. Trends in biochemical sciences *35*, 91-100. https://doi.org/10.1016/j.tibs.2009.09.007.

Hu, C., Petersen, M., Hoyer, N., Spitzweck, B., Tenedini, F., Wang, D., Gruschka, A., Burchardt, L.S., Szpotowicz, E., and Schweizer, M., et al. (2017). Sensory integration and neuromodulatory feedback facilitate Drosophila mechanonociceptive behavior. Nature neuroscience, 1085-1095. https://doi.org/10.1038/nn.4580.

Huang, S. (2019). PhD thesis *2019*.

Huang, S., Piao, C., Beuschel, C.B., Götz, T., and Sigrist, S.J. (2020). Presynaptic Active Zone Plasticity Encodes Sleep Need in Drosophila. Current biology : CB *30*, 1077-1091.e5. https://doi.org/10.1016/j.cub.2020.01.019.

Huang, S., and Sigrist, S.J. (2021). Presynaptic and postsynaptic long-term plasticity in sleep homeostasis. Current opinion in neurobiology *69*, 1-10. https://doi.org/10.1016/j.conb.2020.11.010.

Hussain, A., Pooryasin, A., Zhang, M., Loschek, L.F., La Fortezza, M., Friedrich, A.B., Blais, C.-M., Üçpunar, H.K., Yépez, V.A., and Lehmann, M., et al. (2018). Inhibition of oxidative stress in cholinergic projection neurons fully rescues aging-associated olfactory circuit degeneration in Drosophila. eLife *7*. https://doi.org/10.7554/eLife.32018.

Inagaki, H.K., Kamikouchi, A., and Ito, K. (2009). Methods for quantifying simple gravity sensing in Drosophila melanogaster. Nature protocols *5*, 20-25. https://doi.org/10.1038/nprot.2009.196.

Isabel, G., Pascual, A., and Preat, T. (2004). Exclusive consolidated memory phases in Drosophila. Science (New York, N.Y.) *304*, 1024-1027. https://doi.org/10.1126/science.1094932.

Jackman, S.L., and Regehr, W.G. (2017). The Mechanisms and Functions of Synaptic Facilitation. Neuron *94*, 447-464. https://doi.org/10.1016/j.neuron.2017.02.047.

Jahn, R., and Fasshauer, D. (2012). Molecular machines governing exocytosis of synaptic vesicles. Nature *490*, 201-207. https://doi.org/10.1038/nature11320.

Jenett, A., Rubin, G.M., Ngo, T.-T.B., Shepherd, D., Murphy, C., Dionne, H., Pfeiffer, B.D., Cavallaro, A., Hall, D., and Jeter, J., et al. (2012). A GAL4-driver line resource for Drosophila neurobiology. Cell reports, 991-1001. https://doi.org/10.1016/j.celrep.2012.09.011.

Jennings, B.H. (2011). Drosophila – a versatile model in biology & medicine. Materials Today *14*, 190-195. https://doi.org/10.1016/S1369-7021(11)70113-4.

Johard, H.A.D., Enell, L.E., Gustafsson, E., Trifilieff, P., Veenstra, J.A., and Nässel, D.R. (2008). Intrinsic neurons of Drosophila mushroom bodies express short neuropeptide F: relations to extrinsic neurons expressing different neurotransmitters. The Journal of comparative neurology *507*, 1479-1496. https://doi.org/10.1002/cne.21636.

Kahsai, L., Kapan, N., Dircksen, H., Winther, A.M.E., and Nässel, D.R. (2010). Metabolic stress responses in Drosophila are modulated by brain neurosecretory cells that produce multiple neuropeptides. PloS one *5*, e11480. https://doi.org/10.1371/journal.pone.0011480.

Kahsai, L., and Zars, T. (2011). Learning and memory in Drosophila: behavior, genetics, and neural systems. International review of neurobiology *99*, 139-167. https://doi.org/10.1016/B978-0-12-387003-2.00006-9.

Kandel, E.R. (2001). The molecular biology of memory storage: a dialogue between genes and synapses. Science *294*, 1030-1038. https://doi.org/10.1126/science.1067020.

Kandel, E.R. (2012). The molecular biology of memory: cAMP, PKA, CRE, CREB-1, CREB-2, and CPEB. Molecular brain *5*, 14. https://doi.org/10.1186/1756-6606-5-14.

Kandel, E.R., Dudai, Y., and Mayford, M.R. (2014). The molecular and systems biology of memory. Cell *157*, 163-186. https://doi.org/10.1016/j.cell.2014.03.001.

Kannan, K., and Fridell, Y.-W.C. (2013). Functional implications of Drosophila insulin-like peptides in metabolism, aging, and dietary restriction. Frontiers in physiology *4*, 288. https://doi.org/10.3389/fphys.2013.00288.

Kapan, N., Lushchak, O.V., Luo, J., and Nässel, D.R. (2012). Identified peptidergic neurons in the Drosophila brain regulate insulin-producing cells, stress responses and metabolism by coexpressed short neuropeptide F and corazonin. Cellular and molecular life sciences : CMLS *69*, 4051-4066. https://doi.org/10.1007/s00018-012-1097-z.

Kaupp, U.B. (2010). Olfactory signalling in vertebrates and insects: differences and commonalities. Nature reviews. Neuroscience *11*, 188-200. https://doi.org/10.1038/nrn2789.

Kauwe, G., Tsurudome, K., Penney, J., Mori, M., Gray, L., Calderon, M.R., Elazouzzi, F., Chicoine, N., Sonenberg, N., and Haghighi, A.P. (2016). Acute Fasting Regulates Retrograde Synaptic Enhancement through a 4E-BP-Dependent Mechanism. Neuron *92*, 1204-1212. https://doi.org/10.1016/j.neuron.2016.10.063.

Keene, A.C., Stratmann, M., Keller, A., Perrat, P.N., Vosshall, L.B., and Waddell, S. (2004). Diverse odor-conditioned memories require uniquely timed dorsal paired medial neuron output. Neuron *44*, 521-533. https://doi.org/10.1016/j.neuron.2004.10.006.

Kellar, D., and Craft, S. (2020). Brain insulin resistance in Alzheimer's disease and related disorders: mechanisms and therapeutic approaches. The Lancet Neurology *19*, 758-766. https://doi.org/10.1016/S1474-4422(20)30231-3.

Kittel, R.J., Hallermann, S., Thomsen, S., Wichmann, C., Sigrist, S.J., and Heckmann, M. (2006a). Active zone assembly and synaptic release. Biochemical Society transactions *34*, 939-941. https://doi.org/10.1042/BST0340939.

Kittel, R.J., Wichmann, C., Rasse, T.M., Fouquet, W., Schmidt, M., Schmid, A., Wagh, D.A., Pawlu, C., Kellner, R.R., and Willig, K.I., et al. (2006b). Bruchpilot promotes active zone assembly, Ca2+ channel clustering, and vesicle release. Science *312*, 1051-1054. https://doi.org/10.1126/science.1126308.

Knapek, S., Gerber, B., and Tanimoto, H. (2010). Synapsin is selectively required for anesthesia-sensitive memory. Learning & memory (Cold Spring Harbor, N.Y.) *17*, 76-79. https://doi.org/10.1101/lm.1661810.

Knapek, S., Kahsai, L., Winther, A.M.E., Tanimoto, H., and Nässel, D.R. (2013). Short neuropeptide F acts as a functional neuromodulator for olfactory memory in Kenyon cells of Drosophila mushroom bodies. The Journal of neuroscience : the official journal of the Society for Neuroscience *33*, 5340-5345. https://doi.org/10.1523/JNEUROSCI.2287-12.2013.

Knapek, S., Sigrist, S., and Tanimoto, H. (2011). Bruchpilot, a synaptic active zone protein for anesthesia-resistant memory. The Journal of neuroscience : the official journal of the Society for Neuroscience *31*, 3453-3458. https://doi.org/10.1523/JNEUROSCI.2585-10.2011.

Koh, K., Joiner, W.J., Wu, M.N., Yue, Z., Smith, C.J., and Sehgal, A. (2008). Identification of SLEEPLESS, a sleep-promoting factor. Science (New York, N.Y.) *321*, 372-376. https://doi.org/10.1126/science.1155942.

Konar, A., Singh, P., and Thakur, M.K. (2016). Age-associated Cognitive Decline: Insights into Molecular Switches and Recovery Avenues. Aging and disease *7*, 121-129. https://doi.org/10.14336/AD.2015.1004.

Krashes, M.J., Keene, A.C., Leung, B., Armstrong, J.D., and Waddell, S. (2007). Sequential use of mushroom body neuron subsets during drosophila odor memory processing. Neuron *53*, 103-115. https://doi.org/10.1016/j.neuron.2006.11.021.

Krivanek, T.J., Gale, S.A., McFeeley, B.M., Nicastri, C.M., and Daffner, K.R. (2021). Promoting Successful Cognitive Aging: A Ten-Year Update. Journal of Alzheimer's disease : JAD *81*, 871-920. https://doi.org/10.3233/JAD-201462.

Krukowski, K., Ma, J., Golonzhka, O., Laumet, G.O., Gutti, T., van Duzer, J.H., Mazitschek, R., Jarpe, M.B., Heijnen, C.J., and Kavelaars, A. (2017). HDAC6 inhibition effectively reverses chemotherapy-induced peripheral neuropathy. Pain *158*, 1126-1137. https://doi.org/10.1097/j.pain.0000000000000893.

Kühnau, J. (1976). The flavonoids. A class of semi-essential food components: their role in human nutrition. World review of nutrition and dietetics *24*, 117-191.

Kulkarni, A., Chen, J., and Maday, S. (2018). Neuronal autophagy and intercellular regulation of homeostasis in the brain. Current opinion in neurobiology *51*, 29-36. https://doi.org/10.1016/j.conb.2018.02.008.

Lamb, C.A., Yoshimori, T., and Tooze, S.A. (2013). The autophagosome: origins unknown, biogenesis complex. Nature reviews. Molecular cell biology *14*, 759-774. https://doi.org/10.1038/nrm3696.

Lee, D. (2015). Global and local missions of cAMP signaling in neural plasticity, learning, and memory. Frontiers in pharmacology *6*, 161. https://doi.org/10.3389/fphar.2015.00161.

Lee, K.-S., Kwon, O.-Y., Lee, J.H., Kwon, K., Min, K.-J., Jung, S.-A., Kim, A.-K., You, K.-H., Tatar, M., and Yu, K. (2008). Drosophila short neuropeptide F signalling regulates growth by ERK-mediated insulin signalling. Nature cell biology *10*, 468-475. https://doi.org/10.1038/ncb1710.

Lee, K.-S., You, K.-H., Choo, J.-K., Han, Y.-M., and Yu, K. (2004). Drosophila short neuropeptide F regulates food intake and body size. The Journal of biological chemistry *279*, 50781-50789. https://doi.org/10.1074/jbc.M407842200.

Leidal, A.M., Levine, B., and Debnath, J. (2018). Autophagy and the cell biology of age-related disease. Nature cell biology *20*, 1338-1348. https://doi.org/10.1038/s41556-018-0235-8.

Levine, B., and Kroemer, G. (2008). Autophagy in the pathogenesis of disease. Cell *132*, 27-42. https://doi.org/10.1016/j.cell.2007.12.018.

Lewis, L.P.C., Siju, K.P., Aso, Y., Friedrich, A.B., Bulteel, A.J.B., Rubin, G.M., and Grunwald Kadow, I.C. (2015). A Higher Brain Circuit for Immediate Integration of Conflicting Sensory Information in Drosophila. Current biology : CB *25*, 2203-2214. https://doi.org/10.1016/j.cub.2015.07.015.

Li, B., Yang, Y., Wang, Y., Zhang, J., Ding, J., Liu, X., Jin, Y., Lian, B., Ling, Y., and Sun, C. (2021). Acetylation of NDUFV1 induced by a newly synthesized HDAC6 inhibitor HGC rescues dopaminergic neuron loss in Parkinson models. iScience *24*, 102302. https://doi.org/10.1016/j.isci.2021.102302.

Li, F., Lindsey, J.W., Marin, E.C., Otto, N., Dreher, M., Dempsey, G., Stark, I., Bates, A.S., Pleijzier, M.W., and Schlegel, P., et al. (2020). The connectome of the adult Drosophila mushroom body provides insights into function. eLife *9*. https://doi.org/10.7554/eLife.62576.

Li, L., Tian, X., Zhu, M., Bulgari, D., Böhme, M.A., Goettfert, F., Wichmann, C., Sigrist, S.J., Levitan, E.S., and Wu, C. (2014). Drosophila Syd-1, liprin-α, and protein phosphatase 2A B' subunit Wrd function in a linear pathway to prevent ectopic accumulation of synaptic materials in distal axons. J. Neurosci. *34*, 8474-8487. https://doi.org/10.1523/JNEUROSCI.0409-14.2014.

Li, Y., Wang, S., Li, T., Le Zhu, and Ma, C. (2018). Tomosyn guides SNARE complex formation in coordination with Munc18 and Munc13. FEBS Lett *592*, 1161-1172. https://doi.org/10.1002/1873-3468.13018.

Liang (2019). YongTian Liang_PHD Dissertation.

Liang, L., Li, Y., Potter, C.J., Yizhar, O., Deisseroth, K., Tsien, R.W., and Luo, L. (2013). GABAergic projection neurons route selective olfactory inputs to specific higher-order neurons. Neuron *79*, 917-931. https://doi.org/10.1016/j.neuron.2013.06.014.

Liang, Y., Piao, C., Beuschel, C.B., Toppe, D., Kollipara, L., Bogdanow, B., Maglione, M., Lützkendorf, J., See, J.C.K., and Huang, S., et al. (2021). eIF5A hypusination, boosted by dietary spermidine, protects from premature brain aging and mitochondrial dysfunction. Cell reports *35*, 108941. https://doi.org/10.1016/j.celrep.2021.108941.

Liang, Y., and Sigrist, S. (2018). Autophagy and proteostasis in the control of synapse aging and disease. Current opinion in neurobiology *48*, 113-121. https://doi.org/10.1016/j.conb.2017.12.006.

Lim, A., Rechtsteiner, A., and Saxton, W.M. (2017). Two kinesins drive anterograde neuropeptide transport. Molecular biology of the cell *28*, 3542-3553. https://doi.org/10.1091/mbc.E16-12-0820.

Lin, D.M., and Goodman, C.S. (1994). Ectopic and increased expression of fasciclin II alters motoneuron growth cone guidance. Neuron *13*, 507-523. https://doi.org/10.1016/0896-6273(94)90022-1.

Lipstein, N., Sakaba, T., Cooper, B.H., Lin, K.-H., Strenzke, N., Ashery, U., Rhee, J.-S., Taschenberger, H., Neher, E., and Brose, N. (2013). Dynamic control of synaptic vesicle replenishment and short-term plasticity by Ca(2+)-calmodulin-Munc13-1 signaling. Neuron *79*, 82-96. https://doi.org/10.1016/j.neuron.2013.05.011.

Liu, K.S.Y., Siebert, M., Mertel, S., Knoche, E., Wegener, S., Wichmann, C., Matkovic, T., Muhammad, K., Depner, H., and Mettke, C., et al. (2011). RIM-binding protein, a central part of the active zone, is essential for neurotransmitter release. Science *334*, 1565-1569. https://doi.org/10.1126/science.1212991.

Liu, S., Liu, Q., Tabuchi, M., and Wu, M.N. (2016). Sleep Drive Is Encoded by Neural Plastic Changes in a Dedicated Circuit. Cell *165*, 1347-1360. https://doi.org/10.1016/j.cell.2016.04.013.

Liu, X., and Davis, R.L. (2009). The GABAergic anterior paired lateral neuron suppresses and is suppressed by olfactory learning. Nature neuroscience *12*, 53-59. https://doi.org/10.1038/nn.2235.

Liu, X., Krause, W.C., and Davis, R.L. (2007). GABAA receptor RDL inhibits Drosophila olfactory associative learning. Neuron *56*, 1090-1102. https://doi.org/10.1016/j.neuron.2007.10.036.

Loeffler, D.A. (2019). Influence of Normal Aging on Brain Autophagy: A Complex Scenario. Frontiers in aging neuroscience *11*, 49. https://doi.org/10.3389/fnagi.2019.00049.

Longo, V.D., Antebi, A., Bartke, A., Barzilai, N., Brown-Borg, H.M., Caruso, C., Curiel, T.J., Cabo, R. de, Franceschi, C., and Gems, D., et al. (2015). Interventions to Slow Aging in Humans: Are We Ready? Aging cell *14*, 497-510. https://doi.org/10.1111/acel.12338.

López-Otín, C., Blasco, M.A., Partridge, L., Serrano, M., and Kroemer, G. (2013). The hallmarks of aging. Cell *153*, 1194-1217. https://doi.org/10.1016/j.cell.2013.05.039.

Madeo, F., Carmona-Gutierrez, D., Hofer, S.J., and Kroemer, G. (2019). Caloric Restriction Mimetics against Age-Associated Disease: Targets, Mechanisms, and Therapeutic Potential. Cell metabolism *29*, 592-610. https://doi.org/10.1016/j.cmet.2019.01.018.

Madeo, F., Eisenberg, T., Pietrocola, F., and Kroemer, G. (2018). Spermidine in health and disease. Science (New York, N.Y.) *359*. https://doi.org/10.1126/science.aan2788.

Maglione, M., Kochlamazashvili, G., Eisenberg, T., Rácz, B., Michael, E., Toppe, D., Stumpf, A., Wirth, A., Zeug, A., and Müller, F.E., et al. (2019). Spermidine protects from age-related synaptic alterations at hippocampal mossy fiber-CA3 synapses. Scientific reports *9*, 19616. https://doi.org/10.1038/s41598-019-56133-3.

Mao, Z., and Davis, R.L. (2009). Eight different types of dopaminergic neurons innervate the Drosophila mushroom body neuropil: anatomical and physiological heterogeneity. Frontiers in neural circuits *3*, 5. https://doi.org/10.3389/neuro.04.005.2009.

Mariano, V., Achsel, T., Bagni, C., and Kanellopoulos, A.K. (2020). Modelling Learning and Memory in Drosophila to Understand Intellectual Disabilities. Neuroscience *445*, 12-30. https://doi.org/10.1016/j.neuroscience.2020.07.034.

Martin, F., Boto, T., Gomez-Diaz, C., and Alcorta, E. (2013). Elements of olfactory reception in adult Drosophila melanogaster. Anatomical record (Hoboken, N.J. : 2007) *296*, 1477-1488. https://doi.org/10.1002/ar.22747.

Matkovic, T., Siebert, M., Knoche, E., Depner, H., Mertel, S., Owald, D., Schmidt, M., Thomas, U., Sickmann, A., and Kamin, D., et al. (2013). The Bruchpilot cytomatrix determines the size of the readily releasable pool of synaptic vesicles. The Journal of cell biology *202*, 667-683. https://doi.org/10.1083/jcb.201301072.

Matsunami, H., and Amrein, H. (2003). Taste and pheromone perception in mammals and flies. Genome biology *4*, 220. https://doi.org/10.1186/gb-2003-4-7-220.

Mattson, M.P., and Arumugam, T.V. (2018). Hallmarks of Brain Aging: Adaptive and Pathological Modification by Metabolic States. Cell metabolism *27*, 1176-1199. https://doi.org/10.1016/j.cmet.2018.05.011.

Mattson, M.P., Moehl, K., Ghena, N., Schmaedick, M., and Cheng, A. (2018). Intermittent metabolic switching, neuroplasticity and brain health. Nature reviews. Neuroscience *19*, 63-80. https://doi.org/10.1038/nrn.2017.156.

Mauvezin, C., Ayala, C., Braden, C.R., Kim, J., and Neufeld, T.P. (2014). Assays to monitor autophagy in Drosophila. Methods *68*, 134-139. https://doi.org/10.1016/j.ymeth.2014.03.014.

McCay, C.M., Maynard, L.A., Sperling, G., and Barnes, L.L. (1939). Retarded Growth, Life Span, Ultimate Body Size and Age Changes in the Albino Rat after Feeding Diets Restricted in Calories. The Journal of Nutrition *18*, 1-13. https://doi.org/10.1093/jn/18.1.1.

McGaugh, J.L. (2000). Memory--a century of consolidation. Science (New York, N.Y.) *287*, 248-251. https://doi.org/10.1126/science.287.5451.248.

McGuire, S.E., Deshazer, M., and Davis, R.L. (2005). Thirty years of olfactory learning and memory research in Drosophila melanogaster. Progress in neurobiology *76*, 328-347. https://doi.org/10.1016/j.pneurobio.2005.09.003.

McGuire, S.E., Le, P.T., and Davis, R.L. (2001). The role of Drosophila mushroom body signaling in olfactory memory. Science (New York, N.Y.) *293*, 1330-1333. https://doi.org/10.1126/science.1062622.

McGuire, S.E., Le, P.T., Osborn, A.J., Matsumoto, K., and Davis, R.L. (2003). Spatiotemporal rescue of memory dysfunction in Drosophila. Science (New York, N.Y.) *302*, 1765-1768. https://doi.org/10.1126/science.1089035.

McMahon, H.T., Ushkaryov, Y.A., Edelmann, L., Link, E., Binz, T., Niemann, H., Jahn, R., and Südhof, T.C. (1993). Cellubrevin is a ubiquitous tetanus-toxin substrate homologous to a putative synaptic vesicle fusion protein. Nature *364*, 346-349. https://doi.org/10.1038/364346a0.

Menzies, F.M., Fleming, A., Caricasole, A., Bento, C.F., Andrews, S.P., Ashkenazi, A., Füllgrabe, J., Jackson, A., Jimenez Sanchez, M., and Karabiyik, C., et al. (2017). Autophagy and Neurodegeneration: Pathogenic Mechanisms and Therapeutic Opportunities. Neuron *93*, 1015-1034. https://doi.org/10.1016/j.neuron.2017.01.022.

Mery, F. (2007). Aging and its differential effects on consolidated memory forms in Drosophila. Experimental gerontology *42*, 99-101. https://doi.org/10.1016/j.exger.2006.06.004.

Michalkiewicz, M., Knestaut, K.M., Bytchkova, E.Y., and Michalkiewicz, T. (2003). Hypotension and reduced catecholamines in neuropeptide Y transgenic rats. Hypertension (Dallas, Tex. : 1979) *41*, 1056-1062. https://doi.org/10.1161/01.HYP.0000066623.64368.4E.

Miki, H., Okada, Y., and Hirokawa, N. (2005). Analysis of the kinesin superfamily: insights into structure and function. Trends in Cell Biology *15*, 467-476. https://doi.org/10.1016/j.tcb.2005.07.006.

Minnerly, J., Zhang, J., Parker, T., Kaul, T., and Jia, K. (2017). The cell non-autonomous function of ATG-18 is essential for neuroendocrine regulation of Caenorhabditis elegans lifespan. PLoS genetics *13*, e1006764. https://doi.org/10.1371/journal.pgen.1006764.

Miskiewicz, K., Jose, L.E., Yeshaw, W.M., Valadas, J.S., Swerts, J., Munck, S., Feiguin, F., Dermaut, B., and Verstreken, P. (2014). HDAC6 is a Bruchpilot deacetylase that facilitates neurotransmitter release. Cell reports *8*, 94-102. https://doi.org/10.1016/j.celrep.2014.05.051.

Miśkiewicz, K., Jose, L.E., Bento-Abreu, A., Fislage, M., Taes, I., Kasprowicz, J., Swerts, J., Sigrist, S., Versées, W., and Robberecht, W., et al. (2011). ELP3 controls active zone morphology by acetylating the ELKS family member Bruchpilot. Neuron *72*, 776-788. https://doi.org/10.1016/j.neuron.2011.10.010.

Mitchell, A.P., and Magasanik, B. (1984). Regulation of glutamine-repressible gene products by the GLN3 function in Saccharomyces cerevisiae. Molecular and cellular biology *4*, 2758-2766. https://doi.org/10.1128/mcb.4.12.2758-2766.1984.

Mohseni, N., McMillan, S.C., Chaudhary, R., Mok, J., and Reed, B.H. (2009). Autophagy promotes caspase-dependent cell death during Drosophila development. Autophagy *5*, 329-338. https://doi.org/10.4161/auto.5.3.7444.

Morrison, J.H., and Baxter, M.G. (2012). The ageing cortical synapse: hallmarks and implications for cognitive decline. Nature reviews. Neuroscience *13*, 240-250. https://doi.org/10.1038/nrn3200.

Mukherjee, A., Patel, B., Koga, H., Cuervo, A.M., and Jenny, A. (2016). Selective endosomal microautophagy is starvation-inducible in Drosophila. Autophagy *12*, 1984-1999. https://doi.org/10.1080/15548627.2016.1208887.

Müller, M., Liu, K.S.Y., Sigrist, S.J., and Davis, G.W. (2012). RIM controls homeostatic plasticity through modulation of the readily-releasable vesicle pool. J. Neurosci. *32*, 16574-16585. https://doi.org/10.1523/JNEUROSCI.0981-12.2012.

Murakami, S., Minami-Ohtsubo, M., Nakato, R., Shirahige, K., and Tabata, T. (2017). Two Components of Aversive Memory in Drosophila, Anesthesia-Sensitive and Anesthesia-

Resistant Memory, Require Distinct Domains Within the Rgk1 Small GTPase. J. Neurosci. *37*, 5496-5510. https://doi.org/10.1523/JNEUROSCI.3648-16.2017.

Nässel, D.R., Enell, L.E., Santos, J.G., Wegener, C., and Johard, H.A.D. (2008). A large population of diverse neurons in the Drosophila central nervous system expresses short neuropeptide F, suggesting multiple distributed peptide functions. BMC neuroscience *9*, 90. https://doi.org/10.1186/1471-2202-9-90.

Nässel, D.R., Kubrak, O.I., Liu, Y., Luo, J., and Lushchak, O.V. (2013). Factors that regulate insulin producing cells and their output in Drosophila. Frontiers in physiology *4*, 252. https://doi.org/10.3389/fphys.2013.00252.

Nazir, A., Mukhopadhyay, I., Saxena, D.K., and Chowdhuri, D.K. (2003). Evaluation of the No Observed Adverse Effect Level of Solvent Dimethyl Sulfoxide in Drosophila melanogaster. Toxicology mechanisms and methods *13*, 147-152. https://doi.org/10.1080/15376510309846.

Nicoll, R.A., and Roche, K.W. (2013). Long-term potentiation: peeling the onion. Neuropharmacology *74*, 18-22. https://doi.org/10.1016/j.neuropharm.2013.02.010.

Nieratschker, V., Schubert, A., Jauch, M., Bock, N., Bucher, D., Dippacher, S., Krohne, G., Asan, E., Buchner, S., and Buchner, E. (2009). Bruchpilot in ribbon-like axonal agglomerates, behavioral defects, and early death in SRPK79D kinase mutants of Drosophila. PLoS genetics *5*, e1000700. https://doi.org/10.1371/journal.pgen.1000700.

Nystuen, A.M., Schwendinger, J.K., Sachs, A.J., Yang, A.W., and Haider, N.B. (2007). A null mutation in VAMP1/synaptobrevin is associated with neurological defects and prewean mortality in the lethal-wasting mouse mutant. Neurogenetics *8*, 1-10. https://doi.org/10.1007/s10048-006-0068-7.

Okamoto, K. (2014). Organellophagy: eliminating cellular building blocks via selective autophagy. The Journal of cell biology *205*, 435-445. https://doi.org/10.1083/jcb.201402054.

Olsen, S.R., and Wilson, R.I. (2008). Lateral presynaptic inhibition mediates gain control in an olfactory circuit. Nature *452*, 956-960. https://doi.org/10.1038/nature06864.

Onishi, T., Maeda, R., Terada, M., Sato, S., Fujii, T., Ito, M., Hashikami, K., Kawamoto, T., and Tanaka, M. (2021). A novel orally active HDAC6 inhibitor T-518 shows a therapeutic potential for Alzheimer's disease and tauopathy in mice. Scientific reports *11*, 15423. https://doi.org/10.1038/s41598-021-94923-w.

Ortega, J.M., Genç, Ö., and Davis, G.W. (2018). Molecular mechanisms that stabilize short term synaptic plasticity during presynaptic homeostatic plasticity. eLife *7*. https://doi.org/10.7554/eLife.40385.

Ott, V., Benedict, C., Schultes, B., Born, J., and Hallschmid, M. (2012). Intranasal administration of insulin to the brain impacts cognitive function and peripheral metabolism. Diabetes, obesity & metabolism *14*, 214-221. https://doi.org/10.1111/j.1463-1326.2011.01490.x.

Owald, D., Felsenberg, J., Talbot, C.B., Das, G., Perisse, E., Huetteroth, W., and Waddell, S. (2015). Activity of defined mushroom body output neurons underlies learned olfactory behavior in Drosophila. Neuron *86*, 417-427. https://doi.org/10.1016/j.neuron.2015.03.025.

Owald, D., Fouquet, W., Schmidt, M., Wichmann, C., Mertel, S., Depner, H., Christiansen, F., Zube, C., Quentin, C., and Körner, J., et al. (2010). A Syd-1 homologue regulates pre- and postsynaptic maturation in Drosophila. Journal of Cell Biology *188*, 565-579. https://doi.org/10.1083/jcb.200908055.

Owald, D., and Sigrist, S.J. (2009). Assembling the presynaptic active zone. Current opinion in neurobiology *19*, 311-318. https://doi.org/10.1016/j.conb.2009.03.003.

Pan, H., and Finkel, T. (2017). Key proteins and pathways that regulate lifespan. The Journal of biological chemistry *292*, 6452-6460. https://doi.org/10.1074/jbc.R116.771915.

Panche, A.N., Diwan, A.D., and Chandra, S.R. (2016). Flavonoids: an overview. Journal of nutritional science *5*, e47. https://doi.org/10.1017/jns.2016.41.

Pankiv, S., Clausen, T.H., Lamark, T., Brech, A., Bruun, J.-A., Outzen, H., Øvervatn, A., Bjørkøy, G., and Johansen, T. (2007). p62/SQSTM1 binds directly to Atg8/LC3 to facilitate degradation of ubiquitinated protein aggregates by autophagy. The Journal of biological chemistry *282*, 24131-24145. https://doi.org/10.1074/jbc.M702824200.

Pascual, A., and Préat, T. (2001). Localization of long-term memory within the Drosophila mushroom body. Science *294*, 1115-1117. https://doi.org/10.1126/science.1064200.

Patel, S., DeMaine, S., Heafield, J., Bianchi, L., and Prokop, A. (2017). The droso4schools project: Long-term scientist-teacher collaborations to promote science communication and education in schools. Seminars in cell & developmental biology *70*, 73-84. https://doi.org/10.1016/j.semcdb.2017.07.025.

Pavlov, I.P. Conditioned Reflexes. In.

Peled, E.S., and Isacoff, E.Y. (2011). Optical quantal analysis of synaptic transmission in wild-type and rab3-mutant Drosophila motor axons. Nature neuroscience *14*, 519-526. https://doi.org/10.1038/nn.2767.

Petzoldt, A.G., Götz, T.W.B., Driller, J.H., Lützkendorf, J., Reddy-Alla, S., Matkovic-Rachid, T., Liu, S., Knoche, E., Mertel, S., and Ugorets, V., et al. (2020). RIM-binding protein couples

synaptic vesicle recruitment to release sites. The Journal of cell biology *219*. https://doi.org/10.1083/jcb.201902059.

Piao, C., and Sigrist, S.J. (2021). (M)Unc13s in Active Zone Diversity: A Drosophila Perspective. Frontiers in synaptic neuroscience *13*, 798204. https://doi.org/10.3389/fnsyn.2021.798204.

Pierre-Yves Plaçais, Séverine Trannoy, Guillaume Isabel, Yoshinori Aso, Igor Siwanowicz, Ghislain Belliart-Guérin, Philippe Vernier, Serge Birman, Hiromu Tanimoto, and Thomas Preat (2012). Slow oscillations in two pairs of dopaminergic neurons gate long-term memory formation in Drosophila *2012*.

Piper, M.D.W., and Partridge, L. (2018). Drosophila as a model for ageing. Biochimica et biophysica acta. Molecular basis of disease *1864*, 2707-2717. https://doi.org/10.1016/j.bbadis.2017.09.016.

Plaçais, P.-Y., and Preat, T. (2013). To favor survival under food shortage, the brain disables costly memory. Science *339*, 440-442. https://doi.org/10.1126/science.1226018.

Plaçais, P.-Y., Tredern, É. de, Scheunemann, L., Trannoy, S., Goguel, V., Han, K.-A., Isabel, G., and Preat, T. (2017). Upregulated energy metabolism in the Drosophila mushroom body is the trigger for long-term memory. Nature communications *8*, 15510. https://doi.org/10.1038/ncomms15510.

Poloz, Y., and Stambolic, V. (2015). Obesity and cancer, a case for insulin signaling. Cell death & disease *6*, e2037. https://doi.org/10.1038/cddis.2015.381.

Pooryasin, A., Maglione, M., Schubert, M., Matkovic-Rachid, T., Hasheminasab, S.-M., Pech, U., Fiala, A., Mielke, T., and Sigrist, S.J. (2021). Unc13A and Unc13B contribute to the decoding of distinct sensory information in Drosophila. Nature communications *12*, 1932. https://doi.org/10.1038/s41467-021-22180-6.

Pucciarelli, S., Moreschini, B., Micozzi, D., Fronzo, G.S. de, Carpi, F.M., Polzonetti, V., Vincenzetti, S., Mignini, F., and Napolioni, V. (2012). Spermidine and spermine are enriched in whole blood of nona/centenarians. Rejuvenation Research *15*, 590-595. https://doi.org/10.1089/rej.2012.1349.

Qin, H., Cressy, M., Li, W., Coravos, J.S., Izzi, S.A., and Dubnau, J. (2012). Gamma neurons mediate dopaminergic input during aversive olfactory memory formation in Drosophila. Current biology : CB *22*, 608-614. https://doi.org/10.1016/j.cub.2012.02.014.

Qiu, W.Q., and Folstein, M.F. (2006). Insulin, insulin-degrading enzyme and amyloid-beta peptide in Alzheimer's disease: review and hypothesis. Neurobiology of aging *27*, 190-198. https://doi.org/10.1016/j.neurobiolaging.2005.01.004.

Quade, B., Camacho, M., Zhao, X., Orlando, M., Trimbuch, T., Xu, J., Li, W., Nicastro, D., Rosenmund, C., and Rizo, J. (2019). Membrane bridging by Munc13-1 is crucial for neurotransmitter release. eLife *8*. https://doi.org/10.7554/eLife.42806.

Quinn, W.G., Harris, W.A., and Benzer, S. (1974). Conditioned behavior in Drosophila melanogaster. Proceedings of the National Academy of Sciences of the United States of America *71*, 708-712. https://doi.org/10.1073/pnas.71.3.708.

Quinn, W.G., Sziber, P.P., and Booker, R. (1979). The Drosophila memory mutant amnesiac. Nature *277*, 212-214. https://doi.org/10.1038/277212a0.

Rangarajan, S., Raj, M.L.S., Hernandez, J.M., Grotewold, E., and Gopalan, V. (2004). RNase P as a tool for disruption of gene expression in maize cells. The Biochemical journal *380*, 611-616. https://doi.org/10.1042/BJ20040442.

Reddy-Alla, S., Böhme, M.A., Reynolds, E., Beis, C., Grasskamp, A.T., Mampell, M.M., Maglione, M., Jusyte, M., Rey, U., and Babikir, H., et al. (2017). Stable Positioning of Unc13 Restricts Synaptic Vesicle Fusion to Defined Release Sites to Promote Synchronous Neurotransmission. Neuron *95*, 1350-1364.e12. https://doi.org/10.1016/j.neuron.2017.08.016.

Reiter, L.T., Potocki, L., Chien, S., Gribskov, M., and Bier, E. (2001). A systematic analysis of human disease-associated gene sequences in Drosophila melanogaster. Genome research *11*, 1114-1125. https://doi.org/10.1101/gr.169101.

Rice-Evans, C.A., and Miller, N.J. (1996). Antioxidant activities of flavonoids as bioactive components of food. Biochemical Society transactions *24*, 790-795. https://doi.org/10.1042/bst0240790.

Rizzoli, S.O., and Betz, W.J. (2005). Synaptic vesicle pools. Nature reviews. Neuroscience *6*, 57-69. https://doi.org/10.1038/nrn1583.

Root, C.M., Ko, K.I., Jafari, A., and Wang, J.W. (2011). Presynaptic facilitation by neuropeptide signaling mediates odor-driven food search. Cell *145*, 133-144. https://doi.org/10.1016/j.cell.2011.02.008.

Roote, J., and Prokop, A. (2013). How to design a genetic mating scheme: a basic training package for Drosophila genetics. G3 (Bethesda, Md.) *3*, 353-358. https://doi.org/10.1534/g3.112.004820.

Rosenzweig, E.S., and Barnes, C.A. (2003). Impact of aging on hippocampal function: plasticity, network dynamics, and cognition. Progress in neurobiology *69*, 143-179. https://doi.org/10.1016/S0301-0082(02)00126-0.

Rubinsztein, D.C., Mariño, G., and Kroemer, G. (2011). Autophagy and aging. Cell *146*, 682-695. https://doi.org/10.1016/j.cell.2011.07.030.

Saitoe, M., Horiuchi, J., Tamura, T., and Ito, N. (2005). Drosophila as a novel animal model for studying the genetics of age-related memory impairment. Reviews in the neurosciences *16*, 137-149. https://doi.org/10.1515/revneuro.2005.16.2.137.

Salpietro, V., Lin, W., Delle Vedove, A., Storbeck, M., Liu, Y., Efthymiou, S., Manole, A., Wiethoff, S., Ye, Q., and Saggar, A., et al. (2017). Homozygous mutations in VAMP1 cause a presynaptic congenital myasthenic syndrome. Ann Neurol. *81*, 597-603. https://doi.org/10.1002/ana.24905.

Samson, S.L., and Garber, A.J. (2014). Metabolic syndrome. Endocrinology and metabolism clinics of North America *43*, 1-23. https://doi.org/10.1016/j.ecl.2013.09.009.

Sander, M.C., Fandakova, Y., and Werkle-Bergner, M. (2021). Effects of age differences in memory formation on neural mechanisms of consolidation and retrieval. Seminars in cell & developmental biology *116*, 135-145. https://doi.org/10.1016/j.semcdb.2021.02.005.

Scheunemann, L., Jost, E., Richlitzki, A., Day, J.P., Sebastian, S., Thum, A.S., Efetova, M., Davies, S.-A., and Schwärzel, M. (2012). Consolidated and labile odor memory are separately encoded within the Drosophila brain. J. Neurosci. *32*, 17163-17171. https://doi.org/10.1523/JNEUROSCI.3286-12.2012.

Schroeder, S., Hofer, S.J., Zimmermann, A., Pechlaner, R., Dammbrueck, C., Pendl, T., Marcello, G.M., Pogatschnigg, V., Bergmann, M., and Müller, M., et al. (2021). Dietary spermidine improves cognitive function. Cell reports *35*, 108985. https://doi.org/10.1016/j.celrep.2021.108985.

Schwaerzel, M., Jaeckel, A., and Mueller, U. (2007). Signaling at A-kinase anchoring proteins organizes anesthesia-sensitive memory in Drosophila. The Journal of neuroscience : the official journal of the Society for Neuroscience *27*, 1229-1233. https://doi.org/10.1523/JNEUROSCI.4622-06.2007.

Shang, Y., Donelson, N.C., Vecsey, C.G., Guo, F., Rosbash, M., and Griffith, L.C. (2013). Short neuropeptide F is a sleep-promoting inhibitory modulator. Neuron *80*, 171-183. https://doi.org/10.1016/j.neuron.2013.07.029.

Shen, W., and Ganetzky, B. (2009). Autophagy promotes synapse development in Drosophila. Journal of Cell Biology *187*, 71-79. https://doi.org/10.1083/jcb.200907109.

Shim, J., Gururaja-Rao, S., and Banerjee, U. (2013). Nutritional regulation of stem and progenitor cells in Drosophila. Development *140*, 4647-4656. https://doi.org/10.1242/dev.079087.

Siebert, M., Böhme, M.A., Driller, J.H., Babikir, H., Mampell, M.M., Rey, U., Ramesh, N., Matkovic, T., Holton, N., and Reddy-Alla, S., et al. (2015). A high affinity RIM-binding protein/Aplip1 interaction prevents the formation of ectopic axonal active zones. eLife *4*. https://doi.org/10.7554/eLife.06935.

Sigrist, S., and Ohtsuka, T. (2018). The presynaptic active zone: molecules, plasticity, and diseases. Neuroscience research *127*, 1-2. https://doi.org/10.1016/j.neures.2018.01.004.

Sigrist, S.J., Carmona-Gutierrez, D., Gupta, V.K., Bhukel, A., Mertel, S., Eisenberg, T., and Madeo, F. (2014). Spermidine-triggered autophagy ameliorates memory during aging. Autophagy *10*, 178-179. https://doi.org/10.4161/auto.26918.

Sigrist, S.J., Reiff, D.F., Thiel, P.R., Steinert, J.R., and Schuster, C.M. (2003). Experience-Dependent Strengthening of Drosophila Neuromuscular Junctions. J. Neurosci. *23*, 6546-6556. https://doi.org/10.1523/JNEUROSCI.23-16-06546.2003.

Silbernagl, S., and Despopoulos, A. (1979). Taschenatlas der Physiologie (Stuttgart, New York: Thieme).

Simonsen, A., Cumming, R.C., Brech, A., Isakson, P., Schubert, D.R., and Finley, K.D. (2008). Promoting basal levels of autophagy in the nervous system enhances longevity and oxidant resistance in adult Drosophila. Autophagy *4*, 176-184. https://doi.org/10.4161/auto.5269.

Simpson, C.L., Lemmens, R., Miskiewicz, K., Broom, W.J., Hansen, V.K., van Vught, P.W.J., Landers, J.E., Sapp, P., van den Bosch, L., and Knight, J., et al. (2009). Variants of the elongator protein 3 (ELP3) gene are associated with motor neuron degeneration. Human molecular genetics *18*, 472-481. https://doi.org/10.1093/hmg/ddn375.

Singh, R., and Cuervo, A.M. (2011). Autophagy in the cellular energetic balance. Cell metabolism *13*, 495-504. https://doi.org/10.1016/j.cmet.2011.04.004.

SKINNER, B.F. (1950). Are theories of learning necessary? Psychological review *57*, 193-216. https://doi.org/10.1037/h0054367.

Söderberg, J.A.E., Carlsson, M.A., and Nässel, D.R. (2012). Insulin-Producing Cells in the Drosophila Brain also Express Satiety-Inducing Cholecystokinin-Like Peptide, Drosulfakinin. Frontiers in endocrinology *3*, 109. https://doi.org/10.3389/fendo.2012.00109.

Spano, G.M., Banningh, S.W., Marshall, W., Vivo, L. de, Bellesi, M., Loschky, S.S., Tononi, G., and Cirelli, C. (2019). Sleep Deprivation by Exposure to Novel Objects Increases Synapse Density and Axon-Spine Interface in the Hippocampal CA1 Region of Adolescent Mice. J. Neurosci. *39*, 6613-6625. https://doi.org/10.1523/JNEUROSCI.0380-19.2019.

Stavoe, A.K., Gopal, P.P., Gubas, A., Tooze, S.A., and Holzbaur, E.L. (2019). Expression of WIPI2B counteracts age-related decline in autophagosome biogenesis in neurons. eLife *8*. https://doi.org/10.7554/eLife.44219.

Stavoe, A.K.H., Hill, S.E., Hall, D.H., and Colón-Ramos, D.A. (2016). KIF1A/UNC-104 Transports ATG-9 to Regulate Neurodevelopment and Autophagy at Synapses. Developmental cell *38*, 171-185. https://doi.org/10.1016/j.devcel.2016.06.012.

Stevens, D.R., Wu, Z.-X., Matti, U., Junge, H.J., Schirra, C., Becherer, U., Wojcik, S.M., Brose, N., and Rettig, J. (2005). Identification of the minimal protein domain required for priming activity of Munc13-1. Current biology : CB *15*, 2243-2248. https://doi.org/10.1016/j.cub.2005.10.055.

Stocker, R.F., Heimbeck, G., Gendre, N., and Belle, J.S. de (1997). Neuroblast ablation in Drosophila P[GAL4] lines reveals origins of olfactory interneurons. J. Neurobiol. *32*, 443-456. https://doi.org/10.1002/(SICI)1097-4695(199705)32:5<443::AID-NEU1>3.0.CO;2-5.

Südhof, T.C. (2012). The presynaptic active zone. Neuron *75*, 11-25. https://doi.org/10.1016/j.neuron.2012.06.012.

Tain, L.S., Jain, C., Nespital, T., Froehlich, J., Hinze, Y., Grönke, S., and Partridge, L. (2020). Longevity in response to lowered insulin signaling requires glycine N-methyltransferase-dependent spermidine production. Aging cell *19*, e13043. https://doi.org/10.1111/acel.13043.

Takeuchi, T., Duszkiewicz, A.J., and Morris, R.G.M. (2014). The synaptic plasticity and memory hypothesis: encoding, storage and persistence. Philosophical transactions of the Royal Society of London. Series B, Biological sciences *369*, 20130288. https://doi.org/10.1098/rstb.2013.0288.

Tamura, T., Chiang, A.-S., Ito, N., Liu, H.-P., Horiuchi, J., Tully, T., and Saitoe, M. (2003). Aging Specifically Impairs amnesiac-Dependent Memory in Drosophila. Neuron *40*, 1003-1011. https://doi.org/10.1016/s0896-6273(03)00732-3.

Tanabe, K., Itoh, M., and Tonoki, A. (2017). Age-Related Changes in Insulin-like Signaling Lead to Intermediate-Term Memory Impairment in Drosophila. Cell reports *18*, 1598-1605. https://doi.org/10.1016/j.celrep.2017.01.053.

Taru, H., Iijima, K.-I., Hase, M., Kirino, Y., Yagi, Y., and Suzuki, T. (2002). Interaction of Alzheimer's beta -amyloid precursor family proteins with scaffold proteins of the JNK signaling cascade. The Journal of biological chemistry *277*, 20070-20078. https://doi.org/10.1074/jbc.M108372200.

Tatar, M., Kopelman, A., Epstein, D., Tu, M.P., Yin, C.M., and Garofalo, R.S. (2001). A mutant Drosophila insulin receptor homolog that extends life-span and impairs neuroendocrine function. Science *292*, 107-110. https://doi.org/10.1126/science.1057987.

Templin, A.T., Maier, B., Nishiki, Y., Tersey, S.A., and Mirmira, R.G. (2011). Deoxyhypusine synthase haploinsufficiency attenuates acute cytokine signaling. Cell Cycle *10*, 1043-1049. https://doi.org/10.4161/cc.10.7.15206.

Tomchik, S.M., and Davis, R.L. (2009). Dynamics of learning-related cAMP signaling and stimulus integration in the Drosophila olfactory pathway. Neuron *64*, 510-521. https://doi.org/10.1016/j.neuron.2009.09.029.

Tonoki, A., and Davis, R.L. (2012). Aging impairs intermediate-term behavioral memory by disrupting the dorsal paired medial neuron memory trace. Proceedings of the National Academy of Sciences of the United States of America *109*, 6319-6324. https://doi.org/10.1073/pnas.1118126109.

Tonoki, A., and Davis, R.L. (2015). Aging impairs protein-synthesis-dependent long-term memory in Drosophila. The Journal of neuroscience : the official journal of the Society for Neuroscience *35*, 1173-1180. https://doi.org/10.1523/JNEUROSCI.0978-14.2015.

Tononi, G., and Cirelli, C. (2016). Sleep and Synaptic Down-Selection (Cham (CH)).

Toonen, R.F., and Verhage, M. (2011). Crashpilot underachieves due to acetylation at the nerve terminal. Neuron *72*, 679-681. https://doi.org/10.1016/j.neuron.2011.11.008.

Tsao, C.-H., Chen, C.-C., Lin, C.-H., Yang, H.-Y., and Lin, S. (2018). Drosophila mushroom bodies integrate hunger and satiety signals to control innate food-seeking behavior. eLife *7*. https://doi.org/10.7554/eLife.35264.

Tully, T., Bourtchouladze, R., Scott, R., and Tallman, J. (2003). Targeting the CREB pathway for memory enhancers. Nature reviews. Drug discovery *2*, 267-277. https://doi.org/10.1038/nrd1061.

Tully, T., Preat, T., Boynton, S.C., and Del Vecchio, M. (1994). Genetic dissection of consolidated memory in Drosophila. Cell *79*, 35-47. https://doi.org/10.1016/0092-8674(94)90398-0.

Tully, T., and Quinn, W.G. (1985). Classical conditioning and retention in normal and mutant Drosophila melanogaster. Journal of comparative physiology. A, Sensory, neural, and behavioral physiology *157*, 263-277. https://doi.org/10.1007/BF01350033.

Turrel, O., Goguel, V., and Preat, T. (2018). Amnesiac Is Required in the Adult Mushroom Body for Memory Formation. J. Neurosci., 9202-9214. https://doi.org/10.1523/JNEUROSCI.0876-18.2018.

Ulgherait, M., Rana, A., Rera, M., Graniel, J., and Walker, D.W. (2014). AMPK modulates tissue and organismal aging in a non-cell-autonomous manner. Cell reports *8*, 1767-1780. https://doi.org/10.1016/j.celrep.2014.08.006.

United Nations Department of Economic and Social Affairs, Population Division (2020). World Population Ageing 2019 (New York: United Nations).

Uytterhoeven, V., Kuenen, S., Kasprowicz, J., Miskiewicz, K., and Verstreken, P. (2011). Loss of skywalker reveals synaptic endosomes as sorting stations for synaptic vesicle proteins. Cell *145*, 117-132. https://doi.org/10.1016/j.cell.2011.02.039.

Uytterhoeven, V., Lauwers, E., Maes, I., Miskiewicz, K., Melo, M.N., Swerts, J., Kuenen, S., Wittocx, R., Corthout, N., and Marrink, S.-J., et al. (2015). Hsc70-4 Deforms Membranes to Promote Synaptic Protein Turnover by Endosomal Microautophagy. Neuron *88*, 735-748. https://doi.org/10.1016/j.neuron.2015.10.012.

van der Voet, M., Nijhof, B., Oortveld, M.A.W., and Schenck, A. (2014). Drosophila models of early onset cognitive disorders and their clinical applications. Neuroscience and biobehavioral reviews *46 Pt 2*, 326-342. https://doi.org/10.1016/j.neubiorev.2014.01.013.

Verdile, G., Keane, K.N., Cruzat, V.F., Medic, S., Sabale, M., Rowles, J., Wijesekara, N., Martins, R.N., Fraser, P.E., and Newsholme, P. (2015). Inflammation and Oxidative Stress: The Molecular Connectivity between Insulin Resistance, Obesity, and Alzheimer's Disease. Mediators of inflammation *2015*, 105828. https://doi.org/10.1155/2015/105828.

Vivo, L. de, Bellesi, M., Marshall, W., Bushong, E.A., Ellisman, M.H., Tononi, G., and Cirelli, C. (2017). Ultrastructural evidence for synaptic scaling across the wake/sleep cycle. Science (New York, N.Y.) *355*, 507-510. https://doi.org/10.1126/science.aah5982.

Vivo, L. de, Nagai, H., Wispelaere, N. de, Spano, G.M., Marshall, W., Bellesi, M., Nemec, K.M., Schiereck, S.S., Nagai, M., and Tononi, G., et al. (2019). Evidence for sleep-dependent synaptic renormalization in mouse pups. Sleep *42*. https://doi.org/10.1093/sleep/zsz184.

Vosshall, L.B. (2007). Into the mind of a fly. Nature *450*, 193-197. https://doi.org/10.1038/nature06335.

Waddell, S., Armstrong, J., Kitamoto, T., Kaiser, K., and Quinn, W.G. (2000). The amnesiac Gene Product Is Expressed in Two Neurons in the Drosophila Brain that Are Critical for Memory. Cell *103*, 805-813. https://doi.org/10.1016/S0092-8674(00)00183-5.

Wagh, D.A., Rasse, T.M., Asan, E., Hofbauer, A., Schwenkert, I., Dürrbeck, H., Buchner, S., Dabauvalle, M.-C., Schmidt, M., and Qin, G., et al. (2006). Bruchpilot, a protein with homology to ELKS/CAST, is required for structural integrity and function of synaptic active zones in Drosophila. Neuron *49*, 833-844. https://doi.org/10.1016/j.neuron.2006.02.008.

Wang, Y., Mamiya, A., Chiang, A.-S., and Zhong, Y. (2008). Imaging of an early memory trace in the Drosophila mushroom body. J. Neurosci. *28*, 4368-4376. https://doi.org/10.1523/JNEUROSCI.2958-07.2008.

Wirth, M., Benson, G., Schwarz, C., Köbe, T., Grittner, U., Schmitz, D., Sigrist, S.J., Bohlken, J., Stekovic, S., and Madeo, F., et al. (2018). The effect of spermidine on memory performance in older adults at risk for dementia: A randomized controlled trial. Cortex; a journal devoted to the study of the nervous system and behavior *109*, 181-188. https://doi.org/10.1016/j.cortex.2018.09.014.

Wirth, M., Schwarz, C., Benson, G., Horn, N., Buchert, R., Lange, C., Köbe, T., Hetzer, S., Maglione, M., and Michael, E., et al. (2019). Effects of spermidine supplementation on cognition and biomarkers in older adults with subjective cognitive decline (SmartAge)-study protocol for a randomized controlled trial. Alzheimer's research & therapy *11*, 36. https://doi.org/10.1186/s13195-019-0484-1.

Woitkuhn and Ender, Beuschel, C.B., Maglione, M., Matkovic-Rachid, T., Huang, S., Lehmann, M., Geiger, J.R.P., and Sigrist, S.J. (2020). The Unc13A isoform is important for phasic release and olfactory memory formation at mushroom body synapses. Journal of neurogenetics *34*, 106-114. https://doi.org/10.1080/01677063.2019.1710146.

Wolff, G.H., and Strausfeld, N.J. (2015). Genealogical correspondence of mushroom bodies across invertebrate phyla. Current biology : CB *25*, 38-44. https://doi.org/10.1016/j.cub.2014.10.049.

Wolff, G.H., and Strausfeld, N.J. (2016). Genealogical correspondence of a forebrain centre implies an executive brain in the protostome-deuterostome bilaterian ancestor. Philosophical transactions of the Royal Society of London. Series B, Biological sciences *371*, 20150055. https://doi.org/10.1098/rstb.2015.0055.

Xu, S., Pany, S., Benny, K., Tarique, K., Al-Hatem, O., Gajewski, K., Leasure, J.L., Das, J., and Roman, G. (2018). Ethanol Regulates Presynaptic Activity and Sedation through Presynaptic Unc13 Proteins in Drosophila. eNeuro *5*. https://doi.org/10.1523/ENEURO.0125-18.2018.

Yang, B., Jiang, H., Wang, F., Li, S., Wu, C., Bao, J., Zhu, Y., Xu, Z., Liu, B., and Ren, H., et al. (2019). UNC13A variant rs12608932 is associated with increased risk of amyotrophic

lateral sclerosis and reduced patient survival: a meta-analysis. Neurological sciences : official journal of the Italian Neurological Society and of the Italian Society of Clinical Neurophysiology *40*, 2293-2302. https://doi.org/10.1007/s10072-019-03951-y.

Yang, F., Chu, X., Yin, M., Liu, X., Yuan, H., Niu, Y., and Fu, L. (2014). mTOR and autophagy in normal brain aging and caloric restriction ameliorating age-related cognition deficits. Behavioural brain research *264*, 82-90. https://doi.org/10.1016/j.bbr.2014.02.005.

Yarali, A., Ehser, S., Hapil, F.Z., Huang, J., and Gerber, B. (2009). Odour intensity learning in fruit flies. Proceedings. Biological sciences *276*, 3413-3420. https://doi.org/10.1098/rspb.2009.0705.

Yin, Z., Pascual, C., and Klionsky, D.J. (2016). Autophagy: machinery and regulation. Microbial cell (Graz, Austria) *3*, 588-596. https://doi.org/10.15698/mic2016.12.546.

Young, A.R.J., Chan, E.Y.W., Hu, X.W., Köchl, R., Crawshaw, S.G., High, S., Hailey, D.W., Lippincott-Schwartz, J., and Tooze, S.A. (2006). Starvation and ULK1-dependent cycling of mammalian Atg9 between the TGN and endosomes. Journal of cell science *119*, 3888-3900. https://doi.org/10.1242/jcs.03172.

Yu, D., Akalal, D.-B.G., and Davis, R.L. (2006). Drosophila alpha/beta mushroom body neurons form a branch-specific, long-term cellular memory trace after spaced olfactory conditioning. Neuron *52*, 845-855. https://doi.org/10.1016/j.neuron.2006.10.030.

Yu, D., Keene, A.C., Srivatsan, A., Waddell, S., and Davis, R.L. (2005). Drosophila DPM neurons form a delayed and branch-specific memory trace after olfactory classical conditioning. Cell *123*, 945-957. https://doi.org/10.1016/j.cell.2005.09.037.

Yu, D., Ponomarev, A., and Davis, R.L. (2004). Altered Representation of the Spatial Code for Odors after Olfactory Classical Conditioning. Neuron *42*, 437-449. https://doi.org/10.1016/S0896-6273(04)00217-X.

Yu, Y., Feng, L., Li, J., Lan, X., A, L., Lv, X., Zhang, M., and Chen, L. (2017). The alteration of autophagy and apoptosis in the hippocampus of rats with natural aging-dependent cognitive deficits. Behavioural brain research *334*, 155-162. https://doi.org/10.1016/j.bbr.2017.07.003.

Zars, T., Fischer, M., Schulz, R., and Heisenberg, M. (2000). Localization of a short-term memory in Drosophila. Science (New York, N.Y.) *288*, 672-675. https://doi.org/10.1126/science.288.5466.672.

Zhai, R.G., and Bellen, H.J. (2004). The architecture of the active zone in the presynaptic nerve terminal. Physiology (Bethesda, Md.) *19*, 262-270. https://doi.org/10.1152/physiol.00014.2004.

Zhang, Y.V., Hannan, S.B., Stapper, Z.A., Kern, J.V., Jahn, T.R., and Rasse, T.M. (2016). The Drosophila KIF1A Homolog unc-104 Is Important for Site-Specific Synapse Maturation. Front. Cell. Neurosci. *10*, 207. https://doi.org/10.3389/fncel.2016.00207.

Zhang, Z., Li, X., Guo, J., Li, Y., and Guo, A. (2013). Two clusters of GABAergic ellipsoid body neurons modulate olfactory labile memory in Drosophila. J. Neurosci. *33*, 5175-5181. https://doi.org/10.1523/JNEUROSCI.5365-12.2013.

Zhao, T., Gu, T., Rice, H.C., McAdams, K.L., Roark, K.M., Lawson, K., Gauthier, S.A., Reagan, K.L., and Hewes, R.S. (2008). A Drosophila gain-of-function screen for candidate genes involved in steroid-dependent neuroendocrine cell remodeling. Genetics *178*, 883-901. https://doi.org/10.1534/genetics.107.082487.

Zimmermann, A., Kainz, K., Hofer, S.J., Bauer, M.A., Schroeder, S., Dengjel, J., Pietrocola, F., Kepp, O., Ruckenstuhl, C., and Eisenberg, T., et al. (2019a). 4,4'Dimethoxychalcone: a natural flavonoid that promotes health through autophagy-dependent and -independent effects. Autophagy *15*, 1662-1664. https://doi.org/10.1080/15548627.2019.1632623.

Zimmermann, A., Kainz, K., Hofer, S.J., Bauer, M.A., Schroeder, S., Dengjel, J., Pietrocola, F., Kepp, O., Ruckenstuhl, C., and Eisenberg, T., et al. (2019b). Targeting GATA transcription factors - a novel strategy for anti-aging interventions? Microbial cell (Graz, Austria) *6*, 212-216. https://doi.org/10.15698/mic2019.05.676.

Acknowledgments

First and in particular, I want to thank my supervisor and mentor, Prof. Dr. Stephan J. Sigrist. I am sincerely grateful for the opportunity to work on my PhD studies in his lab. I deeply appreciate your great support, valuable scientific advice, and expertise.
Next, I want to give special thanks to the second reviewer of this PhD thesis, Prof. Dr. Mathias F. Wernet, who kindly accepted this job short term. Additionally, I express my deep gratitude to Prof. Dr. Hans-Joachim Pflüger, who could not undertake this task anymore due to tragic circumstances.
Many thanks to my friends and colleagues. I am particularly grateful to Dr. Niraja Ramesh, Dr. Sheng Huang, and Dr. Oriane Turrel for reading and commenting on my thesis as well as your support. Equally, I want to thank Dr. Atefeh Pooryasin, Chengji Piao, Dr. Anatoli Ender, Dr. Yongtian Liang, and Dr. Lisa Scheunemann. It was a great pleasure and privilege to work with you. Thanks for your help and friendship. Thanks to Sara Mertel, who guided me through the beginning of my PhD thesis, and to Beatrice Rackwitz, who was always very friendly and helpful through all the bureaucracy. Special thanks go to all my Bachelor and Master students, who worked with such great interest and enthusiasm. Here, I want to name only some, my friend Sevim Yildirim-Brochno, Zhiying Zhao, Carry-Ann Kühnapfel, Anita Scholz, and Carolin Jarling. To you and all the others, it was a great time :D And last but absolutely not least, my special thanks to my friend Simona Günther, who cooked endless amounts of food for my flies. Danke für Deine durchgehende Hilfe! And thanks to all the other great people whom I got to know during these years. This was an important part of my life with so many wonderful people. I would never want to miss.

I am extremely thankful for and to my family. Without them, I could not have done this work. First, to my parents Dr. Hans-Werner Beuschel and Kerstin Beuschel, my sister Saskia Cammareri, my brother-in-law Raffael Cammareri, and my grandpa Karl-Heinz Schneider: Danke Euch für Eure durchgehende Unterstützung, die vielen Anrufe, die spannenden Diskussionen und natürlich die großartige Kinderbespaßung. Ich hab Euch alle sehr lieb.

Big thanks also go to my husband's family, Hoang Ba Dang, Minh Chau Dang, Minh Anh Dang, and Minh Thu Dang. Con rất biết ơn vì Ba Mẹ chào đón con vào gia đình và vì quí Ông Bà và Cô tuyệt vời, chu đáo đối với Lucas. Con tạ ơn! Con thực sự mong muốn được học hỏi về nhiều món ăn ngon.

I am incredibly grateful for and to my husband Minh Duc Dang and my child Lucas Khai Dang. Danke für all Eure Geduld, Eure Unterstützung, das viele Tanzen und den großen Spaß mit Euch! Ich freue mich immer sehr darauf, nach getaner Arbeit zu Euch nach Hause zukommen. Ich bin überglücklich, dass es Euch gibt!

Curriculum vitae

The electronic version of this thesis does not contain the curriculum vitae due to data privacy protection. An updated version can be found on LinkedIn or Xing: Christine Beuschel-Dang

List of publications

* These authors contributed equally.

Huang, S., **Beuschel, C.B.**, Pooryasin, A., Piao, C., and Sigrist, S.J. (in submission).
A global form of presynaptic plasticity operates as an on-demand resilience module to optimize brain aging.

Liang, Y., Piao*, C., **Beuschel*, C.B.**, Toppe, D., Kollipara, L.,Bogdanow, B., Maglione, M., Lützkendorf, J., See, J.C.K., Huang, S., Conrad, T.O.F., Kintscher, U., Madeo, F., Liu, F., Sickmann, A., Sigrist, S.J. (2021).
eIF5A hypusination, boosted by dietary spermidine, protects from premature brain aging and mitochondrial dysfunction.
Cell reports 35, 108941. https://doi.org/10.1016/j.celrep.2021.108941.

Petzoldt*, A.G., and Götz*, T.W.B., and Driller*, J.H., and Lützkendorf*, J., Reddy-Alla, S., Matkovic-Rachid, T., Liu, S., Knoche, E., Mertel, S., and Ugorets, V., Lehmann, M., Ramesh, N., **Beuschel, C.B.**, Kuropka, B., Freund, C., Stelzl, U., Loll, B., Liu, F., Wahl, M.C., and Sigrist, S.J. (2020).
RIM-binding protein couples synaptic vesicle recruitment to release sites.
The Journal of cell biology 219. https://doi.org/10.1083/jcb.201902059.

Huang, S., Piao, C., **Beuschel, C.B.**, Götz, T., and Sigrist, S.J. (2020).
Presynaptic active zone plasticity encodes sleep need in Drosophila.
Current biology : CB 30, 1077-1091.e5. https://doi.org/10.1016/j.cub.2020.01.019.

Woitkuhn*, J., and Ender*, A., **Beuschel, C.B.**, Maglione, M., Matkovic-Rachid, T., Huang, S., Lehmann, M., Geiger, J.R.P., and Sigrist, S.J. (2020).
The Unc13A isoform is important for phasic release and olfactory memory formation at mushroom body synapses.
Journal of Neurogenetics 34, 106-114. https://doi.org/10.1080/01677063.2019.1710146.

Bhukel*, A., and **Beuschel*, C.B.**, Maglione, M., Lehmann, M., Juhász, G., Madeo, F., and Sigrist, S.J. (2019).
Autophagy within the mushroom body protects from synapse aging in a non-cell autonomous manner.
Nature communications 10, 1318. https://doi.org/10.1038/s41467-019-09262-2.

Böhme*, M.A., and McCarthy*, A.W., Grasskamp, A.T., **Beuschel, C.B.**, Goel, P., Jusyte, M., Laber, D., Huang, S., Rey, U., and Petzoldt, A.G., et al. (2019).
Rapid active zone remodeling consolidates presynaptic potentiation.
Nature communications 10, 1085. https://doi.org/10.1038/s41467-019-08977-6.

Carmona-Gutierrez*, D., and Zimmermann*, A., Kainz, K., Pietrocola, F., Chen, G., Maglioni, S., Schiavi, A., Nah, J., Mertel, S., **Beuschel, C.B.**, Castoldi, F., Sica, V., Trausinger, G., Raml, R., Sommer, C., Schroeder, S., J. Hofer, S.J., A. Bauer, M.A., Pendl, T., Tadic, J., Dammbrueck, C., Hu, Z., Ruckenstuhl, C., Eisenberg, T., Durand, S., Bossut, N., Aprahamian, F., Abdellatif, M., Sedej, S., Enot, D.P., Wolinski, H., Dengjel, J., Kepp, O., Magnes, C., Sinner, F., Pieber, T.R., Sadoshima, J., Ventura, N., Sigrist, S.J., Kroemer, G., Madeo, F. (2019).
The flavonoid 4,4'-dimethoxychalcone promotes autophagy-dependent longevity across species.
Nature communications 10, 651. https://doi.org/10.1038/s41467-019-08555-w.

Gupta, V.K., Pech, U., Bhukel, A., Fulterer, A., Ender, A., Mauermann, S.F., Andlauer, T.F.M., Antwi-Adjei, E., **Beuschel, C.B.**, Thriene, K., Maglione, M., Quentin, C.,Bushow, R., Schwärzel, M., Mielke, T., Madeo, F., Dengjel, J., Fiala, A., Sigrist, S.J. (2016).
Spermidine suppresses age-associated memory impairment by preventing adverse increase of presynaptic active zone size and release.
PLoS biology 14, e1002563. https://doi.org/10.1371/journal.pbio.1002563.

Appendix

1. List of figures

2. List of tables

3. List of abbreviations

4E-BP	eukaryotic initiation factor 4E binding protein
A	anterior
AA	amino acids
AC	adenylyl cyclase
ACh	acetylcholine
ACT	antennal cerebral tract
AL	antennal lobe
ALS	amyotrophic lateral sclerosis
AMI	age-induced memory impairment
AMN	amnesiac protein
AN	antennal nerve
ANOVA	analysis of variance
APL	anterior paired lateral
Aplip1	APP-like protein interacting protein 1
Atg	autophagy-related
ATP	adenosine triphosphate
ARM	anesthesia-resistant memory
ASM	anesthesia-resistant memory
AZ	active zone
BA	Benzaldehyde
BL	Bloomington Drosophila Stock Center
BRP	Bruchpilot
d	days
C	calyx
C. elegans	*Caenorhabditis elegans*
Ca^{2+}	calcium ion
CaM	calmodulin
cAMP	cyclic adenosine monophosphate
Cas9	CRISPR-associated protein 9
CAST	CAZ-associated structural protein
CAZ	cytomatrix at the active zone
Cf	partition coefficient for final distribution
cm	centimeters
CMG	chaperone-mediated autophagy

CO_2	carbon dioxide
CREB	cAMP response element-binding
CRISPR	clustered regularly interspaced palindromic
CRZ	corazonin
CS	conditioned stimulus
CS^+	shock-associated odor
CS^-	unshocked control odor
Ctrl.	control
D	dorsal
DAN	dopaminergic neuron
Dar	dopamine receptor
DLP	dorsal lateral peptidergic neurons
DMC	4,4'-Dimethodychalcone
DMSO	Dimethylsulfoxide
DNA	desoxyribonucleic acid
DOORS	deafness, onychodystrophy, osteodystrophy, mental retardation, seizures
DPM	dorsal paired medial
DSK	drosulfakinin
DTK	*Drosophila* tachykinin
E3	ubiquitin-protein ligase
EA	Ethyl acetate
EGFP	enhanced green fluorescent protein
eIF5A	eukaryotic translation initiation factor 5A
ELKS	protein-rich of the following amino acids: glutamic acid (E), leucine (L), lysine (K), serine (S)
ELP3	elongator complex protein 3
EM	electron microscopy
EMS	Ethyl methanesulphonate
ERC	ELKS/ RAB6-interacting/ CAST family member
FA	fatty acids
FasII	Fasciclin II
FL	full-length
FOXO	forkhead box subgroup O
GABA	γ-aminobutyric acid
GAP	GTPase activating protein
GFP	green fluorescent protein

GluRIIA	glutamate receptor subunit IIA
GLUT4	glucose transporter 4
h	hour
HDAC6	histone deacetylation 6
HL3	hemolymph-like solution
HMS	Harvard Medical School
Hsc70	heat shock cognate protein 70 kDa
Hspa8	heat shock protein family a member 8
IGF-1	insulin-like growth factor 1
IIS	insulin and IGF-1 signaling
ILP	insulin-like peptide
InR	insulin receptor
INSR	insulin receptor in mammals
IPC	insulin-producing cell
IRS	insulin receptor substrate
ITP	ion transport peptide
K^+	potassium ion
KAT	lysine acetyltransferase
KC	kenyon cells
kDa	kilodalton
KSC	Kyoto Stock Center
LC3	microtubule-associated protein 1 light chain 3B
LH	lateral horn
LN	local interneuron
LNC	lateral neurosecretory cells
LTM	long-term memory
LTP	long-term plasticity
M	medial
M	molar mass [g / mol]
MB	mushroom body
MBON	mushroom body output neuron
MCH	4-Methylcyclohexanol
min	minute
mm	millimeters
mM	millimole
MNC	median neurosecretory cells
mNSC	median neurosecretory cell

MTM	mid-term memory
mTORC1	mammalian TOR complex 1
n	number of independent experiments
N	number of animals
Na^+	sodium ion
NaN_3	sodium azide
Nc82	antibody against the C-term of BRP
nm	nanometers
NMJ	neuronal muscular junction
no	number
NPY	neuropeptide Y
NSF	N-ethylmaleimide-sensitive factor
OADR	old-age dependency ratio
OCT	3-Octanol
OE	overexpression
OR	olfactory receptor
Orco	olfactory receptor co-receptor
ORN	olfactory receptor neuron
p	probability value
P	peduncle
PAM	protocerebral anterior medial
PBS	phosphate-buffered saline
PBT	Triton X-100 in PBS solution
PDE	phosphodiesterase
PDK1	3-phosphoinositide-dependent protein kinase 1
PE	phosphatidylethanolamine
PFA	paraformaldehyde
PI	performance index
PI3K	phosphatidylinositol-3-kinase
PI3P	phosphatidylinositol-3-phosphate
PIP2	phosphatidylinositol-4,5-biphosphate
PIP3	phosphatidylinositol-3,4,5-triphosphate
PN	projection neuron
PPL	protocerebral posterior lateral
RAB	RAS-related in brain
RBP	RIM-binding protein
RDL	resistance to dieldrin

Rheb	RAS homolog enriched in brain
RIM	Rab3-interaction molecules
RNAi	RNA interference
ROS	reactive oxygen species
RRP	readily releasable pool
SEM	standard error of the mean
SILAC	stable isotope labeling of amino acids in cell culture
SNAP-25	synaptosomal-associated protein 25 kDa
SNARE	soluble NSF attachment protein receptor
sNPF	short neuropeptide F
SL	Sigrist laboratory
Spd	Spermidine
Srpk79D	serine-arginine protein kinase at location 79D
STED	stimulated emission depletion microscopy
STM	short-term memory
STP	short-term plasticity
SVs	synaptic vesicles
TAG	triacylglyceride
TOR	target of rapamycin
ts	temperature sensitive
TSC	tuberous sclerosis complex
Ulk1	Unc51-like kinase 1
Upd2	unpaired 2
US	unconditioned stimulus
V	volt
VAMP	vesicle-associated membrane protein
VGCC	voltage-gated calcium channel
vs.	versus
VDRC	Vienna Drosophila Resource Center

4. Replicates of the lifespan experiments

Table 18: Details of lifespan experiments regarding Figure 21a.

food	number of animals	median survival	maximal lifespan	*p*-value
Replicate 1 - Female *w*^{1118} lifespan with 4,4'-Dimethoxychalcone.				
1) control food	115	46	64	1-2: ****$p < 0.0001$ 1-3: ****$p < 0.0001$ 1-4: ****$p < 0.0001$
2) 0.2 mM DMC	114	72	94	
3) 1.0 mM DMC	117	58	88	
4) 2.0 mM DMC	115	58	87	
Replicate 2 - Female *w*^{1118} lifespan with 4,4'-Dimethoxychalcone.				
1) control food	117	58	80	1-2: $^{ns}p = 0.3695$ 1-3: ****$p < 0.0001$ 1-4: $^{ns}p = 0.7772$
2) 0.2 mM DMC	116	58	89	
3) 1.0 mM DMC	115	52	82	
4) 2.0 mM DMC	119	58	83	
Replicate 3 - Female *w*^{1118} lifespan with 4,4'-Dimethoxychalcone.				
1) control food	118	57	87	1-2: ****$p < 0.0001$ 1-3: *$p = 0.0116$ 1-4: ****$p < 0.0001$
2) 0.2 mM DMC	117	70	96	
3) 1.0 mM DMC	116	58	93	
4) 2.0 mM DMC	119	75	91	
Replicate 4 - Female *w*^{1118} lifespan with 4,4'-Dimethoxychalcone.				
1) control food	116	42	62	1-2: ****$p < 0.0001$ 1-3: ****$p < 0.0001$ 1-4: ****$p < 0.0001$
2) 0.2 mM DMC	117	55	88	
3) 1.0 mM DMC	120	62	89	
4) 2.0 mM DMC	117	52	80	
Replicate 5 - Female *w*^{1118} lifespan with 4,4'-Dimethoxychalcone.				
1) control food	115	58	77	1-2: **** $p > 0.0001$ 1-3: *$p = 0.0473$ 1-4: ****$p < 0.0001$
2) 0.2 mM DMC	116	68	98	
3) 1.0 mM DMC	116	60	85	
4) 2.0 mM DMC	120	66	88	

Description: Lifespan of female w^{1118} flies fed with the concentrations 0.2, 1.0, and 2.0 mM DMC since adulthood (each dissolved in 0.1% DMSO). 0.1 % DMSO food served as control.

Figure 107: Replicates of the lifespan experiments for female w^{1118} with DMC.

Replicate 1: Lifespan of females

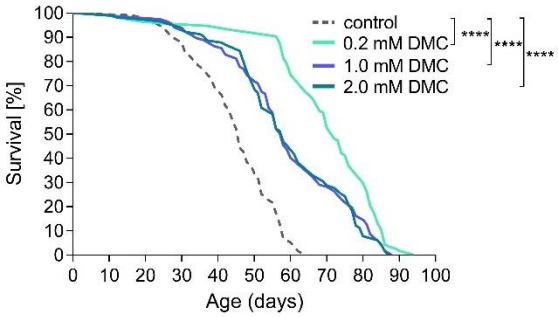

Replicate 2: Lifespan of females

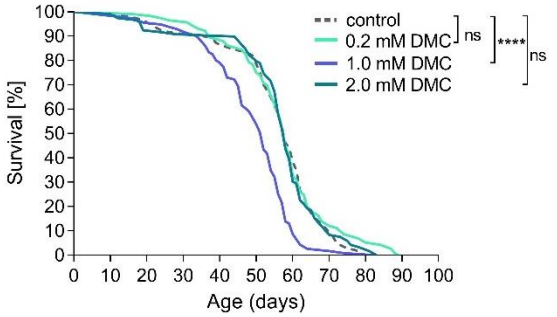

Replicate 3: Lifespan of females

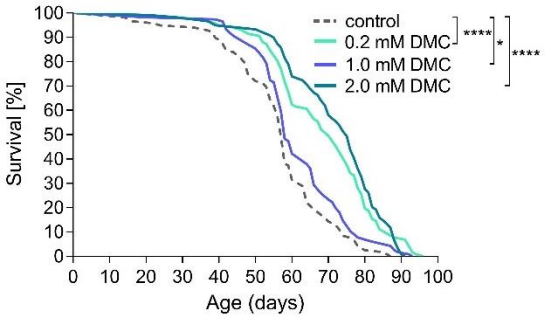

Replicate 4: Lifespan of females

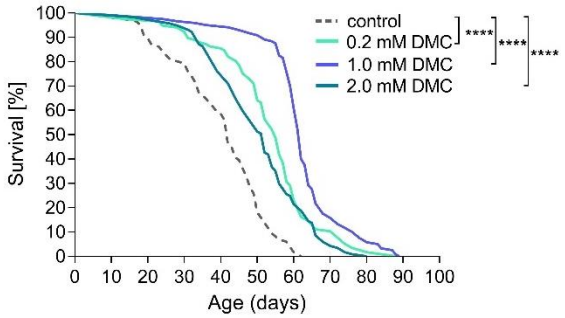

Replicate 5: Lifespan of females

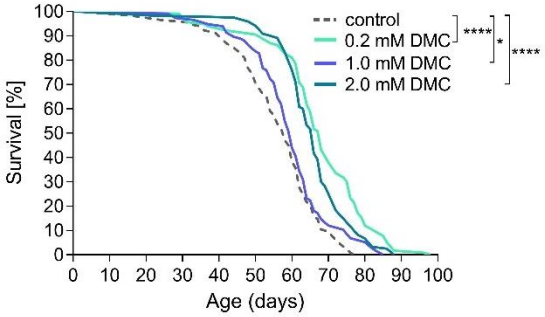

Table 19: Details of lifespan experiments regarding Figure 21b.

food	number of animals	median survival	maximal lifespan	*p*-value
Replicate 1 - Male w^{1118} lifespan with 4,4'-Dimethoxychalcone.				
1) control food	118	54	85	1-2: ****$p < 0.0001$ 1-3: ****$p < 0.0001$ 1-4: ****$p < 0.0001$
2) 0.2 mM DMC	115	64	88	
3) 1.0 mM DMC	117	64	90	
4) 2.0 mM DMC	115	61	86	
Replicate 2 - Male w^{1118} lifespan with 4,4'-Dimethoxychalcone.				
1) control food	119	58	86	1-2: ****$p < 0.0001$ 1-3: $^{ns}p = 0.1118$ 1-4: ****$p < 0.0001$
2) 0.2 mM DMC	114	62	88	
3) 1.0 mM DMC	111	56	94	
4) 2.0 mM DMC	114	64	86	
Replicate 3 - Male w^{1118} lifespan with 4,4'-Dimethoxychalcone.				
1) control food	118	51.5	80	1-2: **$p = 0.0015$ 1-3: $^{ns}p = 0.0958$ 1-4: ****$p < 0.0001$
2) 0.2 mM DMC	116	56	84	
3) 1.0 mM DMC	118	56	80	
4) 2.0 mM DMC	119	64	93	
Replicate 4 - Male w^{1118} lifespan with 4,4'-Dimethoxychalcone.				
1) control food	117	50	68	1-2: $^{ns}p = 0.3566$ 1-3: ****$p < 0.0001$ 1-4: ***$p = 0.0002$
2) 0.2 mM DMC	114	50	89	
3) 1.0 mM DMC	116	62	87	
4) 2.0 mM DMC	118	57	90	
Replicate 5 - Male w^{1118} lifespan with 4,4'-Dimethoxychalcone.				
1) control food	113	58	82	1-2: **$p = 0.0058$ 1-3: $^{ns}p = 0.8523$ 1-4: ****$p < 0.0001$
2) 0.2 mM DMC	117	60	90	
3) 1.0 mM DMC	113	58	87	
4) 2.0 mM DMC	115	62	88	
Description: Lifespan of male w^{1118} flies fed with the concentrations 0.2, 1.0, and 2.0 mM DMC since adulthood (each dissolved in 0.1% DMSO). 0.1 % DMSO food served as control.				

Figure 108: Replicates of the lifespan experiments for male *w*^{1118} with DMC.

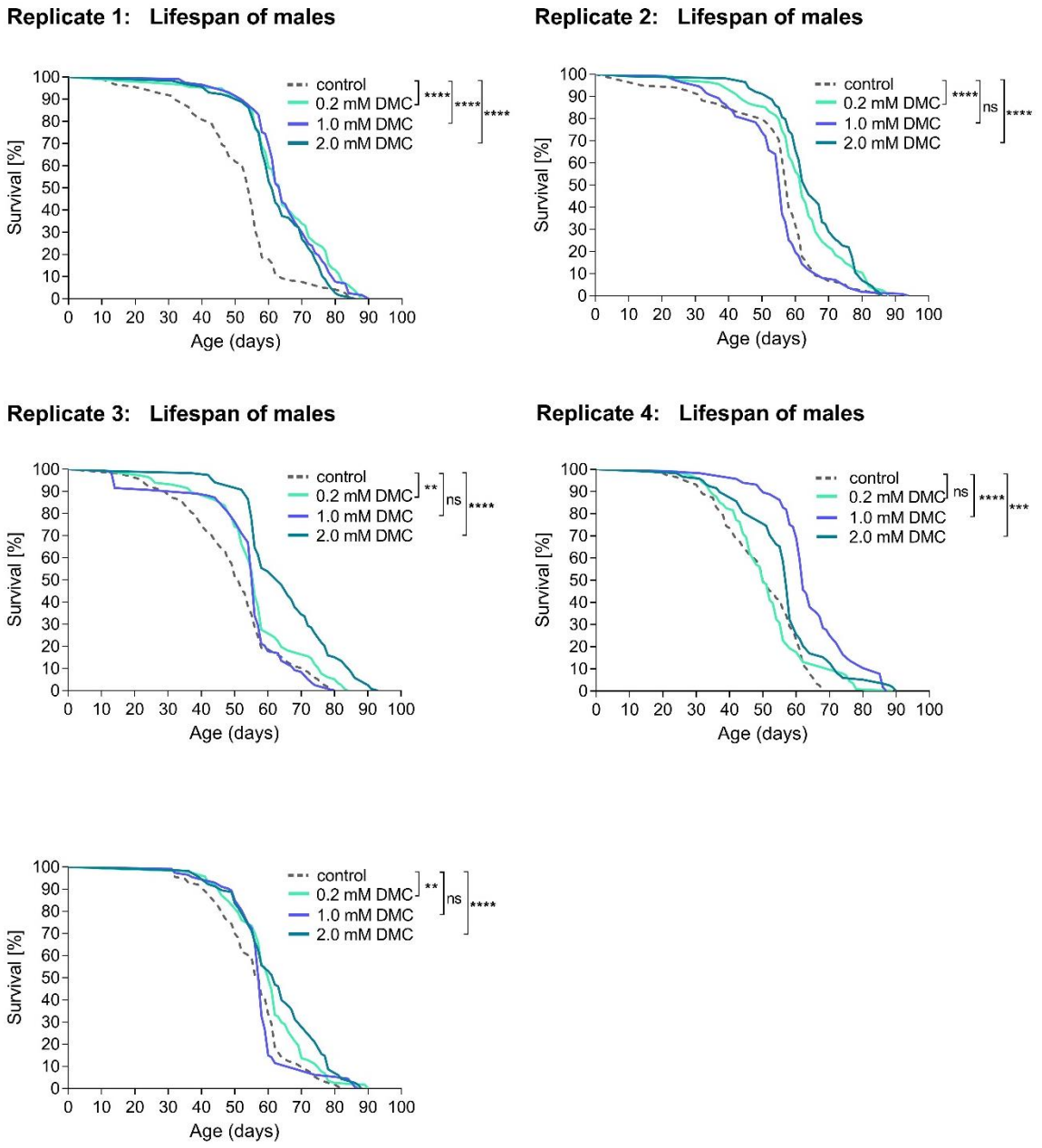

Table 20: Details of lifespan experiments regarding Figure 22.

food	number of animals	median survival	maximal lifespan	*p*-value
Replicate 1 - Female *w*^{1118} lifespan with 4,4'-Dimethoxychalcone from egg deposition.				
1) control food	96	55	77	$^{ns}p = 0.2616$
2) 1.0 mM DMC	97	53	83	

Replicate 2 - Female *w*^{1118} lifespan with 4,4'-Dimethoxychalcone from egg deposition.				
1) control food	98	53	77	****$p < 0.0001$
2) 1.0 mM DMC	99	69	85	
Replicate 3 - Female *w*^{1118} lifespan with 4,4'-Dimethoxychalcone from egg deposition.				
1) control food	96	65	83	****$p < 0.0001$
2) 1.0 mM DMC	99	43	67	
Replicate 4 - Female *w*^{1118} lifespan with 4,4'-Dimethoxychalcone from egg deposition.				
1) control food	100	43	65	****$p < 0.0001$
2) 1.0 mM DMC	97	65	83	
Description: Lifespan of female w^{1118} flies fed with the concentration 1.0 mM DMC since egg deposition (dissolved in 0.1% DMSO). 0.1 % DMSO food served as control.				

Figure 109: Replicates of the lifespan experiments for female *w*^{1118} with 1.0 mM DMC since egg deposition.

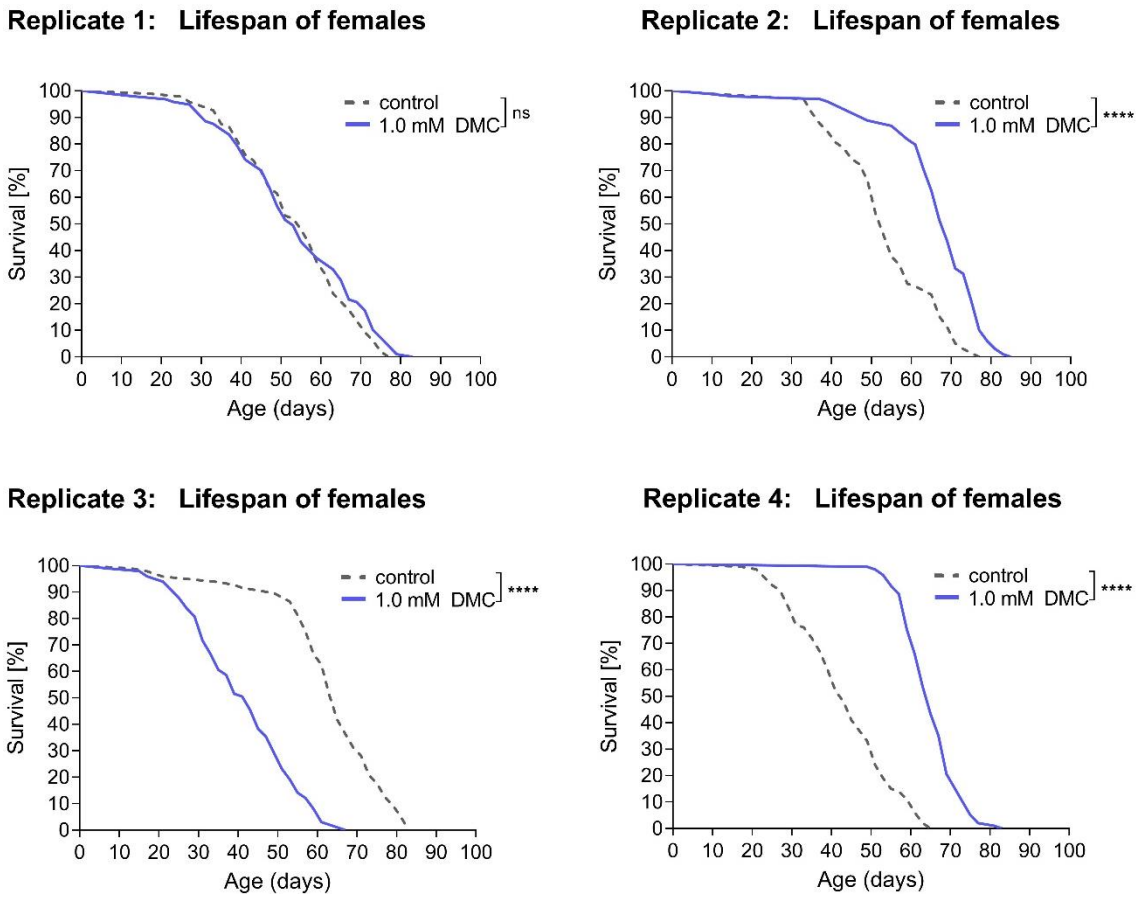

Table 21: Details of lifespan experiments regarding Figure 24a.

food	number of animals	median survival	maximal lifespan	*p*-value
Replicate 1 - Female *w*^{1118} lifespan with 0.1 % Dimethylsulfoxide (control food) versus normal food since egg deposition.				
1) normal food	99	41	79	****$p < 0.0001$
2) 0.1 % DMSO	98	65	91	
Replicate 2 - Female *w*^{1118} lifespan with 0.1 % Dimethylsulfoxide (control food) versus normal food since egg deposition.				
1) normal food	97	51	85	****$p < 0.0001$
2) 0.1 % DMSO	96	43	91	
Replicate 3 - Female *w*^{1118} lifespan with 0.1 % Dimethylsulfoxide (control food) versus normal food since egg deposition.				
1) normal food	97	55	81	$^{ns}p = 0.2152$
2) 0.1 % DMSO	99	71	95	
Replicate 4 - Female *w*^{1118} lifespan with 0.1 % Dimethylsulfoxide (control food) versus normal food since egg deposition.				
1) normal food	93	65	89	****$p < 0.0001$
2) 0.1 % DMSO	90	63	85	
Description: Lifespan of female w^{1118} flies fed with 0.1 % DMSO since adulthood. Normal food served as control.				

Figure 110: Replicates of the lifespan experiments for female *w*^{1118} with 0.1 % DMSO versus normal food since adulthood.

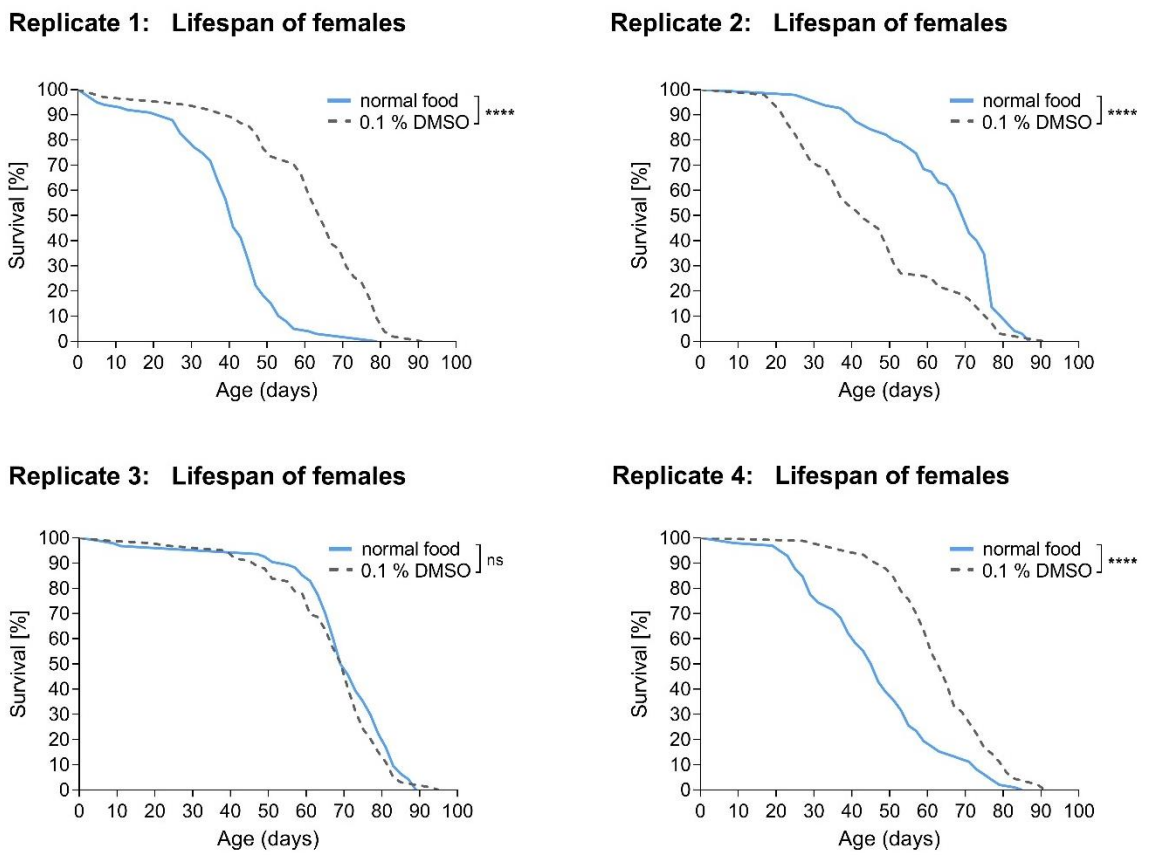

Table 22: Details of the lifespan experiments regarding Figure 24b.

food	number of animals	median survival	maximal lifespan	*p*-value
Replicate 1 - Female *w*^{1118} lifespan with Dimethylsulfoxide from egg deposition.				
1) normal food	94	63	87	1-2: ****$p < 0.0001$ 1-3: ****$p < 0.0001$ 1-4: ****$p < 0.0001$
2) 0.05 % DMSO	99	47	73	
3) 0.1 % DMSO	96	55	77	
4) 0.5 % DMSO	100	41	69	
Replicate 2 - Female *w*^{1118} lifespan with Dimethylsulfoxide from egg deposition.				
1) normal food	95	71	87	1-2: ****$p < 0.0001$ 1-3: ****$p < 0.0001$ 1-4: ****$p < 0.0001$
2) 0.05 % DMSO	98	45	83	
3) 0.1 % DMSO	98	53	77	
4) 0.5 % DMSO	99	44	72	

Replicate 3 - Female w^{1118} lifespan with Dimethylsulfoxide from egg deposition.				
1) normal food	94	70	89	1-2: ****$p < 0.0001$ 1-3: ****$p < 0.0001$ 1-4: ****$p < 0.0001$
2) 0.05 % DMSO	96	49	69	
3) 0.1 % DMSO	96	65	83	
4) 0.5 % DMSO	98	48	75	
Replicate 4 - Female w^{1118} lifespan with Dimethylsulfoxide from egg deposition.				
1) normal food	98	46	85	1-2: *$p = 0.0101$ 1-3: *$p = 0.0143$ 1-4: ****$p < 0.0001$
2) 0.05 % DMSO	96	57	81	
3) 0.1 % DMSO	100	43	65	
4) 0.5 % DMSO	97	35	69	
Description: Lifespan of female w^{1118} flies fed with 0.05 %, 0.1 %, and 0.5 % DMSO since egg deposition. Normal food served as control.				

Figure 111: Replicates of the lifespan experiments for female w^{1118} with different DMSO concentrations since egg deposition.

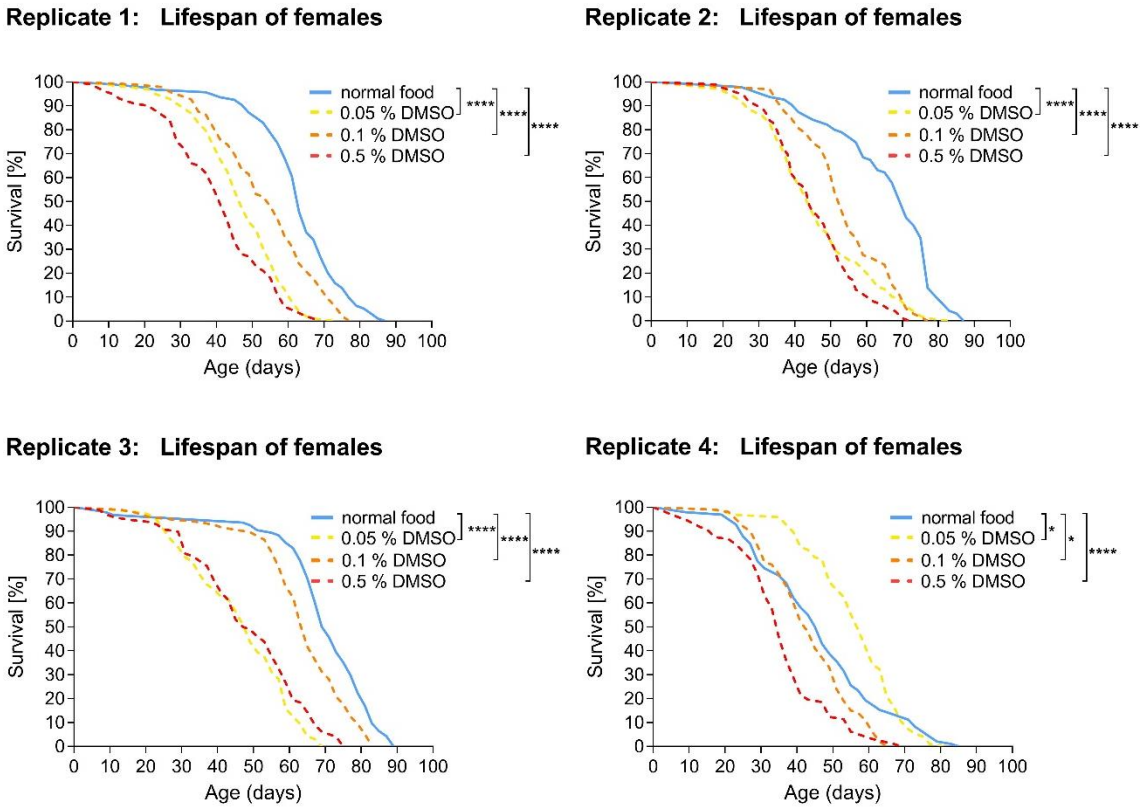

Table 23: Details of lifespan experiments regarding Figure 26a.

food	number of animals	median survival	maximal lifespan	*p*-value
Replicate 1 - Female *atg7*$^{-/-}$ lifespan with 4,4'-Dimethoxychalcone.				
1) control food	90	49	64	1-2: $^{ns}p = 0.0637$ 1-3: $^{ns}p = 0.0805$ 1-4: $^{ns}p = 0.2514$
2) 0.2 mM DMC	94	48	58	
3) 1.0 mM DMC	95	52	64	
4) 2.0 mM DMC	94	50	69	
Replicate 2 - Female *atg7*$^{-/-}$ lifespan with 4,4'-Dimethoxychalcone.				
1) control food	119	64	76	1-2: $^{ns}p = 0.1189$ 1-3: $^{ns}p = 0.3408$ 1-4: $^{ns}p = 0.2190$
2) 0.2 mM DMC	116	66	78	
3) 1.0 mM DMC	119	66	78	
4) 2.0 mM DMC	115	62	76	
Replicate 3 - Female *atg7*$^{-/-}$ lifespan with 4,4'-Dimethoxychalcone.				
1) control food	118	62	76	1-2: $^{ns}p = 0.0598$ 1-3: $^{****}p < 0.0001$ 1-4: $^{ns}p = 0.3308$
2) 0.2 mM DMC	119	64	78	
3) 1.0 mM DMC	119	56	72	
4) 2.0 mM DMC	116	64	76	
Description: Lifespan of female atg7$^{-/-}$ flies fed with the concentrations 0.2, 1.0, and 2.0 mM DMC since adulthood (each dissolved in 0.1% DMSO). 0.1 % DMSO food served as control.				

Figure 112: Replicates of the lifespan experiments for female *atg7*$^{-/-}$ with DMC.

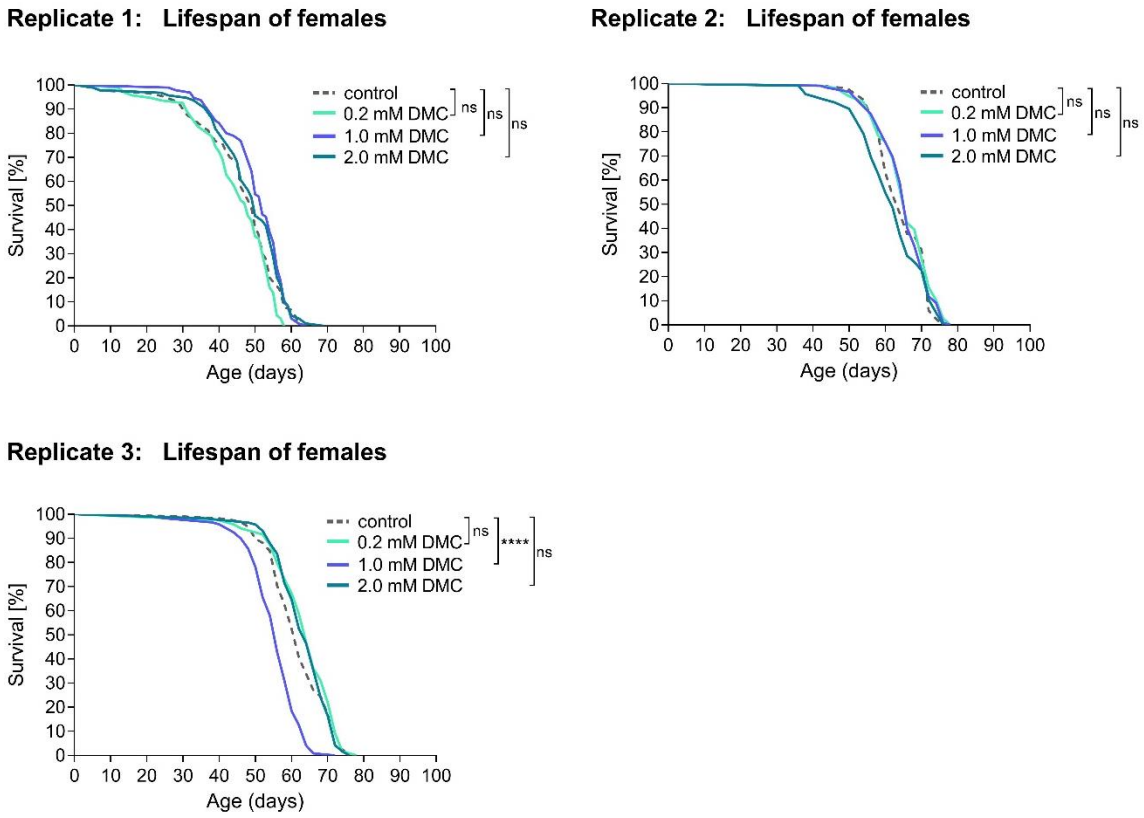

Table 24: Details of lifespan experiments regarding Figure 26b.

food	number of animals	median survival	maximal lifespan	*p*-value
Replicate 1 - Male *atg7*$^{-/-}$ lifespan with 4,4'-Dimethoxychalcone.				
1) control food	96	49	64	1-2: $^{ns}p = 0.3245$ 1-3: $^{ns}p = 0.0731$ 1-4: $^{**}p = 0.0059$
2) 0.2 mM DMC	95	46	62	
3) 1.0 mM DMC	95	50	64	
4) 2.0 mM DMC	96	52.5	68	
Replicate 2 - Male *atg7*$^{-/-}$ lifespan with 4,4'-Dimethoxychalcone.				
1) control food	117	56	72	1-2: $^{***}p = 0.0003$ 1-3: $^{ns}p = 0.3633$ 1-4: $^{ns}p = 0.3224$
2) 0.2 mM DMC	114	60	74	
3) 1.0 mM DMC	117	56	72	
4) 2.0 mM DMC	113	58	72	

Replicate 3 - Male *atg7*$^{-/-}$ lifespan with 4,4'-Dimethoxychalcone.				
1) control food	118	58	72	1-2: $^{ns}p = 0.1558$ 1-3: $^{****}p < 0.0001$ 1-4: $^{***}p < 0.0009$
2) 0.2 mM DMC	119	58	72	
3) 1.0 mM DMC	118	50	66	
4) 2.0 mM DMC	118	54	76	
Description: Lifespan of male atg7$^{-/-}$ flies fed with the concentrations 0.2, 1.0, and 2.0 mM DMC since adulthood (each dissolved in 0.1% DMSO). 0.1 % DMSO food served as control.				

Figure 113: Replicates of the lifespan experiments for male *atg7*$^{-/-}$ with DMC.

Replicate 1: Lifespan of females

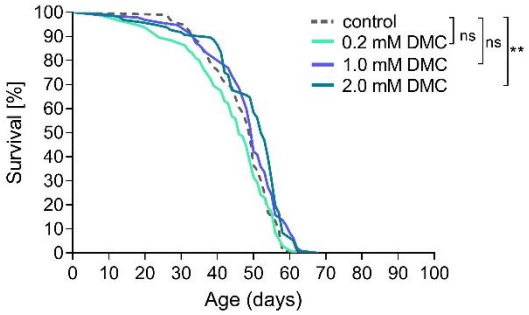

Replicate 2: Lifespan of males

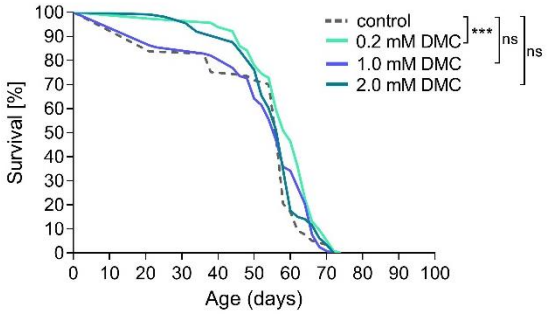

Replicate 3: Lifespan of males

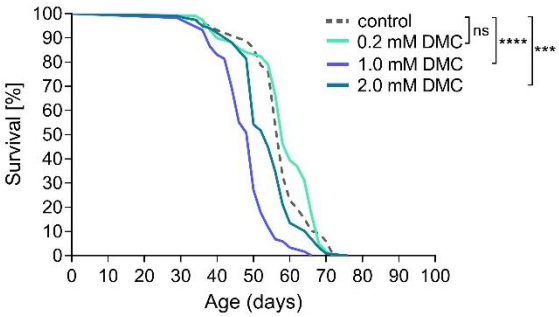

5. Data list of locomotor activity assays

food	number of trials	mean climbing success	test	*p*-value
Figure 28a: **5 seconds climbing with 3-day old female *w*^{1118}.**				
1) control food (0.1 % DMSO)	30	78.65 %	Mann-Whitney test	1-2: $^{*}p = 0.0177$ 1-3: $^{ns}p = 0.6825$ 1-4: $^{ns}p = 0.2597$
2) 0.2 mM DMC	30	69.49 %		
3) 1.0 mM DMC	30	77.16 %		
4) 2.0 mM DMC	30	74.74 %		
5 seconds climbing with 10-day old female *w*^{1118}.				
1) control food (0.1 % DMSO)	30	54.02 %	Mann-Whitney test	1-2: $^{ns}p = 0.3382$ 1-3: $^{ns}p = 0.8683$ 1-4: $^{ns}p = 0.8108$
2) 0.2 mM DMC	30	59.03 %		
3) 1.0 mM DMC	30	53.73 %		
4) 2.0 mM DMC	30	51.97 %		
5 seconds climbing with 20-day old female *w*^{1118}.				
1) control food (0.1 % DMSO)	20	3.38 %	Mann-Whitney test	1-2: $^{***}p = 0.0005$ 1-3: $^{****}p < 0.0001$ 1-4: $^{*}p = 0.0133$
2) 0.2 mM DMC	20	18.91 %		
3) 1.0 mM DMC	20	18.38 %		
4) 2.0 mM DMC	20	9.41 %		
5 seconds climbing with 30-day old female *w*^{1118}.				
1) control food (0.1 % DMSO)	29	0.493 %	Mann-Whitney test	1-2: $^{ns}p = 0.5402$ 1-3: $^{ns}p > 0.9999$ 1-4: $^{ns}p = 0.4238$
2) 0.2 mM DMC	30	1.177 %		
3) 1.0 mM DMC	29	0.246 %		
4) 2.0 mM DMC	30	1.143 %		
Method after Gupta et al., 2013: 15 flies per trial. Test tube with 7 cm label used.				

Figure 28b: **10 seconds climbing with 3-day old female *w^{1118}*.**				
1) control food (0.1 % DMSO)	30	90.09 %	Mann-Whitney test	1-2: $^{ns}p = 0.1714$ 1-3: $^{ns}p = 0.8214$ 1-4: $^{ns}p = 0.5251$
2) 0.2 mM DMC	30	86.34 %		
3) 1.0 mM DMC	30	90.35 %		
4) 2.0 mM DMC	30	88.94 %		
10 seconds climbing with 10-day old female *w^{1118}*.				
1) control food (0.1 % DMSO)	30	83.73 %	Mann-Whitney test	1-2: $^{ns}p = 0.9380$ 1-3: $^{ns}p = 0.8906$ 1-4: $^{ns}p = 0.3614$
2) 0.2 mM DMC	30	84.60 %		
3) 1.0 mM DMC	30	84.19 %		
4) 2.0 mM DMC	30	79.95 %		
10 seconds climbing with 20-day old female *w^{1118}*.				
1) control food (0.1 % DMSO)	20	15.49 %	Mann-Whitney test	1-2: $^{***}p = 0.0002$ 1-3: $^{****}p < 0.0001$ 1-4: $^{**}p = 0.0011$
2) 0.2 mM DMC	20	41.13 %		
3) 1.0 mM DMC	20	50.45 %		
4) 2.0 mM DMC	20	34.26 %		
10 seconds climbing with 30-day old female *w^{1118}*.				
1) control food (0.1 % DMSO)	29	8.08 %	Mann-Whitney test	1-2: $^{ns}p = 0.9658$ 1-3: $^{ns}p = 0.7359$ 1-4: $^{ns}p = 0.7146$
2) 0.2 mM DMC	30	9.11 %		
3) 1.0 mM DMC	29	9.98 %		
4) 2.0 mM DMC	30	8.36 %		
Method after Gupta et al., 2013: 15 flies per trial. Test tube with 7 cm label used.				
Figure 28c: **15 seconds climbing with 3-day old female *w^{1118}*.**				
1) control food (0.1 % DMSO)	30	93.06 %	Mann-Whitney test	1-2: $^{ns}p = 0.2779$ 1-3: $^{ns}p = 0.6311$ 1-4: $^{ns}p = 0.9395$
2) 0.2 mM DMC	30	91.86 %		
3) 1.0 mM DMC	30	93.85 %		
4) 2.0 mM DMC	30	94.21 %		

15 seconds climbing with 10-day old female *w^{1118}*.				
1) control food (0.1 % DMSO)	30	88.17 %	Mann-Whitney test	1-2: $^{ns}p = 0.7325$ 1-3: $^{ns}p = 0.2913$ 1-4: $^{ns}p = 0.4417$
2) 0.2 mM DMC	30	90.16 %		
3) 1.0 mM DMC	30	89.79 %		
4) 2.0 mM DMC	30	85.54 %		
15 seconds climbing with 20-day old female *w^{1118}*.				
1) control food (0.1 % DMSO)	20	20.51 %	Mann-Whitney test	1-2: $^{****}p < 0.0001$ 1-3: $^{****}p < 0.0001$ 1-4: $^{***}p = 0.0002$
2) 0.2 mM DMC	20	50.52 %		
3) 1.0 mM DMC	20	62.81 %		
4) 2.0 mM DMC	20	45.31 %		
15 seconds climbing with 30-day old female *w^{1118}*.				
1) control food (0.1 % DMSO)	29	13.49 %	Mann-Whitney test	1-2: $^{ns}p = 0.3144$ 1-3: $^{ns}p = 0.3349$ 1-4: $^{ns}p = 0.1842$
2) 0.2 mM DMC	30	16.64 %		
3) 1.0 mM DMC	29	17.48 %		
4) 2.0 mM DMC	30	16.85 %		
Method after Gupta et al., 2013: 15 flies per trial. Test tube with 7 cm label used.				
<u>Figure 28d:</u> **15 seconds climbing with 3-day old female *w^{1118}*, fed with normal versus control food.**				
normal food	30	93.47 %	Mann-Whitney test	$^{ns}p = 0.4177$
control food (0.1 % DMSO)	30	93.06 %		
15 seconds climbing with 10-day old female *w^{1118}*, fed with normal versus control food.				
normal food	30	86.21 %	Mann-Whitney test	$^{ns}p = 0.7961$
control food (0.1 % DMSO)	30	88.17 %		
15 seconds climbing with 20-day old female *w^{1118}*, fed with normal versus control food.				
normal food	20	49.46 %	Mann-Whitney test	$^{****}p < 0.0001$
control food (0.1 % DMSO)	20	20.51 %		
15 seconds climbing with 30-day old female *w^{1118}*, fed with normal versus control food.				
normal food	30	17.90 %	Mann-Whitney test	$^{ns}p = 0.3284$
control food (0.1 % DMSO)	29	13.49 %		
Method after Gupta et al., 2013: 15 flies per trial. Test tube with 7 cm label used.				

Figure 29a: **5 seconds climbing with 3-day old male *w*^{1118}.**				
1) control food (0.1 % DMSO)	30	78.89 %	Mann-Whitney test	1-2: $^{ns}p = 0.5381$ 1-3: $^{ns}p = 0.6086$ 1-4: $^{ns}p = 0.8799$
2) 0.2 mM DMC	30	77.31 %		
3) 1.0 mM DMC	30	78.47 %		
4) 2.0 mM DMC	30	79.55		
5 seconds climbing with 10-day old male *w*^{1118}.				
1) control food (0.1 % DMSO)	30	71.90 %	Mann-Whitney test	1-2: $^{ns}p = 0.1053$ 1-3: $^{ns}p = 0.7427$ 1-4: $^{ns}p = 0.9127$
2) 0.2 mM DMC	30	66.75 %		
3) 1.0 mM DMC	30	70.78 %		
4) 2.0 mM DMC	29	73.01 %		
5 seconds climbing with 20-day old male *w*^{1118}.				
1) control food (0.1 % DMSO)	20	34.29 %	Mann-Whitney test	1-2: $^{**}p = 0.0064$ 1-3: $^{ns}p = 0.2656$ 1-4: $^{*}p = 0.0402$
2) 0.2 mM DMC	20	50.35 %		
3) 1.0 mM DMC	20	42.10 %		
4) 2.0 mM DMC	20	47.08 %		
5 seconds climbing with 30-day old male *w*^{1118}.				
2) control food (0.1 % DMSO)	28	31.89 %	Mann-Whitney test	1-2: $^{**}p = 0.0042$ 1-3: $^{ns}p = 0.0527$ 1-4: $^{*}p = 0.0447$
3) 0.2 mM DMC	30	15.51 %		
4) 1.0 mM DMC	29	20.80 %		
5) 2.0 mM DMC	30	19.52 %		
Figure 29b: **10 seconds climbing with 3-day old male *w*^{1118}.**				
1) control food (0.1 % DMSO)	30	88.87 %	Mann-Whitney test	1-2: $^{ns}p = 0.5035$ 1-3: $^{ns}p = 0.7632$ 1-4: $^{ns}p = 0.6418$
2) 0.2 mM DMC	30	89.56 %		
3) 1.0 mM DMC	30	89.27 %		
4) 2.0 mM DMC	30	89.37 %		

10 seconds climbing with 10-day old male *w^{1118}*.				
1) control food (0.1 % DMSO)	30	88.86 %	Mann-Whitney test	1-2: $^{ns}p = 0.1077$ 1-3: $^{ns}p = 0.6592$ 1-4: $^{ns}p = 0.7499$
2) 0.2 mM DMC	30	85.87 %		
3) 1.0 mM DMC	30	86.11 %		
4) 2.0 mM DMC	29	89.21 %		
10 seconds climbing with 20-day old male *w^{1118}*.				
1) control food (0.1 % DMSO)	20	56.49 %	Mann-Whitney test	1-2: $^{*}p = 0.0122$ 1-3: $^{ns}p = 0.2970$ 1-4: $^{**}p = 0.0015$
2) 0.2 mM DMC	20	70.52 %		
3) 1.0 mM DMC	20	63.14 %		
4) 2.0 mM DMC	20	73.90 %		
10 seconds climbing with 30-day old male *w^{1118}*.				
1) control food (0.1 % DMSO)	28	52.23 %	Mann-Whitney test	1-2: $^{ns}p = 0.0670$ 1-3: $^{ns}p = 0.6708$ 1-4: $^{ns}p = 0.0975$
2) 0.2 mM DMC	30	40.90 %		
3) 1.0 mM DMC	29	49.65 %		
4) 2.0 mM DMC	30	42.81 %		
Method after Gupta et al., 2013: 15 flies per trial. Test tube with 7 cm label used.				
Figure 29c: **15 seconds climbing with 3-day old male *w^{1118}*.**				
1) control food (0.1 % DMSO)	30	91.60 %	Mann-Whitney test	1-2: $^{ns}p = 0.6253$ 1-3: $^{ns}p = 0.4046$ 1-4: $^{ns}p = 0.6325$
2) 0.2 mM DMC	30	92.05 %		
3) 1.0 mM DMC	30	93.32 %		
4) 2.0 mM DMC	30	91.83 %		
15 seconds climbing with 10-day old male *w^{1118}*.				
1) control food (0.1 % DMSO)	30	93.76 %	Mann-Whitney test	1-2: $^{*}p = 0.0333$ 1-3: $^{ns}p = 0.4026$ 1-4: $^{ns}p = 0.4669$
2) 0.2 mM DMC	30	89.93 %		
3) 1.0 mM DMC	30	90.54 %		
4) 2.0 mM DMC	29	93.45 %		

15 seconds climbing with 20-day old male *w^{1118}*.				
1) control food (0.1 % DMSO)	20	64.22 %	Mann-Whitney test	1-2: $^{*}p = 0.0390$ 1-3: $^{ns}p = 0.3785$ 1-4: $^{**}p = 0.0027$
2) 0.2 mM DMC	20	75.82 %		
3) 1.0 mM DMC	20	69.95 %		
4) 2.0 mM DMC	20	80.69 %		
15 seconds climbing with 30-day old male *w^{1118}*.				
1) control food (0.1 % DMSO)	28	60.58 %	Mann-Whitney test	1-2: $^{ns}p = 0.0561$ 1-3: $^{ns}p = 0.6026$ 1-4: $^{ns}p = 0.1023$
2) 0.2 mM DMC	30	50.69 %		
3) 1.0 mM DMC	29	59.22 %		
4) 2.0 mM DMC	30	53.33 %		
Method after Gupta et al., 2013: 15 flies per trial. Test tube with 7 cm label used.				
Figure 29d: **15 seconds climbing with 3-day old male *w^{1118}*, fed with normal versus control food.**				
normal food	30	89.67 %	Mann-Whitney test	$^{ns}p = 0.7548$
control food (0.1 % DMSO)	30	91.60 %		
15 seconds climbing with 10-day old male *w^{1118}*, fed with normal versus control food.				
normal food	30	89.67 %	Mann-Whitney test	$^{ns}p = 0.4744$
control food (0.1 % DMSO)	30	91.60 %		
15 seconds climbing with 20-day old male *w^{1118}*, fed with normal versus control food.				
normal food	20	71.64 %	Mann-Whitney test	$^{ns}p = 0.2657$
control food (0.1 % DMSO)	20	64.22 %		
15 seconds climbing with 30-day old male *w^{1118}*, fed with normal versus control food.				
normal food	30	57.65 %	Mann-Whitney test	$^{ns}p = 0.8739$
control food (0.1 % DMSO)	28	60.58 %		
Method after Gupta et al., 2013: 15 flies per trial. Test tube with 7 cm label used.				

column / genotype	number of trials	Cf-value mean	Cf-value median	SEM
Figure 47: **Negative geotaxis performance for *elaV(X)*-Gal4 > UAS-*atg5* RNAi (BL # 34899)**				
1) *atg5* RNAi / +	12	0.9577	0.9680	0.01282
2) *elaV(X)* > *atg5* RNAi	12	0.9042	0.8945	0.01467
Method after Inagaki et al., 2009: 20 flies per trial. Apparatus for negative geotaxis assay.				

6. Data list of memory experiments

Table 25: Details of the memory experiments.

column / genotype	mean ± SEM	median (number)	test	*p*-value
Figure 30: Short-term memory of *w*^{1118} with different 4,4'-Dimethoxychalcone concentrations.				
1) control food (0.1 % DMSO) (3 d)	62.94 ± 2.687	67.20 (29)	two-way ANOVA with Sidak's *post hoc* test	3 days: 1-2: $^{ns}p = 0.5816$ 1-3: $^{ns}p = 0.8239$ 1-4: $^{ns}p = 0.2113$ 30 days: 5-6: $^{ns}p > 0.9999$ 5-7: $^{ns}p = 0.9990$ 5-8: $^{ns}p = 0.4902$ 3 versus 30 days: 1-5: $^{****}p < 0.0001$ 2-6: $^{****}p < 0.0001$ 3-7: $^{****}p < 0.0001$ 4-8: $^{****}p < 0.0001$
2) 0.2 mM DMC (3 d)	69.55 ± 4.152	72.85 (7)		
3) 1.0 mM DMC (3 d)	67.07 ± 3.612	70.18 (12)		
4) 2.0 mM DMC (3 d)	60.59 ± 2.054	70.00 (17)		
5) control food (0.1 % DMSO) (30 d)	46.85 ± 1.258	45.70 (44)		
6) 0.2 mM DMC (30 d)	47.12 ± 2.604	49.95 (16)		
7) 1.0 mM DMC (30 d)	47.79 ± 1.546	49.25 (39)		
8) 2.0 mM DMC (30 d)	43.19 ± 1.538	45.90 (42)		
Method: 3 and 30 days. Raised at 25 °C. Tully Wheel. OCT 1:150, MCH 1:60.				
Figure 31a: Short-term memory of *w*^{1118} for 0.2 mM 4,4'-Dimethoxychalcone.				
1) 3 days	69.55 ± 4.152	72.85 (7)	one-way ANOVA with Sidak's *post hoc* test	1-2: $^{***}p = 0.0004$ 1-3: $^{*}p = 0.0185$ 1-4: $^{***}p = 0.0003$ 1-5: $^{****}p < 0.0001$
2) 10 days	39.04 ± 9.578	39.20 (4)		
3) 20 days	52.84 ± 2.880	54.75 (9)		
4) 30 days	47.12 ± 2.604	49.95 (16)		
5) 70 days	26.30 ± 1.909	25.60 (3)		
Figure 31b: Short-term memory of *w*^{1118} for 1.0 mM 4,4'-Dimethoxychalcone.				
1) 3 days	67.07 ± 3.612	70.18 (12)	one-way ANOVA with Sidak's *post hoc* test	1-2: $^{ns}p = 0.5629$ 1-3: $^{***}p = 0.0008$ 1-4: $^{****}p < 0.0001$ 1-5: $^{****}p < 0.0001$
2) 10 days	61.14 ± 2.359	60.75 (8)		
3) 20 days	52.07 ± 2.313	52.63 (14)		
4) 30 days	47.79 ± 1.546	49.25 (39)		

5) 70 days	10.40 ± 0.000	10.40 (1)		
Figure 31c: Short-term memory of w^{1118} for 2.0 mM 4,4'-Dimethoxychalcone.				
1) 3 days	69.59 ± 2.054	70.00 (17)	Kruskal-Wallis with Dunn's *post hoc* test	1-2: $^{ns}p = 0.6578$ 1-3: $^{***}p = 0.0005$ 1-4: $^{****}p < 0.0001$ 1-5: $^{***}p = 0.0005$
2) 10 days	59.97 ± 4.467	60.23 (8)		
3) 20 days	48.08 ± 2.106	48.95 (14)		
4) 30 days	43.19 ± 1.538	45.90 (42)		
5) 70 days	15.40 ± 0.600	15.40 (2)		
Method: 3, 10, 20, 30, and 70 days. Raised at 25 °C. Tully Wheel. OCT :150, MCH 1:60.				
Figure 32: Short-term memory of w^{1118} for the control food compared to normal food.				
1) 3 days, normal food	57.62 ± 2.648	61.65 (38)	two-way ANOVA with Sidak's *post hoc* test	normal food: 1-3: $^{ns}p > 0.9999$ 1-5: $^{ns}p = 0.6102$ 1-7: $^{****}p < 0.0001$ 1-9: $^{**}p = 0.0056$ 0.1 % DMSO: 2-4: $^{ns}p = 0.9452$ 2-6: $^{ns}p = 0.1282$ 2-8: $^{****}p < 0.0001$ 2-10: $^{****}p < 0.0001$ normal food versus 0.1 % DMSO: 1-2: $^{ns}p = 0.3022$ 3-4: $^{ns}p = 0.9997$ 5-6: $^{ns}p = 0.9895$ 7-8: $^{ns}p = 0.9409$ 9-10: $^{ns}p = 0.9983$
2) 3 days, 0.1% DMSO	62.94 ± 2.687	67.10 (29)		
3) 10 days, normal food	57.55 ± 2.167	57.65 (4)		
4) 10 days, 0.1 % DMSO	59.42 ± 3.551	59.03 (8)		
5) 20 days, normal food	52.03 ± 2.362	53.01 (12)		
6) 20 days, 0.1 % DMSO	54.39 ± 2.336	55.30 (17)		
7) 30 days, normal food	44.82 ± 1.607	45.40 (40)		
8) 30 days, 0.1 % DMSO	46.85 ± 1.258	45.07 (44)		
9) 70 days, normal food	16.00 ± 0.000	16.00 (1)		
10) 70 days, 0.1 % DMSO	21.15 ± 6.250	21.15 (2)		
Method: 3, 10, 20, 30, and 70 days. Raised at 25 °C. Tully Wheel. OCT :150, MCH 1:60.				

Figure 33a: Short-term memory of *appl*-Gal4 > UAS- n-*synaptobrevin* overexpression				
1) n-*synaptobrevin* OE / + (5 d)	70.30 ± 1.621	70.45 (4)	two-way ANOVA with Sidak's *post hoc* test	1-2: $^{ns}p = 0.8594$ 3-4: $^{***}p = 0.0002$ 1-3: $^{****}p < 0.0001$ 2-4: $^{**}p = 0.0.0093$
2) *appl* > n-*synaptobrevin* OE (5 d)	74.30 ± 0.900	74.30 (2)		
3) n-*synaptobrevin* OE / + (20 d)	37.22 ± 3.615	36.05 (12)		
4) *appl* > n-*synaptobrevin* OE (20 d)	52.97 ± 1.874	52.30 (17)		
Two-way ANOVA: Interaction: $^{ns}p = 0.1933$; Row Factor: $^{****}p < 0.0001$; Column Factor: $^{*}p = 0.0328$				
Method: 5 and 20 days. Raised at 29 °C. Tully Wheel. OCT 1:150, MCH 1:60.				
Figure 33b: Short-term memory of 20-day old *appl*-GAl4 > UAS-*cellubrevin* overexpression				
1) *cellubrevin* OE / +	31.07 ± 4.303	34.50 (9)	unpaired t-test	$^{ns}p = 0.8605$
2) *appl* > *cellubrevin* OE	29.65 ± 7.275	30.85 (6)		
Method: 20 days. Raised at 29 °C. Tully Wheel. OCT 1:150, MCH 1:60.				
Figure 34: Short-term memory of 20-day old *appl*-Gal4 > UAS- *unc-104* overexpression (BL # 24786)				
1) *appl* / +	42.42 ± 3.160	46.70 (11)	one-way ANOVA with Sidak's *post hoc* test	1-3: $^{ns}p = 0.8730$ 2-3: $^{**}p = 0.0016$
2) *unc-104* OE / +	30.89 ± 1.868	33.25 (14)		
3) *appl* > *unc-104* OE	44.20 ± 2.877	41.70 (11)		
Method: 20 days. Raised at 29 °C. Tully Wheel. OCT 1:150, MCH 1:60.				
Figure 35a: Short-term memory of *appl*-Gal4 > UAS-*p62/Ref(2)p* overexpression				
1) *appl* / + (5 d)	68.33 ± 3.752	67.25 (6)	two-way ANOVA with Sidak's *post hoc* test	5 days: 1-2: $^{*}p = 0.0375$ 1-3: $^{ns}p = 0.9985$ 2-3: $^{*}p = 0.0164$ 20 days: 4-5: $^{ns}p = 0.7873$ 4-6: $^{ns}p = 0.5717$ 5-6: $^{ns}p = 0.2269$ 5 versus 20 days:
2) *p62/Ref(2)p* OE / + (5 d)	52.76 ± 5.690	54.85 (10)		
3) *appl* > *p62/Ref(2)p* OE (5 d)	68.01 ± 3.404	70.30 (10)		
4) *appl* / + (20 d)	48.27 ± 2.882	49.80 (9)		

5) *p62/Ref(2)p* OE / + (20 d)	44.75 ± 2.993	46.10 (11)		1-4: $^{**}p = 0.0072$ 2-5: $^{ns}p = 0.3385$ 3-6: $^{ns}p = 0.0690$
6) *appl > p62/Ref(2)p* OE (20 d)	54.33 ± 3.929	53.10 (7)		
Two-way ANOVA: Interaction: $^{ns}p = 0.3389$; Row Factor: $^{***}p = 0.0001$; Column Factor: $^{**}p = 0.0062$				
Method: 5 and 20 days. Raised at 29 °C. Tully Wheel. OCT 1:150, MCH 1:60.				
Figure 35b: Short-term memory of 5-day old *appl*-Gal4 > UAS-*p62/ref(2)p* RNAi (BL # 33978)				
1) *appl* / +	67.08 ± 3.901	67.15 (26)	Kruskal-Wallis with Dunn's *post hoc* test	1-3: $^{ns}p = 0.1110$ 2-3: $^{*}p = 0.0308$
2) *p62/Ref(2)p* RNAi / +	43.16 ± 3.004	43.16 (23)		
3) *appl > p62/Ref(2)p* RNAi	55.58 ± 4.140	56.50 (21)		
Method: 5 days. Raised at 29 °C. Tully Wheel. OCT 1:150, MCH 1:55 and 1:60.				
Figure 36: Short-term memory of 20-day old *appl*-Gal4 > UAS-*tomosyn* RNAi (VDRC # 43630)				
1) *appl* / +	39.61 ± 2.370	39.30 (9)	one-way ANOVA with Sidak's *post hoc* test	1-3: $^{ns}p = 0.1367$ 2-3: $^{*}p = 0.0214$
2) *tomosyn* RNAi / +	36.52 ± 2.584	36.60 (11)		
3) *appl > tomosyn* RNAi	47.83 ± 3.619	46.15 (12)		
Method: 20 days. Raised at 29 °C. Tully Wheel. OCT 1:150, MCH 1:60.				
Figure 39a: Short-term memory of 5-day old *CG8005* / + with and without Spermidine				
1) w^{1118} (- Spd)	63.74 ± 2.552	64.10 (12)	two-way ANOVA with Sidak's *post hoc* test	1-2: $^{**}p = 0.0058$ 1-3: $^{ns}p = 0.7405$ 2-4: $^{ns}p = 0.9881$ 3-4: $^{***}p = 0.0005$
2) *CG8005* / + (- Spd)	51.20 ± 2.980	53.10 (13)		
3) w^{1118} (+ Spd)	66.57 ± 2.411	66.90 (12)		
4) *CG8005* / + (+ Spd)	50.66 ± 3.151	51.70 (13)		
Two-way ANOVA: Interaction: $^{ns}p = 0.5537$; Row Factor: $^{ns}p = 0.6869$; Column Factor: $^{****}p < 0.0001$				
Method: 5 days. Raised at 25 °C. T-maze and Tully Wheel. OCT 1:100, MCH 1:100.				
Figure 39b: Short-term memory of 30-day old *CG8005* / + with and without Spermidine				
1) w^{1118} (- Spd)	28.90 ± 2.209	31.45 (22)	two-way ANOVA with Sidak's *post hoc* test	1-2: $^{*}p = 0.0339$ 1-3: $^{*}p = 0.0264$ 2-4: $^{ns}p = 0.0638$ 3-4: $^{*}p = 0.0251$
2) *CG8005* / + (- Spd)	19.50 ± 3.562	22.70 (19)		
3) w^{1118} (+ Spd)	38.41 ± 2.035	39.30 (21)		

4) *CG8005* / + (+ Spd)	28.32 ± 3.218	26.35 (18)		
Two-way ANOVA: Interaction: $^{ns}p = 0.8998$; Row Factor: $^{**}p = 0.0014$; Column Factor: $^{***}p = 0.0007$				
Method: 30 days. Raised at 25 °C. T-maze. OCT 1:100, MCH 1:100.				
Figure 39c: 3 hours Mid-term memory of 5-day old *CG8005* / + with and without Spermidine				
1) w^{1118} (- Spd)	36.88 ± 2.132	35.00 (25)	two-way ANOVA with Sidak's *post hoc* test	1-2: $^{ns}p = 0.0616$ 1-3: $^{ns}p = 0.8022$ 2-4: $^{ns}p = 0.9993$ 3-4: $^{*}p = 0.0142$
2) *CG8005* / + (- Spd)	29.33 ± 2.155	30.60 (26)		
3) w^{1118} (+ Spd)	38.94 ± 2.753	39.70 (25)		
4) *CG8005* / + (+ Spd)	29.45 ± 2.660	31.90 (26)		
Two-way ANOVA: Interaction: $^{ns}p = 0.6907$; Row Factor: $^{ns}p = 0.6564$; Column Factor: $^{***}p = 0.0007$				
Method: 5 days. Raised at 25 °C. T-maze. OCT 1:100, MCH 1:100.				
Figure 39d: 3 hours Mid-term memory of 30-day old *CG8005* / + with and without Spermidine				
1) w^{1118} (- Spd)	11.96 ± 2.530	11.00 (19)	two-way ANOVA with Sidak's *post hoc* test	1-2: $^{ns}p = 0.9488$ 1-3: $^{*}p = 0.0114$ 2-4: $^{ns}p = 0.7322$ 3-4: $^{*}p = 0.0437$
2) *CG8005* / + (- Spd)	10.86 ± 2.770	11.60 (18)		
3) w^{1118} (+ Spd)	22.71 ± 2.854	21.20 (19)		
4) *CG8005* / + (+ Spd)	13.63 ± 2.704	14.60 (17)		
Two-way ANOVA: Interaction: $^{ns}p = 0.1473$; Row Factor: $^{*}p = 0.0154$; Column Factor: $^{ns}p = 0.0657$				
Method: 30 days. Raised at 25 °C. T-maze. OCT 1:100, MCH 1:100.				
Table 3: Innate behavior of *CG8005^{DG05802}* / +				
Olfactory acuity: **OCT** 1) w^{1118}, - Spd, 5 days 2) *CG8005* / +, - Spd, 5 days 3) w^{1118}, + Spd, 5 days 4) *CG8005* / +, + Spd, 5 days	 28.89 ± 4.754 18.70 ± 4.751 26.44 ± 5.417 31.28 ± 4.123	 34.50 (11) 20.00 (11) 22.00 (11) 33.30 (11)	two-way ANOVA with Sidak's *post hoc* test	- / + Spd: 1-3: $^{ns}p = 0.9208$ 2-4: $^{ns}p = 0.1356$ w^{1118} vs. *CG8005*/+: 1-2: $^{ns}p = 0.2600$ 3-4: $^{ns}p = 0.7275$
Olfactory acuity: **MCH** 1) w^{1118}, - Spd, 5 days 2) *CG8005* / +, - Spd, 5 days 3) w^{1118}, + Spd, 5 days 4) *CG8005* / +, + Spd, 5 days	 41.46 ± 5.885 49.73 ± 7.955 53.05 ± 5.793 48.67 ± 5.068	 37.95 (14) 49.90 (12) 50.00 (13) 51.20 (16)	two-way ANOVA with Sidak's *post hoc* test	- / + Spd: 1-3: $^{ns}p = 0.3423$ 2-4: $^{ns}p = 0.9906$ w^{1118} vs. *CG8005*/+: 1-2: $^{ns}p = 0.5869$ 3-4: $^{ns}p = 0.8444$

Olfactory acuity: **OCT**				- / + Spd:
1) w^{1118}, - Spd, 30 days	41.44 ± 4.111	44.65 (14)	two-way	1-3: $^{ns}p = 0.2382$
2) *CG8005* / +, - Spd, 30 days	34.59 ± 3.465	31.15 (14)	ANOVA with	2-4: $^{ns}p = 0.8318$
3) w^{1118}, + Spd, 30 days	32.81 ± 3.621	29.55 (14)	Sidak's *post*	w^{1118} vs. *CG8005*/+:
4) *CG8005* / +, + Spd, 30 days	33.67 ± 2.623	30.45 (12)	*hoc* test	1-2: $^{ns}p = 0.3985$
				3-4: $^{ns}p = 0.6343$
Olfactory acuity: **MCH**				- / + Spd:
1) w^{1118}, - Spd, 30 days	59.36 ± 5.680	62.80 (22)	two-way	1-3: $^{ns}p = 0.7903$
2) *CG8005* / +, - Spd, 30 days	66.10 ± 4.586	61.90 (23)	ANOVA with	2-4: $^{ns}p = 0.3812$
3) w^{1118}, + Spd, 30 days	55.00 ± 5.229	57.15 (22)	Sidak's *post*	w^{1118} vs. *CG8005*/+:
4) *CG8005* / +, + Spd, 30 days	57.28 ± 4.449	57.10 (22)	*hoc* test	1-2: $^{ns}p = 0.5650$
				3-4: $^{ns}p = 0.9373$
Method: 30 days. Raised at 25 °C. T-maze. OCT 1:100, MCH 1:100.				
Figure 40a: Short-term memory of 5-day old *elaV(X)*-Gal4 > UAS-*CG8005* RNAi (VDRC # 103593)				
1) *elaV(X)* / +	41.81 ± 4.067	41.80 (15)	one-way	
2) *CG8005* RNAi / +	51.92 ± 2.101	52.10 (11)	ANOVA with	1-3: $*p = 0.0146$
3) *elaV(X)* > *CG8005* RNAi	29.13 ± 2.261	30.40 (12)	Sidak's *post*	2-3: $****p < 0.0001$
			hoc test	
Method: 5 days. Raised at 29 °C. T-maze. OCT 1:100, MCH 1:100.				
Figure 41a: Short-term memory of *appl*-Gal4 > UAS-*skywalker* overexpression				
1) *skywalker* OE / (5 days)	53.80 ± 4.733	50.10 (10)		
2) *appl* > *skywalker* OE (5 days)	71.64 ± 4.265	70.45 (14)	two-way	1-2: $*p = 0.0121$
3) *skywalker* OE / (20 days)	48.84 ± 3.912	48.80 (18)	ANOVA with	1-3: $^{ns}p = 0.6492$
4) *appl* > *skywalker* OE (20 days)	72.96 ± 3.109	68.20 (15)	Sidak's *post*	2-4: $^{ns}p = 0.9980$
			hoc test	3-4: $***p = 0.0001$
Two-way ANOVA: Interaction: $^{ns}p = 0.5209$; Row Factor: $^{ns}p = 0.5720$; Column Factor: $****p < 0.0001$				
Method: 5 and 20 days. Raised at 29 °C. T-maze and Tully Wheel. OCT 1:100 and MCH 1:100, or OCT 1:150 and MCH 1:55 and 1:75, or OCT 1:150 and EA 1:100.				

Figure 41b: Short-term memory of *ok107*-Gal4 > UAS-*skywalker* overexpression				
1) *skywalker* OE / (5 days)	45.28 ± 4.249	47.50 (5)	two-way ANOVA with Sidak's *post hoc* test	1-2: $^{ns}p = 0.6216$ 1-3: $^{ns}p = 0.5761$ 2-4: $^{ns}p = 0.9889$ 3-4: $^{ns}p = 0.9905$
2) *ok107 > skywalker* OE (5 days)	39.30 ± 7.156	39.95 (4)		
3) *skywalker* OE / (20 days)	39.45 ± 3.831	40.50 (6)		
4) *ok107 > skywalker* OE (20 days)	40.20 ± 2.974	38.30 (5)		
Two-way ANOVA: Interaction: $^{ns}p = 0.4663$; Row Factor: $^{ns}p = 0.5921$; Column Factor: $^{ns}p = 0.5700$				
Method: 5 and 20 days. Raised at 29 °C. T-maze and Tully Wheel. OCT 1:100 and MCH 1:100.				
Figure 42a: Short-term memory of *appl*-Gal4 > UAS-*hsc70-4^{wt}* overexpression				
1) *appl* / + (5 days)	66.30 ± 2.574	66.15 (10)	two-way ANOVA with Sidak's *post hoc* test	1-3: $^{ns}p = 0.2143$ 2-3: $^{*}p = 0.0133$ 4-6: $^{ns}p = 0.9988$ 5-6: $^{**}p = 0.0012$ 1-4: $^{****}p < 0.0001$ 2-5: $^{****}p < 0.0001$ 3-6: $^{****}p < 0.0001$
2) *hsc70-4^{wt}* OE / + (5 days)	51.42 ± 2.195	52.40 (31)		
3) *appl > hsc70-4^{wt}* OE (5 days)	59.41 ± 1.935	57.80 (26)		
4) *appl* / + (20 days)	47.20 ± 1.375	47.25 (22)		
5) *hsc70-4^{wt}* OE / + (20 days)	36.98 ± 1.763	36.70 (30)		
6) *appl > hsc70-4^{wt}* OE (20 days)	46.80 ± 2.295	47.20 (29)		
Two-way ANOVA: Interaction: $^{ns}p = 0.4099$; Row Factor: $^{****}p < 0.0001$; Column Factor: $^{****}p < 0.0001$				
Method: 5 and 20 days. Raised at 29 °C. T-maze and Tully Wheel. OCT 1:150 and EA 1:100, or OCT 1:100 and MCH 1:100.				
Figure 42b: Short-term memory of *ok107*-Gal4 > UAS-*hsc70-4^{wt}* overexpression				
1) *hsc70-4^{wt}* OE / + (5 days)	55.02 ± 2.456	56.00 (19)	two-way ANOVA with Sidak's *post hoc* test	1-2: $^{ns}p = 0.0822$ 1-3: $^{****}p < 0.0001$ 2-4: $^{ns}p = 0.5490$ 3-4: $^{ns}p = 0.2672$
2) *ok107 > hsc70-4^{wt}* (5 days)	47.88 ± 2.628	45.90 (19)		
3) *hsc70-4^{wt}* OE / + (20 days)	37.71 ± 2.523	36.20 (15)		
4) *ok107 > hsc70-4^{wt}* (20 days)	43.93 ± 2.958	45.90 (11)		
Two-way ANOVA: Interaction: $^{*}p = 0.0167$; Row Factor: $^{***}p = 0.0002$; Column Factor: $^{ns}p = 0.8665$				
Method: 5 and 20 days. Raised at 29 °C. T-maze and Tully Wheel. OCT 1:100 and MCH 1:100.				

Figure 43: Short-term memory of *appl*-Gal4 > UAS-*hsc70-4^{D10N}* overexpression				
1) *appl* / + (5 days)	66.91 ± 2.879	66.15 (8)	two-way ANOVA with Sidak's *post hoc* test	1-3: $^{ns}p = 0.9904$ 2-3: $^{ns}p = 0.1808$ 4-6: $^{ns}p = 0.9483$ 5-6: $^{*}p = 0.0289$ 1-4: $^{***}p = 0.0002$ 2-5: $^{**}p = 0.0034$ 3-6: $^{ns}p = 0.1033$
2) *hsc70-4^{D10N}* OE / + (5 days)	33.86 ± 7.657	51.30 (7)		
3) *appl* > *hsc70-4^{D10N}* OE (5 days)	65.18 ± 4.490	64.60 (4)		
4) *appl* / + (20 days)	47.38 ± 1.505	48.00 (17)		
5) *hsc70-4^{D10N}* OE / + (20 days)	33.86 ± 3.513	36.05 (8)		
6) *appl* > *hsc70-4^{D10N}* OE (20 days)	49.98 ± 3.285	54.10 (5)		
Two-way ANOVA: Interaction: $^{ns}p = 0.8697$; Row Factor: $^{****}p < 0.0001$; Column Factor: $^{***}p = 0.0005$				
Method: 5 and 20 days. Raised at 29 °C. Tully Wheel. OCT 1:150 and EA 1:100.				
Figure 44b: Short-term memory of *elaV(X)*-Gal4 > UAS-*atg5* RNAi (BL # 34899)				
1) *atg5* RNAi / + replicate 1: replicate 2:	41.98 ± 1.797 41.32 ± 3.263 42.47 ± 2.086	43.80 (31)	unpaired t-test	$^{***}p = 0.0003$
2) *elaV(X)* > *atg5* RNAi replicate 1: replicate 2:	32.60 ± 1.642 30.89 ± 3.969 33.41 ± 1.591	31.70 (28)		
Method: 10 days. Raised at 29 °C. Tully Wheel. OCT 1:150, MCH 1:60.				
Figure 44c: 1 hour Mid-term memory of *elaV(X)*-Gal4 > UAS-*atg5* RNAi (BL # 34899)				
1) *atg5* RNAi / +	48.16 ± 3.537	48.80 (21)	unpaired t-test	$^{*}p = 0.0111$
2) *elaV(X)* > *atg5* RNAi	36.77 ± 2.316	37.00 (20)		
Method: 10 days. Raised at 29 °C. T-maze. OCT 1:150, MCH 1:60.				

Figure 45b: 1 hour Mid-term memory of *elaV(X)*-Gal4 > UAS-*atg5* RNAi for 10 and 30 days (BL # 34899)				
1) *atg5* RNAi / + (10 days)	40.94 ± 2.760	38.30 (21)	two-way ANOVA with Sidak's *post hoc* test	1-2: ****$p < 0.0001$ 1-3: ****$p < 0.0001$ 2-3: $^{ns}p = 0.6878$ 2-4: $^{ns}p = 0.1880$ 3-4: *$p = 0.0202$
2) *elaV(X)* > *atg5* RNAi (10 days)	16.68 ± 2.351	16.05 (26)		
3) *atg5* RNAi / + (30 days)	21.32 ± 2.118	21.50 (22)		
4) *elaV(X)* > *atg5* RNAi (30 days)	5.90 ± 4.970	8.60 (7)		
Two-way ANOVA: Interaction: $^{ns}p = 0.1546$; Row Factor: ****$p < 0.0001$; Column Factor: ****$p < 0.0001$				
Method: 10 and 30 days. Raised at 29 °C. T-maze. OCT 1.100, MCH 1:100.				
Figure 45c: 1 hour Anesthesia-resistant memory of *elaV(X)*-Gal4 > UAS-*atg5* RNAi (BL # 34899)				
1) *atg5* RNAi / + (10 days)	7.29 ± 3.434	5.60 (13)	one-way ANOVA with Tukey's *post hoc* test	1-2: $^{ns}p = 0.9623$ 1-3: $^{ns}p = 0.6599$ 2-3: $^{ns}p = 0.4807$
2) *elaV(X)* > *atg5* RNAi (10 days)	6.39 ± 1.570	6.05 (16)		
3) *atg5* RNAi / + (30 days)	10.55 ± 2.415	10.80 (11)		
Method: 10 and 30 days. Raised at 29 °C. T-maze. OCT 1.100, MCH 1:100.				
Figure 45d: 1 hour Anesthesia-sensitive memory of *elaV(X)*-Gal4 > UAS-*atg5* RNAi (BL # 34899)				
1) *atg5* RNAi / + (10 days)	33.65 ± 3.434	35.34 (13)	one-way ANOVA with Tukey's *post hoc* test	1-2: ****$p < 0.0001$ 1-3: ****$p < 0.0001$ 2-3: $^{ns}p = 0.9901$
2) *elaV(X)* > *atg5* RNAi (10 days)	10.29 ± 1.570	10.63 (16)		
3) *atg5* RNAi / + (30 days)	10.77 ± 2.415	10.52 (11)		
Method: ASM values were calculated as the MTM median minus the particular ARM values.				

Figure 46: Short-term memory of 5-day old elaV(X)-Gal4 > UAS-atg5 RNAi (BL # 34899)				
1) *atg5* RNAi / +	59.69 ± 2.086	59.80 (15)	unpaired t-test	****$p < 0.0001$
2) *elaV(X)* > *atg5* RNAi	41.35 ± 3.167	41.05 (12)		
Method: 5 days. Raised at 29 °C. T-maze and Tully Wheel. OCT 1.150, MCH 1:55 and 1:75.				
Table 4: Innate behavior of *elaV(X)*-Gal4 > UAS-*atg5* RNAi (BL # 34899)				
Shock reactivity:				
1) *atg5* RNAi / +	77.68 ± 4.012	78.80 (9)	unpaired t-test	$^{ns}p = 0.9368$
2) *elaV(X)* > *atg5* RNAi	77.31 ± 2.626	79.40 (12)		
Olfactory acuity: **OCT**				
1) *atg5* RNAi / +	22.63 ± 4.085	22.20 (9)	unpaired t-test	$^{ns}p = 0.8402$
2) *elaV(X)* > *atg5* RNAi	21.22 ± 5.824	20.65 (6)		
Olfactory acuity: **MCH**				
1) *atg5* RNAi / +	24.59 ± 6.726	21.20 (13)	unpaired t-test	$^{ns}p = 0.5927$
2) *elaV(X)* > *atg5* RNAi	19.55 ± 6.205	12.70 (11)		
Method: 10 days. Raised at 29 °C. T-maze and Tully Wheel. OCT 1:150, MCH 1:60.				
Figure 48a: Short-term memory of *gmr*-Gal4 > UAS-*atg5* RNAi (BL # 34899)				
1) *atg5* RNAi / +	49.31 ± 3.576	45.95 (8)	unpaired t-test	$^{ns}p = 0.3963$
2) *gmr* > *atg5* RNAi	55.66 ± 5.128	52.70 (5)		
Method: 10 days. Raised at 29 °C. T-maze and Tully Wheel. OCT 1:100, MCH 1:100.				
Figure 48b: Short-term memory of *gh146*-Gal4 > UAS-*atg5* RNAi (BL # 34899)				
1) *atg5* RNAi / +	52.64 ± 1.642	52.00 (15)	unpaired t-test	$^{ns}p = 0.1017$
2) *gh146* > *atg5* RNAi	58.73 ± 3.456	57.35 (12)		
Method: 10 days. Raised at 29 °C. Tully Wheel. OCT 1:150, MCH 1:55.				
Figure 49b: Short-term memory of *vt030559*-Gal4 > UAS-*atg5* RNAi (BL # 34899)				
1) *atg5* RNAi / +	47.54 ± 2.795	46.40 (11)	unpaired t-test	****$p < 0.0001$
2) *vt030559* > *atg5* RNAi	28.43 ± 1.977	28.70 (9)		
Method: 10 days. Raised at 29 °C. T-maze and Tully Wheel. OCT 1:100, MCH 1:100.				

Figure 49c: 1 hour Mid-term memory of *vt030559*-Gal4 > UAS-*atg5* RNAi (BL # 34899)				
1) *atg5* RNAi / +	38.37 ± 1.993	38.70 (16)	unpaired t-test	$^{**}p = 0.0033$
2) *vt030559* > *atg5* RNAi	24.34 ± 4.568	20.55 (8)		
Method: 10 days. Raised at 29 °C. T-maze. OCT 1:100, MCH 1:100.				
Figure 50a: 1 hour Anesthesia-resistant memory of *vt030559*-Gal4 > UAS-*atg5* RNAi (BL # 34899)				
1) *vt030559* / +	14.70 ± 3.217	14.10 (7)	one-way ANOVA with Sidak's *post hoc* test	1-3: $^{ns}p = 0.9783$ 2-3: $^{ns}p = 0.5105$
2) *atg5* RNAi / +	21.30 ± 2.735	18.50 (12)		
3) *vt030559* > *atg5* RNAi	15.83 ± 1.923	16.90 (3)		
Method: 10 days. Raised at 29 °C. T-maze. OCT 1:100, MCH 1:100.				
Figure 50b: 1 hour Anesthesia-sensitive memory of *vt030559*-Gal4 > UAS-*atg5* RNAi (BL # 34899)				
1) *vt030559* / +	22.80 ± 3.217	23.40 (7)	one-way ANOVA with Sidak's *post hoc* test	1-3: $^{*}p = 0.0145$ 2-3: $^{ns}p = 0.0855$
2) *atg5* RNAi / +	21.80 ± 2.936	20.20 (12)		
3) *vt030559* > *atg5* RNAi	4.717 ± 1.923	3.650 (3)		
Method: ASM values were calculated as the MTM median minus the particular ARM values.				
Figure 51a: Short-term memory of *ok107*-Gal4 > UAS-*atg5* RNAi (BL # 34899)				
1) *atg5* RNAi / +	42.29 ± 1.767	44.35 (32)	unpaired t-test	$^{*}p = 0.0209$
replicate 1:	42.07 ± 3.114			
replicate 2:	42.47 ± 2.086			
2) *ok107*-Gal4 > *atg5* RNAi	36.05 ± 1.956	37.90 (29)		
replicate 1:	34.76 ± 2.915			
replicate 2:	36.84 ± 2.646			
Method: 10 days. Raised at 29 °C. Tully Wheel. OCT 1:150, MCH 1:60.				
Figure 51b: Short-term memory of 5-day old *ok107*-Gal4 > UAS-*atg5* RNAi (BL # 34899)				
1) *atg5* RNAi / +	57.10 ± 2.256	55.50 (19)	unpaired t-test	$^{**}p = 0.0091$
2) *ok107* > *atg5* RNAi	46.99 ± 2.867	45.70 (20)		
Method: 5 days. Raised at 29 °C. T-maze and Tully Wheel. OCT 1:150, MCH 1:55 and 1:75.				

Figure 52b: Short-term memory of *mb247*-Gal80 ;; *ok107*-Gal4 > UAS-*atg5* RNAi (BL # 34899)				
1) *mb247*-Gal80 / + ;; *ok107*-Gal4 / +	52.63 ± 2.933	49.75 (8)	one-way ANOVA with Sidak's *post hoc* test	1-3: $^{**}p = 0.0013$ 2-3: $^{ns}p = 0.3585$
2) *atg5* RNAi / +	32.38 ± 2.543	31.30 (13)		
3) *mb247*-Gal80 ;; *ok107*-Gal4 > *atg5* RNAi	37.08 ± 2.620	39.05 (12)		
Method: 10 days. Raised at 29 °C. T-maze and Tully Wheel. OCT 1:100, MCH 1:100.				
Figure 52c: 1 hour Mid-term memory of *mb247*-Gal80 ;; *ok107*-Gal4 > UAS-*atg5* RNAi (BL # 34899)				
1) *mb247*-Gal80 / + ;; *ok107*-Gal4 / +	52.70 ± 5.428	56.80 (5)	one-way ANOVA with Sidak's *post hoc* test	1-3: $^{ns}p = 0.7069$ 2-3: $^{ns}p = 0.9226$
2) *atg5* RNAi / +	46.42 ± 4.124	49.70 (11)		
3) *mb247*-Gal80 ;; *ok107*-Gal4 > *atg5* RNAi	48.12 ± 2.549	47.10 (13)		
Method: 10 days. Raised at 29 °C. T-maze. OCT 1:100, MCH 1:100.				
Figure 53a: Short-term memory of *mb247*-Gal4 > UAS-*atg5* RNAi (BL # 34899)				
1) *atg5* RNAi / +	35.07 ± 2.704	38.20 (12)	unpaired t-test	$^{ns}p = 0.3514$
2) *mb247*-Gal4 > *atg5* RNAi	38.99 ± 3.080	39.80 (13)		
Method: 10 days. Raised at 29 °C. Tully Wheel. OCT 1:150, MCH 1:60.				
Figure 53b: 1 hour Mid-term memory of *mb247*-Gal4 > UAS-*atg5* RNAi (BL # 34899)				
1) *atg5* RNAi / +	53.40 ± 8.669	54.20 (3)	unpaired t-test	$^{ns}p = 0.7644$
2) *mb247*-Gal4 > *atg5* RNAi	56.00 ± 3.260	54.75 (4)		
Method: 10 days. Raised at 29 °C. T-maze. OCT 1:150, EA 1:100.				
Figure 54: Short-term memory of *tub*-Gal80^{ts} ;; *ok107*-Gal4 > UAS-*atg5* RNAi (BL # 34899)				
1) *tub*-Gal80^{ts} / + ;; *ok107*-Gal4 / +	33.03 ± 5.281	29.60 (3)	Kruskal-Wallis with Dunn's *post hoc* test	1-3: $^{ns}p > 0.9999$ 2-3: $^{ns}p > 0.9999$
2) *atg5* RNAi / +	34.73 ± 1.631	35.70 (13)		
3) *tub*-Gal80^{ts} ;; *ok107*-Gal4 > *atg5* RNAi	32.46 ± 3.614	32.00 (10)		

Method: 10 days. Raised at 18 °C, after eclosion at 29 °C. T-maze. OCT 1:100, MCH 1:100.				
Table 5: Innate behavior of *atg5* knockdown in specific neuronal areas (BL # 34899)				
Olfactory acuity: **OCT** 1) *atg5* RNAi / + 2) *gh146* > *atg5* RNAi Olfactory acuity: **MCH** 1) *atg5* RNAi / + 2) *gh146* > *atg5* RNAi	 52.14 ± 5.870 36.70 ± 3.845 38.07 ± 5.315 29.16 ± 5.910	 54.90 (12) 39.65 (16) 37.00 (15) 28.30 (14)	 unpaired t-test unpaired t-test	 *p = 0.0303 ^{ns}p = 0.2710
Method: 10 days. Raised at 29 °C. T-maze. OCT 1:100, MCH 1:100.				
Olfactory acuity: **OCT** 1) *atg5* RNAi / + 2) *vt030559* > *atg5* RNAi Olfactory acuity: **MCH** 1) *atg5* RNAi / + 2) *vt030559* > *atg5* RNAi	 34.56 ± 10.22 39.15 ± 13.20 61.54 ± 6.915 54.88 ± 5.965	 46.80 (8) 37.20 (6) 58.40 (8) 52.60 (4)	 unpaired t-test unpaired t-test	 ^{ns}p = 0.7845 ^{ns}p = 0.5507
Method: 10 days. Raised at 29 °C. T-maze. OCT 1:100, MCH 1:100.				
Olfactory acuity: **OCT** 1) *atg5* RNAi / + 2) *ok107* > *atg5* RNAi Olfactory acuity: **MCH** 1) *atg5* RNAi / + 2) *ok107* > *atg5* RNAi	 22.63 ± 4.085 20.32 ± 5.798 24.59 ± 6.726 18.97 ± 5.136	 22.20 (9) 18.50 (5) 21.20 (13) 17.20 (11)	 unpaired t-test unpaired t-test	 ^{ns}p = 0.7457 ^{ns}p = 0.5258
Method: 10 days. Raised at 29 °C. T-maze and Tully Wheel. OCT 1:150, MCH 1:60.				
Olfactory acuity: **OCT** 1) *mb247*-Gal80 / + ;; *ok107*-Gal4 / + 2) *atg5* RNAi / + 3) *mb247*-Gal80 ;; *ok107*-Gal4 > *atg5* RNAi Olfactory acuity: **MCH** 1) *mb247*-Gal80 / + ;; *ok107*-Gal4 / + 2) *atg5* RNAi / + 3) *mb247*-Gal80 ;; *ok107*-Gal4 > *atg5* RNAi	 52.77 ± 4.117 44.03 ± 9.636 56.24 ± 5.648 57.93 ± 3.425 58.00 ± 8.286 42.31 ± 5.420	 54.30 (7) 48.65 (6) 58.05 (10) 58.75 (8) 58.80 (8) 43.20 (9)	 one-way ANOVA with Sidak's *post hoc* test one-way ANOVA with Sidak's *post hoc* test	 1-3: ^{ns}p = 0.9085 2-3: ^{ns}p = 0.3603 1-3: ^{ns}p = 0.1488 2-3: ^{ns}p = 0.1463
Method: 10 days. Raised at 29 °C. T-maze. OCT 1:100, MCH 1:100.				

Olfactory acuity: **OCT**				
1) *tub*-Gal80^{ts} / + ;; *ok107*-Gal4 / +	63.74 ± 10.86	55.90 (5)	one-way ANOVA with Sidak's *post hoc* test	1-3: $^{ns}p = 0.3860$ 2-3: $^{ns}p = 0.8662$
2) *atg5* RNAi / +	49.46 ± 9.698	55.85 (8)		
3) *tub*-Gal80^{ts} ;; *ok107*-Gal4 > *atg5* RNAi	42.23 ± 12.33	40.30 (6)		
Olfactory acuity: **MCH**				
1) *tub*-Gal80^{ts} / + ;; *ok107*-Gal4 / +	71.80 ± 9.503	62.70 (3)	Kruskal-Wallis with Dunn's *post hoc* test	1-3: $^{ns}p = 0.1766$ 2-3: $^{ns}p = 0.3806$
2) *atg5* RNAi / +	33.43 ± 5.040	31.70 (9)		
3) *tub*-Gal80^{ts} ;; *ok107*-Gal4 > *atg5* RNAi	46.20 ± 6.229	50.00 (7)		
Method: 10 days. Raised at 18 °C, after eclosion at 29 °C. T-maze. OCT 1:100 and MCH 1:100.				
Figure 55b: Short-term memory of 5-day old *elaV(X)*-Gal4 > UAS-*atg9* RNAi (BL # 34901)				
1) *atg9* RNAi / +	64.01 ± 3.409	65.00 (9)	unpaired t-test	$^{*}p = 0.0498$
2) *elaV(X)* > *atg9* RNAi	53.86 ± 3.374	51.60 (10)		
Method: 5 days. Raised at 29 °C. Tully Wheel: OCT 1:150, MCH 1:55. T-maze: OCT 1:150, MCH 1:75.				
Figure 55c: Short-term memory of *elaV(X)*-Gal4 > UAS-*atg9* RNAi (BL # 34901)				
1) *atg9* RNAi / +	51.84 ± 2.467	51.30 (17)	unpaired t-test	$^{*}p = 0.0103$
2) *elaV(X)* > *atg9* RNAi	37.95 ± 4.629	38.90 (15)		
Method: 10 days. Raised at 29 °C. Tully Wheel. OCT 1:150, MCH 1:60 and 1:55.				
Figure 55d: 1 hour Mid-term memory of *elaV(X)*-Gal4 > UAS-*atg9* RNAi (BL # 34901)				
1) *atg9* RNAi / +	53.23 ± 4.582	52.90 (13)	unpaired t-test	$^{*}p = 0.0267$
2) *elaV(X)* > *atg9* RNAi	40.22 ± 3.068	39.00 (13)		
Method: 10 days. Raised at 29 °C. T-maze (and Tully Wheel). OCT 1:150 and MCH 1:75, or OCT 1:100 and MCH 1:100.				
Figure 55e: 1 hour Anesthesia-resistant memory of *elaV(X)*-Gal4 > UAS-*atg9* RNAi (BL # 34901)				
1) *atg9* RNAi / +	25.47 ± 4.083	22.00 (11)	unpaired t-test	$^{ns}p = 0.6757$
2) *elaV(X)* > *atg9* RNAi	27.81 ± 3.455	27.40 (9)		
Method: 10 days. Raised at 29 °C. T-maze. OCT 1:100, MCH 1:100.				

Figure 55f: 1 hour Anesthesia-sensitive memory of *elaV(X)*-Gal4 > UAS-*atg9* RNAi (BL # 34901)				
1) *atg9* RNAi / +	27.43 ± 4.083	30.90 (11)	unpaired t-test	$^{**}p = 0.0085$
2) *elaV(X)* > *atg9* RNAi	11.19 ± 3.455	11.60 (9)		
Method: ASM values were calculated as the MTM median minus the particular ARM values.				
Table 6: Innate behavior of *elaV(X)*-Gal4 > UAS-*atg9* RNAi (BL # 34901)				
Shock reactivity:				
1) *atg9* RNAi / +	88.62 ± 2.648	89.70 (6)	unpaired t-test	$^{ns}p = 0.3412$
2) *elaV(X)* > *atg9* RNAi	85.14 ± 2.302	85.85 (8)		
Olfactory acuity: **OCT**				
1) *atg9* RNAi / +	27.26 ± 3.823	24.40 (14)	unpaired t-test	$^{ns}p = 0.4809$
2) *elaV(X)* > *atg9* RNAi	23.34 ± 3.853	23.30 (17)		
Olfactory acuity: **MCH**				
1) *atg9* RNAi / +	50.28 ± 8.450	52.00 (10)	unpaired t-test	$^{ns}p = 0.9190$
2) *elaV(X)* > *atg9* RNAi	49.11 ± 7.583	58.80 (13)		
Method: 10 days. Raised at 29 °C. Tully Wheel. OCT 1:150, MCH 1:60.				
Figure 56b: Short-term memory of *gh146* > UAS-*atg9* RNAi (BL # 34901)				
1) *atg9* RNAi / +	51.97 ± 7.183	54.65 (8)	unpaired t-test	$^{ns}p = 0.2231$
2) *gh146* > *atg9* RNAi	61.57 ± 3.636	63.10 (10)		
Method: 10 days. Raised at 29 °C. T-maze and Tully Wheel. OCT 1:150, MCH 1:55 and 1:75.				
Figure 57a: Short-term memory of 5-day old *vt030559*-Gal4 > UAS-*atg9* RNAi (BL # 34901)				
1) *vt030559* / +	48.48 ± 2.980	46.30 (8)	one-way ANOVA with Sidak's *post hoc* test	1-3: $^{*}p = 0.0371$ 2-3: $^{**}p = 0.0091$
2) *atg9* RNAi / +	54.26 ± 5.380	54.40 (5)		
3) *vt030559* > *atg9* RNAi	34.98 ± 3.986	33.70 (8)		
Method: 5 days. Raised at 29 °C. T-maze. OCT 1:100, MCH 1:100.				
Figure 57b: Short-term memory of 10-day old *vt030559*-Gal4 > UAS-*atg9* RNAi (BL # 34901)				
1) *vt030559* / +	47.25 ± 1.344	46.30 (4)	one-way ANOVA with Sidak's *post hoc* test	1-3: $^{*}p = 0.0212$ 2-3: $^{**}p = 0.0026$
2) *atg9* RNAi / +	45.30 ± 2.222	43.85 (16)		
3) *vt030559* > *atg9* RNAi	35.81 ± 1.679	37.00 (15)		
Method: 10 days. Raised at 29 °C. T-maze and Tully Wheel. OCT 1:100, MCH 1:100.				

Figure 58d: 1 hour Mid-term memory of *ok107*-Gal4 > UAS-*atg9* RNAi (BL # 34901)				
1) *atg9* RNAi / +	54.27 ± 5.316	52.90 (11)	unpaired t-test	*p = 0.0175
2) *ok107* > *atg9* RNAi	39.35 ± 3.263	39.40 (17)		
Method: 10 days. Raised at 29 °C. T-maze (and Tully Wheel). OCT 1:150 and MCH 1:75, or OCT 1:100 and MCH 1:100.				
Figure 58e: 1 hour Anesthesia-resistant memory of *ok107*-Gal4 > UAS-*atg9* RNAi (BL # 34901)				
1) *atg9* RNAi / +	23.38 ± 3.468	22.00 (15)	unpaired t-test	^{ns}p = 0.5349
2) *ok107* > *atg9* RNAi	20.86 ± 2.197	19.90 (17)		
Method: 10 days. Raised at 29 °C. T-maze. OCT 1:150 and MCH 1:75, or OCT 1:100 and MCH 1:100.				
Figure 58f: 1 hour Anesthesia-sensitive memory of *ok107*-Gal4 > UAS-*atg9* RNAi (BL # 34901)				
1) *atg9* RNAi / +	29.52 ± 3.468	30.90 (15)	unpaired t-test	*p = 0.0102
2) *ok107* > *atg9* RNAi	18.54 ± 2.197	19.50 (17)		
Method: ASM values were calculated as the MTM median minus the particular ARM values.				
Figure 59: Short-term memory of *ilp2*-Gal4 > UAS-*atg9* RNAi (BL # 34901)				
1) *atg9* RNAi / +	52.78 ± 4.254	53.70 (11)	unpaired t-test	^{ns}p = 0.0597
2) *ilp2* > *atg9* RNAi	63.73 ± 2.411	62.45 (8)		
Method: 10 days. Raised at 29 °C. T-maze and Tully Wheel. OCT 1:100, MCH 1:100.				
Figure 60: Short-term memory of *gmr*-Gal4 > UAS-*atg9* RNAi (BL # 34901)				
1) *atg9* RNAi / +	50.85 ± 4.077	45.10 (12)	unpaired t-test	^{ns}p = 0.2302
2) *gmr* > *atg9* RNAi	57.28 ± 3.317	56.50 (13)		
Method: 10 days. Raised at 29 °C. T-maze and Tully Wheel. OCT 1:100, MCH 1:100.				
Figure 61a: Short-term memory of *mb147*-Gal80 ;; *ok107*-Gal4 > UAS-*atg9* RNAi (BL # 34901)				
1) *mb247*-Gal80 / + ;; *ok107*-Gal4 / +	55.33 ± 4.366	53.70 (10)	one-way ANOVA with	1-3: *p = 0.0149 2-3: ^{ns}p = 0.9347
2) *atg9* RNAi / +	41.29 ± 2.351	41.60 (14)		

3) *mb247*-Gal80 ;; *ok107*-Gal4 > *atg9* RNAi	42.63 ± 2.788	44.40 (16)	Sidak's *post hoc* test	
Method: 10 days. Raised at 29 °C. T-maze and Tully Wheel. OCT 1:100, MCH 1:100.				
Figure 61b: 1 hour Mid-term memory of *mb147*-Gal80 ;; *ok107*-Gal4 > UAS-*atg9* RNAi (BL # 34901)				
1) *mb247*-Gal80 / + ;; *ok107*-Gal4 / +	53.34 ± 3.424	50.20 (14)	one-way ANOVA with Sidak's *post hoc* test	1-3: ***p = 0.0005 2-3: ^{ns}p = 0.1581
2) *atg9* RNAi / +	42.50 ± 4.061	42.40 (9)		
3) *mb247*-Gal80 ;; *ok107*-Gal4 > *atg9* RNAi	32.79 ± 1.505	33.85 (8)		
Method: 10 days. Raised at 29 °C. T-maze. OCT 1:100, MCH 1:100.				
Figure 62a: Short-term memory of 5-day old *mb247*-Gal4 > UAS-*atg9* RNAi (BL # 34901)				
1) *atg9* RNAi / +	64.60 ± 6.901	62.40 (3)	unpaired t-test	^{ns}p = 0.4171
2) *mb247* > *atg9* RNAi	72.33 ± 5.055	73.90 (3)		
Method: 5 days. Raised at 29 °C. T-maze and Tully Wheel. OCT 1:150, MCH 1:55 or 1:75.				
Figure 62b: Short-term memory of 10-day old *mb247*-Gal4 > UAS-*atg9* RNAi (BL # 34901)				
1) *atg9* RNAi / +	51.97 ± 7.183	54.65 (8)	unpaired t-test	^{ns}p = 0.3236
2) *mb247* > *atg9* RNAi	59.87 ± 4.124	60.40 (11)		
Method: 10 days. Raised at 29 °C. T-maze and Tully Wheel. OCT 1:150, MCH 1:55 or 1:75.				
Figure 63a: Short-term memory of *tub*-Gal80^{ts} ;; *ok107*-Gal4 > UAS-*atg9* RNAi (BL # 34901)				
1) *tub*-Gal80^{ts} / + ;; *ok107*-Gal4 / +	40.03 ± 3.146	42.35 (12)	one-way ANOVA with Sidak's *post hoc* test	1-3: ^{ns}p = 0.2743 2-3: ^{ns}p = 0.2040
2) *atg9* RNAi / +	29.22 ± 2.856	25.10 (11)		
3) *tub*-Gal80^{ts} ;; *ok107*-Gal4 > *atg9* RNAi	35.00 ± 1.847	35.40 (20)		
Method: 10 days. Raised at 29 °C. T-maze and Tully Wheel. OCT 1:100, MCH 1:100.				

Figure 63b: 1 hour Mid-term memory of *tub*-Gal80^{ts} ;; *ok107*-Gal4 > UAS-*atg9* RNAi (BL # 34901)				
1) *tub*-Gal80^{ts} / + ;; *ok107*-Gal4 / +	30.75 ± 2.670	32.50 (13)	one-way ANOVA with Sidak's *post hoc* test	1-3: $^{ns}p = 0.2067$ 2-3: $^{ns}p = 0.9997$
2) *atg9* RNAi / +	37.03 ± 2.736	39.95 (14)		
3) *tub*-Gal80^{ts} ;; *ok107*-Gal4 > *atg9* RNAi	37.11 ± 2.751	34.60 (18)		
Method: 10 days. Raised at 18 °C, after eclosion at 29 °C. T-maze. OCT 1:100, MCH 1:100.				
Table 7: Innate behavior of *atg9* knockdown in specific neuronal areas (BL # 34901)				
Olfactory acuity: **OCT**				
1) *atg9* RNAi / +	22.74 ± 5.672	28.60 (17)	unpaired t-test	$^{ns}p = 0.8905$
2) *gh146* > *atg9* RNAi	23.84 ± 5.540	19.10 (16)		
Olfactory acuity: **MCH**				
1) *atg9* RNAi / +	36.55 ± 5.867	36.50 (22)	unpaired t-test	$^{ns}p = 0.6661$
2) *gh146* > *atg9* RNAi	33.17 ± 4.863	37:20 (19)		
Method. 10 days. Raised at 29 °C. T-maze. OCT 1:100, MCH 1:00.				
Olfactory acuity: **OCT**				
1) *atg9* RNAi / +	27.26 ± 3.823	24.40 (14)	unpaired t-test	$^{ns}p = 0.4809$
2) *ok107* > *atg9* RNAi	33.79 ± 5.352	23.30 (17)		
Olfactory acuity: **MCH**				
1) *atg9* RNAi / +	50.28 ± 8.450	52.00 (10)	unpaired t-test	$^{ns}p = 0.9190$
2) *ok107* > *atg9* RNAi	49.11 ± 7.583	58.80 (13)		
Method: 10 days. Raised at 29 °C. Tully Wheel. OCT 1:150, MCH 1:60				
Olfactory acuity: **OCT**				
1) *atg9* RNAi / +	31.64 ± 7.345	32.20 (14)	unpaired t-test	$^{ns}p = 0.5546$
2) *ilp2* > *atg9* RNAi	37.08 ± 5.098	33.30 (13)		
Olfactory acuity: **MCH**				
1) *atg9* RNAi / +	27.25 ± 7.087	28.50 (14)	unpaired t-test	$^{ns}p = 0.4940$
2) *ilp2* > *atg9* RNAi	33.94 ± 6.010	31.10 (11)		
Method: 10 days. Raised at 29 °C. T-maze. OCT 1:100, MCH 1:100.				

Olfactory acuity: **OCT**				
1) *mb247*-Gal80 / + ;; *ok107*-Gal4 / +	62.03 ± 3.664	61.55 (8)	one-way ANOVA with Sidak's *post hoc* test	1-3: $^{*}p = 0.0103$
2) *atg9* RNAi / +	55.01 ± 4.433	55.00 (9)		2-3: $^{ns}p = 0.0882$
3) *mb247*-Gal80 ;; *ok107*-Gal4 > *atg9* RNAi	41.14 ± 4.401	45.90 (5)		
Olfactory acuity: **MCH**				
1) *mb247*-Gal80 / + ;; *ok107*-Gal4 / +	80.33 ± 5.647	85.60 (8)	Kruskal-Wallis with Dunn's *post hoc* test	1-3: $^{*}p = 0.0418$
2) *atg9* RNAi / +	73.10 ± 5.499	73.30 (9)		2-3: $^{ns}p = 0.2785$
3) *mb247*-Gal80 ;; *ok107*-Gal4 > *atg9* RNAi	54.74 ± 8.696	53.30 (5)		
Method: 10 days. Raised at 29 °C. T-maze. OCT 1:100, MCH 1:100.				
Olfactory acuity: **OCT**				
1) *tub*-Gal80^{ts} / + ;; *ok107*-Gal4 / +	74.78 ± 10.05	81.30 (5)	Kruskal-Wallis with Dunn's *post hoc* test	1-3: $^{ns}p = 0.4596$
2) *atg9* RNAi / +	61.97 ± 3.831	63.30 (9)		2-3: $^{ns}p = 0.3677$
3) *tub*-Gal80^{ts} ;; *ok107*-Gal4 > *atg9* RNAi	68.51 ± 1.808	70.25 (10)		
Olfactory acuity: **MCH**				
1) *tub*-Gal80^{ts} / + ;; *ok107*-Gal4 / +	78.16 ± 6.858	85.50 (7)	Kruskal-Wallis with Dunn's *post hoc* test	1-3: $^{ns}p = 0.1863$
2) *atg9* RNAi / +	57.13 ± 9.724	48.30 (9)		2-3: $^{ns}p > 0.9999$
3) *tub*-Gal80^{ts} ;; *ok107*-Gal4 > *atg9* RNAi	66.50 ± 6.313	74.60 (8)		
Method: 10 days. Raised at 18 °C, after eclosion at 29 °C. T-maze. OCT 1:100, MCH 1:100.				
Figure 64: Short-term memory of *ok107*-Gal4 > UAS-*atg1* overexpression (BL # 51655)				
1) *ok107* / +	58.91 ± 4.174	58.95 (8)	Mann-Whitney test	$^{ns}p = 0.1893$
2) *ok107* > *atg1* OE	37.94 ± 11.88	20.00 (7)		
Method: 5 days. Raised at 29 °C. T-maze and Tully Wheel. OCT 1:100, MCH 1:100.				
Figure 66c: Short-term memory of *sNPF^{c00448}* (BL # 85000)				
1) *w^{1118}*	66.42 ± 2.355	57.50 (13)	unpaired t-test	$^{**}p = 0.0017$
2) *sNPF^{c00448}*	55.18 ± 2.091	57.50 (12)		
Method: 5 days. Raised at 25 °C. T-maze and Tully Wheel. OCT 1:100, MCH 1:100.				

Figure 66d: 1 hour Mid-term memory of *sNPF^{c00448}* (BL # 85000)				
1) *w^{1118}*	60.29 ± 4.203	62.45 (14)	unpaired t-test	**p* = 0.0100
2) *sNPF^{c00448}*	44.37 ± 3.828	44.37 (13)		
Method: 5 days. Raised at 25 °C. T-maze. OCT 1:100, MCH 1:100.				
Figure 66e: 1 hour Anesthesia-resistant memory of *sNPF^{c00448}* (BL # 85000)				
1) *w^{1118}*	26.07 ± 3.016	32.30 (13)	unpaired t-test	^{ns}p = 0.3684
2) *sNPF^{c00448}*	23.01 ± 1.163	23.00 (12)		
Method: 5 days. Raised at 25 °C. T-maze. OCT 1:100, MCH 1:100.				
Figure 66f: 1 hour Anesthesia-sensitive memory of *sNPF^{c00448}* (BL # 85000)				
1) *w^{1118}*	36.38 ± 3.016	30.15 (13)	unpaired t-test	****p* = 0.0002
2) *sNPF^{c00448}*	21.36 ± 1.163	21.37 (12)		
Method: ASM values were calculated as the MTM median minus the particular ARM values.				
Table 8: Innate behavior of *sNPF^{c00448}* (BL # 85000)				
Olfactory acuity: **OCT**				
1) *w^{1118}*	33.21 ± 6.258	35.10 (17)	unpaired t-test	*****p* < 0.0001
2) *sNPF^{c00448}*	-4.118 ±4.783	-1.600 (17)		
Olfactory acuity: **MCH**				
1) *w^{1118}*	48.33 ± 3.852	47.80 (12)	unpaired t-test	***p* = 0.0014
2) *sNPF^{c00448}*	27.83 ± 4.110	30.90 (11)		
Method: 5 days. Raised at 25 °C. T-maze. OCT 1:100, MCH 1:100.				
Chapter II.2.5.1: Short-term memory of *ok107*-Gal4 > UAS- *sNPF* RNAi				
1) *ok107* / +	53.55 ± 1.667	54.15 (12)	one-way ANOVA with Sidak's *post hoc* test	
2) *sNPF* RNAi / +	49.82 ± 3.158	52.80 (9)		1-3: ^{ns}p = 0.3602 2-3: ^{ns}p = 0.9508
3) *ok107* > *sNPF* RNAi	48.67 ± 3.137	50.30 (14)		
Method: 10 days. Raised at 29 °C. Tully Wheel. OCT 1:100, MCH 1:100.				

Chapter II.2.5.1: 1 hour Mid-term memory of *ok107*-Gal4 > UAS- *sNPF* RNAi				
1) *ok107* / +	65.73 ± 0.367	66.10 (3)	one-way ANOVA with Sidak's *post hoc* test	1-3: $^{ns}p = 0.0825$ 2-3: $^{ns}p = 0.7577$
2) *sNPF* RNAi / +	50.08 ± 3.307	50.95 (6)		
3) *ok107* > *sNPF* RNAi	53.14 ± 3.381	53.00 (8)		
Method: 10 days. Raised at 29 °C. T-maze. OCT 1:100, MCH 1:100.				
Figure 67c: Short-term memory of *ok107*-Gal4 > UAS- *sNPF R RNAi*				
1) *sNPF R* RNAi / +	49.58 ± 3.229	47.35 (10)	unpaired t-test	****$p < 0.0001$
2) *ok107* > *sNPF R* RNAi	20.83 ± 2.715	23.20 (10)		
Method: 10 days. Raised at 29 °C. T-maze and Tully Wheel. OCT 1:100, MCH 1:100.				
Figure 67d: 1 hour Mid-term memory of *ok107*-Gal4 > UAS- *sNPF R RNAi*				
1) *ok107* / +	43.73 ± 3.103	44.00 (4)	one-way ANOVA with Sidak's *post hoc* test	1-3: **$p = 0.0011$ 2-3: ****$p < 0.0001$
2) *sNPF R* RNAi / +	53.54 ± 4.257	51.50 (13)		
3) *ok107* > *sNPF R* RNAi	18.77 ± 2.204	16.25 (18)		
Method: 10 days. Raised at 29 °C. T-maze. OCT 1:100, MCH 1:100.				
Figure 67e: 1 hour Anesthesia-resistant memory of *ok107*-Gal4 > UAS- *sNPF R RNAi*				
1) *ok107* / +	21.84 ± 3.597	21.60 (8)	one-way ANOVA with Sidak's *post hoc* test	1-3: $^{ns}p = 0.2738$ 2-3: $^{ns}p = 0.0976$
2) *sNPF R* RNAi / +	23.22 ± 2.615	23.50 (11)		
3) *ok107* > *sNPF R* RNAi	16.30 ± 1.882	15.85 (14)		
Method: 10 days. Raised at 29 °C. T-maze. OCT 1:100, MCH 1:100.				
Figure 67f: 1 hour Anesthesia-sensitive memory of *ok107*-Gal4 > UAS- *sNPF R RNAi*				
1) *ok107* / +	22.16 ± 3.597	22.40 (8)	one-way ANOVA with Sidak's *post hoc* test	1-3: ****$p < 0.0001$ 2-3: ****$p < 0.0001$
2) *sNPF R* RNAi / +	28.28 ± 2.615	28.00 (11)		
3) *ok107* > *sNPF R* RNAi	-0.0533 ± 1.752	0.250 (15)		
Method: ASM values were calculated as the MTM median minus the particular ARM values.				

Figure 68a: Short-term memory of *vt030559*-Gal4 > UAS- *sNPF R* RNAi				
1) *sNPF R* RNAi / +	45.54 ± 2.835	43.30 (14)	unpaired t-test	****$p < 0.0001$
2) *vt030559* > *sNPF R* RNAi	24.59 ± 2.484	24.95 (12)		
Method: 10 days. Raised at 29 °C. T-maze and Tully Wheel. OCT 1:100, MCH 1:100.				
Figure 68b: 1 hour Mid-term memory of *vt030559*-Gal4 > UAS- *sNPF R* RNAi				
1) *sNPF R* RNAi / +	35.98 ± 2.904	34.60 (22)	unpaired t-test	**$p = 0.0010$
2) *vt030559* > *sNPF R* RNAi	23.20 ± 2.273	22.10 (26)		
Method: 10 days. Raised at 29 °C. T-maze. OCT 1:100, MCH 1:100.				
Figure 68c: 1 hour Anesthesia-resistant memory of *vt030559*-Gal4 > UAS- *sNPF R* RNAi				
1) *sNPF R* RNAi / +	13.24 ± 1.929	13.00 (21)	unpaired t-test	$^{ns}p = 0.6828$
2) *vt030559* > *sNPF R* RNAi	14.38 ± 1.967	15.90 (18)		
Method: 10 days. Raised at 29 °C. T-maze. OCT 1:100, MCH 1:100.				
Figure 68d: 1 hour Anesthesia-sensitive memory of *vt030559*-Gal4 > UAS- *sNPF R* RNAi				
1) *sNPF R* RNAi / +	21.36 ± 1.929	21.60 (21)	unpaired t-test	****$p < 0.0001$
2) *vt030559* > *sNPF R* RNAi	7.722 ± 1.967	6.20 (18)		
Method: ASM values were calculated as the MTM median minus the particular ARM values.				
Figure 69: Short-term memory of *ilp2*-Gal4 > UAS- *sNPF R* RNAi				
1) *sNPF R* RNAi / +	46.91 ± 4.033	44.60 (21)	Mann-Whitney test	$^{ns}p = 0.4284$
2) *vt030559* > *sNPF R* RNAi	46.39 ± 4.684	51.70 (21)		
Method: 10 days. Raised at 29 °C. T-maze and Tully Wheel. OCT 1:100, MCH 1:100.				
Figure 70a: Short-term memory of *mb247*-Gal80 ;; *ok107*-Gal4 > UAS- *sNPF R* RNAi				
1) *mb247*-Gal80 / + ;; *ok107*-Gal4 / +	53.52 ± 3.044	53.50 (11)	one-way ANOVA with Sidak's *post hoc* test	1-3: *$p = 0.0169$ 2-3: $^{ns}p = 0.5558$
2) *sNPF R* RNAi / +	46.02 ± 3.208	43.00 (13)		
3) *mb247*-Gal80 ;; *ok107*-Gal4 > *sNPF R* RNAi	42.22 ± 2.323	41.80 (15)		
Method: 10 days. Raised at 29 °C. T-maze and Tully Wheel. OCT 1:100, MCH 1:100.				

Figure 70b: 1 hour Mid-term memory of *mb247*-Gal80 ;; *ok107*-Gal4 > UAS- *sNPF R* RNAi				
1) *mb247*-Gal80 / + ;; *ok107*-Gal4 / +	38.23 ± 3.366	38.75 (16)	one-way ANOVA with Sidak's *post hoc* test	1-3: $^{ns}p = 0.1464$ 2-3: $^{ns}p = 0.2469$
2) *sNPF R* RNAi / +	36.78 ± 2.518	34.80 (19)		
3) *mb247*-Gal80 ;; *ok107*-Gal4 > *sNPF R* RNAi	30.58 ± 2.843	30.55 (16)		
Method: 10 days. Raised at 29 °C. T-maze. OCT 1:100, MCH 1:100.				
Figure 70c: 1 hour Anesthesia-resistant memory of *mb247*-Gal80 ;; *ok107*-Gal4 > UAS- *sNPF R* RNAi				
1) *mb247*-Gal80 / + ;; *ok107*-Gal4 / +	18.47 ± 1.610	17.60 (21)	one-way ANOVA with Sidak's *post hoc* test	1-3: $^{ns}p = 0.7944$ 2-3: $^{ns}p = 0.3733$
2) *sNPF R* RNAi / +	13.24 ± 1.929	13.00 (21)		
3) *mb247*-Gal80 ;; *ok107*-Gal4 > *sNPF R* RNAi	16.78 ± 2.313	18.10 (19)		
Method: 10 days. Raised at 29 °C. T-maze. OCT 1:100, MCH 1:100.				
Figure 70d: 1 hour Anesthesia-sensitive memory of *mb247*-Gal80 ;; *ok107*-Gal4 > UAS- *sNPF R* RNAi				
1) *mb247*-Gal80 / + ;; *ok107*-Gal4 / +	12.08 ± 1.610	12.95 (21)	one-way ANOVA with Sidak's *post hoc* test	1-3: $^{**}p = 0.0015$ 2-3: $^{ns}p = 0.9865$
2) *sNPF R* RNAi / +	21.56 ± 1.929	21.80 (21)		
3) *mb247*-Gal80 ;; *ok107*-Gal4 > *sNPF R* RNAi	21.97 ± 2.313	20.65 (19)		
Method: ASM values were calculated as the MTM median minus the particular ARM values.				
Figure 71: Short-term memory of *tub*-Gal80^{ts} ;; *ok107*-Gal4 > UAS- *sNPF R* RNAi				
1) *tub*-Gal80^{ts} / + ;; *ok107*-Gal4 / +	27.71 ± 3.368	23.60 (15)	one-way ANOVA with Sidak's *post hoc* test	1-3: $^{ns}p = 0.1676$ 2-3: $^{ns}p = 0.3228$
2) *sNPF R* RNAi / +	25.80 ± 2.861	27.75 (18)		
3) *tub*-Gal80^{ts} ;; *ok107*-Gal4 > *sNPF R* RNAi	20.11 ± 2.861	20.50 (18)		
Method: 10 days. Raised at 29 °C. T-maze and Tully Wheel. OCT 1:100, MCH 1:100.				

Table 9: Innate behavior of *sNPF* receptor knockdown in different areas				
Replicate 1				
Olfactory acuity: **OCT**				
1) *sNPF R* RNAi / +	70.44 ± 3.513	68.80 (17)	unpaired t-test	****$p < 0.0001$
2) *ok107 > sNPF R* RNAi	37.40 ± 3.636	34.75 (22)		
Olfactory acuity: **MCH**				
1) *sNPF R* RNAi / +	87.04 ± 2.267	88.20 (12)	unpaired t-test	***$p = 0.0005$
2) *ok107 > sNPF R* RNAi	59.03 ± 4.683	62.35 (28)		
Method: 10 days. Raised at 29 °C. T-maze. OCT 1:100, MCH 1:100.				
Replicate 2				
Olfactory acuity: **OCT**				
1) *sNPF R* RNAi / +	72.00 ± 8.729	80.75 (8)	unpaired t-test	***$p = 0.0009$
2) *ok107 > sNPF R* RNAi	24.71 ± 7.449	31.60 (9)		
Olfactory acuity: **MCH**				
1) *sNPF R* RNAi / +	88.22 ± 1.790	85.90 (9)	unpaired t-test	****$p < 0.0001$
2) *ok107 > sNPF R* RNAi	40.14 ± 4.157	35.20 (9)		
Method: 10 days. Raised at 29 °C. T-maze. OCT 1:100, MCH 1:100.				
Olfactory acuity: **OCT**				
1) *sNPF R* RNAi / +	70.33 ± 5.857	69.60 (12)	unpaired t-test	***$p = 0.0009$
2) *vt030559 > sNPF R* RNAi	36.94 ± 6.466	37.30 (12)		
Olfactory acuity: **MCH**				
1) *sNPF R* RNAi / +	76.08 ± 4.885	83.35 (14)	unpaired t-test	*$p = 0.0277$
2) *vt030559 > sNPF R* RNAi	53.26 ± 8.863	61.90 (12)		
Method: 10 days. Raised at 29 °C. T-maze. OCT 1:100, MCH 1:100.				
Olfactory acuity: **OCT**				
1) *sNPF R* RNAi / +	60.39 ± 5.068	61.20 (9)	unpaired t-test	$^{ns}p = 0.2469$
2) *ilp2 > sNPF R* RNAi	49.50 ± 6.892	53.10 (12)		
Olfactory acuity: **MCH**				
1) *sNPF R* RNAi / +	93.88 ± 1.076	94.55 (8)	unpaired t-test	*$p = 0.0319$
2) *ilp2 > sNPF R* RNAi	86.66 ± 2.830	85.70 (8)		
Method: 10 days. Raised at 29 °C. T-maze. OCT 1:100, MCH 1:100.				

Olfactory acuity: **OCT**				
1) *mb247*-Gal80 / + ;; *ok107*-Gal4 / +	54.87 ± 7.412	50.30 (10)	one-way ANOVA with Sidak's *post hoc* test	1-3: $^{ns}p = 0.3584$ 2-3: $^{ns}p = 0.3389$
2) *sNPF R* RNAi / +	57.13 ± 5.541	61.50 (7)		
3) *mb247*-Gal80 ;; *ok107*-Gal4 > *sNPF R* RNAi	39.01 ± 10.41	32.40 (12)		
Olfactory acuity: **MCH**				
1) *mb247*-Gal80 / + ;; *ok107*-Gal4 / +	63.94 ± 7.238	67.85 (10)	one-way ANOVA with Sidak's *post hoc* test	1-3: $^{ns}p = 0.0800$ 2-3: $^{ns}p = 0.0865$
2) *sNPF R* RNAi / +	65.40 ± 6.073	62.50 (8)		
3) *mb247*-Gal80 ;; *ok107*-Gal4 > *sNPF R* RNAi	33.02 ± 13.41	36.85 (12)		
Method: 10 days. Raised at 29 °C. T-maze. OCT 1:100, MCH 1:100.				
Olfactory acuity **OCT**				
1) *tub*-Gal80^{ts} / + ;; *ok107*-Gal4 / +	79.16 ± 4.305	82.90 (14)	Kruskal-Wallis with Dunn's *post hoc* test	1-3: $^{ns}p = 0.9778$ 2-3: $^{ns}p = 0.9519$
2) *sNPF R* RNAi / +	67.02 ± 5.510	64.50 (16)		
3) *tub*-Gal80^{ts} ;; *ok107*-Gal4 > *sNPF R* RNAi	73.55 ± 5.054	77.10 (13)		
Olfactory acuity: **MCH**				
1) *tub*-Gal80^{ts} / + ;; *ok107*-Gal4 / +	70.43 ± 7.699	82.80 (16)	Kruskal-Wallis with Dunn's *post hoc* test	1-3: $^{ns}p > 0.9999$ 2-3: $^{ns}p = 0.8625$
2) *sNPF R* RNAi / +	69.30 ± 6.143	69.55 (16)		
3) *tub*-Gal80^{ts} ;; *ok107*-Gal4 > *sNPF R* RNAi	82.03 ± 4.681	89.50 (13)		
Method: 10 days. Raised at 29 °C. T-maze. OCT 1:100, MCH 1:100.				
Figure 72a: Short-term memory for 10-day old *ok107 > sNPF* overexpression				
1) *sNPF* OE / +	58.20 ± 6.239	67.50 (4)	unpaired t-test	$^{**}p = 0.0010$
2) *ok107 > sNPF* OE	34.39 ± 2.662	49.20 (13)		
Method: 10 days. Raised at 29 °C. T-maze. OCT 1:100 and MCH 1:100.				

Figure 72b: 1 hour Mid-term memory of *ok107 > sNPF* overexpression				
1) *sNPF* OE / + (5 days)	67.20 ± 3.554	63.30 (9)	two-way ANOVA with Sidak's *post hoc* test	days: 1-2: $^{ns}p = 0.0841$ 3-4: $^{ns}p = 0.2039$ 5-6: $^{*}p = 0.0285$ *sNPF* OE / +: 1-3: $^{ns}p = 0.0745$ 1-5: $^{****}p < 0.0001$ 3-5: $^{ns}p = 0.5851$ *ok107 > sNPF* OE: 2-4: $^{**}p = 0.0090$ 2-6: $^{****}p < 0.0001$ 4-6: $^{ns}p = 0.8149$
2) *ok107 > sNPF* OE (5 days)	57.21 ± 3.080	55.15 (16)		
3) *sNPF* OE / + (10 days)	52.45 ± 1.932	51.65 (4)		
4) *ok107 > sNPF* OE (10 days)	38.65 ± 2.521	37.65 (4)		
5) *sNPF* OE / + (20 days)	45.26 ± 2.944	44.00 (11)		
6) *ok107 > sNPF* OE (20 days)	33.87 ± 2.911	35.90 (15)		
Two-way ANOVA: Interaction: $^{ns}p = 0.9077$; Row Factor: $^{****}p < 0.0001$; Column Factor: $^{***}p = 0.0007$				
Method: 5, 10, and 20 days. Raised at 29 °C. T-maze. OCT 1:100 and MCH 1:100.				
Figure 72c: 1 hour Anesthesia-resistant memory of 20-day old *ok107 > sNPF* overexpression				
1) *ok107* / +	18.11 ± 2.771	17.80 (15)	Kruskal-Wallis with Dunn's *post hoc* test	1-3: $^{ns}p > 0.9999$ 2-3: $^{ns}p > 0.9999$
2) *sNPF* OE / +	16.82 ± 2.659	16.60 (17)		
3) *ok107 > sNPF* OE	18.03 ± 3.496	14.30 (18)		
Method: 20 days. Raised at 29 °C. T-maze. OCT 1:100 and MCH 1:100.				
Figure 72d: 1 hour Anesthesia-resistant memory of 20-day old *ok107 > sNPF* overexpression				
1) *ok107* / +	17.54 ± 2.771	17.85 (15)	Kruskal-Wallis with Dunn's *post hoc* test	1-3: $^{ns}p = 0.9039$ 2-3: $^{ns}p = 0.1858$
2) *sNPF* OE / +	27.18 ± 2.659	27.40 (17)		
3) *ok107 > sNPF* OE	17.87 ± 3.496	21.60 (18)		
Method: ASM values were calculated as the MTM median minus the particular ARM values.				

Figure 73a: 1 hour Mid-term memory for two copies *sNPF* overexpression in the mushroom body				
1) *sNPF* OE / + ; *sNPF* OE / + (5 days)	46.10 ± 2.410	47.00 (23)	two-way ANOVA with Sidak's *post hoc* test	days: 1-2: $^{**}p = 0.0033$ 3-4: $^{ns}p = 0.1404$ 5-6: $^{ns}p = 0.0535$ 2x *sNPF* OE / +: 1-3: $^{ns}p = 0.5063$ 1-5: $^{ns}p = 0.5228$ 3-5: $^{ns}p = 0.9996$ *ok107* > 2x *sNPF* OE: 2-4: $^{ns}p = 0.8652$ 2-6: $^{ns}p = 0.9250$ 4-6: $^{ns}p = 0.9996$
2) *ok107* > *sNPF* OE ; *sNPF* OE (5 days)	32.87 ± 4.220	32.30 (18)		
3) *sNPF* OE / + ; *sNPF* OE / + (10 days)	40.64 ± 2.804	40.60 (13)		
4) *ok107* > *sNPF* OE ; *sNPF* OE (10 days)	29.00 ± 4.742	31.20 (7)		
5) *sNPF* OE / + ; *sNPF* OE / + (20 days)	41.08 ± 2.857	30.10 (16)		
6) *ok107* > *sNPF* OE / + ; *sNPF* OE / + (20 days)	30.48 ± 1.995	31.90 (16)		
Two-way ANOVA: Interaction: $^{ns}p = 0.9029$; Row Factor: $^{ns}p = 0.3002$; Column Factor: $^{****}p < 0.0001$				
Method: 5, 10, and 20 days. Raised at 29 °C. T-maze. OCT 1:100 and MCH 1:100.				
Figure 73b: 1 hour Anesthesia-resistant memory for two copies *sNPF* overexpression in the mushroom body				
1) *sNPF* OE / + ; *sNPF* OE / + (5 days)	27.90 ± 2.352	26.35 (20)	two-way ANOVA with Sidak's *post hoc* test	1-3: $^{***}p = 0.0003$ 2-4: $^{****}p < 0.0001$ 1-2: $^{ns}p = 0.9910$ 3-4: $^{ns}p = 0.2603$
2) *ok107* > *sNPF* OE ; *sNPF* OE (5 days)	28.27 ± 2.460	29.50 (21)		
3) *sNPF* OE / + ; *sNPF* OE / + (20 days)	16.15 ± 2.096	16.90 (25)		
4) *ok107* > *sNPF* OE ; *sNPF* OE (20 days)	11.81 ± 1.348	9.800 (21)		
Two-way ANOVA: Interaction: $^{ns}p = 0.2696$; Row Factor: $^{****}p < 0.0001$; Column Factor: $^{ns}p = 0.3507$				
Method: 5 and 20 days. Raised at 29 °C. T-maze. OCT 1:100 and MCH 1:100.				

Figure 73c: 1 hour Anesthesia-sensitive memory for two copies *sNPF* overexpression in the mushroom body				
1) *sNPF* OE / + ; *sNPF* OE / + (5 days)	19.11 ± 2.351	20.65 (20)	two-way ANOVA with Sidak's *post hoc* test	1-3: $^{ns}p = 0.5634$ 2-4: $^{****}p < 0.0001$ 1-2: $^{****}p < 0.0001$ 3-4: $^{ns}p = 0.7748$
2) *ok107 > sNPF* OE ; *sNPF* OE (5 days)	4.033 ± 2.460	2.800 (21)		
3) *sNPF* OE / + ; *sNPF* OE / + (20 days)	21.95 ± 2.096	21.20 (25)		
4) *ok107 > sNPF* OE ; *sNPF* OE (20 days)	20.09 ± 1.348	22.10 (21)		
Two-way ANOVA: Interaction: $^{**}p = 0.0025$; Row Factor: $^{****}p < 0.0001$; Column Factor: $^{***}p = 0.0001$				
Method: ASM values were calculated as the MTM median minus the particular ARM values.				
Figure 74a: Short-term memory of *ilp2* (BL # 30881)				
1) w^{1118}	55.74 ± 2.218	56.75 (20)	unpaired t-test	$^{****}p < 0.0001$
2) *ilp2*	31.21 ± 2.326	31.60 (19)		
Method: 5 days. Raised at 25 °C. T-maze and Tully Wheel. OCT 1:100, MCH 1:100.				
Figure 74b: Short-term memory of *ilp2-3* (BL # 30888)				
1) w^{1118}	64.12 ± 2.339	64.30 (19)	unpaired t-test	$^{****}p < 0.0001$
2) *ilp2-3*	40.25 ± 3.084	41.50 (15)		
Method: 5 days. Raised at 25 °C. T-maze and Tully Wheel. OCT 1:100, MCH 1:100.				
Figure 74c: Short-term memory of *ilp3* (BL # 30882)				
1) w^{1118}	52.39 ± 3.148	51.55 (16)	Mann-Whitney test	$^{****}p < 0.0001$
2) *ilp3*	32.55 ± 3.275	36.40 (17)		
Method: 5 days. Raised at 25 °C. T-maze and Tully Wheel. OCT 1:100, MCH 1:100.				
Figure 74d: Short-term memory of 5-day old of *ilp5* flies (BL # 30884)				
1) w^{1118}	54.03 ± 2.456	53.20 (15)	unpaired t-test	$^{ns}p = 0.5483$
2) *ilp5*	56.12 ± 2.390	57.55 (14)		
Method: 5 days. Raised at 25 °C. T-maze and Tully Wheel. OCT 1:100, MCH 1:100.				

Figure 74e: Short-term memory of 5-day old *w^{Dah}* ;; *ilp2-3,5* flies				
1) *w^{Dah}*	57.29 ± 2.933	60.50 (13)	unpaired t-test	*p = 0.0148
2) *w^{Dah}* ;; *ilp2-3,5*	46.44 ± 2.919	44.75 (14)		
Method: 5 days. Raised at 25 °C. T-maze and Tully Wheel. OCT 1:100, MCH 1:100.				
Figure 74f: Short-term memory of *ilp7* (BL # 30887)				
1) *w^{1118}*	54.99 ± 2.825	55.70 (15)	unpaired t-test	****p < 0.0001
2) *ilp7*	33.34 ± 2.942	33.50 (13)		
Method: 5 days. Raised at 25 °C. T-maze and Tully Wheel. OCT 1:100, MCH 1:100.				
Figure 76a: 1 hour Mid-term memory of *ilp2* (BL # 30881)				
1) *w^{1118}*	57.96 ± 4.028	56.20 (11)	unpaired t-test	****p < 0.0001
2) *ilp2*	28.17 ± 2.299	29.60 (13)		
Method: 5 days. Raised at 25 °C. T-maze. OCT 1:100, MCH 1:100.				
Figure 76b: 1 hour Mid-term memory of *ilp2-3* (BL # 30888)				
1) *w^{1118}*	65.94 ± 4.893	69.50 (9)	unpaired t-test	***p = 0.0009
2) *ilp2-3*	44.02 ± 2.986	42.30 (11)		
Method: 5 days. Raised at 25 °C. T-maze. OCT 1:100, MCH 1:100.				
Figure 76c: 1 hour Mid-term memory of 5-day old *ilp5* flies (BL # 30884)				
1) *w^{1118}*	41.78 ± 5.413	46.75 (8)	unpaired t-test	^{ns}p = 0.3806
2) *ilp5*	48.34 ± 4.632	51.40 (7)		
Method: 5 days. Raised at 25 °C. T-maze. OCT 1:100, MCH 1:100.				
Figure 76d: 1 hour Anesthesia-resistant memory of *ilp2* (BL # 30881)				
1) *w^{1118}*	24.00 ± 2.248	25.10 (11)	unpaired t-test	**p = 0.0090
2) *ilp2*	14.65 ± 2.279	13.30 (15)		
Method: 5 days. Raised at 25 °C. T-maze. OCT 1:100, MCH 1:100.				

Figure 76e: 1 hour Anesthesia-resistant memory of *ilp2-3* (BL # 30888)				
1) w^{1118}	28.58 ± 3.293	29.25 (12)	Mann-Whitney test	****$p < 0.0001$
2) *ilp2-3*	6.154 ± 3.698	7.100 (13)		
Method: 5 days. Raised at 25 °C. T-maze. OCT 1:100, MCH 1:100.				
Figure 76f: 1 hour Anesthesia-sensitive memory of *ilp2* (BL # 30881)				
1) w^{1118}	32.44 ± 2.484	29.40 (11)	unpaired t-test	****$p < 0.0001$
2) *ilp2*	14.95 ± 2.279	16.30 (15)		
Method: ASM values are calculated as the MTM median minus the particular ARM values.				
Figure 76g: 1 hour Anesthesia-sensitive memory of *ilp2-3* (BL # 30888)				
1) w^{1118}	37.37 ± 3.293	36.69 (12)	Mann-Whitney test	$^{ns}p = 0.7283$
2) *ilp2-3*	36.15 ± 3.698	35.20 (13)		
Method: ASM values were calculated as the MTM median minus the particular ARM values.				
Figure 77a: Short-term memory of 30-day old *ilp5* (BL # 30884)				
2) w^{1118} (30 days)	45.84 ± 3.903	52.00 (11)	unpaired t-test	$^{ns}p = 0.4006$
3) *ilp5* (30 days)	42.10 ± 1.921	42.10 (11)		
Method: 5 and 30 days. Raised at 25 °C. T-maze and Tully Wheel. OCT 1:100, MCH 1:100.				
Figure 77b: Short-term memory of 30-day old w^{Dah} ;; *ilp2-3,5* flies				
1) w^{Dah}	45.12 ± 2.887	45.80 (13)	unpaired t-test	*$p = 0.0148$
2) w^{Dah} ;; *ilp2-3,5*	29.47 ± 5.093	33.45 (14)		
Method: 30 days. Raised at 25 °C. T-maze and Tully Wheel. OCT 1:100, MCH 1:100.				
Figure 77c: 1 hour Mid-term memory of aged *ilp5* (BL # 30884)				
2) w^{1118} (30 days)	27.89 ± 3.766	25.50 (7)	unpaired t-test	$^{ns}p = 0.9543$
3) *ilp5* (30 days)	28.16 ± 2.714	28.80 (7)		
Method: 5 and 30 days. Raised at 25 °C. T-maze. OCT 1:100, MCH 1:100.				

Figure 77d: 1 hour Mid-term memory of 30-day old *w^{Dah}* ;; *ilp2-3,5* flies				
1) *w^{Dah}*	26.35 ± 4.438	26.25 (4)	unpaired t-test	^{ns}p = 0.1762
2) *w^{Dah}* ;; *ilp2-3,5*	18.65 ± 2.351	19.10 (4)		
Method: 30 days. Raised at 25 °C. T-maze. OCT 1:100, MCH 1:100.				
Table 11: Innate behavior of the experimental insulin-like peptide groups				
Shock reactivity:				
1) *w^{1118}*	91.02 ± 1.666	92.20 (9)	Mann-Whitney test	^{ns}p = 0.9838
2) *ilp2*	91.00 ± 1.946	91.20 (10)		
Method: 5 days. Raised at 25 °C. Tully Wheel.				
Olfactory acuity: **OCT**				
1) *w^{1118}*	61.74 ± 6.908	63.60 (10)	unpaired t-test	^{ns}p = 0.7086
2) *ilp2*	57.78 ± 7.608	65.35 (12)		
Olfactory acuity: **MCH**				
1) *w^{1118}*	70.10 ± 4.717	74.60 (13)	unpaired t-test	^{ns}p = 0.1558
2) *ilp2*	80.13 ± 4.757	85.30 (10)		
Method: 5 days. Raised at 25 °C. T-maze. OCT 1:100, MCH 1:100.				
Shock reactivity:				
1) *w^{1118}*	83.40 ± 3.929	88.05 (12)	Mann-Whitney test	^{ns}p = 0.5273
2) *ilp3*	86.80 ± 3.857	91.20 (10)		
Method: 5 days. Raised at 25 °C. Tully Wheel.				
Olfactory acuity: **OCT**				
1) *w^{1118}*	46.74 ± 3.025	45.30 (14)	unpaired t-test	^{ns}p = 0.1074
2) *ilp3*	39.92 ± 2.709	39.10 (13)		
Olfactory acuity: **MCH**				
1) *w^{1118}*	60.41 ± 6.641	65.20 (15)	Mann-Whitney test	^{ns}p = 0.3094
2) *ilp3*	56.37 ± 4.231	51.10 (15)		
Method: 5 days. Raised at 25 °C. T-maze. OCT 1:100, MCH 1:100.				
Shock reactivity:				
1) *w^{1118}*	78.30 ± 1.713	78.00 (21)	unpaired t-test	^{ns}p = 0.1396
2) *ilp2-3*	74.05 ± 2.173	72.50 (24)		
Method: 5 days. Raised at 25 °C. T-maze.				

Olfactory acuity: **OCT**				
1) w^{1118}	78.38 ± 3.615	76.45 (10)	unpaired t-test	$^{ns}p = 0.6329$
2) *ilp2-3*	75.65 ± 4.301	74.75 (10)		
Olfactory acuity: **MCH**				
1) w^{1118}	81.51 ± 3.140	80.55 (10)	unpaired t-test	$^{ns}p = 0.1194$
2) *ilp2-3*	87.35 ± 1.703	87.70 (10)		
Method: 5 days. Raised at 25 °C. T-maze. OCT 1:100, MCH 1:100.				
Shock reactivity:				
1) w^{1118}	71.85 ± 3.686	70.80 (10)	unpaired t-test	$^{ns}p = 0.1168$
2) *ilp5*	80.01 ± 3.309	83.80 (10)		
Method: 5 days. Raised at 25 °C. T-maze and Tully Wheel.				
Olfactory acuity: **OCT**				
1) w^{1118}	43.78 ± 3.843	42.90 (14)	unpaired t-test	$^{ns}p = 0.6329$
2) *ilp5*	51.90 ± 5.535	52.80 (12)		
Olfactory acuity: **MCH**				
1) w^{1118}	60.58 ± 5.883	65.20 (17)	Mann-Whitney test	$^{ns}p = 0.1920$
2) *ilp5*	46.13 ± 7.443	55.75 (18)		
Method: 5 days. Raised at 25 °C. T-maze. OCT 1:100, MCH 1:100.				
Shock reactivity:				
1) w^{1118}	89.16 ± 2.562	91.30 (10)	unpaired t-test	$^{ns}p = 0.2759$
2) *ilp2-3,5*	92.44 ± 1.145	91.80 (9)		
Method: 5 days. Raised at 25 °C. Tully Wheel.				
Olfactory acuity: **OCT**				
1) w^{1118}	39.36 ± 8.668	49.70 (8)	unpaired t-test	$^{ns}p = 0.9137$
2) *ilp2-3,5*	40.61 ± 7.387	31.95 (10)		
Olfactory acuity: **MCH**				
1) w^{1118}	69.28 ± 7.964	75.55 (10)	unpaired t-test	$^{ns}p = 0.6113$
2) *ilp2-3,5*	73.98 ± 3.572	77.10 (9)		
Method: 5 days. Raised at 25 °C. T-maze. OCT 1:100, MCH 1:100.				

Figure 80a: Short-term memory for *w^{1118}*				
1) 5-days	59.23 ± 0.8485	60.25 (176)	Kruskal-Wallis with Dunn's *post hoc* test	1-2: ***p = 0.0009 1-3: ****p < 0.0001 2-3: **p = 0.0035
2) 20 days	48.57 ± 2.432	50.40 (29)		
3) 30 days	37.55 ± 1.250	37.65 (107)		
Method: 5, 20, and 30 days. Raised at 25 °C. Pooled from 2014 – 2021.				
Figure 80b: 1 hour Mid-term memory for *w^{1118}*				
1) 5-days	54.09 ± 3.083	57.75 (38)	one-way ANOVA with Tukey's *post hoc* test	1-2: ****p < 0.0001 1-3: ****p < 0.0001 2-3: ^{ns}p = 0.3208
2) 20 days	28.10 ± 3.031	29.40 (27)		
3) 30 days	20.31 ± 2.793	18.80 (15)		
Method: 5, 20, and 30 days. Raised at 25 °C. Pooled from 2014 – 2021.				
Figure 80c: 3 hour Mid-term memory for *w^{1118}*				
1) 5-days	35.87 ± 1.304	34.90 (107)	Kruskal-Wallis with Dunn's *post hoc* test	1-2: ****p < 0.0001 1-3: ****p < 0.0001 2-3: **p = 0.0092
2) 20 days	19.32 ± 2.203	22.05 (56)		
3) 30 days	11.60 ± 1.218	12.00 (97)		
Method: 5, 20, and 30 days. Raised at 25 °C. Pooled from 2014 – 2021.				
Figure 81: Short-term memory of 1x BRP (*w^{1118}* x *brp^{c04298}*) (HMS # c04298)				
1) *w^{1118}* (5 days)	62.20 ± 3.044	64.20 (9)	two-way ANOVA with Sidak's *post hoc* test	1-2: ^{ns}p = 0.3045 1-3: *p < 0.0138 3-4: ^{ns}p = 0.2896 2-4: *p < 0.0497
2) 1x BRP (5 days)	52.82 ± 6.440	54.65 (6)		
3) *w^{1118}* (20 days)	45.47 ± 4.909	48.00 (10)		
4) 1x BRP (20 days)	36.84 ± 2.909	39.40 (8)		
Two-way ANOVA: Interaction: ^{ns}p = 0.9332; Row Factor: ***p = 0.0009; Column Factor: ^{ns}p = 0.0519				
Method: 5 and 20 days. Raised at 25 °C. T-maze and Tully Wheel. OCT 1:100, MCH 1:100.				

Figure 82a: Short-term memory of *brp^{83}*, *r58h05*-Gal4 > UAS-*brp^{B3}* RNAi				
1) 2x BRP (*w^{1118}*)	58.01 ± 1.628	56.45 (36)	one-way ANOVA with Sidak's *post hoc* test	1-2: $^{****}p < 0.0001$ 1-3: $^{ns}p = 0.3031$ 2-3: $^{***}p = 0.0001$
2) 4x BRP	39.77 ± 2.478	39.00 (23)		
3) 4x BRP , *r58h05* > *brp^{B3}* RNAi	53.47 ± 2.211	52.10 (23)		
Method: 5 days. Raised at 25 °C. T-maze and Tully Wheel. OCT 1:100, MCH 1:100.				
Figure 82b: 1 hour Mid-term memory of *brp^{83}*, *r58h05*-Gal4 > UAS-*brp^{B3}* RNAi				
1) 2x BRP (*w^{1118}*)	59.13 ± 2.455	60.05 (16)	one-way ANOVA with Sidak's *post hoc* test	1-2: $^{****}p < 0.0001$ 1-3: $^{***}p = 0.0004$ 2-3: $^{**}p = 0.0091$
2) 4x BRP	30.03 ± 3.709	31.75 (16)		
3) 4x BRP , *r58h05* > *brp^{B3}* RNAi	42.46 ± 2.063	41.50 (16)		
Method: 5 days. Raised at 25 °C. T-maze. OCT 1:100, MCH 1:100.				
Figure 82c: Short-term memory of *brp^{83}*, *r58h05*-Gal4 > UAS-*brp^{B3}* RNAi in comparison to its genetic controls				
1) *r58h05* / +	49.20 ± 3.397	48.85 (12)	one-way ANOVA with Sidak's *post hoc* test	1-3: $^{ns}p = 0.8806$ 2-3: $^{ns}p = 0.9995$ 3-4: $^{ns}p = 0.9995$ 1-4: $^{ns}p = 0.7526$ 2-4: $^{ns}p = 0.9884$
2) *brp^{B3}* RNAi / +	52.76 ± 3.702	53.00 (11)		
3) *r58h05* > *brp^{B3}* RNAi	54.31 ± 4.338	53.40 (11)		
4) 4x BRP , *r58h05* > *brp^{B3}* RNAi	55.90 ± 4.292	52.20 (9)		
Method: 5 days. Raised at 25 °C. T-maze and Tully Wheel. OCT 1:100, MCH 1:100.				
Figure 82d: 1 hour Mid-term memory of *brp^{83}*, *r58h05*-Gal4 > UAS-*brp^{B3}* RNAi in comparison to its genetic controls				
1) *r58h05* / +	47.10 ± 3.486	47.00 (8)	one-way ANOVA with Sidak's *post hoc* test	1-3: $^{ns}p = 0.8641$ 2-3: $^{ns}p = 0.9660$ 3-4: $^{ns}p > 0.9999$ 1-4: $^{ns}p = 0.8332$
2) *brp^{B3}* RNAi / +	39.75 ± 3.312	39.75 (8)		
3) *r58h05* > *brp^{B3}* RNAi	42.86 ± 2.819	42.50 (14)		

4) 4x BRP , *r58h05 > brp^{B3}* RNAi	42.60 ± 2.362	42.85 (14)		2-4: $^{ns}p = 0.9769$
Method: 5 days. Raised at 25 °C. T-maze. OCT 1:100, MCH 1:100.				
Figure 83a: Short-term memory of *sss^{P1}* (BL # 16588)				
1) 2x BRP (*w^{1118}*)	47.53 ± 2.868	49.95 (14)	unpaired t-test	$^{ns}p = 0.2412$
2) *sss*	43.13 ± 2.106	40.95 (12)		
Method: 5-8 days. Raised at 25 °C. T-maze and Tully-Wheel. 1-minute rest between all steps of the memory test. OCT 1:100, MCH 1:100.				
Figure 83b: Short-term memory of *sss^{P1}* ; 4x BR				
1) 2x BRP (*w^{1118}*)	49.59 ± 2.349	48.00 (17)	one-way ANOVA with Sidak's *post hoc* test	1-2: $^{*}p = 0.0314$ 1-3: $^{ns}p = 0.9892$ 1-4: $^{***}p = 0.0002$ 2-4: $^{ns}p = 0.4100$ 3-4: $^{**}p = 0.0021$
2) 4x BRP	37.48 ± 2.590	38.30 (18)		
3) *sss*	47.20 ± 3.380	47.20 (15)		
4) *sss* ; 4x BRP	30.21 ± 4.089	28.50 (16)		
Method: 4 days. Raised at 25 °C. T-maze and Tully-Wheel. 1-minute rest between all steps of the memory test. OCT 1:100, MCH 1:100.				
Figure 83c: Short-term memory of *sss^{P1}* ; *brp^{83}*				
1) 2x BRP (*w^{1118}*)	55.76 ± 3.880	57.70 (10)	one-way ANOVA with Sidak's *post hoc* test	1-2: $^{ns}p > 0.9999$ 1-3: $^{ns}p = 0.9839$ 1-4: $^{ns}p = 0.9114$ 2-4: $^{ns}p = 0.8661$ 3-4: $^{ns}p = 0.5966$
2) 3x BRP	55.01 ± 3.994	56.55 (8)		
3) *sss*	52.94 ± 1.507	53.60 (8)		
4) *sss* ; 3x BRP	59.77 ± 3.214	60.95 (10)		
Method: 5 days. Raised at 25 °C. T-maze and Tully-Wheel. 1-minute rest between all steps of the memory test. OCT 1:100, MCH 1:100.				
Figure 83d: 3 hours Mid-term memory of *sss^{P1}* (BL # 16588)				
1) 2x BRP (*w^{1118}*)	26.72 ± 2.343	26.40 (12)	unpaired t-test	$^{****}p < 0.0001$
2) *sss*	8.375 ± 2.534	5.350 (12)		
Method: 5-8 days. Raised at 25 °C. T-maze. 1-minute rest between all steps of the memory test. OCT 1:100, MCH 1:100.				

Figure 83e: 3 hours Mid-term memory of *sss^{P1}* ; *brp^{83}*				
1) 2x BRP (*w^{1118}*)	28.12 ± 2.155	26.55 (18)	one-way ANOVA with Sidak's *post hoc* test	1-2: $^{ns}p = 0.0685$ 1-3: $^{*}p = 0.0325$ 1-4: $^{*}p = 0.0151$ 2-4: $^{ns}p = 0.9981$ 3-4: $^{ns}p > 0.9999$
2) 4x BRP	19.98 ± 3.028	18.55 (16)		
3) *sss*	18.90 ± 1.622	17.60 (15)		
4) *sss* ; 4x BRP	18.83 ± 1.985	21.50 (21)		
Method: 3-5 days. Raised at 25 °C. T-maze. 1-minute rest between all steps of the memory test. OCT 1:100, MCH 1:100.				
Figure 83f: 3 hours Mid-term memory of *sss^{P1}* ; 3x BRP				
1) 2x BRP (*w^{1118}*)	35.07 ± 2.077	32.75 (16)	one-way ANOVA with Sidak's *post hoc* test	1-2: $^{ns}p = 0.2131$ 1-3: $^{***}p = 0.0001$ 1-4: $^{*}p = 0.0236$ 2-4: $^{***}p = 0.0002$ 3-4: $^{****}p < 0.0001$
2) 3x BRP	28.96 ± 2.500	28.10 (11)		
3) *sss*	18.90 ± 2.952	17.80 (11)		
4) *sss* ; 3x BRP	45.39 ± 2.799	44.80 (11)		
Method: 3-7 days. Raised at 25 °C. T-maze. 1-minute rest between all steps of the memory test. OCT 1:100, MCH 1:100.				
Figure 83g: 3 hours Anesthesia-resistant memory of *sss^{P1}* (BL # 16588)				
1) 2x BRP (*w^{1118}*)	14.93 ± 2.695	13.50 (10)	unpaired t-test	$^{ns}p = 0.4310$
2) *sss*	12.04 ± 2.368	11.30 (10)		
Method: 5-8 days. Raised at 25 °C. T-maze. 1-minute rest between all steps of the memory test. OCT 1:100, MCH 1:100.				
Figure 83h: 3 hours Anesthesia-resistant memory of *sss^{P1}* ; *brp^{83}*				
1) 2x BRP (*w^{1118}*)	15.35 ± 2.871	15.70 (12)	one-way ANOVA with Sidak's *post hoc* test	1-2: $^{ns}p = 0.9344$ 1-3: $^{ns}p = 0.8435$ 1-4: $^{ns}p = 0.1508$ 2-4: $^{ns}p = 0.6036$ 3-4: $^{ns}p = 0.7502$
2) 4x BRP	12.39 ± 2.789	13.60 (12)		
3) *sss*	11.62 ± 1.658	11.55 (12)		
4) *sss* ; 4x BRP	7.308 ± 2.766	9.550 (12)		
Method: 3-5 days. Raised at 25 °C. T-maze. 1-minute rest between all steps of the memory test. OCT 1:100, MCH 1:100.				

Figure 83i: 3 hours Anesthesia-resistant memory of *sss^{P1}* ; 3x BRP				
1) 2x BRP (*w^{1118}*)	23.60 ± 3.313	26.90 (17)	Kruskal-Wallis with Dunn's *post hoc* test	1-2: $^{ns}p = 0.0864$ 1-3: $^{ns}p > 0.9999$ 1-4: $^{ns}p > 0.9999$ 2-4: $^{ns}p = 0.3981$ 3-4: $^{ns}p > 0.9999$
2) 3x BRP	17.88 ± 1.146	18.30 (11)		
3) *sss*	20.51 ± 3.597	23.25 (12)		
4) *sss* ; 3x BRP	23.82 ± 3.404	23.70 (12)		
Method: 3-7 days. Raised at 25 °C. T-maze. 1-minute rest between all steps of the memory test. OCT 1:100, MCH 1:100.				
Figure 83j: 3 hours Anesthesia-sensitive memory of *sss^{P1}* (BL # 16588)				
1) 2x BRP (*w^{1118}*)	11.47 ± 2.695	12.90 (10)	unpaired t-test	$^{****}p < 0.0001$
2) *sss*	-6.690 ± 2.368	-5.950 (10)		
Method: 5-8 days. Raised at 25 °C. T-maze. 1-minute rest between all steps of the memory test. OCT 1:100, MCH 1:100.				
Figure 83k: 3 hours Anesthesia-sensitive memory of *sss^{P1}* ; *brp^{83}*				
1) 2x BRP (*w^{1118}*)	11.20 ± 2.871	10.85 (12)	one-way ANOVA with Sidak's *post hoc* test	1-2: $^{ns}p = 0.6117$ 1-3: $^{ns}p = 0.5775$ 1-4: $^{ns}p = 0.9314$ 2-4: $^{ns}p = 0.1516$ 3-4: $^{ns}p = 0.1365$
2) 4x BRP	6.158 ± 2.789	4.950 (12)		
3) *sss*	5.983 ± 1.658	6.050 (12)		
4) *sss* ; 4x BRP	14.19 ± 2.766	11.95 (12)		
Method: 3-5 days. Raised at 25 °C. T-maze. 1-minute rest between all steps of the memory test. OCT 1:100, MCH 1:100.				
Figure 83l: 3 hours Anesthesia-sensitive memory of *sss^{P1}* ; 3x BRP				
1) 2x BRP (*w^{1118}*)	9.150 ± 3.313	5.850 (17)	Kruskal-Wallis with Dunn's *post hoc* test	1-2: $^{ns}p > 0.9999$ 1-3: $^{ns}p = 0.1493$ 1-4: $^{ns}p = 0.0567$ 2-4: $^{ns}p = 0.5387$ 3-4: $^{****}p < 0.0001$
2) 3x BRP	10.22 ± 1.146	9.800 (11)		
3) *sss*	-2.708 ±3.597	-5.450 (12)		
4) *sss* ; 3x BRP	20.98 ± 3.404	21.10 (12)		
Method: 3-7 days. Raised at 25 °C. T-maze. 1-minute rest between all steps of the memory test. OCT 1:100, MCH 1:100.				

Figure 84a: Short-term memory of 30-day old *sss* ; 3x BRP				
1) 2x BRP (w^{1118})	42.86 ± 1.315	43.60 (7)	one-way ANOVA with Tukey's *post hoc* test	1-2: $^{**}p = 0.0053$ 1-3: $^{ns}p = 0.6828$ 2-3: $^{**}p = 0.0017$
2) 3x BRP	32.19 ± 2.631	28.95 (8)		
3) *sss* ; 3x BRP	45.64 ± 2.017	45.64 (5)		
Method: 30 days. Raised at 25 °C. T-maze and Tully Wheel. 1-minute rest between all steps of the memory test. OCT 1:100, MCH 1:100.				
Figure 84b: 3 hours Mid-term memory of 30-day old *sss* ; 3x BRP				
1) 2x BRP (w^{1118})	12.64 ± 4.464	13.30 (9)	one-way ANOVA with Tukey's *post hoc* test	1-2: $^{ns}p = 0.9948$ 1-3: $^{ns}p = 0.9490$ 2-3: $^{ns}p = 0.9219$
2) 3x BRP	13.18 ± 3.477	17.45 (8)		
3) *sss* ; 3x BRP	10.72 ± 3.644	9.300 (5)		
Method: 30 days. Raised at 25 °C. T-maze. 1-minute rest between all steps of the memory test. OCT 1:100, MCH 1:100.				
Figure 84c: 3 hours Anesthesia-resistant memory of 30-day old *sss* ; 3x BRP				
1) 2x BRP (w^{1118})	14.00 ± 3.124	13.30 (8)	one-way ANOVA with Tukey's *post hoc* test	1-2: $^{ns}p = 0.6570$ 1-3: $^{ns}p = 0.4082$ 2-3: $^{ns}p = 0.8277$
2) 3x BRP	10.06 ± 3.484	11.40 (8)		
3) *sss* ; 3x BRP	6.850 ± 3.182	5.700 (4)		
Method: 30 days. Raised at 25 °C. T-maze. 1-minute rest between all steps of the memory test. OCT 1:100, MCH 1:100.				
Figure 84d: 3 hours Anesthesia-sensitive memory of 30-day old *sss* ; 3x BRP				
1) 2x BRP (w^{1118})	-0.70 ± 3.124	0.000 (8)	one-way ANOVA with Tukey's *post hoc* test	1-2: $^{ns}p = 0.1940$ 1-3: $^{ns}p = 0.8336$ 2-3: $^{ns}p = 0.6442$
2) 3x BRP	7.388 ± 3.484	6.050 (8)		
3) *sss* ; 3x BRP	2.450 ± 3.182	3.600 (4)		
Method: 30 days. Raised at 25 °C. T-maze. 1-minute rest between all steps of the memory test. OCT 1:100, MCH 1:100.				
Figure 85a: Short-term memory of *r13f02 > sss* RNAi ; 3x BRP				
1) 2x BRP (w^{1118})	66.84 ± 3.557	66.15 (12)	one-way ANOVA with Sidak's *post hoc* test	1-4: $^{ns}p > 0.9999$ 2-4: $^{ns}p = 0.9995$ 3-4: $^{*}p = 0.0472$
2) 3x BRP , *r13f02* / +	66.38 ± 3.193	66.90 (10)		
3) *sss* RNAi / + ; 3x BRP	52.10 ± 4.159	52.75 (10)		

4) *r13f02* > *sss* RNAi ; 3x BRP	66.96 ± 5.219	72.90 (10)		
Method: 5 days. Raised at 25 °C. T-maze. 1-minute rest between all steps of the memory test. OCT 1:100, MCH 1:100.				
Figure 85b: 3 hours Mid-term memory of *r13f02* > *sss* RNAi ; 3x BRP				
1) 2x BRP (*w*^{1118})	26.96 ± 5.117	28.45 (14)	one-way ANOVA with Sidak's *post hoc* test	1-4: $^{ns}p = 0.4624$ 2-4: $^{ns}p = 0.3347$ 3-4: $^{ns}p = 0.7020$
2) 3x BRP , *r13f02* / +	28.88 ± 5.911	32.10 (11)		
3) *sss* RNAi / + ; 3x BRP	25.02 ± 2.915	26.05 (12)		
4) *r13f02* > *sss* RNAi ; 3x BRP	18.81 ± 3.654	18.15 (14)		
Method: 5 days. Raised at 25 °C. T-maze. 1-minute rest between all steps of the memory test. OCT 1:100, MCH 1:100.				
Figure 86a: Short-term memory of sss ; 3x BRP , *r13f02* > *sss* OE				
1) 2x BRP (*w*^{1118})	58.21 ± 2.743	57.80 (10)	one-way ANOVA with Tukey's *post hoc* test	1-2: $^{ns}p = 0.9826$ 1-3: $^{*}p = 0.0184$ 2-3: $^{**}p = 0.0082$
2) *sss* ; 3x BRP , *r13f02* / +	59.89 ± 2.626	58.40 (12)		
3) *sss* ; 3x BRP , *r13f02* > *sss* OE	47.17 ± 2.576	48.30 (12)		
Method: 5 days. Raised at 25 °C. T-maze and Tully Wheel. 1-minute rest between all steps of the memory test. OCT 1:100, MCH 1:100.				
Table 12: Innate behavior in the context of the conducted experiments.				
Olfactory acuity: **OCT**				
1) 2x BRP (*w*^{1118})	38.37 ± 4.341	40.70 (23)	one-way ANOVA with Tukey's *post hoc* test	1-2: $^{ns}p = 0.9578$ 1-3: $^{ns}p = 0.6393$ 2-3: $^{ns}p = 0.8494$
2) 4x BRP	40.29 ± 5.220	39.20 (13)		
3) 4x BRP , r58h05 > *brp*^{B3} RNAi	44.44 ± 5.013	45.55 (14)		
Olfactory acuity: **MCH**				
1) 2x BRP (*w*^{1118})	65.09 ± 5.586	67.10 (15)	Kruskal-Wallis with Dunn's *post hoc* test	1-2: $^{ns}p > 0.9999$ 1-3: $^{ns}p > 0.9999$ 2-3: $^{ns}p > 0.9999$
2) 4x BRP	64.20 ± 5.220	67.10 (13)		
3) 4x BRP , r58h05 > *brp*^{B3} RNAi	68.81 ± 5.356	76.25 (14)		
Method: 5 days. Raised at 25 °C. T-maze. OCT 1:100, MCH 1:100.				

Odor acuity: **OCT**				
1) *r58h05* / +	35.50 ± 3.838	33.85 (12)	Kruskal-Wallis with Dunn's *post hoc* test	1-3: $^{ns}p > 0.9999$ 2-3: $^{ns}p = 0.6431$ 1-4: $^{ns}p > 0.9999$ 2-4: $^{ns}p > 0.9999$ 3-4: $^{ns}p > 0.9999$
2) brp^{B3} RNAi / +	46.17 ± 6.096	51.90 (13)		
3) *r58h05* > brp^{B3} RNAi	35.20 ± 5.837	34.50 (13)		
4) 4x BRP , *r58h05* > brp^{B3} RNAi	38.26 ± 5.476	39.90 (8)		
Odor acuity: **MCH**				
1) *r58h05* / +	70.43 ± 3.206	71.80 (11)	Kruskal-Wallis with Dunn's *post hoc* test	1-3: $^{ns}p > 0.9999$ 2-3: $^{ns}p > 0.9999$ 1-4: $^{ns}p > 0.9999$ 2-4: $^{ns}p > 0.9999$ 3-4: $^{ns}p > 0.9999$
2) brp^{B3} RNAi / +	63.90 ± 7.265	72.55 (12)		
3) *r58h05* > brp^{B3} RNAi	73.07 ± 2.873	72.40 (11)		
4) 4x BRP , *r58h05* > brp^{B3} RNAi	73.07 ± 9.182	76.0 (3)		
Method: 5 days. Raised at 25 °C. T-maze. OCT 1:100, MCH 1:100.				
Odor acuity: **OCT**				
1) 2x BRP (w^{1118})	36.98 ± 2.556	39.10 (32)	unpaired t-test	$^{ns}p = 0.241$
2) *sss*	31.36 ± 4.062	30.60 (30)		
Odor acuity: **MCH**				
1) 2x BRP (w^{1118})	37.17 ± 3.411	37.30 (41)	unpaired t-test	$^{*}p = 0.0381$
2) *sss*	27.20 ± 3.907	25.30 (31)		
Method: 5 days. Raised at 25 °C. T-maze. 1-minute rest between all steps of the memory test. OCT 1:100, MCH 1:100.				
Shock reactivity:				1-2: $^{ns}p = 0.9966$
1) 2x BRP (w^{1118})	79.76 ± 2.863	81.35 (14)	one-way ANOVA with Sidak's *post hoc* test	1-3: $^{ns}p = 0.5988$
2) 4x BRP	81.61 ± 3.886	81.70 (10)		1-4: $^{ns}p = 0.9720$
3) *sss*	73.80 ± 1.296	73.80 (12)		2-4: $^{ns}p = 0.8583$
4) *sss* ; 4x BRP	76.80 ± 4-467	81.45 (10)		3-4: $^{ns}p = 0.9742$
Method: 5 days. Raised at 25 °C. T-maze and Tully-Wheel. 1-minute rest between all steps of the memory test. OCT 1:100, MCH 1:100.				
Odor acuity: **OCT**				1-2: $^{**}p = 0.0033$
1) 2x BRP (w^{1118})	17.39 ± 4.873	16.20 (16)	one-way ANOVA with Sidak's *post hoc* test	1-3: $^{ns}p > 0.9999$
2) 4x BRP	41.12 ± 5.237	37.60 (13)		1-4: $^{**}p = 0.0014$
3) *sss*	16.66 ± 3.862	12.70 (9)		2-4: $^{ns}p = 0.9986$
4) *sss* ; 4x BRP	43.52 ± 4.635	44.30 (12)		3-4: $^{**}p = 0.0051$

Odor acuity: **MCH**			one-way ANOVA with Sidak's *post hoc* test	1-2: $^{ns}p = 0.1834$
1) 2x BRP (w^{1118})	71.32 ± 5.086	69.85 (14)		1-3: $^{**}p = 0.0058$
2) 4x BRP	51.24 ± 7.933	44.70 (12)		1-4: $^{ns}p = 0.9015$
3) *sss*	38.46 ± 7.043	34.75 (12)		2-4: $^{ns}p = 0.7601$
4) *sss* ; 4x BRP	62.75 ± 7.376	62.90 (12)		3-4: $^{ns}p = 0.0839$
Method: 5 days. Raised at 25 °C. T-maze. 1-minute rest between all steps of the memory test. OCT 1:100, MCH 1:100.				
Shock reactivity:				1-2: $^{ns}p = 0.9179$
1) 2x BRP (w^{1118})	78.48 ± 3.831	80.55 (10)	one-way	1-3: $^{ns}p = 0.9179$
2) 3x BRP	82.79 ± 2.698	83.45 (8)	ANOVA with	1-4: $^{ns}p = 0.9441$
3) *sss*	74.58 ± 2.216	73.75 (8)	Sidak's *post*	2-4: $^{ns}p = 0.9999$
4) *sss* ; 3x BRP	81.82 ± 3.154	84.85 (10)	*hoc* test	3-4: $^{ns}p = 0.4673$
Method: 5 days. Raised at 25 °C. T-maze and Tully-Wheel. 1-minute rest between all steps of the memory test. OCT 1:100, MCH 1:100.				
Odor acuity: **OCT**			one-way ANOVA with Sidak's *post hoc* test	1-2: $^{ns}p = 0.9389$
1) 2x BRP (w^{1118})	18.66 ± 4.771	17.45 (16)		1-3: $^{ns}p = 0.9699$
2) 3x BRP	24.82 ± 6.386	23.95 (12)		1-4: $^{ns}p = 0.9951$
3) *sss*	13.00 ± 6.447	20.40 (9)		2-4: $^{ns}p = 0.8485$
4) *sss* ; 3x BRP	22.22 ± 6.054	22.20 (11)		3-4: $^{ns}p = 0.9992$
Odor acuity: **MCH**			one-way ANOVA with Sidak's *post hoc* test	1-2: $^{ns}p = 0.9873$
1) 2x BRP (w^{1118})	50.55 ± 7.643	55.75 (14)		1-3: $^{**}p = 0.0026$
2) 3x BRP	44.31 ± 8.520	57.90 (13)		1-4: $^{ns}p > 0.9999$
3) *sss*	5.260 ± 7.603	9.450 (10)		2-4: $^{ns}p = 0.9783$
4) *sss* ; 3x BRP	51.63 ± 9.292	60.30 (12)		3-4: $^{**}p = 0.0029$
Method: 5 days. Raised at 25 °C. T-maze. 1-minute rest between all steps of the memory test. OCT 1:100, MCH 1:100.				
Shock reactivity:				
1) 2x BRP (w^{1118})	50.01 ± 4.289	47.60 (10)	one-way	1-4: $^{**}p = 0.0094$
2) 3x BRP , *r13f02* / +	57.69 ± 4.474	57.80 (10)	ANOVA with	2-4: $^{ns}p = 0.2375$
3) *sss* RNAi / + ; 3x BRP	60.01 ± 3.439	59.15 (10)	Sidak's *post*	3-4: $^{ns}p = 0.4668$
4) *r13f02 > sss* RNAi ; 3x BRP	67.33 ± 3.095	71.65 (10)	*hoc* test	
Method: 5 days. Raised at 25 °C. T-maze. 1-minute rest between all steps of the memory test. OCT 1:100, MCH 1:100.				

Odor acuity: **OCT**				
1) 2x BRP (*w*^{1118})	27.61 ± 6.400	24.00 (10)	one-way	1-4: $^{ns}p > 0.9999$
2) 3x BRP , *r13f02* / +	34.50 ± 4.813	28.30 (12)	ANOVA with	2-4: $^{ns}p = 0.7158$
3) *sss* RNAi / + ; 3x BRP	47.05 ± 4.399	50.05 (10)	Sidak's *post*	3-4: $^{*}p = 0.0399$
4) r13f02 > *sss* RNAi ; 3x BRP	27.59 ± 4.975	26.85 (10)	*hoc* test	
Odor acuity: **MCH**				
1) 2x BRP (*w*^{1118})	48.38 ± 11.91	46.10 (12)	one-way	1-4: $^{ns}p > 0.9999$
2) 3x BRP , *r13f02* / +	48.63 ± 8.200	54.65 (12)	ANOVA with	2-4: $^{ns}p > 0.9999$
3) *sss* RNAi / + ; 3x BRP	44.59 ± 9.340	46.50 (14)	Sidak's *post*	3-4: $^{ns}p = 0.9849$
4) r13f02 > *sss* RNAi ; 3x BRP	48.98 ± 10.07	41.10 (12)	*hoc* test	
Method: 5 days. Raised at 25 °C. T-maze. 1-minute rest between all steps of the memory test. OCT 1:100, MCH 1:100.				
Shock reactivity:				
1) 2x BRP (*w*^{1118})	74.89 ± 4.109	75.00 (7)	Kruskal-Wallis	1-2: $^{ns}p > 0.9999$
2) *sss* ; 3x BRP , *r13f02* / +	71.68 ± 3.523	76.15 (8)	with Dunn's	2-3: $^{ns}p = 0.6747$
3) *sss* ; 3x BRP , *r13f02* > *sss* OE	70.25 ± 3.465	71.30 (8)	*post hoc* test	2-3: $^{ns}p > 0.9999$
Method: 5 days. Raised at 25 °C. T-maze. 1-minute rest between all steps of the memory test. OCT 1:100, MCH 1:100.				
Odor acuity: **OCT**				
1) 2x BRP (*w*^{1118})	18.21 ± 7.434	19.65 (14)	one-way	1-2: $^{ns}p = 0.7096$
2) *sss* ; 3x BRP , *r13f02* / +	24.71 ± 4.958	24.00 (14)	ANOVA with	1-3: $^{ns}p = 0.9956$
3) *sss* ; 3x BRP , *r13f02* > *sss* OE	17.48 ± 4.578	17.15 (14)	Tukey's *post hoc* test	2-3: $^{ns}p = 0.6543$
Odor acuity: **MCH**				
1) 2x BRP (*w*^{1118})	64.45 ± 4.225	63.25 (8)	Kruskal-Wallis	1-2: $^{ns}p = 0.1191$
2) *sss* ; 3x BRP , *r13f02* / +	80.01 ± 4.504	80.35 (10)	with Dunn's	1-3: $^{ns}p = 0.4481$
3) *sss* ; 3x BRP , *r13f02* > *sss* OE	71.47 ± 7.796	76.95 (10)	*post hoc* test	2-3: $^{ns}p > 0.9999$
Method: 5 days. Raised at 25 °C. T-maze. 1-minute rest between all steps of the memory test. OCT 1:100, MCH 1:100.				
Figure 88a: Short-term memory of *appl*-Gal4 > UAS-*hdac6* RNAi for 5 and 30 days (RNAi line 1, BL # 31053)				
1) *hdac6* RNAi / + (5 d)	50.80 ± 2.379	50.30 (14)	two-way	1-2: $^{****}p < 0.0001$
2) *appl* > *hdac6* RNAi (5 d)	67.21 ± 1.787	66.00 (15)	ANOVA with Sidak's *post*	1-3: $^{****}p < 0.0001$ 2-4: $^{****}p < 0.0001$
3) *hdac6* RNAi / + (30 d)	23.44 ± 1.803	23.05 (18)	*hoc* test	3-4: $^{****}p < 0.0001$

4) *appl* > *hdac6* RNAi (30 d)	37.64 ± 2.855	39.90 (14)		
Two-way ANOVA: Interaction: $^{ns}p = 0.6181$; Row Factor: $^{****}p < 0.0001$; Column Factor: $^{****}p < 0.0001$				
Method: 5 and 30 days. Raised at 29 °C. Tully Wheel. OCT 1:150, MCH 1:60.				
Figure 88b: Short-term memory of *ok107*-Gal4 > UAS-*hdac6* RNAi for 5 and 30 days (RNAi line 1, BL # 31053)				
1) *hdac6* RNAi / + (5 d)	50.80 ± 2.379	50.30 (14)	two-way ANOVA with Sidak's *post hoc* test	1-2: $^{ns}p = 0.8796$ 1-3: $^{****}p < 0.0001$ 2-4: $^{****}p < 0.0001$ 3-4: $^{ns}p > 0.8506$
2) *ok107* > *hdac6* RNAi (5 d)	48.97 ± 2.937	47.30 (15)		
3) *hdac6* RNAi / + (30 d)	23.44 ± 1.803	23.05 (18)		
4) *ok107* > *hdac6* RNAi (30 d)	25.44 ± 3.648	20.70 (16)		
Two-way ANOVA: Interaction: $^{ns}p = 0.5013$; Row Factor: $^{****}p < 0.0001$; Column Factor: $^{ns}p = 0.9897$				
Method: 5 and 30 days. Raised at 29 °C. Tully Wheel. OCT 1:150, MCH 1:60.				
Figure 88c: Short-term memory of *appl*-Gal4 > UAS-*hdac6* RNAi for 5 and 30 days (RNAi line 2, BL # 34702)				
1) *hdac6* RNAi / + (5 d)	55.30 ± 2.940	57.30 (6)	two-way ANOVA with Sidak's *post hoc* test	1-2: $^{ns}p = 0.4647$ 1-3: $^{**}p = 0.0076$ 2-4: $^{**}p = 0.0021$ 3-4: $^{ns}p = 0.9606$
2) *appl* > *hdac6* RNAi (5 d)	62.63 ± 2.362	57.75 (6)		
3) *hdac6* RNAi / + (30 d)	37.14 ± 3.577	40.40 (11)		
4) *appl* > *hdac6* RNAi (30 d)	38.58 ± 6.617	40.00 (6)		
Two-way ANOVA: Interaction: $^{ns}p = 0.5012$; Row Factor: $^{****}p < 0.0001$; Column Factor: $^{ns}p = 0.3184$				
Method: 5 and 30 days. Raised at 29 °C. Tully Wheel. OCT 1:150, MCH 1:60.				
Figure 88d: Short-term memory of *ok107*-Gal4 > UAS-*hdac6* RNAi for 5 and 30 days (RNAi line 2, BL # 34702)				
1) *hdac6* RNAi / + (5 d)	55.30 ± 2.940	57.30 (6)	two-way ANOVA with Sidak's *post hoc* test	1-2: $^{ns}p = 0.1434$ 1-3: $^{**}p = 0.0070$ 2-4: $^{ns}p = 0.0535$ 3-4: $^{ns}p = 0.0912$
2) *ok107* > *hdac6* RNAi (5 d)	42.08 ± 4.977	40.60 (4)		
3) *hdac6* RNAi / + (30 d)	37.14 ± 3.577	40.40 (11)		
4) *ok107* > *hdac6* RNAi (30 d)	24.70 ± 5.783	18.10 (5)		
Two-way ANOVA: Interaction: $^{ns}p = 0.9325$; Row Factor: $^{***}p = 0.0008$; Column Factor: $^{*}p = 0.0107$				

Method: 5 and 30 days. Raised at 29 °C. Tully Wheel. OCT 1:150, MCH 1:60.				
Figure 89a: Short-term memory of *appl*-Gal4 > UAS-*hdac6* overexpression				
1) *appl* / +	54.00 ± 4.591	61.25 (20)	one-way ANOVA with Tukey's *post hoc* test	1-3: $^{ns}p = 0.5151$ 2-3: $^{**}p = 0.0063$
2) *hdac6* OE / +	42.98 ± 1.754	43.90 (23)		
3) *appl* > *hdac6* OE	53.17 ± 1.745	54.20 (24)		
Method: 5. Raised at 29 °C. Tully Wheel. OCT 1:150, MCH 1:60.				
Figure 89b: Short-term memory of *elaV(X)*-Gal4 > UAS-*hdac6* overexpression				
1) *elaV(X)* / +	47.84 ± 2.294	48.50 (21)	Kruskal-Wallis with Dunn's *post hoc* test	1-3: $^{ns}p = 0.1329$ 2-3: $^{ns}p = 0.9436$
2) *hdac6* OE / +	42.98 ± 1.754	43.90 (23)		
3) *elaV(X)* > *hdac6* OE	42.06 ± 2.472	40.30 (20)		
Method: 5. Raised at 29 °C. Tully Wheel. OCT 1:150, MCH 1:60.				
Figure 90a: Short-term memory of *appl*-Gal4 > UAS-*elp3* RNAi (RNAi line 1, BL # 35488)				
1) *appl* > EGFP	40.39 ± 2.924	38.60 (9)	one-way ANOVA with Sidak's *post hoc* test	1-3: $^{**}p = 0.0041$ 2-3: $^{*}p = 0.0288$
2) *elp3* RNAi / +	44.42 ± 2.408	43.80 (13)		
3) *appl* > *elp3* RNAi	53.67 ± 2.706	54.50 (13)		
Method: 5. Raised at 29 °C. Tully Wheel. OCT 1:150, MCH 1:60.				
Figure 90b: Short-term memory of *elaV(X)*-Gal4 > UAS-*elp3* RNAi (RNAi line 2, VDRC # 106128)				
1) *elaV(X)* / +	59.05 ± 2.284	56.10 (8)	one-way ANOVA with Sidak's *post hoc* test	1-3: $^{**}p = 0.0015$ 2-3: $^{ns}p = 0.5572$
2) *elp3* RNAi / +	46.93 ± 2.394	46.10 (7)		
3) *elaV(X)* > *elp3* RNAi	42.83 ± 3.912	47.10 (6)		
Method: 5. Raised at 29 °C. Tully Wheel. OCT 1:150, MCH 1:60.				
Figure 90c: Short-term memory of *ok107*-Gal4 > UAS-*elp3* RNAi (RNAi line 2, VDRC # 106128)				
1) *ok107* / +	46.00 ± 3.826	44.70 (10)	one-way ANOVA with Sidak's *post hoc* test	1-3: $^{ns}p = 0.7746$ 2-3: $^{ns}p = 0.6971$
2) *elp3* RNAi / +	46.93 ± 2.394	46.10 (7)		
3) *ok107* > *elp3* RNAi	42.91 ± 3.480	43.55 (8)		

Method: 5. Raised at 29 °C. Tully Wheel. OCT 1:150, MCH 1:60.				
Figure 90d: 3 hours Mid-term memory of *appl*-Gal4 > UAS-*elp3* RNAi (RNAi line 1, BL # 35488)				
1) *appl* > EGFP	20.14 ± 2.415	17.30 (16)	one-way ANOVA with Sidak's *post hoc* test	1-3: $^{ns}p = 0.4553$ 2-3: $^{ns}p = 0.8959$
2) *elp3* RNAi / +	14.95 ± 2.390	14.45 (20)		
3) *appl* > *elp3* RNAi	16.29 ± 2.236	16.50 (22)		
Method: 5. Raised at 29 °C. Tully Wheel. OCT 1:150, MCH 1:60.				
Figure 90e: 3 hours Mid-term memory of *elaV(X)*-Gal4 > UAS-*elp3* RNAi (RNAi line 2, VDRC # 106128)				
1) *elaV(X)* / +	37.20 ± 8.100	37.20 (2)	one-way ANOVA with Sidak's *post hoc* test	1-3: $^{ns}p = 0.7466$ 2-3: $^{ns}p = 0.9984$
2) *elp3* RNAi / +	31.55 ± 2.105	31.10 (13)		
3) *elaV(X)* > *elp3* RNAi	31.78 ± 5.238	28.95 (6)		
Method: 5. Raised at 29 °C. Tully Wheel. OCT 1:150, MCH 1:60.				
Figure 90f: 3 hours Mid-term memory of *ok107*-Gal4 > UAS-*elp3* RNAi (RNAi line 2, VDRC # 106128)				
1) *ok107* / +	33.38 ± 3.273	35.90 (12)	one-way ANOVA with Sidak's *post hoc* test	1-3: $^{ns}p = 0.2251$ 2-3: $^{ns}p = 0.1182$
2) *elp3* RNAi / +	32.02 ± 2.476	32.30 (11)		
3) *ok107* > *elp3* RNAi	39.10 ± 2.677	40.40 (9)		
Method: 5. Raised at 29 °C. Tully Wheel. OCT 1:150, MCH 1:60.				
Table 13: Innate behavior for the conducted ELP3 and HDAC6 tests				
<u>Shock reactivity:</u> 1) *hdac6* RNAi / + (5 days) 2) *appl* > *hdac6* RNAi (5 days) 3) *hdac6* RNAi / + (30 days) 4) *appl* > *hdac6* RNAi (30 days)	 85.97 ± 2.050 94.86 ± 1.020 65.10 ± 5.303 82.88 ± 4.993	 87.55 (10) 93.70 (9) 63.60 (9) 85.70 (8)	two-way ANOVA with Sidak's *post hoc* test	1-2: $^{ns}p = 0.1690$ 1-3: $^{***}p = 0.0005$ 2-4: $^{ns}p = 0.0632$ 3-4: $^{**}p = 0.0045$
Method: RNAi line 1 (BL # 31053). *5 and 30 days. Raised at 29 °C. Tully Wheel.*				
<u>Odor acuity:</u> **OCT** 1) *hdac6* RNAi / + (5 days) 2) *appl* > *hdac6* RNAi (5 days) 3) *hdac6* RNAi / + (30 days) 4) *appl* > *hdac6* RNAi (30 days)	 25.30 ± 6.071 29.67 ± 8.024 20.98 ± 6.292 25.10 ± 5.526	 28.50 (6) 29.67 (6) 28.50 (6) 25.10 (6)	two-way ANOVA with Sidak's *post hoc* test	1-2: $^{ns}p = 0.8720$ 1-3: $^{ns}p = 0.8747$ 2-4: $^{ns}p = 0.8610$ 3-4: $^{ns}p = 0.8853$

Odor acuity: **MCH**				
1) *hdac6* RNAi / + (5 days)	53.16 ± 5.467	58.45 (6)	two-way	1-2: $^{ns}p = 0.2739$
2) *appl* > *hdac6* RNAi (5 days)	40.92 ± 4.859	44.15 (6)	ANOVA with	1-3: $^{**}p = 0.0017$
3) *hdac6* RNAi / + (30 days)	21.28 ± 5.857	23.10 (6)	Sidak's *post*	2-4: $^{ns}p = 0.0775$
4) *appl* > *hdac6* RNAi (30 days)	23.02 ± 6.656	22.85 (6)	*hoc* test	3-4: $^{ns}p = 0.9722$
Method: RNAi line 1 (BL # 31053). *5 and 30 days. Raised at 29 °C. Tully Wheel. OCT 1:150, MCH 1:60.*				
Shock reactivity:				
1) *hdac6* RNAi / + (5 days)	85.97 ± 2.050	87.55 (10)	two-way	1-2: $^{ns}p = 0.6170$
2) *ok107* > *hdac6* RNAi (5 days)	90.26 ± 3.024	94.30 (8)	ANOVA with	1-3: $^{***}p = 0.0001$
3) *hdac6* RNAi / + (30 days)	64.91 ± 4.747	63.40 (10)	Sidak's *post*	2-4: $^{ns}p = 0.2151$
4) *ok107* > *hdac6* RNAi (30 days)	73.07 ± 2.659	76.30 (7)	*hoc* test	3-4: $^{**}p = 0.0054$
Method: RNAi line 1 (BL # 31053). *5 and 30 days. Raised at 29 °C. Tully Wheel*				
Odor acuity: **OCT**				
1) *hdac6* RNAi / + (5 days)	25.30 ± 6.071	28.50 (6)	two-way	
2) *ok107* > *hdac6* RNAi (5 days)	10.73 ± 6.931	15.20 (6)	ANOVA with	1-2: $^{ns}p = 0.1598$
3) *hdac6* RNAi / + (30 days)	20.98 ± 6.292	28.50 (6)	Sidak's *post*	1-3: $^{ns}p = 0.8366$
4) *ok107* > *hdac6* RNAi (30 days)	16.10 ± 2.722	14.90 (7)	*hoc* test	2-4: $^{ns}p = 0.7447$
Odor acuity: **MCH**				3-4: $^{ns}p = 0.7828$
1) *hdac6* RNAi / + (5 days)	53.16 ± 5.467	58.45 (6)	two-way	
2) *ok107* > *hdac6* RNAi (5 days)	36.04 ± 9.411	45.80 (5)	ANOVA with	1-2: $^{ns}p = 0.2094$
3) *hdac6* RNAi / + (30 days)	21.28 ± 5.857	23.10 (6)	Sidak's *post*	1-3: $^{**}p = 0.0079$
4) *ok107* > *hdac6* RNAi (30 days)	6.586 ± 6.971	0.9000 (7)	*hoc* test	2-4: $^{*}p = 0.0151$
				3-4: $^{ns}p = 0.2510$
Method: RNAi line 1 (BL # 31053). *5 and 30 days. Raised at 29 °C. Tully Wheel. OCT 1:150, MCH 1:60.*				
Odor acuity: **OCT**			one-way	
1) *appl* > EGFP	28.23 ± 4.983	30.40 (4)	ANOVA with	1-3: $^{ns}p = 0.9850$
2) *elp3* RNAi / +	24.88 ± 8.481	24.00 (4)	Sidak's *post*	2-3: $^{ns}p = 0.9895$
3) *appl* > *elp3* RNAi	26.40 ± 7.938	27.45 (8)	*hoc* test	

Odor acuity: **MCH** 1) *appl* > EGFP 2) *elp3* RNAi / + 3) *appl* > *elp3* RNAi	22.85 ± 5.818 43.05 ± 10.22 31.29 ± 8.162	23.15 (4) 39.60 (4) 23.05 (8)	one-way ANOVA with Sidak's *post hoc* test	1-3: $^{ns}p = 0.7604$ 2-3: $^{ns}p = 0.5940$
Method: RNAi line 1 (BL # 35488). *5 days. Raised at 29 °C. Tully Wheel. OCT 1:150, MCH 1:60.*				
Figure 91a: Short-term memory of hypomorph *aplip1^{ek4}* in the background of *aplip1* null-mutation (*Df(3L)BSC799)*				
1) *w^{1118}*	73.10 ± 2.810	71.80 (14)	unpaired t-test	****$p < 0.0001$
2) *aplip1^{ek4}* , *Df(3L)BSC799*	43.00 ± 4.659	40.05 (12)		
Method: 5 days. Raised at 25 °C. T-maze and Tully Wheel. OCT 1:100, MCH 1:100.				
Figure 91b: Short-term memory of *ok107*-Gal4 > *UAS-aplip1* RNAi (VDRC # 50007)				
1) *ok107* / +	68.60 ± 3.619	68.40 (9)	one-way ANOVA with Sidak's *post hoc* test	1-3: *$p = 0.0111$ 2-3: $^{ns}p = 0.1075$
2) *aplip1* RNAi / +	62.75 ± 3.042	63.20 (12)		
3) *ok107* > *aplip1* RNAi	53.25 ± 3.821	51.00 (11)		
Method: 5 days. Raised at 29 °C. T-maze and Tully Wheel. OCT 1:100, MCH 1:100				
Figure 91c: Short-term memory of *mb247*-Gal4 > *UAS-aplip1* RNAi (VDRC # 50007)				
1) *mb247* / +	75.37 ± 3.991	70.20 (7)	one-way ANOVA with Sidak's *post hoc* test	1-3: ***$p = 0.0001$ 2-3: *$p = 0.0134$
2) *aplip1* RNAi / +	62.12 ± 3.416	65.00 (9)		
3) *mb247* > *aplip1* RNAi	44.14 ± 5.360	45.20 (14)		
Method: 5 days. Raised at 29 °C. T-maze and Tully Wheel. OCT 1:100, MCH 1:100				
Table 14: Innate behavior of the experimental Aplip1 deficient flies				
Olfactory acuity: **OCT** 1) *w^{1118}* 2) *aplip1^{EY11248}* , *Df(3L)BSC799*	40.78 ± 5.316 47.31 ± 6.886	38.30 (17) 48.00 (11)	unpaired t-test	$^{ns}p = 0.4554$
Olfactory acuity: **MCH** 1) *w^{1118}* 2) *aplip1^{EY11248}* , *Df(3L)BSC799*	86.90 ± 1.418 88.20 ± 2.660	85.70 (9) 90.70 (9)	unpaired t-test	$^{ns}p = 0.6720$
Method: 5 days. Raised at 25 °C. T-maze. OCT 1:100, MCH 1:100.				

Olfactory acuity: **OCT**			Kruskal-Wallis with Dunn's *post hoc* test	1-3: $^{ns}p > 0.9999$ 2-3: $^{**}p = 0.0073$
1) *ok107* / +	24.60 ± 3.504	24.60 (37)		
2) *aplip1* RNAi / +	37.87 ± 3.493	39.70 (57)		
3) *ok107* > *aplip1* RNAi	23.91 ± 3.254	18.50 (54)		
Olfactory acuity: **MCH**			one-way ANOVA with Sidak's *post hoc* test	1-3: $^{ns}p = 0.8754$ 2-3: $^{ns}p = 0.9570$
1) *ok107* / +	76.28 ± 3.656	79.20 (9)		
2) *aplip1* RNAi / +	71.21 ± 5.031	76.70 (15)		
3) *ok107* > *aplip1* RNAi	72.90 ± 3.360	72.05 (14)		
Method: 5 days. Raised at 29 °C. T-maze. OCT 1:100, MCH 1:100.				
Olfactory acuity: **OCT**			one-way ANOVA with Sidak's *post hoc* test	1-3: $^{ns}p = 0.6049$ 2-3: $^{*}p = 0.0407$
1) *mb247* / +	16.26 ± 4.299	14.30 (32)		
2) *aplip1* RNAi / +	37.87 ± 3.493	39.70 (57)		
3) *mb247* > *aplip1* RNAi	29.45 ± 3.947	23.20 (36)		
Olfactory acuity: **MCH**			one-way ANOVA with Sidak's *post hoc* test	1-3: $^{ns}p = 0.0678$ 2-3: $^{ns}p = 0.2723$
1) *mb247* / +	70.02 ± 6.238	70.40 (9)		
2) *aplip1* RNAi / +	71.21 ± 5.031	76.70 (15)		
3) *mb247* > *aplip1* RNAi	57.40 ± 7.355	63.30 (9)		
Method: 5 days. Raised at 29 °C. T-maze. OCT 1:100, MCH 1:100.				
Figure 92a: Short-term memory of *srpk79D* null-mutant				
1) w^{1118}	61.21 ± 2.458	61.25 (14)	unpaired t-test	$^{****}p < 0.0001$
2) $srpk79D^{VN}$	25.44 ± 2.687	29.70 (11)		
Method: 5 days. Raised at 25 °C. T-maze and Tully Wheel. OCT 1:100, MCH 1:100.				
Figure 92b: Olfactory acuity with 3-Octanol of *srpk79D* null-mutant				
1) w^{1118}	50.13 ± 5.370	47.50 (13)	unpaired t-test	$^{**}p = 0.0071$
2) $srpk79D^{VN}$	32.14 ± 2.486	30.70 (12)		
Method: 5 days. Raised at 25 °C. T-maze. OCT 1:100, MCH 1:100.				
Figure 92c: Olfactory acuity with 4-Methylcyclohexanol of *srpk79D* null-mutant				
1) w^{1118}	78.88 ± 5.275	84.60 (13)	Mann-Whitney test	$^{ns}p = 0.0720$
2) $srpk79D^{VN}$	68.04 ± 3.913	74.10 (15)		
Method: 5 days. Raised at 25 °C. T-maze. OCT 1:100, MCH 1:100.				

Figure 92d: 1 hour Mid-term memory of *srpk79D* null-mutant				
1) w^{1118}	63.68 ± 3.609	66.45 (8)	unpaired t-test	****$p < 0.0001$
2) *srpk79D*^{VN}	22.77 ± 2.866	21.40 (11)		
Method: 5 days. Raised at 25 °C. T-maze. OCT 1:100, MCH 1:100.				
Figure 92e: 1 hour Anesthesia-resistant memory of *srpk79D* null-mutant				
1) w^{1118}	25.34 ± 2.041	26.55 (10)	unpaired t-test	****$p < 0.0001$
2) *srpk79D*^{VN}	4.936 ± 1.925	4.100 (11)		
Method: 5 days. Raised at 25 °C. T-maze. OCT 1:100, MCH 1:100.				
Figure 92f: 1 hour Anesthesia-sensitive memory of *srpk79D* null-mutant				
1) w^{1118}	41.16 ± 2.041	39.95 (10)	unpaired t-test	****$p < 0.0001$
2) *srpk79D*^{VN}	16.46 ± 1.925	17.30 (11)		
Method: ASM values were calculated as the MTM median minus the particular ARM values.				
Figure 93a: Short-term memory of *ok107*-Gal4 > UAS-*srpk79D* RNAi (VDRC # 47544)				
1) *ok107* / +	45.78 ± 2.805	47.10 (10)	one-way ANOVA with Sidak's *post hoc* test	1-3: $^{ns}p = 0.3804$ 2-3: $^{**}p = 0.0092$
2) *srpk79D* RNAi / +	51.50 ± 1.668	51.10 (11)		
3) *ok107* > *srpk79D* RNAi	41.55 ± 2.458	42.40 (11)		
Method: 5 days. Raised 29 °C. T-maze and Tully Wheel. OCT 1:100, MCH 1:100.				
Figure 93b: Short-term memory of *mb247*-Gal4 > UAS-*srpk79D* RNAi (VDRC # 47544)				
1) *mb247* / +	45.65 ± 3.236	45.60 (10)	one-way ANOVA with Sidak's *post hoc* test	1-3: $^{ns}p = 0.9989$ 2-3: $^{ns}p = 0.2486$
2) *srpk79D* RNAi / +	51.50 ± 1.668	51.10 (11)		
3) *mb247* > *srpk79D* RNAi	45.81 ± 2.861	48.55 (10)		
Method: 5 days. Raised 29 °C. T-maze and Tully Wheel. OCT 1:100, MCH 1:100.				
Table 15: Innate behavior of UAS-*srpk79D* RNAi in the mushroom body (VDRC # 47544)				
Olfactory acuity: **OCT** 1) *ok107* / + 2) *srpk79D* RNAi / + 3) *ok107* > *srpk79D* RNAi	 28.73 ± 7.479 33.84 ± 8.324 61.82 ± 6.944	 38.30 (7) 37.85 (8) 62.95 (6)	one-way ANOVA with Sidak's *post hoc* test	1-3: $^{*}p = 0.0198$ 2-3: $^{*}p = 0.0433$

Olfactory acuity: **MCH** 1) *ok107* / + 2) *srpk79D* RNAi / + 3) *ok107* > *srpk79D* RNAi	 53.71 ± 8.064 78.73 ± 7.558 82.86 ± 4.263	 53.30 (8) 82.30 (7) 86.70 (7)	 Kruskal-Wallis with Dunn's *post hoc* test	 1-3: $^{*}p = 0.0361$ 2-3: $^{ns}p > 0.9999$
Method: 5 days. Raised 29 °C. T-maze. OCT 1:100, MCH 1:100.				
Olfactory acuity: **OCT** 1) *mb247* / + 2) *srpk79D* RNAi / + 3) *mb247* > *srpk79D* RNAi Olfactory acuity: **MCH** 1) *mb247* / + 2) *srpk79D* RNAi / + 3) *mb247* > *srpk79D* RNAi	 28.73 ± 10.18 33.84 ± 8.324 44.53 ± 4.616 50.40 ± 7.226 78.73 ± 7.558 73.89 ± 6.490	 31.95 (8) 37.85 (8) 46.50 (7) 56.15 (8) 82.30 (7) 77.30 (7)	 one-way ANOVA with Sidak's *post hoc* test Kruskal-Wallis with Dunn's *post hoc* test	 1-3: $^{ns}p = 0.3589$ 2-3: $^{ns}p = 0.6154$ 1-3: $^{ns}p = 0.0619$ 2-3: $^{ns}p > 0.9999$
Method: 5 days. Raised 29 °C. T-maze. OCT 1:100, MCH 1:100.				
Figure 95a: 3-Octanol odor acuity for *unc13* rescues in an *unc13* null mutation background				
1) w^{1118}	35.91 ± 4.144	33.30 (16)	Kruskal-Wallis with Dunn's *post hoc* test	1-3: $^{ns}p > 0.9999$ 2-3: $^{*}p = 0.0140$ 1-2: $^{**}p = 0.0025$
2) unc13 rescue	11.86 ± 5.500	9.400 (14)		
3) *unc13B* deletion	35.29 ± 4.319	34.70 (9)		
Method: 5 days. Raised at 25 °C. Tully Wheel. OCT 1:150.				
Figure 95b: 4-Methylcyclohexanol odor acuity for *unc13* rescues in an *unc13* null mutation background				
1) w^{1118}	52.76 ± 5.959	57.60 (19)	one-way ANOVA with Sidak's *post hoc* test	1-3: $^{ns}p = 0.5741$ 2-3: $^{ns}p = 0.4407$ 1-2: $^{*}p = 0.0363$
2) unc13 rescue	31.25 ± 6.282	33.35 (14)		
3) *unc13B* deletion	43.38 ± 5.990	55.88 (10)		
Method: 5 days. Raised at 25 °C. Tully Wheel. MCH 1:60 and 1:55 and 1:75.				
Figure 95c: Short-term memory for *unc13* rescues in an *unc13* null mutation background				
1) w^{1118}	70.54 ± 1.243	69.30 (42)	one-way ANOVA with Sidak's *post hoc* test	1-3: $^{****}p < 0.0001$ 2-3: $^{**}p = 0.0017$ 1-2: $^{****}p < 0.0001$
2) unc13 rescue	53.46 ± 1.321	54.40 (74)		
3) *unc13B* deletion	44.18 ± 2.553	45.30 (20)		
Method: 5 days. Raised at 25 °C. Tully Wheel. OCT 1:150, MCH 1:60.				

Figure 96a: Short-term memory of UAS-*unc13A* RNAi in olfactory co-receptors				
1) *or83b* / +	47.54 ± 3.889	45.30 (10)	one-way ANOVA with Sidak's *post hoc* test	1-3: $^{ns}p = 0.9953$ 2-3: $^{ns}p = 0.5367$
2) *unc13A* RNAi / +	41.10 ± 5.150	37.90 (10)		
3) *or83b* > *unc13A* RNAi	48.14 ± 5.531	49.30 (10)		
Method: 5 days. Raised at 29 °C. T-maze. BA 1:1000, MCH 1:500.				
Figure 96b: Short-term memory of UAS-*unc13A* RNAi in the projection neurons				
1) *gh146* / +	45.38 ± 2.809	46.00 (9)	one-way ANOVA with Sidak's *post hoc* test	1-3: $^{**}p = 0.0035$ 2-3: $^{****}p < 0.0001$
2) *unc13A* RNAi / +	58.10 ± 3.146	59.60 (10)		
3) *gh146* > *unc13A* RNAi	30.67 ± 2.852	31.35 (10)		
Method: 7 days. Raised at 29 °C. T-maze. BA 1:500, MCH 1:100.				
Figure 96c: Short-term memory of UAS-*unc13A* RNAi in the mushroom body				
1) *ok107* / +	54.28 ± 2.705	55.25 (6)	one-way ANOVA with Sidak's *post hoc* test	1-3: $^{****}p < 0.0001$ 2-3: $^{****}p < 0.0001$
2) *unc13A* RNAi / +	51.45 ± 2.732	50.30 (11)		
3) *ok107* > *unc13A* RNAi	26.83 ± 3.416	30.85 (12)		
Method: 6 days. Raised at 25 °C. T-maze and Tully Wheel. OCT 1:100, MCH 1:100.				
Figure 96d: Short-term memory of UAS-*unc13B* RNAi in olfactory co-receptors				
1) *or83b* / +	47.54 ± 3.889	45.30 (10)	one-way ANOVA with Sidak's *post hoc* test	1-3: $^{ns}p = 0.9787$ 2-3: $^{ns}p = 0.8573$
2) *unc13B* RNAi / +	45.72 ± 3.442	44.75 (10)		
3) *or83b* > *unc13B* RNAi	48.62 ± 4.879	44.45 (10)		
Method: 5 days. Raised at 29 °C. T-maze. BA 1:1000, MCH 1:500.				
Figure 96e: Short-term memory of UAS-*unc13B* RNAi in the projection neurons				
1) *gh146* / +	47.95 ± 2.924	46.40 (11)	one-way ANOVA with Sidak's *post hoc* test	1-3: $^{ns}p = 0.3906$ 2-3: $^{***}p = 0.0004$
2) *unc13B* RNAi / +	62.98 ± 3.806	64.60 (11)		
3) *gh146* > *unc13B* RNAi	41.67 ± 3.745	38.30 (10)		
Method: 7 days. Raised at 29 °C. T-maze. BA 1:500, MCH 1:100.				

Figure 96f: Short-term memory of UAS-*unc13B* RNAi in the mushroom body				
1) *ok107* / +	58.55 ± 2.205	55.90 (17)	one-way ANOVA with Sidak's *post hoc* test	1-3: ****$p < 0.0001$ 2-3: **$p = 0.0098$
2) *unc13B* RNAi / +	50.43 ± 2.550	52.80 (21)		
3) *ok107* > *unc13B* RNAi	39.61 ± 3.076	38.10 (17)		
Method: 6 days. Raised at 25 °C. T-maze and Tully Wheel. OCT 1:100, MCH 1:100.				
Figure 97a: 3 hours Mid-term memory of UAS-*unc13A* RNAi in the projection neurons				
1) *gh146* / +	22.36 ± 3.162	19.35 (10)	one-way ANOVA with Sidak's *post hoc* test	1-3: $^{ns}p = 0.9266$ 2-3: ***$p = 0.0005$
2) *unc13A* RNAi / +	42.06 ± 4.057	41.70 (10)		
3) *gh146* > *unc13A* RNAi	20.56 ± 3.638	23.45 (10)		
Method: 7 days. Raised at 29 °C. T-maze. BA 1:500, MCH 1:100.				
Figure 97b: 3 hours Anesthesia-resistant memory of UAS-*unc13A* RNAi in the projection neurons				
1) *gh146* / +	20.64 ± 4.132	21.20 (10)	one-way ANOVA with Sidak's *post hoc* test	1-3: $^{ns}p = 0.9359$ 2-3: $^{ns}p = 0.5926$
2) *unc13A* RNAi / +	17.89 ± 3.489	16.70 (10)		
3) *gh146* > *unc13A* RNAi	22.13 ± 1.441	22.35 (10)		
Method: 7 days. Raised at 29 °C. T-maze. BA 1:500, MCH 1:100.				
Figure 97c: 3 hours Anesthesia-sensitive memory of UAS-*unc13A* RNAi in the projection neurons				
1) *gh146* / +	-1.290 ± 4.132	-1.850 (10)	one-way ANOVA with Sidak's *post hoc* test	1-3: $^{ns}p = 0.8174$ 2-3: ****$p < 0.0001$
2) *unc13A* RNAi / +	23.81 ± 3.489	25.00 (10)		
3) *gh146* > *unc13A* RNAi	1.320 ± 1.441	1.100 (10)		
Method: ASM values were calculated as the MTM median minus the particular ARM values.				
Figure 97d: 3 hours Mid-term memory of UAS-*unc13B* RNAi in the projection neurons				
1) *gh146* / +	22.36 ± 3.162	19.35 (10)	one-way ANOVA with Sidak's *post hoc* test	1-3: $^{ns}p = 0.1885$ 2-3: $^{ns}p = 0.3672$
2) *unc13B* RNAi / +	39.27 ± 4.546	34.75 (10)		
3) *gh146* > *unc13B* RNAi	31.96 ± 4.092	29.45 (10)		

Method: 7 days. Raised at 29 °C. T-maze. BA 1:500, MCH 1:100.				
Figure 97e: 3 hours Anesthesia-resistant memory of UAS-*unc13B* RNAi in the projection neurons				
1) *gh146* / +	20.50 ± 5.236	20.10 (8)	one-way ANOVA with Sidak's *post hoc* test	1-3: $^{ns}p = 0.9680$ 2-3: $^{ns}p = 0.9871$
2) *unc13B* RNAi / +	18.41 ± 2.326	17.05 (10)		
3) *gh146* > *unc13B* RNAi	19.19 ± 4.255	20.60 (10)		
Method: 7 days. Raised at 29 °C. T-maze. BA 1:500, MCH 1:100.				
Figure 97f: 3 hours Anesthesia-sensitive memory of UAS-*unc13B* RNAi in the projection neurons				
1) *gh146* / +	-1.150 ± 5.236	-0.7500 (8)	one-way ANOVA with Sidak's *post hoc* test	1-3: $^{ns}p = 0.1119$ 2-3: $^{ns}p = 0.4690$
2) *unc13B* RNAi / +	16.34 ± 2.326	17.70 (10)		
3) *gh146* > *unc13B* RNAi	10.26 ± 4.255	8.850 (10)		
Method: ASM values were calculated as the MTM median minus the particular ARM values.				
Figure 98a: 3 hours Mid-term memory of UAS-*unc13A* RNAi in the mushroom body				
1) *ok107* / +	24.95 ± 3.204	22.65 (10)	one-way ANOVA with Sidak's *post hoc* test	1-3: ****$p < 0.0001$ 2-3: ****$p < 0.0001$
2) *unc13A* RNAi / +	22.16 ± 2.421	21.60 (16)		
3) *ok107* > *unc13A* RNAi	-3.700 ± 3.221	-1.900 (17)		
Method: 6 days. Raised at 25 °C. T-maze. OCT 1:100, MCH 1:100.				
Figure 98b: 3 hours Anesthesia-resistant memory of UAS-*unc13A* RNAi in the mushroom body				
1) *ok107* / +	16.76 ± 3.727	12.10 (10)	one-way ANOVA with Sidak's *post hoc* test	1-3: *$p = 0.0161$ 2-3: **$p = 0.0084$
2) *unc13A* RNAi / +	17.20 ± 2.206	16.80 (12)		
3) *ok107* > *unc13A* RNAi	5.883 ± 2.141	6.150 (12)		
Method: 6 days. Raised at 25 °C. T-maze. OCT 1:100, MCH 1:100.				

Figure 98c: 3 hours Anesthesia-sensitive memory of UAS-*unc13A* RNAi in the mushroom body				
1) *ok107* / +	5.890 ± 3.727	10.55 (10)	one-way ANOVA with Sidak's *post hoc* test	1-3: $^{**}p = 0.0025$ 2-3: $^{**}p = 0.0046$
2) *unc13A* RNAi / +	4.400 ± 2.206	4.800 (12)		
3) *ok107* > *unc13A* RNAi	-7.783 ± 2.141	-8.050 (12)		
Method: ASM values were calculated as the MTM median minus the particular ARM values.				
Figure 98d: 3 hours Mid-term memory of UAS-*unc13B* RNAi in the mushroom body				
1) *ok107* / +	25.90 ± 2.379	23.95 (14)	one-way ANOVA with Sidak's *post hoc* test	1-3: $^{**}p = 0.0040$ 2-3: $^{**}p = 0.0013$
2) *unc13B* RNAi / +	26.55 ± 2.267	28.20 (17)		
3) *ok107* > *unc13B* RNAi	14.67 ± 2.436	14.10 (17)		
Method: 6 days. Raised at 25 °C. T-maze. OCT 1:100, MCH 1:100.				
Figure 98e: 3 hours Anesthesia-resistant memory of UAS-*unc13B* RNAi in the mushroom body				
1) *ok107* / +	12.92 ± 2.142	11.65 (14)	one-way ANOVA with Sidak's *post hoc* test	1-3: $^{ns}p = 0.4442$ 2-3: $^{ns}p = 0.0854$
2) *unc13B* RNAi / +	16.88 ± 2.298	18.30 (12)		
3) *ok107* > *unc13B* RNAi	8.421 ± 3.618	8.250 (14)		
Method: 6 days. Raised at 25 °C. T-maze. OCT 1:100, MCH 1:100.				
Figure 98f: 3 hours Anesthesia-sensitive memory of UAS-*unc13B* RNAi in the mushroom body				
1) *ok107* / +	11.03 ± 2.142	12.30 (14)	one-way ANOVA with Sidak's *post hoc* test	1-3: $^{ns}p = 0.9966$ 2-3: $^{ns}p = 0.3131$
2) *unc13B* RNAi / +	11.33 ± 2.298	9.900 (12)		
3) *ok107* > *unc13B* RNAi	5.679 ± 3.618	5.850 (14)		
Method: ASM values were calculated as the MTM median minus the particular ARM values.				

Figure 99a: 1 hour Mid-term memory of UAS-*unc13A* RNAi in the mushroom body				
1) *ok107* / +	39.91 ± 2.529	42.05 (14)	one-way ANOVA with Sidak's *post hoc* test	1-3: ****$p < 0.0001$ 2-3: ****$p < 0.0001$
2) *unc13A* RNAi / +	43.08 ± 3.502	40.50 (13)		
3) *ok107* > *unc13A* RNAi	12.88 ± 1.964	14.25 (12)		
Method: 6 days. Raised at 25 °C. T-maze. OCT 1:100, MCH 1:100.				
Figure 99: 1 hour Anesthesia-resistant memory of UAS-*unc13A* RNAi in the mushroom body				
1) *ok107* / +	10.66 ± 3.119	10.20 (12)	one-way ANOVA with Sidak's *post hoc* test	1-3: *$p = 0.0101$ 2-3: *$p = 0.0227$
2) *unc13A* RNAi / +	9.650 ± 2.043	11.35 (12)		
3) *ok107* > *unc13A* RNAi	1.250 ± 1.043	-0.150 (14)		
Method: 6 days. Raised at 25 °C. T-maze. OCT 1:100, MCH 1:100.				
Figure 99c: 1 hour Anesthesia-sensitive memory of UAS-*unc13A* RNAi in the mushroom body				
1) *ok107* / +	31.39 ± 3.119	31.85 (12)	one-way ANOVA with Sidak's *post hoc* test	1-3: ****$p < 0.0001$ 2-3: ****$p < 0.0001$
2) *unc13A* RNAi / +	30.85 ± 2.043	29.15 (12)		
3) *ok107* > *unc13A* RNAi	13.00 ± 1.487	14.40 (14)		
Method: ASM values were calculated as the MTM median minus the particular ARM values.				
Figure 99d: 1 hour Mid-term memory of UAS-*unc13B* RNAi in the mushroom body				
1) *ok107* / +	45.64 ± 4.364	44.40 (10)	one-way ANOVA with Sidak's *post hoc* test	1-3: **$p = 0.0064$ 2-3: *$p = 0.0415$
2) *unc13B* RNAi / +	41.51 ± 2.694	42.60 (13)		
3) *ok107* > *unc13B* RNAi	31.49 ± 2.581	30.60 (16)		
Method: 6 days. Raised at 25 °C. T-maze. OCT 1:100, MCH 1:100.				
Figure 99e: 1 hour Anesthesia-resistant memory of UAS-*unc13B* RNAi in the mushroom body				
1) *ok107* / +	14.84 ± 3.031	13.70 (13)	one-way ANOVA with Sidak's *post hoc* test	1-3: **$p = 0.0042$ 2-3: $^{ns}p = 0.0539$
2) *unc13B* RNAi / +	11.09 ± 2.548	11.70 (13)		
3) *ok107* > *unc13B* RNAi	2.579 ± 2.317	2.150 (14)		
Method: 6 days. Raised at 25 °C. T-maze. OCT 1:100, MCH 1:100.				

Figure 99f: 1 hour Anesthesia-sensitive memory of UAS-*unc13B* RNAi in the mushroom body				
1) *ok107* / +	29.56 ± 3.031	30.70 (13)	one-way ANOVA with Sidak's *post hoc* test	1-3: $^{ns}p = 0.8976$ 2-3: $^{ns}p = 0.5812$
2) *unc13B* RNAi / +	31.51 ± 2.548	30.90 (13)		
3) *ok107* > *unc13B* RNAi	28.02 ± 2.317	28.45 (14)		
Method: ASM values were calculated as the MTM median minus the particular ARM values.				
Table 16: Innate behavior of the UAS-*unc13A* and *B* RNAi in different areas of the olfactory memory system				
Olfactory acuity: **BA**			one-way ANOVA with Sidak's *post hoc* test	
1) *or83b* / +	45.53 ± 8.583	39.20 (6)		1-3: $^{ns}p = 0.4855$
2) *unc13A* RNAi / +	42.82 ± 5.614	44.55 (6)		2-3: $^{ns}p = 0.6522$
3) *or83b* > *unc13A* RNAi	34.20 ± 7.071	38.75 (6)		
Olfactory acuity: **MCH**			one-way ANOVA with Sidak's *post hoc* test	
1) *or83b* / +	49.60 ± 9.651	45.75 (4)		1-3: $^{ns}p = 0.3905$
2) *unc13A* RNAi / +	41.50 ± 12.63	46.65 (4)		2-3: $^{ns}p = 0.6740$
3) *or83b* > *unc13A* RNAi	27.88 ± 12.38	35.85 (4)		
Method: 5 days. Raised at 29 °C. T-maze. BA 1:1000, MCH 1:500.				
Olfactory acuity: **BA**			one-way ANOVA with Sidak's *post hoc* test	
1) *or83b* / +	45.53 ± 8.583	39.20 (6)		1-3: $^{ns}p = 0.4422$
2) *unc13B* RNAi / +	36.58 ± 7.290	40.00 (6)		2-3: $^{ns}p = 0.9024$
3) *or83b* > *unc13B* RNAi	31.87 ± 8.460	29.80 (6)		
Olfactory acuity: **MCH**			one-way ANOVA with Sidak's *post hoc* test	
1) *or83b* / +	49.60 ± 9.651	45.75 (4)		1-3: $^{ns}p = 0.5922$
2) *unc13B* RNAi / +	41.15 ± 7.609	44.75 (6)		2-3: $^{ns}p = 0.9237$
3) *or83b* > *unc13B* RNAi	36.77 ± 9.811	43.05 (6)		
Method: 5 days. Raised at 29 °C. T-maze. BA 1:1000, MCH 1:500.				
Olfactory acuity: **BA**			Kruskal-Wallis with Dunn's *post hoc* test	
1) *gh146* / +	39.19 ± 6.651	34.50 (21)		1-3: $^{ns}p = 0.8742$
2) *unc13A* RNAi / +	71.84 ± 5.780	76.00 (18)		2-3: $^{*}p = 0.0328$
3) *gh146* > *unc13A* RNAi	47.40 ± 7.398	52.25 (18)		
Olfactory acuity: **MCH**			Kruskal-Wallis with Dunn's *post hoc* test	
1) *gh146* / +	43.86 ± 5.224	48.80 (24)		1-3: $^{ns}p > 0.9999$
2) *unc13A* RNAi / +	74.37 ± 4.030	74.37 (21)		2-3: $^{***}p = 0.0006$

3) *gh146* > *unc13A* RNAi	44.84 ± 6.018	44.84 (22)		
Method: 7 days. Raised at 29 °C. T-maze. BA 1:500, MCH 1:100.				
Olfactory acuity: **BA**			one-way	
1) *gh146* / +	42.00 ± 7.004	42.20 (19)	ANOVA with	1-3: $^{ns}p = 0.9327$
2) *unc13B* RNAi / +	65.33 ± 5.361	72.35 (18)	Sidak's *post*	2-3: $^{*}p = 0.0470$
3) *gh146* > *unc13B* RNAi	44.88 ± 5.857	43.90 (18)	*hoc* test	
Olfactory acuity: **MCH**				
1) *gh146* / +	43.86 ± 5.224	48.80 (24)	Kruskal-Wallis	1-3: $^{ns}p > 0.9999$
2) *unc13B* RNAi / +	66.03 ± 5.432	77.30 (22)	with Dunn's	2-3: $^{**}p = 0.0057$
3) *gh146* > *unc13B* RNAi	42.46 ± 6.325	47.95 (22)	*post hoc* test	
Method: 7 days. Raised at 29 °C. T-maze. BA 1:500, MCH 1:100.				
Shock reactivity:			one-way	
1) *ok107* / +	90.95 ± 2.387	93.40 (12)	ANOVA with	1-3: $^{ns}p = 0.8717$
2) *unc13A* RNAi / +	87.07 ± 2.445	89.80 (13)	Sidak's *post*	2-3: $^{ns}p = 0.7181$
3) *ok107* > *unc13A* RNAi	89.42 ± 2.045	90.20 (13)	*hoc* test	
Method: 4 days. Raised at 25 °C. Tully Wheel.				
Olfactory acuity: **OCT**			one-way	
1) *ok107* / +	45.52 ± 5.280	46.60 (10)	ANOVA with	1-3: $^{ns}p = 0.7304$
2) *unc13A* RNAi / +	44.90 ± 4.163	47.35 (10)	Sidak's *post*	2-3: $^{ns}p = 0.6643$
3) *ok107* > *unc13A* RNAi	49.83 ± 3.048	50.40 (10)	*hoc* test	
Olfactory acuity: **MCH**				
1) *ok107* / +	71.71 ± 4.584	78.15 (16)	Kruskal-Wallis	1-3: $^{ns}p > 0.9999$
2) *unc13A* RNAi / +	64.60 ± 5.519	72.40 (21)	with Dunn's	2-3: $^{ns}p > 0.9999$
3) *ok107* > *unc13A* RNAi	71.40 ± 4.197	74.00 (19)	*post hoc* test	
Method: 6 days. Raised at 25 °C. T-maze. OCT 1:100, MCH 1:100.				
Shock reactivity:			one-way	
1) *ok107* / +	90.95 ± 2.387	93.40 (12)	ANOVA with	1-3: $^{ns}p = 0.2011$
2) *unc13B* RNAi / +	91.46 ± 1.530	92.20 (13)	Sidak's *post*	2-3: $^{ns}p = 0.2731$
3) *ok107* > *unc13B* RNAi	95.05 ± 1.188	94.80 (13)	*hoc* test	
Method: 4 days. Raised at 25 °C. Tully Wheel.				
Olfactory acuity: **OCT**				
1) *ok107* / +	45.40 ± 3.920	47.75 (14)	one-way	1-3: $^{ns}p = 0.4807$
2) *unc13B* RNAi / +	37.24 ± 3.330	36.30 (14)	ANOVA with	2-3: $^{ns}p = 0.9736$
3) *ok107* > *unc13B* RNAi	38.54 ± 5.680	42.95 (14)	Sidak's *post*	
			hoc test	

Olfactory acuity: **MCH** 1) *ok107* / + 2) *unc13B* RNAi / + 3) *ok107* > *unc13B* RNAi	 71.71 ± 4.584 67.12 ± 4.763 71.16 ± 4.233	 78.15 (16) 68.00 (18) 73.95 (16)	Kruskal-Wallis with Dunn's *post hoc* test	1-3: $^{ns}p > 0.9999$ 2-3: $^{ns}p > 0.9999$
Method: 6 days. Raised at 25 °C. T-maze. OCT 1:100, MCH 1:100.				
Figure 102a: Short-term memory of UAS-*unc13A* C-term expressed in the mushroom body				
1) *ok107* / +	43.34 ± 1.971	45.50 (32)	Kruskal-Wallis with Dunn's *post hoc* test	1-3: ****$p < 0.0001$ 1-4: *$p = 0.0390$ 2-3: ****$p < 0.0001$ 3-4: ****$p < 0.0001$
2) *unc13A* RNAi / +	53.77 ± 1.926	54.70 (27)		
3) *ok107* > *unc13A* C-term -GFP , *unc13A* RNAi	15.42 ± 2.373	17.50 (25)		
4) *ok107* > *unc13A* C-term -GFP	53.44 ± 3.083	53.60 (29)		
Method: 6 days. Raised at 29 °C. T-maze. OCT 1:100, MCH 1:100.				
Figure 102b: Olfactory acuity with 3-Octanol for UAS-*unc13A* C-term expressed in the mushroom body				
1) *ok107* / +	48.03 ± 4.372	49.90 (16)	one-way ANOVA with Sidak's *post hoc* test	1-3: $^{ns}p = 0.5256$ 1-4: $^{ns}p = 0.9975$ 2-3: $^{ns}p = 0.9655$ 3-4: $^{ns}p = 0.6873$
2) *unc13A* RNAi / +	41.32 ± 6.658	41.45 (18)		
3) *ok107* > *unc13A* C-term -GFP , *unc13A* RNAi	36.84 ± 4.578	39.25 (18)		
4) *ok107* > *unc13A* C-term -GFP	45.76 ± 6.002	48.60 (19)		
Method: 6 days. Raised at 29 °C. T-maze. OCT 1:100, MCH 1:100.				

Figure 102c: Olfactory acuity with 4-Methylcyclohexanol for UAS-*unc13A* C-term expressed in the mushroom body				
1) *ok107* / +	61.65 ± 4.438	67.10 (15)	one-way ANOVA with Sidak's *post hoc* test	1-3: $^{ns}p = 0.7280$ 1-4: $^{ns}p = 0.5652$ 2-3: $^{ns}p = 0.9751$ 3-4: $^{ns}p = 0.0579$
2) *unc13A* RNAi / +	50.72 ± 5.599	54.05 (18)		
3) *ok107* > *unc13A* C-term -GFP , *unc13A* RNAi	54.14 ± 4.945	53.60 (18)		
4) *ok107* > *unc13A* C-term -GFP	71.03 ± 3.557	73.55 (16)		
Method: 6 days. Raised at 29 °C. T-maze. OCT 1:100, MCH 1:100.				
Figure 102d: 1 hour Mid-term memory of UAS-*unc13A* C-term expressed in the mushroom body				
1) *ok107* / +	43.06 ± 3.359	43.30 (9)	one-way ANOVA with Sidak's *post hoc* test	1-3: $^{****}p < 0.0001$ 1-4: $^{ns}p = 0.7966$ 2-3: $^{****}p < 0.0001$ 3-4: $^{****}p < 0.0001$
2) *unc13A* RNAi / +	50.57 ± 3.953	52.10 (11)		
3) *ok107* > *unc13A* C-term -GFP , *unc13A* RNAi	15.86 ± 2.907	18.80 (11)		
4) *ok107* > *unc13A* C-term -GFP	48.31 ± 2.694	48.80 (7)		
Method: 6 days. Raised at 29 °C. T-maze. OCT 1:100, MCH 1:100.				
Figure 102e: 1 hour Anesthesia-resistant memory of UAS-*unc13A* C-term expressed in the mushroom body				
1) *ok107* / +	17.71 ± 2.243	19.40 (13)	one-way ANOVA with Sidak's *post hoc* test	1-3: $^{*}p = 0.0198$ 1-4: $^{**}p = 0.0013$ 2-3: $^{***}p = 0.0009$ 3-4: $^{****}p < 0.0001$
2) *unc13A* RNAi / +	21.84 ± 2.958	21.05 (14)		
3) *ok107* > *unc13A* C-term -GFP , *unc13A* RNAi	5.233 ± 2.609	3.700 (12)		
4) *ok107* > *unc13A* C-term -GFP	33.68 ± 3.171	36.70 (13)		
Method: 6 days. Raised at 29 °C. T-maze. OCT 1:100, MCH 1:100.				

Figure 102f: 1 hour Anesthesia-sensitive memory of UAS-*unc13A* C-term expressed in the mushroom body				
1) *ok107* / +	25.59 ± 2.243	23.90 (13)	one-way ANOVA with Sidak's *post hoc* test	1-3: $^{**}p = 0.0066$ 1-4: $^{*}p = 0.0458$ 2-3: $^{***}p = 0.0001$ 3-4: $^{ns}p = 0.9065$
2) *unc13A* RNAi / +	30.26 ± 2.958	31.05 (14)		
3) *ok107* > *unc13A* C-term -GFP , *unc13A* RNAi	12.00 ± 2.787	14.85 (12)		
4) *ok107* > *unc13A* C-term -GFP	15.12 ± 3.171	12.10 (13)		
Method: 6 days. Raised at 29 °C. T-maze. OCT 1:100, MCH 1:100.				
Figure 102g: 3 hours Mid-term memory of UAS-*unc13A* C-term expressed in the mushroom body				
1) *ok107* / +	37.46 ± 5.176	41.50 (10)	one-way ANOVA with Sidak's *post hoc* test	1-3: $^{***}p = 0.0006$ 1-4: $^{ns}p = 0.9814$ 2-3: $^{*}p = 0.0122$ 3-4: $^{***}p = 0.0001$
2) *unc13A* RNAi / +	31.78 ± 4.200	29.80 (10)		
3) *ok107* > *unc13A* C-term -GFP , *unc13A* RNAi	14.34 ± 2.741	15.70 (11)		
4) *ok107* > *unc13A* C-term -GFP	40.19 ± 3.411	37.35 (10)		
Method: 6 days. Raised at 29 °C. T-maze. OCT 1:100, MCH 1:100.				
Figure 102h: 3 hours Anesthesia-resistant memory of UAS-*unc13A* C-term expressed in the mushroom body				
1) *ok107* / +	15.27 ± 1.783	15.55 (12)	one-way ANOVA with Sidak's *post hoc* test	1-3: $^{ns}p = 0.2919$ 2-3: $^{*}p = 0.0112$ 3-4: $^{****}p < 0.0001$ 1-4: $^{*}p = 0.0144$
2) *unc13A* RNAi / +	21.82 ± 3.768	18.50 (12)		
3) *ok107* > *unc13A* C-term -GFP , *unc13A* RNAi	6.900 ± 3.229	10.10 (12)		
4) *ok107* > *unc13A* C-term -GFP	29.75 ± 4.072	24.75 (12)		
Method: 6 days. Raised at 29 °C. T-maze. OCTt 1:100, MCH 1:100.				

Figure 102i: 3 hours Anesthesia-sensitive memory of UAS-*unc13A* C-term expressed in the mushroom body				
1) *ok107* / +	26.23 ± 1.783	25.95 (12)	one-way ANOVA with Sidak's *post hoc* test	1-3: $^{**}p = 0.0024$ 1-4: $^{**}p = 0.0011$ 2-3: $^{ns}p = 0.9996$ 3-4: $^{ns}p = 0.9984$
2) *unc13A* RNAi / +	7.983 ± 3.768	11.30 (12)		
3) *ok107* > *unc13A* C-term -GFP , *unc13A* RNAi	8.800 ± 3.229	5.600 (12)		
4) *ok107* > *unc13A* C-term -GFP	7.600 ± 4.072	12.60 (12)		
Method: ASM values were calculated as the MTM median minus the particular ARM values.				
Figure 103c: Short-term memory of UAS-*unc13A* N-term^{DN} expressed in the mushroom body				
1) *ok107* / +	58.97 ± 2.268	59.40 (7)	one-way ANOVA with Sidak's *post hoc* test	1-3: $^{****}p < 0.0001$ 2-3: $^{****}p < 0.0001$
2) *unc13A* N-term^{DN} -GFP / +	63.00 ± 3.860	67.00 (7)		
3) *ok107* > *unc13A* N-term^{DN} -GFP	28.13 ± 4.015	23.35 (8)		
Method: 6 days. Raised at 25 °C. T-maze and Tully Wheel. OCT 1:100, MCH 1:100.				
Figure 103a: Olfactory acuity with 3-Octanol for UAS-*unc13A* N-term^{DN} expressed in the mushroom body				
1) *ok107* / +	43.80 ± 5.499	49.45 (18)	one-way ANOVA with Sidak's *post hoc* test	1-3: $^{**}p = 0.0032$ 2-3: $^{***}p = 0.0003$
2) *unc13A* N-term^{DN} -GFP / +	49.91 ± 5.386	52.25 (18)		
3) *ok107* > *unc13A* N-term^{DN} -GFP	18.08 ± 5.476	12.55 (18)		
Method: 6 days. Raised at 25 °C. T-maze. OCT 1:100.				

Figure 103b: Olfactory acuity with 4-Methylcyclohexanol for UAS-*unc13A* N-term^{DN} expressed in the mushroom body				
1) *ok107* / +	72.81 ± 4.607	74.25 (18)	Kruskal-Wallis with Dunn's *post hoc* test	1-3: $^{ns}p = 0.0849$ 2-3: $^{ns}p = 0.2595$
2) *unc13A* N-term^{DN} -GFP / +	71.22 ± 3.272	70.55 (18)		
3) *ok107* > *unc13A* N-term^{DN} -GFP	58.41 ± 5.403	63.30 (18)		
Method: 6 days. Raised at 25 °C. T-maze. MCH 1:100.				
Figure 104b: Short-term memory of UAS-*unc13A* N-term^{DN} expressed in the mushroom body, restricted to the adulthood				
1) *tub*-Gal80^{ts} / + ;; *ok107* / +	53.87 ± 3.719	54.30 (12)	one-way ANOVA with Sidak's *post hoc* test	1-3: $^{ns}p = 0.1872$ 2-3: $^{ns}p = 0.3322$
2) *unc13A* N-term^{DN} -GFP / +	52.38 ± 2.146	51.70 (12)		
3) *tub*-Gal80^{ts} ;; ok107 > *unc13A* N-term^{DN} -GFP	46.44 ± 3.188	47.95 (12)		
Method: 6 days. Raised at 18 °C, after eclosion at 29 °C. T-maze and Tully Wheel. OCT 1:100, MCH 1:100.				
Figure 104c: 1 hour Mid-term memory of UAS-*unc13A* N-term^{DN} expressed in the mushroom body, restricted to the adulthood				
1) *tub*-Gal80^{ts} / + ;; *ok107* / +	39.11 ± 2.911	38.95 (16)	Kruskal-Wallis with Dunn's *post hoc* test	1-3: $^{*}p = 0.0171$ 2-3: $^{ns}p = 0.1123$
2) *unc13A* N-term^{DN} -GFP / +	36.88 ± 3.667	36.00 (15)		
3) *tub*-Gal80^{ts} ;; *ok107* > *unc13A* N-term^{DN} -GFP	26.42 ± 3.422	23.15 (16)		
Method: 6 days. Raised at 18 °C, after eclosion at 29 °C. T-maze. OCT 1:100, MCH 1:100.				

Figure 104d: 1 hour Anesthesia-resistant memory of UAS-*unc13A* N-term^{DN} expressed in the mushroom body, restricted to the adulthood				
1) *tub*-Gal80^{ts} / + ;; *ok107* / +	8.264 ± 3.588	8.750 (14)	one-way ANOVA with Sidak's *post hoc* test	1-3: $^{ns}p = 0.7962$ 2-3: $^{ns}p = 0.8387$
2) *unc13A* N-term^{DN} -GFP / +	12.61 ± 2.632	11.65 (14)		
3) *tub*-Gal80^{ts} ;; *ok107* > *unc13A* N-term^{DN} -GFP	10.58 ± 1.921	8.800 (16)		
Method: 6 days. Raised at 18 °C, after eclosion at 29 °C. T-maze. OCT 1:100, MCH 1:100.				
Figure 104e: 1 hour Anesthesia-sensitive memory of UAS-*unc13A* N-term^{DN} expressed in the mushroom body, restricted to the adulthood				
1) *tub*-Gal80^{ts} / + ;; *ok107* / +	30.69 ± 3.588	30.20 (14)	one-way ANOVA with Sidak's *post hoc* test	1-3: $^{****}p < 0.0001$ 2-3: $^{*}p = 0.0145$
2) *unc13A* N-term^{DN} -GFP / +	23.39 ± 2.632	24.35 (14)		
3) *tub*-Gal80^{ts} ;; *ok107* > *unc13A* N-term^{DN} -GFP	12.57 ± 1.921	14.35 (16)		
Method: ASM values were calculated as the MTM median minus the particular ARM values.				
Table 17: Innate behavior for the conducted C- or N-terminus of Unc13A, expressed in the mushroom body				
<u>Shock reactivity:</u> 1) *ok107* / + 2) *unc13A* RNAi / + 3) *ok107* > *unc13A* C-term -GFP , *unc13A* RNAi 4) *ok107* > *unc13A* C-term-GFP	 85.49 ± 1.639 73.70 ± 2.689 79.52 ± 2.734 79.48 ± 3.372	 85.40 (12) 70.00 (12) 81.20 (12) 79.05 (12)	one-way ANOVA with Sidak's *post hoc* test	1-3: $^{ns}p = 0.4065$ 2-3: $^{ns}p = 0.4330$ 3-4: $^{ns}p > 0.9999$ 1-4: $^{ns}p = 0.3997$
Method: 5 days. Raised at 29 °C. T-maze.				
<u>Shock reactivity:</u> 1) *ok107* / + 2) *unc13A* N-term^{DN} -GFP / + 3) *ok107* > *unc13A* N-term^{DN} -GFP	 91.42 ± 2.136 81.85 ± 3.155 88.91 ± 1.691	 89.55 (6) 81.85 (6) 88.75 (10)	one-way ANOVA with Sidak's *post hoc* test	1-3: $^{ns}p = 0.6767$ 2-3: $^{ns}p = 0.0696$
Method: 6 days. Raised at 25 °C. Tully Wheel.				

Shock reactivity: 1) *tub*-Gal80^{ts} / + ;; ok107 / + 2) *unc13A* N-term^{DN} -GFP / + 3) *tub*-Gal80^{ts} ;; ok107 > *unc13A* N-term^{DN} -GFP	95.08 ± 1.045 85.13 ± 1.794 93.32 ± 1.068	96.75 (10) 86.45 (10) 94.35 (10)	Kruskal-Wallis with Dunn's *post hoc* test	1-3: $^{ns}p = 0.3902$ 2-3: $^{*}p = 0.0153$
Method: 6 days. Raised at 18 °C, after eclosion at 29 °C. Tully Wheel.				
Olfactory acuity: **OCT** 1) *tub*-Gal80^{ts} / + ;; ok107 / + 2) *unc13A* N-term^{DN} -GFP / + 3) *tub*-Gal80^{ts} ;; ok107 > *unc13A* N-term^{DN} -GFP	44.03 ± 9.953 38.93 ± 8.790 26.60 ± 10.15	53.35 (12) 44.85 (12) 11.80 (12)	one-way ANOVA with Sidak's *post hoc* test	1-3: $^{ns}p = 0.3763$ 2-3: $^{ns}p = 0.6063$
Olfactory acuity: **MCH** 1) *ok107* / + 2) *unc13A* N-term^{DN} -GFP / + 3) *ok107 > unc13A* N-term^{DN} -GFP	43.23 ± 5.946 42.79 ± 3.546 44.72 ± 5.438	41.25 (12) 41.45 (12) 42.55 (12)	one-way ANOVA with Sidak's *post hoc* test	1-3: $^{ns}p = 0.9737$ 2-3: $^{ns}p = 0.9561$
Method: 6 days. Raised at 18 °C, after eclosion at 29 °C. T-maze. OCT 1:100, MCH 1:100.				